1993

Observed And Calculated Behaviour Of A Geotextile Reinforced Embankment On A Soft Compressible Soil

Carthigesu Thiagarajah Gnanendran

OBSERVED AND CALCULATED BEHAVIOUR OF A GEOTEXTILE REINFORCED EMBANKMENT ON A SOFT COMPRESSIBLE SOIL

by

Carthigesu Thiagarajah Gnanendran

Faculty of Engineering Science

Submitted in partial fulfilment

of the requirement for the degree of

Doctor of Philosophy

Faculty of Graduate Studies

The University of Western Ontario

London, Ontario

August 1993

ISBN 0-315-83955-4

ABSTRACT

An instrumented test embankment was constructed to failure on a soft compressible organic clayey silt deposit at Sackville, New Brunswick, Canada in Sept./ Oct., 1989. This embankment consisted of an unreinforced section and a section reinforced with a relatively high strength polyester woven geotextile. The instrumentation, field performance and analyses of these embankments are examined in this thesis.

The observed responses of pore pressure, settlement, heave and lateral displacements in the foundation soil and the strain in the geotextile are correlated and failure of each embankment is discussed. An account of the development and propagation of cracks in relation to the construction and the interpretation of failure for each embankment is also discussed. The excess pore pressure response and soil deformations showed some evidence of the susceptibility of the soil to progressive failure. The actual failure was of a plastic (or visco-plastic) type and no classical-type of abrupt failure was encountered during the construction of either of these embankments.

A numerical model is developed to perform fully coupled large strain elasto-plastic consolidation analysis with Modified cam-clay material behaviour using 15-noded cubic strain triangular elements. The viscous/creep effects and the potential strain softening behaviour of the soil are not considered in this numerical model. The test embankment was back analyzed using information obtained from the field investigation together with engineering properties of the soils and geotextile obtained from laboratory tests. The results of finite element analysis using this model are shown to be in reasonable agreement with the observed performance. The deformations at large depth and the large settlements and heaves observed in the field at high embankment thicknesses could not be predicted

satisfactorily using this model.

Finite element analyses are used to study the sensitivity of embankment behaviour to variations in the foundation soil and embankment fill properties. The influence of the variation of over consolidation ratio (OCR), the coefficient of earth pressure at rest (K_0), angle of internal friction, Poisson's ratio and the permeability of the foundation soil as well as the effective friction angle of the embankment fill are examined. This sensitivity study indicated that the effective friction angle (ϕ'), K_0 and OCR of the foundation soil are all important parameters and therefore should be measured or estimated carefully. Furthermore, uncertainties regarding the Poisson's ratio did not affect the results of the analysis significantly but the uncertainties regarding permeabilities of the foundation soil or effective friction angle may have a significant influence on the behaviour of such reinforced embankments on soft soil.

Both small strain and large strain undrained finite element models are also used to back analyze the reinforced embankment. The effect of changing the undrained shear strength profile on the behaviour of this embankment is examined. The failure of the reinforced embankment could be predicted accurately by a small strain undrained finite element analysis using the mean shear strength profile (between the field vane and the CAU triaxial and constant volume direct simple shear tests in the lab).

DEDICATION

to my family

ACKNOWLEDGEMENTS

The author wishes to express his sincere gratitude and appreciation to his advisor Dr. R. Kerry Rowe for his guidance, encouragement and continuous support throughout the course of this study.

Valuable suggestions and encouragement given by Dr. K. Y. Lo and Dr. I. D. Moore are gratefully appreciated.

Special thanks go to Dr. A. O. Landva, Dr. A. J. Valsangkar for their participation in the construction and field monitoring of the embankment.

Thanks are due to Dr. Tim Law for providing the data from the site investigation performed by NRC under his direction.

The construction and monitoring of the test embankment was funded by the Natural Science and Engineering Research Council of Canada by means of Strategic Grant STR12092 to Dr. A. O. Landva, Dr. Tim Law, Dr. R. Kerry Rowe, Dr. Arun Valsangkar and Dr. P. LaRochelle. Additional funding came from the Natural Science and Engineering Research Council of Canada under Grant No. A1007 awarded to Dr. R. Kerry Rowe.

The author wishes to acknowledge Dr. J. P. Carter and Dr. N. P. Balaam for developing the original version of the program AFENA, from coding written by R. L. Taylor (Zienkiewicz, 1977). The version of AFENA used in this thesis was a modified version of that originally developed by Dr. J. P. Carter and Dr. N. P. Balaam.

Many thanks are due to the following people for their assistance during the course of study and preparation of the thesis:

To Mr. Gary Lusk for his assistance and co-operation during the laboratory testing program and for his superb draftsmanship in preparing some of the figures presented in this thesis.

To Mr. Paul Ho for his assistance during the testing of the geotextile.

To Mr. K. White for his assistance in the installation of instruments and monitoring of the embankment during the field investigation.

To Dr. J. Govindarajan, Ms. Colleen Bretzlaff, Mr. Dan Corrin, Mr. George Jelich and Mr. Barry Kay for their invaluable assistance with the computing facilities at the University of Western of Ontario.

To Mr. S. Hinchberger, Mr. N. Prebaharan and all other friends for their encouragement and moral support.

Finally, with heartfelt love and gratitude, the author wishes to thank his wife Aathirai and daughters Abbyrhamy, Lokiny and Subashini for their understanding, encouragement and patience throughout the course of this study.

TABLE OF CONTENTS

LIST OF TABLES

LIST OF FIGURES

NOTATION

A, B, C, A1,B1	the constants to relate the hydraulic conductivity with void ratio i.e. $k_y = A * (B - e)^C$ when the soil is normally consolidated and $k_y = A1 * e^{B1}$ when the soil is overconsolidated
A_f	Skempton's pore pressure parameter at failure (i.e. $\Delta u/\Delta\sigma_1$ at failure)
$\overline{B}$	empirical pore pressure parameter ($\Delta u/\Delta\sigma_1$)
c'	apparent cohesion
C_u	undrained shear strength
C_c	gradient of the compression line in the e - log p′ plot
C_s	gradient of the swelling line in the e - log p′ plot
e	void ratio
e_{cs}	void ratio at critical state line at p′ = 1 kPa
E′	Young's modulus in terms of effective stresses
E_u	undrained modulus of the foundation soil
ε	normal strain
ε_v	volumetric strain
ε_x	normal strain in x - direction
ε_y	normal strain in y - direction
γ_{xy}	shear strain
ϕ'	effective friction angle of the soil
ϕ_u	undrained angle of internal friction for the foundation soil
ψ	angle of dilatancy

FS	factor of safety
G	shear modulus
G_s	specific gravity of soil solids
γ	unit weight of soil
I_p	plasticity index
I_L	liquidity index
J	geosynthetic tensile modulus (kN/m)
k_x, k_y or k_h, k_v	permeability in the horizontal and vertical direction
K	parameter of Janbu's equation for Young's modulus of the embankment fill
K_o	coefficient of effective lateral earth pressure at rest
K_a	coefficient of active earth pressure
κ	gradient of the swelling line in the e - ln p′ plot
λ	gradient of the compression line in the e - ln p′ plot
M	critical state friction constant, $M = \frac{6 \sin\phi'}{3 - \sin\phi'}$
p′	mean normal effective stress = $(\sigma_1' + \sigma_2' + \sigma_3')/3$
p_c'	isotropic preconsolidation pressure
P_a	atmospheric pressure
q	generalized deviator stress $= [(\sigma_1' - \sigma_2')^2 + (\sigma_2' - \sigma_3')^2 + (\sigma_1' - \sigma_3')^2]^{\frac{1}{2}}$
OCR	over consolidation ratio
ν or ν'	Poisson's ratio

ρ_c	rate of increase in undrained shear strength with depth
σ_{xx}	normal stress in the x - plane x - direction
σ_{yy}	normal stress in the y - plane y - direction
σ_{xy}	shear stress in x - plane y - direction
σ_1' and σ_3'	major and minor principal effective stresses respectively
σ_1 and σ_3	major and minor principal total stresses respectively
t	time
u	pore water pressure
w	water content
w_n	natural water content (%)
w_p	plastic limit (%)
w_L	liquid limit (%)

CHAPTER 1

INTRODUCTION

1.1 GENERAL

Soft compressible organic clayey silt/silty clay deposits are widely distributed in Canada. The construction of embankments on such soft compressible soil deposits appears to be affected by gradual growth of the plastic region and the potential softening behaviour of these deposits. The construction costs associated with the need for stage loading and/or the height and slope restrictions associated with the construction of conventional embankments on these soils are substantial. The magnitude of this problem has necessitated the development of practical engineering solutions, including the use of geosynthetic reinforcement. It is becoming a common practice to make use of geotextiles to improve the stability and performance of embankments constructed on such deposits.

Full scale instrumented structures and the measurements obtained from them would provide a reliable method to investigate the validity of theories and assumptions applied in engineering analysis and design. In addition, full scale measurements often provide a sound basis for development of improved solutions to engineering problems. Despite the research that has been conducted into the stability of fills on soft clays, there are still many unanswered questions concerning the behaviour of embankments on organic silts/clays; and there are very few cases where instrumented reinforced and unreinforced embankments have been constructed to failure at the same site (a noted exception being the Almere embankment, SCW, 1981; Rowe and Soderman, 1984).

An instrumented test embankment was constructed between Sackville and Aulac

in the Province of New Brunswick, Canada in September/October 1989. The objective of this test embankment was to provide a case record of deformation and progressive failure for both reinforced and unreinforced embankment sections constructed on a soft compressible soil. The design, instrumentation, construction and monitoring of this test embankment are described in this thesis. The soil profile obtained from the field investigation conducted at this site and the soil parameters determined from a laboratory investigation on samples retrieved from the site prior to construction of this embankment are also described in this thesis.

In order to make reasonable predictions of the stability and deformations of geotextile reinforced embankments on soft compressible organic soils, it is necessary to use a method of analysis which is sophisticated enough to accurately model their complex behaviour. The results of finite element analyses performed using both small strain and large strain undrained models to predict the behaviour of this test embankment are reported. For the type of foundation soil under investigation, there could be significant consolidation during construction. Therefore, a numerical model was developed to perform fully coupled large strain elasto-plastic Biot consolidation analysis with Modified cam-clay material behaviour using 15-noded cubic strain triangular elements and the resulting calculated behaviour is compared with the observed behaviour of the test embankment.

Finite element analyses have also been used in this thesis to study the sensitivity of embankment behaviour to variations in the foundation soil and embankment fill properties. In particular, the influence of the variation of over consolidation ratio, the coefficient of earth pressure at rest, angle of internal friction, Poisson's ratio and the permeability of the foundation soil as well as the effective friction angle of the embankment fill are examined in light of the vertical and horizontal deformations, excess

pore pressures and the geotextile strain.

1.2 OUTLINE OF THE THESIS

Finite element and limit equilibrium methods available for the analysis of geotextile reinforced embankments are critically reviewed in chapter 2. The details of the limit equilibrium method used for the design of the test embankment is also briefly described in this chapter.

The observed behaviour of the unreinforced section of the test embankment is described in chapter 3. The overall site conditions, foundation soil properties, the properties of the fill material, construction detaiis and the data collection procedures adopted at the site are also discussed in this chapter. The pore pressure responses, settlement, heave and lateral displacements of the unreinforced section are correlated and failure of the embankment is discussed.

The behaviour of the reinforced section of the test embankment is reported in chapter 4. The construction sequence adopted, the observed pore pressure response, the variation in both the vertical and horizontal displacements of selected points on the ground surface as well as in the foundation soil, and the horizontal displacement profile along vertically placed inclinometers are presented. An account of the development and propagation of cracks in relation to the construction and the manner in which initial failure and rotational failure of the embankment were interpreted is also described.

A relatively high strength polyester woven geotextile (Nicolon style 68300) was used as reinforcement. Instrumentation of the geotextile and the geotextile strain responses observed in the field are described in chapter 5. The properties of the geotextile

reinforcement and the geotextile-fill interface are also discussed in this chapter.

A laboratory testing programme was also developed and carried out at the Geotechnical Laboratory of the University of Western Ontario to determine additional soil parameters required for the analyses. In this investigation, triaxial, direct simple shear, consolidation and permeability tests were performed using the large diameter undisturbed samples retrieved from the site. The details of this investigation and the results obtained therefrom are reported in chapter 6.

Chapter 7 contains a brief description of both undrained and consolidation finite element models used for the small strain and large strain analyses reported in this thesis.

The predicted behaviour of the test embankment from a fully coupled large strain elasto-plastic Biot consolidation finite element analysis is compared with the field observations in chapter 8.

The sensitivity of the calculated behaviour of the reinforced embankment to variations in the foundation soil and the embankment fill parameters are examined in chapter 9. The sensitivity to the undrained shear strength profile is also examined in this chapter.

Finally, the conclusions drawn from the work reported in the previous chapters and recommendations for future work are presented in chapter 10.

CHAPTER 2

REVIEW OF METHODS OF ANALYSIS

2.1 INTRODUCTION

Geosynthetic reinforced embankments constructed on soft soil foundation may be analyzed using either limit equilibrium or finite element methods. Both have advantages and disadvantages. In this chapter the use of limit equilibrium and finite element approaches in predicting the performance of geosynthetic reinforced embankments is examined.

The term 'progressive failure' has been used in chapters 3 and 4 to describe the observed behaviour of both unreinforced and reinforced test embankments constructed at Sackville, New Brunswick. Different definitions have been used for this term in the past by various researchers. Initially, Terzaghi (1936) postulated a mechanism of progressive failure in stiff fissured clays. In his discussion of the process of softening, the time element is implied for progressive failure to occur. On the other hand, Terzaghi and Peck (1948), Taylor (1948), Bishop (1967), appeared to consider progressive failure in the context of spreading of yield zones in space.

In this thesis, the term 'progressive failure' is defined as the process of successive failure of individual soil elements in a soil mass. The term progressive refers both to space and time. Various mechanisms have been proposed in the past for the occurrence of progressive failure. For example, Bjerrum (1967) discussed the existence of high horizontal effective stress in overconsolidated clays as a mechanism of progressive failure. In a later investigation, Lo (1972) suggested that the material should possess a

strain-softening post-peak stress-strain relationship as a necessary condition for the occurrence of progressive failure. The cause or the particular mechanism involved for the progressive failure are not investigated in this thesis but only the evidence of its occurrence from the observed excess pore pressure and deformational responses of the foundation soil with time are discussed. In essence, the term 'progressive failure' implies the gradual growth of plastic region with space and time at constant load. This could be due to strain softening, time dependent (i.e. creep) strength loss (caused by visco-plastic behaviour of the soil) or due to some other mechanism.

2.2 LIMIT EQUILIBRIUM METHOD

Limit equilibrium methods have been used extensively to assess the short term stability of geosynthetic reinforced embankments constructed on soft soil foundations (e.g. Fowler, 1982; Haliburton, 1981; Jewell, 1982; Ingold, 1982; Milligan and La Rochelle, 1984; Rowe and Soderman, 1985; Low et al., 1990; Kaniraj and Abdullah, 1992 and others).

The various methods are similar in that limiting equilibrium is examined for the system of external forces acting on an assumed failure mass. In general, the following failure mechanisms are examined in these methods: 1) bearing capacity failure of the foundation involving the entire embankment; 2) lateral sliding of a block along the embankment-reinforcement interface, foundation-reinforcement interface or along a weak zone or layer within the foundation soil, and 3) a slip circle type failure mechanism through the embankment and foundation soil.

The majority of these limit equilibrium methods are total stress analysis ($\phi = 0$) and assume an approximated circular arc type of failure surface. The slip circle type of

failure mechanism is the focus of the following discussion.

A typical slip circle type failure mechanism is shown in Fig. 2.1. The external forces acting on the failure mass and involved in the moment equilibrium are: the weight of the failure mass, W, the soil shear force mobilized along the circular arc failure surface and the force representing the geotextile, T. The factor of safety against collapse is defined as the ratio of the restoring moment due to the soil shear strength and the reinforcement force, to the overturning moment due to the weight of the failure mass.

It is generally agreed that the reinforcement force can be assumed to act at the intersection of the failure surface and the plane of the geotextile and acts in a direction which increases the restoring moment. There is still debate regarding the inclination (orientation) and magnitude of this force. The majority of the methods (e.g. Brakel et al., 1982, Ingold, 1982, Jewell, 1982, Milligan and La Rochelle, 1982 among others) assume that the reinforcement force acts in its original orientation (usually horizontal). Some methods (e.g. Haliburton, 1981 and Fowler, 1982) assume that the reinforcement force acts tangential to the slip surface. They argue that the local deformations associated with the formation of a slip surface result in a local reorientation of the geotextile so that it is tangent to the slip circle. There are a few other methods which assume a somewhat intermediate orientation for the reinforcement force (e.g. Stabilenka design charts by Enka Industrial Systems Group, 1987 which assume that the reinforcement force acts parallel to the bisector between the horizontal and the tangential directions). Still other methods (e.g. Rowe and Soderman, 1985) consider both tangential and horizontal orientations. Rowe and Soderman (1985) concluded that the soil-structure interaction plays an important role in the mobilization of geotextile force and considered its effect approximately in terms of an allowable compatible strain. However, complete consideration of soil-structure interaction is not possible by limit equilibrium techniques alone. More recent methods

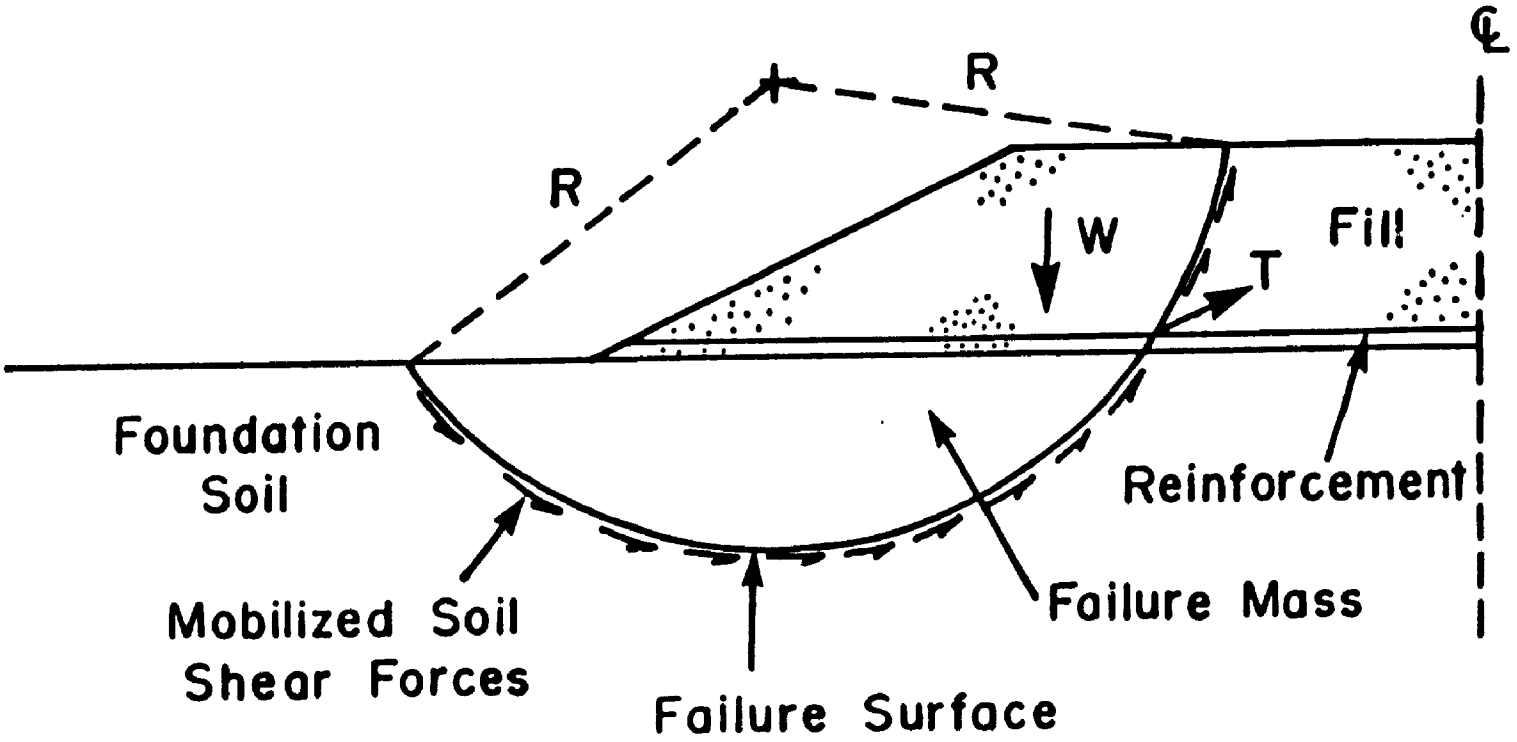

FIG. 2.1 TYPICAL SLIP CIRCLE TYPE MECHANISM

(e.g. Low et al., 1990) considers all three orientations mentioned above.

The reinforcement orientation which provides the best agreement with observed embankment behaviour is dependent on the particular case. However, the assumption that the reinforcement remains in its original (horizontal) orientation is the most conservative and the assumption that the reinforcement force is tangential to the slip circle is the other extreme. The bisector orientation assumption is in between the two.

In a slip circle type limit equilibrium analysis, a reinforced embankment is considered to have failed along a circular mechanism through the soil and the shear strength is mobilized along this failure surface. It is typically assumed that the reinforcement has either failed in tension or pulled out of the soil. A number of recommendations can be found in the literature regarding what limiting reinforcement force should be used in limit equilibrium calculations. Some investigators (e.g. Haliburton, 1981 and Fowler, 1982) consider the geotextile to have failed when its ultimate tensile strength is reached. Others (e.g. Jewell, 1982; Ingold, 1982; Milligan and La Rochelle, 1984) suggest limiting the force in the geotextile to some fraction of its ultimate tensile strength to reduce the likelihood of geotextile creep to rupture. Based on a review of available information, Bonaparte and Christopher (1987) suggest values of limiting strain which are dependent on foundation soil type for use in limit equilibrium calculations.

The failure heights determined using this slip circle approach are plastic collapse heights. This method, as in all limit equilibrium analysis approaches, gives no indication of the deformations of the reinforced embankment prior to and during failure. In some instances, the embankment may actually have failed due to excessive displacement prior to reaching the collapse height predicted using limit equilibrium analysis. In some cases,

extremely large displacements may be required to cause failure of the geosynthetic reinforcement. Having recognized this possibility, Jewell (1982) suggests that the limiting strain in the geosynthetic should be limited to such a value which could be expected under conditions of strain compatibility of the soil and geotextile reinforcement. However, Jewell (1982) does not indicate how to determine an appropriate value of allowable geosynthetic strain for a given situation. Rowe and Soderman (1985) have proposed a technique which may be used to estimate an "allowable compatible strain" for use in limit equilibrium calculations for reinforced embankments constructed on soft homogeneous clayey foundations.

A limit equilibrium analysis program, REAP (Reinforced Embankment Analysis Program), based on a modified version of a method proposed by Jewell (1982) developed by Myllevelle and Rowe (1988) was used for the design of both the unreinforced and reinforced sections of the test embankment constructed at Sackville, New Brunswick. It was also used to evaluate the Factor of Safety for the observed failure surface through back analysis as reported in a subsequent chapter of this thesis.

The limit equilibrium method (REAP) considers the overall undrained stability of a reinforced embankment on a cohesive deposit. Details of the basic assumptions, theory and computer implementation of the analysis can be found elsewhere (see Myllevelle and Rowe, 1988). The method essentially considers moment equilibrium about the centre of the slip circle under consideration. The overturning moments are considered to be made up of two components, one being that due to embankment fill and the other due to a thrust force within the embankment fill itself (see Fig. 2.2 for the general arrangement of the limit equilibrium problem). The restoring moments are derived from the reinforcement and shear strength of the clay foundation along the assumed failure surface. The reinforcement force is assumed to act horizontally and to be the minimum of: 1) sum of

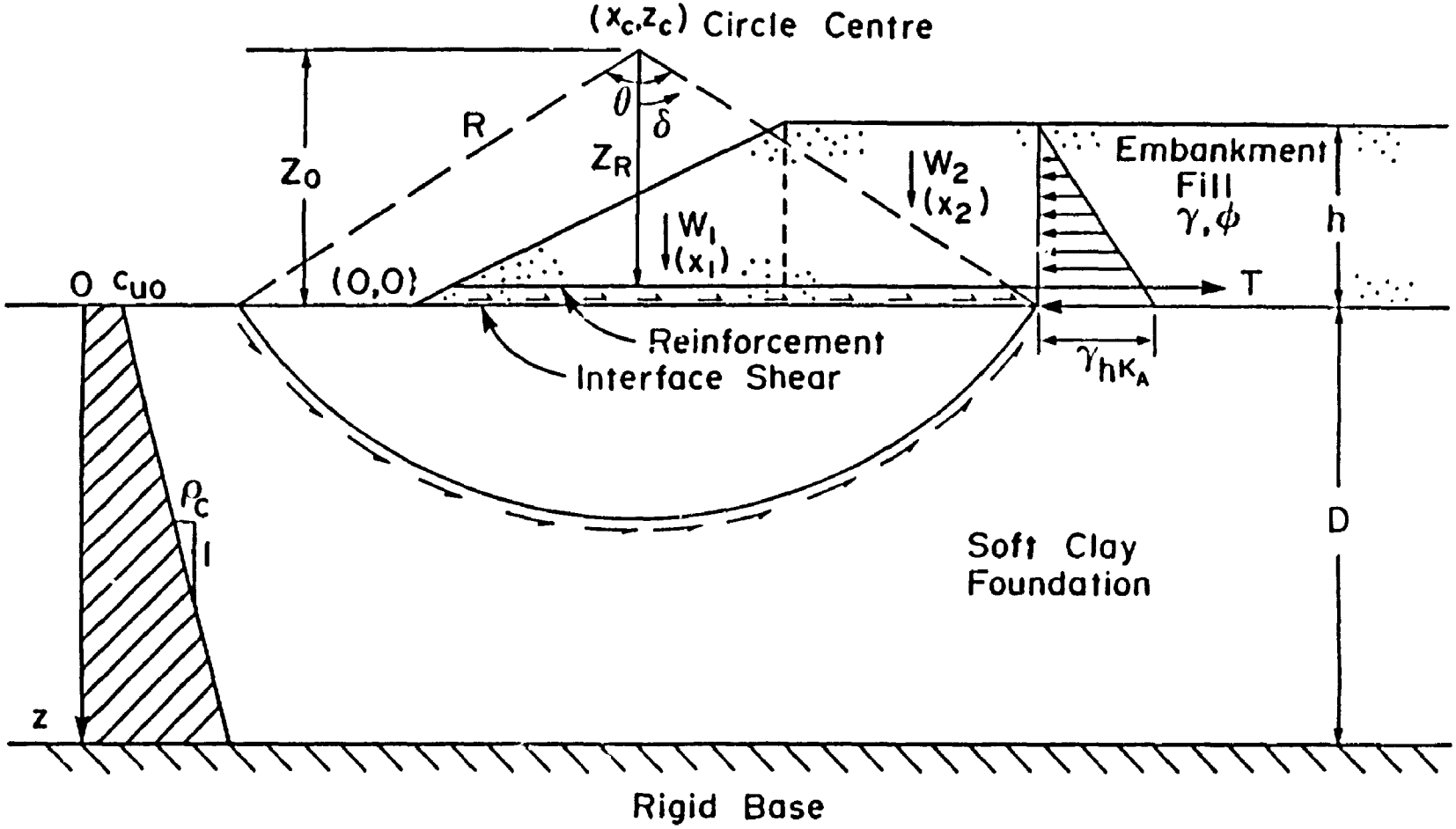

FIG. 2.2 GENERAL ARRANGEMENT OF THE LIMIT EQUILIBRIUM METHOD, REAP (AFTER MYLLEVILLE AND ROWE, 1988)

thrust force in fill and clay fill interface shear; or 2) the pullout capacity of the reinforcement; or 3) the allowable reinforcement force (governed by strength). For unreinforced embankments, REAP gives essentially the same Factor of Safety (or collapse height) and critical circle as simplified Bishop's Method of Slices.

In general, limit equilibrium methods are easy to use and require less time and effort in a design situation. However, they do not provide any information about deformations of the soil or of the geosynthetic. The tensile force developed in the reinforcement depends on the deformations that occur both within the soil medium and within the geosynthetic. Consequently, a limit equilibrium technique which disregards the deformation characteristics of the soil-reinforcement system cannot be rigorously employed to evaluate the behaviour of this system. Furthermore, the deformational characteristics of the two elements (i.e. the reinforcement and the soil) are such that concomitant failure will not occur in the two elements. This mathematical inconsistency can be avoided only by recourse to numerical methods of stress analysis which takes into account both the constitutive responses of the geosynthetic and the soil mass (i.e. both the embankment and the foundation soil).

2.3 FINITE ELEMENT METHOD

In principle, the finite element techniques are attractive because they can model the stress and strain conditions throughout the reinforced soil system. The finite element method has been used to analyze reinforced embankments by many investigators (e.g. Andrawes et al., 1980; Bell et al., 1977; Rowe, 1982, 1984; Rowe and Soderman, 1984; Monnet et al., 1986; Humphrey and Holtz, 1989; Hird and Kwok, 1989; Rowe and Mylleville, 1990 and others). Despite some similarities, these approaches differ considerably with regard to the assumptions implicit in the finite element formulations. In

particular, different levels of sophistication have been adopted with regard to the modelling of nonlinearity, plastic failure, large deformations (i.e. small and large strain theory), the geosynthetic, and the soil-geosynthetic interface conditions (i.e. geosynthetic-soil interaction). The assumptions made regarding these factors may significantly affect the results of a particular analysis and therefore their validity need to be assessed for any specific application.

Early work done by Andrawes et al. (1980) used small strain theory to analyze model tests. The model tests consisted of placing a geotextile-reinforced granular embankment on a compressible rubber foundation. The granular fill and rubber foundation were assumed to be a hyperbolic elastic material. The load deformation behaviour of the geotextile was modelled using a polynomial function and the relative tangential displacement at the geotextile-soil interface was governed by a hyperbolic elastic model. It is not surprising that reasonable results were obtained using this model since rubber, unlike real soils, is a nonlinear elastic material.

Bell et al. (1977) and Boutrup and Holtz (1983) have examined a 1.4 m high geotextile-reinforced embankment constructed on a 2.7 m thick deposit of muskeg using a nonlinear, large deformation analysis. Bell et al. used a linear orthotropic elastic model for the embankment fill whereas Boutrup and Holtz used an elasto-plastic model with a Drucker-Prager failure criterion. A series of multi-linear elastic truss members were used to model the geotextile and no provision was made for slip at the geotextile-soil interface. The geometry was updated during the analysis. Based on the analysis, Bell et al. concluded that the low modulus geotextile (~ 50 kN/m) used did not reduce the embankment settlement significantly and the main function of the geotextile was to prevent local bearing failure. Boutrup and Holtz also suggested that the settlements were not substantially affected by the reinforcement even for somewhat higher geotextile

modulus values (88 kN/m and 300 kN/m). The practical value of the results presented by Bell et al. and Boutrup and Holtz is somewhat diminished due to the fact that the parameters adopted for the peat were estimated from the results of laboratory unconfined compression tests and field vane tests. The results of these tests are very difficult to interpret due to the relatively high permeability and the high compressibility of the muskeg.

A parametric study of embankments constructed using surface reinforcement was performed by Ohta et al. (1980). A small strain finite element computer program was used for the analysis. An elasto-plastic model was used for the foundation soil. The stiffness of the embankment was neglected. The reinforcement was represented by a 0.5 m thick elastic layer. Based on the results of this study, Ohta et al. concluded that the surface reinforcement could considerably reduce the deformation and increase the bearing capacity of the foundation. However, the elastic layer used to simulate the reinforcement would result in excessive flexural rigidity and therefore did not adequately model a reinforcing sheet.

Monnet et al. (1986) have simulated the construction of both geotextile-reinforced and unreinforced embankments on a 5 m thick clay deposit using a small strain finite element computer program. The soil was assumed to be an elasto-plastic material with a Drucker-Prager failure criterion and the geotextile was modelled using a series of linear elastic bar elements. The geotextile-soil interface was modelled using an elasto-plastic isoparametric interface element. It was concluded that the use of even a relatively low modulus geotextile (200 kN/m) resulted in decreased settlements and a substantial increase in the embankment failure height. The increase of strength with depth of the foundation soil used was 4.5 kPa/m which is significantly higher than usually expected in soft plastic clays. The conclusion of increased failure height may be overly optimistic for

cases involving lower modulus geotextiles since the deformation of the embankment was not considered in the analysis.

An elasto-plastic soil model with a Mohr-Coulomb failure criterion has been used successfully to model the soil behaviour during the "construction" of reinforced embankments on soft foundations. For example, Rowe and Soderman (1984) used an elasto-plastic soil model to successfully analyze both an unreinforced and geotextile reinforced sections of two test embankments constructed at Almere, The Netherlands. Rowe et al. (1984) also used an elasto-plastic soil model and large deformation finite element theory to back analyze several geotextile reinforced sections of a road embankment constructed in stages on a very soft compressible peat deposit (i.e. Bloomington Road, near Aurona, Ontario).

Rowe and Mylleville (1989 and 1990) have used a similar elasto-plastic soil model to perform parametric studies to investigate the influence of geosynthetic modulus on the behaviour of reinforced embankments and particularly its influence on the strain developed in the reinforcement and the shear strain developed in the foundation. Mylleville and Rowe (1991) have also examined the effect of geosynthetic modulus on the behaviour of reinforced embankments constructed on very soft brittle clay deposits using a similar elasto-plastic model.

More recently, Mylleville (1991) has used an elasto-plastic soil model with Mohr-Coulomb failure criterion and large deformation finite element theory to back-analyze the Stage I construction of the Hubrey Road embankment (near London, Ontario). This embankment was constructed on a very soft compressible deposit of peat and organic silt. The immediate (end of construction phase) behaviour was successfully predicted and partial dissipation of pore pressures during construction was considered in this analysis.

However, in this analysis, the excess pore pressures immediately after construction were calculated using the relationship, $\Delta u = \overline{B}\ \Delta\sigma_1$, where Δu is the excess pore pressure at a point; $\Delta\sigma_1$ is the increase in total major principal stress at that point; and $\overline{B}$ is an empirical pore pressure parameter, instead of using an appropriate large deformation consolidation theory. The fully drained response was also examined and compared with the observed behaviour just prior to Stage II construction of this embankment by Mylleville. Good agreement between the predictions and the measured field performance was reported.

In order to model the entire response of a reinforced embankment system up to collapse, it is necessary to adopt a finite element formulation and constitutive model which (i) models the stress-dependent properties of the embankment material; (ii) correctly models plastic failure and plastic flow in both the embankment fill and foundation; and (iii) allows for potential slip at the reinforcement-soil interface (see Rowe and Soderman, 1987).

In this thesis, the finite element analysis is used to study the behaviour of the test embankment constructed at Sackville, New Brunswick. Small strain as well as large deformation elasto-plastic finite element formulations have been used to analyze this test embankment. Higher order (i.e. cubic strain triangular) elements were used for the foundation in these analyses. The undrained behaviour was studied using the Mohr-Coulomb failure criterion. Consolidation behaviour of the foundation was investigated using fully coupled Biot's consolidation theory with Modified Cam Clay material behaviour. Details regarding the actual model used are discussed in chapter 7.

CHAPTER 3

DETAILS OF THE TEST EMBANKMENT AND THE OBSERVED BEHAVIOUR OF THE UNREINFORCED EMBANKMENT

3.1 INTRODUCTION

In September/October 1989, a test embankment was constructed between Sackville and Aulac in the Province of New Brunswick, Canada. The objective of this test embankment was to provide a case record of deformation and progressive failure for both reinforced and unreinforced embankment sections constructed on a soft compressible soil. The observed behaviour of the unreinforced section of the test embankment is described in this chapter. The behaviour of the reinforced section is reported in chapter 4.

Both this chapter and chapter 4 focus on describing the properties of the insitu soil evident from field tests and conventional index tests, the field instrumentation and the observed response during construction. The results of more elaborate laboratory investigations are reported in chapter 6 and finite element analyses of the two embankments are reported in chapters 8 and 9. The data collected from various instruments are presented in a manner suitable for interpretation and comparison. A plastic type of failure, different from the previous case histories (reported by La Rochelle et al., 1974, Ortigao et al., 1984 and Keenan et al., 1986) was observed in this test embankment. In this chapter, the pore pressure responses, settlement, heave and lateral displacements of the unreinforced section are correlated and failure of the embankment is discussed. Finally, the extent of the interaction between the unreinforced and reinforced sections and interpretation of rotational failure of the unreinforced section is examined. Field observations on the development and propagation of cracks are detailed in chapter 4.

3.2 SITE CONDITIONS AND SOIL PROFILE

The test site is situated in an area of intertidal salt marsh deposit (Rampton and Paradis, 1981), locally known as "Marshland". The construction area chosen was reasonably flat for the most part but was bounded by creeks on the northern and eastern boundaries (see Fig. 3.1). The eastern part of the site had a mild downward slope towards the creek. An initial investigation conducted by Dr. A. Landva of UNB (University of New Brunswick) during June 1989 indicated that there was a root mat underlain by organic clayey silt/silty clay whose strength increased with depth. This investigation included Static Cone Penetration Tests (Cone tests) at two locations (see Fig. 3.2 for locations, denoted as "UNB Cone Tests"). To minimize the fill required to cause failure, the root mat on the northern side of the embankment (see Fig. 3.1) was cut to a depth of 1 to 1.2 m on an approximately 1.3 to 1.8 m square grid.

An NRC team headed by Dr. K. T. Law conducted a series of field tests at the above site during August 1989. These tests included cone penetration tests at five locations and pressure meter test at one location (see Fig. 3.2). These cone tests indicated that there was a significant difference in strength over the site. A Laval University team, headed by Dr. P. La Rochelle, also conducted field tests at the site which included field vane tests at one location and piezocone tests at two locations. Both these teams collected large diameter (200 mm Dia.) samples for use in laboratory investigations and some of the samples collected by Laval University were used for the laboratory investigation reported in chapter 6. The foundation soil was investigated to a maximum depth of 25 m. The bedrock lies at a depth greater than 25 m.

Field vane tests were performed in Sept. 1989 and the data collected from these tests at three locations (V4, V5 and V6) along the proposed unreinforced section are

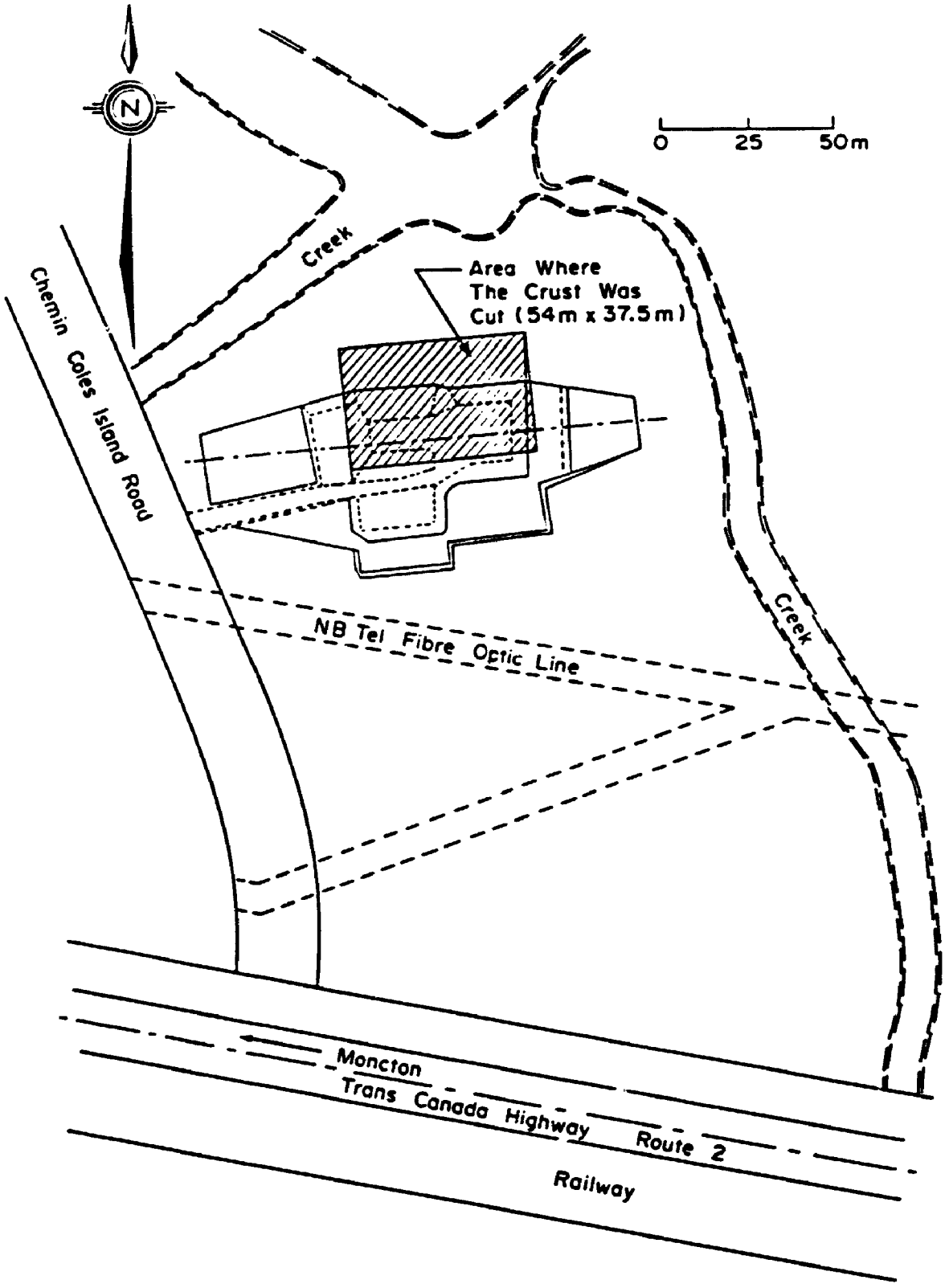

FIG. 3.1 THE SITE PLAN

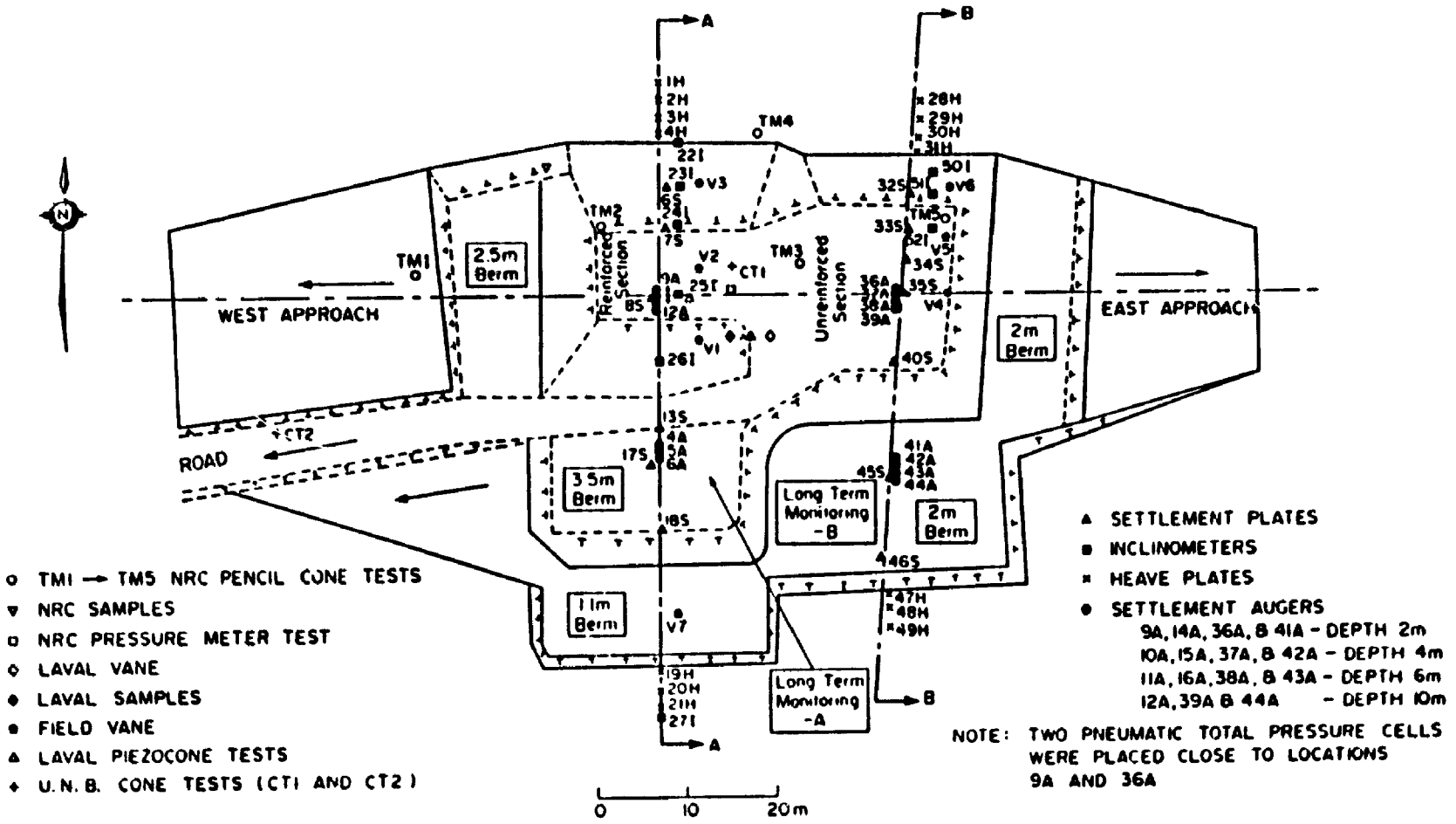

FIG. 3.2 LAYOUT OF INSTRUMENTATION - PLAN

shown in Fig. 3.3. For ease of comparison, the data obtained for the reinforced section (vane locations V1, V2, V3 and V7) are also presented in Fig. 3.3. The locations where the vane tests and cone tests were performed are shown on Fig. 3.2. A typical borehole log of the foundation soil profile, the initial UNB cone data (June 1989) and the profiles of Atterberg limits, water and organic contents and cone data determined at UNB (courtesy Dr. A. Landva) from NRC samples (see Fig. 3.2 for location) are presented in Fig. 3.3 (see also Fig. 3.4 for the plasticity chart). It is noted that the liquidity index of the soil exceeds 1 at depths ranging from 1 to 6 m. A summary of the results from self boring pressuremeter tests conducted by NRC is presented in Table 3.1 and the NRC cone data presented in Fig. 3.5 (courtesy Dr. K. T. Law).

3.3 DESIGN

The design of the test embankment configuration was based on limit equilibrium analysis using the cone data obtained during the initial site investigation of June 1989 and was revised, at the site, when the field vane data was obtained just prior to the commencement of construction in Sept. 1989. A limit equilibrium analysis program (REAP) developed for the analysis of reinforced and unreinforced embankment behaviour (Mylleville and Rowe, 1988) was used for the design of the test fill configuration.

The test embankment consisted of a 25 m long unreinforced section and a 25 m long reinforced section connected by a reinforced transition. The embankment configuration was designed in such a way that failure would take place only on the northern side. This was a critical design constraint because of the very close proximity of the N.B. Tel fibre optic cable just south of the embankment (see Fig. 3.1). Berms were provided in the east, west and the southern sides as detailed in Fig. 3.2 (see also Fig. 3.6). One berm was selected for the monitoring of long term behaviour and is being monitored

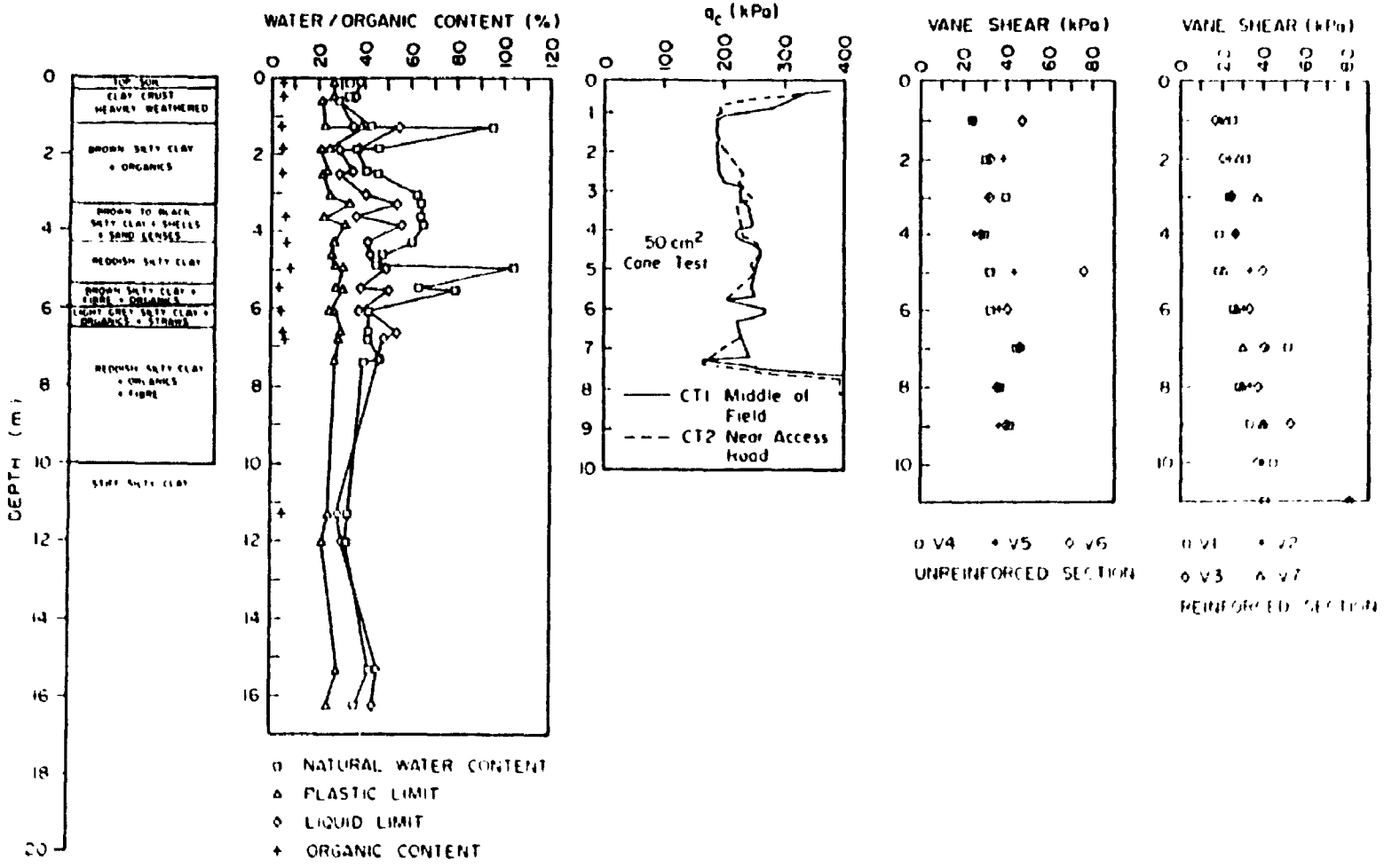

FIG. 3.3 THE SOIL PROFILE

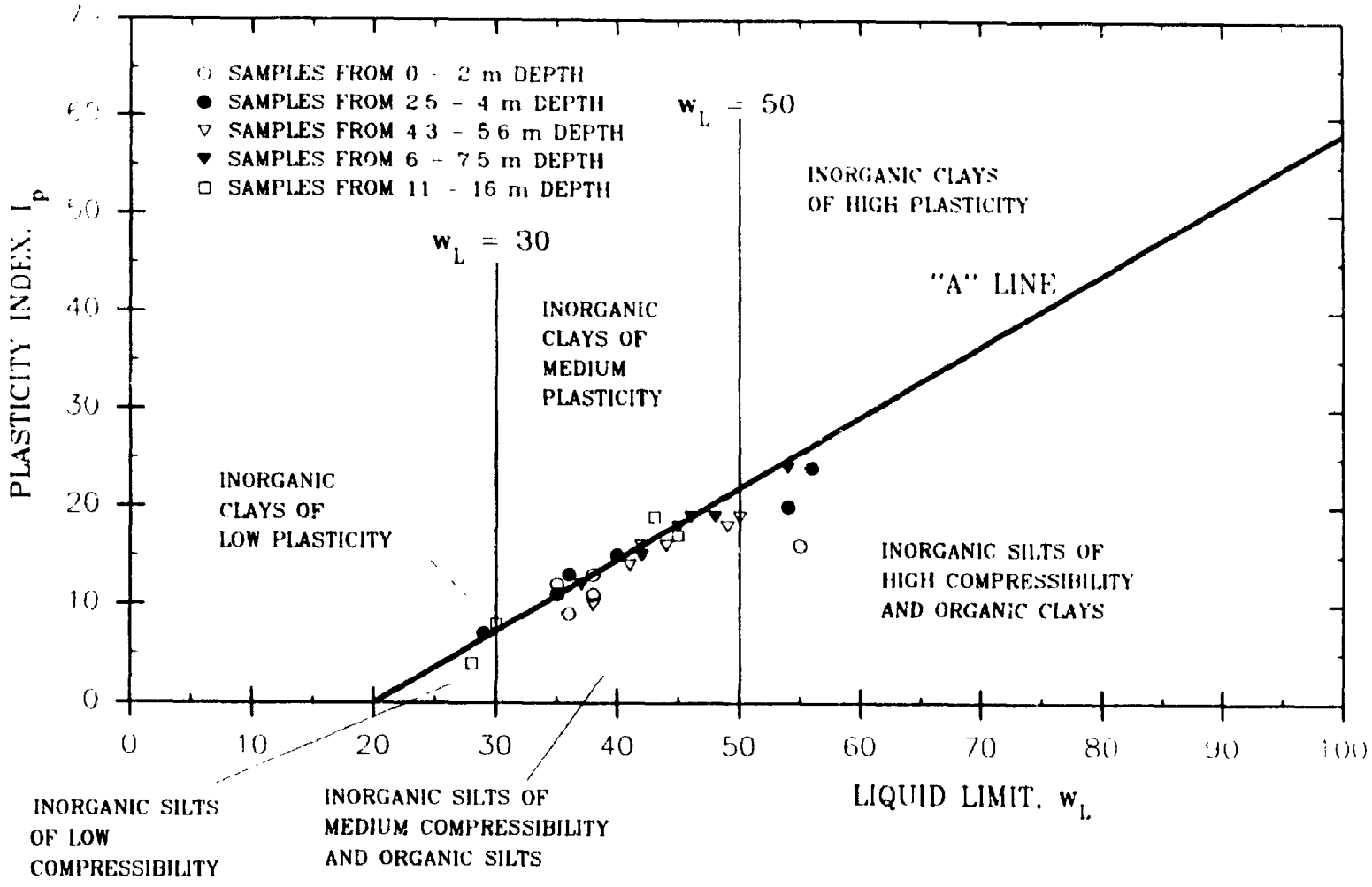

FIG. 3.4 THE PLASTICITY CHART FOR UNB DATA

Table 3.1 Self Boring Pressuremeter Test Results (NRC Data, courtesy Dr. K.T. Law)

Depth (m)	K_0	G_{ur} MPa	E' (ν = .3) (MPa)	E_u (ν = .5) (MPa)	(ϕ'_{cv}= 25)		(ϕ'_{cv}= 30)		(ϕ'_{cv}= 35)	
					ϕ'	δ	ϕ'	δ	ϕ'	δ
2.4	0.68	1.57	4.09	4.72	31.9	7.8	34.3	5.1	37.1	2.6
3.9	0.76	2.04	5.31	6.13	29.0	4.5	31.4	1.7	34.1	-1.1
3.9	0.76	2.04	5.31	6.13	29.0	4.5	31.4	1.7	34.1	-1.1
5.4	0.79	2.81	7.30	8.43	26.6	1.8	29.0	-1.2	31.6	-4.1
5.4	0.79	2.81	7.30	8.43	26.6	1.8	29.0	-1.2	31.6	-4.1
6.9	0.81	3.87	10.07	11.62	24.7	-0.3	27.0	-3.4	29.6	-6.4
12.1	0.88	9.86	25.63	29.57	22.0	-3.3	24.1	-6.6	26.6	-9.7

K_0 : Coefficient of horizontal earth pressure at rest.
E' : Drained Young's modulus.
E_u : Undrained Young's modulus.
G_{ur} : Unload reload shearing modulus.
γ : Poisson's ratio.
ϕ' : Angle of shearing resistance.
δ : Angle of dilation.
ϕ'_{cv} : Critical state angle of shearing resistance. (constant volume shearing)

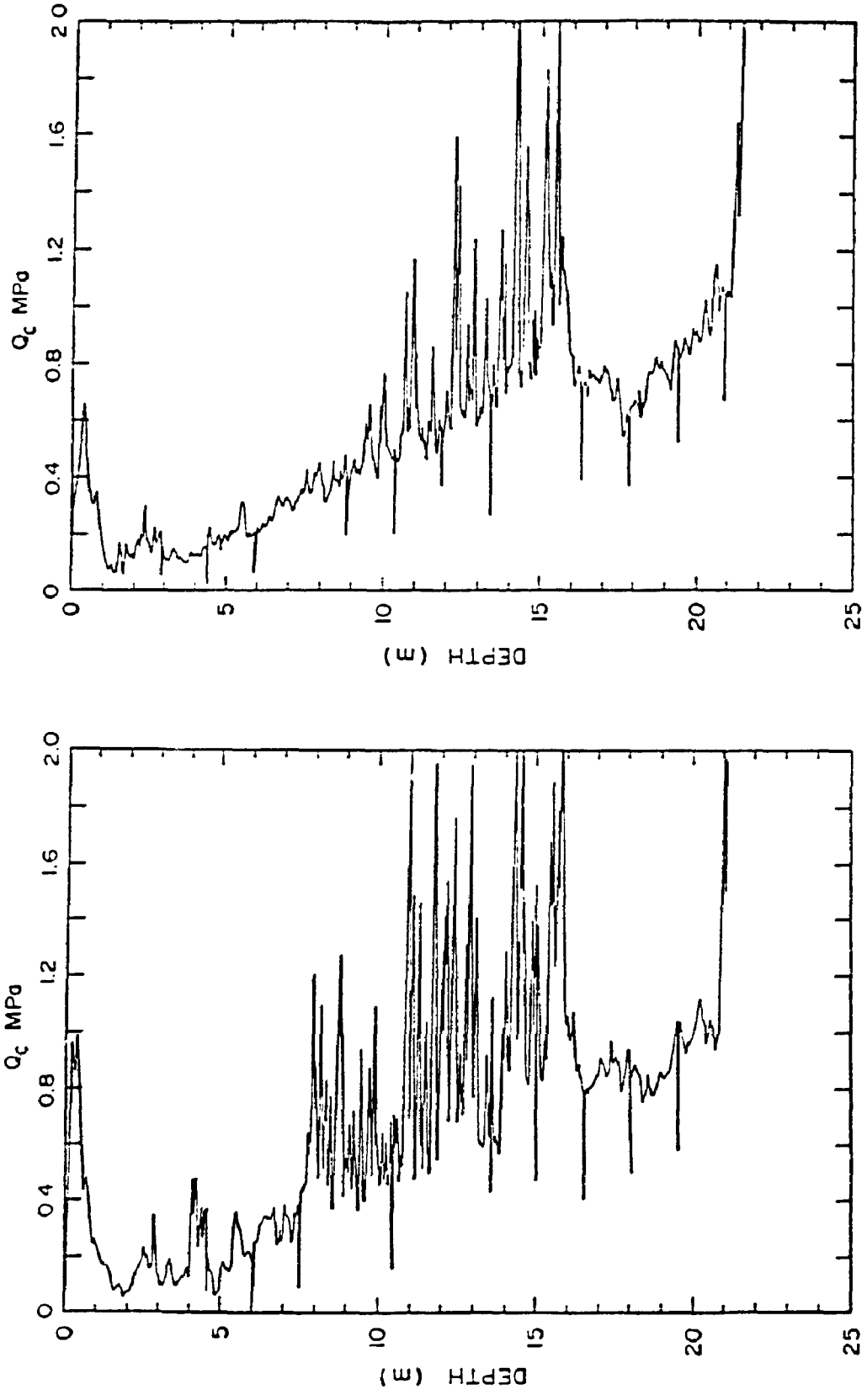

FIG. 3.5 CONE DATA FROM NRC INVESTIGATION (DR. K. T. LAW)

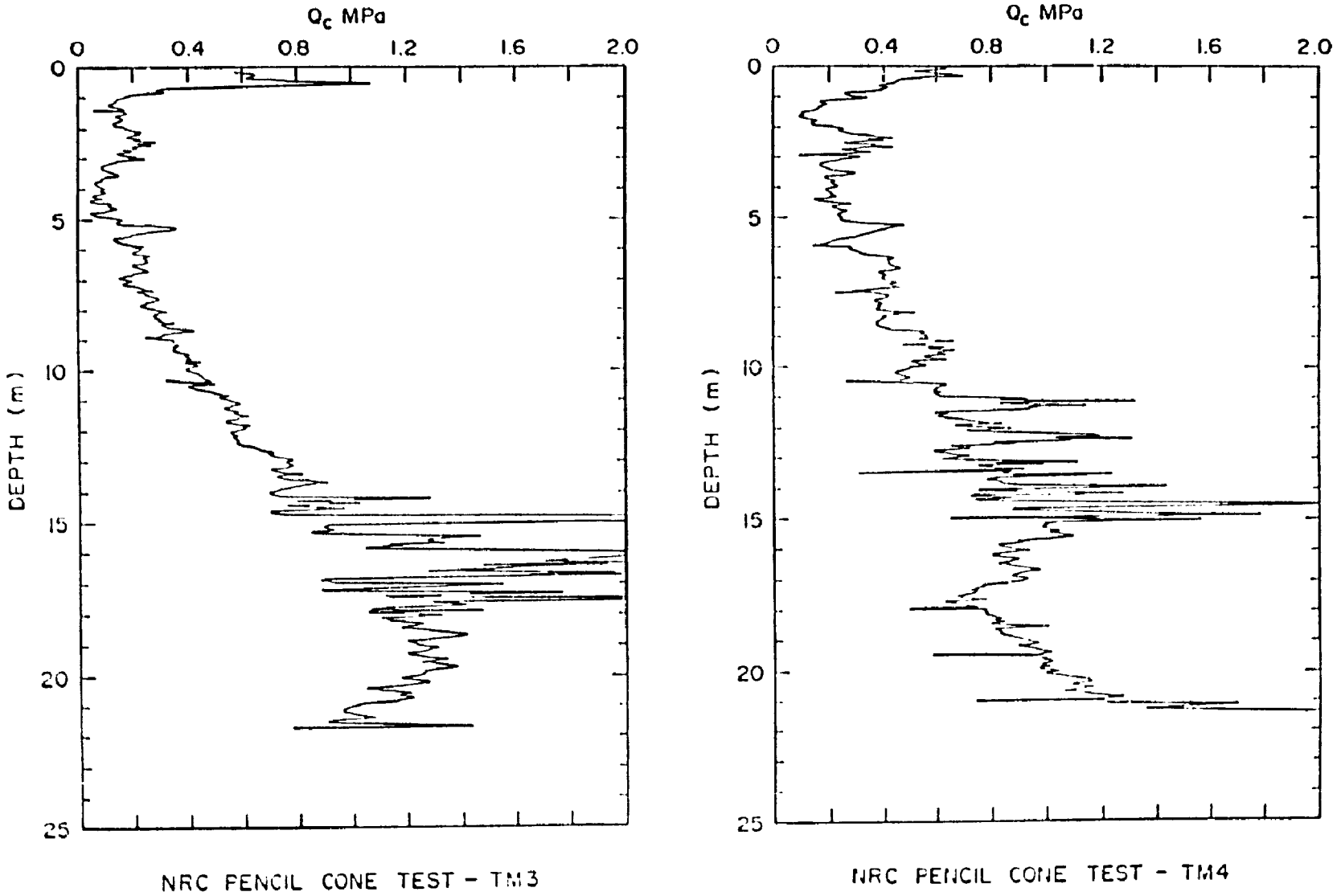

FIG. 3.5 CONE DATA FROM NRC INVESTIGATION (DR. K. T. LAW)

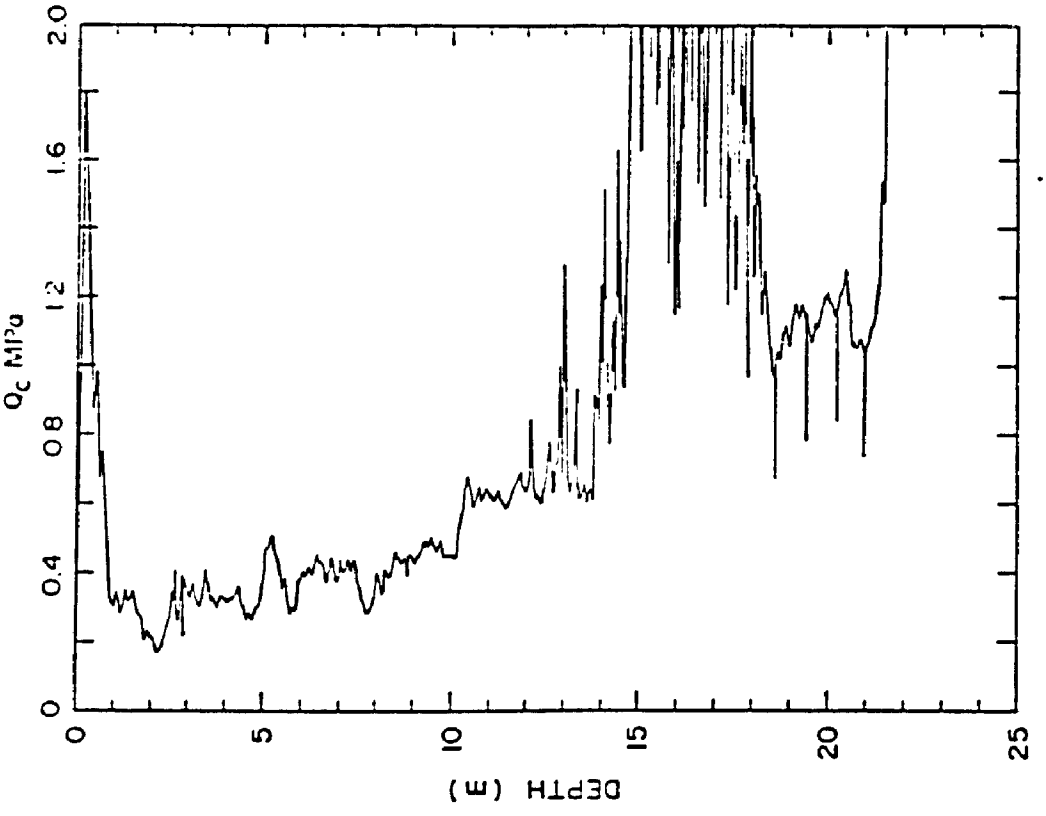

FIG. 3.5 CONE DATA FROM NRC INVESTIGATION (DR. K. T. LAW)

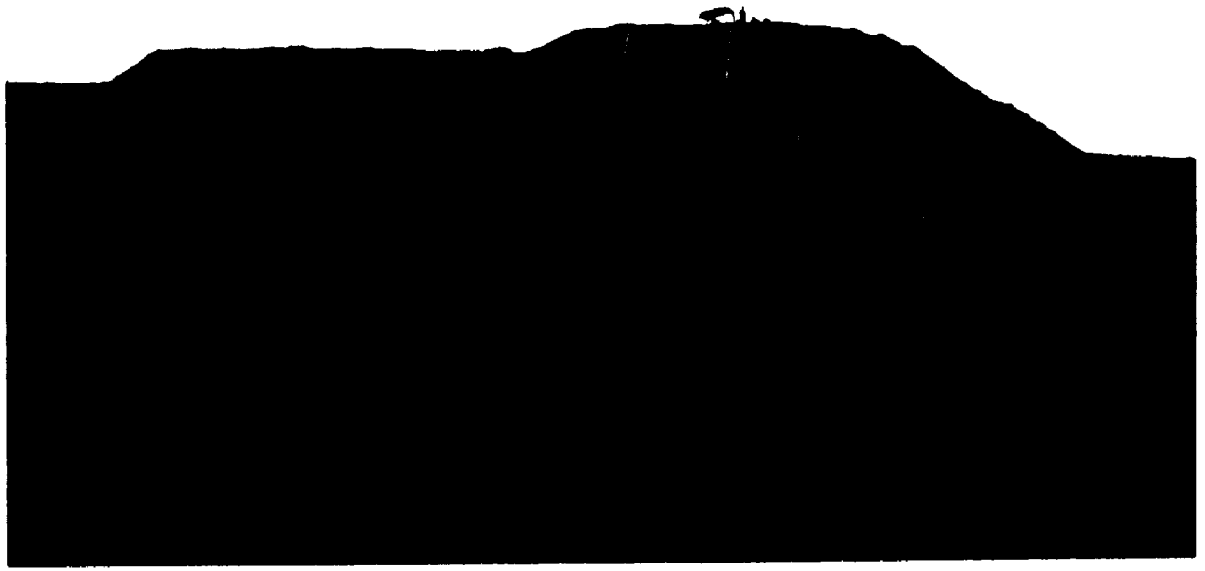

FIGURE 3.6 A TYPICAL VIEW OF THE TEST EMBANKMENT FROM THE NORTH-EAST

periodically The final layout of fill and the cross section of the unreinforced section are shown in Figures 3.2 and 3.7 respectively. Although it would have been highly desirable to have longer sections and to have completely separated the reinforced and unreinforced sections, the site constraints, the variability of the deposit, and limitations on available fill (budget) constrained the design to 25 m long reinforced and unreinforced sections side by side. It should be recognized that this does not represent ideal plane strain conditions and, in particular, the response of the unreinforced section may have been influenced to some extent by the failure of the reinforced section (which was failed first). Despite these limitations it was considered preferable to obtain data from both an unreinforced and a reinforced section than to simply obtain data for only one case and a wider section since the variability of the deposit (as described below) would itself preclude ideal plane strain conditions from being achieved at this site.

Both the NRC cone data and vane data indicated that the soil strength varied over the site - being approximately 30% higher beneath what was selected to be the unreinforced section (see Fig. 3.3) than beneath the reinforced section. Based on this information, it was considered best to arrange the sections such that the stronger soil was beneath the unreinforced section thereby minimizing the difference in fill thickness required to fail the two sections and as far as possible, increasing the extent to which plane strain conditions would be approximated. Limit equilibrium analyses performed on the basis of vane strength indicated that the failure height of the unreinforced section range between 7 and 11.4 m and that of the reinforced section range between 6.6 and 11.1 m. The range represents a reasonable interpretation of the vane data. The failure heights were indicated as 9.2 and 8.2 m respectively for the unreinforced and reinforced sections based on an average vane strength profile beneath each section (see Fig. 3.3 for vane strength profiles).

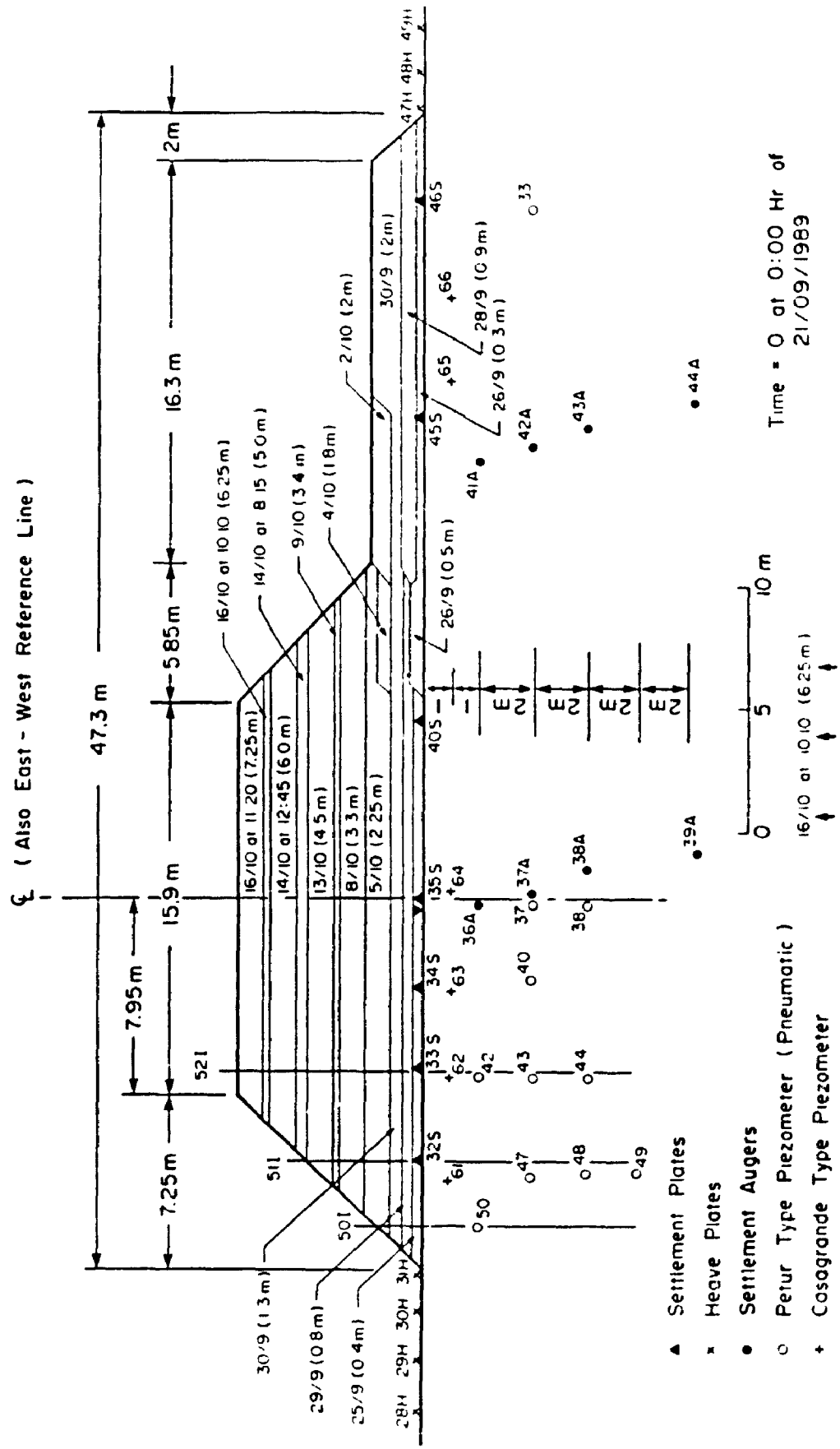

FIG. 3.7 LAYOUT OF INSTRUMENTATION AND SEQUENCE OF CONSTRUCTION

The instrument layout was selected based on the results of the limit equilibrium analysis performed with the initial (June 1989) cone data and previous field experience together with the results of finite element analyses (Rowe et al, 1984, Rowe and Soderman, 1984 and 1986). The layout of piezometers were based on an examination of generic finite element (sensitivity) analyses for reinforced embankment behaviour.

Particular care was taken in the design of the fill height and berms on the south side of the embankment (i.e. adjacent to the N.B. Tel fiber optic cable) to ensure an adequate factor of safety against failure. A number of instruments (e.g. heave plates 19H, 20H, 21H, 47H, 48H, 49H and inclinometer 27I - see Fig. 3.2) were installed on the south to provide warning of any potential problems. These instruments were carefully monitored during construction and no movement of any significance was observed (i.e. the observed largest horizontal and vertical displacements were less than 0.07 and 0.04 m respectively).

3.4 INSTRUMENTATION

The embankment was instrumented to allow monitoring of the construction procedure and the collection of data necessary for detailed interpretation and for future analysis of the behaviour of the embankment. The instrumentation included piezometers, settlement plates, augers, heave plates. inclinometer casings and a total pressure cell. Details regarding the location of instruments for monitoring the unreinforced section are shown in Figs. 3.2 and 3.7. These instruments were installed in June 1989 (i.e. approximately 3 months before construction).

To monitor the development of excess pore pressures in the foundation subsoil, a total of 10 pneumatic (PETUR^{TM} P-102 wellpoint type) piezometers were installed at

various depths along the centre line of the unreinforced section as shown in Fig. 3.7. In addition to these pneumatic piezometers, 6 Casagrande type piezometers were also installed, as backup, at a depth of 1 m from the ground level (see Figs. 3.2 and 3.7). Pneumatic piezometer leads were directed out from beneath the embankment to allow monitoring of embankment response without interfering with the construction. Two pneumatic piezometer reading stations one on the north and the other on the south of the embankment were used to facilitate the data collection process.

Four heave plates, five settlement plates and four augers at different depths were installed on the main part (i.e. northern side) of the unreinforced section in order to monitor the movement of the specific points on the ground surface and the foundation soil. Another set of four augers at different depths, two settlement plates and three heave plates were installed on the berm (i.e. southern) side of the embankment (see Figs. 3.2 and 3.7).

Lateral displacement of the foundation subsoil was monitored with three vertical inclinometers that were installed close to the toe of the embankment (see Figs. 3.2 and 3.7). The 88 mm diameter plastic inclinometer casings consisted of 3 m long sections joined by plastic couplings. Inclinometer casings were installed up to a depth of about 10 m where a stratum of stiff clayey silt/silty clay was encountered. A pneumatic total pressure cell was installed close to the centre line of the unreinforced section to measure the pressure imposed by the fill on the foundation subsoil.

3.5 EMBANKMENT CONSTRUCTION

Prior to construction, the instrumentation was monitored until the initial performance of the instruments was considered to be satisfactory and zero readings were defined. Initially, a 0.5 m thick gravel access road was formed, avoiding the instrumented

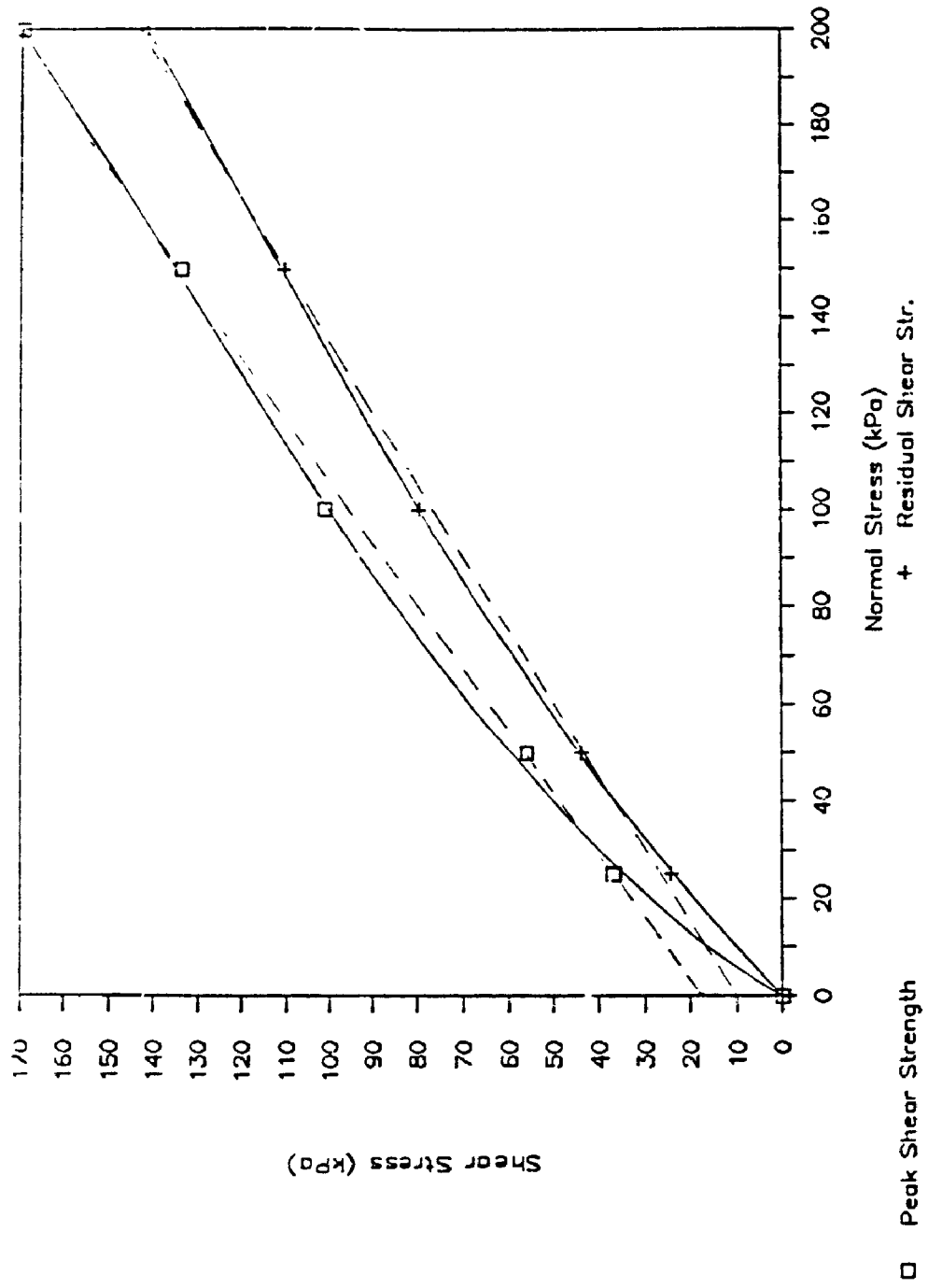

FIG. 3.11 SHEAR STRENGTH ENVELOPE OF FILL

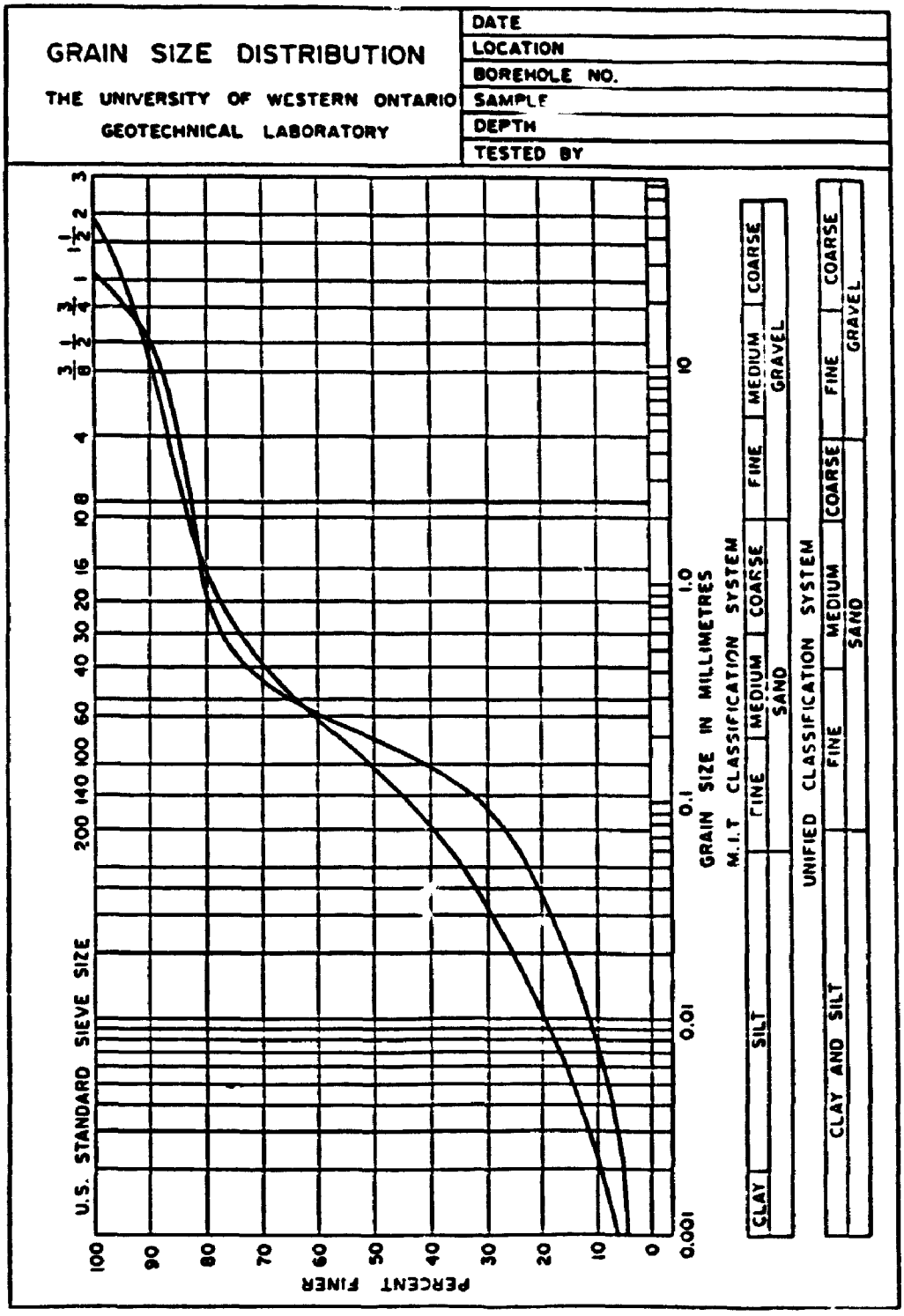

FIG. 3.8 TYPICAL GRADING CURVES OF FILL

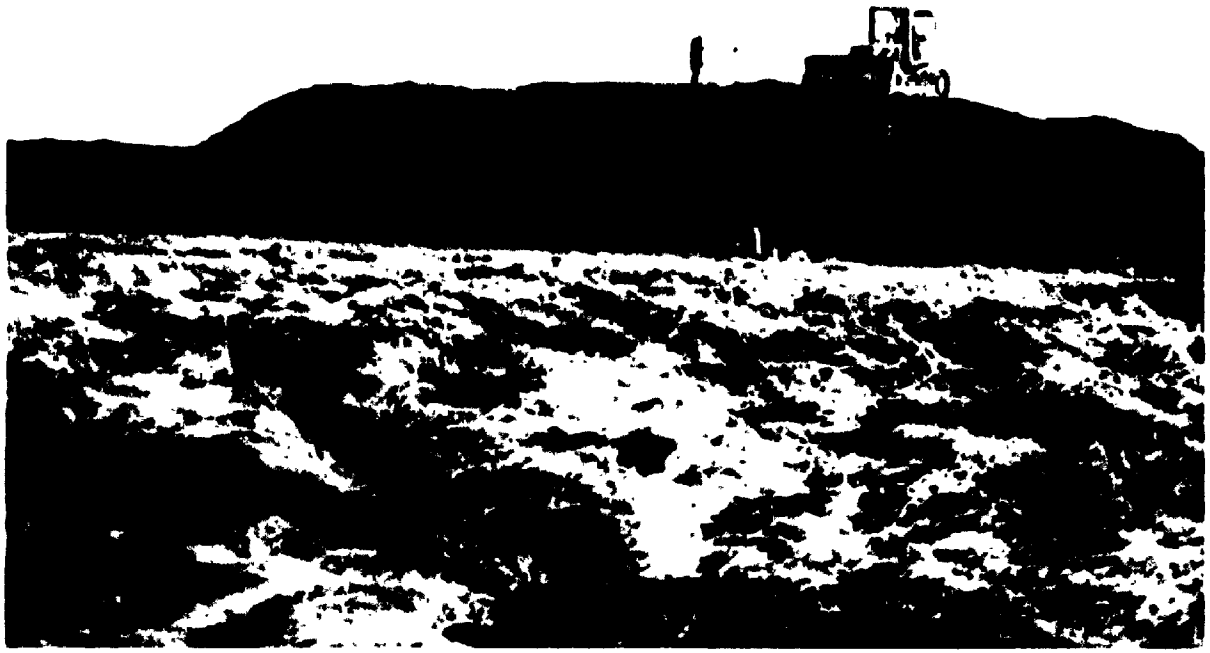

FIGURE 3.9 A TYPICAL VIEW OF THE EMBANKMENT UNDER CONSTRUCTION - VIEW FROM THE NORTH

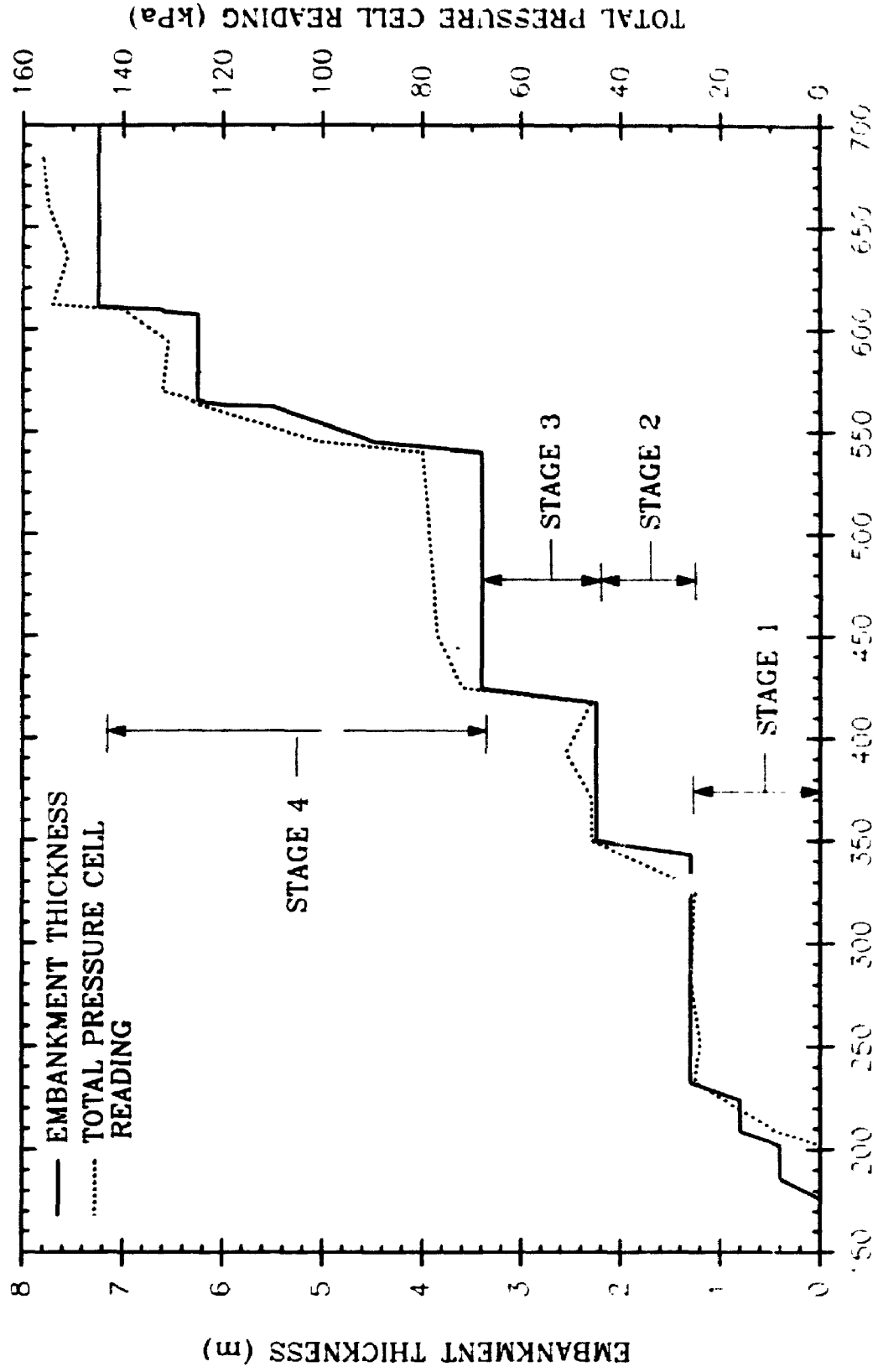

FIG 3.10 VARIATION OF EMBANKMENT THICKNESS AND TOTAL PRESSURE CELL READING WITH TIME – UNREINFORCED SECTION

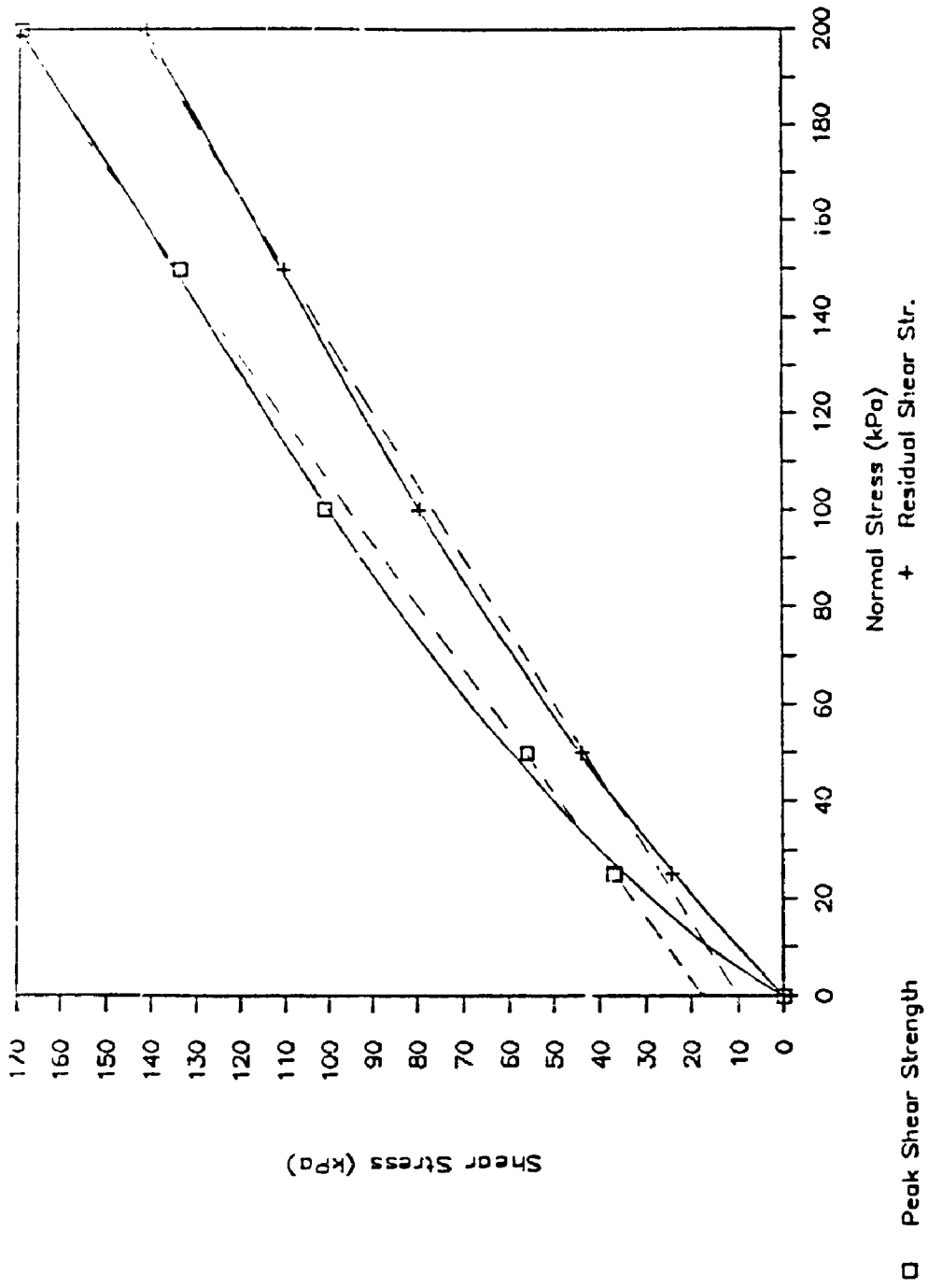

FIG. 3.11 SHEAR STRENGTH ENVELOPE OF FILL

Owing to the curved nature of the strength envelope, strength parameters for low normal stresses must be obtained directly from the strength envelope (see Fig. 3.11) and not from the extrapolated straight line fit given above.

The piezometers and the position monitoring devices (i.e. settlement plates, heave plates and augers) were monitored at least twice a day when the construction was in progress, but more frequently at later stages of construction when there was evidence of rapid movement. A set of readings was made on all the instruments after placement of each layer of fill.

3.6 RESULTS AND PERFORMANCE OF INSTRUMENTATION

3.6.1 Embankment thickness and Total pressure

Fill thicknesses were monitored by observing the position of the surface of fill against the fill thickness scale markings made on the settlement plate extension pipes. The variation of thickness of the main part (i.e. northern side) of the unreinforced section of the embankment (hereafter called the embankment thickness) with time is shown in Fig. 3.10. For ease of comparison, the variation in the total pressure on the foundation soil surface, as measured by the total pressure cell, with time is superimposed on the same figure.

The results of the total pressure cell were found to be reasonably consistent with the pressures calculated based on thickness and unit weight of the fill. The total pressure cell continued to function well until the end of construction. It can be observed that the total pressure cell reading is in general close to the calculated pressure.

construction despite the relatively rapid rate of construction. Very rapid build up of pore pressure was evident in all these three piezometers as the fill was raised from 3.4 to 6.25 m and particularly after 560 hours (i.e. after the embankment reached a thickness of 5.5 m). Unfortunately, piezometers 37 and 40 ceased to function after about 600 hours; this failure of the piezometers is considered to have been the result of the large deformations which occurred around this time.

Fig. 3.13 indicates that the build up of excess pore pressure is greater in piezometer 44, placed at 6 m depth, than at piezometer 42, placed at a depth of 2 m, (i.e. $u_{44} > u_{42}$). This difference is considered to be the result of some pore pressure dissipation. Support for this hypothesis can be drawn from the greater rate of dissipation of excess pore pressure in piezometer 42 (after the end of construction) compared to piezometer 44 and the fact that piezometer 42 is much closer to the drainage boundary. Piezometer 44 indicated excess pore pressures close to the applied vertical stress at the ground surface for embankment thicknesses between 1.3 m and about 5m. No increase in excess pore pressure was observed in either piezometer for construction of the embankment above 6.25 m suggesting that the soil approached failure at this embankment thickness.

Fig. 3.14 shows that the excess pore pressure responses for piezometers 48 and 49 were very similar. Piezometer 49 showed slightly higher excess pore pressure than piezometer 48 most of the time. Piezometers 47, 48 and 49 were placed on a vertical line beneath the slope of the embankment (see Fig. 3.7). The deeper piezometers reflect an increase in pore pressure in excess of that expected due to the fill directly above the piezometers. This is considered to be a result of the increased pore pressure beneath the main portion of the embankment. An additional factor in the difference in excess pore pressures at the three depths is the shorter drainage paths for the shallower piezometers

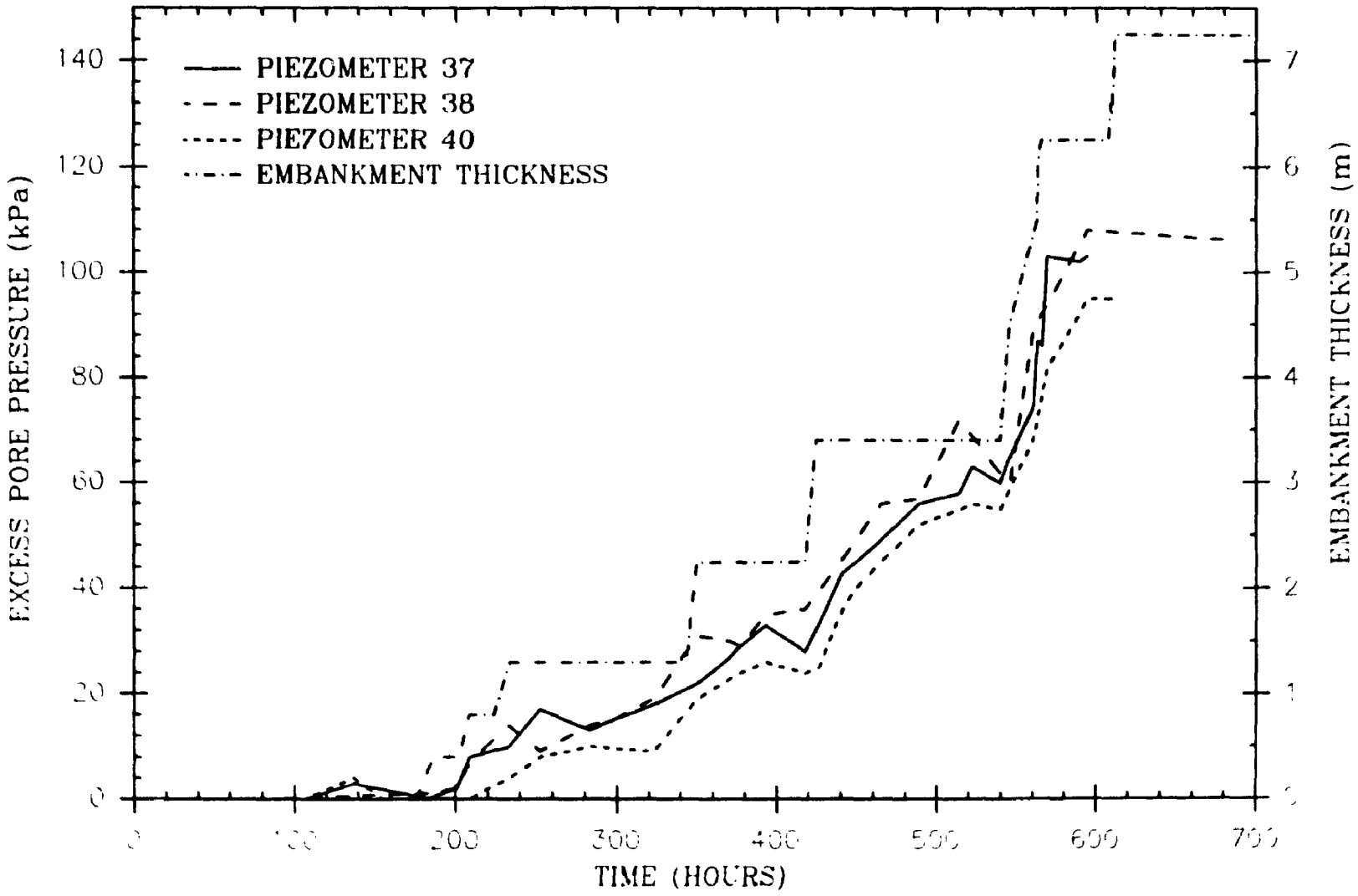

FIG 3.12 VARIATION OF EXCESS PORE PRESSURE WITH TIME FOR PIEZOMETERS 37, 38 AND 40

resulting in more rapid dissipation of excess pore pressure.

It is noted that dissipation of excess pore pressure during early stages of construction has previously been reported by Leroueil et al. (1978a) and Ortigao et al. (1983), among others. Leroueil et al. (1978b) analyzed this typical behaviour and attributed the dissipation to the initially overconsolidated state of the foundation soil at early stages and its change to normally consolidated state at later stages of construction.

Piezometer 50, which is located beneath the toe of the embankment showed some increase in pore pressure but, as would be expected, the level of excess pore pressure is consistently lower than at piezometers beneath the embankment.

The excess pore pressure response of piezometer 33 placed beneath the southern berm of the embankment is shown in Fig. 3.15. For ease of comparison with the construction sequence, the variations of berm and main embankment thicknesses with time are superimposed in this figure. The excess pore pressure increased in piezometer 33 up to about 43 kPa during 100 - 230 hours in direct response to the construction of the berm. This increase was similar to the calculated vertical stress at the ground surface based on the fill thickness and unit weight. The excess pore pressure dissipated quite rapidly to about 6 kPa during 230 - 320 hours when there was no further addition of fill on the berm. However, it showed some significant increase in excess pore pressure when the main embankment was raised above the berm thickness of 2 m. The magnitude of the increase is substantially less than the increase directly beneath the embankment and reflects the two dimensional nature of the excess pore pressures which result from construction of the main embankment.

Variation of parameter $\overline{B}$ (= change in excess pore pressure/change in vertical

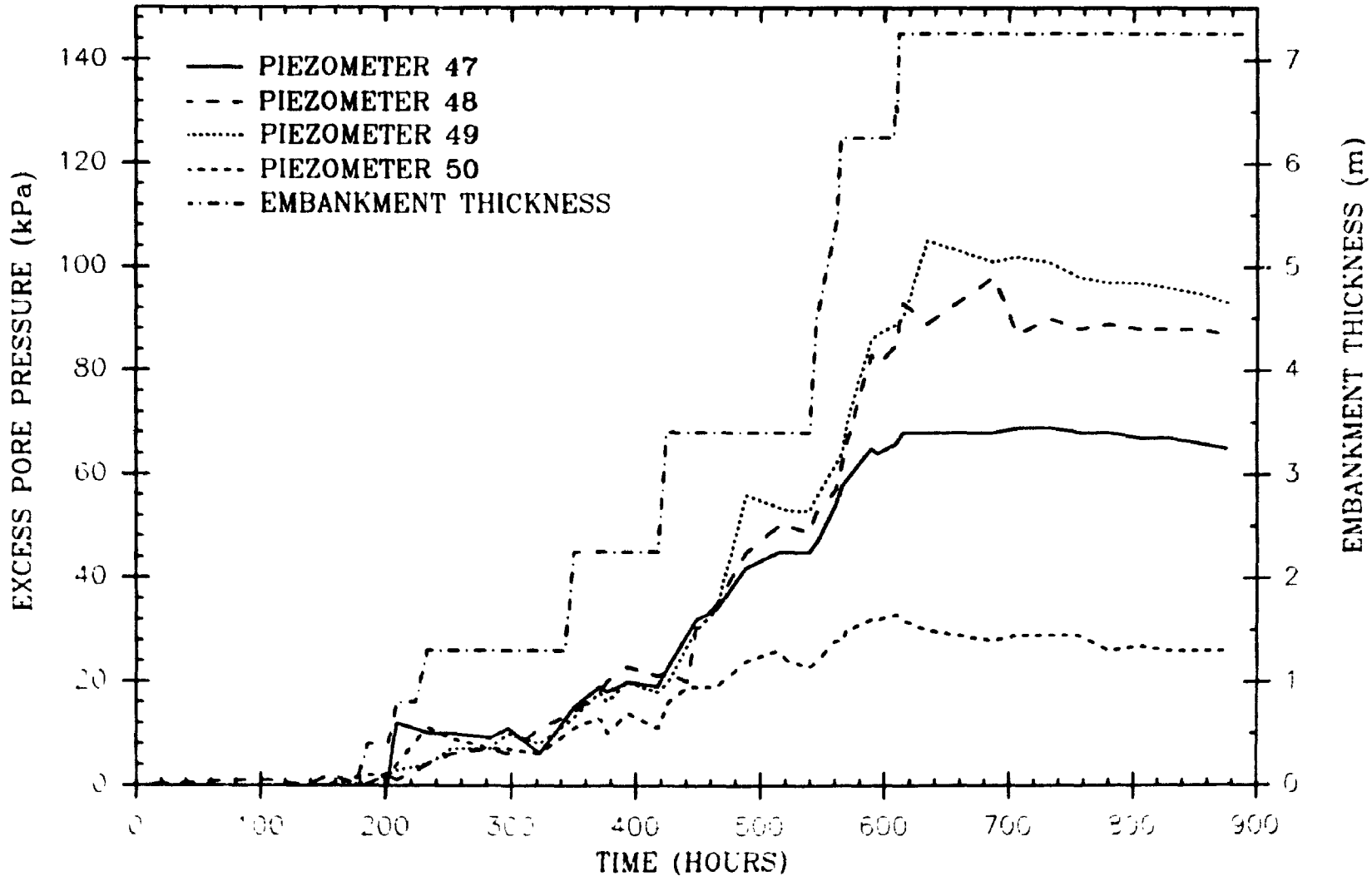

FIG 3.14 VARIATION OF EXCESS PORE PRESSURE WITH TIME FOR PIEZOMETERS 47, 48, 49 AND 50

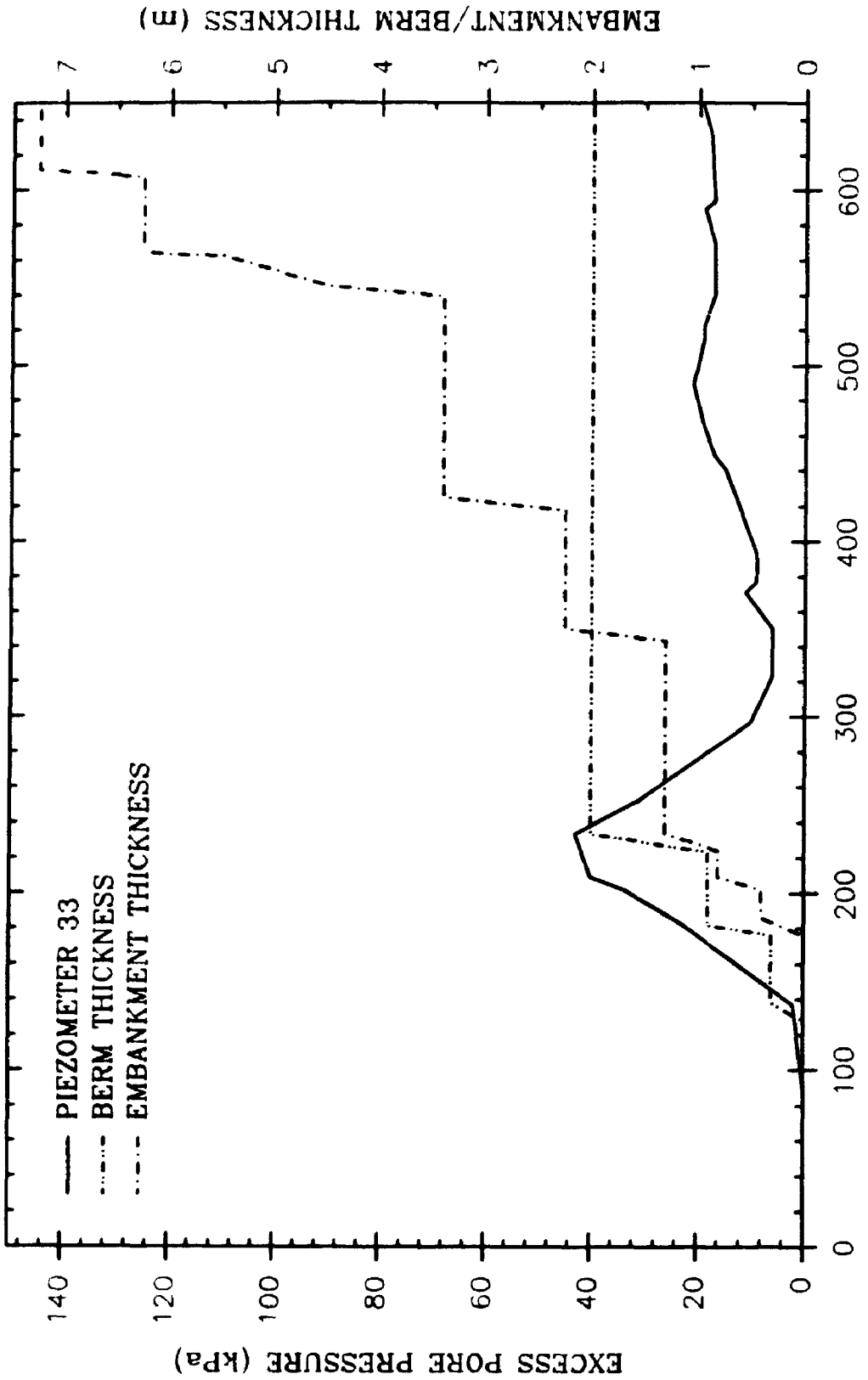

FIG. 3.15 VARIATION OF EXCESS PORE PRESSURE WITH TIME FOR PIEZOMETER 33

construction despite the relatively rapid rate of construction. Very rapid build up of pore pressure was evident in all these three piezometers as the fill was raised from 3.4 to 6.25 m and particularly after 560 hours (i.e. after the embankment reached a thickness of 5.5 m). Unfortunately, piezometers 37 and 40 ceased to function after about 600 hours; this failure of the piezometers is considered to have been the result of the large deformations which occurred around this time.

Fig. 3.13 indicates that the build up of excess pore pressure is greater in piezometer 44, placed at 6 m depth, than at piezometer 42, placed at a depth of 2 m, (i.e. $u_{44} > u_{42}$). This difference is considered to be the result of some pore pressure dissipation. Support for this hypothesis can be drawn from the greater rate of dissipation of excess pore pressure in piezometer 42 (after the end of construction) compared to piezometer 44 and the fact that piezometer 42 is much closer to the drainage boundary. Piezometer 44 indicated excess pore pressures close to the applied vertical stress at the ground surface for embankment thicknesses between 1.3 m and about 5m. No increase in excess pore pressure was observed in either piezometer for construction of the embankment above 6.25 m suggesting that the soil approached failure at this embankment thickness.

Fig. 3.14 shows that the excess pore pressure responses for piezometers 48 and 49 were very similar. Piezometer 49 showed slightly higher excess pore pressure than piezometer 48 most of the time. Piezometers 47, 48 and 49 were placed on a vertical line beneath the slope of the embankment (see Fig. 3.7). The deeper piezometers reflect an increase in pore pressure in excess of that expected due to the fill directly above the piezometers. This is considered to be a result of the increased pore pressure beneath the main portion of the embankment. An additional factor in the difference in excess pore pressures at the three depths is the shorter drainage paths for the shallower piezometers

resulting in more rapid dissipation of excess pore pressure.

It is noted that dissipation of excess pore pressure during early stages of construction has previously been reported by Leroueil et al. (1978a) and Ortigao et al. (1983), among others. Leroueil et al. (1978b) analyzed this typical behaviour and attributed the dissipation to the initially overconsolidated state of the foundation soil at early stages and its change to normally consolidated state at later stages of construction.

Piezometer 50, which is located beneath the toe of the embankment showed some increase in pore pressure but, as would be expected, the level of excess pore pressure is consistently lower than at piezometers beneath the embankment.

The excess pore pressure response of piezometer 33 placed beneath the southern berm of the embankment is shown in Fig. 3.15. For ease of comparison with the construction sequence, the variations of berm and main embankment thicknesses with time are superimposed in this figure. The excess pore pressure increased in piezometer 33 up to about 43 kPa during 100 - 230 hours in direct response to the construction of the berm. This increase was similar to the calculated vertical stress at the ground surface based on the fill thickness and unit weight. The excess pore pressure dissipated quite rapidly to about 6 kPa during 230 - 320 hours when there was no further addition of fill on the berm. However, it showed some significant increase in excess pore pressure when the main embankment was raised above the berm thickness of 2 m. The magnitude of the increase is substantially less than the increase directly beneath the embankment and reflects the two dimensional nature of the excess pore pressures which result from construction of the main embankment.

Variation of parameter $\overline{B}$ (= change in excess pore pressure/change in vertical

stress on the original ground at the centre line of the embankment $= \frac{\Delta u}{\Delta \gamma H}$) with time for piezometers 37 and 40 (which were placed in the region close to the centre line) are presented in Fig. 3.16. The changes in pore pressure and vertical stress are relative to those existing at 525 hours since it was after this time that the embankment was constructed quite rapidly from 3.4 to 7.25 m (with a brief stoppage of construction at 6.25 m thickness). It is considered that the foundation soil exhibited essentially an "elastic" response up to about 3.4 m thickness, as discussed later in this chapter. Piezometer 37 showed a very rapid increase of the parameter $\overline{B}$ up to about 570 hours (and especially between about 560 - 570 hours) as the embankment was raised from 5.5 to 6.25 m and reached a maximum of 0.77 at about 595 hours, after being constant at about 0.75 for a period of about 20 hours. Piezometer 40 also showed a very rapid increase up to a maximum of 0.75 at 595 hours. This response suggest that the embankment approached failure during 570-595 hours, i.e. at the thickness of 6.25 m.

The piezometers 37 and 40 did not give reasonable readings when the embankment thickness was raised above 6.25 m - probably due to breakage of the lines caused by large movements occurring at this time. The other 10 piezometers are still functioning well and are being monitored periodically.

3.6.3 Inclinometer data

The inclinometer casings were monitored with an automated inclinometer probe and readout unit obtained from Terra Technology Corp. It had the capability to record, store, file, and reduce inclinometer data on the spot. Built-in software allowed for comparison of data and on-screen display of the displacement profile in the field itself. The equipment generally worked well and the data were collected reasonably fast. As a precautionary measure, another inclinometer probe and digital readout unit (a "Sinco"

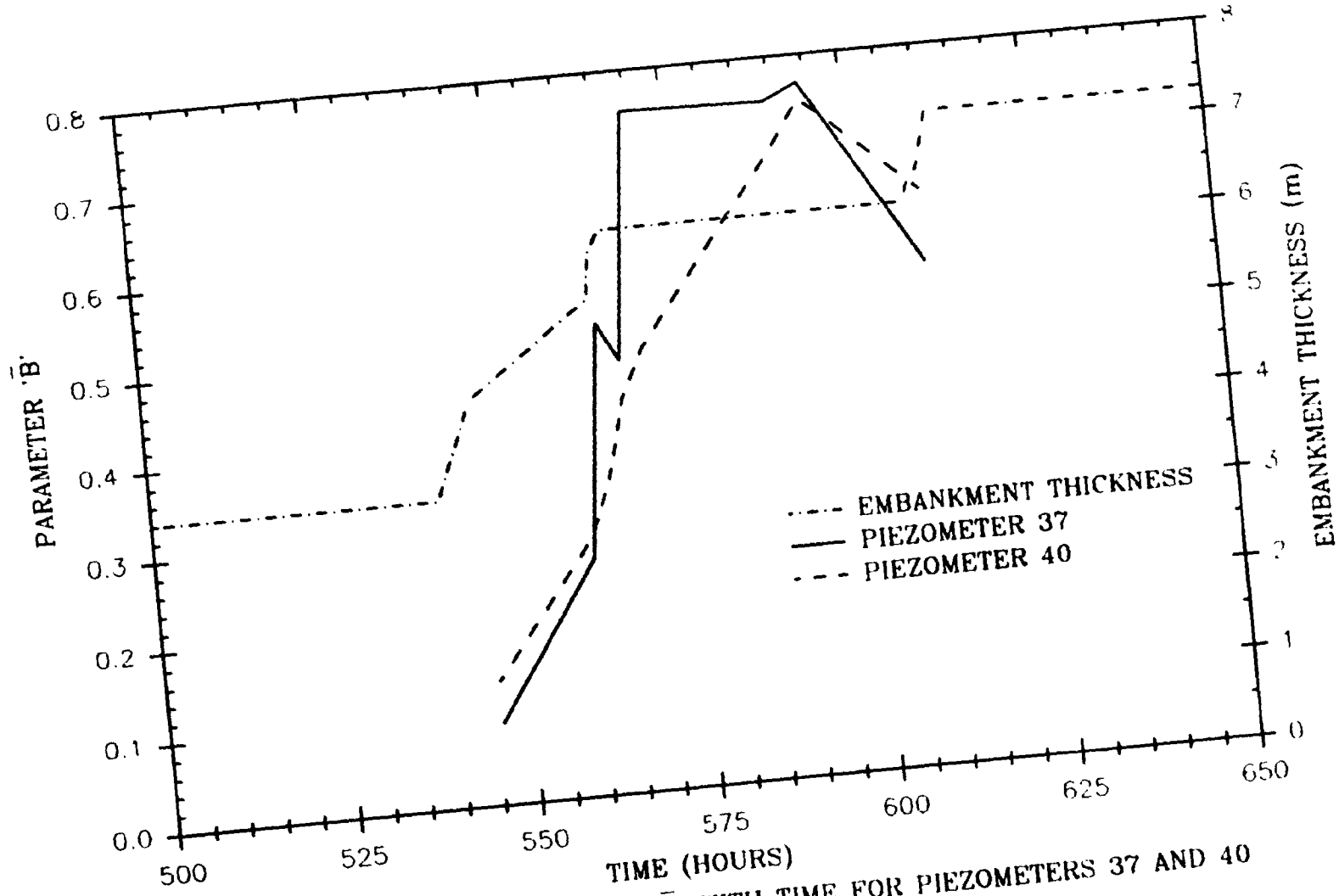

FIG. 3.16 VARIATION OF PARAMETER 'B̄' WITH TIME FOR PIEZOMETERS 37 AND 40 (BASED ON TIME = 525 HOURS)

manual data collection unit) made by Slope Indicator Co. was used as a backup. Initial data were collected with both units at the beginning of construction to facilitate any future change in the equipment if it became necessary.

Inclinometer casings were installed (on September 7, 1989) at three locations in the region where large horizontal displacements were expected to occur. Two of them were placed along the slope of the embankment, one close to the toe and the other close to the shoulder, and the third one was placed on the crest but close to the shoulder (see Fig. 3.7). Large lateral displacements were encountered in the inclinometers when the embankment thickness was raised to about 5m. Marche and Chapuis (1974) suggested that lateral displacements can be considered a good indicator of the development of failure conditions in the foundation. However, Tavenas et al. (1979) have suggested that the development of large lateral displacements is related to the passage of the clay from an overconsolidated to a normally consolidated state, i.e. a phenomenon not directly related to the FOS (factor of safety) of the foundation. The inclinometers provided useful data prior to the onset of initial failure (i.e. up to a thickness of 5 m). However, due to the relatively large movements, the inclinometers became blocked between a fill thickness of 5 and 6 m and could no longer be monitored. Hence, a crude probe consisting of a dead weight tied to a scaled tape was used to determine the depth to inclinometer blockage and hence provide some indication of the depth to the failure zone. The variation of horizontal displacement with depth obtained from the different inclinometers are shown in Figures 3.17, 3.18 and 3.19. For ease of comparison, the horizontal displacement profiles at different embankment thicknesses are superimposed on each of these figures. The depth of the blockage determined from the crude probing exercise at later stages of construction are also shown on these figures.

The horizontal displacements were comparatively small (less than 0.25 m) when

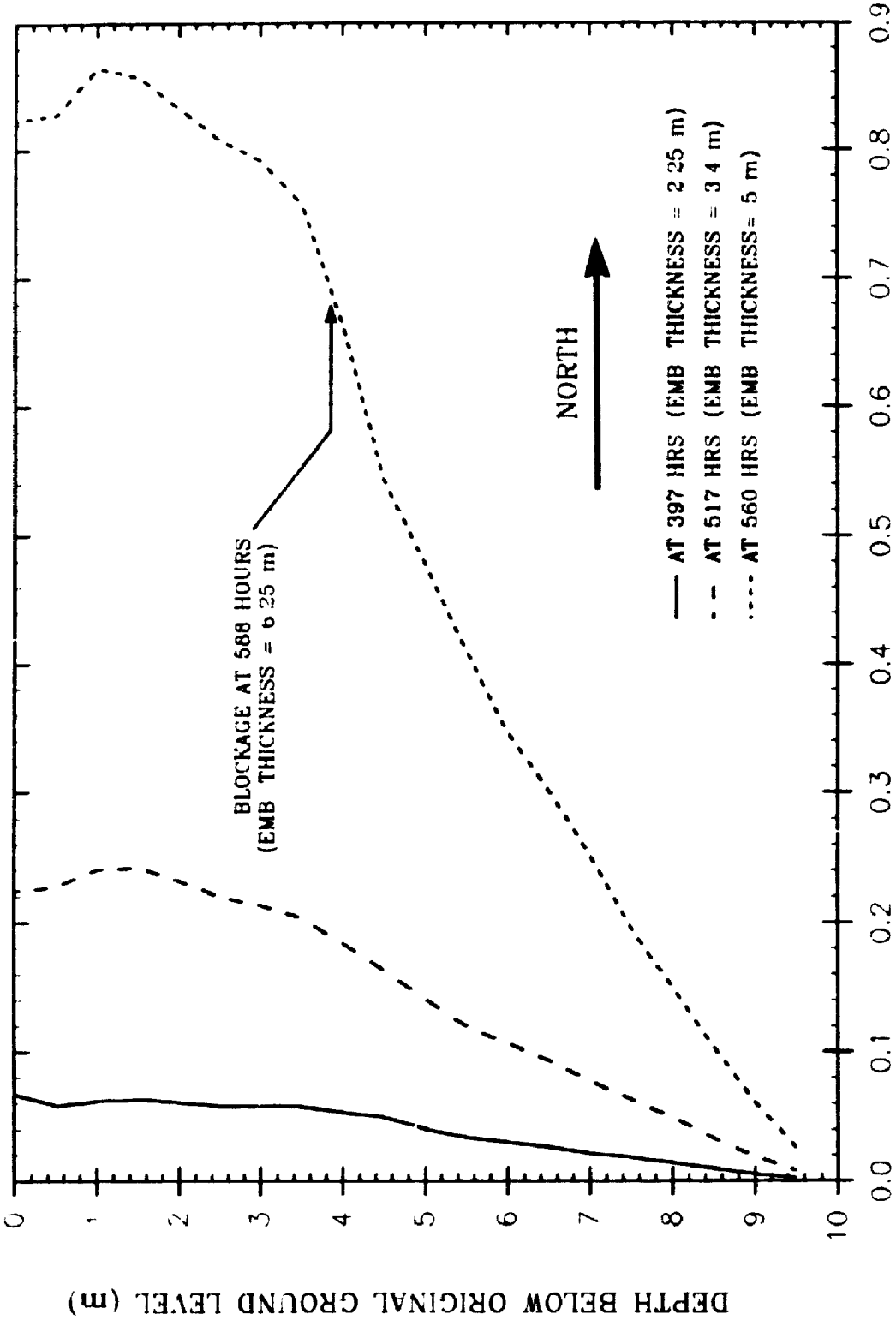

FIG. 3.17 VARIATION OF HORIZONTAL DISPLACEMENT WITH DEPTH A DIFFERENT EMB. THICKNESSES FOR INCLINOMETER 501

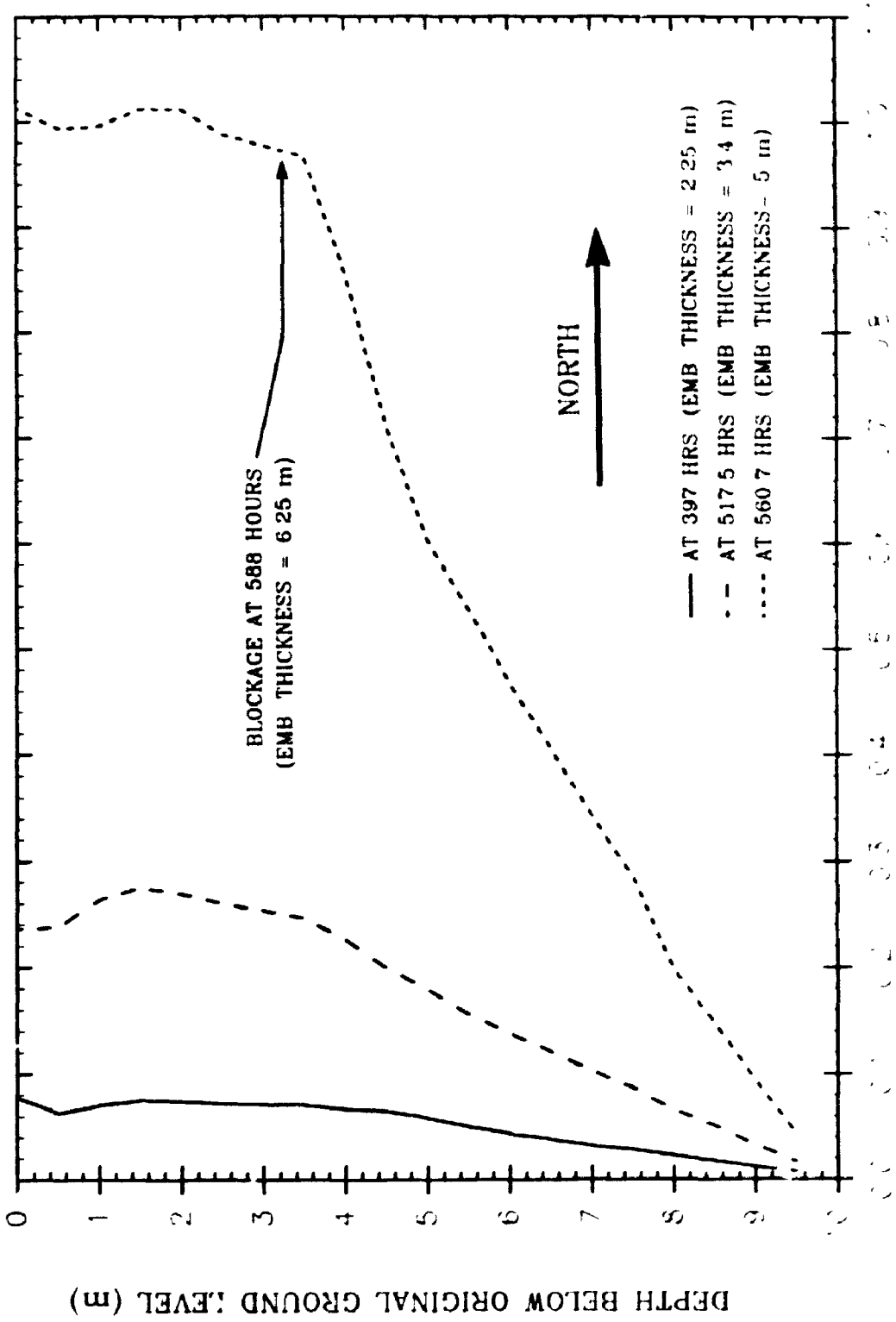

FIG 3 18 VARIATION OF HORIZONTAL DISPLACEMENT WITH DEPTH AT DIFFERENT EMB THICKNESSES FOR INCLINOMETER 511

3.20 and 3.21 indicate that the settlement of all the monitoring points increased with time and increasing fill thickness. It can be observed that the settlements at the ground surface monitoring points (i.e. settlement plates 32S, 33S, 34S and 35S) were less than 0.3 m until the embankment thickness was increased above 3.4 m. The plots indicate that there was a slight gradual increase in settlement between stages of construction when there was no addition of fill (i.e. at fill thicknesses 1.3, 2.3 and 3.4 m). The increase in settlement with time at a height of 3.4 m was, at least in part, due to loading of the reinforced section to failure during this period (i.e. the fill thickness of the reinforced section was increased from 3.4 to 9.5 m).

The settlement at plate 32S (located beneath the embankment slope) did not increase as much as the other monitoring points. The settlement at plates 33S, 34S and 35S increased rapidly with increase in fill thickness beyond 3.4 m during stage 4 construction (see Fig. 3.20). A rapid increase in settlement was evident after about 560 hours (i.e. for fill thicknesses greater than 5.5 m). When the fill thickness was raised to about 6.25 m, the settlement increased to as high as 0.9 m. Failure of the embankment appear to have initiated at this embankment thickness of about 5.5 m as evidenced by the blockage of the inclinometer casings between a thickness of 5 and 6 m and by the very rapid increase in settlement when the fill thickness was raised above 5.5 m (see Figs. 3.20 and 3.21). However the failure was not dramatic and additional fill could be placed. At a fill thickness of 7.25 m, the largest settlement of more than 1.4 m was recorded at settlement plate 35S. Settlements were also large at monitoring points 33S (max. settlement = 1.37 m) and 34S (max. settlement = 1.3 m). Visually, the maximum settlement appeared to have occurred between plates 35S and 40S just south of plate 35S (see Fig. 3.22).

The settlement of the augers exhibited a response similar to the settlement plate

the embankment thickness was raised to 3.4 m as evidenced by inclinometer 501 shown in Fig. 3.17. A rapid increase in the horizontal displacement, to as high as 0.85 m, was observed when the embankment thickness was raised to 5 m. Comparison of the horizontal displacement profiles at different embankment thicknesses indicate a gradual initiation of a failure zone at a depth of about 3.5 m from the ground surface. This observation is further confirmed by the measurements of the depth of blockage performed at later stages of construction.

The horizontal displacement profiles for the inclinometers 511 and 521 shown in Figures 3.18 and 3.19 respectively indicated a similar response to that discussed for inclinometer 501. Fig. 3.18 shows the initiation of a failure zone at a depth of about 3.5 m more clearly than the other two inclinometers. Fig. 3.19 shows evidence of significant movements to a depth of about 3 m. Based on the shape of the deformed profile at 5 m and the location of the blockage at 6.25 m it would appear that the failure at this location passed through the foundation at a depth of about 1 m.

3.6.4 Settlement data

The movement of settlement plates/augers and heave plates was monitored using electronic distance measuring apparatus (distomat) which permitted monitoring of the horizontal and vertical movement of the monitoring points. Readings could be taken quickly and were automatically recorded on a computer. The equipment generally worked very well.

The variation of settlement with time for the settlement plates 32S, 33S, 34S and 35S are presented in Fig. 3.20 (i.e. Figs. 3.20a and 3.20b). A similar plot for the augers 36A, 37A, 38A and 39A are shown in Fig. 3.21 (i.e. Figs. 3.21a and 3.21b). Both Figs.

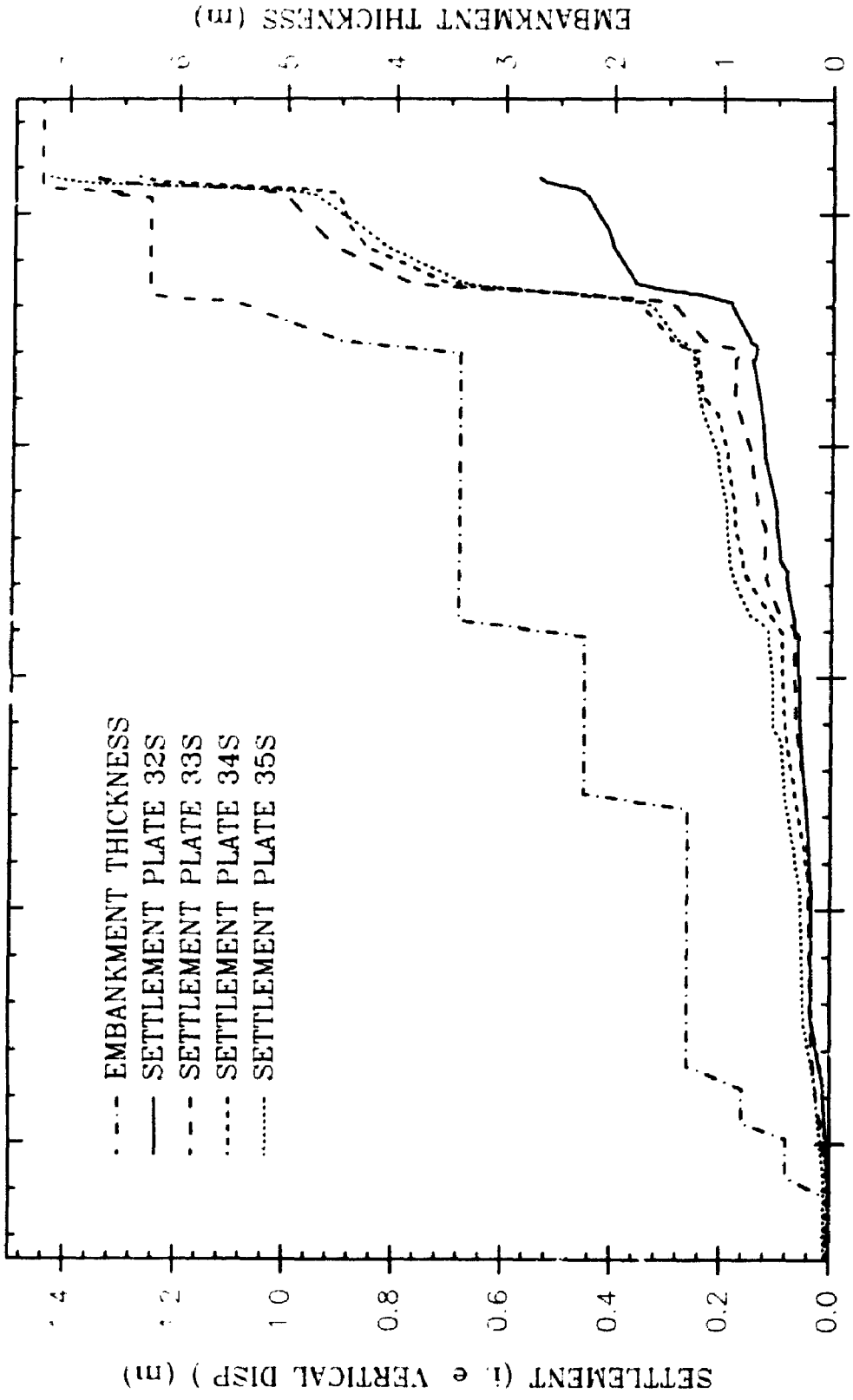

FIG. 3.20a VARIATION OF SETTLEMENT WITH TIME FOR SETTLEMENT PLATES 32S, 33S, 34S AND 35S

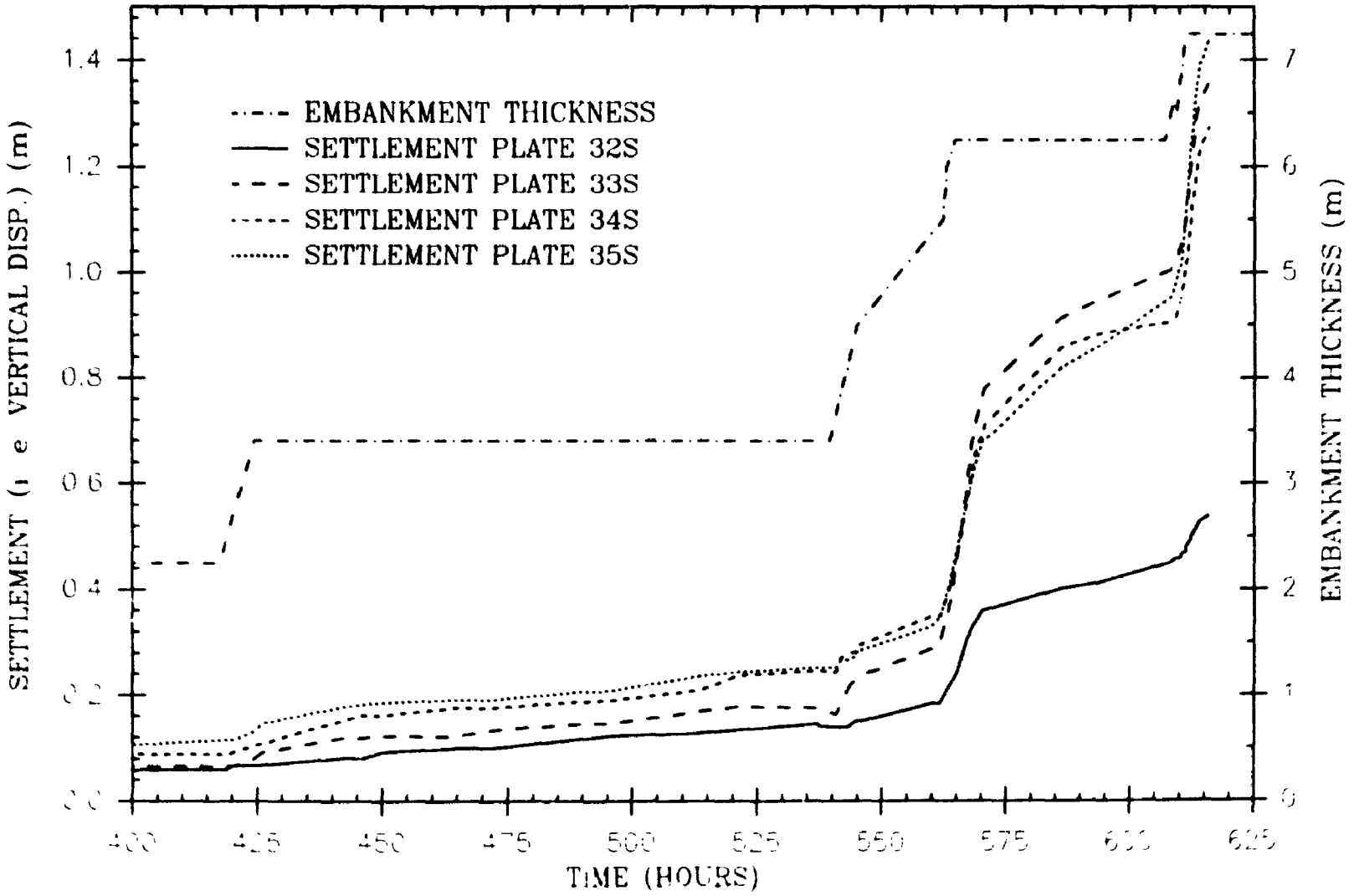

FIG 3.20b VARIATION OF SETTLEMENT WITH TIME FOR SETTLEMENT PLATES 32S, 33S, 34S AND 35S

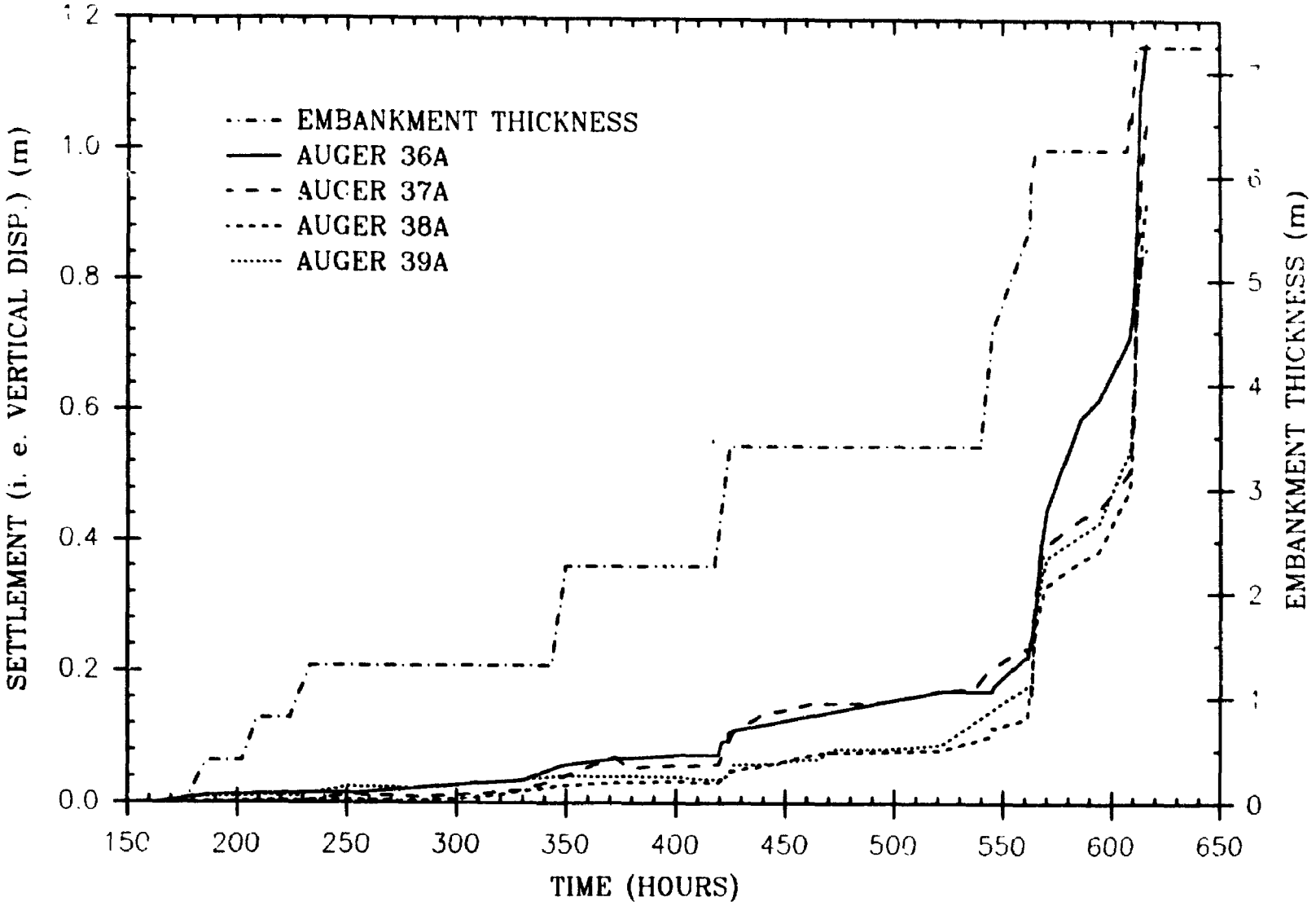

FIG. 3.21a VARIATION OF SETTLEMENT WITH TIME FOR AUGERS 36A, 37A, 38A AND 39A

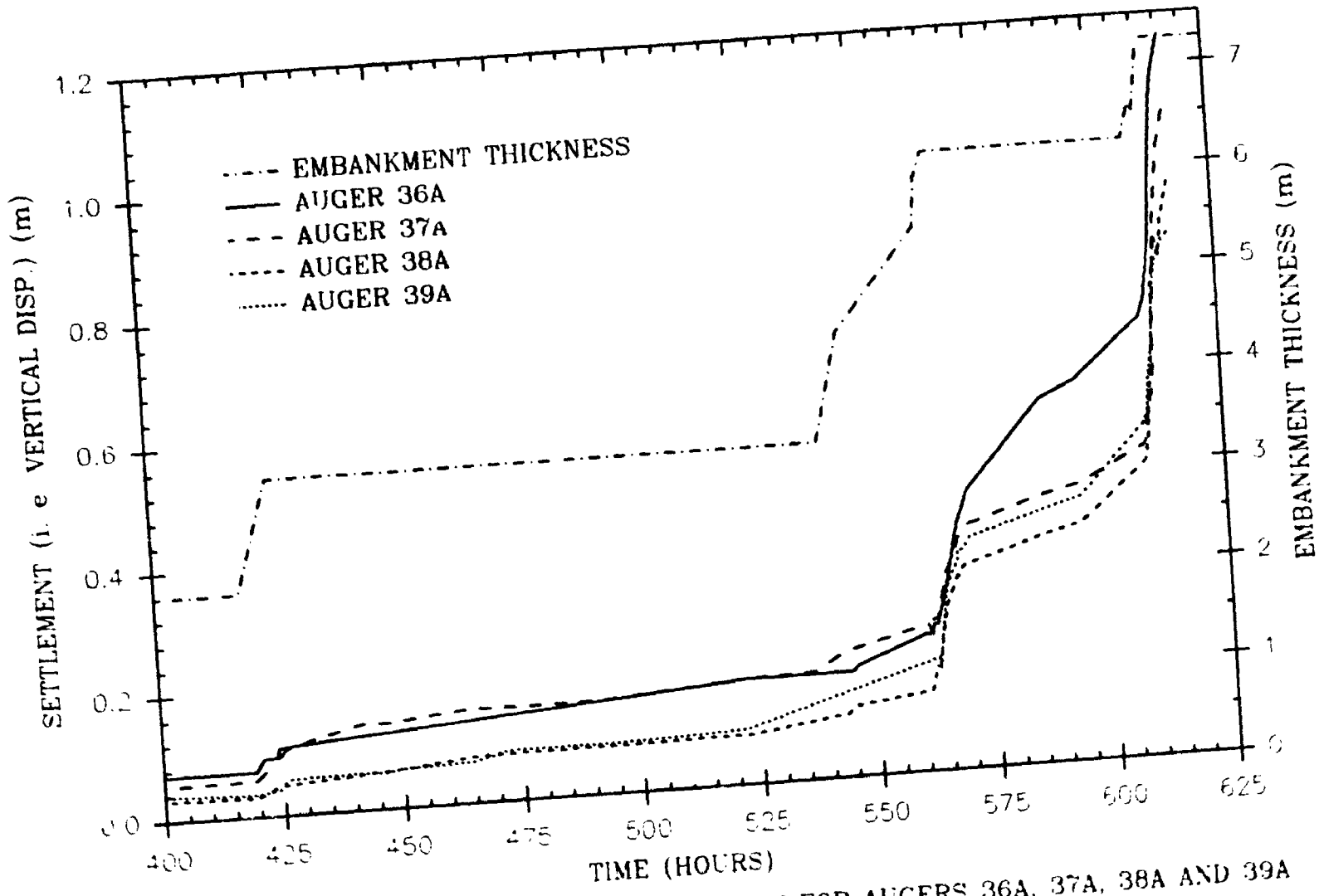

FIG. 3.21b VARIATION OF SETTLEMENT WITH TIME FOR AUGERS 36A, 37A, 38A AND 39A

3.20 and 3.21 indicate that the settlement of all the monitoring points increased with time and increasing fill thickness. It can be observed that the settlements at the ground surface monitoring points (i.e. settlement plates 32S, 33S, 34S and 35S) were less than 0.3 m until the embankment thickness was increased above 3.4 m. The plots indicate that there was a slight gradual increase in settlement between stages of construction when there was no addition of fill (i.e. at fill thicknesses 1.3, 2.3 and 3.4 m). The increase in settlement with time at a height of 3.4 m was, at least in part, due to loading of the reinforced section to failure during this period (i.e. the fill thickness of the reinforced section was increased from 3.4 to 9.5 m).

The settlement at plate 32S (located beneath the embankment slope) did not increase as much as the other monitoring points. The settlement at plates 33S, 34S and 35S increased rapidly with increase in fill thickness beyond 3.4 m during stage 4 construction (see Fig. 3.20). A rapid increase in settlement was evident after about 560 hours (i.e. for fill thicknesses greater than 5.5 m). When the fill thickness was raised to about 6.25 m, the settlement increased to as high as 0.9 m. Failure of the embankment appear to have initiated at this embankment thickness of about 5.5 m as evidenced by the blockage of the inclinometer casings between a thickness of 5 and 6 m and by the very rapid increase in settlement when the fill thickness was raised above 5.5 m (see Figs. 3.20 and 3.21). However the failure was not dramatic and additional fill could be placed. At a fill thickness of 7.25 m, the largest settlement of more than 1.4 m was recorded at settlement plate 35S. Settlements were also large at monitoring points 33S (max. settlement = 1.37 m) and 34S (max. settlement = 1.3 m). Visually, the maximum settlement appeared to have occurred between plates 35S and 40S just south of plate 35S (see Fig. 3.22).

The settlement of the augers exhibited a response similar to the settlement plate

FIGURE 3.22 ROTATIONAL FAILURE OF THE UNREINFORCED SECTION

points. The settlement of augers 36A and 37A were almost the same until about 560 - 565 hours. The settlement of augers 38A and 39A were also very similar during the same period. However, there are intervals of time during which period the settlement of auger 37A placed at a depth of 4 m appears to be slightly greater than that of 36A which is placed at a depth of 2 m. A similar observation can be made concerning the augers 38A and 39A. This minor anomaly is a result of the method of monitoring, as discussed below. The movement of the augers was inferred by monitoring the top of the rods (about 12 mm dia, hexagonal cross section, made of aluminum) fixed to the augers. These rods were protected in steel pipe casings (50 mm dia.). The accuracy of survey measurements of the location of the top of the rods is affected by the wind causing movement of the rod while measurements were being taken. The effect of wind was only significant when the overprojection of the pipe above the fill level (or ground level at the beginning of construction) and the rod above the protection pipe were large. This occurred for periods during construction when it was necessary to add a new extension to the pipe and rod and before the fill was brought up sufficiently to stop significant movement of the pipe due to wind. This is considered to be the cause of the anomaly whereby the settlement at 4 m (37A) appears to exceed that at 2 m (36A) at some point in time.

A marked increase in the settlement of auger 36A compared to the other augers is observed after 565 hours indicating a more rapid deformation of the upper 2 m of the foundation soil (see Fig. 3.21). The final readings of the settlement indicate the expected descending order (i.e. 1.17, 1.04, 0.93 and 0.85 m for the augers 36A, 37A, 38A and 39A respectively). Moreover, comparison of Figs. 3.20 and 3.21 indicate a close agreement between the settlement of auger 36A (placed at a depth of 2 m) with the settlement plate 35S which is closest to it. The largest settlement recorded at settlement plate 35S was 1.44 m and the corresponding largest "settlement" at auger 36A was 1.17 m. It is noted that, although the failure surfaces inferred from inclinometer data and surface

observations, appears to have been shallow, extensive "undrained" plastic deformation appears to have occurred as is evident by the "settlement" of 0.85 m even at a depth of 10 m and by the large horizontal deformation that were evident when the fill thickness was in excess of 7 m. It is noted that although the augers are primarily intended to measure vertical deformations, the development of sliding (and the consequent lateral movement) will also be reflected in the "settlement" readings. An examination of all the available data would suggest that a significant component of the "deep settlements" noted above may in fact be largely a reflection of the large lateral movement which occurred above this depth.

3.6.5 Heave and horizontal displacement

The settlements were accompanied by heave observed in the region close to the toe (see Figure 3.23, i.e. Figs. 3.23a and 3.23b). Heave plates were installed at selected points in this region as detailed previously (see Figs. 3.2 and 3.7). Displacement of each heave plate was measured by monitoring the movement of the top of the 0.5 m pipe fixed perpendicular to the plate (i.e. the pipe initially vertical). The horizontal displacements along two mutually perpendicular axes were also obtained from the survey data. The absolute horizontal displacements calculated from these data are plotted against time in Figure 3.24 (i.e. Figs. 3.24a and 3.24b).

Fig. 3.23 indicates that the vertical displacement (i. e.heave) was small, less than 0.1 m, up to about 490 hours (an embankment thickness of 3.4 m). A small increase in heave is also observed between the stages of construction, similar to settlement observations. A moderate increase of heave (up to a maximum of 0.28 m at heave plate 29H) was observed during the early portion of stage 4 construction (up to about 561 hours). The heave increased very rapidly (by about 0.37 m at heave plate 29H) during the

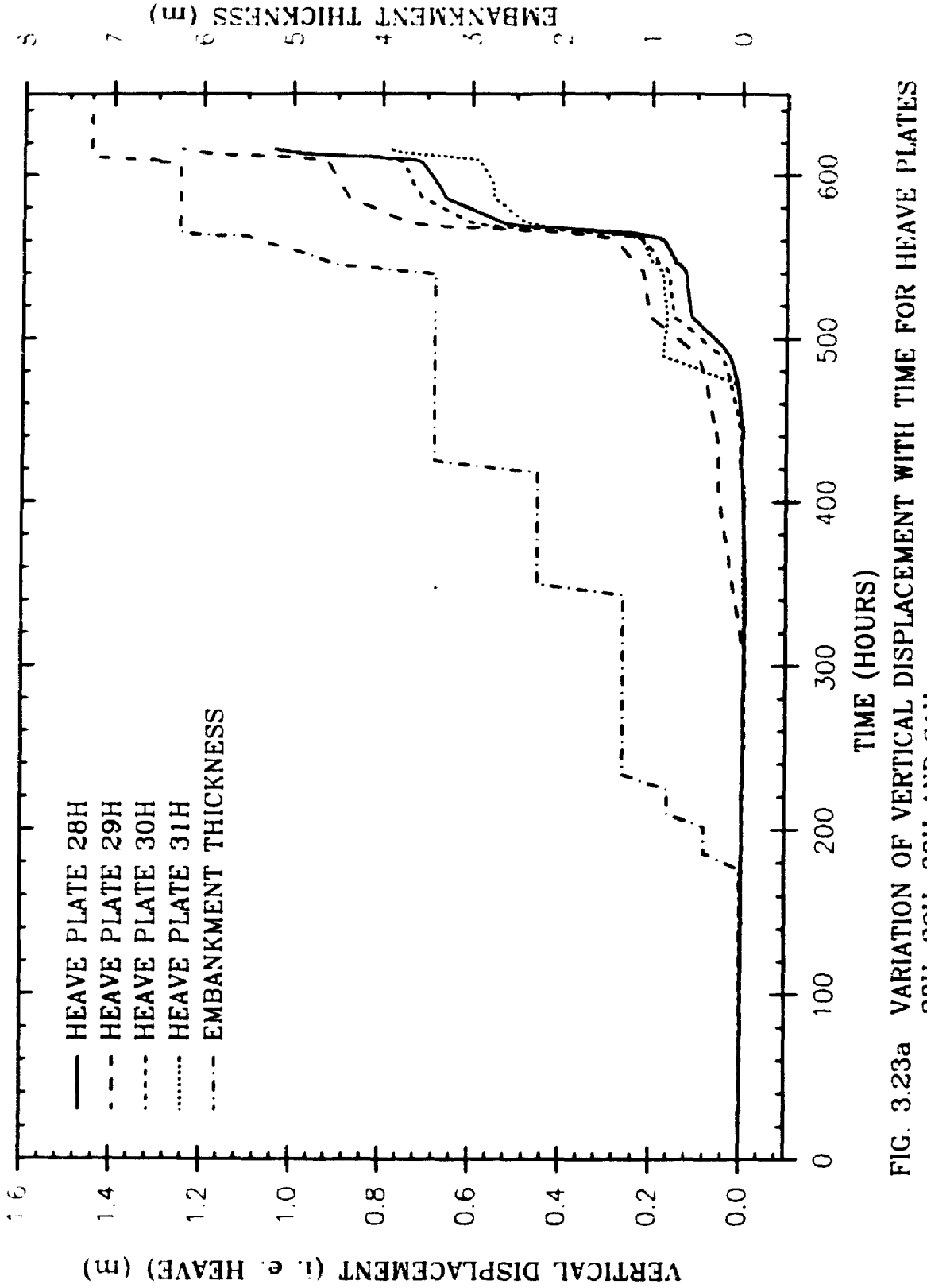

FIG. 3.23a VARIATION OF VERTICAL DISPLACEMENT WITH TIME FOR HEAVE PLATES 28H, 29H, 30H AND 31H

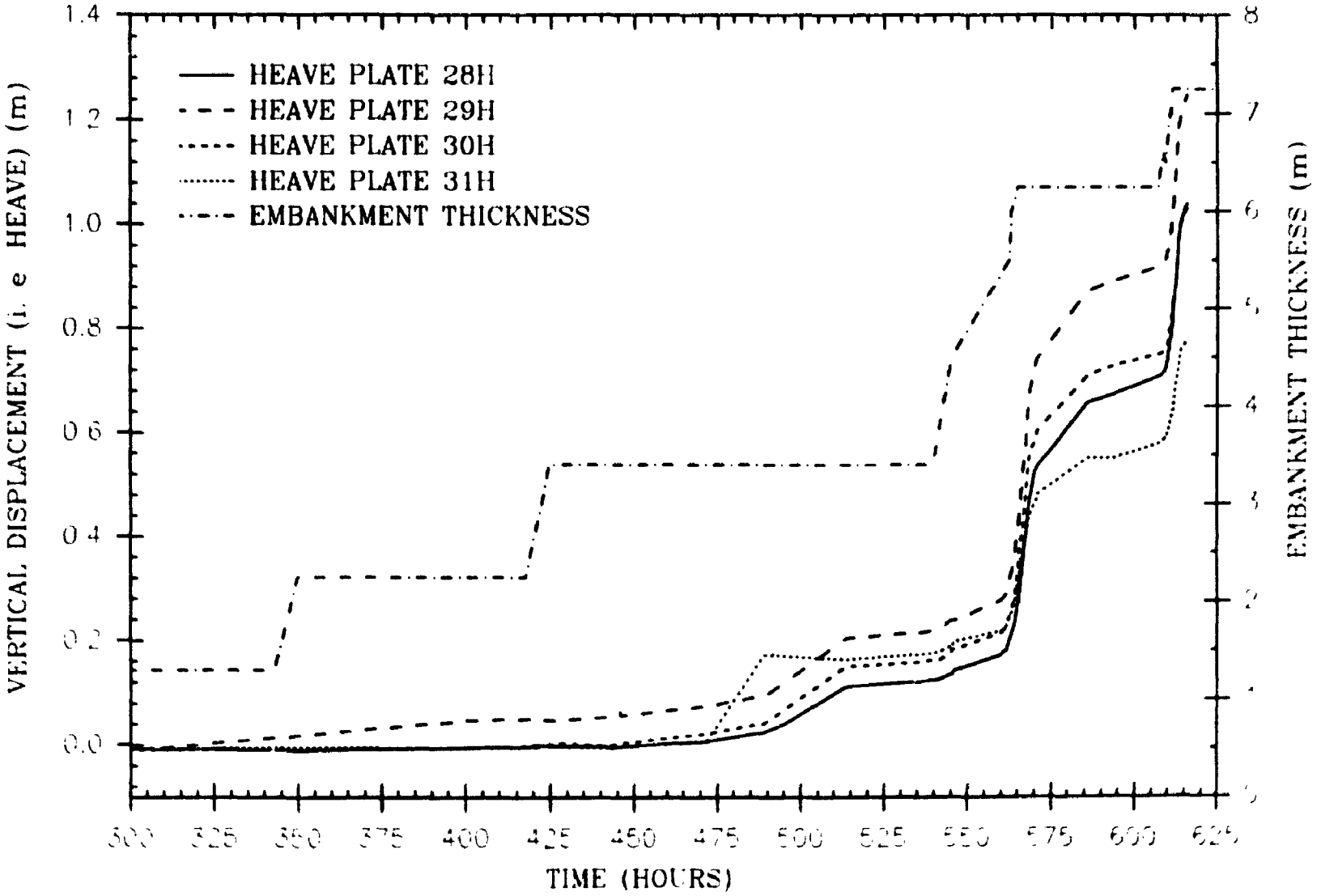

FIG 3.23b VARIATION OF VERTICAL DISPLACEMENT WITH TIME FOR HEAVE PLATES 28H, 29H, 30H AND 31H

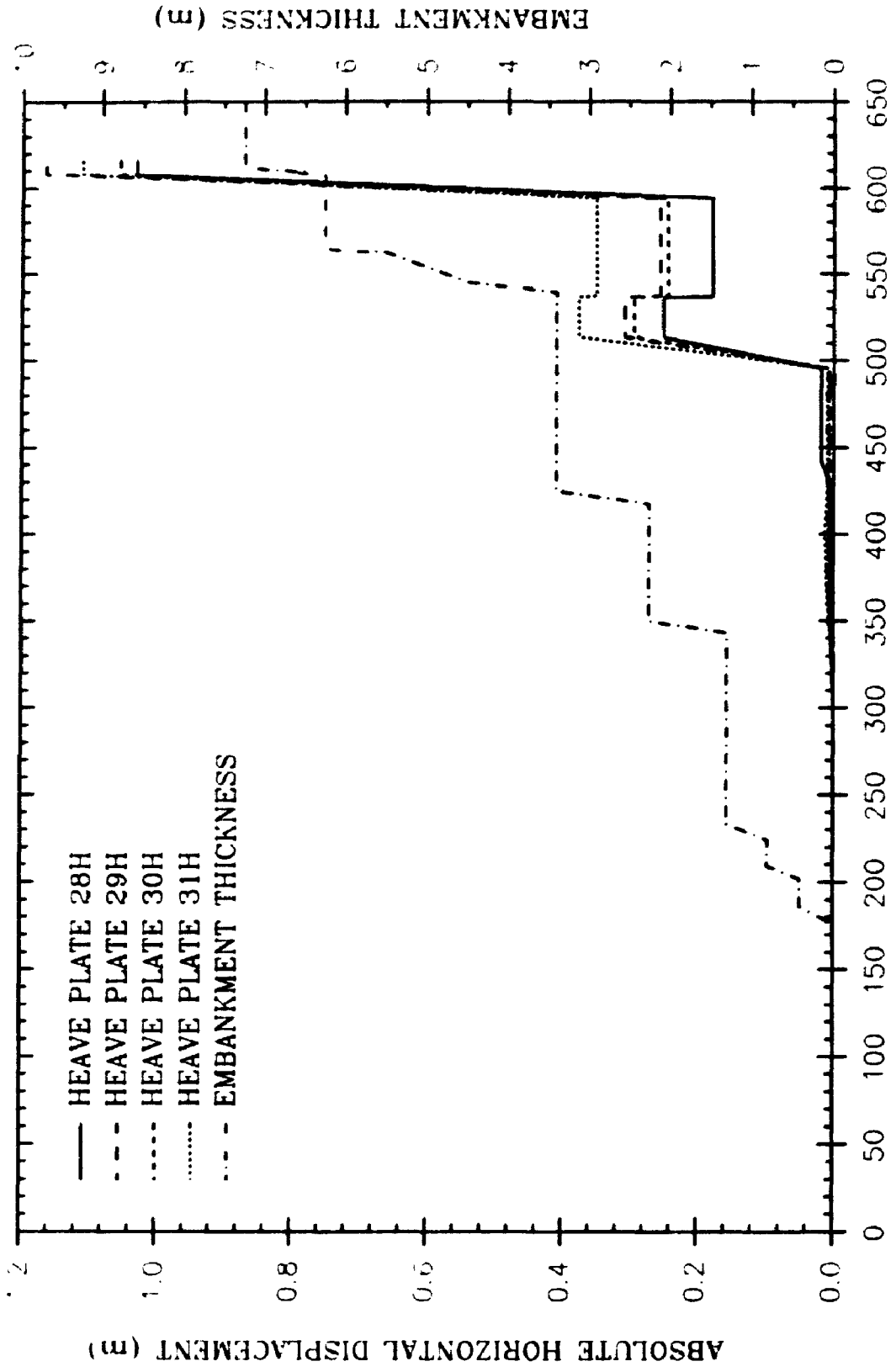

FIG 3.24a VARIATION OF HORIZONTAL DISPLACEMENT WITH TIME FOR HEAVE PLATES 28H, 29H, 30H AND 31H

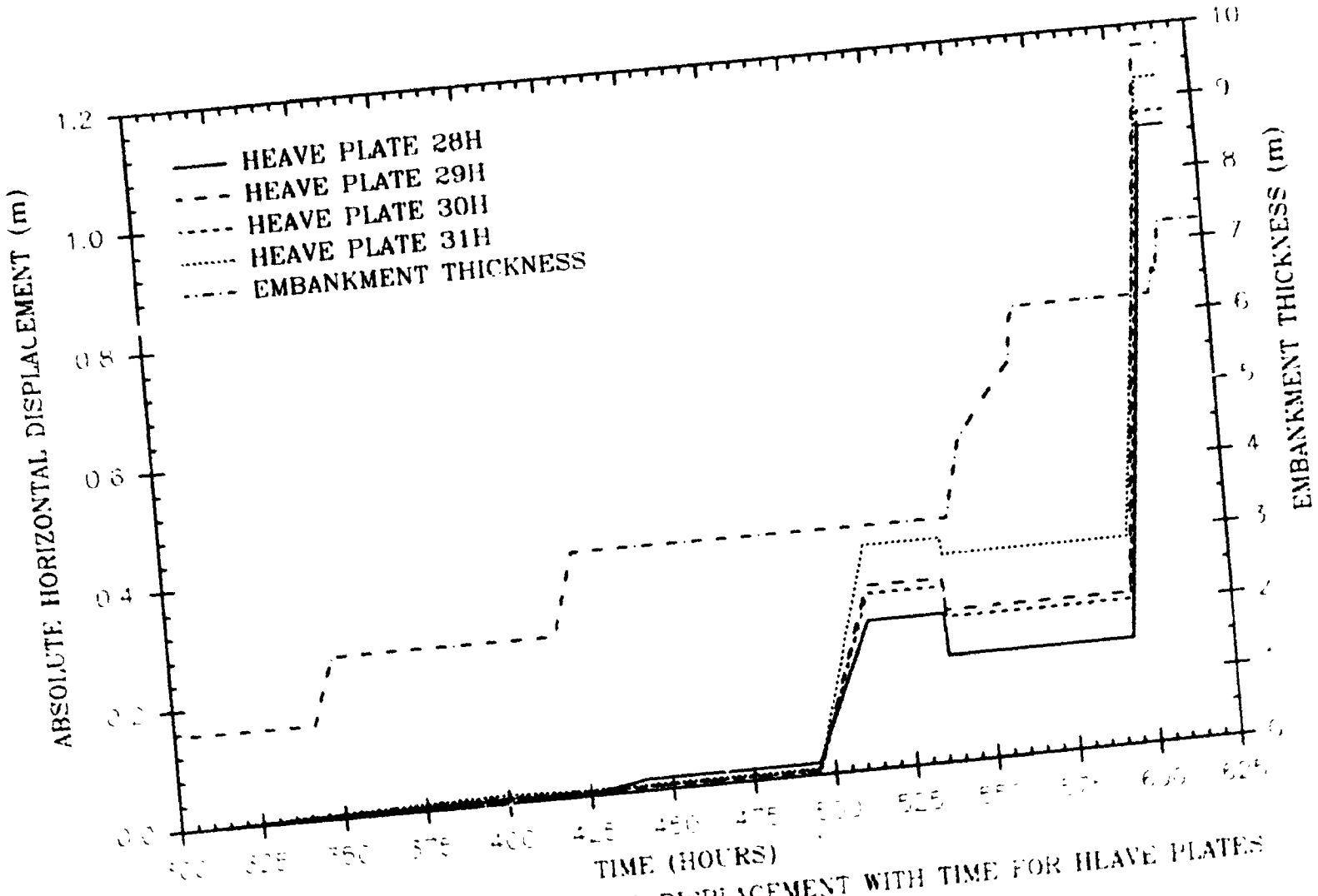

FIG 3.24b VARIATION OF HORIZONTAL DISPLACEMENT WITH TIME FOR HEAVE PLATES 28H, 29H, 30H AND 31H

time interval 561 - 568 hours which reflects the increase of embankment thickness from 5.5 m to 6.3 m. Settlement and inclinometer data suggested the initiation of failure during this period as discussed previously. The rate of heaving slowed down a little until 608 hours. Another period of very rapid increase in heave was observed during 608 - 616 hours. For example, the heave increased by about 0.33 m in heave plate 29H when the fill thickness was increased from 6.45 to 7.25 m during this time interval of rapid movement.

A similar pattern of behaviour for the variation of absolute horizontal displacement (hereafter called the horizontal displacement) with time was exhibited by all the four heave plates (see Fig. 3.24). The horizontal displacement of the heave plates were negligible (less than 2 mm) until about 495 hours when the embankment thickness was raised up to 3.4 m in the first three stages of construction. A marked increase in the horizontal displacement, as high as 0.35 m in heave plate 31H, was observed in all the four heave plates during the period of approximately 495 - 513 hours.

The horizontal displacement plotted in Fig. 3.24 is the cumulative effect of the actual displacement and the negative displacement introduced by the tilting. Thus, the apparent drop in the horizontal displacement implied by Fig. 3.24 at about 537 hours (which is preceded, and followed, by periods of constant horizontal displacements (i.e. during the time intervals 513 - 537 hours and 537 - 594 hours) is the result of tilting of the monitoring point during the formation of the wave-like heave zone which was formed during this period (i.e. between fill thicknesses of 3.4 and 6 m). (The monitoring point for each heave plate was 0.5 m above the ground surface and hence a tilt of the plate caused by the heave of the ground resulted in a corresponding negative horizontal displacement at the monitoring point. Thus for example a tilt of 20^{0} to the south combined with a horizontal movement of the ground by 17 cm to the north would give a net displacement of zero at the monitoring point on the heave plate). It is worth noting that the vertical

displacement will not be significantly affected by this tilting.

A rapid increase in the horizontal displacement (as high as 0.91 m at heave plate 29H) was observed as the embankment was raised from 6.25 to 7.25 m (595 - 610 hours). This would appear to correspond to failure of the embankment.

3.6.6 Displacements on the berm side of embankment

The settlement on the berm side of the embankment was comparatively small (< 0.1 m) as is evident from the settlement plots for settlement plates 45S and 46S (Fig. 3.25) and for the augers 41A, 42A, 43A and 44A placed in the foundation soil beneath the berm (Fig. 3.26). Settlement plate 46S placed comparatively closer to the toe of the berm showed significantly lower settlement than settlement plate 45S placed well away from the toe of the berm. Both settlement plates showed an increase in settlement with time (up to about 350 hours) as long as the main embankment thickness was less than the berm thickness. Subsequent increases in the main embankment thickness slowed and then reversed the settlement trends beneath the berm. The apparent decrease in settlement is attributed to incremental heave induced by construction of the main embankment. The augers showed a pattern similar to the settlement plates. In addition, a descending pattern of settlement with depth was observed. The largest settlement was about 0.05 m and was indicated by auger 41A.

The vertical displacement observed in the heave plates placed on the southern side of the embankment were even smaller as indicated in Fig. 3.27. The largest heave observed was about 0.04 m at heave plate 49H. Very small settlements (< 0.02 m) were observed in the heave plates during the initial stages of construction. Heave plate 47H placed closer to the toe indicated the largest settlement.

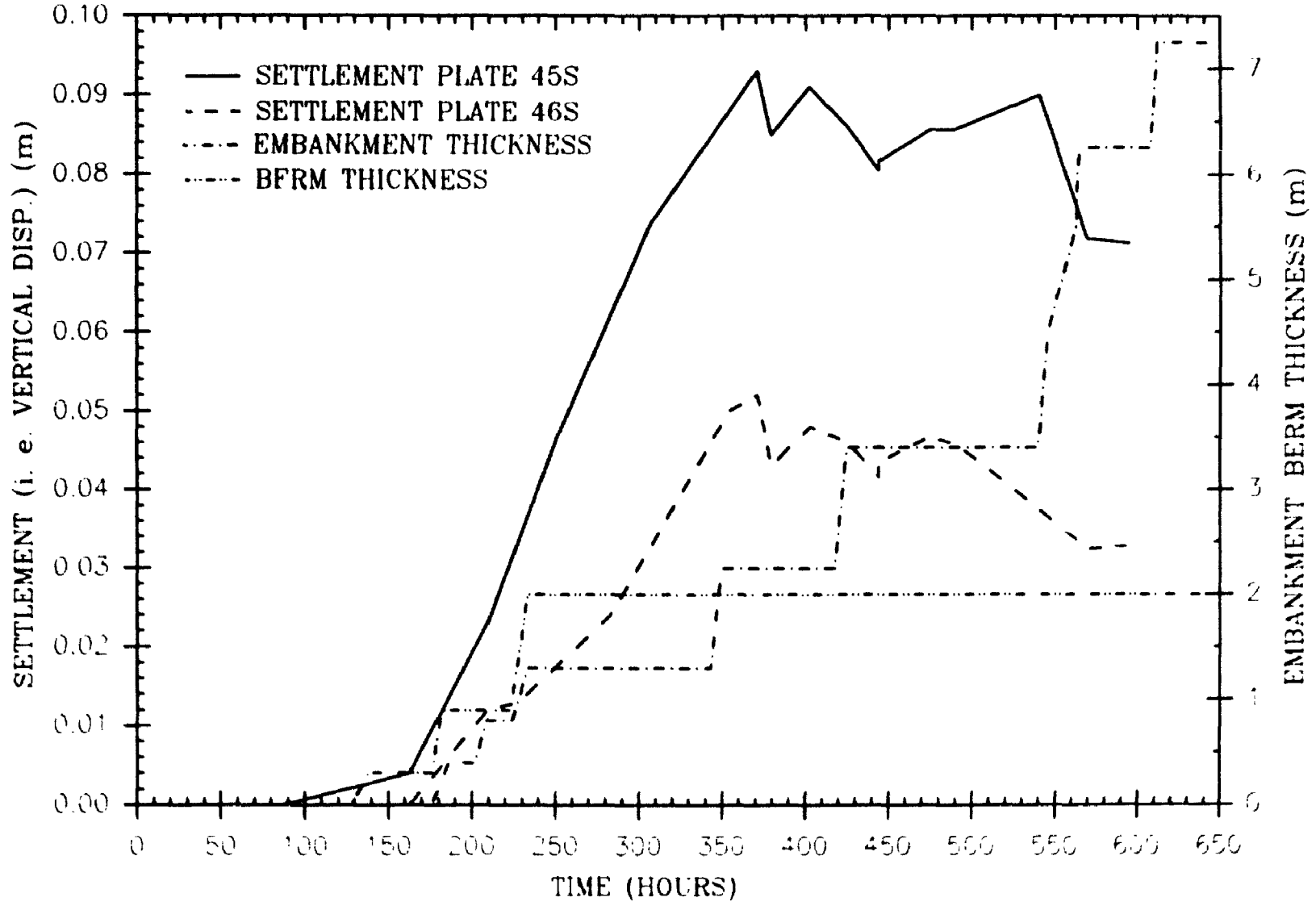

FIG 3.25 VARIATION OF SETTLEMENT WITH TIME FOR SETTLEMENT PLATES 45S AND 46S

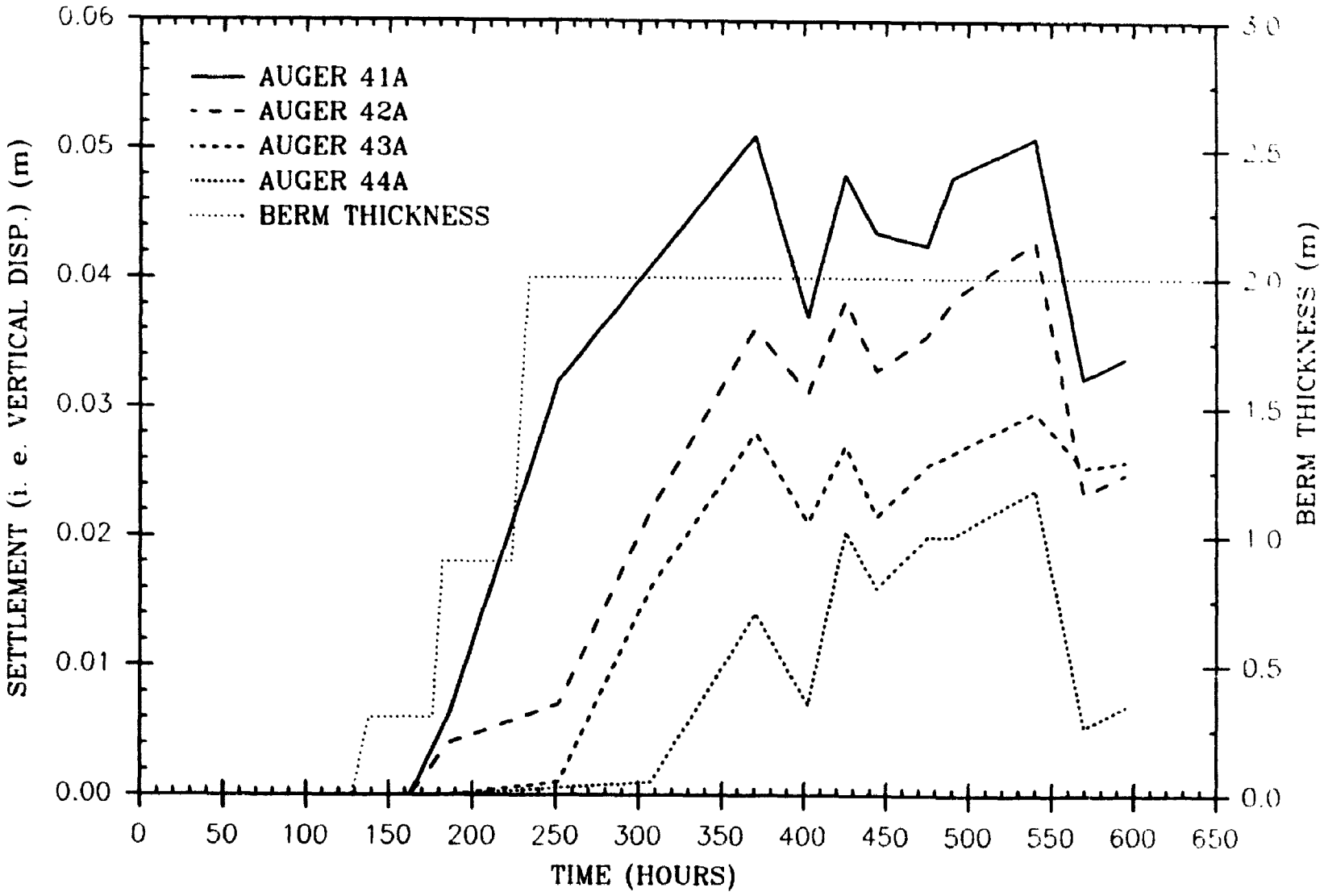

FIG. 3.26 VARIATION OF SETTLEMENT WITH TIME FOR AUGERS 41A, 42A, 43A AND 44A

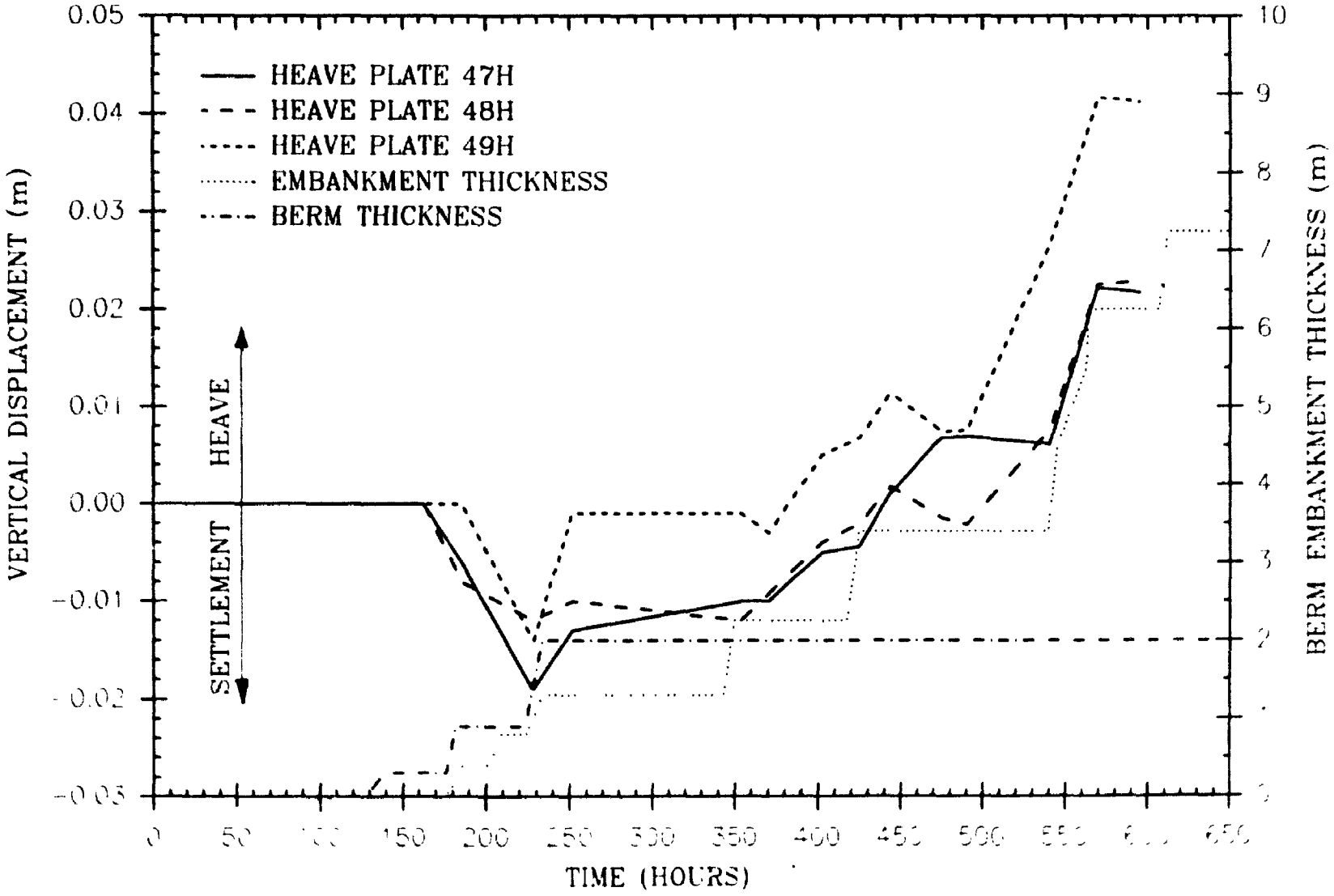

FIG 3.27 VARIATION OF VERTICAL DISPLACEMENT WITH TIME FOR HEAVE PLATES 47H, 48H AND 49H

3.7 UNREINFORCED EMBANKMENT FAILURE

The variation of settlement at settlement plates 32S, 33S, 34S and 35S with embankment thickness is shown in Fig. 3.28. A reasonably linear relationship is indicated during the early stages of construction up to 3.4 m, probably due to elastic behaviour of the foundation soil. This is consistent with the finding of Tavenas et al. (1974) who demonstrated that foundations behave elastically up to a critical height approximately equal to 50% of the failure height. When the embankment was increased from 3.4 m to 5.4 m there was initially a thickness - settlement response similar to that in the initial phase of loading. From 5.4 m there was an increased rate of settlement which became even more evident at a thickness of 6.1 m. The embankment continued to settle very rapidly even when the construction was stopped for a brief period at 6.25 m thickness. The failure appeared to be of a visco plastic nature, and the time dependent undrained response appears to reflect a combination of plastic failure and "undrained creep". To confirm this type of failure, more fill was added and the movement of the embankment closely monitored. Movement of the embankment was also monitored physically by observing the movement of the marks made on the auger rods with respect to the top of their protection pipes. Construction was stopped when very rapid movements were observed at a thickness of 7.25 m.

The variation of vertical displacement with embankment thickness at the heave plates placed north of the toe is shown in Fig. 3.29. The heave was very small (except at heave plate 29H) compared to the settlement up to 3.4 m thickness. The heave responses indicate that nonlinear behaviour started to occur between 3.4 m and 4.5 m thickness, well before the 5.4 m thickness indicated by the settlement responses. The gradual flattening of the settlement and heave responses close to 6.25 m thickness during the construction from 3.4 to 6.25 m thickness suggest that the failure thickness of the embankment was close to

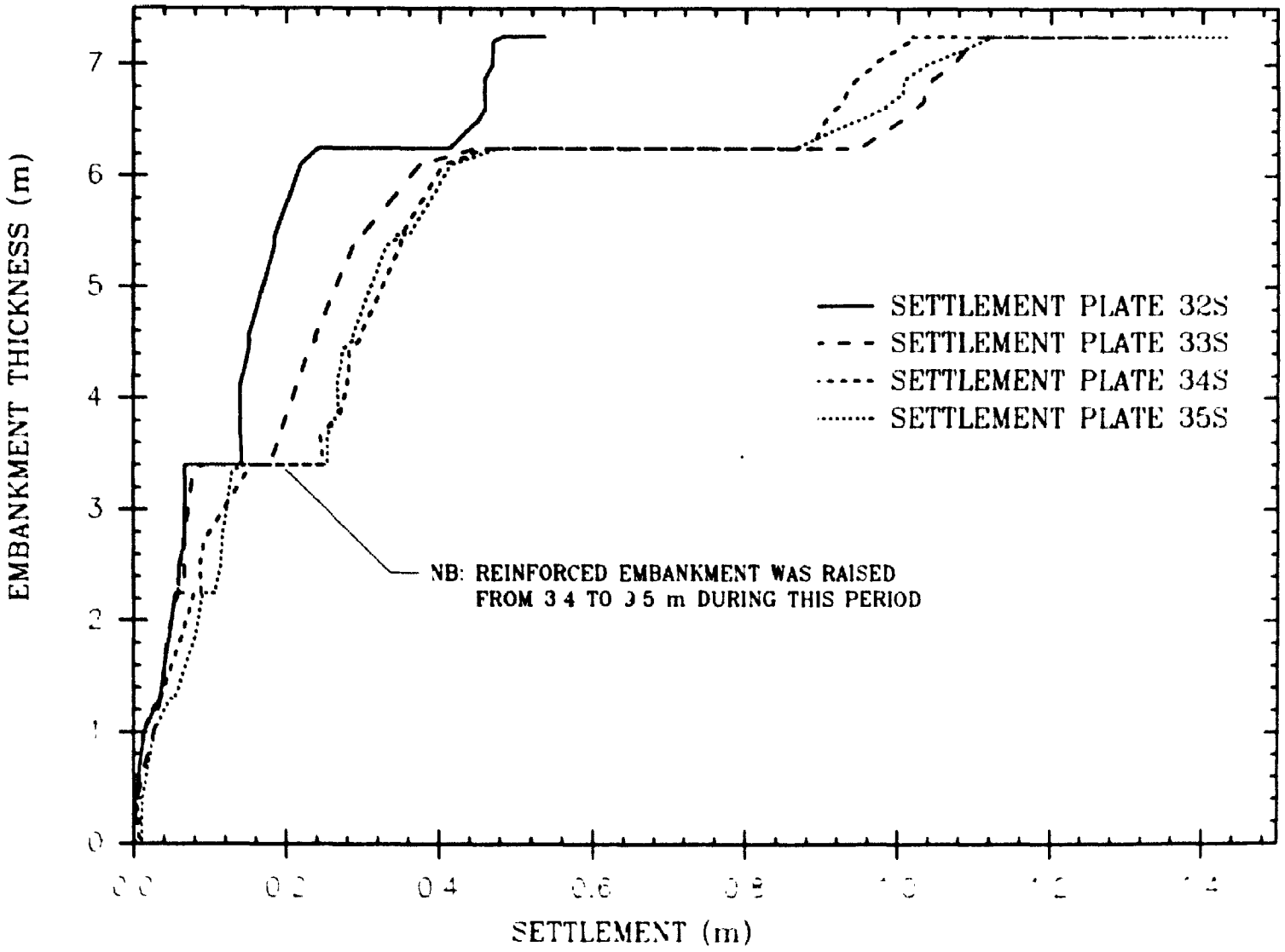

FIG 3 28 VARIATION OF SETTLEMENT WITH EMBANKMENT THICKNESS FOR SETTLEMENT PLATES 32S, 33S, 34S AND 35S

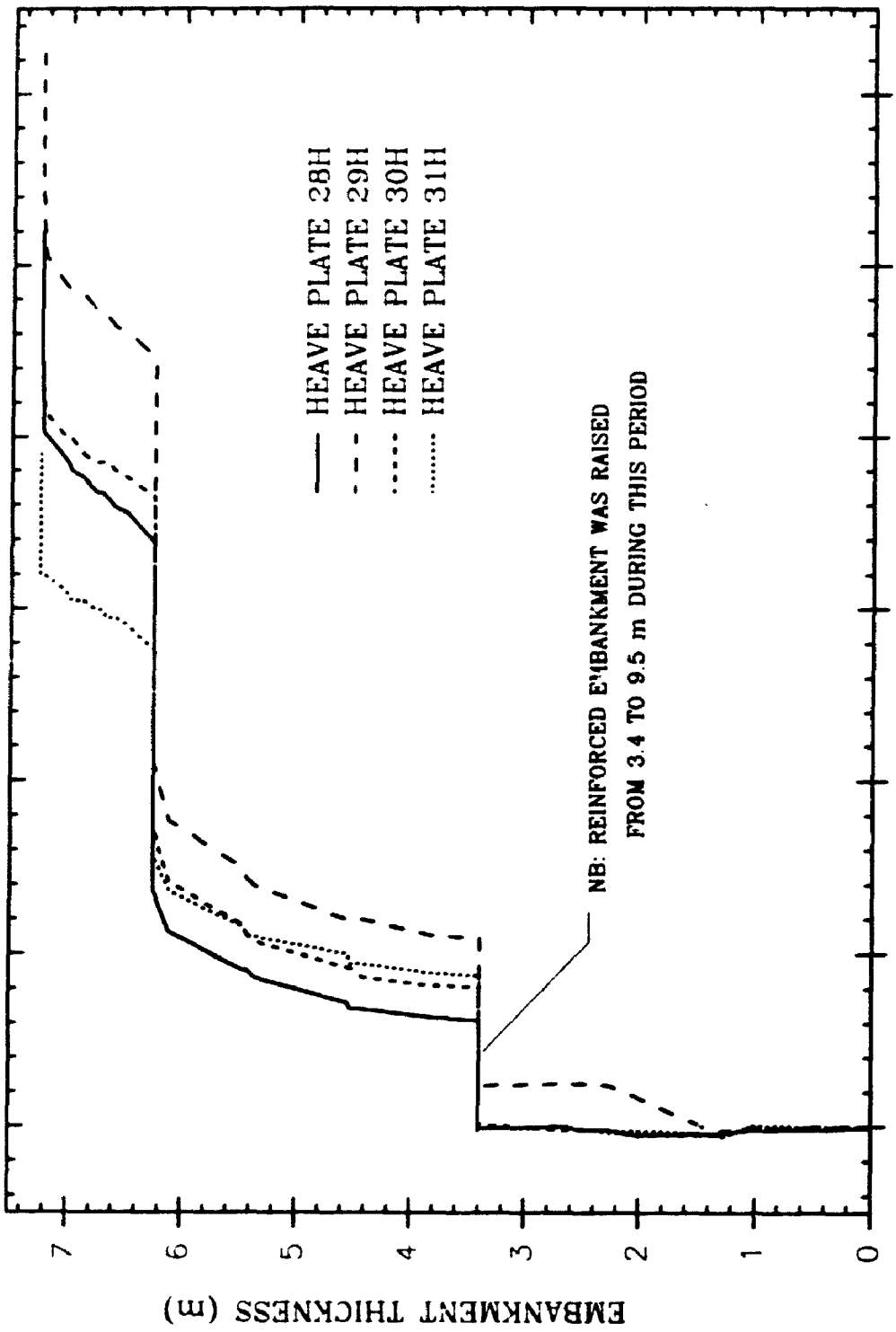

FIG. 3.29 VARIATION OF VERTICAL DISPLACEMENT WITH EMBANKMENT THICKNESS FOR HEAVE PLATES 28H, 29H, 30H AND 31H

6.25 m. However, a definite failure thickness cannot be interpreted from these figures because of the absence of a clear flattening of the curves during the construction afterwards up to 7.25 m thickness.

The net embankment height (hereafter called the embankment height) is defined as the elevation of the crest of the embankment with reference to the maximum elevation of the ground near the toe (i.e. net embankment height at a particular instant = embankment thickness - settlement - maximum heave near the toe at that particular instant). This can be determined from the embankment thickness, settlement and heave data and is plotted against the embankment thickness for different settlement plates in Fig. 3.30. The embankment height increased linearly with embankment thickness during the first three stages of construction as evident from this figure, probably due to the elastic behaviour of the foundation soil as discussed previously. The variation was reasonably linear during stage four construction until the embankment thickness reached 6.1 m. A rapid flattening of the variation of embankment height with thickness is observed at an embankment thickness of 6.1 m (i.e. at about 5.4 m net height) indicating the onset of failure of the embankment. This thickness corresponds to the time of 565 hours (see Fig. 3.10). At this time very rapid increases in settlement (see Figs. 3.20 and 3.21) as well as heave (see Fig. 3.23) were observed as reported earlier. However, the variation of parameter $\overline{B}$ with time (see Fig. 3.16) suggested the initiation of failure between 570 - 595 hours (i.e. at 6.25 m embankment thickness). The embankment height remained constant at about 5.4 m until the embankment was raised to 6.25 m thickness, indicating a plastic type of failure of the embankment. The net height decreased dramatically (to about 4.5 m) when there was no addition of fill at 6.25 m thickness (i.e. between 565 and 607 hours).

To confirm the failure of the embankment, more fill was added on October 16, 1989 (starting at about 607 hours). The embankment height increased gradually again, but

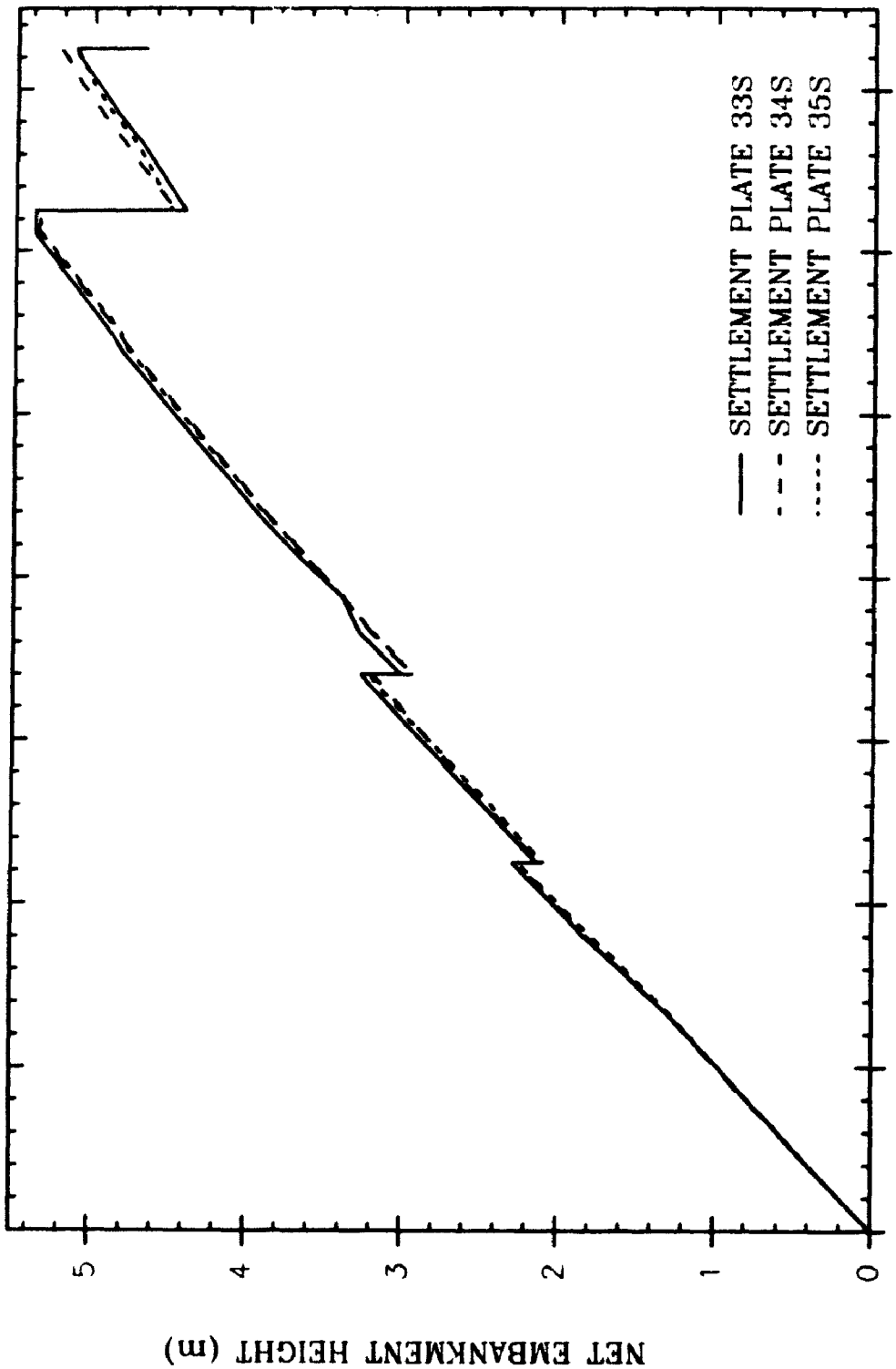

FIG. 3.30 VARIATION OF NET EMBANKMENT HEIGHT WITH EMBANKMENT THICKNESS FOR SETTLEMENT PLATES 33S, 34S AND 35S

at a lesser gradient up to a maximum of about 5.2 m. The construction was stopped at 7.25 m thickness when very rapid settlement and heave was observed as discussed previously (see Figs. 3.20 and 3.23). The embankment height dropped to about 4.8 m within 2 hours. It was evident that the embankment had already failed and that this failure was of a plastic type (or visco-plastic type). It was clear that the embankment could not be constructed significantly above the net height of 5.4 m, which was reached first at 6.1 m thickness.

Construction of the reinforced section close by had some influence on the behaviour of the unreinforced section, particularly during the brief stoppage of work at 3.4 m thickness, as evident from the extension of cracks from the reinforced section into the unreinforced section observed on Oct. 12, 1989 (see Fig. 3.31). Two major cracks were observed on the crest of the unreinforced section, marked as A and B in Fig. 3.32, when its thickness was increased to 6.25 m (i.e. on Oct. 15, 1989). A close look at the shape of the cracks A and B (see Fig. 3.32), as compared with those observed on Oct. 12 (see Fig. 3.31), shows that they have changed course and become approximately parallel to the longitudinal axis of the embankment in the central region of the unreinforced embankment portion when the embankment was raised to 6.25 m. It can be observed that the parallel nature is well pronounced for the crack B, which is considered to be directly associated with failure of the unreinforced embankment (crack B is evident to the left side of Fig. 3.22). This observation suggests that the influence of the reinforced section on the behaviour of the unreinforced section was not very significant, at least after Oct. 12, and the cracks A and B found on Oct. 15 in the mid region of the unreinforced part of the test embankment really represent two failure surfaces for the unreinforced section.

Failure of the unreinforced section was of the plastic type. To identify the most critical failure surface and to confirm the failure, fill was further added to the unreinforced section on Oct. 16, 1989. Construction was stopped at 7.25 m thickness when very rapid

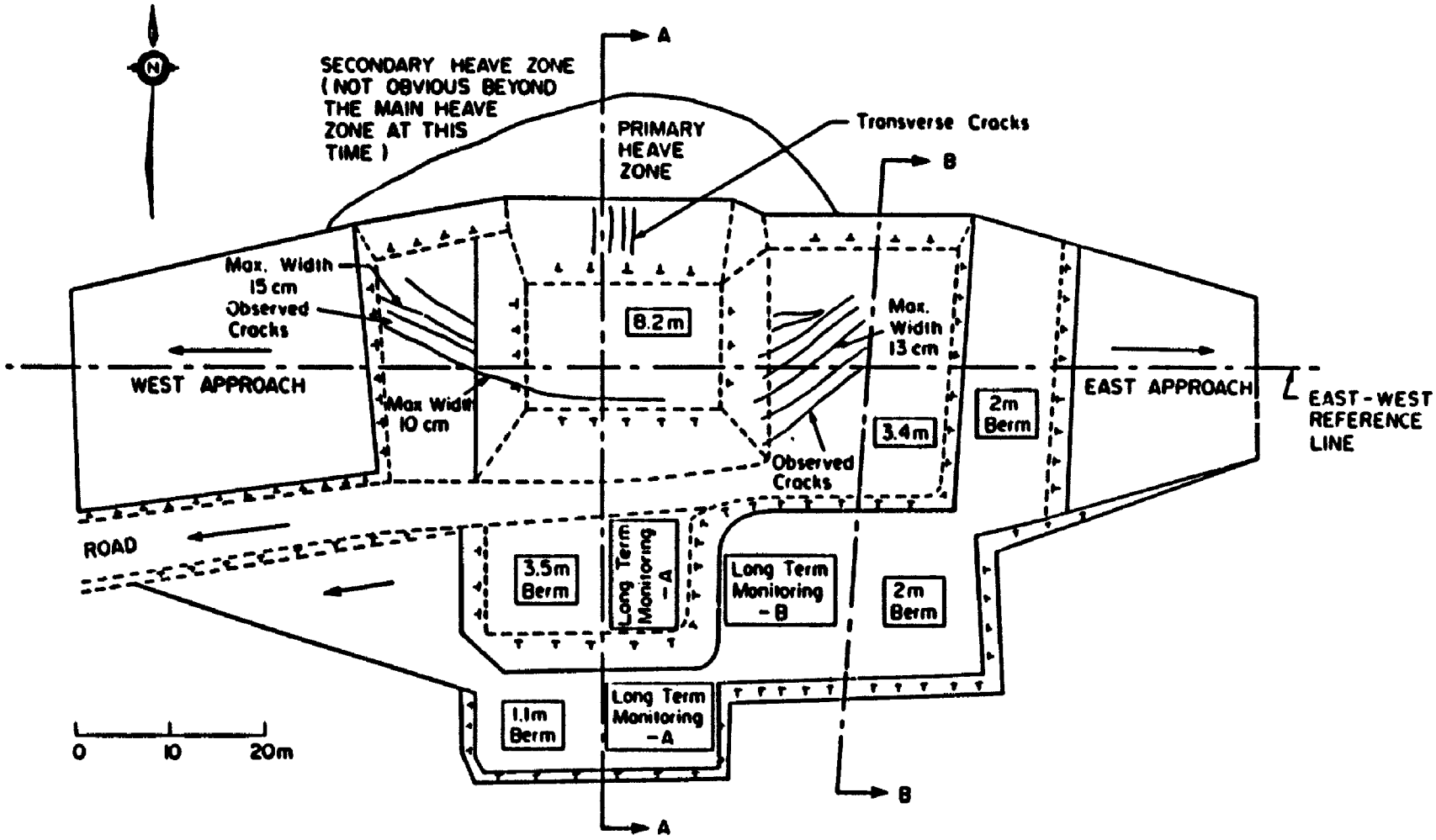

FIG. 3.31 MAPPING OF OBSERVED CRACKS ON OCT. 12, 1989 (518 HOURS)

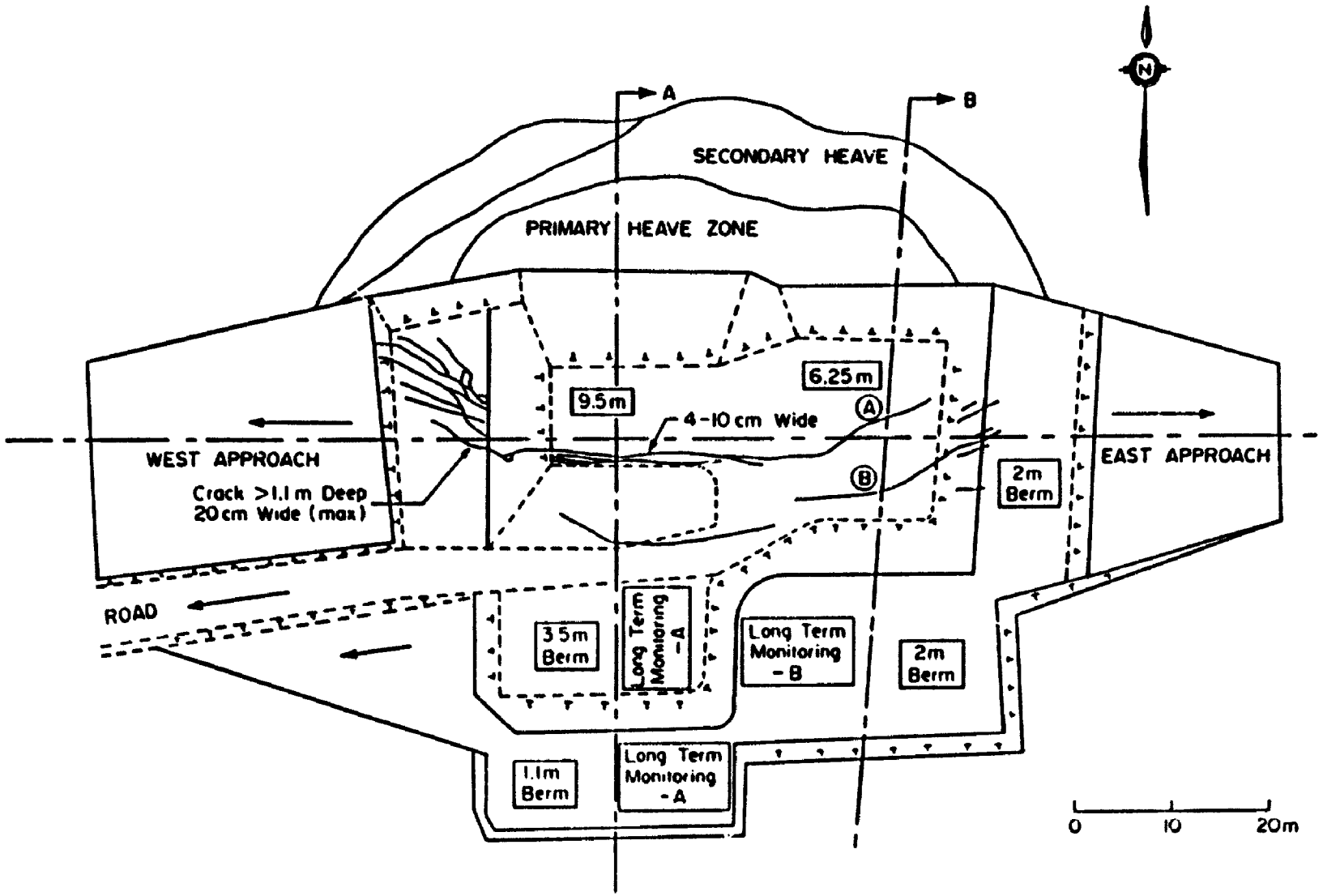

FIG. 3.32 MAPPING OF OBSERVED CRACKS AT FAILURE - OCT. 15, 1989 (588 HRS.)

movements were observed. Rotational failure of the unreinforced embankment along crack A was confirmed by the rotational-type deformation of the crest with a maximum depression along crack A on the new surface (see Fig. 3.22). Crack B was also found to open up again on the new surface confirming the existence of a secondary failure surface for the unreinforced embankment. The apparent circular type failure surfaces established from the cracks and the inclinometer data are presented in Fig. 3.33.

The failure thickness of 6.1 m indicated by this field investigation is significantly lower than the 9.2 m failure thickness indicated by limit equilibrium analysis performed on the basis of average vane strength profile (and below the range 7.0 - 11.4 m, determined for the range of vane strengths) of the soil beneath the unreinforced section. A limit equilibrium analysis performed on the basis of the same average vane strength profile for the foundation soil (for a 7.25 m thick embankment) indicated factors of safety of about 1.35 and 1.95 respectively for the above primary and secondary failure surfaces inferred from the field investigation (see Fig. 3.33). It is noted that the plasticity index of the soil ranged between 9 and 19% (see Fig. 3.3) with an average of about 14% and the corresponding Bjerrum's correction for the vane strength will not have a significant effect on either the calculated failure thickness or the factor of safety (see Bjerrum, 1973). It is considered that the susceptibility of the soil to some strain softening and progressive failure could have contributed for the lower failure thickness observed in this field investigation. It is noted that considerable caution is required for the design of embankment on soft organic clayey silt deposits if such design is based on vane strength and on the use of simple limit equilibrium design procedures.

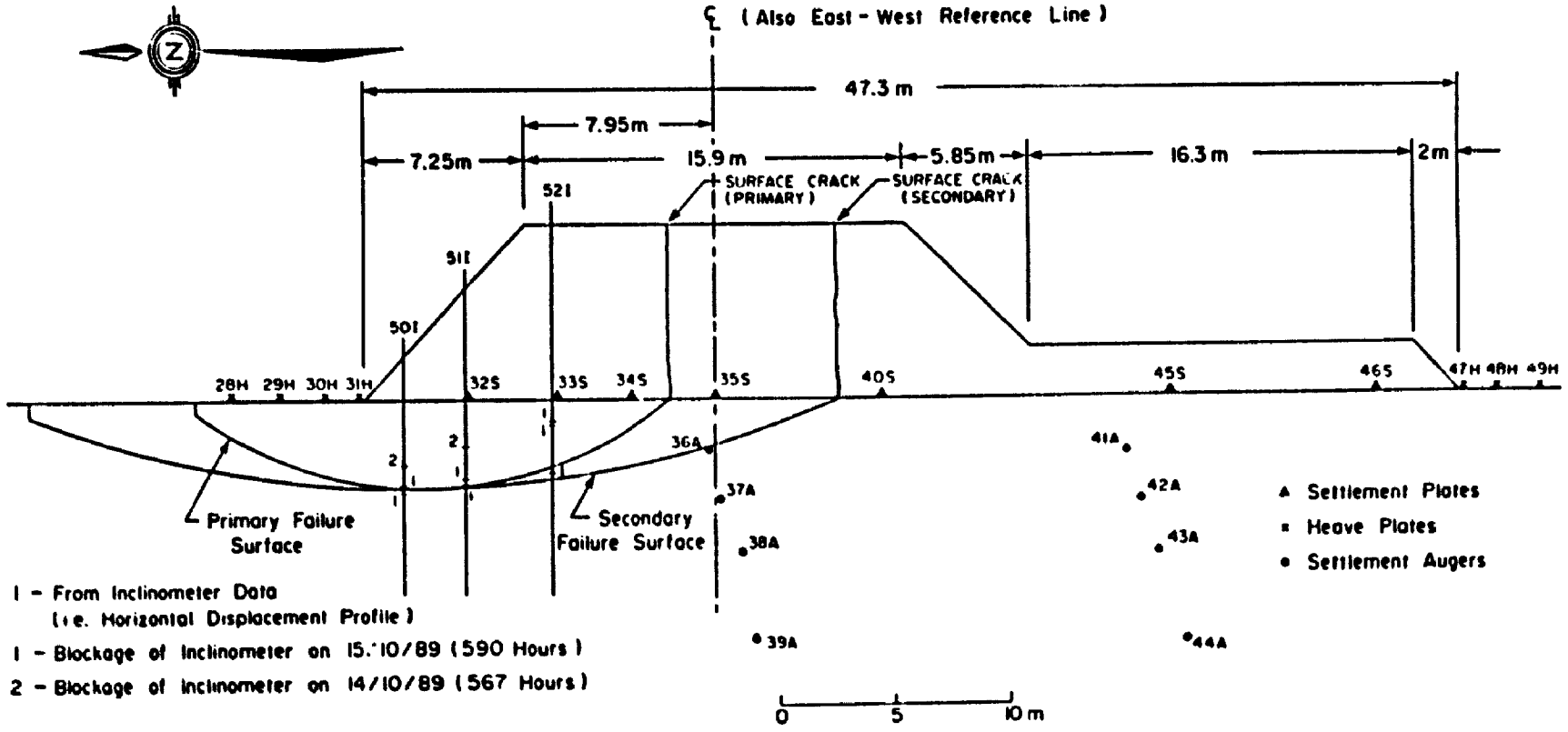

FIG. 3.33 INFERRED FAILURE SURFACES FOR THE UNREINFORCED EMBANKMENT

3.8 GENERAL COMMENTS ON THE PERFORMANCE OF INSTRUMENTATION

The position monitoring devices (i.e. the settlement plates, augers and heave plates) performed very well during the entire construction and monitoring period. The electronic distance-measuring apparatus allowed quick readings and automatic recording on a computer.

The inclinometers provided useful data up to about 5 m thickness and could not be monitored afterwards due to the relatively large movements. The pneumatic piezometers functioned well and provided useful data for most of the construction period, at least up to about 6.25 m thickness. Out of the 10 pneumatic piezometers functioning at the beginning of construction, 8 are still functioning and appear to be giving reasonable readings. These piezometers are still being monitored by UNB under the direction of Dr. A. O. Landva. The pneumatic total pressure cell also functioned well and provided useful data throughout the construction and monitoring period. The Casagrande piezometers were found to be slow to respond to the rapid construction and did not provide much useful data.

3.9 SUMMARY AND CONCLUSIONS

The instrumentation and field performance of the unreinforced section of the test embankment constructed at Sackville, N.B. has been described. Details concerning the site conditions, foundation soil properties, properties of the fill material and details of construction and data collection have been given. This section was instrumented with piezometers, settlement plates, augers, heave plates, inclinometers and a total pressure cell (see Figs. 3.2 and 3.7). Details of the instrumentation and their responses with

construction have been described.

The embankment behaved elastically up to a thickness of about 3.4 m. The reinforced section was constructed to failure when the unreinforced section was at a constant thickness of 3.4 m. Due to the proximity of the reinforced and unreinforced sections (an unfortunate necessity due to site conditions and other limitations) there was some interaction between the two sections. However, fortunately, the rotational failure of the unreinforced section could be clearly delineated.

The unreinforced section was constructed rapidly from 3.4 to 6.25 m thickness. An examination of pore pressure, heave and settlement responses suggest that the embankment failed at a thickness of 6.1 - 6.25 m. The net height could not be raised above a maximum of 5.4 m (attained at about 6.1 m thickness) even though the fill thickness was increased from 6.25 to 7.25 m. The failure was of a plastic (or visco-plastic) type and no classical-type abrupt failure was encountered during the construction of this embankment.

It is noted that although the failure surfaces inferred from inclinometer data and surface observations appears to have been shallow, extensive plastic deformation is implied by the settlement augers even at a depth of 10 m. It is considered that much of this apparent settlement may be due to lateral movement which occurred above this depth.

The height to which the embankment could be constructed is substantially less than would be expected from conventional vane strength data. This, coupled with the pore pressure response, suggests that progressive failure may have been a significant factor affecting the performance of this embankment.

CHAPTER 4

OBSERVED BEHAVIOUR OF THE REINFORCED EMBANKMENT

4.1 INTRODUCTION

The behaviour of the unreinforced section of a test embankment constructed in Sackville, New Brunswick was examined in chapter 3. The overall site conditions, foundation soil properties, the properties of the fill material, construction details and data collection procedures adopted at the site were described in that chapter. The instrumentation and observed behaviour of the geotextile reinforced section of the test embankment are presented in this chapter.

A relatively high strength polyester woven geotextile (Nicolon style 68300) was used as reinforcement. Instrumentation of the geotextile and the geotextile strain responses are described in chapter 5, but a brief discussion is presented in this chapter. The construction sequence adopted, the observed pore pressure response, the variation in both the vertical and horizontal displacements of selected points on the ground surface as well as in the foundation soil, and the horizontal displacement profile along vertically placed inclinometers are presented in this chapter. An account of the development and propagation of cracks in relation to the construction and the manner in which initial failure and rotational failure of the embankment were interpreted is also described.

4.2 INSTRUMENTATION

To facilitate monitoring of the construction and to observe the performance of the geotextile, field instruments were installed in the mid 4 m portion of the 25 m long

reinforced part of the test embankment. The design of embankment configuration and the layout of instrumentation were similar to that previously discussed for the unreinforced section in chapter 3. The instrumentation of the reinforced section consisted of piezometers, settlement plates, augers, heave plates, inclinometer casings and a total pressure cell and strain gauges on the geotextile. The layout of the instrumentation of the reinforced section is shown in Fig. 4.1 (see also Fig. 3.2 in chapter 3 for the plan view of the test embankment and Fig. 5.1 in chapter 5 for the layout of instrumentation on the geotextile).

A total of 32 (Petur type) pneumatic piezometers (at various depths) and 9 Casagrande type piezometers (at a depth of 1 m) were installed to monitor the pore pressures as shown in Fig. 4.1. Only two of the pneumatic piezometers (1 and 14, not shown on Fig. 4.1) were not functioning at the beginning of construction. A pneumatic type total pressure cell was installed on the mid region of the reinforced portion close to the centre line of the embankment to measure the total pressure imposed by the fill on the foundation subsoil.

Movement of the ground was monitored by measuring the displacement of heave plates (1H, 2H, 3H and 4H in the northern side) and settlement plates (6S, 7S and 8S in the north and 13S, 17S and 18S in the south, under the berms). Five inclinometers (22I, 23I, 24I, 25I and 26I) were installed, close to the north side toe of the embankment, to monitor the horizontal movement of the foundation subsoil. The inclinometer casings were installed up to a depth ranging from 8 to 11 m where a relatively stiff clayey silt/silty clay stratum was encountered. Four settlement augers were placed to the north (9A, 10A, 11A and 12A) and three to the south (14A, 15A and 16A) of the embankment in order to obtain vertical displacement of selected points in the foundation subsoil. An additional inclinometer (27I) and three heave plates (19H, 20H and 21H) were installed on the

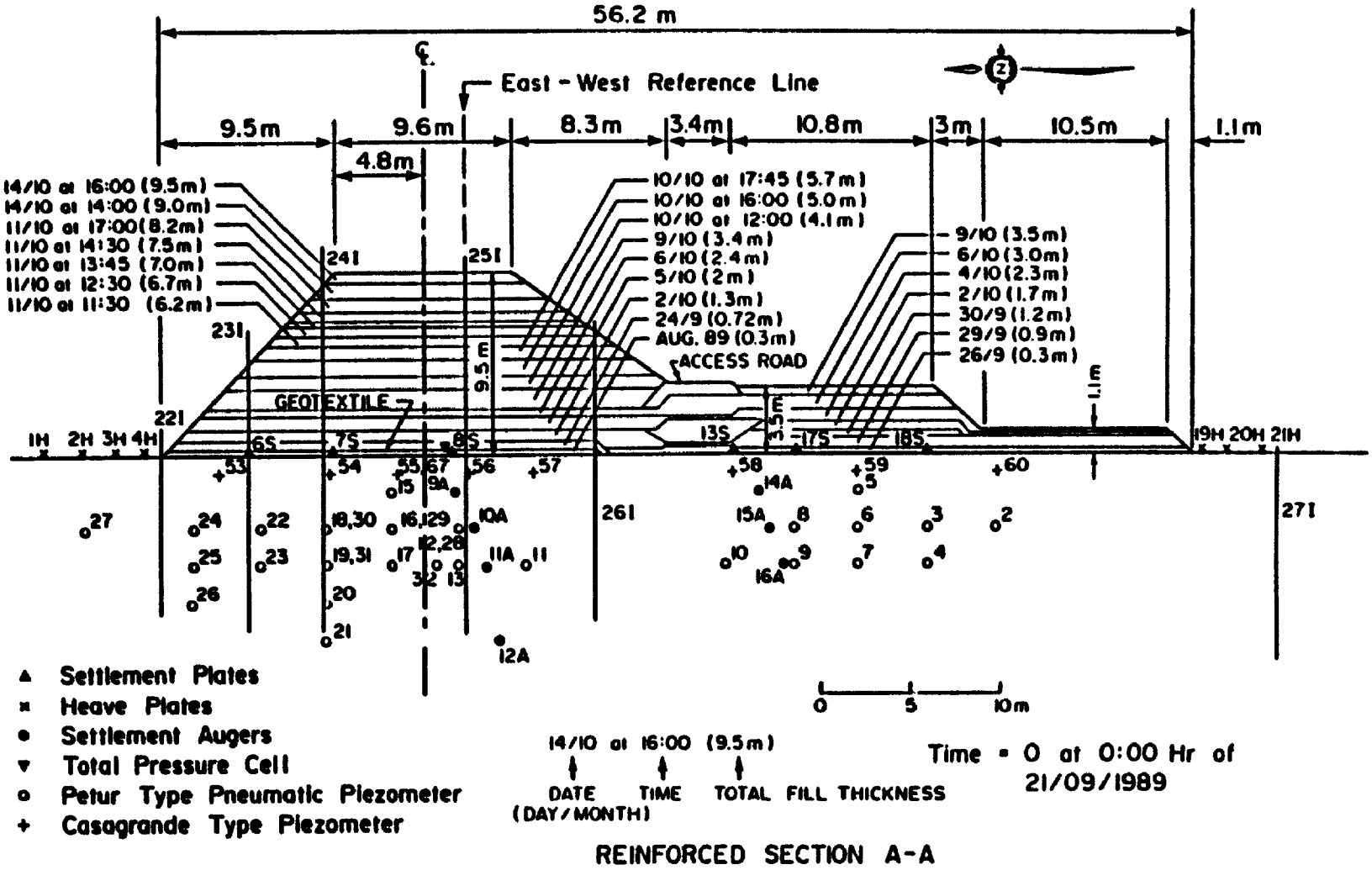

FIG. 4.1 INSTRUMENTATION LAYOUT AND CONSTRUCTION SEQUENCE OF REINFORCED EMBANKMENT

southern side of the embankment to monitor the movements and provide warning of any potential problems for the N.B. Tel fibre optic cable situated just south of the embankment (see chapter 3 for more detail).

Geotextile strains were monitored both in the transverse and longitudinal directions. A total of 34 electrical, 7 electromechanical and 7 mechanical strain gauges were installed on the geotextile to measure the strain in the transverse direction (see Fig. 5.1). The details concerning the design, configuration and installation of the electromechanical and mechanical gauges and the responses of all the gauges are described in chapter 5.

4.3 REINFORCED EMBANKMENT CONSTRUCTION

As previously described for the unreinforced section (see chapter 3), vertical cuts of 1 - 1.2 m deep on an approximate 1.3 - 1.8 m square grid were made through the surface crust/root mat on the northern side of the reinforced part of the embankment to minimize the effect of this surface crust/root mat and hence reduce the amount of fill required to cause failure (see chapter 3 for the plan showing the areal extent of the root-mat). To reduce the cost of the fill, a locally available fill material (gravelly silty sand with some clay, with properties as presented in chapter 3) was used for most of the construction work. However, to simulate the standard construction practice and to allow adequate interaction between the geotextile and the surrounding soil, a 0.3 - 0.5 m thick layer of good quality granular fill material (see Fig. 4.2) was used both below and above the geotextile. Field density measurements on this granular fill material indicated a unit weight of 18 kN/m^3. The natural water content of the granular fill, obtained from bulk samples, averaged 7.6%. Direct shear tests performed on saturated bulk samples of granular fill indicated the strength properties as $c' = 0$, $\phi' = 42.3^o$

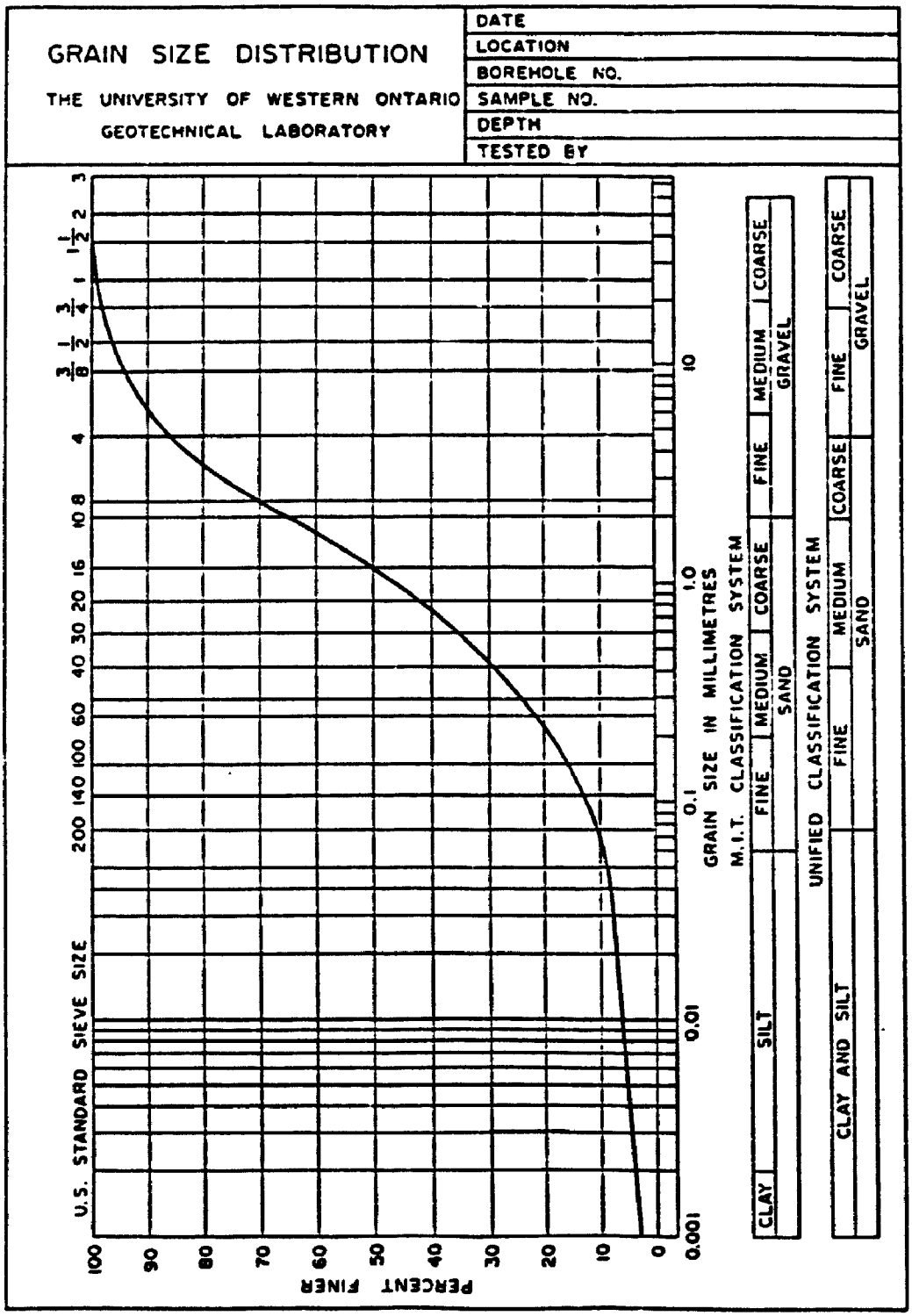

FIG. 4.2 GRADING CURVE OF GRANULAR FILL

The reinforcement selected for this project was a Nicolon (style 6830O) polyester woven geotextile with a unit weight of 631 g/sq. m. The geotextile was factory sewn into a 23m x 30 m rectangular section and delivered to a storage area close to the site. The tensile strength properties determined from tensile tests performed on samples of this geotextile are given in chapter 5 (see Table 5.1).

The electrical strain gauges were installed (allowing only short lead wires) under dry conditions in the storage area. The mechanical and electromechanical ring gauges were installed after the geotextile was placed in position at the site. Long lead wire electrical connections for the electrical and electromechanical gauges were installed at the site by field soldering.

A 0.3 -0.5 m thick granular "working platform" was placed to provide a level surface on the area to be covered by the geotextile (the variability in fill thickness reflected very local topographic variations). Since the electrical strain gauges were quite delicate, considerable care was taken during transport and placement of geotextile in the field. Installation procedures and the precautions adopted during the installation of the gauges and embankment construction to avoid damages and prolong the life of the strain gauges are described in chapter 5. A 0.4 m thick "upper layer" of granular fill was carefully placed over the geotextile without allowing passage of either the trucks or the bull dozer directly on the geotextile. To avoid damage to the strain gauges, spreading of this granular fill over the gauges was performed manually.

As mentioned in chapter 3, a 0.5 m thick gravel access road was initially constructed (see Fig. 3.2). A 0.3 m thick blanket of the same gravel fill was placed on the waterlogged areas found on the southern side of the section. The access road was raised as the work progressed. The construction of the different berms was followed by

construction of the northern side of the reinforced section to failure. At least one complete set of readings was taken from all strain gauges on the geotextile as well as all other instruments placed in the reinforced section after placement of each layer of fill.

The sequence of construction adopted for the reinforced embankment and its southern berm is indicated in Fig. 4.1. The reinforced section, which reached a thickness of 9.5 m on Oct. 14, 1989, was found to have dropped 0.1 m, close to settlement plate 8S, on Oct. 15, 1989. The deformations continued and by 16 October 1989, a large depression (of about 0.6 m maximum depth) and cracks of 4 - 10 cm width were observed on the crest of the embankment close to settlement plate 8S. To verify the propagation of cracks and to confirm the observed plastic-type failure of the embankment, additional fill was placed as necessary to relevel the entire crest width of the embankment. The final fill thickness observed close to settlement plate 8S on Oct. 16, 1989, was 10.1 m. The other areas showed an average thickness of 9.5 m.

4.4 PERFORMANCE OF INSTRUMENTATION AND RESULTS

4.4.1 Embankment thickness and Total pressure

Fill thicknesses were monitored throughout the construction period. The variation of thickness of the main part (i.e. northern side) of the reinforced section of the embankment (hereafter called the embankment thickness) with time is shown in Fig. 4.3. For ease of comparison, the variation of the total pressure on the foundation soil (as measured by the total pressure cell) with time is superimposed on the same figure. The total pressure cell reading is reasonably consistent with pressures calculated from the fill thickness and unit weight (It should be noted that the pressure cell was placed on top of the 0.3 m thick working mat and hence should underestimate the total thickness by about

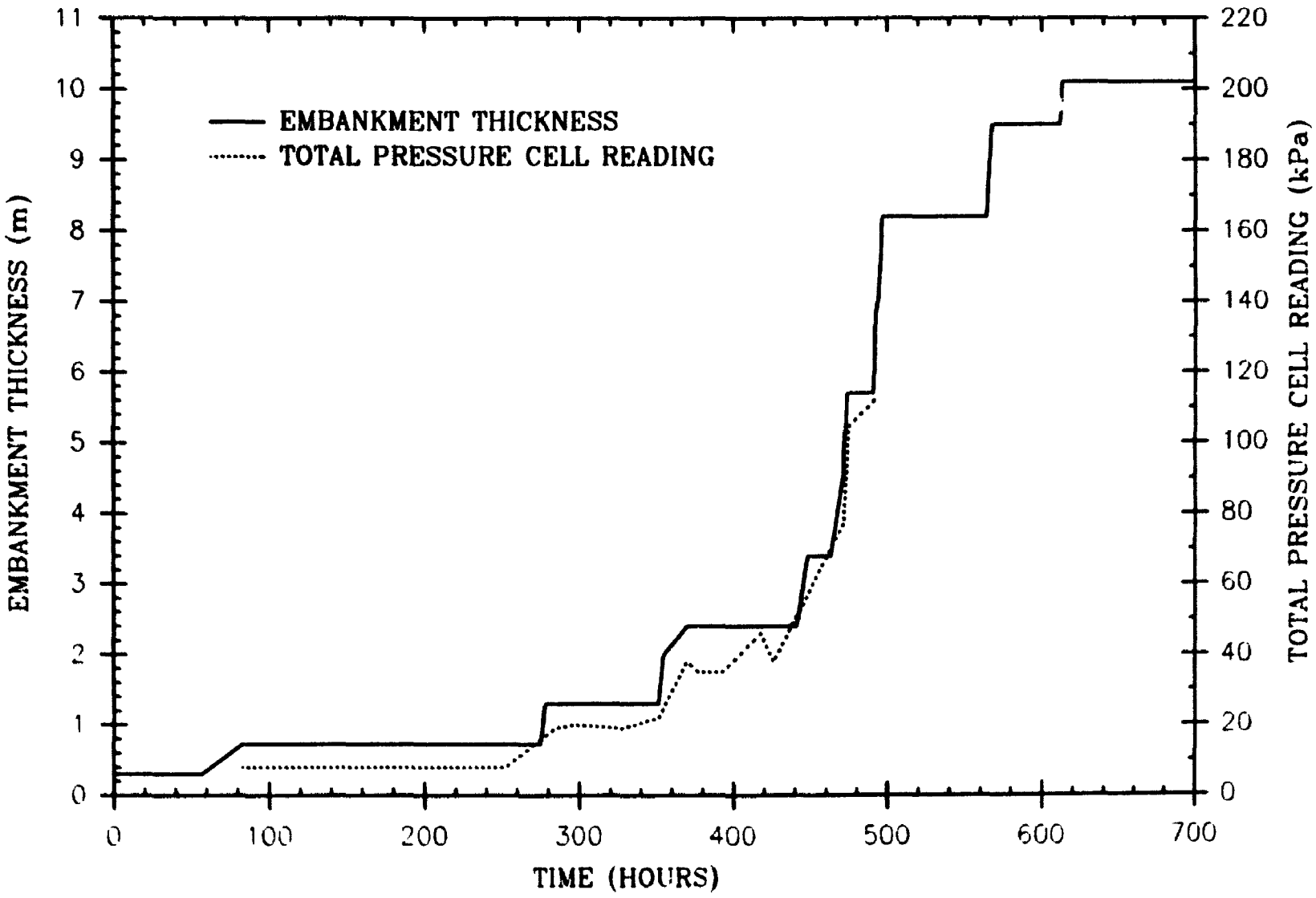

FIG. 4 3 VARIATION OF EMBANKMENT THICKNESS AND TOTAL PRESSURE CELL READING WITH TIME

0.3 m). The total pressure cell failed to function when the embankment thickness was raised above 5.5 m; it is suspected that this is because of a breakage of the hydraulic line which in turn was caused by the large movements which occurred at this time.

4.4.2 Pore pressures

The variation of excess pore pressure (determined from the pore pressure measurements) with time for different pneumatic piezometers placed beneath the main part of the reinforced section are shown in Figs. 4.4, 4.5, 4.6, 4.7 and 4.8. The location of the piezometers are shown in Fig. 4.1. For ease of comparison with the sequence of construction, the variation of fill thickness with time is also superimposed on these figures. The vertical axis scales of these figures have the same number of divisions.

The initial 0.3-0.5 m thick working pad at the reinforced section was constructed about 5 weeks in advance of the commencement of placement of the remainder of the fill and the excess pore pressure appear to have largely dissipated during this period. For convenience of presentation, the monitoring data are presented in terms of the time commencing at 0:00 hrs. on 21 September 1989, at which time 0.3 m granular working mat had been placed at the reinforced section but no fill had been placed at the unreinforced section and no additional fill had been placed at the reinforced section.

These figures indicate that the excess pore pressures in all the piezometers were small (typically less than 30% of the increase in vertical stress) up to about 260 hours during which time the embankment thickness was increased to 0.7 m. A gradual build-up of excess pore pressure is evident during the next two stages of construction when the thickness was increased to 1.3 and 2.4 m respectively. During these loading stages, the increase in excess pore pressure was up to 70% of the increase in vertical stress. There

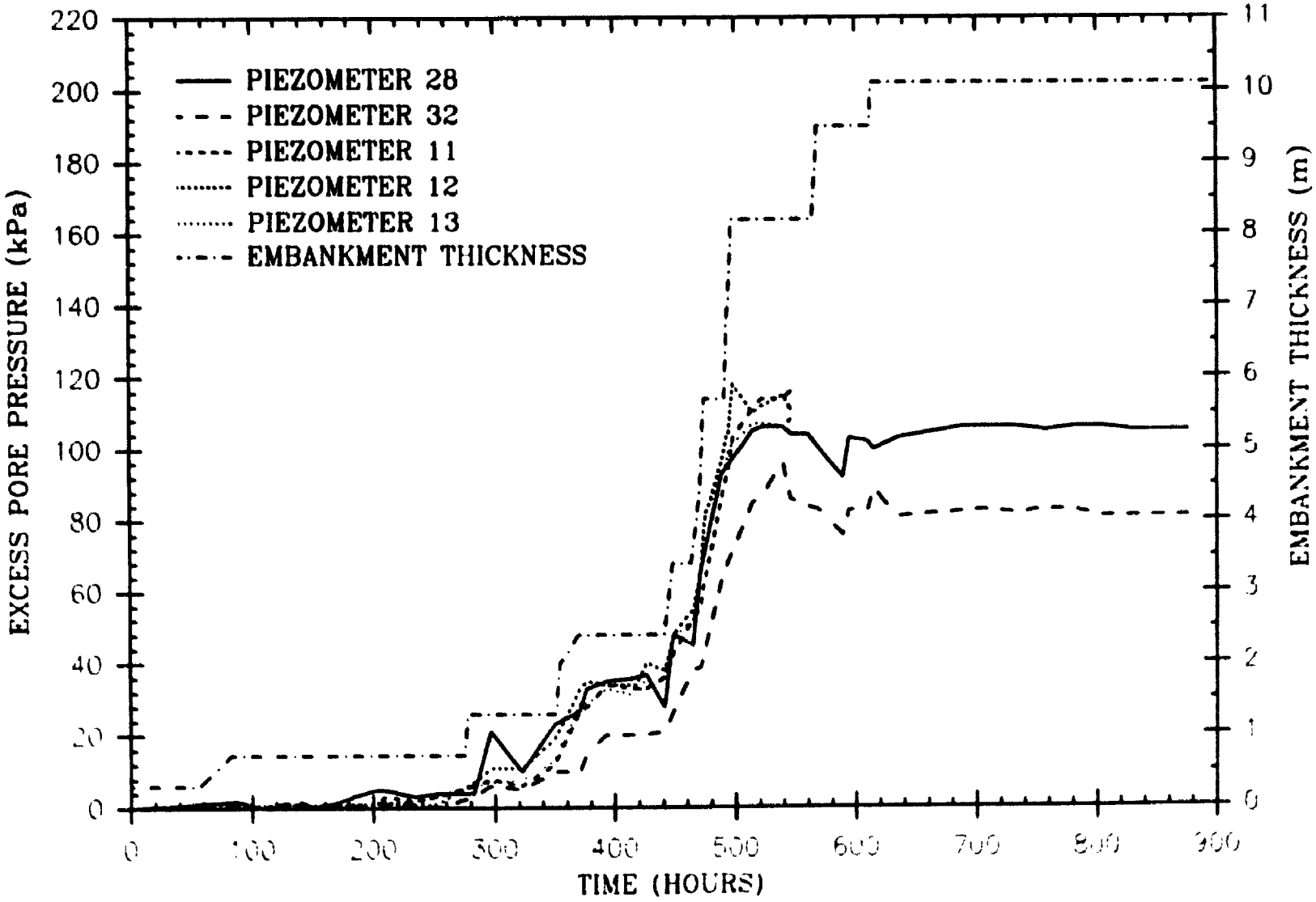

FIG 4.4 VARIATION OF EXCESS PORE PRESSURE WITH TIME FOR PIEZOMETERS 28, 32, 11, 12 AND 13

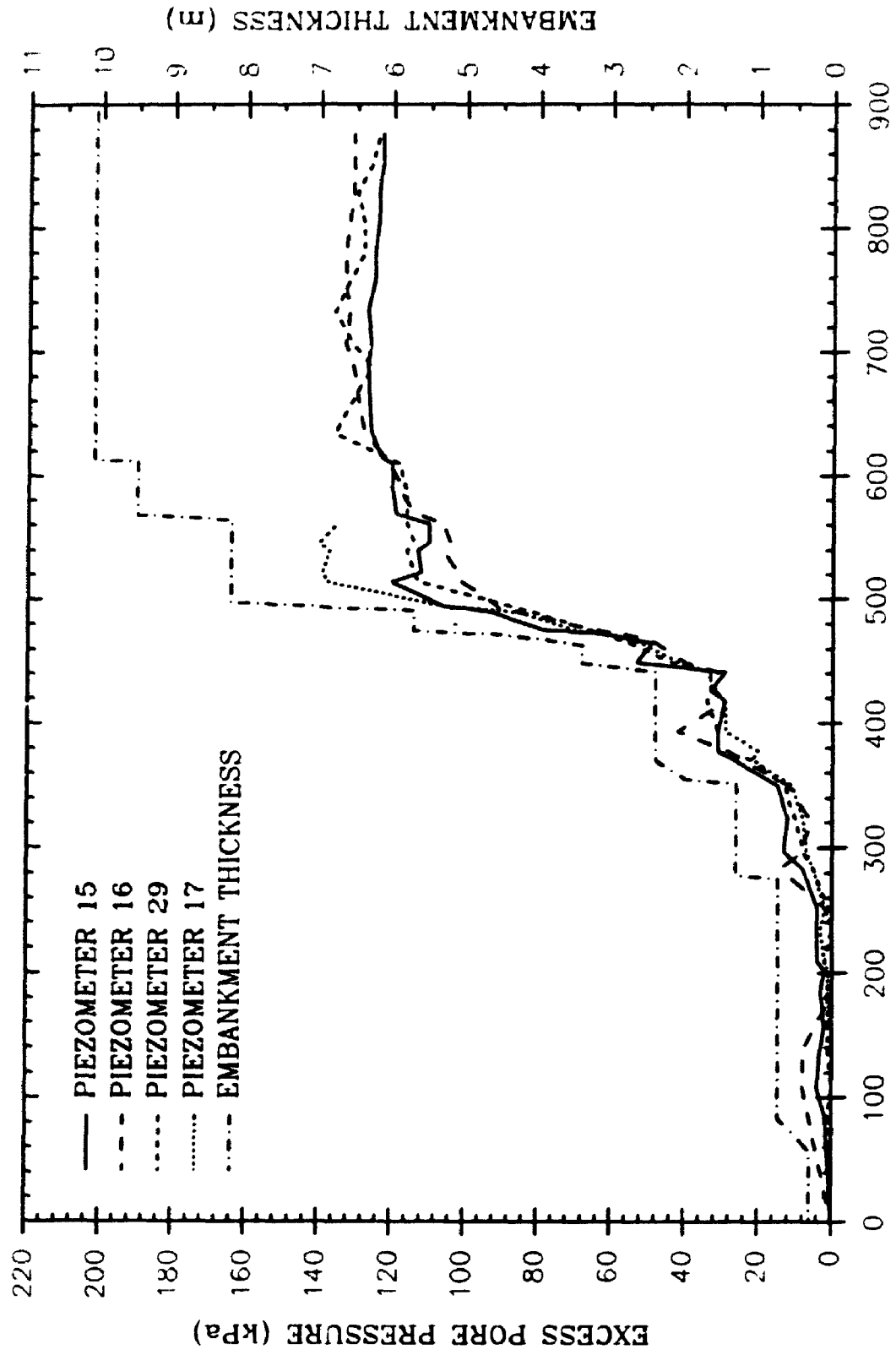

FIG. 4.5 VARIATION OF EXCESS PORE PRESSURE WITH TIME FOR PIEZOMETERS 15, 16, 29 AND 17

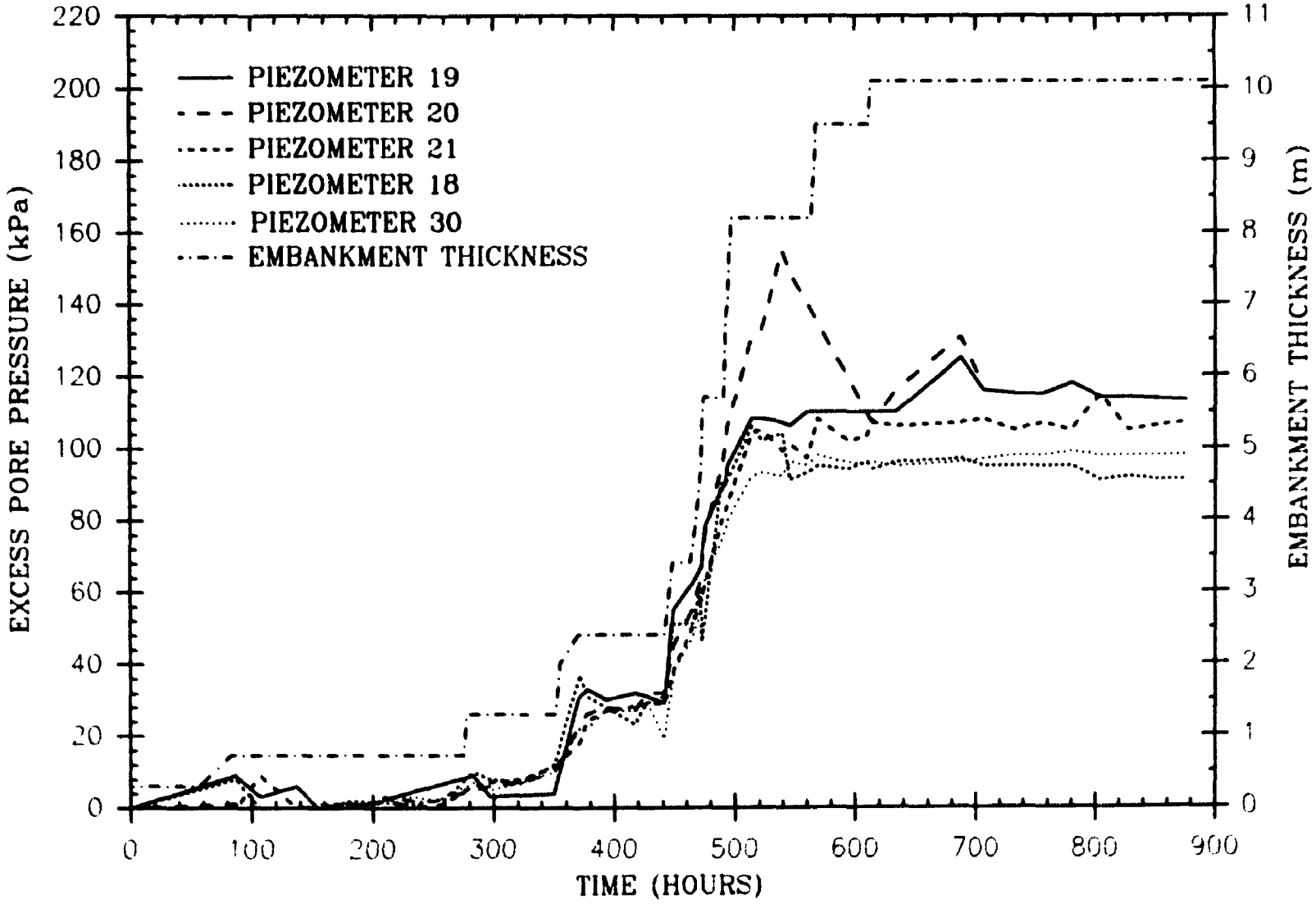

FIG. 4 6 VARIATION OF EXCESS PORE PRESSURE WITH TIME FOR PIEZOMETERS 18, 30, 19, 20 AND 21

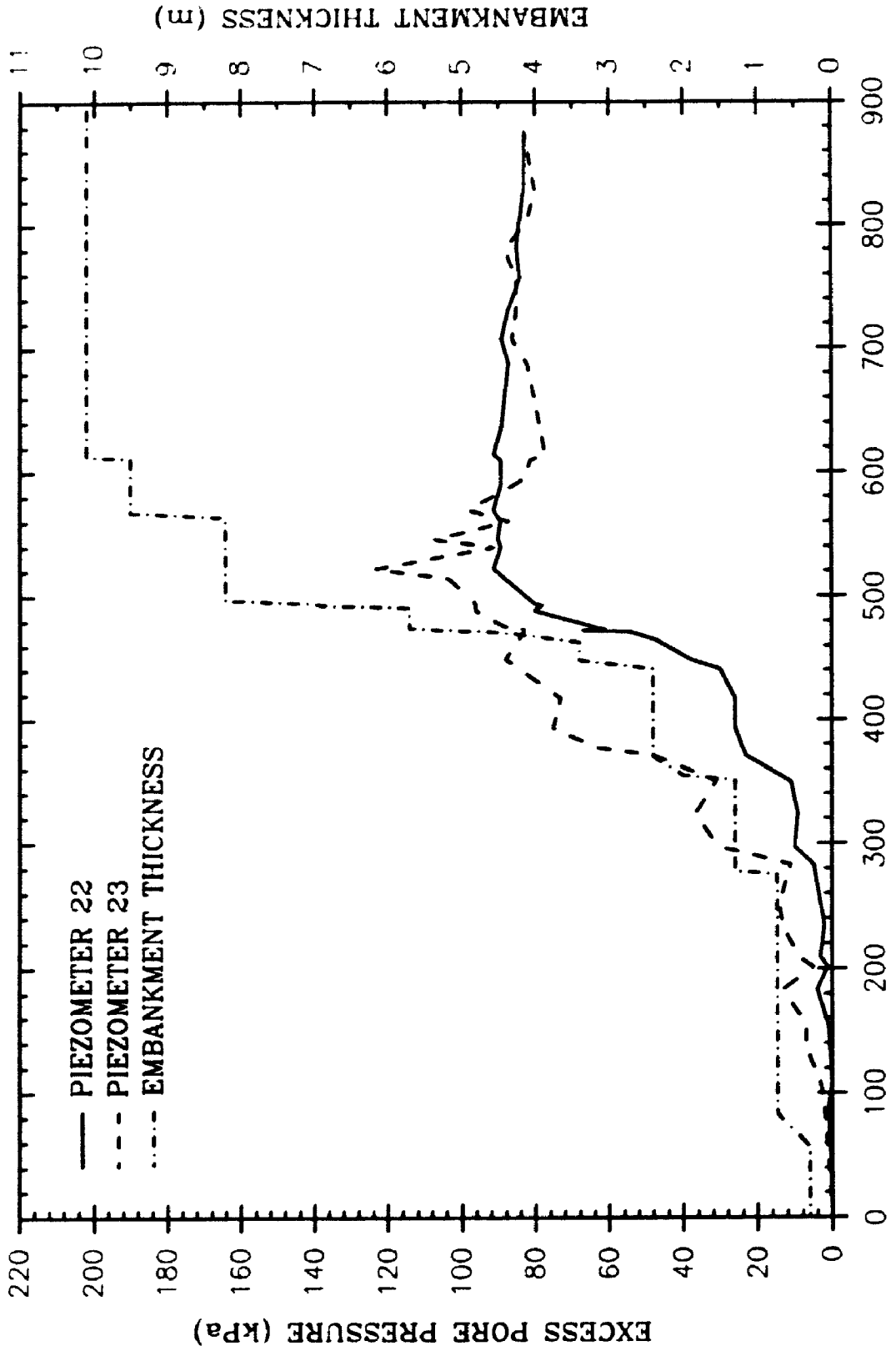

FIG. 4.7 VARIATION OF EXCESS PORE PRESSURE WITH TIME FOR PIEZOMETERS 22 AND 23

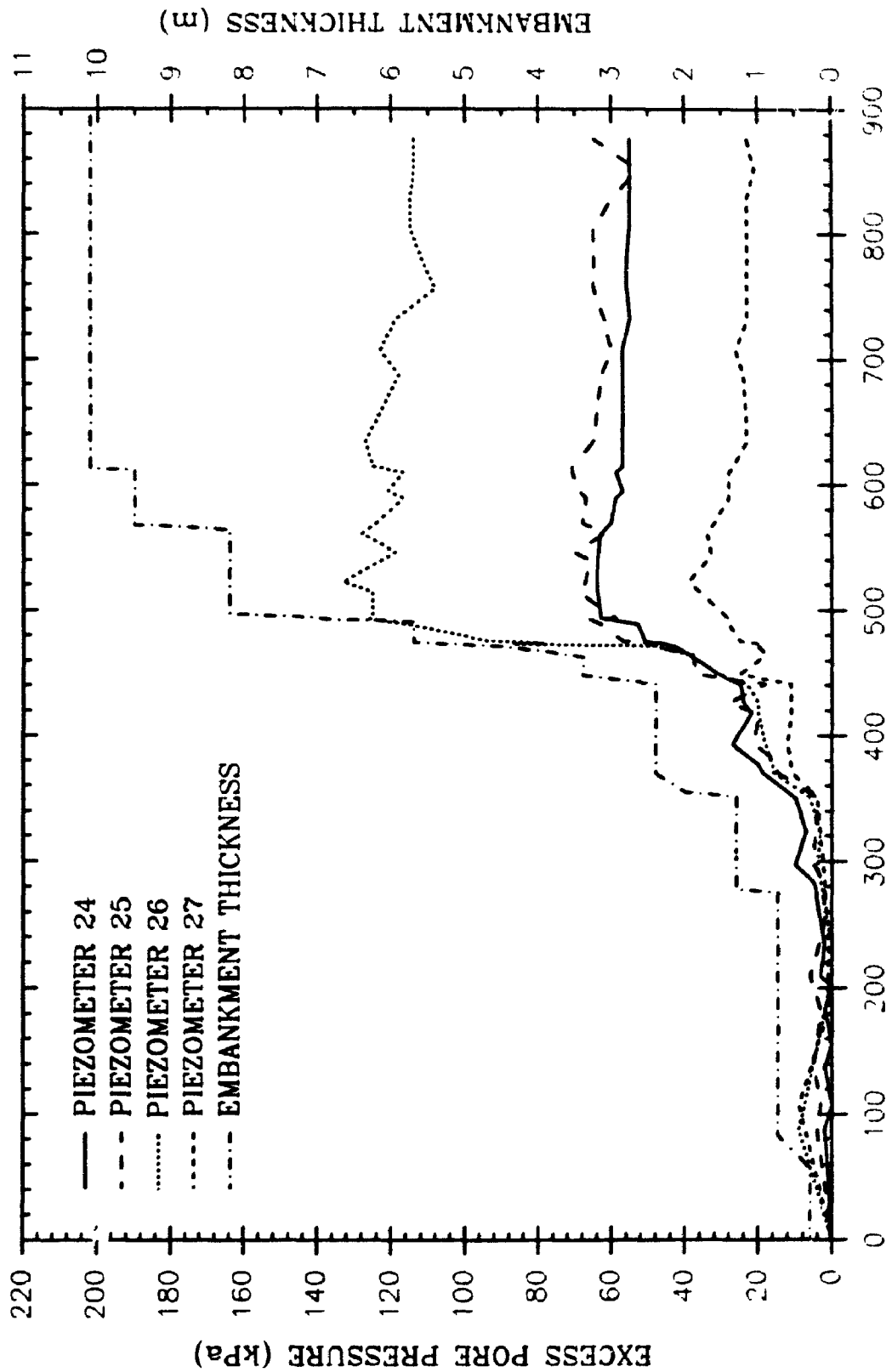

FIG. 4.8 VARIATION OF EXCESS PORE PRESSURE WITH TIME FOR PIEZOMETERS 24, 25, 26 AND 27

appears to have been some dissipation of excess pore pressure during the short periods when no fill was being placed at this section for fill thicknesses of 1.3 and 2.4 m. Similar excess pore pressure responses during early stages of construction have been reported by previous investigators such as Leroueil et al. (1978a) and Ortigao et al. (1983). At the St. Albans fill (located on sensitive clay), Leroueil et al. (1978b) attributed the high early dissipation of excess pore pressure to the initially overconsolidated state of the foundation soil at early stages of construction. The change to lower dissipation rates at latter stages of construction were attributed to a change in soil as it becomes normally consolidated. A similar type of behaviour is evident at the Sackville embankment reported here.

The embankment was subsequently raised from 2.4 to 3.4 m. It was then constructed quite rapidly from 3.4 m and it is considered to have approached failure before it reached 8.2 m thickness as discussed later in this chapter. Figs. 4.4, 4.5 and 4.6 indicate a very rapid build-up of pore pressure after about 440 hours in response to the rapid construction of the embankment from a thickness of 2.4 m to 8.2 m during 426 - 497 hours. A time lag between the addition of fill and the build-up of pore pressure is evident from the pore pressure responses. Although there was no addition of fill during 475 - 490 hours at the embankment thickness of 5.7 m, these figures did not indicate any dissipation of excess pore pressure in this period. Construction of the embankment to 8.2 m gave rise to the maximum excess pore pressures. There is some evidence that the excess pore pressures recorded by some piezometers may have begun to dissipate at about 515 hours. As discussed subsequently, the embankment approached failure during its rapid construction from 3.4 m to 8.2 m thickness (during 463 - 497 hours) and that the rate of construction was fast enough to impart near undrained behaviour during this time period.

The excess pore pressure responses indicated by piezometers 11, 12, 13 and 28 (see Fig. 4.4) were very similar even though the piezometers were placed at different

depths (4 and 6 m) and locations. Piezometer 32 placed at 6 m depth consistently indicated smaller excess pore pressure than piezometer 28 placed at 4 m depth or piezometers 13 and 17 (see Fig. 4.5) which were either side of piezometer 32 at 6m depth. However the trend observed in piezometer 32 was very similar to that in the other piezometer and it appears to have typically underestimated excess pore pressure by about 20 kPa. Piezometers 11, 12, 13 and 17 all failed while the embankment was at a thickness of 8.2 m. It would appear that these failures were the result of the large deformation causing the pressure line to break. Some dissipation of excess pore pressure is suggested by the response of piezometers 28 and 32 between 540 and 589 hours. This may be pore pressure dissipation in response to the fact that no fill was added between 497 and 564 hours at embankment thickness 8.2 m. A small increase in the excess pore pressure is observed in both piezometers 28 and 32 during about 589 - 594 hours in response to the construction of the embankment from 8.2 to 9.5 m during 564 - 568 hours. Recognizing the stick-slip nature of piezometer response, an alternative interpretation of the pore pressure response at thicknesses of 8.2 m and 9.5 m is that the excess pore pressure remained essentially constant following construction to a thickness of 8.2 m for the period from about 515 hours to 900 hours. Some support for this hypothesis is evident from Fig. 4.5.

Fig. 4.5 shows that the excess pore pressure responses at piezometers 15, 16, 17 and 29 were very similar even though they were installed at varying depths. Piezometer 15 placed at 2 m depth showed a larger increase in excess pore pressure than piezometers 16 and 29 placed at 4 m depth during 460 - 515 hours (in response to the construction from 3.4 m to 8.2 m thickness). Piezometer 15 also showed evidence of dissipation of excess pore pressure after about 515 hours. In contrast, piezometers 16 and 29 showed continuous increase in excess pore pressure although there was no addition of fill during 497 - 564 hours. Piezometer 15 showed a lower excess pore pressure than piezometers 16

and 29 after about 610 hours until the end of the monitoring period. Piezometer 15 appears to have been subject to more dissipation than piezometers 16 and 29, particularly during the early stages of construction. This is probably due to the shorter drainage path since piezometer 15 is 2m closer to the surface than piezometers 16 and 29. Piezometers 16 and 29 were placed about 1 m apart in the longitudinal direction but at about the same location in the section; under ideal conditions one would expect an identical response from these piezometers. Although there is some difference in the excess pore pressure during 510 - 570 hours, they generally show similar behaviour right from the beginning of construction until the end of the monitoring period (see Fig. 4.5). It is of some interest to note that after filling to 9.5 m thickness, the excess pore pressures remained essentially constant until the end of the monitoring period. This type of response has been previously observed in soils susceptible to strain softening and progressive failure (see Lo 1966 and Fisher et al. 1982a and 1982b).

Piezometers 18 and 30 were placed about 1 m apart in the longitudinal direction but at the same location along the section. Fig. 4.6 shows that the excess pore pressure responses of piezometers 18 and 30 are very close to each other throughout the construction and monitoring period providing confirmation of the magnitude and nature of the excess pore pressure response. Piezometers 18, 19, 20 and 21 placed at 4 m, 6 m, 8 m and 10 m depths respectively indicate very similar excess pore pressure responses up to about 490 hours. Piezometer 20 showed the greatest increase in pore pressure during 440 - 540 hours. Examination of the erratic responses after 500 hours would suggest that the piezometer may have been malfunctioning and as a consequence the pore pressure reported in response to construction from 5.7 to 8.2 m may not be real. However an alternative explanation for this response could arise from the existence of a very compressible zone in the deposit near piezometer 20. Collapse of the structure of this local zone might give a response similar to that observed.

Fig. 4.7 indicate that piezometer 23 placed at 6 m depth is indicating a much larger excess pore pressure during the early stages of construction compared to piezometer 22 which is placed 2 m directly above it (see Fig. 4.1). Both the inferred build-up and the dissipation of excess pore pressure appear to be unusual for piezometer 23 and it is suspected that the piezometer was defective. However, as noted above, an alternative hypothesis that this response is the result of collapse of a local compressive zone in the organic clayey silt can not be excluded at this time. Piezometer 22 showed increases in excess pore pressure (in direct response to the construction of embankment) very similar to piezometers 18 and 30 up to a thickness of 3.4 m but subsequently showed lesser increases of excess pore pressure. Its location below the slope of the embankment (see Fig. 4.1) is considered to be the reason for this behaviour.

Piezometer 27 placed at a depth of 4 m just outside the embankment did not show large build-up of pore pressure but did indicate significant direct response to the sequence of construction of the embankment (see Figs. 4.1 and 4.8). The excess pore pressure in piezometers 24, 25 and 26 placed close to the toe of the embankment at depths 4, 6 and 8 m respectively are very close to each other during the early stages of construction up to about 470 hours. Piezometer 26 indicated a very large build-up of excess pore pressure during 470 -490 hours (about 75 kPa) apparently in response to the rapid construction from a fill thickness of 3.4 m to 5.7 m between 463 - 475 hours. It is suspected that piezometer 26 was malfunctioning after about 470 hours. The increase in pore pressure during the next stage of construction from 5.7 to 8.2 m in piezometer 26 as well as in 24 and 25 was small. Although the authors consider that the response of piezometers 26 and 20 is probably spurious during the period from about 470 hours, the similarity of the response at these two piezometers, which are at the same depth, is noted and the data have not been removed in case subsequent interpretation/analysis reveals some rational explanation for the response of piezometers 20, 23 and 26. As previously noted, one

hypothesis is that this may be the result of local variations in compressibility and collapse of this soil at a depth of 6 - 8 m between piezometers 20 and 26.

Typical excess pore pressure responses of the piezometers placed in the berm side of the embankment are shown in Figures 4.9 and 4.10. The construction of the berms were completed by about 450 hours in several stages. Fig. 4.9 indicates that the excess pore pressures in piezometers 8, 9 and 10 increased gradually up to about 520 hours but remained relatively constant thereafter. It would appear that the excess pore pressure observed at these piezometers reflect excess pore pressures due to the main embankment and the berm. In particular, comparing Figs. 4.9 and 4.10, it is evident that there is a decrease in excess pore pressure with distance away from the main embankment (e.g. compare the response of piezometers 10, 9 and 7 which are all at 6 m depth and all have approximately the same thickness of fill directly above).

The variation of the parameter $\overline{B}$ [= change in excess pore pressure with reference to zero time/change in vertical stress on the original ground surface at the centre line of the embankment with reference to zero time $= \frac{\Delta u}{\Delta \gamma H}$] with time for selected piezometers in the region close to the centre line is presented in Fig. 4.11. Since the total pressure cell failed to function at about 480 hours, the change in vertical stress was based on fill thickness and unit weight for the determination of parameter $\overline{B}$. Piezometers 15, 16 and 28 showed similar responses throughout the construction and monitoring period. (Piezometer 32 exhibited the same pattern of behaviour but gave lower $\overline{B}$ values compared to the other three piezometers as a result of the lower excess pore pressure as previously discussed.) The $\overline{B}$-value for piezometers 15, 16 and 28 indicated direct responses to the sequence of construction. Since the original 0.3 m thick granular blanket had been left in place for a considerable period of time, the calculation of $\overline{B}$ was taken with reference to the conditions after this sand blanket was in place. The placement of the

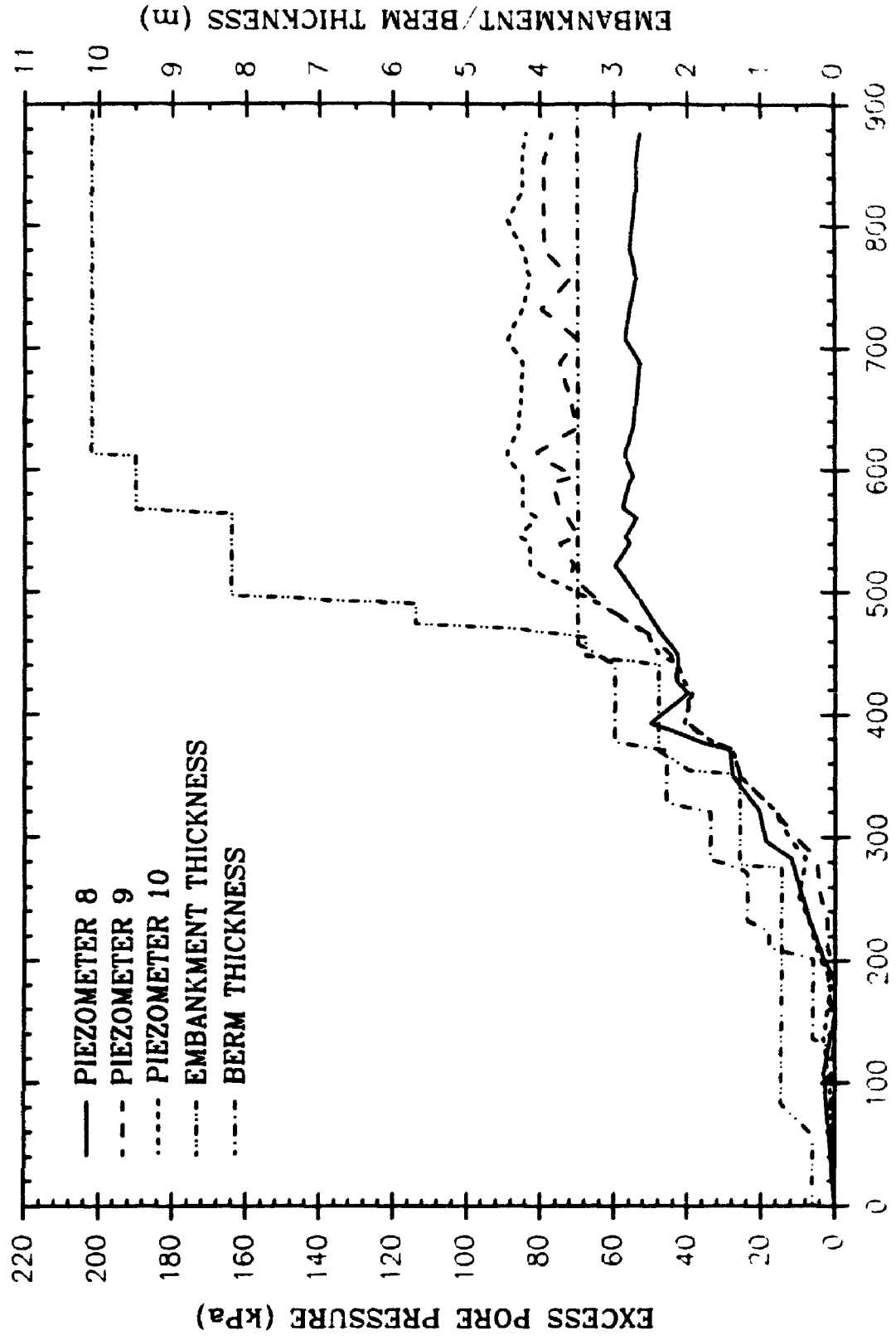

FIG 4.9 VARIATION OF EXCESS PORE PRESSURE WITH TIME FOR PIEZOMETERS 8, 9 AND 10

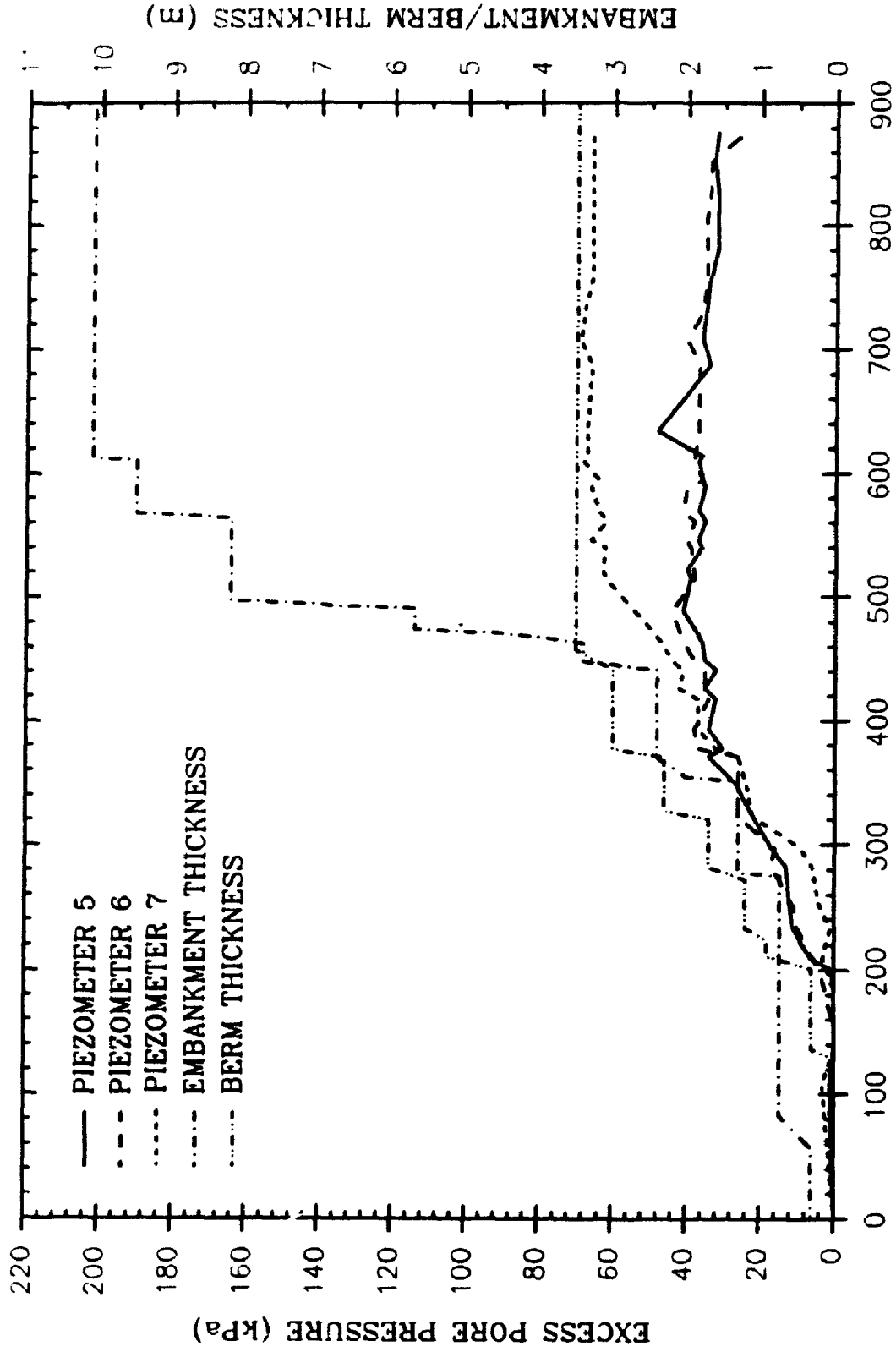

FIG. 4.10 VARIATION OF EXCESS PORE PRESSURE WITH TIME FOR PIEZOMETERS 5, 6 AND 7

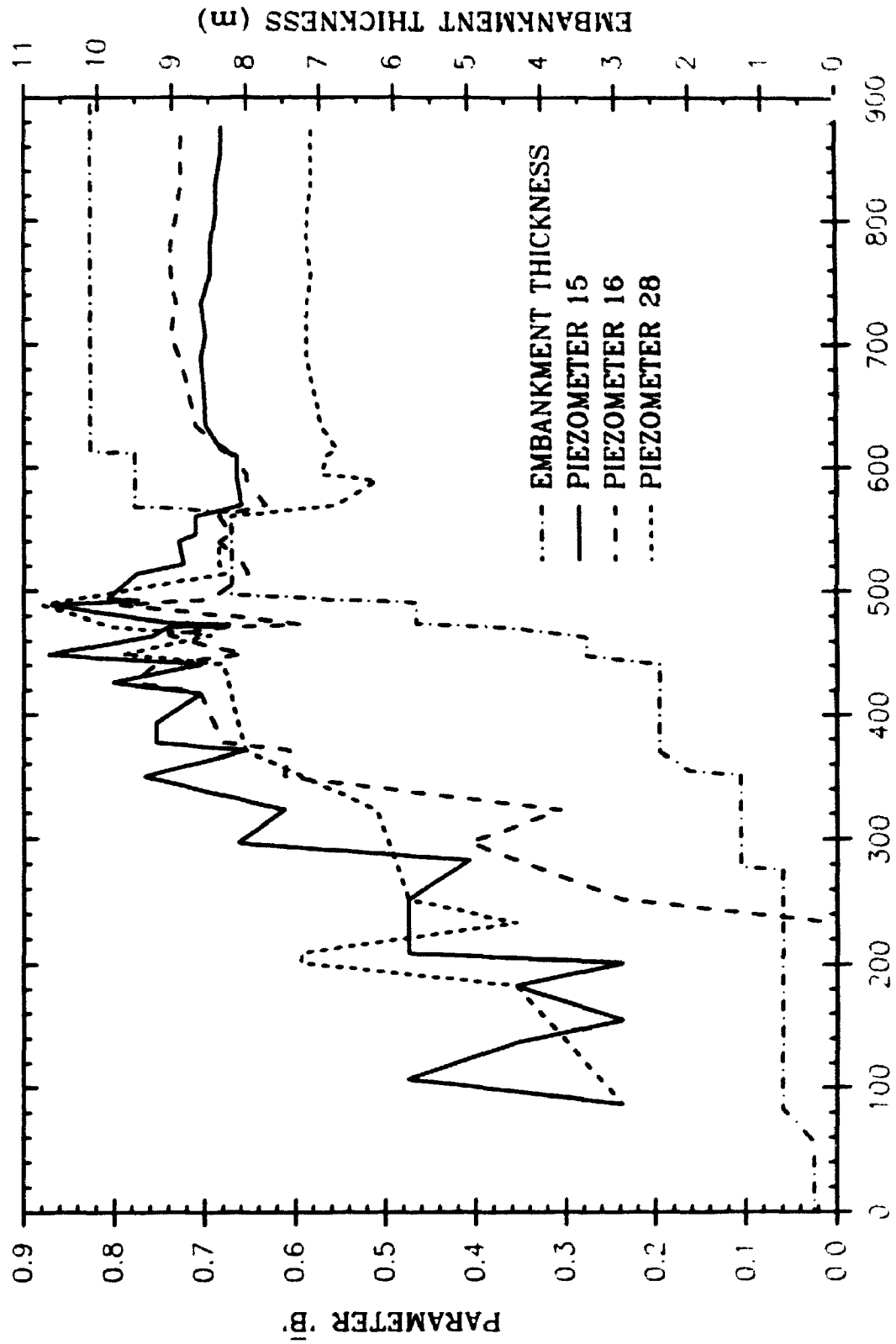

FIG 4.11 VARIATION OF PARAMETER 'B' WITH TIME FOR PIEZOMETERS 15, 16 AND 28

0.4 m granular blanket above the geotextile took a relatively long period of time (26 hours) because of the hand placement required to minimize damage to the strain gauges on the geotextile. Thus, because of the slow rate of loading and the apparent overconsolidated nature of the soil at this stress level, the $\overline{B}$-value was relatively low (typically between 0.2 and 0.4) during this construction phase. As a result of raising the embankment to 1.3 m, the $\overline{B}$-value increased to between 0.51 and 0.66. Raising the embankment to 2.4 m gave $\overline{B}$-values of between 0.66 and 0.80. The largest $\overline{B}$-values, of 0.87, 0.79 and 0.88 for piezometers 15, 16 and 28 respectively were obtained at about 488 hours suggesting that the soil mass (but not the embankment) approached failure as a result of increasing the embankment thickness to 5.7 m. Increasing the embankment thickness from 5.7 to 8.2 m did not result in any increase in $\overline{B}$-value. In fact the $\overline{B}$-value decreased somewhat to between 0.65 and 0.77 and further decreased to between 0.51 and 0.66 prior to the placement of the final fill thickness. Increasing the embankment thickness to 9.5 m apparently resulted in a slight increase in $\overline{B}$-value to between 0.58 and 0.73. The $\overline{B}$-value remained relatively constant at this final value for the remainder of the monitoring period as shown on Fig. 4.11 (i.e. almost 300 hours).

The $\overline{B}$-values shown in Fig. 4.11 were all calculated relative to fill placed after the initial 0.3 m granular layer. The $\overline{B}$-values were also calculated with reference to increase in fill thickness and excess pore pressures relative to the values that existed at 425 hours (i.e. for an embankment height of 2.4 m) and the results are presented in Fig. 4.12. The same trends are evident but the magnitude of the calculated $\overline{B}$-values changed. Thus the maximum value of between 0.8 and 0.9 was obtained at a fill thickness of 5.7 m. After all fill had been placed, a relatively constant value of between 0.44 (piezometer 28) and 0.66 (piezometer 16) was obtained.

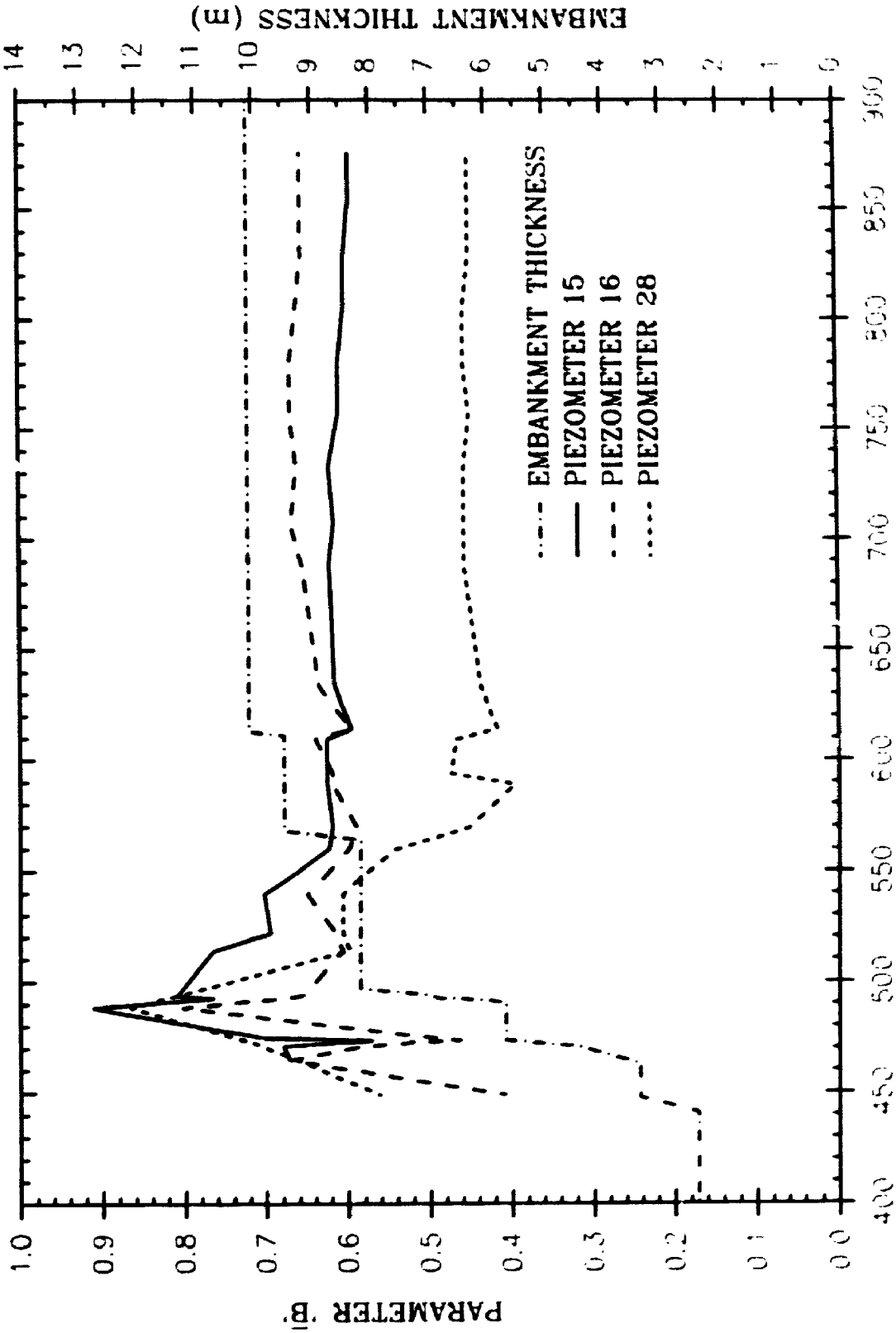

FIG 4.12 VARIATION OF PARAMETER 'B' WITH TIME FOR PIEZOMETERS 15, 16 AND 28
(BASED ON TIME = 425 HOURS)

4.4.3 Inclinometer data

Inclinometer casings were installed (on September 7, 1989) at four locations in the region where large lateral displacements were expected to occur (see Figs. 4.1 and 3.2). The variation of horizontal displacement with depth obtained from the inclinometers 22I, 23I, 25I and 26I is shown in Figs. 4.13, 4.14, 4.15 and 4.16 respectively. The horizontal displacement profiles at three different embankment thicknesses are shown on each of these figures. The depth of the blockage determined from the crude probing exercise at later stages of construction is also shown. Large horizontal displacements were observed in the inclinometers when the thickness of the embankment was about 5.7 m, indicating failure of the soil mass. In fact the movement became so large at the thickness of 5.7 m that the inclinometers became blocked and could not be monitored in the normal fashion for subsequent fill thicknesses. It was not possible to probe inclinometer 24I during the rapid construction of the embankment from 4.5 to 5.7 m between 471 and 475 hours owing to the interference of the construction activity nearby. This inclinometer was also blocked when an attempt was made to monitor it at a fill thickness of 5.7 m.

Comparison of these figures with the results reported for the unreinforced section in chapter 3 indicate that the horizontal displacements for a given fill thickness were significantly higher than that observed in the unreinforced section even at low embankment thicknesses. This is the result of the lower soil strength at the reinforced section as discussed in chapter 3. Maximum horizontal displacements of about 0.2 m and 0.5 m at embankment thicknesses of 2.4 and 3.4 m respectively were observed at inclinometer 22I which was located at the toe of the embankment. This inclinometer gave the largest maximum horizontal displacements, compared to all the other inclinometers, at all stages of construction. This observation supports the use of inclinometer at the toe as an indicator of imminent failure. This has been reported by, for instance, Kirby and Lambe

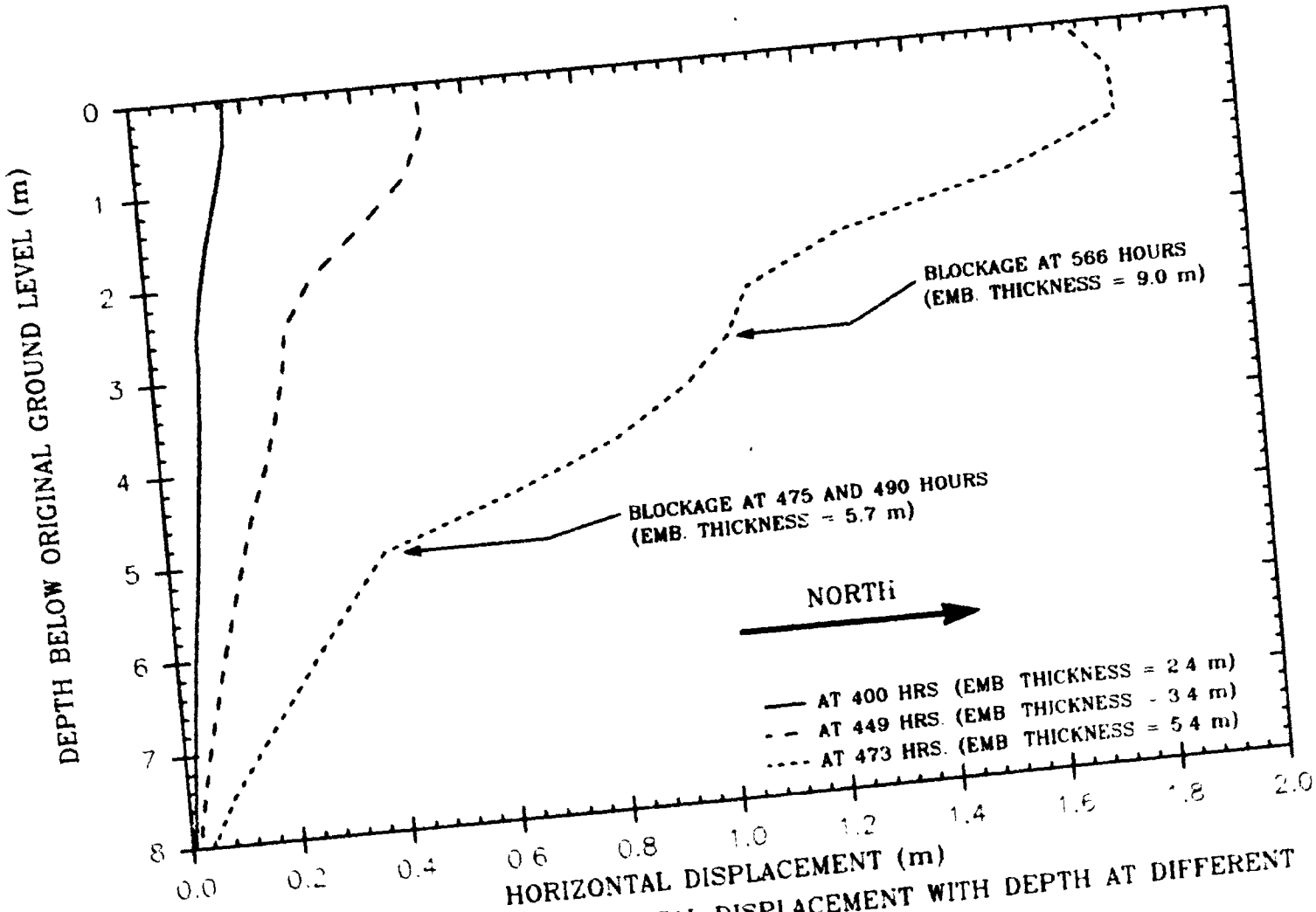

FIG 4.13 VARIATION OF HORIZONTAL DISPLACEMENT WITH DEPTH AT DIFFERENT EMB. THICKNESSES FOR INCLINOMETER 221

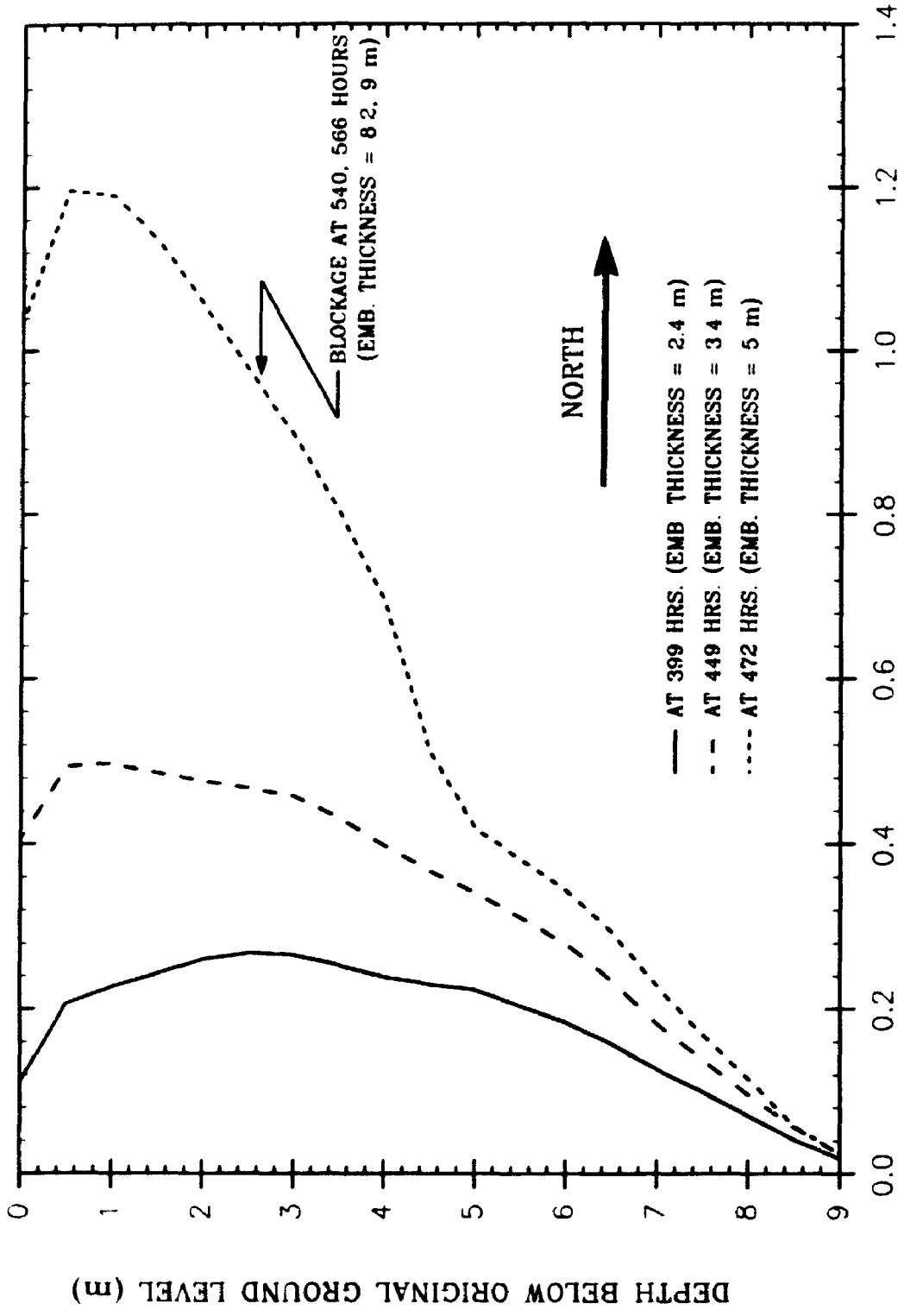

FIG. 4.14 VARIATION OF HORIZONTAL DISPLACEMENT WITH DEPTH AT DIFFERENT EMB. THICKNESSES FOR INCLINOMETER 23I

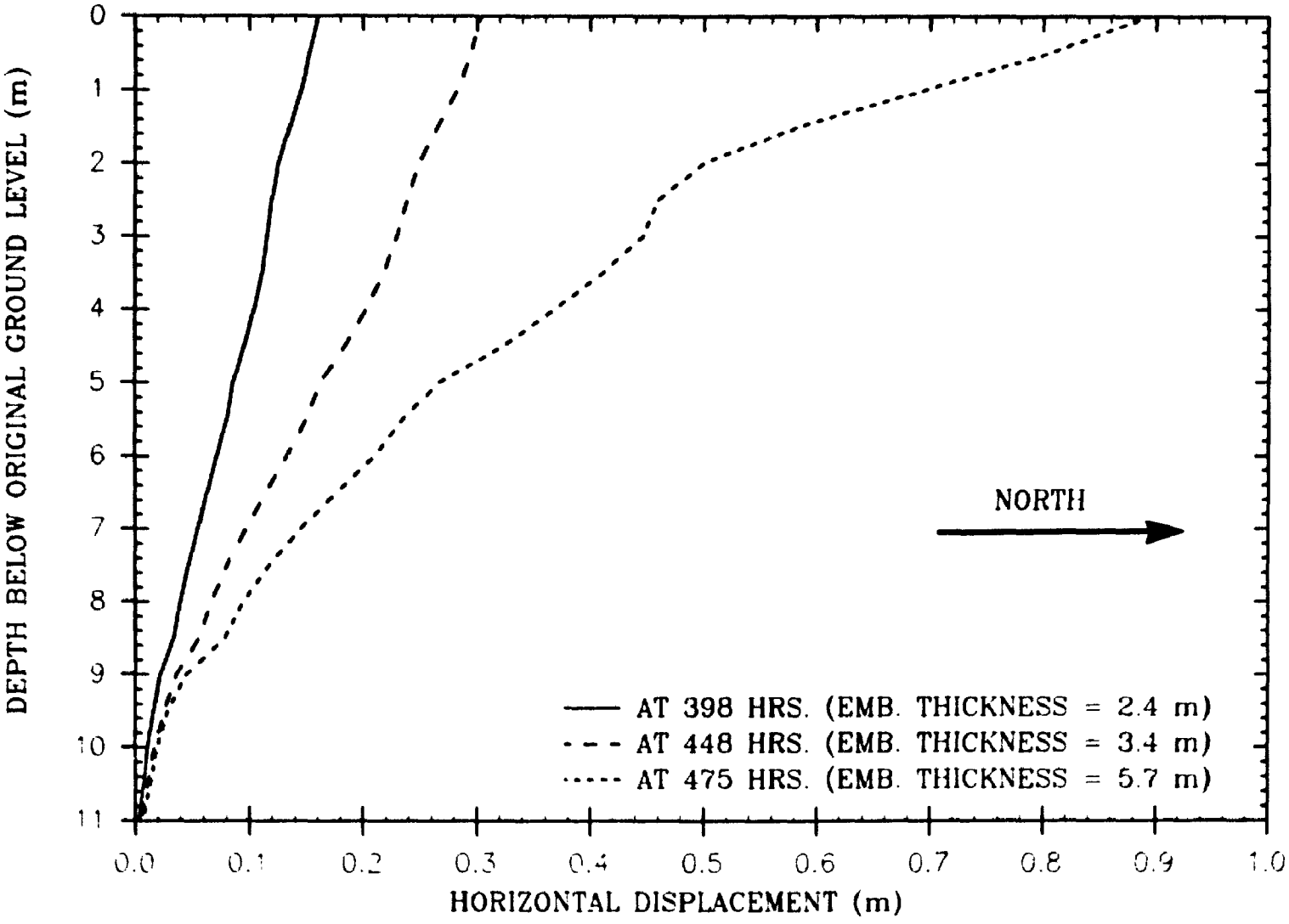

FIG 4 15 VARIATION OF HORIZONTAL DISPLACEMENT WITH DEPTH AT DIFFERENT EMB. THICKNESSES FOR INCLINOMETER 251

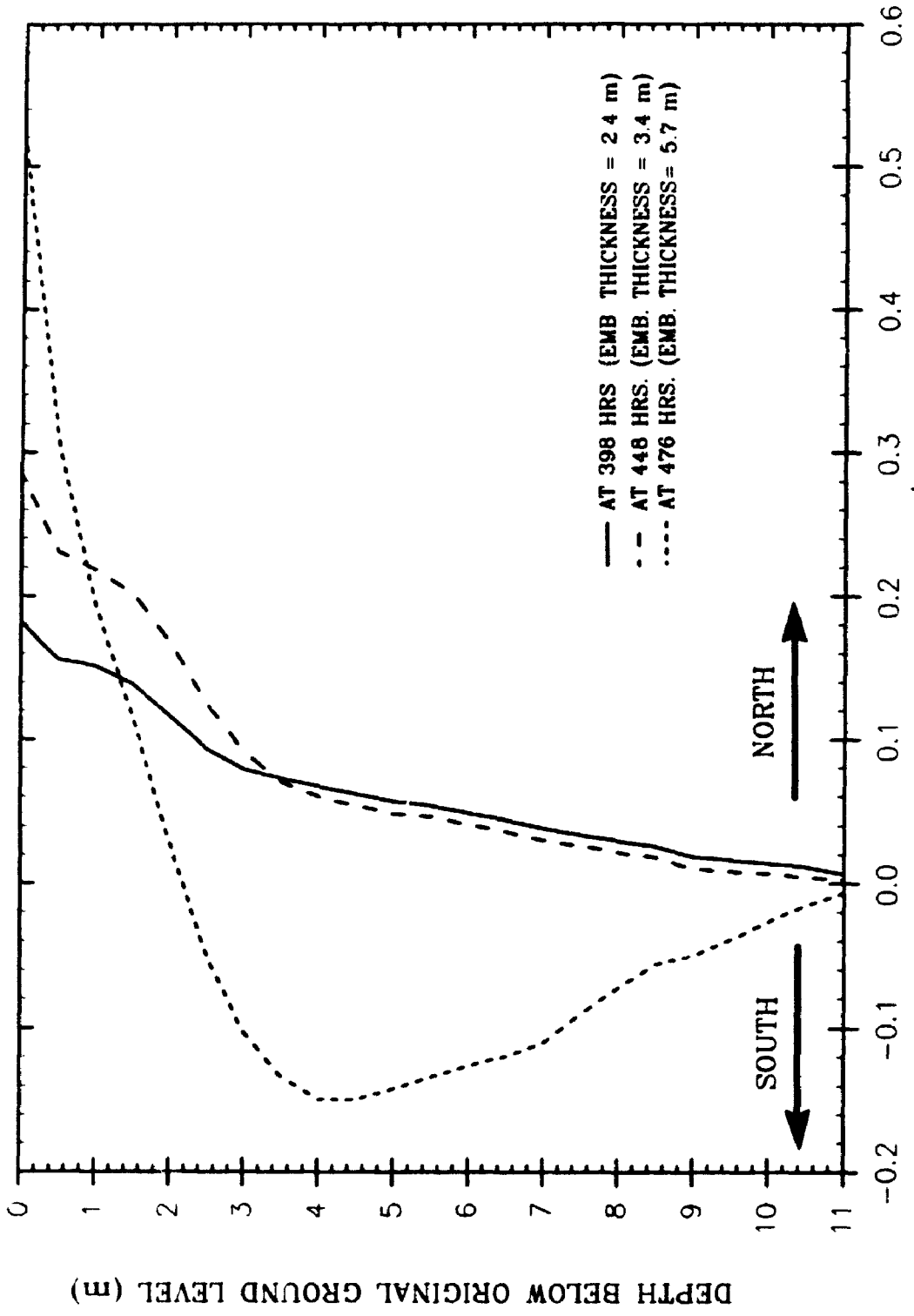

FIG. 4.16 VARIATION OF HORIZONTAL DISPLACEMENT WITH DEPTH AT DIFFERENT EMB. THICKNESSES FOR INCLINOMETER 261

(1972), and a control method has been suggested by Marche and Chapuis (1974) for the construction of embankment on soft foundations.

Very large horizontal displacements (up to a maximum of about 1.77 m) were detected at inclinometer 22I when the embankment thickness was increased to 5.4 m (see Fig. 4.13). The horizontal displacement profile of inclinometer 22I indicated the initiation of two failure surfaces; the first at a depth of approximately 2.5 - 3 m and the second at a depth of 5 m from the ground surface. The crude probing exercise carried out at later stages of construction also indicated similar results.

The horizontal displacement profile of inclinometer 23I at an embankment thickness of 5 m (see Fig. 4.14) indicated the apparent initiation of a shear surface at about 4.5 - 5 m depth. The probe did not go below 3.5 m from the original ground surface when this inclinometer was probed at 5.7 m thickness (i.e. at about 475 hours). The crude probing at later stages of construction (i.e. at embankment thicknesses of 8.2 and 9 m) indicated the existence of a failure surface at a depth of about 3 m. The displacement profile at 5 m embankment thickness did not indicate any failure zone at 3 m depth. However, the displacement profiles at 3.4 m and 2.3 m embankment thicknesses are suggesting some evidence for the initiation of shear at about 3 m depth.

The data presented in Fig. 4.15 for a fill thickness of 5.7 m suggest the initiation of a failure zone at a depth of 2 - 2.5 m in inclinometer 25I. This could not be verified with the crude probe because at subsequent fill thicknesses blockage occurred within the fill indicating a failure zone at about 1.9 m above the ground level at this location.

Inclinometer 26I, placed south of the east-west reference line, showed comparatively smaller horizontal displacements, especially up to 3.4 m embankment

thickness (see Figs. 4.1 and 4.16). A change in the direction of lateral movement was evident in inclinometer 26I when the embankment thickness was increased from 3.4 to 5.7 m (see Fig. 4.16). This inclinometer also became blocked and could not be monitored in the normal fashion after 5.7 m thickness.

It should also be noted that the inclinometers indicate that significant movements were occurring to depth of at least 7 m prior to shearing of the inclinometers (discussed above).

4.4.4 Settlement data

The variation of settlement with time are presented for plates 6S, 7S and 8S in Fig. 4.17 (i.e. Figs. 4.17a and 4.17b). Very similar small settlement responses are exhibited by all the settlement plates up to a time of about 470 hours (3.4 m thickness). Up to this time the same fill thickness had been placed above each settlement plate (see Fig. 4.1). As the fill thickness increased beyond 3.4 m, settlement plate 6S experienced less stress change (and hence settlement) than plates 7S and 8S. Settlement plates 7S and 8S showed very similar responses up to about 512 hours which reflects the construction of the embankment up to 8.2 m thickness. The shoulder of the embankment approached settlement plate 7S when the fill thickness was increased to about 8.2 m and passed over it when the fill thickness was increased above 8.2 m (see Fig. 4.1).

Tavenas et al. (1974) suggested that soft clay foundations should behave elastically up to a critical height approximately equal to 50% of the failure height. It can be observed that the settlements of the ground monitoring points were less than 0.2 m when the embankment was constructed up to 3.4 m (at a time of about 448 hours), probably exhibiting elastic behaviour. A similar order of magnitude for the maximum horizontal

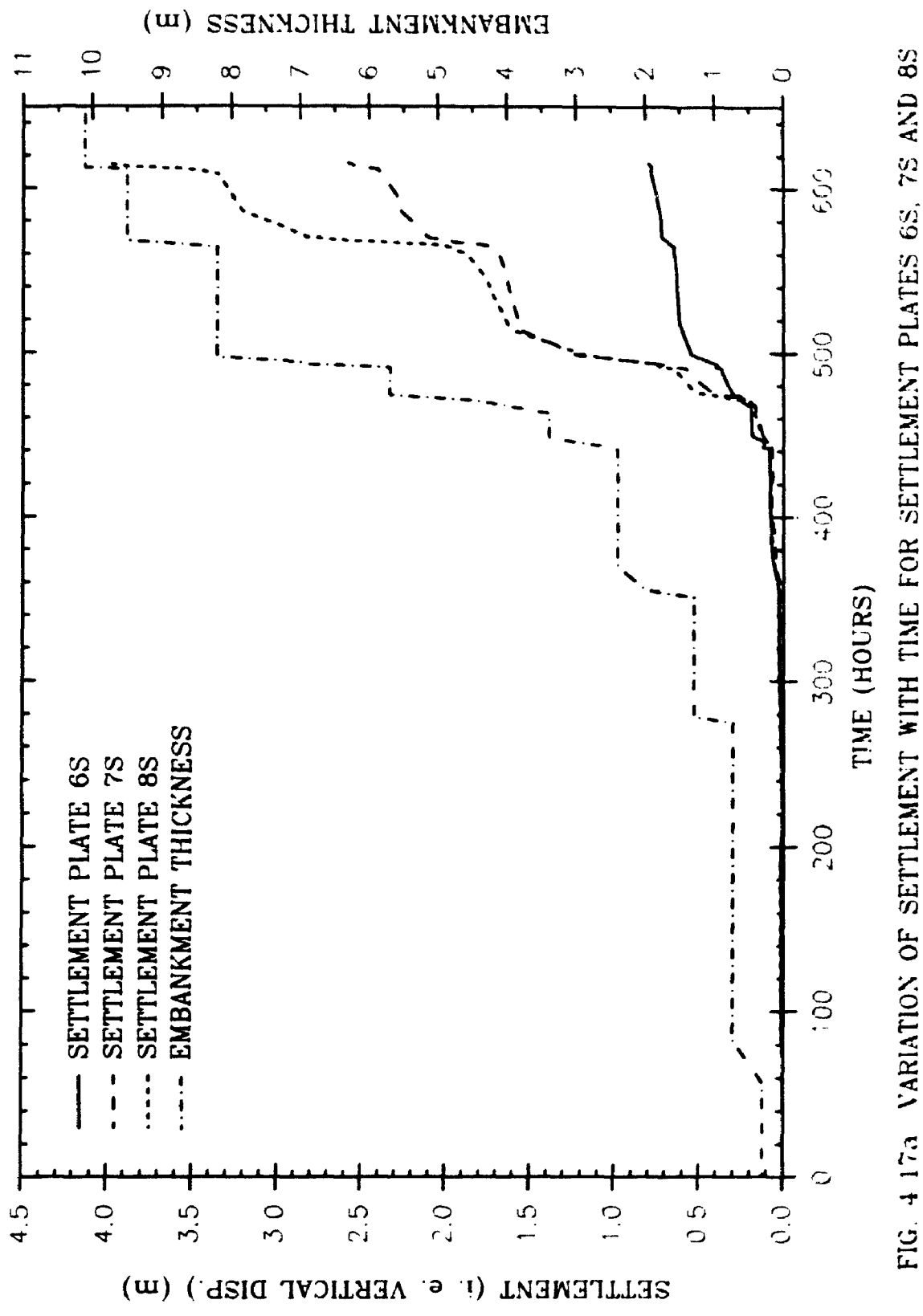

FIG. 4.17a VARIATION OF SETTLEMENT WITH TIME FOR SETTLEMENT PLATES 6S, 7S AND 8S

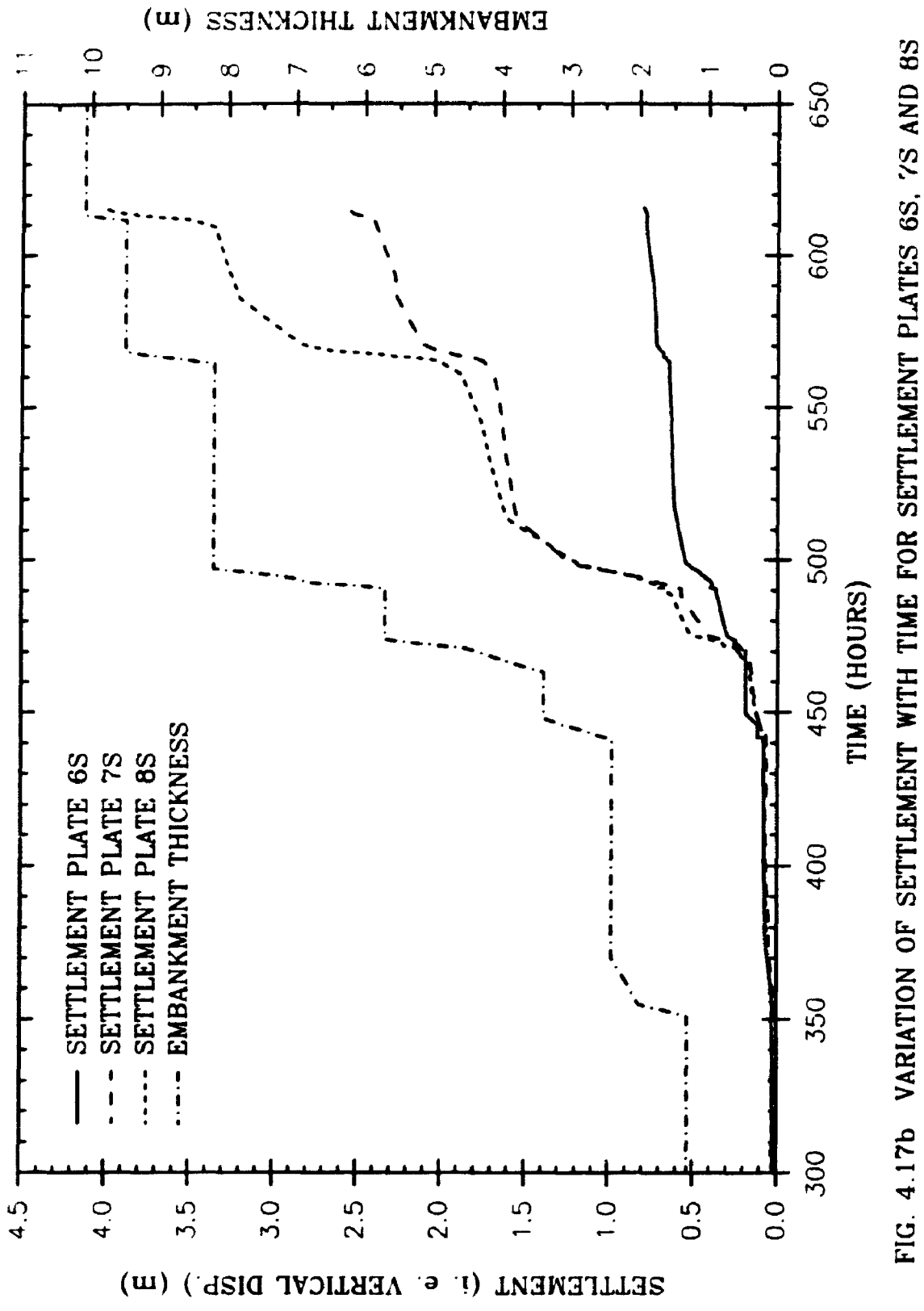

FIG. 4.17b VARIATION OF SETTLEMENT WITH TIME FOR SETTLEMENT PLATES 6S, 7S AND 8S

displacements at the inclinometers was also observed up to this embankment thickness (as previously discussed). The unreinforced section showed a similar response, as reported in chapter 3.

Both settlement plates 7S and 8S indicated a rapid increase in settlement (from about 0.2 m to 0.65 m) between 470 and 490 hours apparently in response to the rapid construction from 3.4 m to 5.7 m thickness between 463 and 473 hours. Rapid build-up of pore pressure was also observed in the piezometers placed in the foundation soil (e.g. piezometers 15, 16, 28 and 32) during this period, as previously discussed.

A very rapid increase in settlement from about 0.65 m to 1.6 m was evident at both settlement plates 7S and 8S between 490 and 512 hours (in response to the construction of the embankment from 5.7 m to 8.2 m between 490 and 497 hours). Settlement plate 8S showed significantly larger continuing settlement than settlement plate 7S even though no additional fill was placed between 497 and 564 hours. A significant depression around settlement plate 8S was observed during this period. Large horizontal displacements, as evidenced by the blockage of inclinometer casings, were also observed at a thickness of 8.2 m, as previously discussed, and the embankment had apparently failed. However, there was no evidence of classical-type (abrupt) failure similar to those reported by several investigators, for instance, La Rochelle et al. 1974, Ortigao et al. 1984 and Keenan et al. 1986, among others.

A very rapid increase in settlement at plate 8S (from 2.0 to 2.8 m) occurred between 565 and 570 hours when more fill was added to increase the thickness from 8.2 to 9.5 m. Although there was no addition of fill between 568 and 609 hours, the settlement increased from 2.8 to 3.2 m between 568 and 586 hours, followed by a milder increase up to 3.35 m between 586 and 609 hours. The total settlement during the period 564 - 609

hours was about 1.35 m which was in excess of the 1.3 m thick fill added during this period, indicating a plastic-type of failure such as that identified by Rowe and Soderman (1987) for reinforced embankments on soft soils.

A large depression and severe cracking developed as a result of increasing the embankment thickness to 9.5 m. Although the embankment was considered to have failed, further fill was added between 609 and 613 hours, increasing the thickness to 10.1 m at location of depression near settlement plate 8S. Very rapid settlement was observed at settlement plate 8S between 609 and 616 hours. Fill was not added in other areas, including the area surrounding settlement plate 7S, and there was no significant change in response of settlement plate 7S during this period.

Settlement augers 9A, 10A, 11A and 12A placed at depths of 2, 4, 6 and 10 m respectively indicated a pattern of settlement response with time similar to the settlement plates but less than at settlement plate 8S which was placed at the ground surface (see Figs. 4.18, 4.17 and 4.1). Settlements were small (less than 0.1 m) in all the four augers up to about 470 hours (i.e. an embankment thickness of 3.4 m). Fig. 4.18 indicates that the settlement of the foundation subsoil decreases with depth (i.e. the settlement is less in the auger placed deeper compared to that placed at shallow depth). Augers 9A and 10A gave a very similar settlement - time response throughout the monitoring period. Augers 11A and 12A gave similar responses especially up to about 566 hours.

Very rapid settlement is observed in augers 9A and 10A between 491 and 497 hours apparently in response to the rapid construction of embankment from 5.7 m to 8.2 m. Augers 11A and 12A did not show evidence of rapid settlement during this period but indicated moderate increases in settlement, which suggests that significant plastic deformation occurred between augers 10A and 11A (i.e. 4 - 6 m) during this period. All

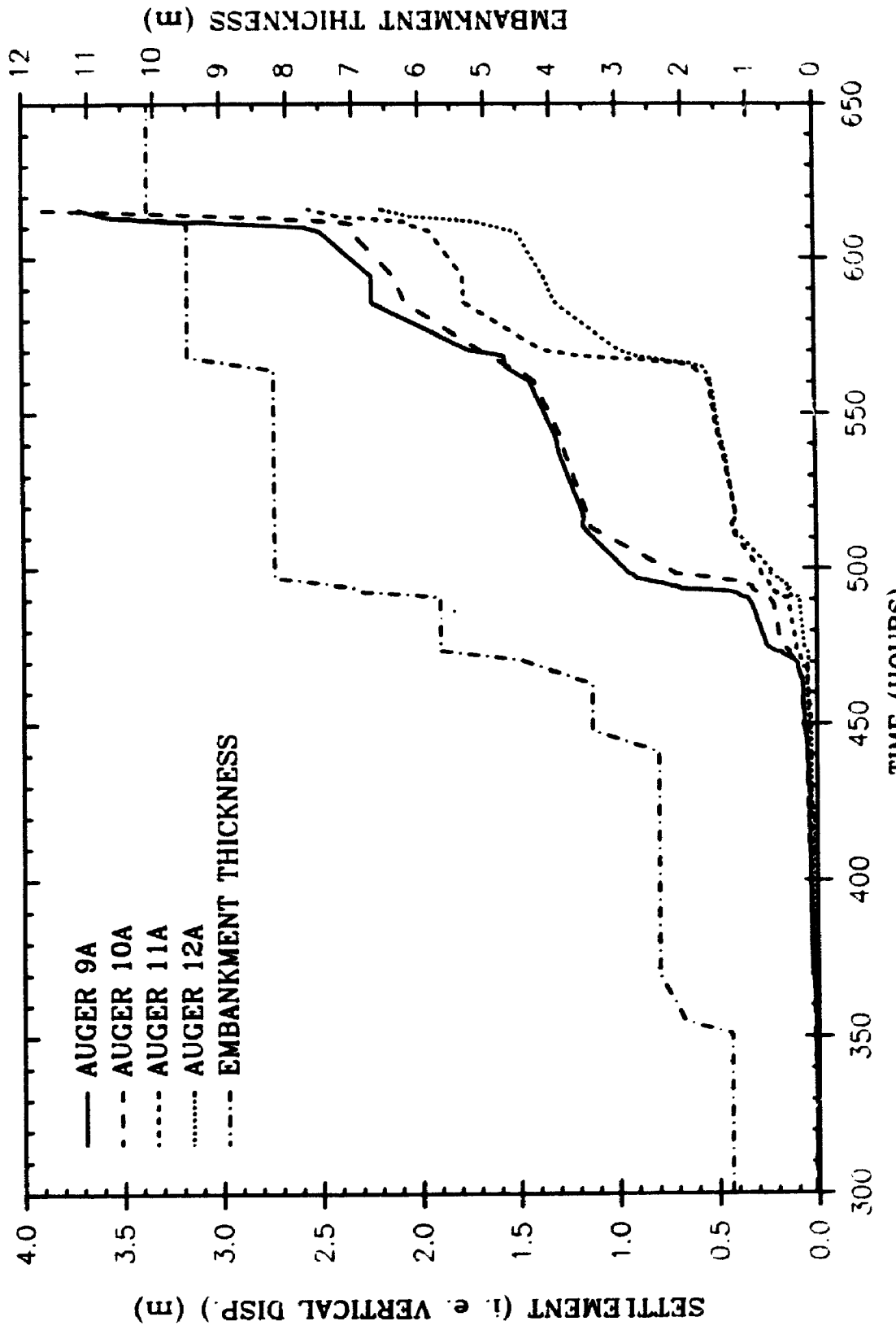

FIG. 4.18 VARIATION OF SETTLEMENT WITH TIME FOR AUGERS 9A, 10A, 11A AND 12A

the four augers indicated very rapid settlement when the thickness of the embankment was raised to 10.1 m between 610 and 613 hours. Settlement of auger 9 increased from 2.6 to 3.6 m during this 3 hour period indicating 1 m settlement for the addition of 0.6 m thick fill. This plastic-type failure is similar to that predicted for reinforced embankments on soft soils by Rowe and Soderman (1987).

Augers 11A and 12A indicated very rapid settlement (about 0.65 m at auger 11A) between 566 and 570 hours in response to the construction of the embankment from 8.2 to 9.5 m between 564 and 568 hours. Only moderate settlements (i.e. about 0.19 m and 0.15 m at augers 9A and 10A respectively) were indicated by augers 9A and 10A during this period. It is noted that although the augers are primarily intended to measure vertical deformations, the development of sliding (and the consequent lateral movement) will also be reflected in the "settlement" readings. An examination of all the available data would suggest that a significant component of the "deep settlements" noted above (i.e. at augers 11A and 12A placed at 6 and 10 m depth) may in fact be largely a reflection of the large lateral movement which occurred above this depth.

Settlement plates 13S, 17S and 18S placed beneath the berm indicated much smaller settlement than the settlement observed in the main embankment at settlement plates 7S and 8S (see Figs. 4.18 and 4.19). Settlement plates 17S and 18S showed very similar responses up to about 450 hours, i.e. until construction of the berm was completed. Settlement plate 17S showed subsequent increases in settlement which (by comparison with the results of 18S) can be attributed to the effect of loading of the main embankment rather than consolidation. Settlement of plate 18S was quite small over the entire test period (see Fig. 4.19). Settlement plate 13S, which was placed close to the access road, showed comparatively larger settlement than plates 17S and 18S up to 450 hours when the berm was completed. This is probably due to the truck traffic close by. Subsequently,

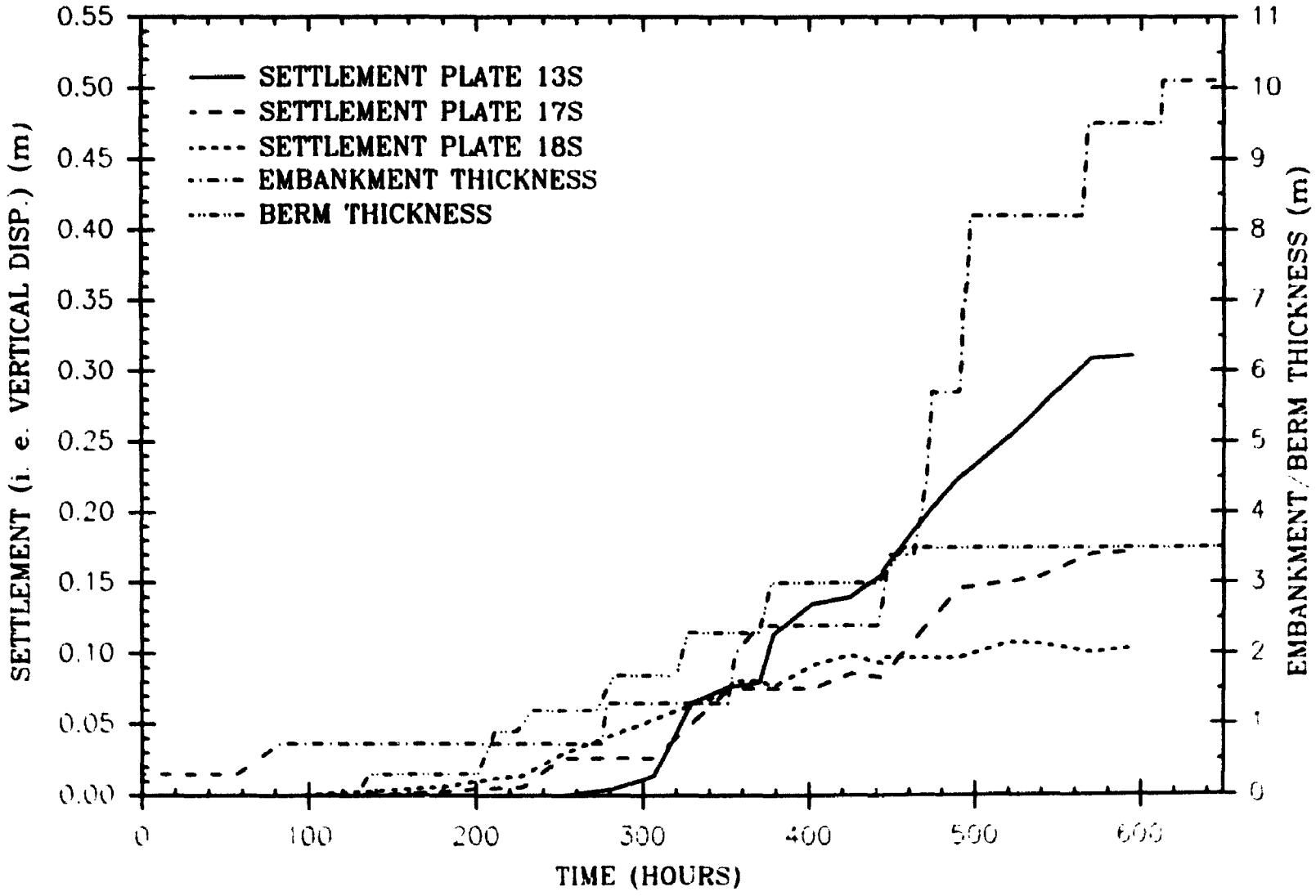

FIG 4.19 VARIATION OF SETTLEMENT WITH TIME FOR SETTLEMENT PLATES 13S, 17S AND 18S

plate 13S showed much larger increase in settlement, apparently being influenced more by the main embankment than were plates 17S and 18S. It is noted that there is no settlement data for plate 13S prior to 260 hours. This is because the original plate was damaged by a truck and had to be replaced. The settlement shown for plate 13S do not include the settlement which occurred prior to 260 hours.

Augers 14A, 15A and 16A placed closer to settlement plate 13S indicated much lower settlements than settlement plate 13S (see Figs. 4.20 and 4.19). In general, the settlement of auger 14A placed at 2 m depth was greater than that of auger 15A placed at 4 m depth which was in turn greater than that of auger 16A placed at 6 m depth. All these augers also showed evidence of some influence from the main embankment construction after about 450 hours.

4.4.5 Heave and horizontal displacement

All four heave plates (placed close to the toe of the embankment) indicated similar pattern of vertical displacement (i.e. heave) with time as shown in Fig. 4.21. Heave was negligible up to about 440 hours by which time the embankment had been constructed to 2.4 m thickness. Similarly, low settlement at the settlement plates and small horizontal displacements in the inclinometers were observed during this period as discussed previously. These low strains can be attributed to the elastic behaviour of the foundation. Moderate increase of heave was observed afterwards up to about 472 hours which represents an embankment thickness of 5 m. Very rapid increase in heave was observed between 472 and 475 hours, apparently in response to the construction of the embankment from 5 to 5.7 m. The heave continued to increase quite rapidly when there was no addition of fill between 475 and 490 hours. These rapid movements suggest that the soil beneath the embankment had approached failure at 5.7 m thickness. The pore pressure

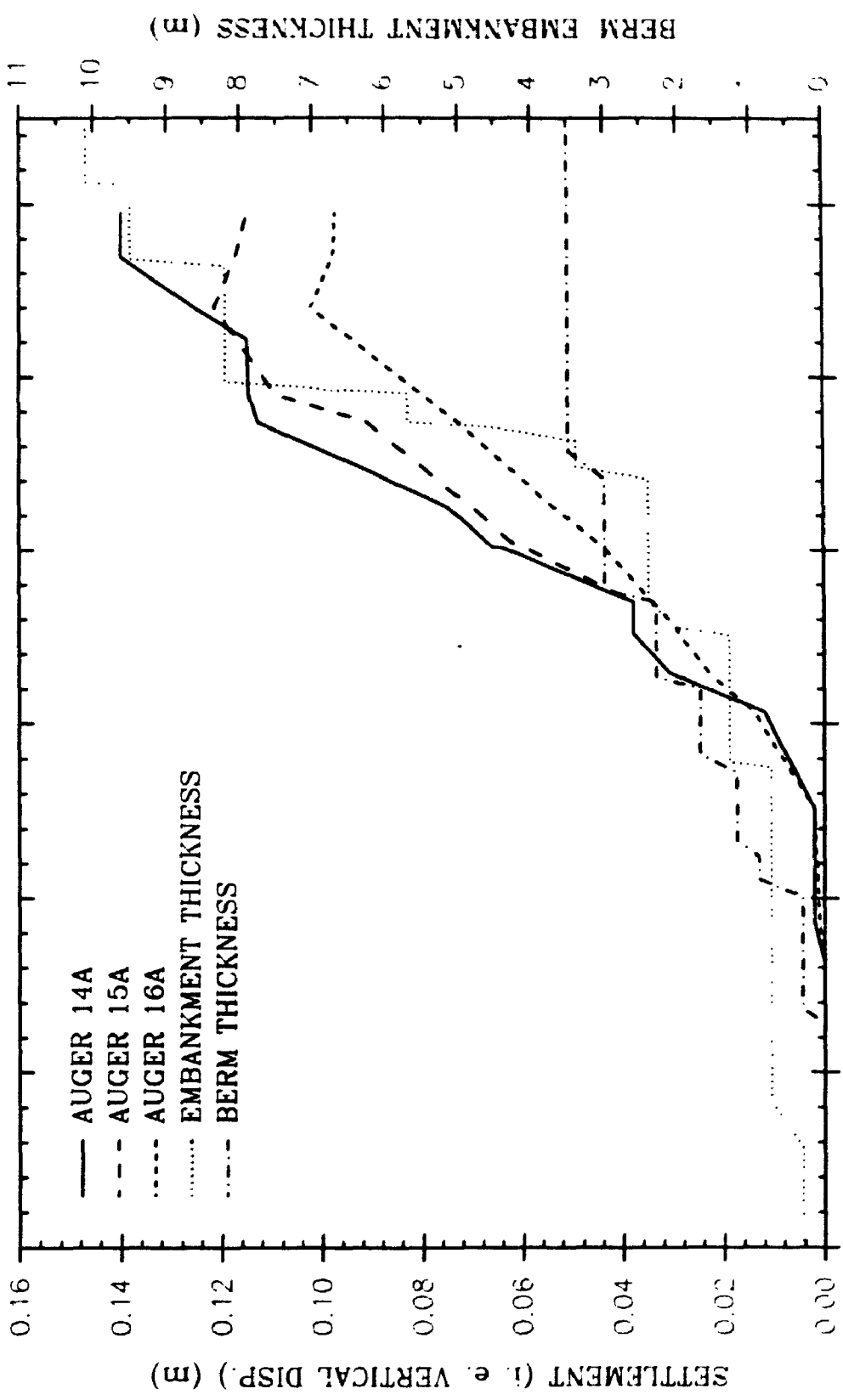

FIG 4.20 VARIATION OF SETTLEMENT WITH TIME FOR AUGERS 14A, 15A AND 16A

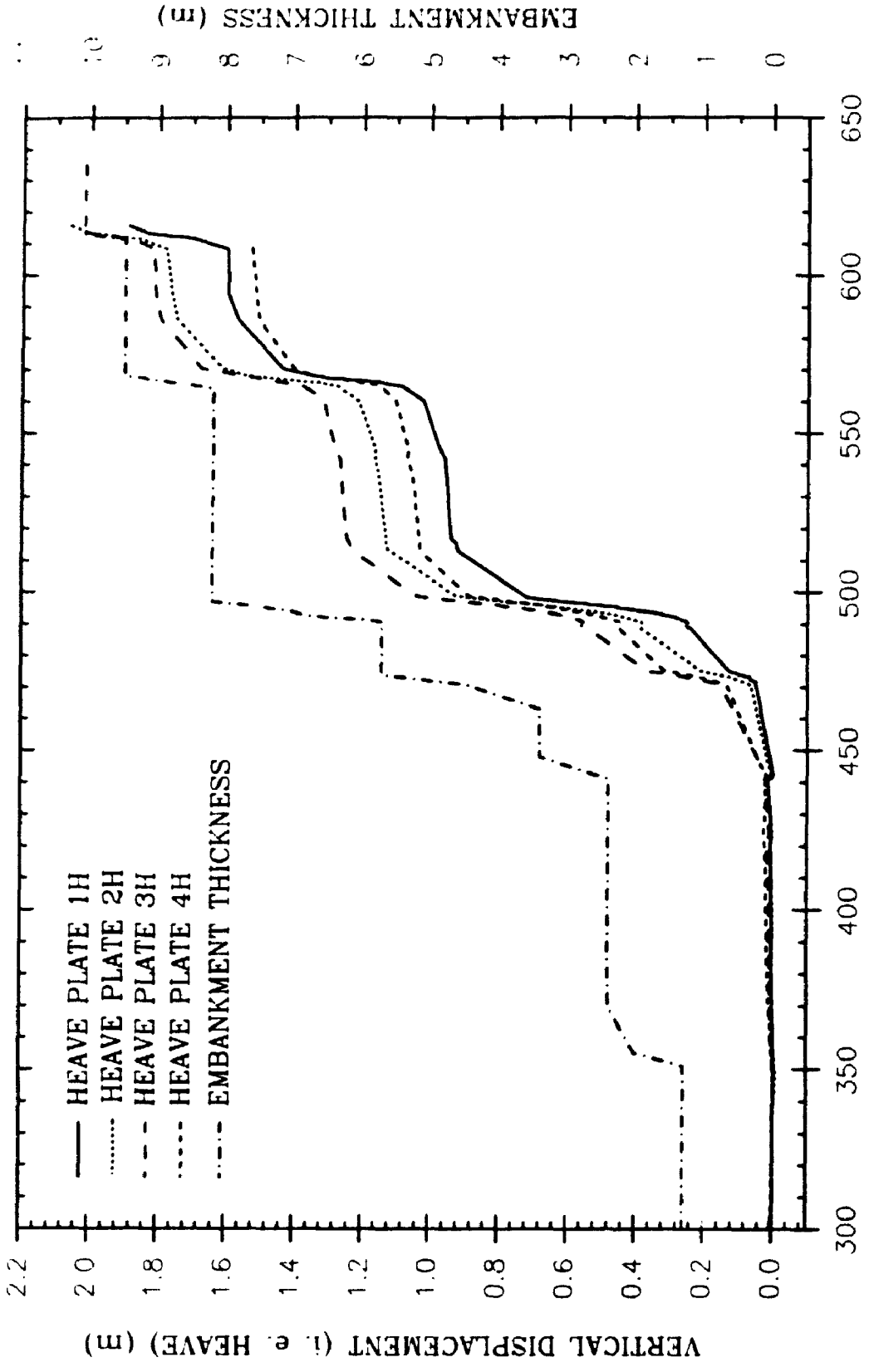

FIG. 4.21 VARIATION OF VERTICAL DISPLACEMENT WITH TIME FOR HEAVE PLATES 1H, 2H, 3H AND 4H

responses also indicated a similar phenomenon, as discussed previously.

As the embankment thickness was increased beyond 5.7 m, the heave increased in direct response to the addition of fill. Very rapid heave was observed at all four heave plates when the embankment was constructed rapidly from 5.7 to 8.2 m (490 - 497 hours) and from 8.2 to 9.5 m (564 - 568 hours). Evidence for rotational type failure occurred when the embankment thickness reached 8.2 m. At this thickness a crack opened up in the ground north of the embankment at the outer limit of the major heave zone. Cracks on the crest also were observed at this stage. Another crack in the ground further north developed when the embankment was lifted to 9.5 m thickness, indicating the development of a secondary failure surface. Details of the crack propagation and the interpretation of failure height are presented in a later section of this chapter.

All four heave plates showed a very similar pattern of horizontal displacement variation with time up to about 565 hours (see Fig. 4.22). The horizontal displacements were very small (< 0.03 m) up to about 470 hours (i.e. until the embankment reached 3.4 m). Horizontal displacement increased in direct response to the addition of fill from 470 to 520 hours as the embankment thickness was increased from 3.4 to 8.2 m. Very large increases in horizontal displacement (as high as 1.14 m at heave plates 2 and 3) were observed between 498 and 513 hours apparently in response to the construction from 5.7 to 8.2 m between 490 and 497 hours. After reaching 8.2 m embankment thickness, there was an apparent decrease (of about 0.13 m) in the horizontal displacement during the time interval 517 - 537 hours. This would appear to be tne result of tilting of the heave plates (as discussed in chapter 3) and the reduction in horizontal movement due to sinking of the embankment near the toe.

The heave plates 19H, 20H and 21H placed on the southern (i.e berm) side of the

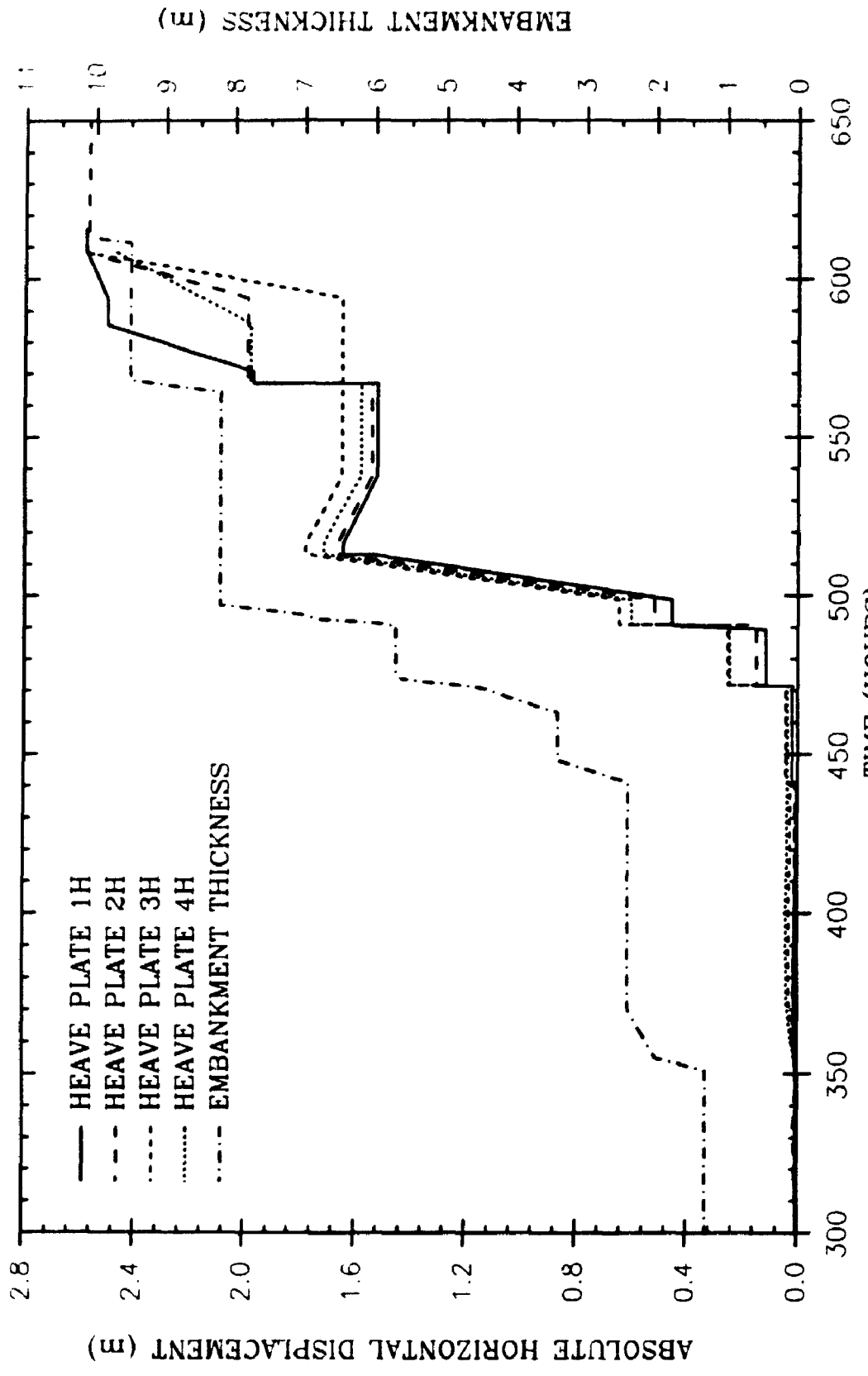

FIG. 4.22 VARIATION OF HORIZONTAL DISPLACEMENT WITH TIME FOR HEAVE PLATES 1H, 2H, 3H AND 4H

embankment showed very small vertical displacements (< 0.04 m) throughout the construction and monitoring period (see Fig. 4.23). All the three heave plates indicated very small (< 0.03 m) settlement (i.e. negative heave) during the early stages of construction. The settlement in heave plate 19H placed closer to the toe was larger than that of heave plate 20H placed 2 m south of it (see Figs. 4.1 and 3.2 for location of heave plates). Heave plate 21H placed further away from the toe indicated the largest settlement.

4.4.6 Geotextile strain

A detailed account of the measured geotextile strains and their relation to the sequence of construction are presented in chapter 5. A typical variation of geotextile strain (in the transverse direction) with embankment thickness is presented in Fig. 4.24. This figure summarizes the range of strains, obtained from different types of gauges (i. e. electrical, mechanical and electromechanical ring gauges) installed between 16.6 and 17.6 m from the toe of the embankment, against the embankment thickness (see Fig. 5.1 for the details regarding the layout of strain gauges). The mean (i. e. the average) as well as the lower and upper limits of the strain readings are presented separately. Significant increases of the slopes for the lower limit and average plots were observed at about 4.1 m thickness, indicating that the embankment apparently started to move (or yield) at about 4.1 m thickness. The gauges in the region 16.6 - 17.6 m from the embankment toe indicate a relatively consistent pattern of strain - thickness behaviour up to 8.2 m thickness. It can be observed that the general trend of the strain - thickness variation observed before the brief stoppage of construction at 5.7 m thickness (i. e. between 475 and 490 hours) was continued again after about 7 m thickness. This continuation of the same trend suggest that the sequence of construction employed at the site did not have any significant influence on the overall behaviour of the reinforced embankment.

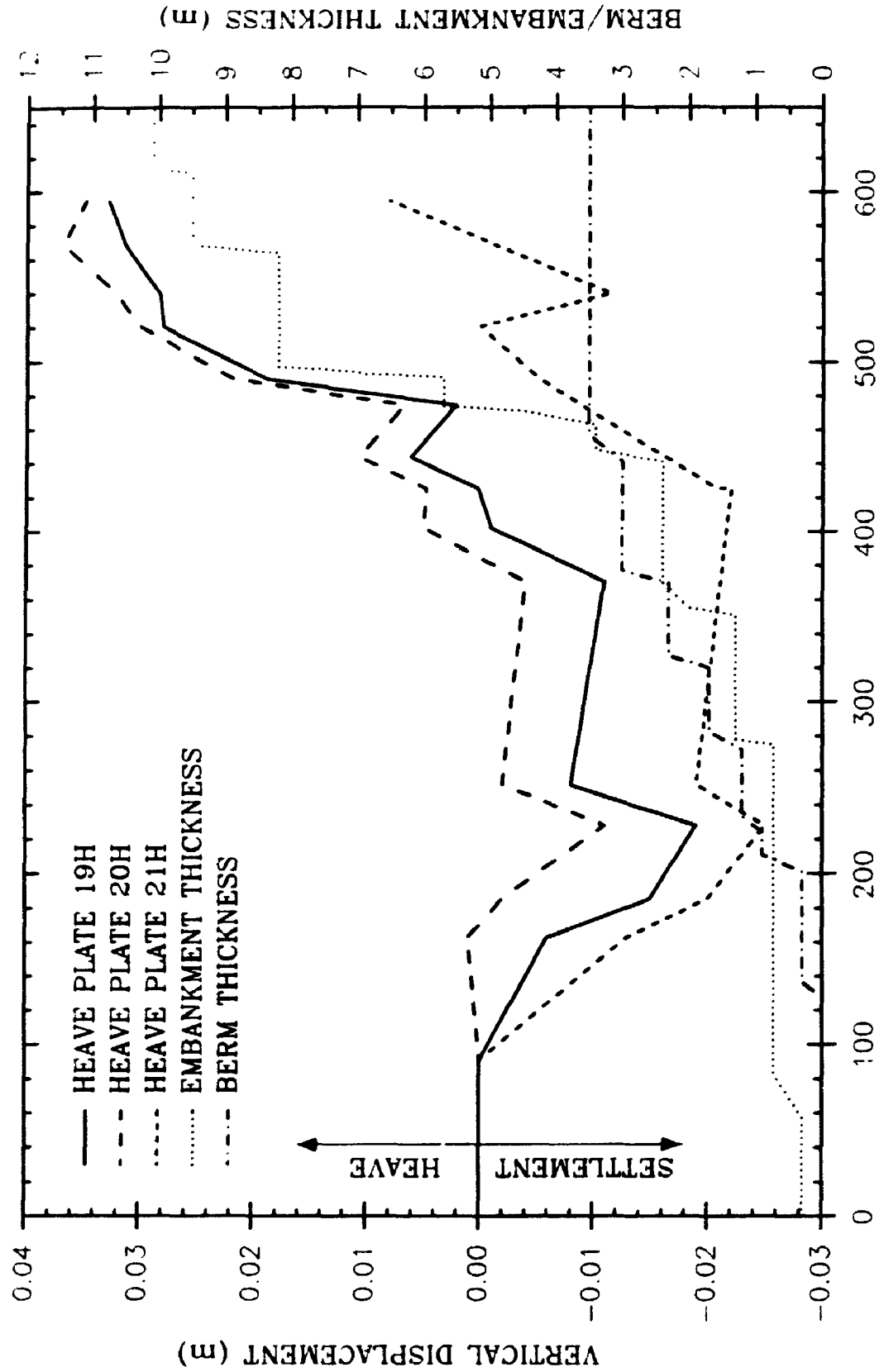

FIG. 4.23 VARIATION OF VERTICAL DISPLACEMENT WITH TIME FOR HEAVE PLATES 19H, 20H AND 21H

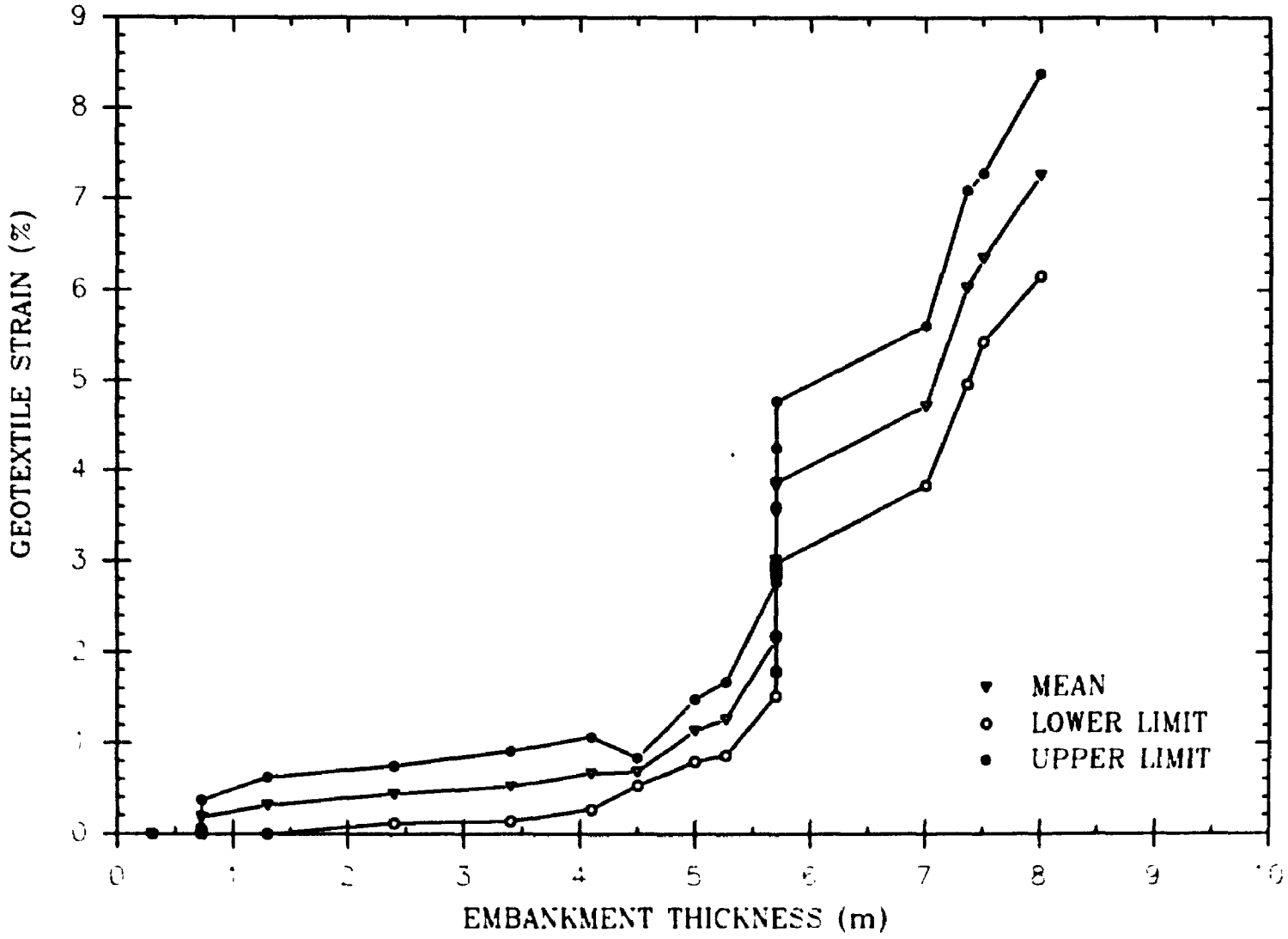

FIGURE 4 24 TYPICAL VARIATION OF GEOTEXTILE STRAIN WITH EMBANKMENT THICKNESS (FOR GAUGES BETWEEN 16 6 AND 17 6 m FROM EMBANKMENT TOE)

A summary of the average, upper limit and lower limit strains at different critical embankment thicknesses are presented in Table 4.1. It is evident from this table that the geotextile strain (in the transverse direction) increased with the load up to an embankment thickness of about 8.2 m, in all the regions across the geotextile. It was suspected that the geotextile either yielded between points M5 and M6 or otherwise underwent a local failure around monitoring point M6 at about 8.2 m thickness (see chapter 5).

It could be inferred from Table 4.1 that the strains were comparatively small (the average was less than about 0.72%) up to an embankment thickness of 3.4 m. The average value of strain increased to less than about 1.0%, 1.95% and 2.95% when the embankment thickness was increased to 4.1 m (i. e. at 468 hours), 5.0 m (i. e. at 472 hours) and 5.7 m (i. e. at 475 hours) respectively suggesting the initiation of movement or (or yielding) of the foundation soil during the construction of the embankment above 4.1 m. Large increase of the average value of strain, from 2.95% to 4.86%, at 5.7 m thickness is evidenced indicating that the soil approached failure at about 5.7 m thickness. The excess pore pressure and both vertical and horizontal displacement responses also indicated that the soil approached failure at about 5.7 m thickness. Considering the magnitude of the strains, it would appear that the contribution of the geotextile to the stability of the embankment was not significant up to about 3.4 m thickness but that its contribution increased gradually after about 4.1 m thickness. The strain increased to as high as about 8.6% when the embankment was raised to 8.2 m thickness. It is apparent that the role of geotextile in providing stability to the embankment increased significantly after 5.7 m thickness.

It was inferred from the strain distribution profiles (i. e. the variation of transverse geotextile strain across the North - South centre line axis of the reinforced section at different stages of construction) that the location of maximum strain was between about 17 and 19 m from the toe during early stages of construction (i. e. up to 3.4 m thickness).

TABLE 4.1 SUMMARY OF GEOTEXTILE STRAIN VERSUS EMBANKMENT THICKNESS ACROSS THE GEOTEXTILE

DISTANCE FROM EMBANKMENT TOE (m)	AVERAGE (MEAN) Strain Thickness (%)							MAXIMUM (UPPER LIMIT) Strain Thickness (%)						MINIMUM (LOWER LIMIT) Strain Thickness (%)					
	3.4 m	4.1 m	5 m	5.7 m (475 hrs)	5.7 m (490 hrs)	8.2 m	Approximate thickness at change of slope	3.4 m	4.1 m	5.0 m	5.7 m (475 hrs)	5.7 m (490 hrs)	Approximate thickness at change of slope	3.4 m	4.1 m	5 m	5.7 m (475 hrs)	5.7 m (490 hrs)	Approximate thickness at change of slope
20.9-22.5	0.40	0.67	0.72				4.1 m	0.64	0.79	1.17	1.63	4.2	3.4 - 4.1 m	0.25	0.31	0.43			
18-19.5	0.5	0.96	1.94	**	3.51		4.1 m	1.26	2.29	4.64	**	5.07	3.4 m	0.32	0.49	0.87	1.84	1.95	5 - 5.7 m
16.6-17.6	0.52	0.87	1.43	2.15	3.88		4.1 m	0.91	1.07	2.02	2.77	4.77	4.1 m	0.14	0.27	0.79	1.52	2.98	4.1 m
14.6-15.6	0.41	0.76	1.68	2.95	4.86	8.61*	3.4 m	1.14	2.02				3.4 m	0.12	0.23	**	0.94	2.19	5.35 m
13.6-14.2	0.18	0.48	1.31	2.34	4.3*	7.66*	3.4 m	0.27	0.61				3.4 m	0.09	0.17	0.96			3.4, 5 m
11.8-12.6	0.34	0.69	1.10	2.06	4.56	8.53*	3.4, 5 m	0.53	0.88	1.42	3.29		3.4, 5 m	0.16	0.43	0.78	2.42	6.02	5.0 m
9.8-10.9	0.44	0.75	1.11	1.97			5.0 m	0.46	1.03	1.69	2.26		5.0 m	0.42	0.47	0.74	1.69		5.0 m
8.15-9.5	0.57	1.04	1.53	2.4	3.93*	6.44*	3.4 m	0.67	1.11	1.74			3.4 m	0.46	0.96	1.31			3.4 m
4.7	0.45	0.90	0.98	1.25	1.57		5.7 m												

* SINGLE GAUGE STILL FUNCTIONING

** DATA NOT COLLECTED OR INSUFFICIENT DATA AT THAT TIME

The location of this maximum strain shifted towards the centre line of the embankment to between about 14 and 19 m when the thickness was raised above 4.1 m and further shifted to between about 12 and 15 m from the toe when the thickness was increased above 5.7 m (see chapter 5).

4.5 GENERAL COMMENTS ON FIELD OBSERVATION

Initial indications of significant plastic deformation in the soil was provided by the large increases in horizontal displacements in the inclinometers and the rapid increase in geotextile strain when the embankment was raised from 5 to 5.7 m. An increase in the maximum strain along the geotextile from about 2% (at about 472 hours) to 3% (at about 475 hours) was observed during this construction phase on Oct. 10, 1989 (see Table 4.1, average strain data). The maximum strain further increased overnight to about 4.9% (on Oct. 11, 1989, i.e. at about 490 hours). The first indication that failure of the soil was being approached occurred when the embankment thickness was 5.7 m. The inclinometer casings 22, 23 and 24 were found to be blocked at this thickness. At the start of work on the following morning (October 11, 1989), extensive but thin (maximum width of 1 - 2 cm) tension cracks were observed on the east and west berms of the reinforced section. Some very thin tension cracks were also observed at the south end of the reinforced section near the Casagrande piezometer 57C (i.e. about 3.6 m south of centre line, see Fig. 3.2).

The cracks on the west berm increased to a maximum width of 1 cm when the embankment thickness was increased to 6.2 m (Oct. 11, 1989 at 11:20 am). Sinking of the toe of the embankment and visible heaving at heave plate 1H were observed when the thickness was increased to about 7 m. Tension cracks in the transverse (i.e. north - south) direction closer to Casagrande piezometer 53C (i.e. about 3.2 m from the toe), probably

caused by the extensive heaving, were observed. The tension crack on the east berm of the reinforced section increased to a width of 4 - 5 cm and extended to about 3 m into the unreinforced section. The tension crack on the west berm increased to a maximum width of 6 cm when the thickness was lifted to 7.5 m. The fill was lifted to a thickness of 8.2 m at the close of work on Oct. 11, 1989. Extensive cracking as mapped in Fig. 4.25 was observed on the following morning (October 12, 1989). The observed severe cracking of the ground at the limit of the heave zone is also mapped on this figure. At the outer limit of the heave zone, the ground heaved up and split giving the appearance of a thrust fault with a vertical discontinuity of about 0.4 m, along one of the cuts initially made in the crust to break up the root-mat. Fill was not added on the 12th and 13th of Oct., 1989 due to rain. At the beginning of work on Oct. 14, 1989, it was observed that the crack close to the Casagrande piezometer 57C (i.e. at 2.6 - 3.1 m from the centre line) has widened to a maximum of 3 cm and a distance of 6.6 m (from the N-S axis) to the east (see Fig. 4.25).

The thickness of the unreinforced section was increased from 3.4 m to 6.25 m on Oct. 14, 1989. This was immediately followed by the building of the reinforced section from 8.2 to 9.5 m on the same day. It was obvious that the reinforced section has already failed as evidenced by the severe cracking towards the west berm (see Fig. 4.26), rotational-type deformation of the crest with maximum depression closer to settlement plate 8S and severe cracking of the ground north of the embankment toe. The ground projected out at the outer limits of two distinct heave zones as shown in Fig. 4.27, indicating the existence of two failure surfaces apparently of circular nature. The mapping of the cracks observed in both the reinforced and unreinforced sections are shown in Fig. 4.28. An apparent circular failure surface inferred from the inclinometer data (i.e. from both the horizontal displacement and blockage of the probe) and the crack patterns, is shown in Fig. 4.29. Two circular type failure surfaces were evident in the reinforced section, the primary (initial) one apparently passing through the reinforcement and the

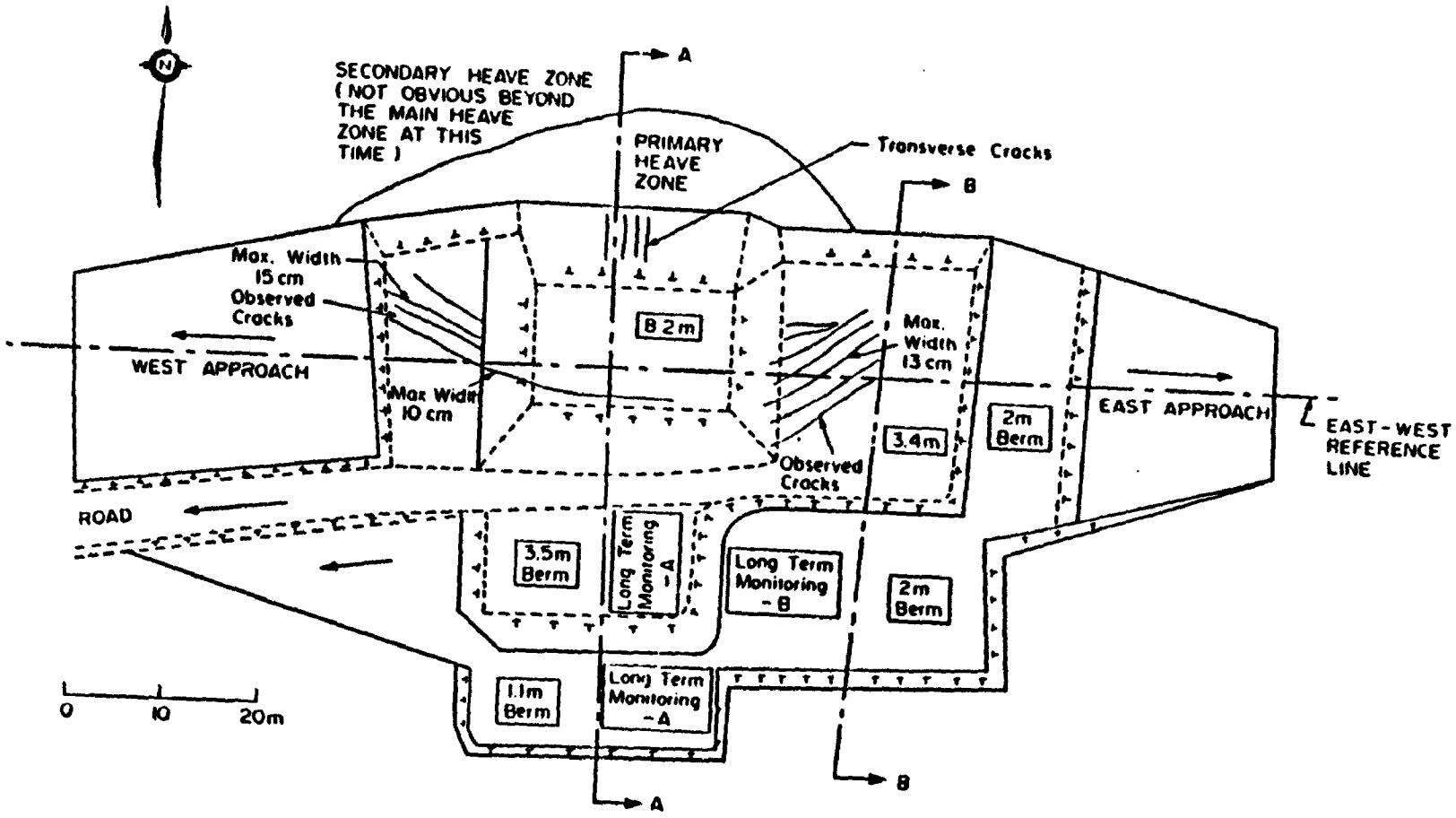

FIG. 4.25 MAPPING OF OBSERVED CRACKS ON OCT.12, 1989 (518 HOURS)

FIGURE 4.26 VIEW OF THE FAILED REINFORCED EMBANKMENT FROM WEST BERM

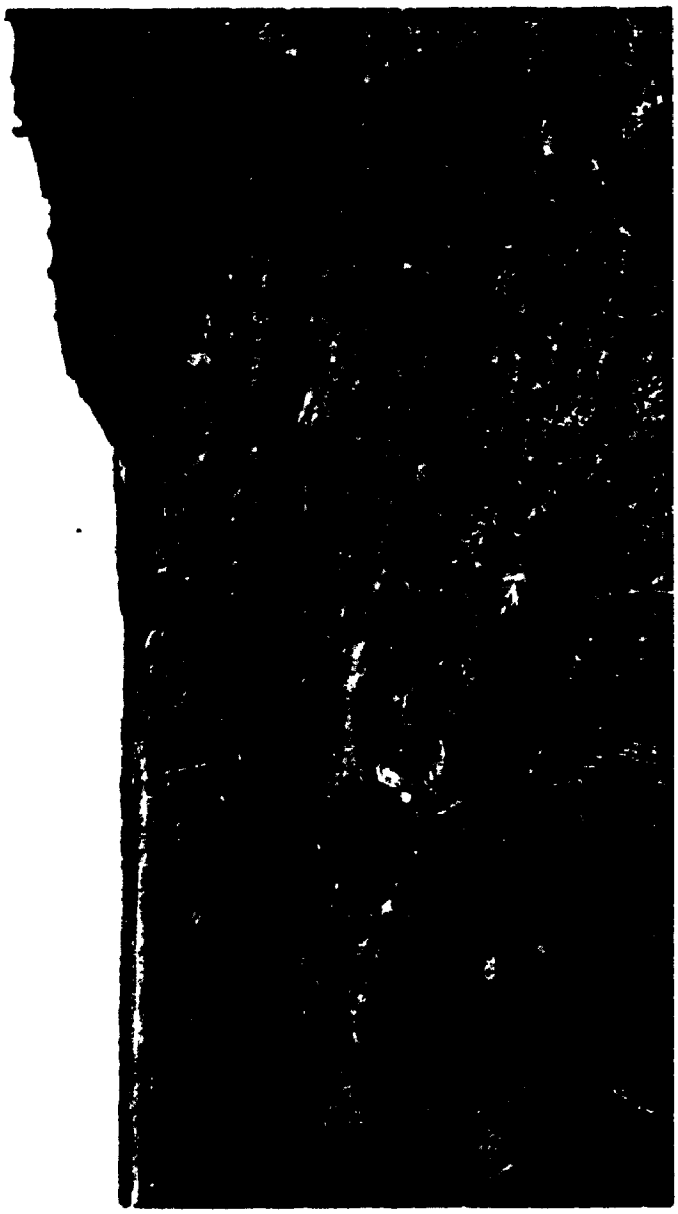

FIGURE 4.27 HEAVE FAILURE OBSERVED ON THE GROUND NORTH OF THE EMBANKMENT

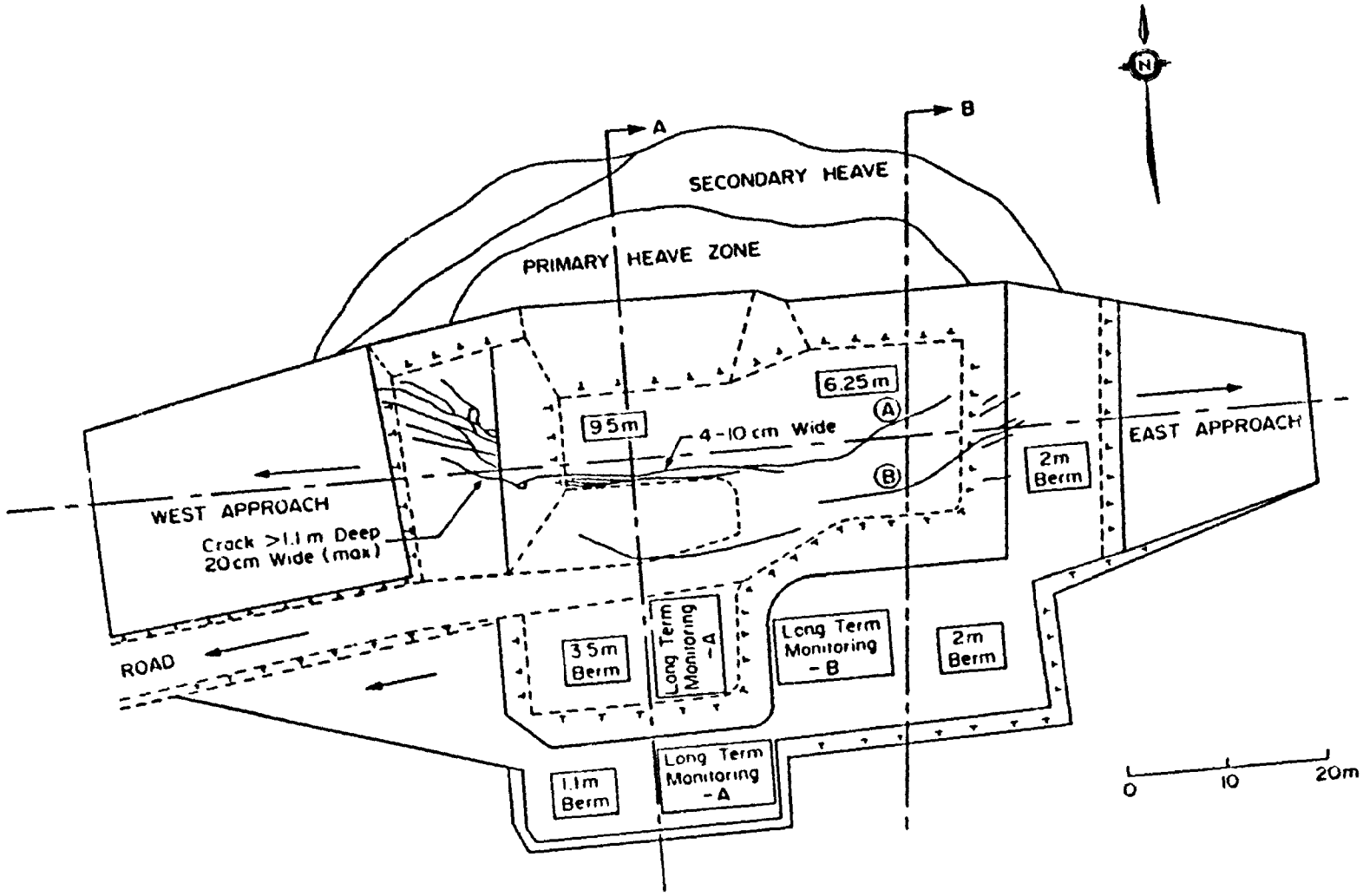

FIG. 4.28 MAPPING OF OBSERVED CRACKS AT FAILURE - OCT.15, 1989 (588 HRS.)

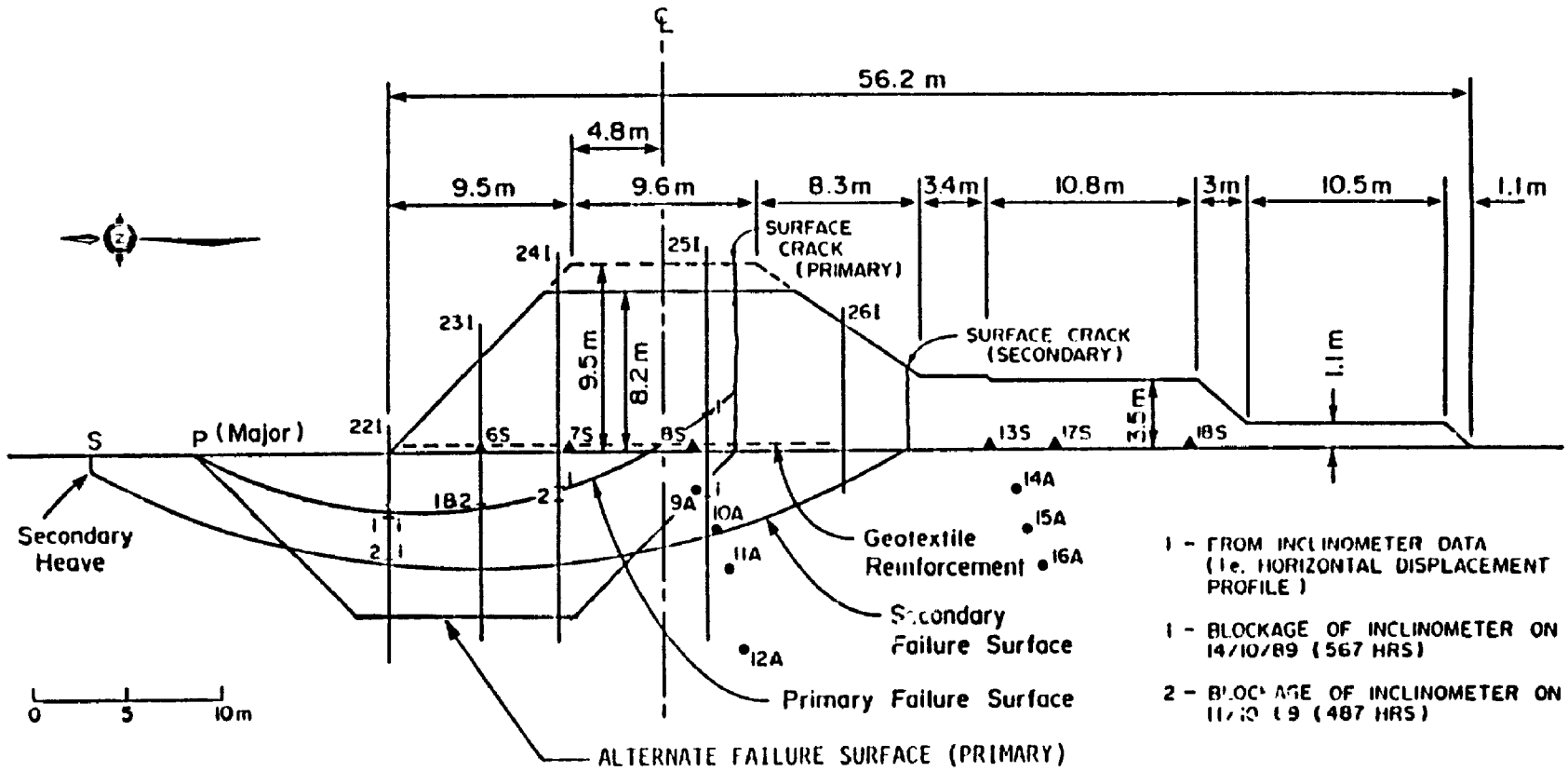

FIG. 4.29 INFERRED FAILURE SURFACES FOR THE REINFORCED EMBANKMENT

other secondary one passing closer to the edge of the reinforcement. A potential deep seated non-circular failure mechanism is also shown.

It is noted that the inferred primary (circular type) failure surface intersects the geotextile reinforcement at a distance of about 14.3 m from the toe which falls within the range (12 - 15 m) where the strain measurements indicated the occurrence of maximum geotextile strain (see also chapter 5).

A limit equilibrium analysis performed on the basis of average vane strength profile for the soil beneath the reinforced section (for a 8.2 m thick embankment) indicated factors of safety of about 1.46 and 1.21 respectively for the above primary and secondary failure surfaces inferred from the field investigation (see Fig. 4.29). The factor of safety for the deep seated wedge mechanism estimated on the basis of the same strength profile is about 1.54. It was reported in chapter 3 that the plasticity index of the soil ranged between 9 and 19% with an average of about 14% and the corresponding Bjerrum's correction for the vane strength will not have a significant effect on the factor of safety (see Bjerrum, 1973).

4.6 FAILURE OF THE REINFORCED EMBANKMENT SECTION

Variation of settlement of the main embankment, i.e. at settlement plates 7S and 8S and auger 9A, with embankment thickness are shown in Fig. 4.30. An approximately linear relationship between settlement and the embankment thickness was observed up to about 3.4 m thickness. There is a gradual increase in the rate of settlement for embankment thicknesses between 3.4 and 5.5 m. As 5.7 m was approached there was a pronounced change in settlement behaviour. The variation of heave of the ground north of the toe of the embankment (i.e. at heave plates 1H, 2H, 3H and 4H) with embankment

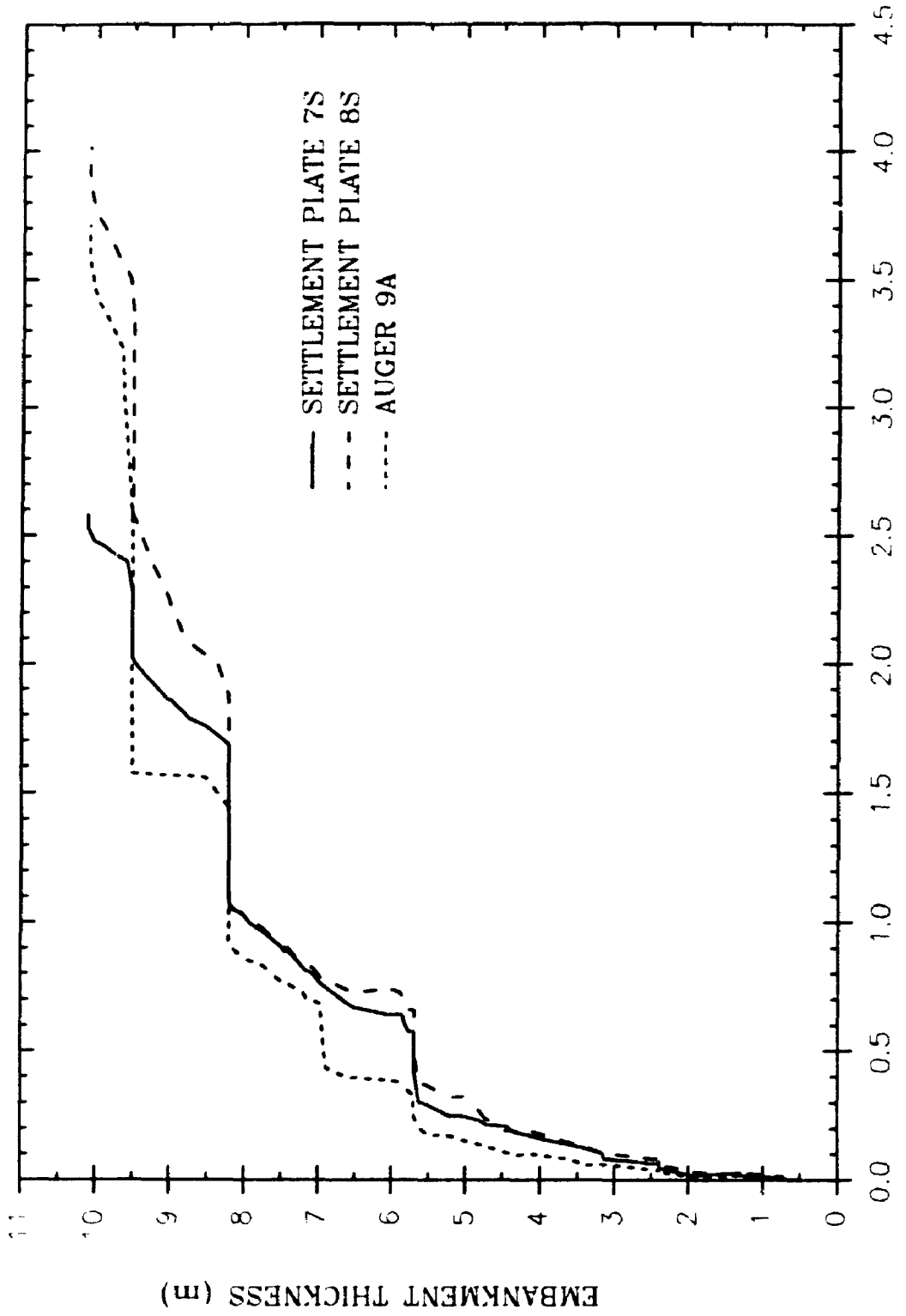

FIGURE 4.30 VARIATION OF SETTLEMENT WITH EMBANKMENT THICKNESS FOR SETTLEMENT PLATES 7S AND 8S AND AUGER 9A

thickness shown in Fig. 4.31 indicated a somewhat similar behaviour. The heaves were negligible up to about 1.7 m thickness. The flattening of the curve between 5.5 and 5.7 m thickness was well pronounced at heave plate 1H. Although there was a very brief stoppage of work, for about 16 hours, at the embankment thickness of 5.7 m, it is apparent that failure of the embankment was initiated at about 5.7 m thickness. Initiation of failure at the embankment thickness of 5.7 m was also evident from the excess pore pressure responses, particularly the variation of parameter $\overline{B}$ with time shown in Figs. 4.11 and 4.12, and the inclinometer data as discussed previously.

A linear relationship for the variation of net embankment height with the embankment thickness up to about 3.4 m thickness is evidenced in Fig. 4.32. The net height is defined as the elevation of the crest of the embankment with reference to the maximum elevation of the ground near the toe (i.e. net embankment height at a particular instant = embankment thickness - settlement - maximum heave near the toe at that particular instant). This confirms our earlier observation that the foundation indicated elastic behaviour up to about 3.4 m thickness. There was a shift in the net height versus thickness response close to 5.7 m embankment thickness. It is believed that it was caused by the brief stoppage of work at 5.7 m thickness as well as the geotextile becoming more effective in providing the required stability to the embankment (as evidenced by large increase of geotextile strain at this stage). However, although there is strong evidence of failure in the soil there is no evidence that the embankment itself had failed at a thickness of about 5.7 m since additional fill could be added without any significant change in the rate of increase in net embankment height with fill thickness until a fill thickness of about 6.5 m.

Increased influence of the geotextile in providing for the stability to the embankment afterwards was evident from the rapid increase in the geotextile strain during

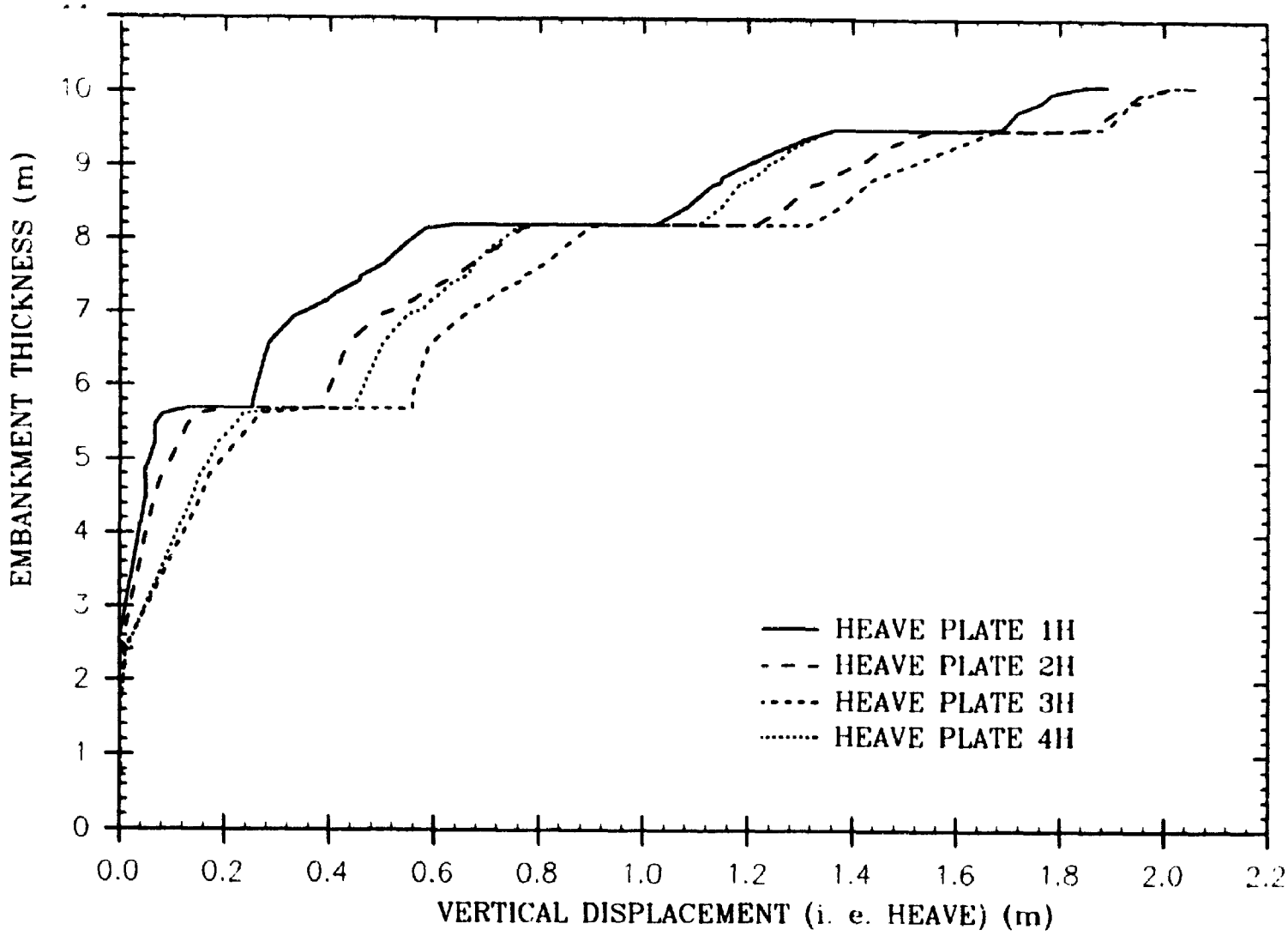

FIGURE 4.31 VARIATION OF VERTICAL DISPLACEMENT WITH EMBANKMENT THICKNESS FOR HEAVE PLATES 1H, 2H, 3H AND 4H

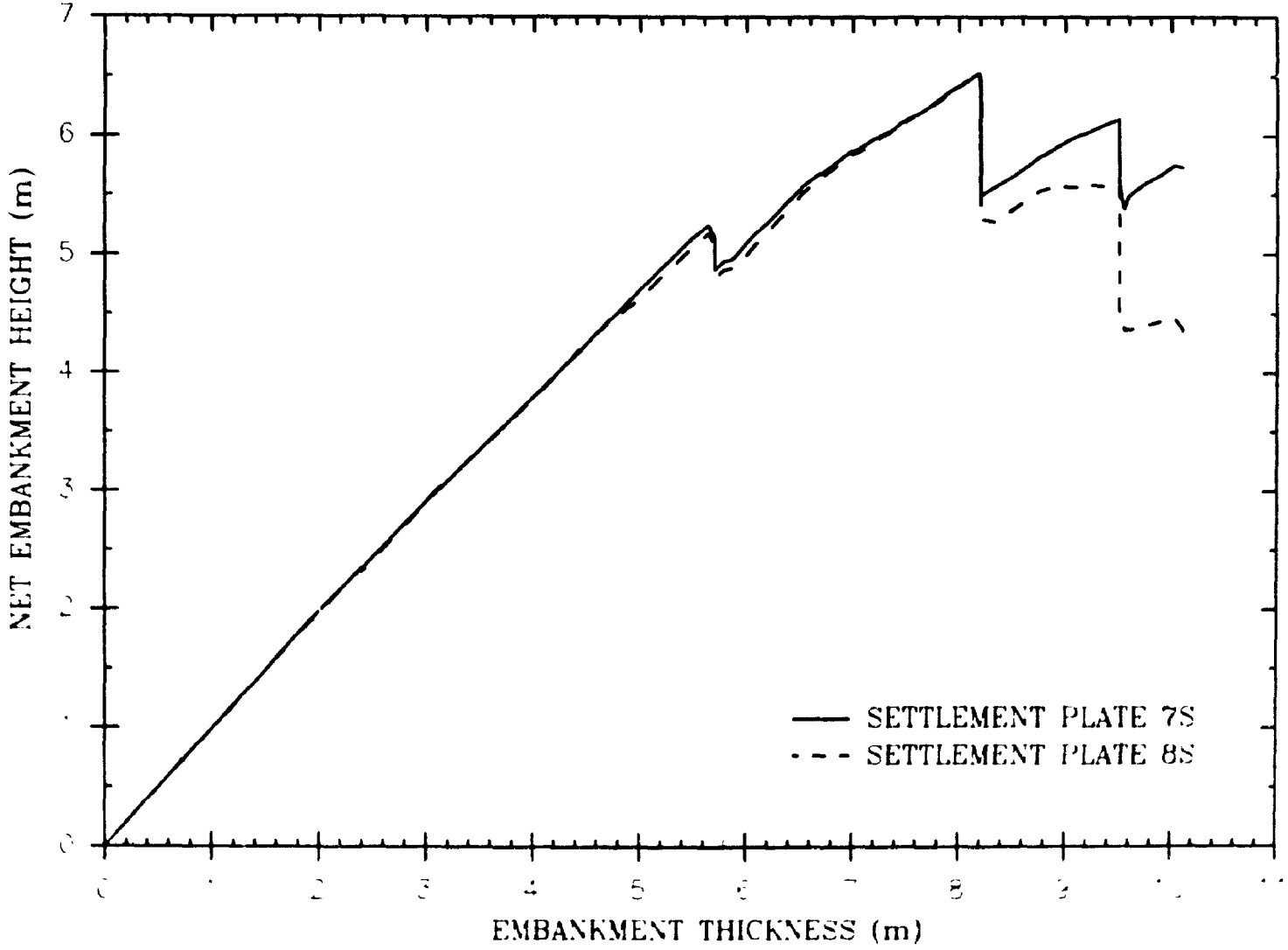

FIGURE 4.32 VARIATION OF NET EMBANKMENT HEIGHT WITH EMBANKMENT THICKNESS FOR SETTLEMENT PLATES 7S AND 8S

the construction of the embankment from 5.7 m to 8.2 m. It is considered that it was possible to construct the embankment beyond the thickness of 5.7 m only because of the influence of the geotextile. A change in slope for the net embankment height versus thickness plot was observed at a thickness of about 6.5 m (i.e. at a net embankment height of about 5.5 m). However, the embankment continued to stand intact until the thickness was increased to 8.2 m. Evidence for the initiation of rotational type failure occurred when the embankment thickness reached 8.2 m. At this thickness, a crack opened up on the ground at the outer limit of the major heave zone, north of the embankment. Cracks on the crest of the embankment were also observed as detailed earlier (see Fig. 4.25).

The variation of net embankment height with thickness followed along the same slope when the thickness was raised above 8.2 m (Fig. 4.32). However, a marked change in the slope of the net height versus thickness plot was observed (especially at settlement plate 8S) at a thickness of about 8.75 m, i.e. at a net height of 5.5 m, indicating the onset of failure of the embankment. When the thickness was increased further, the net height at settlement plate 8S remained the same indicating that the net height of the embankment could not be increased above 5.6 m. The embankment could therefore be considered to have failed at a net height of 5.6 m with the corresponding thickness of 8.75 m. This was a plastic-type failure, the type predicted for reinforced embankments on soft soils by Rowe and Soderman (1987).

At 9.5 m thickness, a rotational failure was evidenced from the rotational-type deformation of the crest, up to a maximum depth of about 0.5 m closer to settlement plate 8S, and an apparently associated rotational-type deformation of the ground north of the toe at the outer limit of the major heave zone (see Figs. 4.26 and 4.27). Another crack on the ground further north from the toe and a crack south of the crest were observed at 9.5 m thickness, indicating the development of a secondary failure surface (see Fig. 4.28)

apparently passing outside the geotextile reinforcement. At this stage, very large increases in settlement, up to a maximum settlement of about 4.0 m, and heave at the monitoring points were also observed (see Figs. 4.30 and 4.31).

It is noted that the failure thickness of 8.75 m indicated by this field investigation is significantly above the 8.2 m failure thickness determined from limit equilibrium analysis on the basis of average vane strength profile (and well within the range of 6.6 - 11.1 m determined from the range of vane strength profile). It was observed that the failure thickness of the unreinforced embankment was significantly less than that determined from a similar limit equilibrium analysis (see chapter 3). This observation coupled with the pore pressure and geotextile strain responses (discussed earlier) suggest that the relative benefits of reinforcement may be even greater for the type of (soft compressible organic clayey silt) soils investigated in this test embankment than they are for perfectly plastic or work hardening soils.

4.7 GENERAL COMMENTS ON THE PERFORMANCE OF INSTRUMENTATION

The position monitoring devices (i.e. the settlement plates, augers and heave plates) performed very well during the entire construction and monitoring period. The electronic distance measuring apparatus allowed quick readings and automatic recording on a computer. Failure of the embankment was associated with large deformations (e.g. settlement exceeded 4 m in plate 8S, heave exceeded 2 m and the horizontal displacement exceeded 1.1 m at heave plate 4H) as discussed previously, and alternative deformation monitoring devices (e.g. profilometers) would have failed well before the embankment deformations were complete.

The inclinometers provided useful data up to about 5.7 m thickness and could not be monitored afterwards owing to the relatively large movements. However, they provided a clear indication for the onset of initial failure of the foundation soil. All the pneumatic piezometers functioned well and provided useful data for most of the construction period, at least up to about 8.2 m thickness. Out of the 30 pneumatic piezometers functioning at the beginning of construction, 25 were still functioning and appeared to be giving reasonable readings. These piezometers are still being monitored by U.N.B under the direction of Dr. A. O. Landva.

The Casagrande piezometers were found to be slow to respond to the rapid construction and the data collected from them were not given any significance for the interpretation of the behaviour.

4.8 SUMMARY AND CONCLUSIONS

The instrumentation and field performance of the geotextile reinforced section of the test embankment constructed at Sackville, N.B. has been described. The site conditions, foundation soil properties, properties of the fill material and details of construction and data collection were described in chapter 3. The reinforced section was instrumented with a number of piezometers, settlement plates, augers, heave plates, inclinometers and a total pressure cell (see Fig. 4.1). Details of the instrumentation, their responses with construction and their performance has been described. A relatively high strength polyester woven geotextile (Nicolon style 68300) was used as reinforcement. This was instrumented with a number of electrical, electromechanical and mechanical gauges. The responses of the strain gauges and their performance are described in chapter 5.

The embankment behaved elastically up to about 3.4 m thickness as evident from settlement responses. The inclinometer data and the geotextile strains indicated significant plastic deformation in the soil during the construction of the embankment from 5 to 5.7 m. The geotextile strain responses suggested that the role of geotextile in providing stability to the embankment increased significantly during this construction phase. Even though there was some evidence for dissipation of excess pore pressure during the early stages of construction, there was no indication of dissipation after 2.4 m thickness. The excess pore pressure responses suggested that the foundation soil approached failure at a thickness of about 5.7 m. The inclinometers also indicated large horizontal displacements and became blocked at this thickness. The role of the geotextile in maintaining embankment stability increased dramatically after 5.7 m thickness. It was apparent that it was possible to construct the embankment above 5.7 m thickness only because of the influence of the geotextile, and the reinforced embankment failed at a thickness of about 8.75 m (i.e. at a net height of 5.6 m). The excess pore pressure responses showed some evidence for the susceptibility of the soil to progressive failure but the actual failure was of a plastic type and no classical-type of abrupt failure was encountered during the construction of this embankment. The fact that the failure thickness of the unreinforced embankment was below the predicted range and that the reinforced embankment was well within the predicted range (and significantly above the predicted thickness for the average strength profile) suggests that the relative benefits of reinforcement may be even greater for the type of soils investigated in this test embankment (soft compressible organic clayey silt) than they are for perfectly plastic or work hardening soils.

The instrumentation was in general very successful and it is considered that this field investigation has great potential to enhance the understanding of the behaviour of reinforced embankments on soft organic clayey silt deposits. In particular it has provided

considerable data concerning pore pressures, vertical and horizontal displacement and geotextile strain which can be used in detailed analyses and to aid in the development of improved design methods on geotextile reinforced embankments.

CHAPTER 5

INSTRUMENTATION OF THE GEOTEXTILE AND MONITORING OF GEOTEXTILE STRAIN

5.1 INTRODUCTION

The overall observed behaviour of the reinforced section of the test embankment constructed at Sackville, New Brunswick was described in chapter 4. A relatively high strength polyester woven geotextile was used as the reinforcement which was instrumented with a number of electrical, electromechanical and mechanical gauges. This chapter provides details concerning the instrumentation and monitoring of the geotextile.

5.2 INSTRUMENTATION OF GEOTEXTILE

Geotextile strains were monitored both in the transverse and longitudinal directions. A total of 34 electrical, 7 electromechanical and 7 mechanical strain gauges (to be described below) were installed on the geotextile to measure the strain in the transverse direction. The strain in the longitudinal direction was monitored with four electrical gauges installed at different locations. The electrical gauges were of electrical resistance type (100 mm long gauges manufactured by Micro-Measurements Division, Measurements Group Inc. - Type EP-08-40CBY-120). These gauges are easily damaged and despite considerable care, 5 of the original 38 were damaged during transport and placement of the geotextile in the field. The location of the electrical gauges, together with the electromechanical (ring type) and mechanical strain gauges are shown on Fig. 5.1 (the gauges that did not provide reliable data have been omitted from this figure).

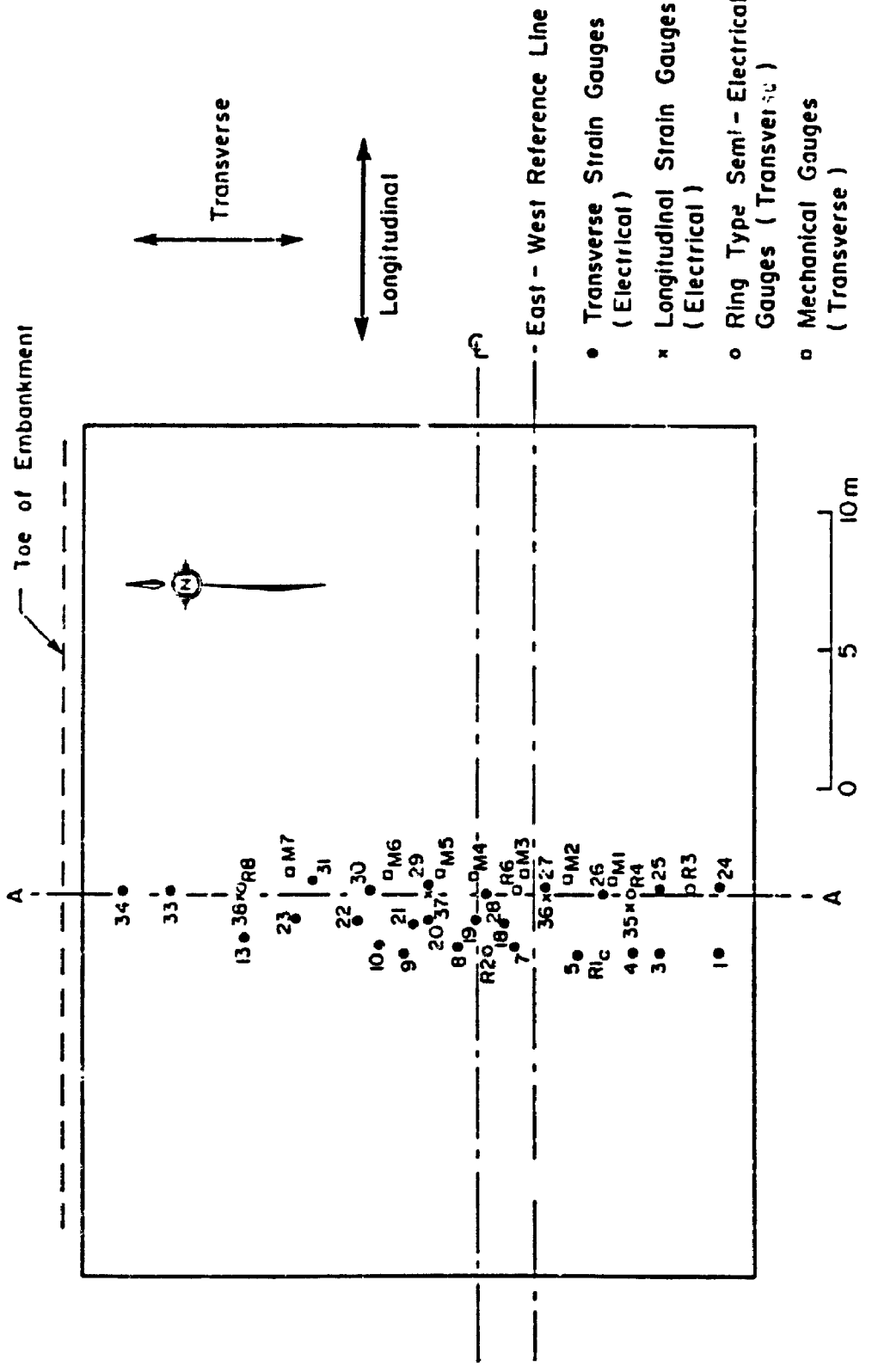

FIG. 5.1 PLAN OF GEOTEXTILE REINFORCEMENT AND LAYOUT OF STRAIN GAUGES

The electromechanical gauge consisted of a thin metal ring fastened to the geotextile, at two diametrically opposite places, by means of fastening plates welded to the ring and small bolts and nuts. The ring end of the fastening plate was narrow and had a 90^{o} angle projection symmetrical to its centre line to provide a gap between the geotextile and the ring (see Fig. 5.2). The strain induced in the ring caused by the deformation of geotextile was measured with two electrical strain gauges (30 mm long strain gauges manufactured by Showa Measuring Instruments Co. Ltd. - Type N11-FA-30-120-11) installed diametrically opposite to each other on the outer surface of the ring. The electrical strain gauges fixed on the ring were calibrated (against the displacement between the support ends of the ring, and hence the strain in the geotextile) to allow an inference of the strain in the geotextile to be made from the observed strain in the strain gauges on the ring. The ring was calibrated by inducing known displacements between the supports using a micrometer arrangement (see Fig. 5.3) and then recording the corresponding readings of the electrical strain gauges. The ring gauges were protected with metal cover pans in the field.

The mechanical gauges monitored the physical movement (and relative movement) of seven points on the geotextile. Each reference point consisted of a 10 mm Dia. bolt passed through the weave of the geotextile and fastened to two stainless steel plates (80 x 80 x 1 mm thick) on either face of the geotextile (see Fig. 5.4). A piano wire was securely fastened to the reference point and directed outside the embankment in the transverse direction. The other end of the wire was connected to a spring which was in turn connected to a fixed reference point outside the embankment. A small but consistent tension was applied to the wire with the use of this spring. The portion of the wire within the embankment was protected with a 20 mm Dia. PVC tubing and a reference bead was mounted on the piano wire outside the toe of the embankment. The reference points were staggered along the East-West direction so that any local failure or damage of the

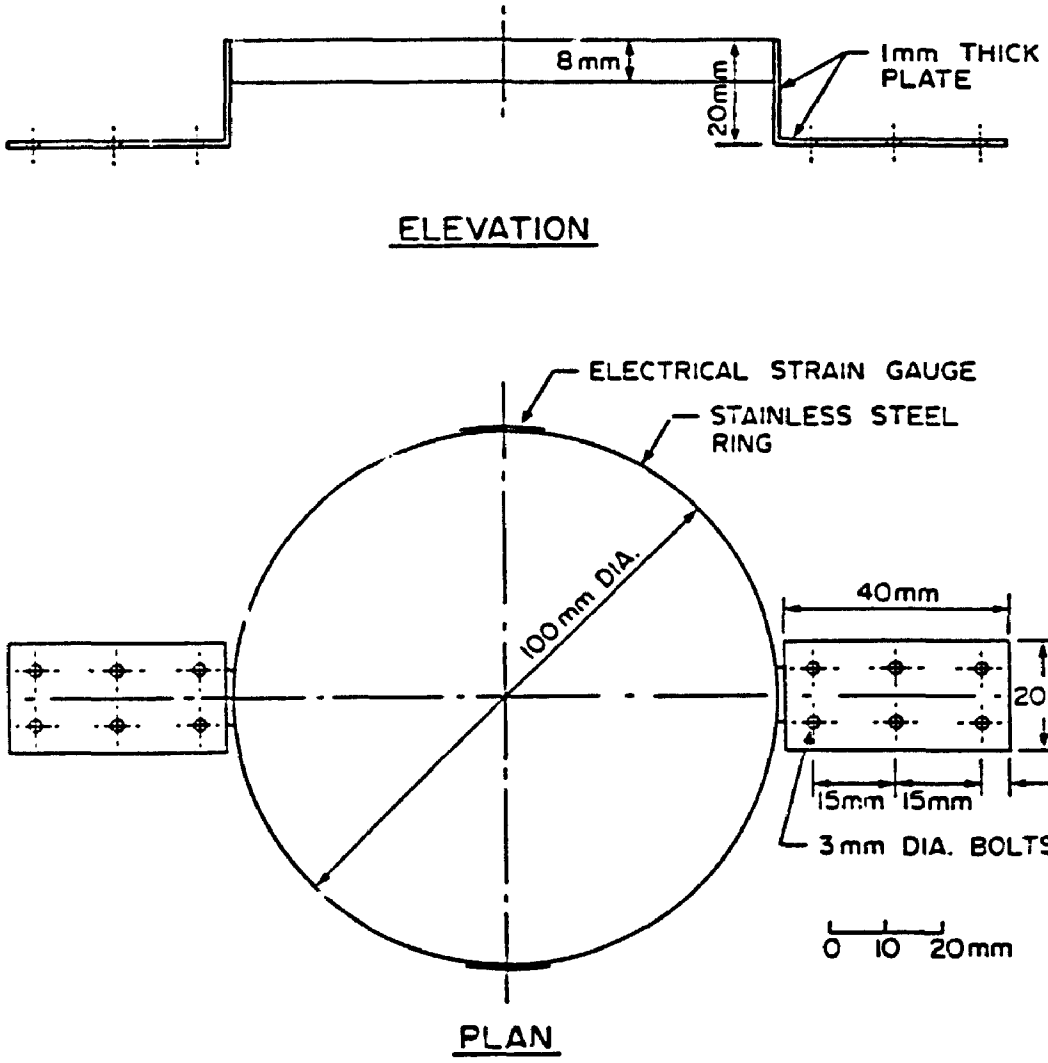

FIG. 5.2 DETAILS OF ELECTROMECHANICAL STRAIN GAUGE

FIGURE 5.3 ARRANGEMENT USED FOR THE CALIBRATION OF RING GAUGES

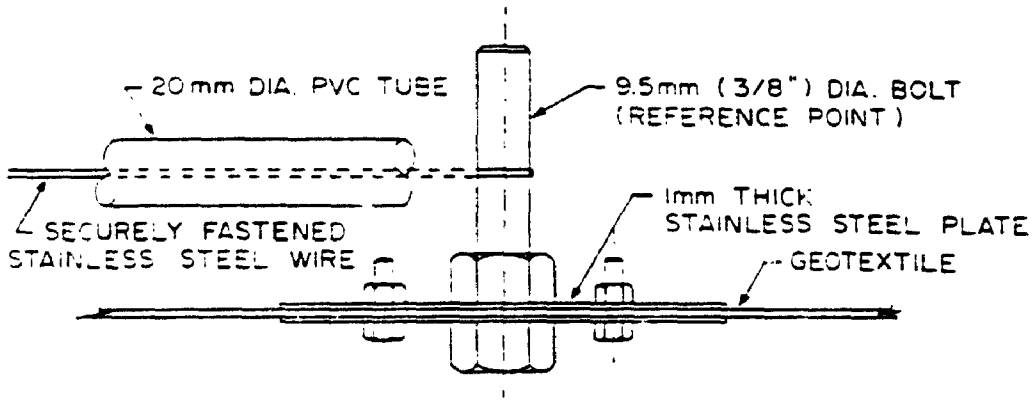

SECTIONAL VIEW OF INSTALLED REFERENCE POINT

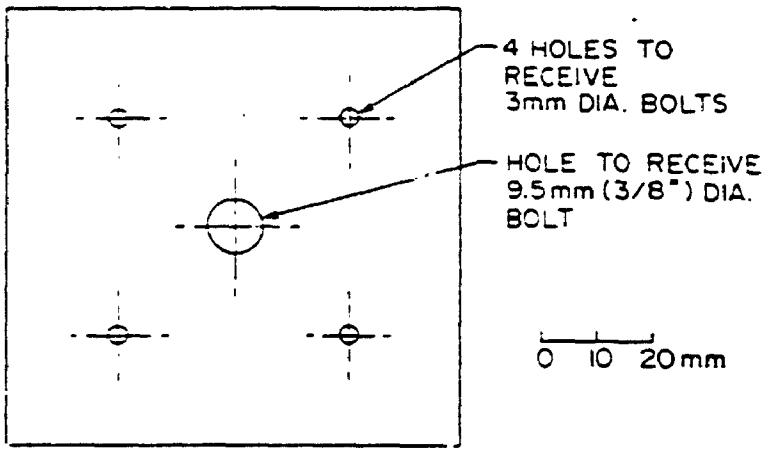

PLAN VIEW OF A STAINLESS STEEL PLATE

FIG. 5.4 DETAILS OF MECHANICAL GAUGE REFERENCE POINT

geotextile would not affect the gauges in the other regions. Each reference point had a separate wire and a separate protective tubing. The physical displacement of the reference bead (i.e. the physical displacement of the reference point) was monitored with respect to the fixed reference point outside the embankment during the entire construction and monitoring period and the corresponding strains were inferred based on the initial length between the reference points (the absolute movement of the reference point was also monitored).

5.3 COMMENTS ON INSTALLATION OF STRAIN GAUGE AND CONSTRUCTION CONSIDERATIONS

The reinforcement used on this project was Nicolon style 68300 multifilament polyester woven geotextile with a unit weight of 631 g/sq. m. The geotextile was factory sewn into 23m x 30 m rectangular section and delivered to a storage area close to the site. A typical tensile force - elongation plot obtained from a wide strip tensile test (Draft CGSB Standard, 1986) performed on a 200 mm wide sample of this geotextile is shown in Fig. 5.5. The average tensile strength properties of this geotextile, determined from five tensile tests, are summarized in Table 5.1. The elastic modulus reported in this table is the slope of the linear (offset) portion of the tensile force - elongation plot.

The geotextile-granular fill interface friction angle (ϕ'_{int}) was determined to be 41.9^{o} using a modified direct shear apparatus (see Fisher, 1985 for the details of the apparatus). The test procedure described by Rowe et al. (1985) was followed for this laboratory determination.

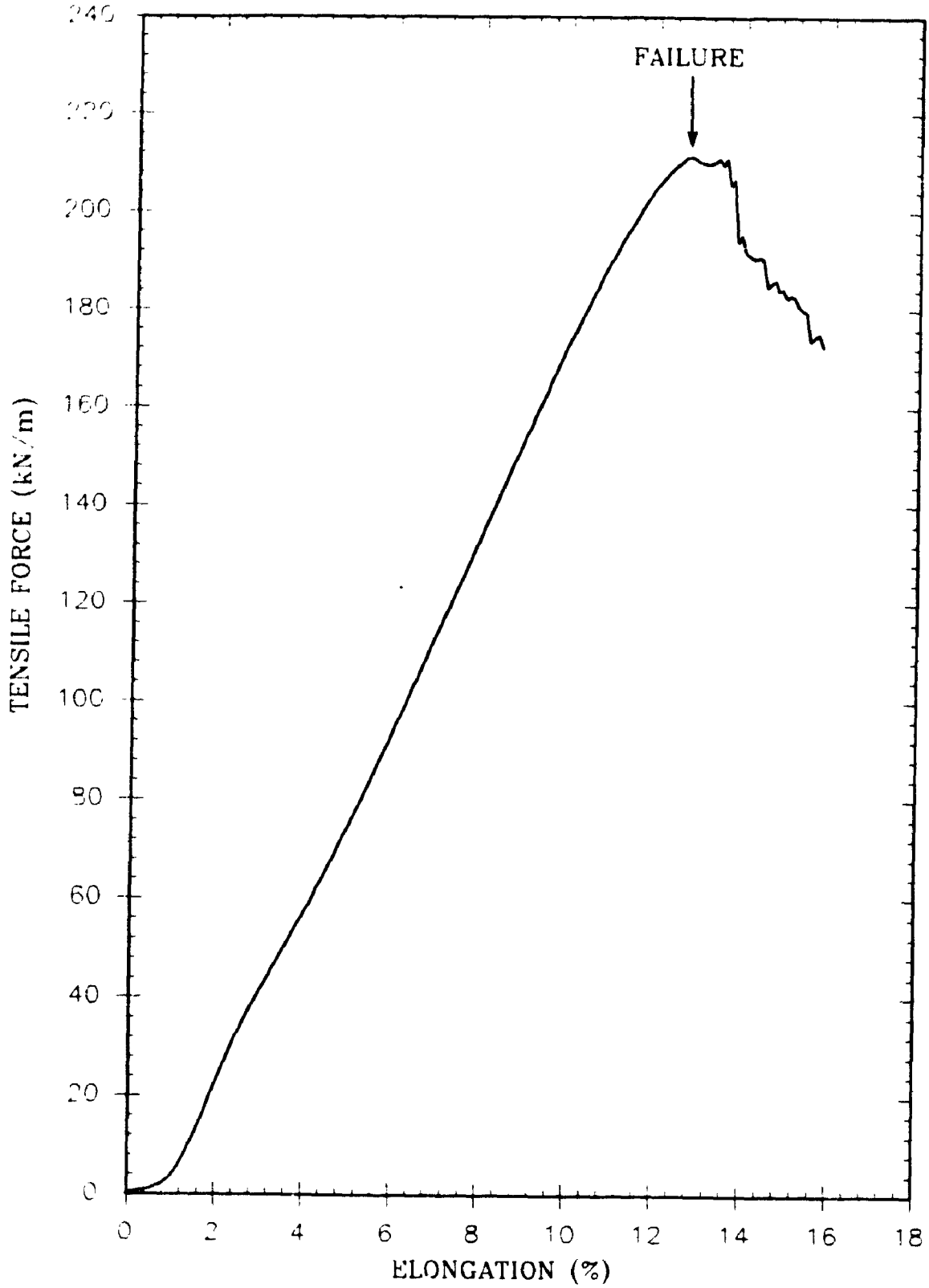

FIG. 5.5 A TYPICAL TENSILE FORCE Vs. ELONGATION PLOT

Table 5.1: Properties of the geotextile

Tensile strength	216 kN/m
Failure strain	13%
Elastic modulus	1920 kN/m
Initial modulus	257 kN/m
Secant modulus(0-5% strain)	1466 kN/m
Secant modulus (0-10%strain)	1678 kN/m

The electrical strain gauges were installed allowing only short lead wires and protected with Dow Corning 3145 RTV adhesive/sealant, under dry conditions in a storage area. All the precautions suggested by Sluimer and Risseew (1982) and Schimelfenyg et. al., (1990) were followed during the installation process. The electrical gauges were installed on the geotextile in a dry storage area near the site. Once installed, the geotextile was transported to the site and placed on a 0.3 -0.5 m thick granular "working platform" which served to provide a level surface. The fastening plates for fixing the electromechanical ring gauges also were bolted to the geotextile prior to moving the geotextile to the site. The mechanical and electromechanical ring gauges were installed after the geotextile was placed in position at the site. Long lead wire electrical connections for the electrical and electromechanical gauges were installed at the site by field soldering. All protective measures such as waterproofing of all the soldering connections with shrink tubing and applying waterproof coatings, encasing the lead cables of the mechanical gauges with plastic tubes and the covering of electromechanical ring gauges with heavy duty metal cover pans were undertaken in a systematic manner to prolong the life of the gauges.

To accommodate large deformations, the lead wires of the electrical and electromechanical gauges were taken along zig-zag paths, in addition to providing extra lengths of wire on a zig-zag form closer to the gauges. The lead wires of the electrical and electromechanical gauges were directed to two data collection stations, one located close to inclinometer 23I and the other close to the inclinometer 26I, and passed through 100 mm Dia. PVC pipes to the top of the embankment (see Figs. 3.2 and 4.1). These pipes were extended with the use of PVC couplings as the construction progressed.

A 0.4 m thick "upper layer" of granular fill was carefully placed over the geotextile without allowing passage of either the trucks or the bull dozer directly on the geotextile. To avoid damage to the strain gauges, spreading of this granular fill directly over the gauges was performed manually for the first lift of fill.

The electrical and electromechanical gauges were monitored with Vishay strain indicator boxes. To facilitate faster reading, the lead wires of the strain gauges were connected through "switch and balance units" (10 channels/strain gauges per unit) to the strain indicator boxes (one strain indicator box per switch and balance unit). Initial readings of all the strain gauges were recorded before placement of any fill over the geotextile.

5.4 GEOTEXTILE STRAIN DEVELOPMENT WITH TIME

The variation of geotextile strain as measured from different strain gauges with time are shown in Figs. 5.6 to 5.15. The layout of strain gauges on the geotextile reinforcement is shown in Fig. 5.1. For ease of comparison with the construction sequence, the variation of fill thickness with time is also superimposed on these figures and the measurements will be discussed in groups according to the distance of the group

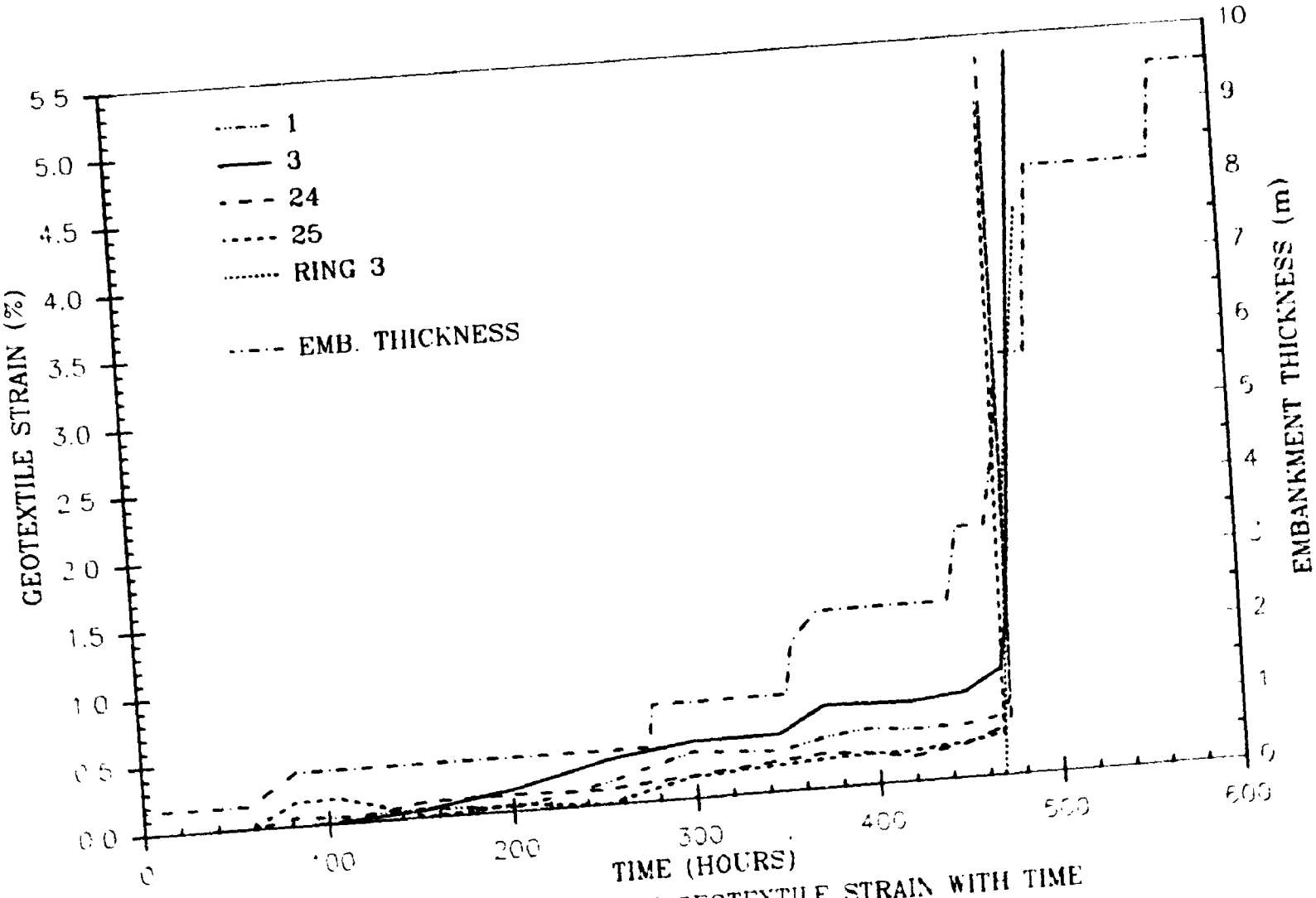

FIG. 5.6 VARIATION OF GEOTEXTILE STRAIN WITH TIME FOR STRAIN GAUGES 1, 3, 24, 25 AND RING 3

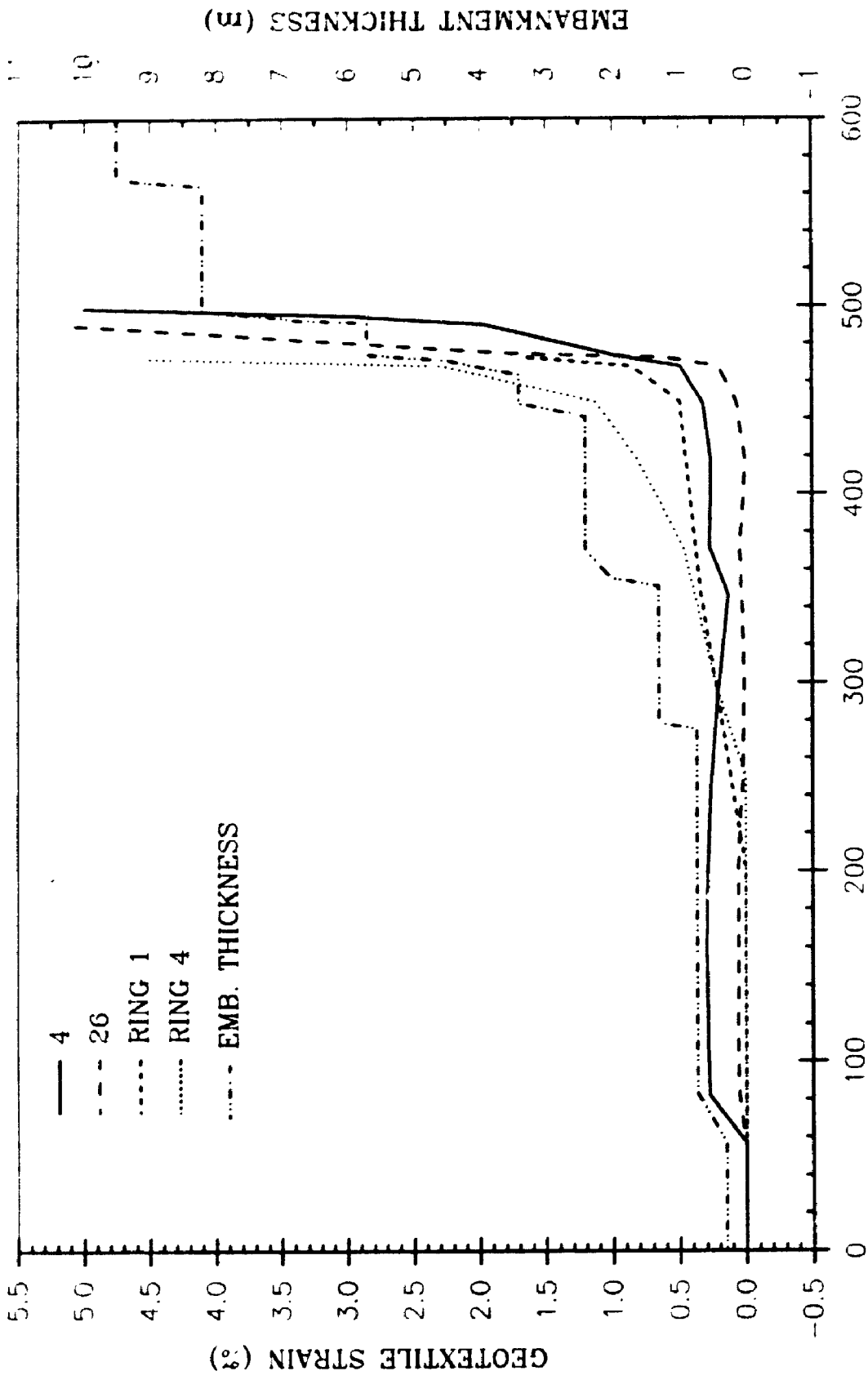

FIG. 5.7 VARIATION OF GEOTEXTILE STRAIN WITH TIME FOR GAUGES 4, 26, RING 1 AND RING 4

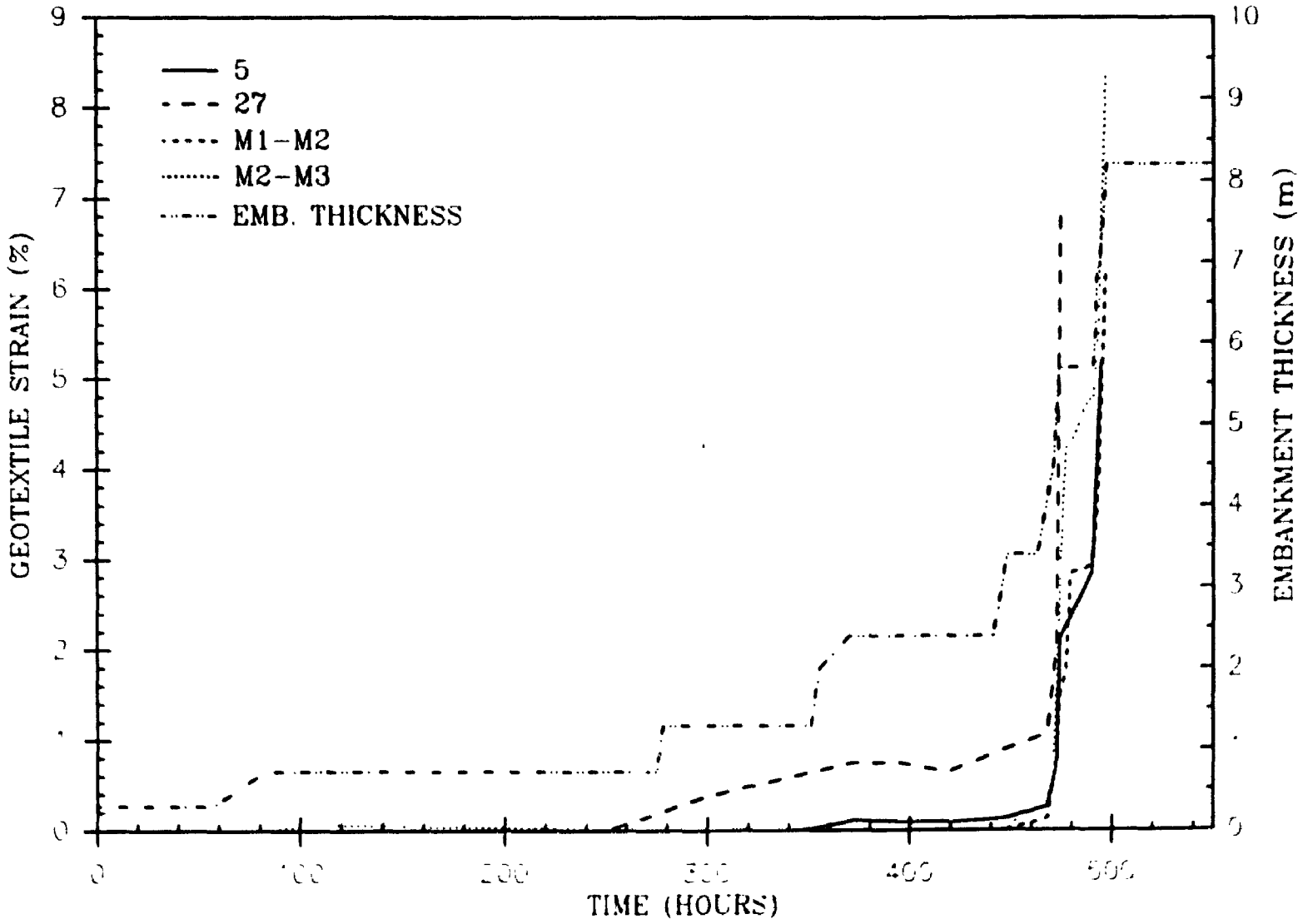

FIG 5.8 VARIATION OF GEOTEXTILE STRAIN WITH TIME FOR GAUGES 5, 27, M1–M2 AND M2–M3

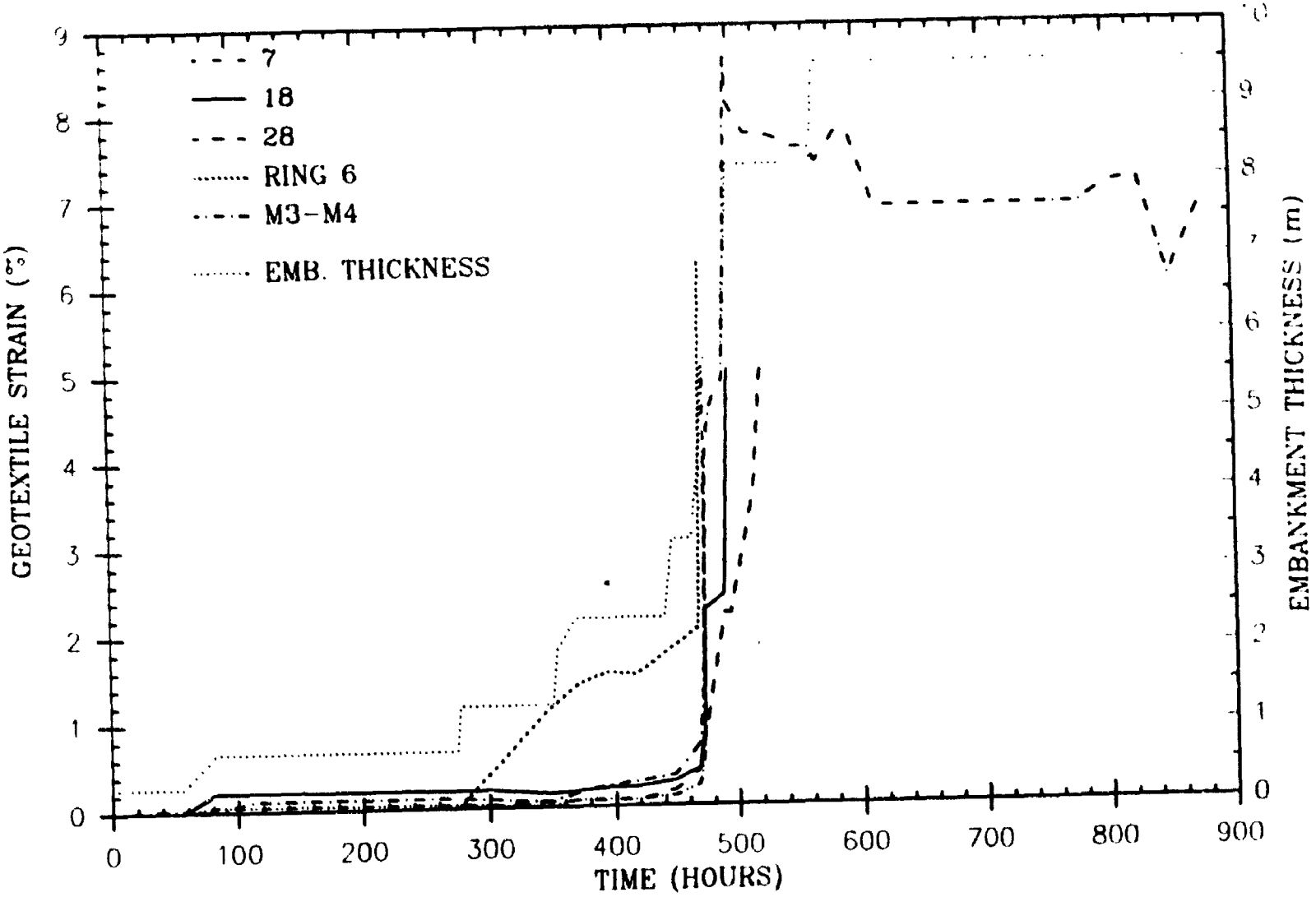

FIG. 5.9 VARIATION OF GEOTEXTILE STRAIN WITH TIME FOR GAUGES 7, 18, 28, RING 6 AND M3-M4

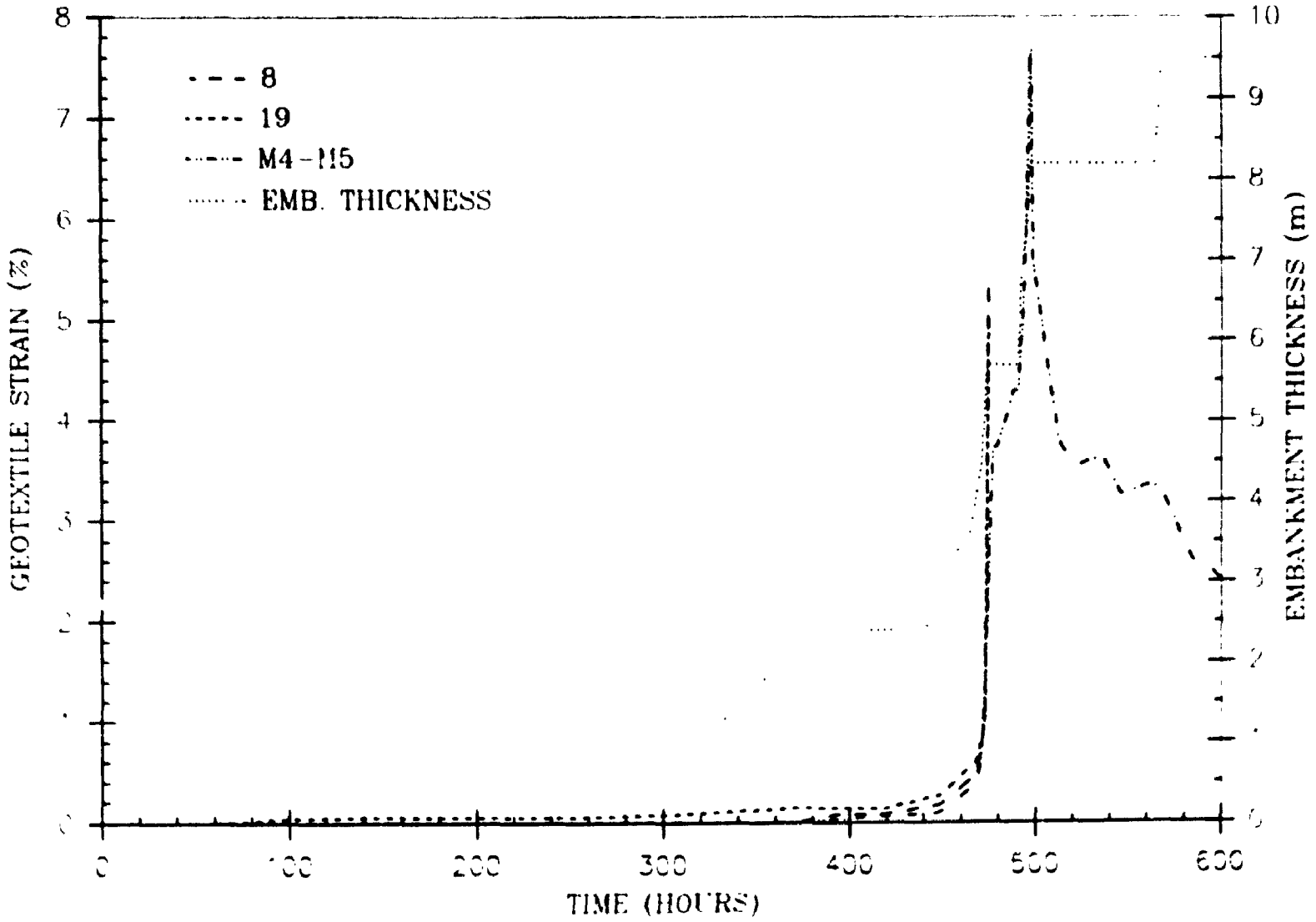

FIG 5.10 VARIATION OF GEOTEXTILE STRAIN WITH TIME FOR GAUGES 8, 19 AND M4-M5

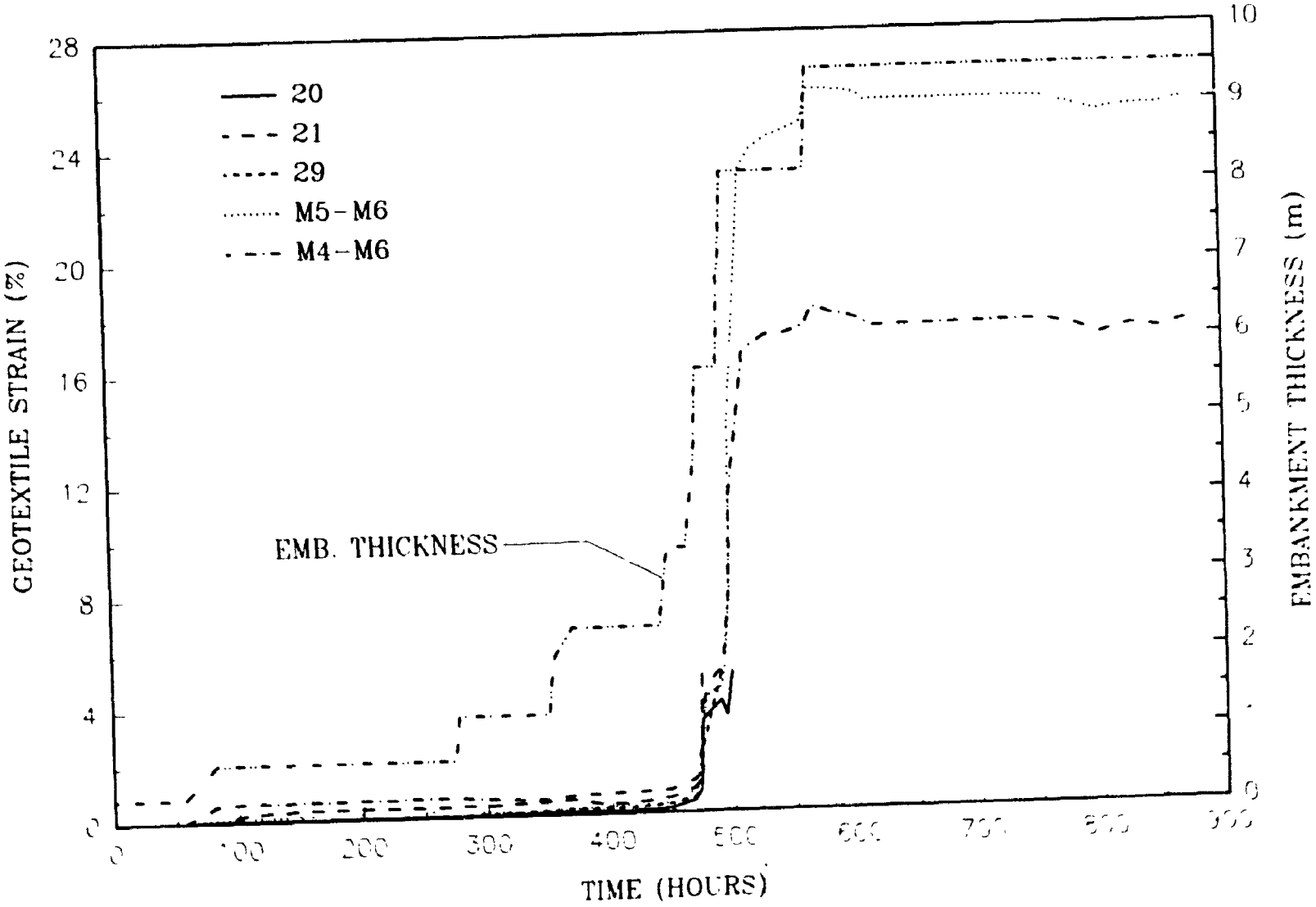

FIG 5.11a VARIATION OF GEOTEXTILE STRAIN WITH TIME FOR GAUGES 20, 21, 29, M5-M6 AND M4-M6

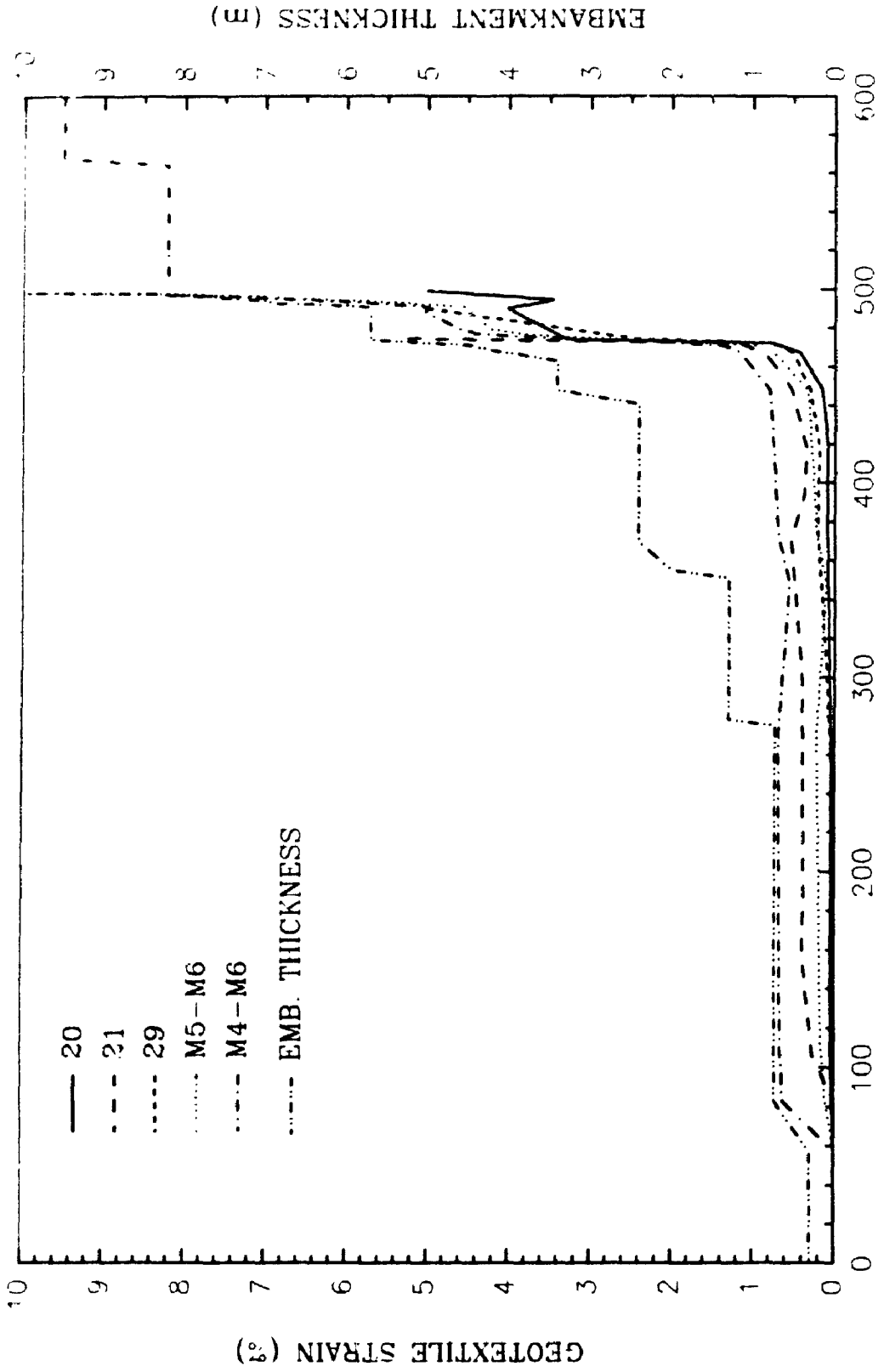

FIG. 5.11b VARIATION OF GEOTEXTILE STRAIN WITH TIME FOR GAUGES 20, 21, 29, M5–M6 AND M4–M6

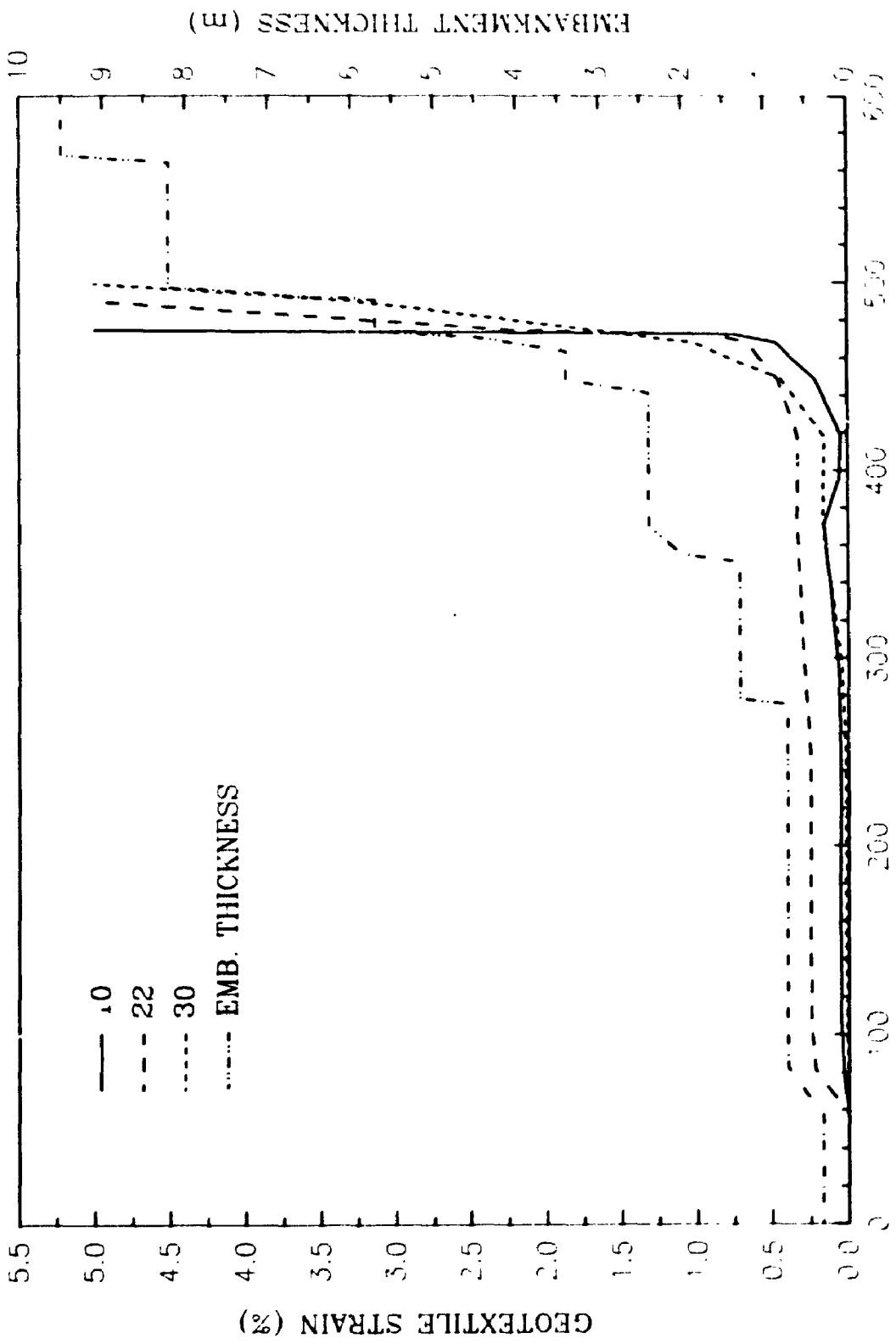

FIG 5.12 VARIATION OF GEOTEXTILE STRAIN WITH TIME FOR STRAIN GAUGES 10, 22 AND 30

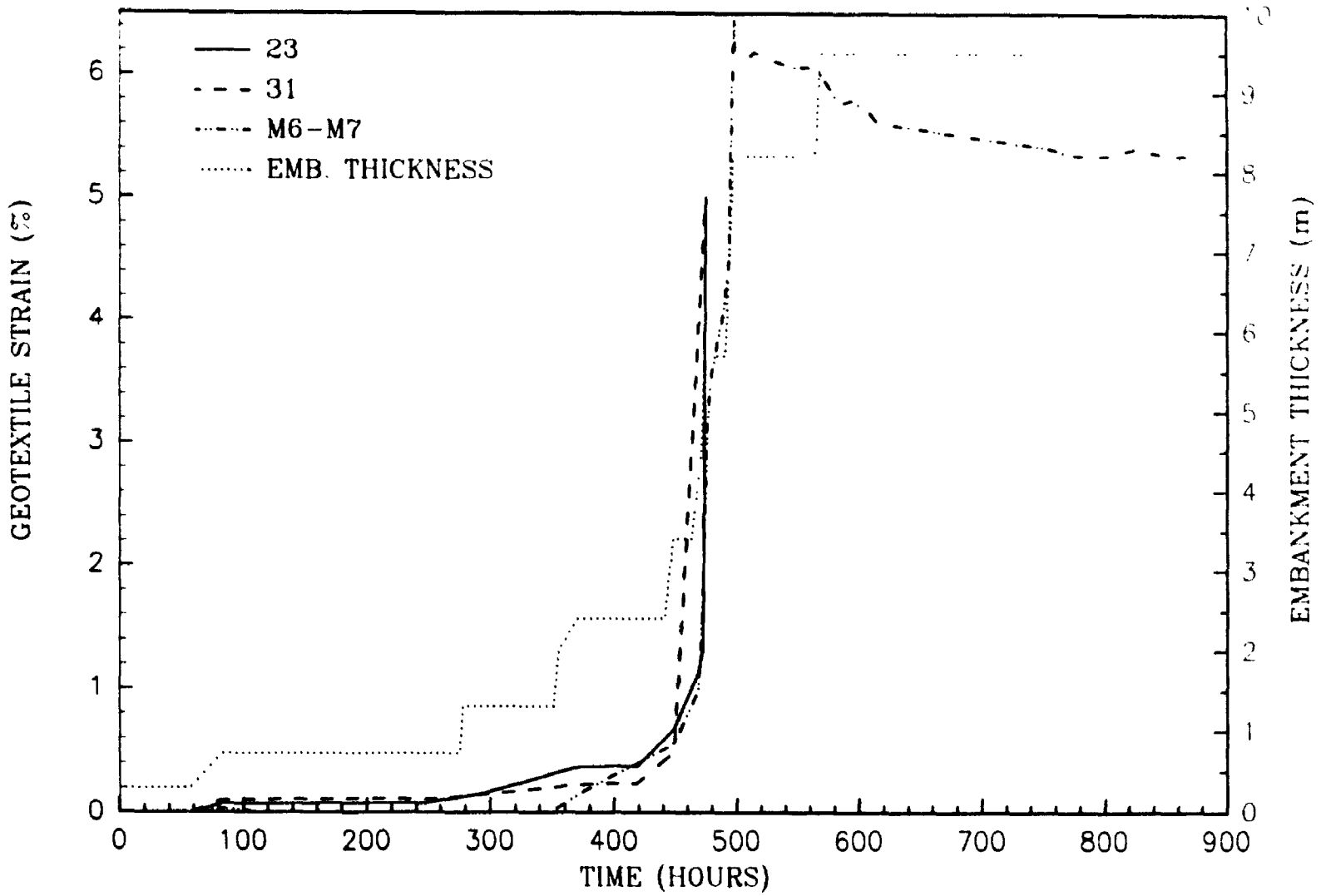

FIG. 5.13 VARIATION OF GEOTEXTILE STRAIN WITH TIME FOR GAUGES 23, 31 AND M6-M7

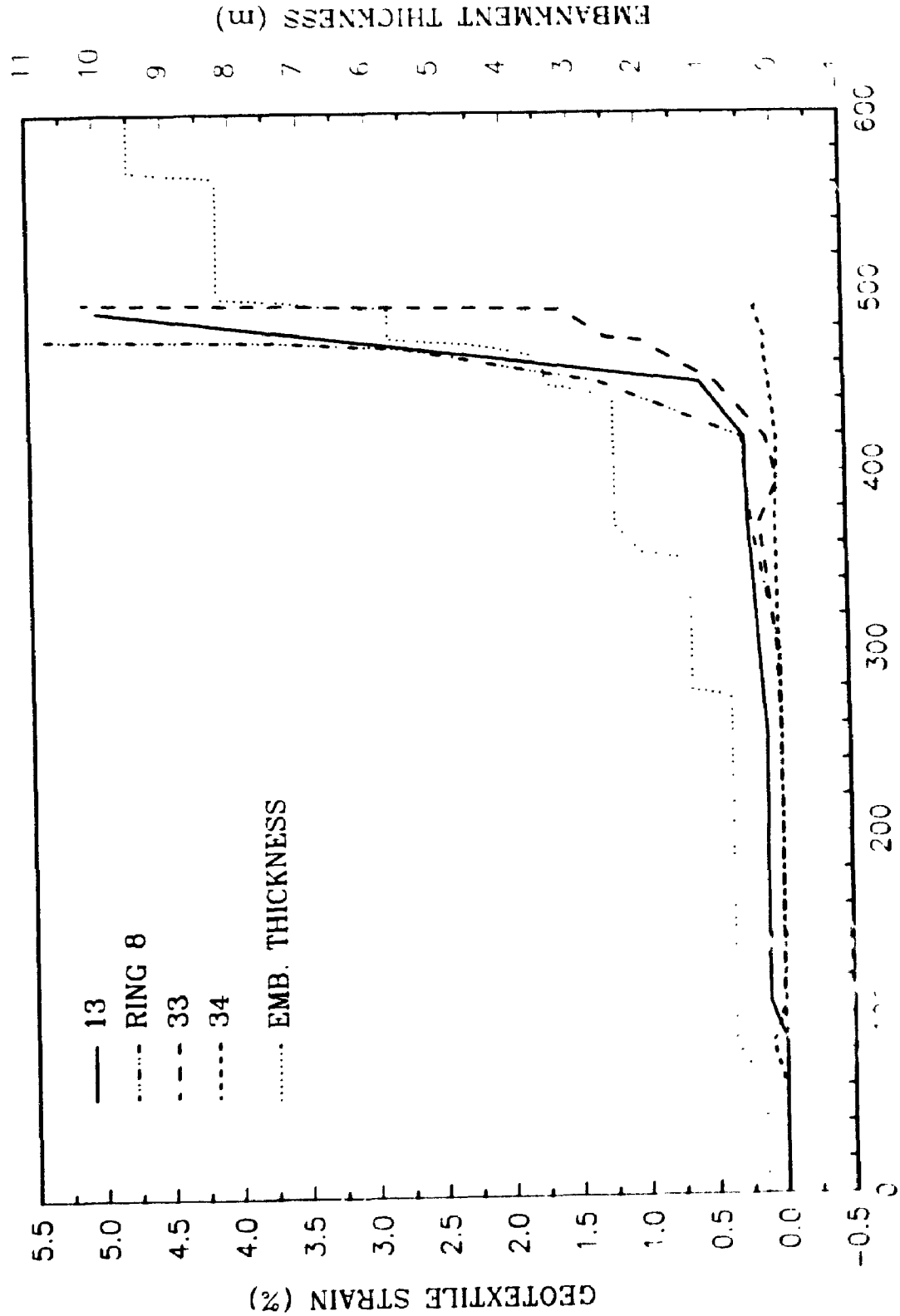

FIG 5.14 VARIATION OF GEOTEXTILE STRAIN WITH TIME FOR GAUGES 13, 33, 34 AND RING 8

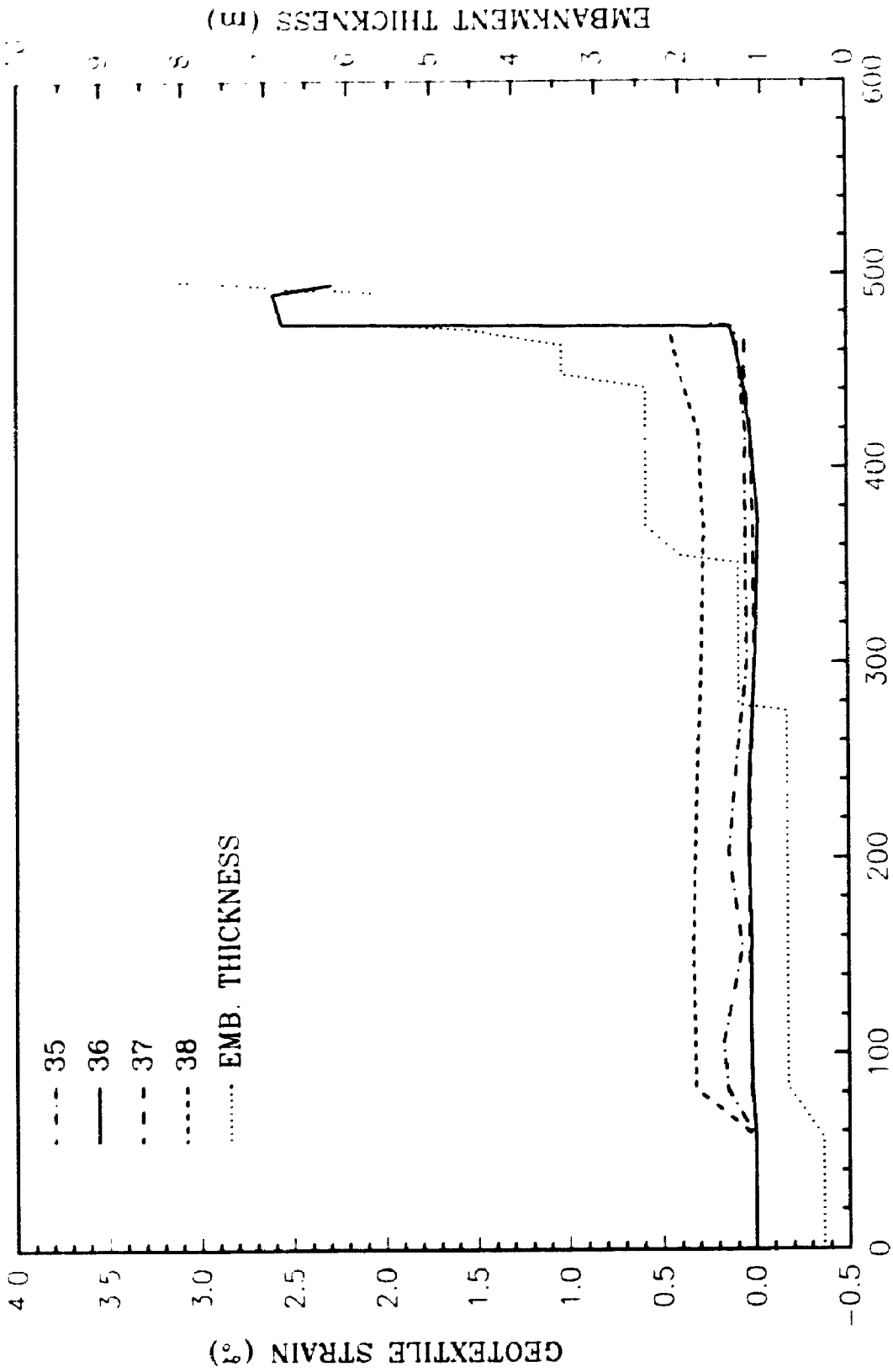

FIG. 5.15 VARIATION OF GEOTEXTILE STRAIN WITH TIME FOR LONGITUDINAL GAUGES 35, 36, 37 AND 38

of gauges from the toe of the embankment.

Drops in strain readings were recorded in many gauges between 83 - 275 hours when the embankment was at a constant thickness of 0.7 m. This is considered to be due to self-adjustment of the geotextile eliminating the initial slackness and any small wrinkles induced during installation. During early stages of construction (up to about 3.4 m thickness), the foundation soil underwent some consolidation as evidenced by the dissipation of pore pressures (see chapters 3 and 4). It is speculated that consolidation also may have contributed to the decrease of strain at 0.7 m thickness.

All these figures indicate that the strains in the geotextile were comparatively small (< 1.3%, except ring 6 which indicated strains of up to about 2%) up until 448 hours when the embankment reached 3.4 m thickness. The strain increased rapidly (in some cases to above 5%) when the embankment thickness was increased from 3.4 to 5.7 m between 448 and 475 hours. Many of the electrical strain gauges became defective when the embankment was constructed from about 5 to 5.7 m (between 472 - 475 hours). Excessive horizontal and vertical displacements in the inclinometers and settlement monitoring points were observed during this construction phase as reported in chapter 4. It was not possible to monitor most of the electrical strain gauges after 5.7 m thickness, probably due to the damages caused to the cables by excessive movements.

5.4.1 Gauges between 20.5 and 22.5 m from the toe of embankment

The strain - time responses indicated by all the gauges in this region are shown in Fig. 5.6. The strains in these gauges (1, 3, 24, 25 and ring 3) were less than about 0.8% until 468 hours when the embankment was constructed up to about 4.1 m thickness. The strain in gauge 3 was significantly larger than that of gauge 1 during this period. However,

gauges 24 and 25 indicated a somewhat lower strain than gauges 1 and 3, and ring 3 did not show any significant strain during this period. Rapid increase in the geotextile strain was observed in these gauges between 468 and 475 hours (i.e. during the construction of the embankment from 4.1 to 5.7 m) and between 475 and 490 hours (when the fill thickness was constant at 5.7 m). An increase of strain from about 0.3 to 5% was recorded at gauge 24 between 468 and 472 hours (i.e. when the fill thickness was increased from 4.1 to 5 m). Gauges 1 and 25 indicated a maximum strain of about 5% and gauge 24 indicated a maximum strain of about 5.3% when they ceased to function at about 475 hours (i.e. 5.7 m embankment thickness). Between 475 and 490 hours, the embankment fill thickness was held constant at a thickness of 5.7 m. Both vertical and horizontal deformations occurred during this period and the strain in gauge 3 and ring 3 continued to increase rapidly. Neither of these gauges could be monitored after 490 hours (i.e. above 5.7 m thickness).

5.4.2 Gauges between 18 and 19.5 m from the toe of embankment

Fig. 5.7 shows the strain - time response of all the gauges (4, 26, ring 1 and ring 4) in this region. Gauges 4. 26 and ring 1 indicated small strains (< 0.5%) during the construction of the embankment up to 3.4 m thickness followed by a rapid increase in strain. Gauges 26 and 4 indicated strains of about 1.75 and 1.04% respectively at 475 hours (5.7 m thickness). A continuous large increase of strain from about 1.75 to 5% was indicated by gauge 26 between 475 and 490 hours as the embankment deformed at a constant fill thickness of 5.7 m; it is suspected that this gauge became defective during this period.

The strain at gauge 4 increased from about 1 to 2% between 475 and 490 hours (fill thickness of 5.7 m). The strain then increased from 2% to 5% between 490 and 499 hours

as the embankment was constructed from 5.7 m to 8.2 m thickness. This gauge malfunctioned and could not be monitored after 499 hours.

Ring 4 indicated strains of less than about 1.1% until 448 hours when the embankment was constructed up to 3.4 m thickness. The strain in ring 4 continued to increase (i.e. from about 1.1 to 1.8%) during the period 448-463 hours when the fill thickness remained constant at 3.4 m. This strain continued to increase slowly (up to 2.3%) until 468 hours as the fill thickness was increased to 4.1 m. However as the thickness was increased from 4.1 m to 5 m (468 - 472 hours) there was a rapid increase of strain from 2.3 to 4.6%. Ring 1 also indicated a rapid increase of strain from 0.85 to 1.6% during the same period. Both these ring gauges ceased to function after 472 hours (i.e. above 5 m thickness).

5.4.3 Gauges between 16.6 and 17.6 m from the toe of embankment

The strain - time responses of all the gauges (5, 27, M1-M2 and M2-M3) in this region are shown in Fig. 5.8. The electrical strain gauges 5 and 27 indicated strains of less than about 1% until 468 hours; i.e. until the embankment was constructed up to 4.1 m. Gauge 27 indicated a rapid increase in strain from about 2.1 to 6.9% between 472 and 475 hours during which time the embankment was constructed rapidly from 5 to 5.7 m thickness and it is suspected that this gauge became defective as the embankment approached 5.7 m thickness. Gauge 5 showed an increase of strain from 0.7 to 2.1% between 472 and 475 hours when the thickness was increased from 5 to 5.7 m. The mechanical gauges M1-M2 and M2-M3 did not indicate any significant strain until about 448 hours (3.4 m thickness) but showed rapid increases in strain up to about 1.5 and 2.8% respectively when the thickness was increased to 5.7 m (at about 475 hours).

Gauge 5 and both mechanical gauges indicated rapid increases in strain between 490 and 497 hours when the embankment thickness was increased from 5.7 to 8.2 m. Gauge 5 could not be monitored after 497 hours. The mechanical gauges M1 and M2 could not be monitored after 497 hours due to large movements (i.e. when movement of points M1 and M2 relative to the toe of the embankment exceeded 1 m and the monitoring point on the gauge wire disappeared into the embankment).

5.4.4 Gauges between 14.6 and 15.6 m from the toe of embankment

The electrical gauges 7, 18 and 28 and the mechanical gauge M3-M4 installed in this region indicated strains of less than about 1% until 468 hours (i.e. up to about 4.1 m thickness) but showed rapid increases of strain afterwards (see Fig. 5.9). Ring 6 showed negligible strain up to about 275 hours (0.7 m thickness) followed by an increase comparatively larger than the other gauges in this region up to about 468 hours (i.e. 4.1 m thickness). All the gauges, except gauge 28, in this region indicated large increase of strain between 468 and 472 hours when the embankment was constructed rapidly from 4.1 to 5.7 m thickness. Gauge 7 and ring 6 ceased to function at about 475 hours (i.e. 5.7 m embankment thickness).

Large increases of strain were observed in gauges 18 and M3-M4 between 490 and 497 hours when the embankment thickness was increased from 5.7 to 8.2 m. A drop in strain was observed in gauge M3-M4 when the fill thickness approached 8.2 m (i.e. at about 497 hours) which was followed by a continuous decrease in strain until additional fill was placed. There was a small increase in strain (from 7.4 to 7.7%) between 568 and 584 hours apparently in response to the increase in fill thickness from 8.2 to 9.5 m between 564 and 568 hours. However, the strain then decreased from 7.7 to 6.9% between 594 and 615 hours and remained relatively constant at about 6.9% after 615 hours.

A comparatively small strain increase (0.4 to 0.9%) was recorded at gauge 28 between 468 and 475 hours (during which period the fill thickness was increased from 4.1 to 5.7 m). However, it indicated a continuous increase in strain from 0.9 to 2.2% between 475 and 490 hours (i.e. when the fill thickness was constant at 5.7 m). Again, it indicated a small strain increase (from 2.2 to 2.5%) between 494 and 499 hours during which period the fill thickness was increased from 5.7 to 8.2 m. The strain continued to increase from (2.5 to 5%) between 499 and 521 hours during the brief stoppage of construction at the reinforced section of the embankment at 8.2 m thickness and this gauge could not be monitored afterwards.

5.4.5 Gauges between 13.6 and 14.2 m from the toe of embankment

Fig. 5.10 shows the strain - time response of the gauges 8, 19 and M4-M5 in this region. Gauges 8 and 19 indicated strains of less than about 1% until 472 hours (5 m embankment thickness) and a rapid increase to about 5% when the embankment thickness was increased to 5.7 m (475 hours); but both these gauges ceased to function after 475 hours. The mechanical gauge M4-M5 also indicated small strains (< 0.7%) up to 471 hours (4.5 m thickness) and a rapid increase in strain to about 2.3% when the embankment thickness was increased to 5.7 m (i.e. at 475 hours). The strain in gauge M4-M5 continued to increase rapidly (up to about 3.7%) until 477 hours followed by a moderate increase up to about 4.3% until 490 hours when the fill thickness remained constant at 5.7 m. Further rapid increase in strain (from 4.3 to about 7.7%) was observed in this gauge between 490 and 498 hours during which period the fill thickness had been increased from 5.7 to 8.2 m. A rapid decrease of strain was recorded in this gauge afterward; this was probably due to the large movement of the monitoring point M5 caused by the yielding of the geotextile close to it as discussed later in this chapter. It should be noted that the decreasing trend continued even when additional fill was placed between 564 and 568

hours to increase the thickness from 8.2 to 9.5 m.

5.4.6 Gauges between 11.8 and 12.6 m from the toe of embankment

All the gauges in this region (i.e. gauges 20, 21, 29 and M5-M6) indicated strains of less than about 1.4% until 472 hours (i.e. 5 m thickness) followed by a rapid increase of strain (see Figs. 5.11a and 5.11b). The strain in gauge 21 increased rapidly from about 1.2 to 5.4% between 472 and 475 hours when the fill thickness was increased from 5 to 5.7 m and this gauge ceased to function after 475 hours. Gauge 29 indicated a rapid increase of strain from about 0.8 to 2.4% during the same period (i.e. between 472 and 475 hours) followed by a continuous increase in strain (up to about 5%) until 490 hours when the fill thickness remained constant at 5.7 m and it ceased to function after 490 hours. Gauge 20 indicated a rapid increase of strain from about 0.7 to 3.3% between 472 and 475 hours during which period the embankment thickness was increased from 5 to 5.7 m. This gauge also indicated an increase of strain from 3.3 to 4% between 475 and 490 hours when the fill thickness was constant at 5.7 m. It indicated a drop of strain from 4 to 3.5% between 490 - 495 hours (i.e. during the construction from 5.7 to 7.5 m) followed by a rapid increase of strain to about 5% when the fill thickness was increased to 8.2 m (497 hours) and it could not be monitored after 499 hours (8.2 m thickness). This drop of strain could be attributed to the yielding of the geotextile in the nearby region as discussed later in this chapter.

The mechanical gauge M5-M6 indicated a rapid increase of strain (from about 1.4 to 2.5%) between 472 and 475 hours during which period the embankment was constructed from 5 to 5.7 m thickness. Although the fill thickness was constant at 5.7 m between 475 and 490 hours the deformations continued and were accompanied by a rapid increase of strain (up to 4.2%) until 479 hours followed by a moderate increase (up to

about 4.6%) until 490 hours. The strain in this gauge increased from 4.6 to about 8.5% between 490 and 497 hours (i e. during the construction of the embankment from 5.7 to 8.2 m thickness). Large increase of strain (from about 8.5 to 13.9%, see Fig. 5.11a) was recorded in this gauge between 497 and 498 hours followed by a very large increase of strain (from 13.9 to 23%) between 498 and 512 hours (when the thickness remained constant at 8.2 m); this suggest that the geotextile tore/yielded at about 498 hours.

5.4.7 Gauges between 9.8 and 10.9 m from the toe of embankment

The variation of strain with time for the gauges 10, 22 and 30 in this region are shown in Fig. 5.12. All these gauges indicated strains of less than about 1% until 468 hours (i.e. 4.1 m fill thickness). Rapid increases of strain were indicated between 468 and 475 hours in all these three gauges (i.e. when the thickness was increased from 4.1 to 5.7 m). An increase of strain from about 0.74 to 5% was recorded in gauge 10 between 472 and 475 hours and it is suspected that this gauge became defective when the thickness approached 5.7 m (i.e. at about 475 hours). Gauges 22 and 30 indicated an increase of strain from 0.9 to 2.2% and 1.5 to 1.7% respectively during the same interval of time (i.e. 472 - 475 hours). A continuous rapid increase of strain (from about 2.2 to 5%) was recorded in gauge 22 between 475 and 490 hours when the embankment thickness remained constant at 5.7 m and this gauge could no longer be monitored after 490 hours. Gauge 30 indicated a rapid increase of strain from 1.7 to 3.3% during the same interval of time (i.e. between 475 and 490 hours when the fill thickness was constant at 5.7 m) followed by a rapid increase of strain from 3.3 to about 5% between 490 and 499 hours during which time the thickness had been increased from 5.7 to 8.2 m and it could not be monitored afterwards.

5.4.8 Gauges between 8.15 and 9.5 m from the toe of embankment

The strain - time responses of the gauges 23, 31 and M6-M7 in this region are shown in Fig. 5.13. All these gauges indicated small strains (< 0.7%) until 448 hours (i.e. 3.4 m fill thickness) followed by a rapid increase in strain between 448 and 475 hours (i.e. when the fill thickness was increased from 3.4 to 5.7 m). Neither of the electrical gauges 23 and 31 could be monitored after 475 hours (5.7 m thickness). The strain in the mechanical gauge continued to increase from 2.4 to 3.9% between 475 and 490 hours when the fill thickness was constant at 5.7 m. This gauge indicated a rapid increase in strain (from 3.9 to 6.4%) between 490 and 497 hours when the fill thickness was increased from 5.7 to 8.2 m. A significant drop in the strain was observed in this gauge at about 497 hours when the fill thickness approached 8.2 m which was followed by a continuous decease in strain during the brief stoppage of construction (at the reinforced embankment section) between 497 and 564 hours (8.2 m thickness) as well as afterwards (including the period of further addition of fill to increase the thickness from 8.2 to 9.5 m between 564 and 568 hours). However, it indicated a relatively constant strain of about 5.3% after 755 hours.

It was noted earlier that the strain readings in the mechanical gauge M4-M5 decreased rapidly after the embankment was constructed to 8.2 m thickness (i.e. after 497 hours, see Fig. 5.10). A very large increase of strain, from about 8.5 to above 23% (much higher than the 13% failure strain observed during laboratory tensile tests, see Fig. 5.5), was recorded in gauge M5-M6 between 498 and 512 hours) at 8.2 m thickness (see Fig. 5.11) and it is hypothesized that the geotextile tore/yielded in this region (i.e. near M5). Note that the inferred circular type (primary) failure surface passes through M4 (or near M4, see Fig. 5.16) and it is likely that there is a (shear) failure zone surrounding this failure surface which could extend between M3 and M5.

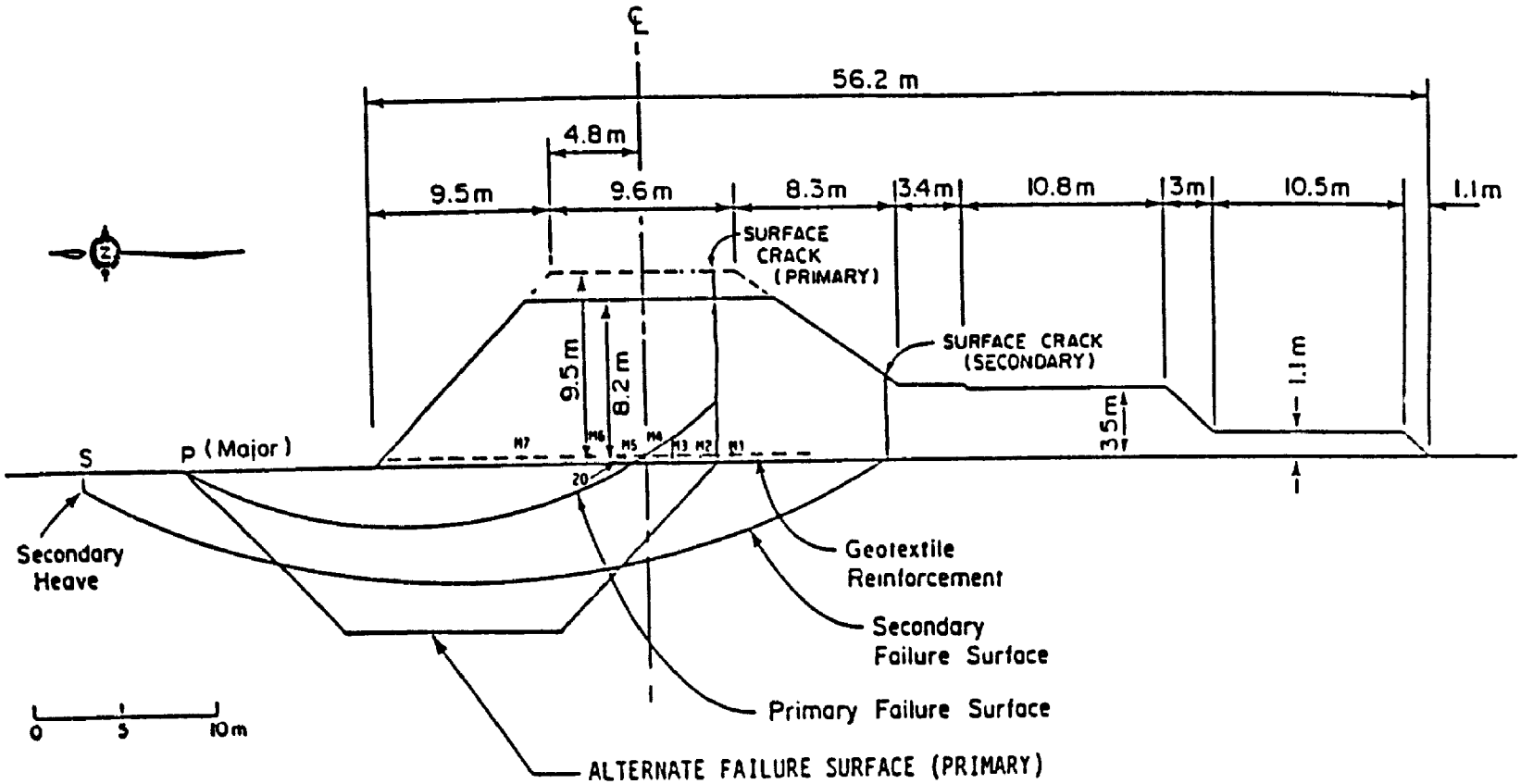

NOTE: FOR CLARITY, ONLY A FEW (SELECTED) GAUGES ARE SHOWN ON THIS FIGURE

FIG. 5.16 INFERRED FAILURE SURFACES OF THE REINFORCED EMBANKMENT AND THE LOCATION OF MECHANICAL STRAIN GAUGES

It was reported that this reinforced embankment showed evidence for rotational type failure at a thickness of about 8.2 m but it failed at a thickness of about 8.75 m and the failure was of plastic type (see chapter 4). Since it was possible to construct up to 9.5 m thickness without any abrupt failure of the embankment, it appears that if the geotextile did rupture close to M5 (i.e. at a distance of about 13 m from the toe), it did not have a dramatic effect on the embankment performance (i.e. the energy released by any such break was absorbed in the soil-reinforcement system).

5.4.9 Gauges between 2.7 and 7.7 m from the toe of embankment

The strain - time responses of the gauges (13, 33, 34 and ring 8) installed in this region are shown in Fig. 5.14. Both the gauges 13 and ring 8 placed at a similar distance from the toe (of about 7.7 m) indicated strains of less than about 1.3% until 448 hours; i.e. until the embankment was constructed up to 3.4 m thickness. Both these gauges indicated rapid increases of strain after 448 hours. An increase of strain from about 0.6 to 3.3% was indicated by gauge 13 between 448 and 475 hours (i.e. when the fill thickness was increased from 3.4 to 5.7 m). The increasing trend continued during the period 475 - 490 hours when the fill thickness remained constant at 5.7 m and this gauge could not be monitored after 490 hours (i.e. when the fill thickness was increased to above 5.7 m). Ring 8 indicated an increase of strain from about 1.3 to 2.2% between 448 and 463 hours (i.e. when the fill thickness remained constant at 3.4 m) followed by an increase of strain from about 2.2 to 2.7% between 463 and 468 hours when the fill thickness was increased from 3.4 to 4.1 m. A rapid increase of strain from 2.7 to 5.4% was recorded between 468 and 475 hours (when the fill thickness was increased from 4.1 to 5.7 m) and this gauge ceased to function after 475 hours (above 5.7 m fill thickness).

Gauge 33 indicated small strains (of less than about 0.45%) until 448 hours (3.4 m

thickness). It indicated moderate increases of strain from 0.45 to 0.9%, from 0.9 to 1.3% and from 1.3 to 1.6% during the periods 448 - 468 hours (i.e. when the fill thickness was increased from 3.4 to 4.1 m), 468 - 475 hours (i.e. when the fill thickness was increased from 4.1 to 5.7 m) and 475 - 490 hours (i.e. when the fill thickness was constant at 5.7 m) respectively. This gauge being located closer to the toe was beneath the shoulder of the embankment for thicknesses above 4.3 m and the surrounding soil did not experience any significant strain or deformation (see the settlement response of settlement plate 6S, chapter 4). The comparatively small increases of strain observed in this gauge can be attributed to the small deformation (or strain) in the surrounding soil. Gauge 34, placed much closer to the toe, indicated smaller strains (< 0.2%) until 495 hours (i.e. 7.5 m thickness) and ceased to function afterwards. However, gauge 33 indicated rapid increases of strain from about 1.6 to 5.1% between 490 and 494 hours (when the fill thickness was increased from 5.7 to about 7.5 m) and it could not be monitored afterwards. This large increase of strain can be due to the development of anchorage force closer to the edge of the geotextile caused by large deformation (or strain).

5.4.10 Longitudinal gauges

Fig. 5.15 shows the strain - time responses of the longitudinal gauges 35, 36, 37 and 38. Gauges 35, 37 and 38 all indicated low strain (< 0.5%) until they ceased to function at about 475, 472 and 468 hours respectively (i.e. 5.7 m, 5 m and 4.1 m thickness respectively); the failure of the gauge was attributed to damage to the wires as a result of the large transverse movements. This behaviour suggests that approximated plane strain conditions existed in the instrumented mid zone (i.e. middle 4m portion) of the 25 m long reinforced embankment, during its construction up to 5.7 m thickness.

Gauge 36 also indicated very low strain (< 0.15%) until 475 hours (i.e. up to about

5.7 m thickness) but showed an increase afterwards. However, it was not clear whether this increase was due to longitudinal strain in the geotextile or was due to damage to the electrical connections and/or cable caused by large transverse movements.

5.5 COMMENTS ON THE VARIATION OF GEOTEXTILE STRAIN WITH EMBANKMENT THICKNESS

The variation of geotextile strain (in the transverse direction, as measured from various gauges) with the embankment thickness is presented in Figs. 5.17 to 5.25. For the convenience of presenting and interpreting the data, the entire instrumented width of geotextile in the transverse direction (i.e. North - South direction) has been divided into several narrow bands parallel to the toe (or longitudinal axis) of the embankment (see Fig. 5.1 for location of gauges). Each of these figures indicate the strains, obtained from different types of gauges (i.e. electrical, mechanical and electromechanical ring gauges) installed in the corresponding narrow band of geotextile, versus the embankment thickness. The mean (i.e. the average) as well as the lower and upper limits of the strain readings are presented separately so that the range of measured geotextile strain at different embankment thicknesses could be interpreted. Most of the electrical and electromechanical ring gauges could not be monitored during the later stages of construction (i.e. especially after 5.7 m thickness) as discussed previously and the limited available data after this stage are presented either as an average, minimum or maximum depending on the amount of data and the magnitude of the data from the electromechanical and mechanical gauges relative to the electrical gauges prior to failure of the latter.

The variation in strain with thickness (e.g. see Fig. 5.19) was similar both before and after the brief stoppage of construction at 5.7 m thickness (i.e. between 475 and 490

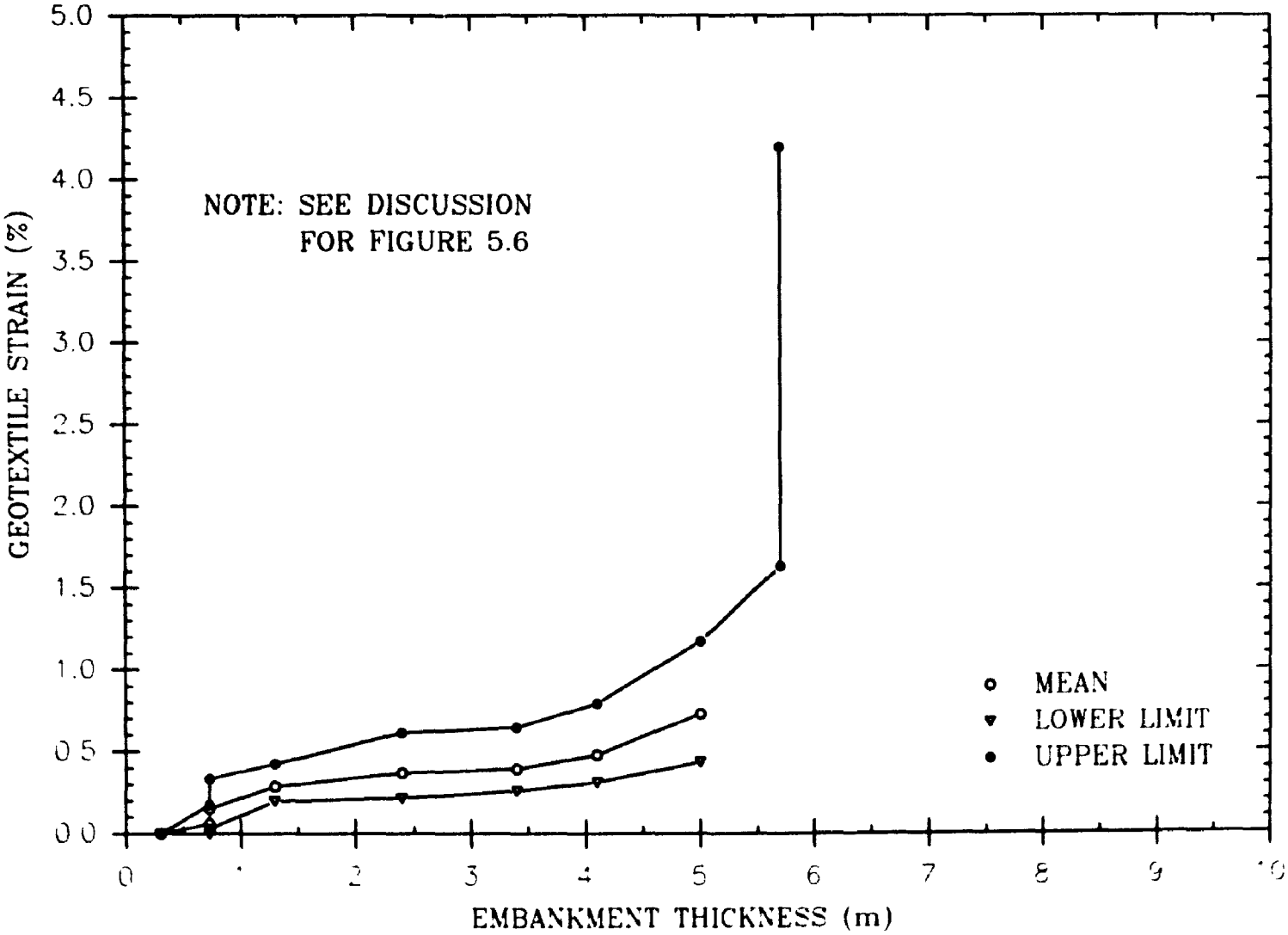

FIG. 5.17 VARIATION OF GEOTEXTILE STRAIN WITH EMBANKMENT THICKNESS FOR GAUGES BETWEEN 20.5 AND 22.5 m FROM EMBANKMENT TOE

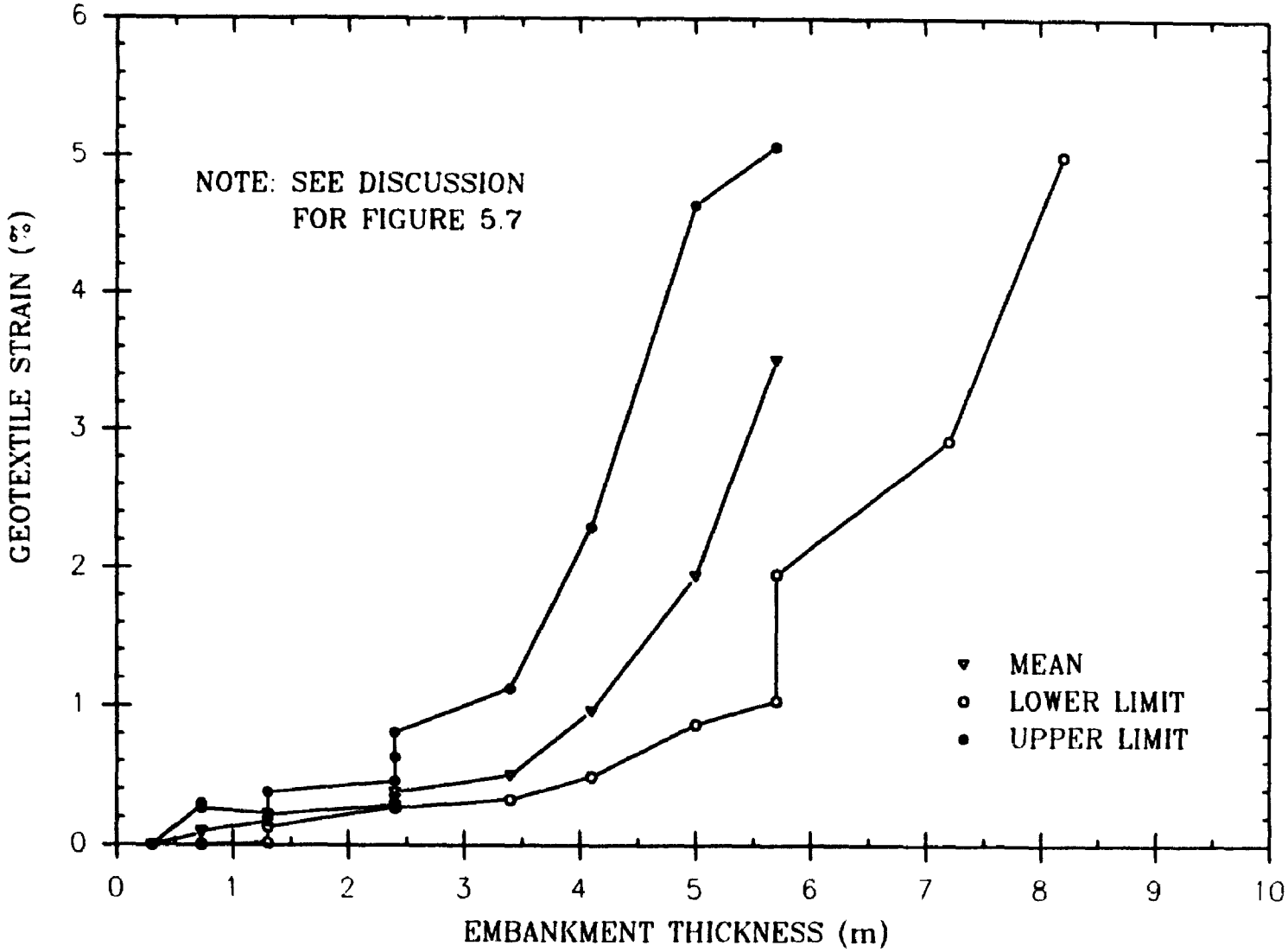

FIG. 5.18 VARIATION OF GEOTEXTILE STRAIN WITH EMBANKMENT THICKNESS FOR GAUGES BETWEEN 18 AND 19.5 m FROM EMBANKMENT TOE

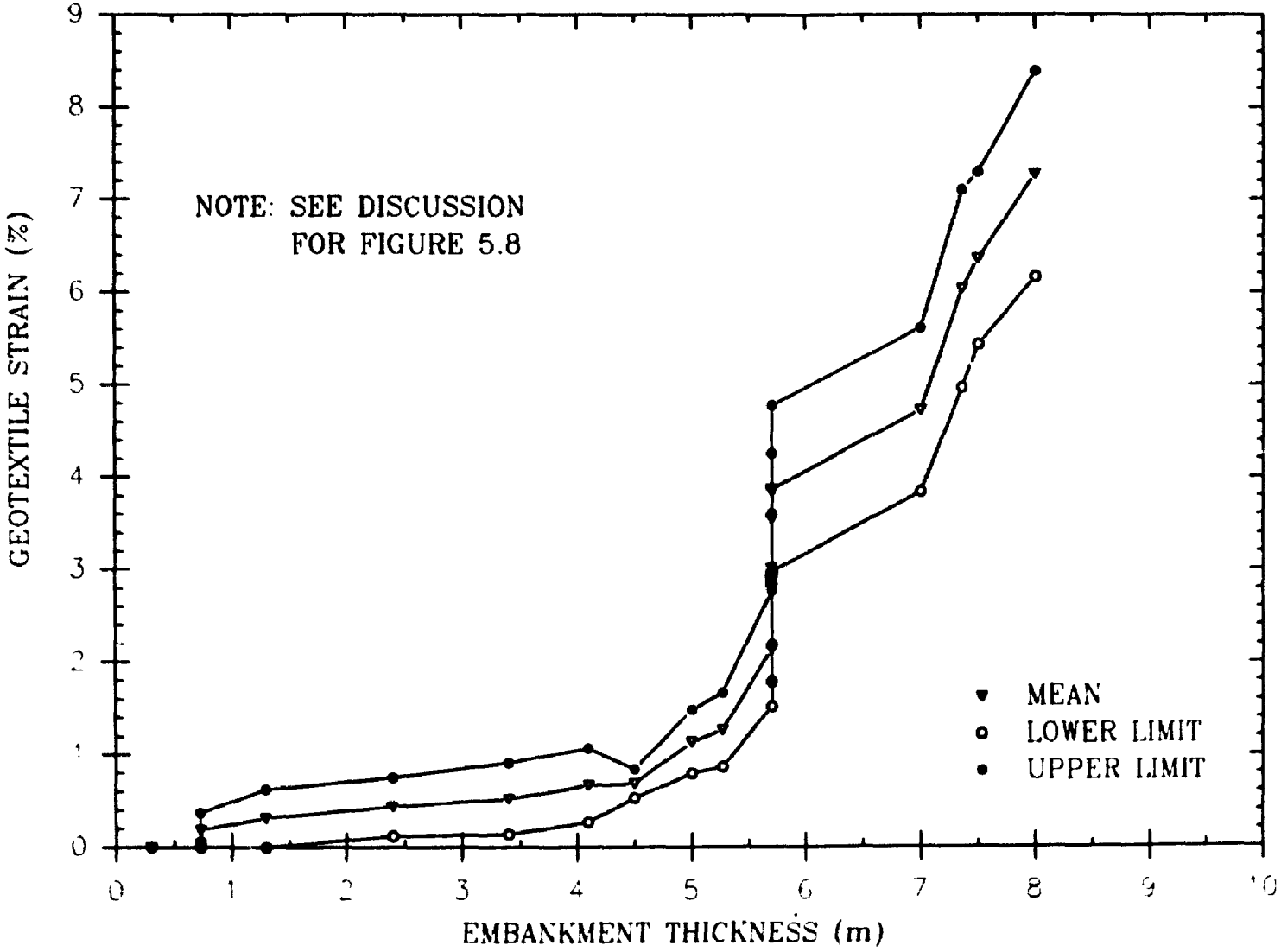

FIG. 5.19 VARIATION OF GEOTEXTILE STRAIN WITH EMBANKMENT THICKNESS FOR GAUGES BETWEEN 16 6 AND 17 6 m FROM EMBANKMENT TOE

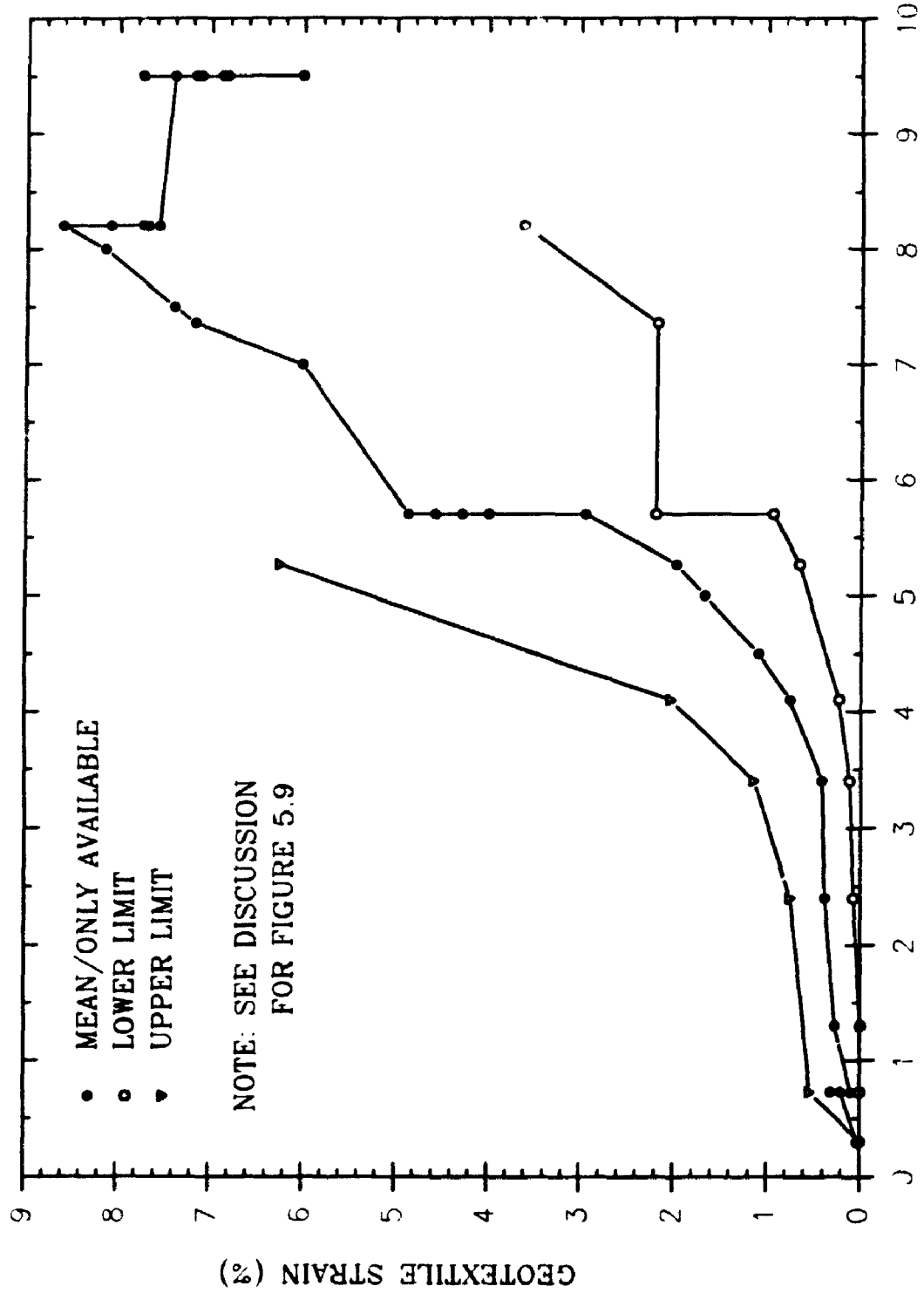

FIG. 5.20 VARIATION OF GEOTEXTILE STRAIN WITH EMBANKMENT THICKNESS FOR GAUGES BETWEEN 14.6 AND 15.6 m FROM EMBANKMENT TOE

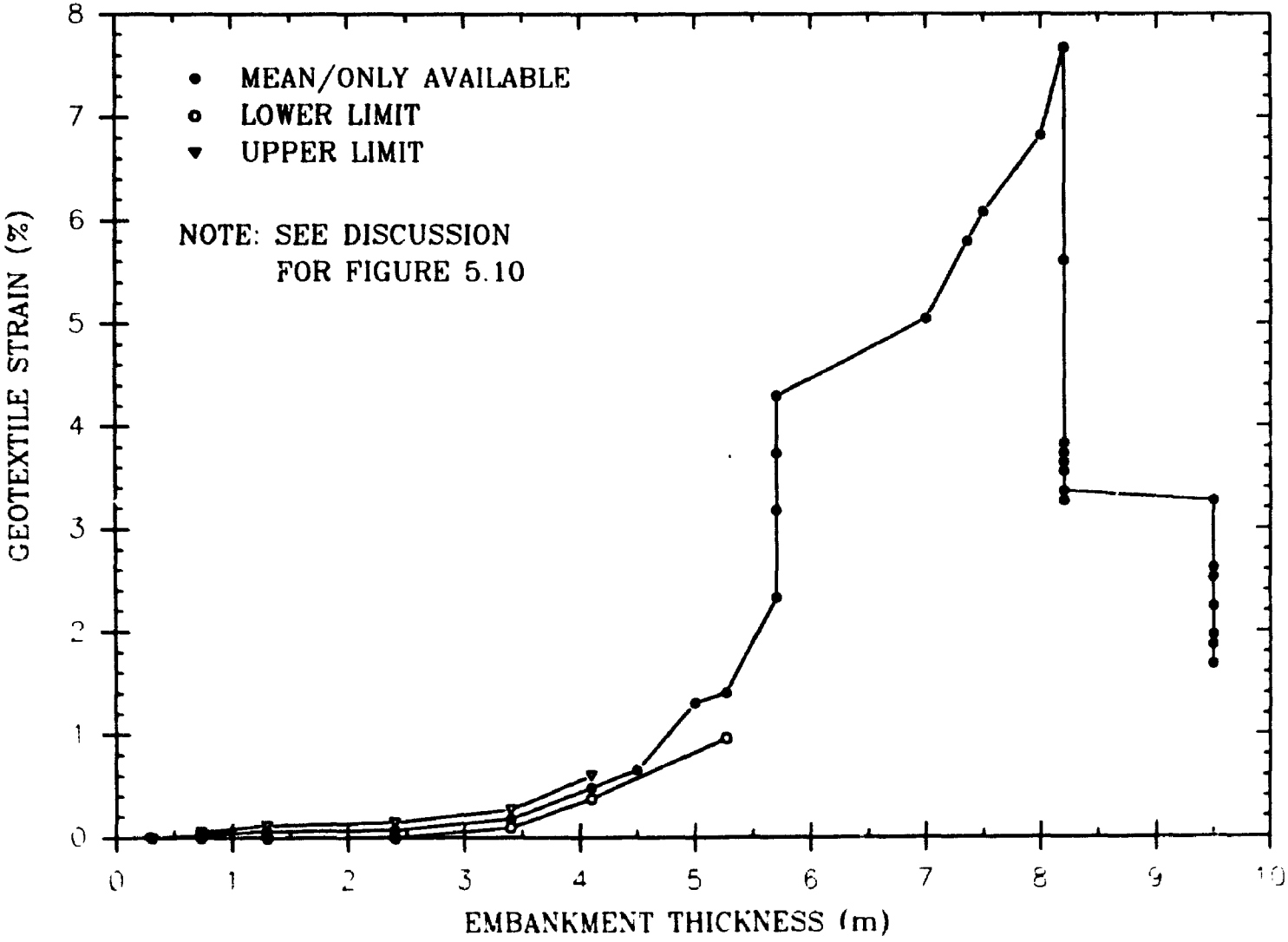

FIG. 5.21 VARIATION OF GEOTEXTILE STRAIN WITH EMBANKMENT THICKNESS FOR GAUGES BETWEEN 13.6 AND 14.2 m FROM EMBANKMENT TOE

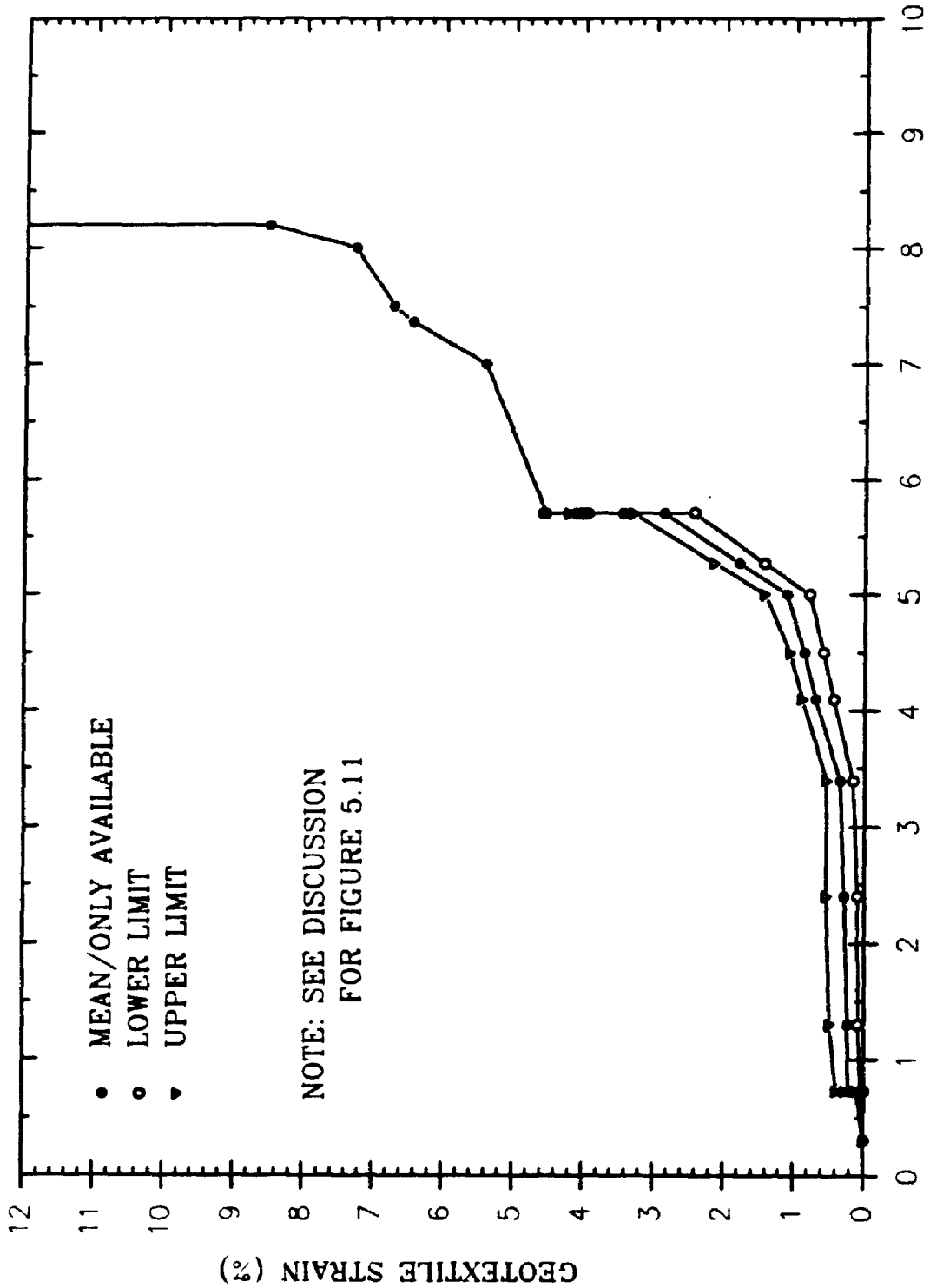

FIG. 5.22 VARIATION OF GEOTEXTILE STRAIN WITH EMBANKMENT THICKNESS FOR GAUGES BETWEEN 11.8 AND 12.6 m FROM EMBANKMENT TOE

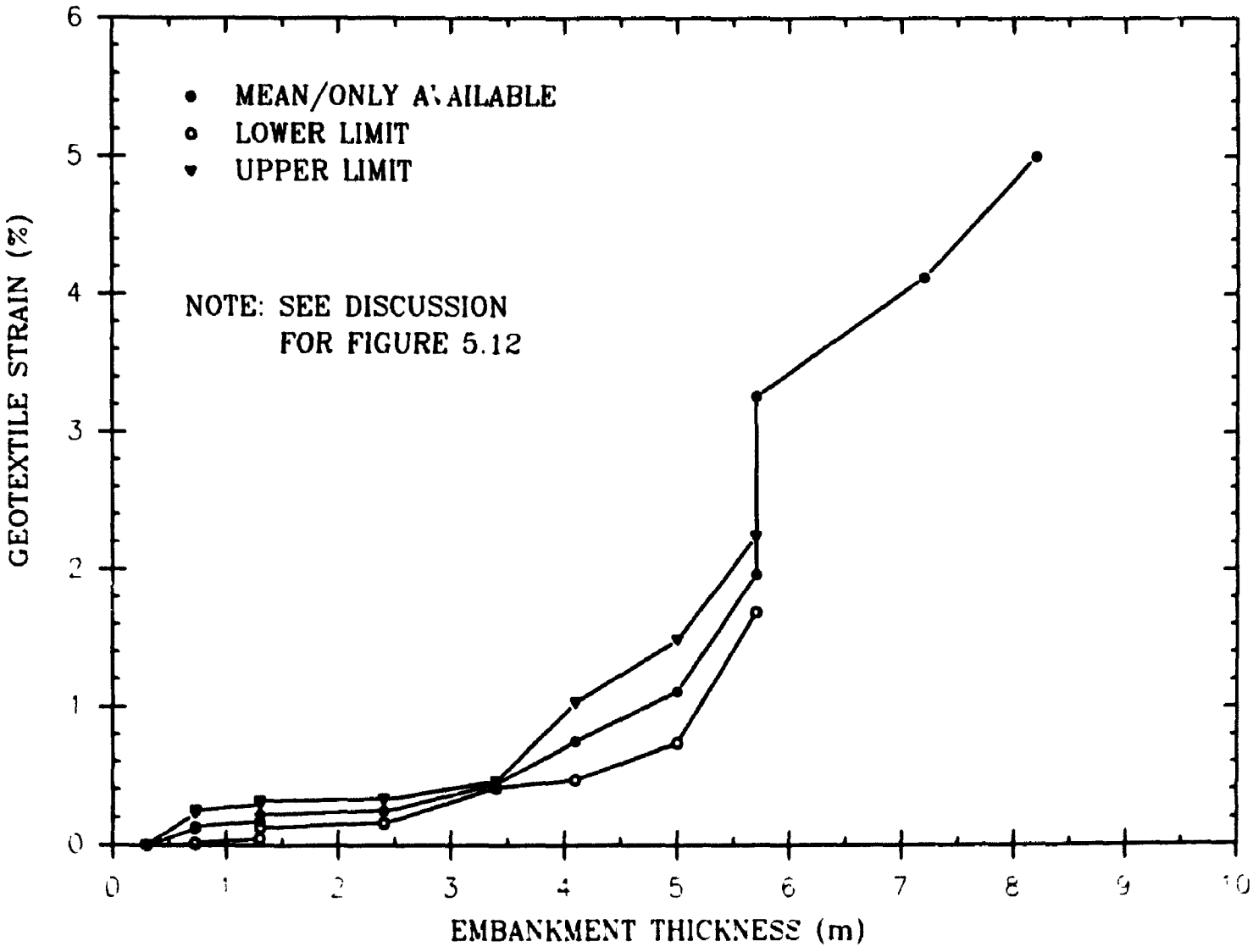

FIG 5.23 VARIATION OF GEOTEXTILE STRAIN WITH EMBANKMENT THICKNESS FOR GAUGES BETWEEN 9.8 AND 10.9 m FROM EMBANKMENT TOE

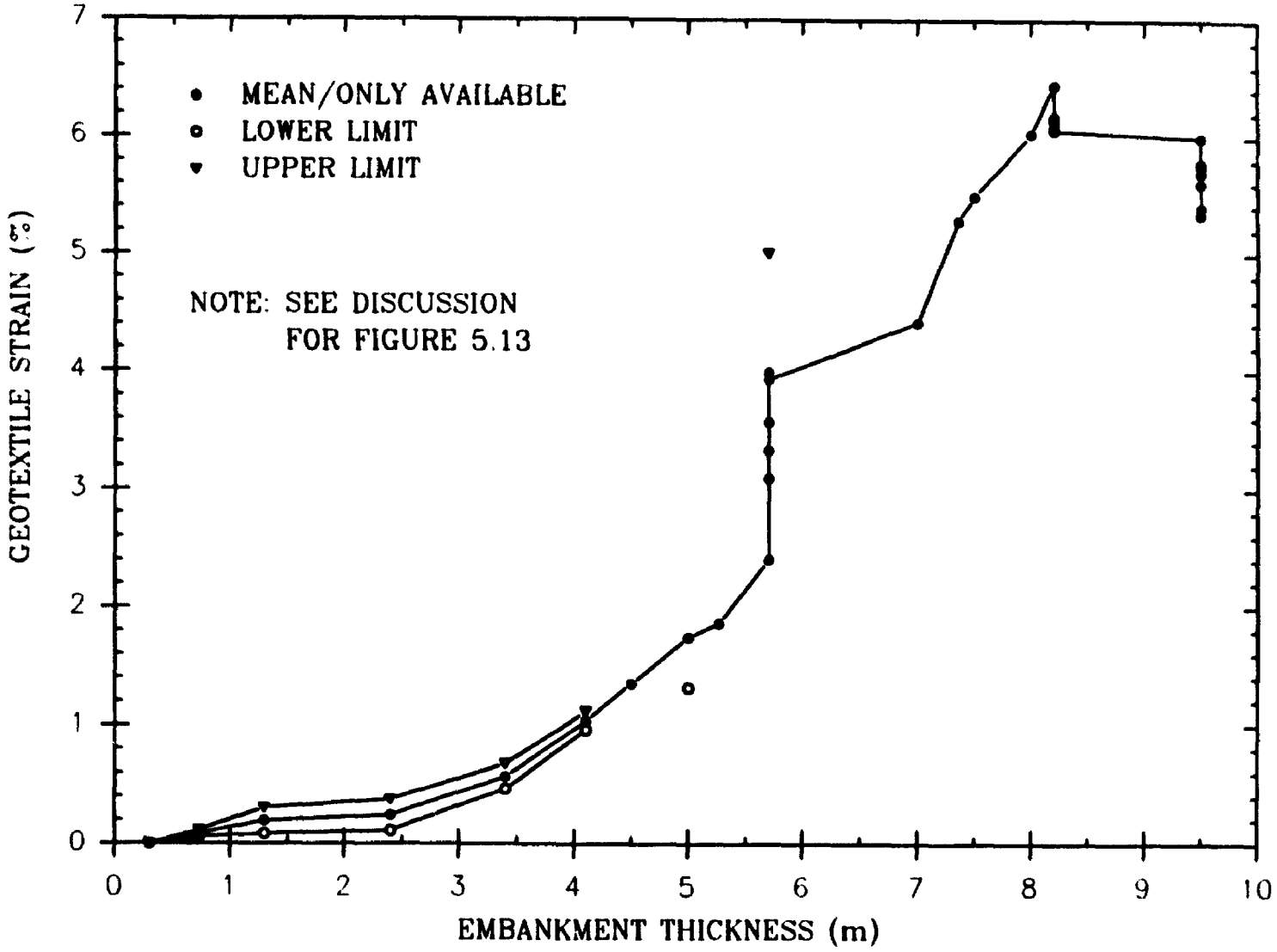

FIG. 5.24 VARIATION OF GEOTEXTILE STRAIN WITH EMBANKMENT THICKNESS FOR GAUGES BETWEEN 8.15 AND 9.5 m FROM EMBANKMENT TOE

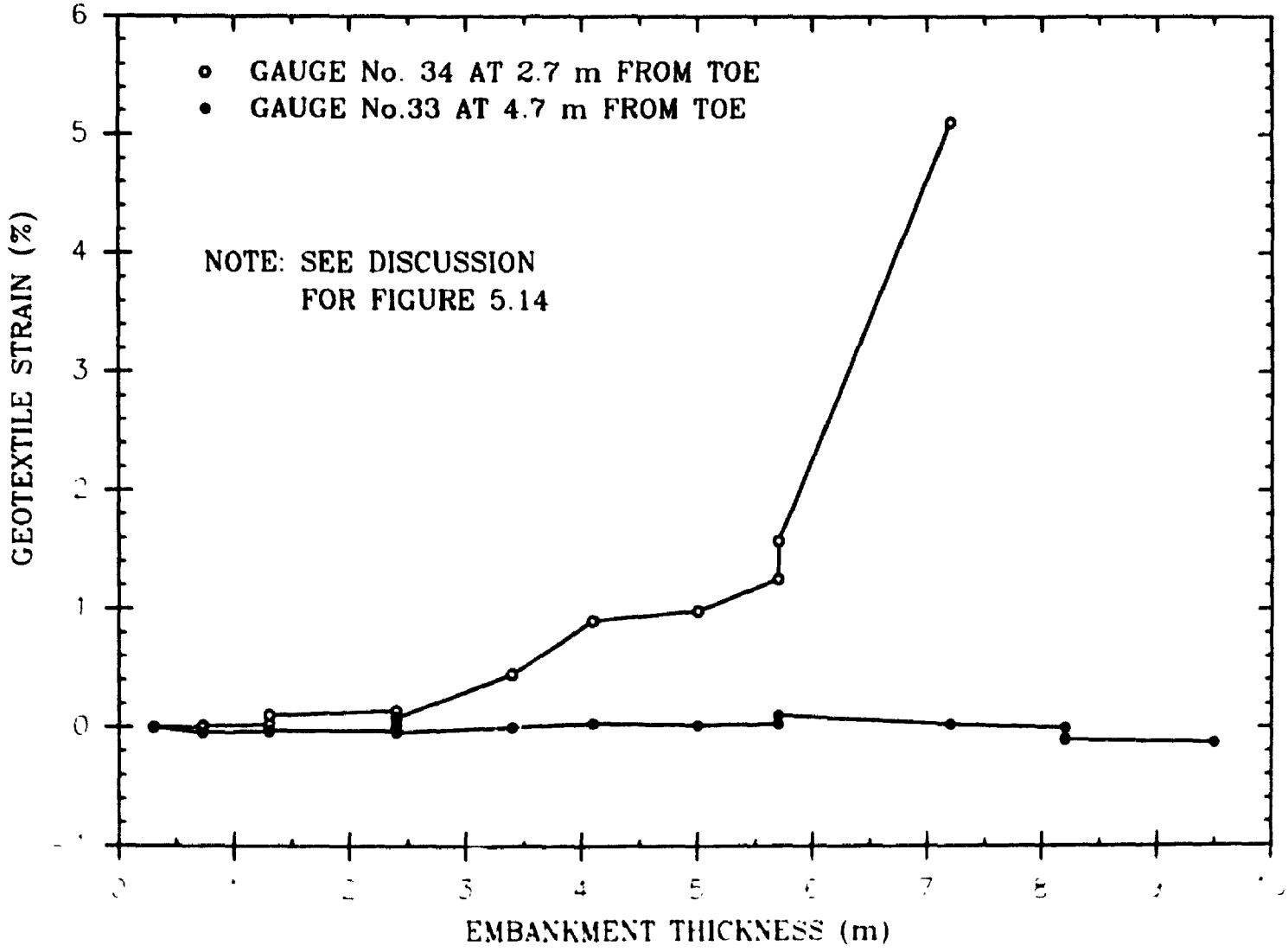

FIG 5.25 VARIATION OF GEOTEXTILE STRAIN WITH EMBANKMENT THICKNESS FOR GAUGES AT 2.7 AND 4.7 m FROM EMBANKMENT TOE

hours). This continuation of the same trend suggests that the sequence of construction employed at the site did not significantly influence the overall behaviour of the reinforced embankment. Although this continuation of the same trend is most evident in Fig. 5.19, a similar pattern of behaviour was apparent from other plots (see Figs. 5.20 to 5.24). A significant increases of the slope of the strain versus thickness plots was observed between 3.4 and 5 m (e.g. at about 4.1 m thickness for the gauges shown in Fig. 5.19), indicating that the embankment apparently started to move (i.e. the foundation yielded) when the thickness was between 3.4 and 5 m.

A summary of the average, upper limit and lower limit strains at different critical embankment thicknesses, as extracted from the strain versus thickness relationships (i.e. Figs. 5.17 to 5.25), is presented in Table 5.2. This shows that the geotextile strain (in the transverse direction) increased with the load up to an embankment thickness of about 8.2 m, in all the regions (i.e. narrow bands considered) across the geotextile. Decreases in strain were recorded in two regions (i.e. 14.6 - 15.6 m and 13.6 - 14.2 m from embankment toe - see Figs. 5.20 and 5.21), and a large increase of strain in one region, i.e. 11.8 - 12.6 from embankment toe (see Fig. 5.22). when the embankment was raised above 8.2 m thickness. Most of the electrical and electromechanical ring gauges ceased to function before 8.2 m thickness and these large decreases above 8.2 m thickness were recorded in the mechanical gauges M3-M4 and M4-M5 and the large increase was recorded in gauge M5-M6 as discussed previously. It was hypothesized that the geotextile yielded between points M5 and M6 at about 8.2 m thickness.

It could be inferred from Table 5.2 that the strains were comparatively small (the average was less than about 0.72%) up to an embankment thickness of 3.4 m. The average value of strain increased to less than about 1%, 2% and 3% when the embankment thickness was increased to 4.1 m (i.e. at 468 hours), 5.0 m (i.e. at 472 hours) and 5.7 m

TABLE 5.2 SUMMARY OF GEOTEXTILE STRAIN VERSUS EMBANKMENT THICKNESS ACROSS THE GEOTEXTILE

DISTANCE FROM EMBANKMENT TOE (m)	AVERAGE (MEAN) Strain Thickness (%)							MAXIMUM (UPPER LIMIT) Strain Thickness (%)						MINIMUM (LOWER LIMIT) Strain Thickness (%)					
	3.4 m	4.1 m	5 m	5.7 m (475 hrs)	5.7 m (490 hrs)	8.2 m	Approximate thickness at change of slope	3.4 m	4.1 m	5.0 m	5.7 m (475 hrs)	5.7 m (490 hrs)	Approximate thickness at change of slope	3.4 m	4.1 m	5 m	5.7 m (475 hrs)	5.7 m (490 hrs)	Approximate thickness at change of slope
20.5-22.5	0.40	0.47	0.72				4.1 m	0.64	0.79	1.17	1.63	4.2	3.4 - 4.1 m	0.25	0.31	0.43			
18-19.5	0.5	0.96	1.94	**	3.51		4.1 m	1.26	2.29	4.64	**	5.07	3.4 m	0.32	0.49	0.87	1.04	1.95	5 - 5.7 m
16.6-17.6	0.52	0.67	1.43	2.15	3.88		4.1 m	0.91	1.07	2.02	2.77	4.77	4.1 m	0.14	0.27	0.79	1.52	2.98	4.1 m
14.6-15.6	0.42	0.76	1.68	2.95	4.86	8.61*	3.4 m	1.14	2.02				3.4 m	0.12	0.23	**	0.94	2.19	5.35 m
13.6-14.2	0.18	0.48	1.31	2.34	4.3*	7.66*	3.4 m	0.27	0.61				3.4 m	0.09	0.37	0.96			3.4, 5 m
11.8-12.6	0.34	0.69	1.10	2.86	4.54	8.53*	3.4, 5 m	0.53	0.88	1.42	3.29		3.4, 5 m	0.16	0.43	0.78	2 42	4.02	5 0 m
9.8-10.9	0.44	0.75	1.11	1.97			5.0 m	0.46	1.03	1.69	2.24		5.0 m	0.42	0.47	0.74	1.69		5.0 m
8.15-9.5	0.57	1.04	1.53	2.4	3.93*	6.44*	3.4 m	0.67	1.11	1.74			3.4 m	0.46	0.96	1.31			3.4 m
4.7	0.45	0.90	0.98	1.25	1.57		5.7 m												

* SINGLE GAUGE STILL FUNCTIONING

** DATA NOT COLLECTED OR INSUFFICIENT DATA AT THAT TIME

(i.e. at 475 hours) respectively suggesting the initiation of movement (or yielding) of the foundation soil during the construction of the embankment above 4.1 m. It would appear that the geotextile was not required to contribute significantly to the stability of the embankment up to about 3.4 m thickness but that this contribution increased gradually after about 4.1 m thickness. Large increase of the average value of strain, from about 3% to 4.5%, at 5.7 m thickness is evidenced indicating that the soil approached failure at about 5.7 m thickness. The excess pore pressure and both vertical and horizontal displacement responses also indicated that the soil approached failure at about 5.7 m thickness (see chapter 4). The strain increased to over 8.5% when the embankment was raised to 8.2 m thickness. It is apparent that the role of geotextile in providing stability to the embankment increased dramatically after 5.7 m thickness. In chapter 4 it was suggested that the construction of the embankment above 5.7 m thickness was possible only due to the influence of the geotextile and the strain data also show some evidence for this conclusion.

5.6 GEOTEXTILE STRAIN DISTRIBUTION

The variation of geotextile strain along the transverse (i.e. North - South) direction of geotextile reinforcement (i.e. the strain distribution profile) at different stages of construction are presented in Figs. 5.26 to 5.35. The average and both upper and lower limits of the strains, inferred from the strain versus thickness data, are plotted separately to facilitate interpreting the range of strain at each location along the (North - South) centre line of the geotextile at different stages of construction. It should be noted that the strain distribution shown in Fig. 5.35 was when the embankment thickness was increased to 8.2 m (i.e. 498 hours) and the maximum strain in the geotextile increased rapidly to about 13.9% in about 0.8 hour while the thickness was constant at 8.2 m (see Figs. 5.11 and 5.22 also).

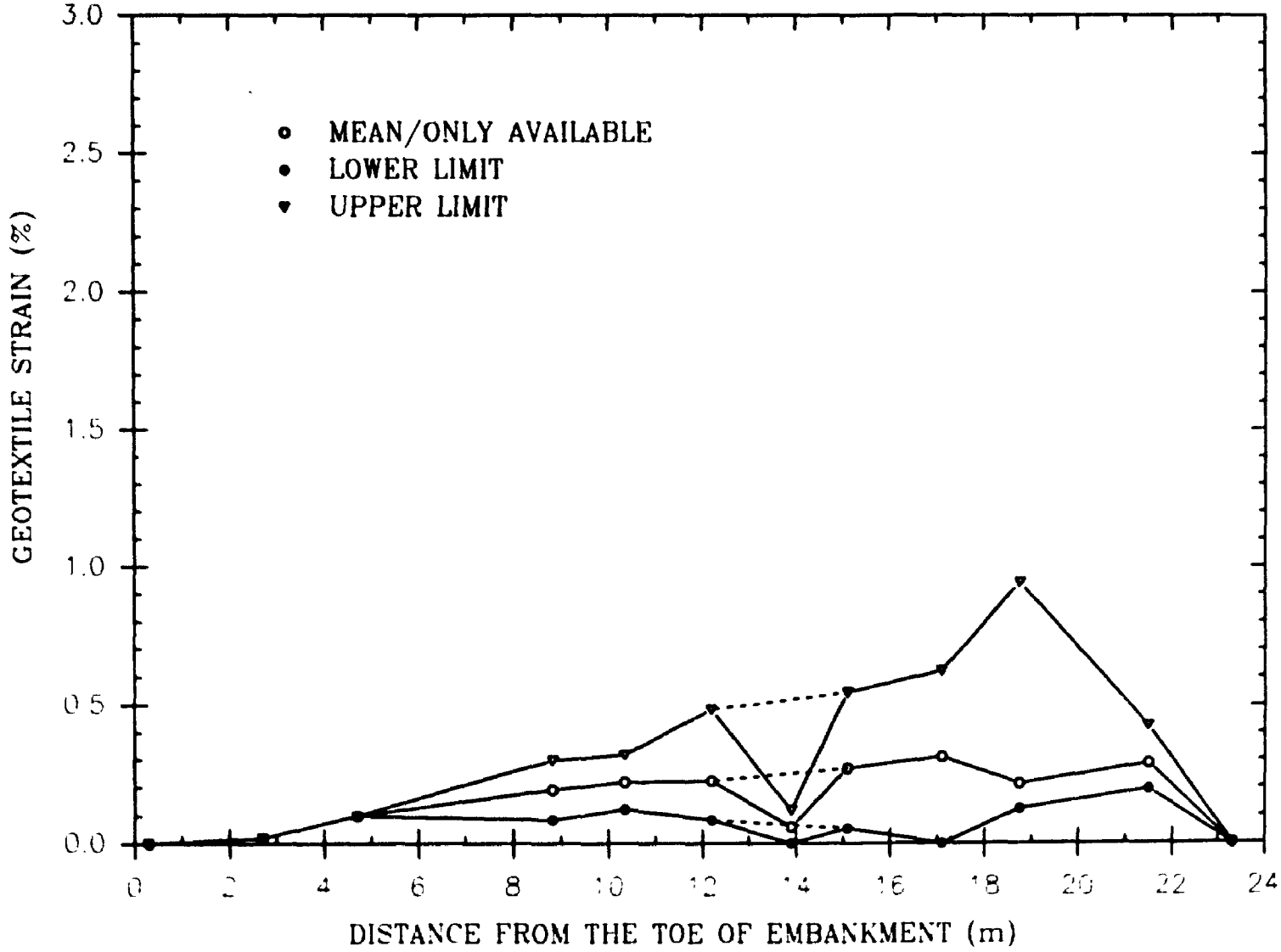

FIG 5.26 GEOTEXTILE STRAIN DISTRIBUTION AT EMBANKMENT THICKNESS = 1.3 m (349 HOURS)

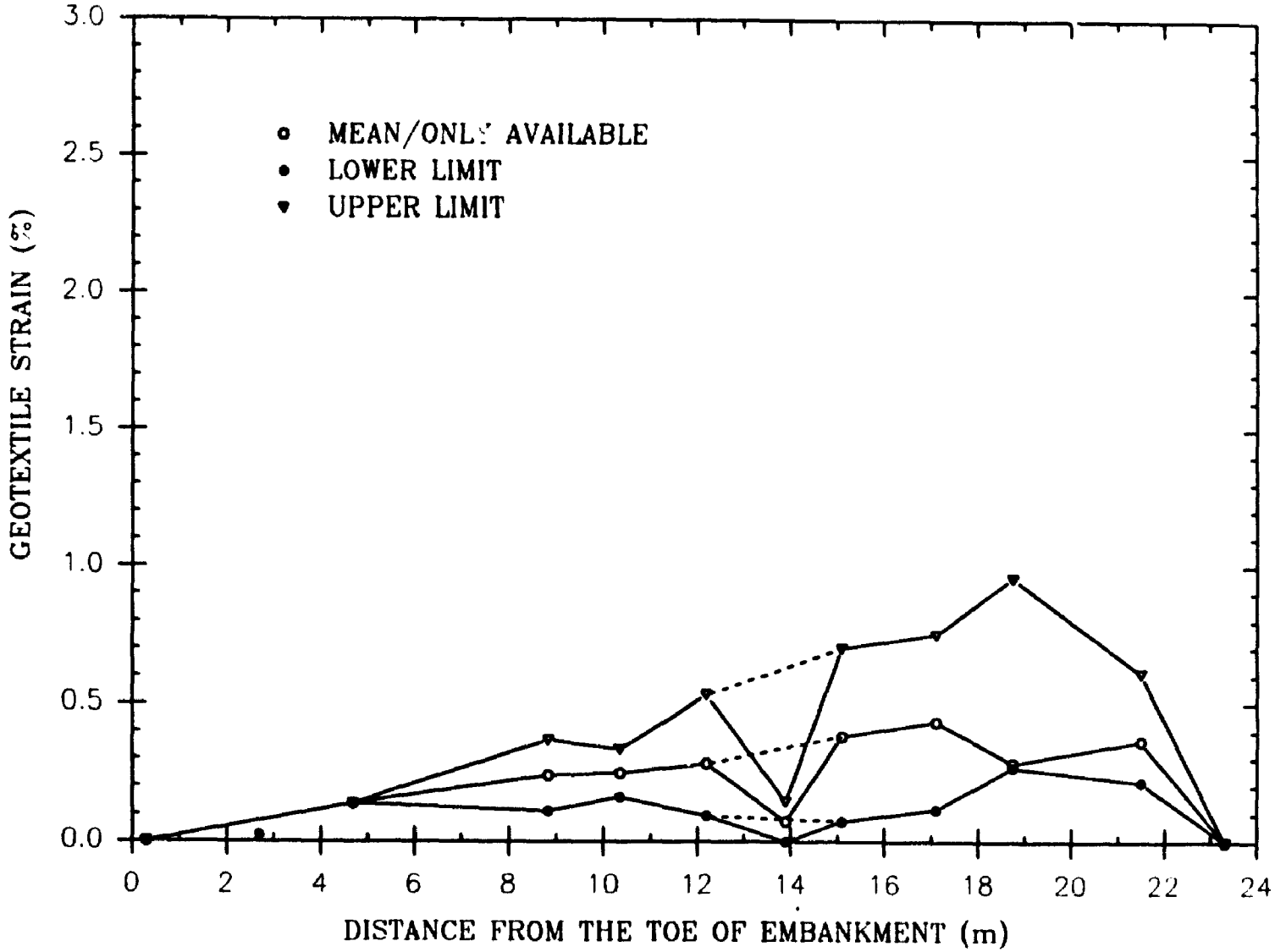

FIG. 5.27 GEOTEXTILE STRAIN DISTRIBUTION AT EMBANKMENT THICKNESS = 2.4 m (372 HOURS)

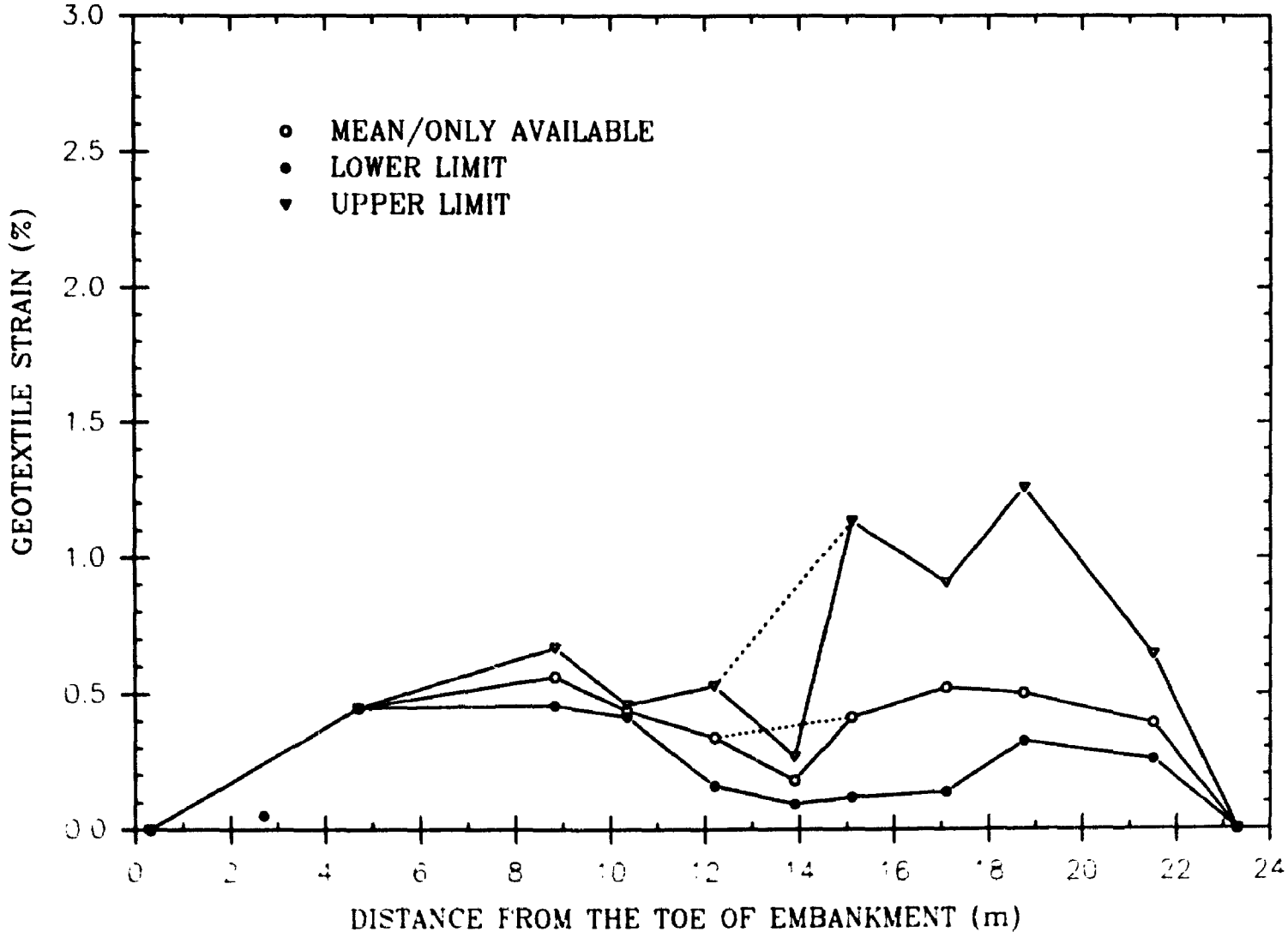

FIG. 5.28 GEOTEXTILE STRAIN DISTRIBUTION AT EMBANKMENT THICKNESS = 3.4 m (448 HOURS)

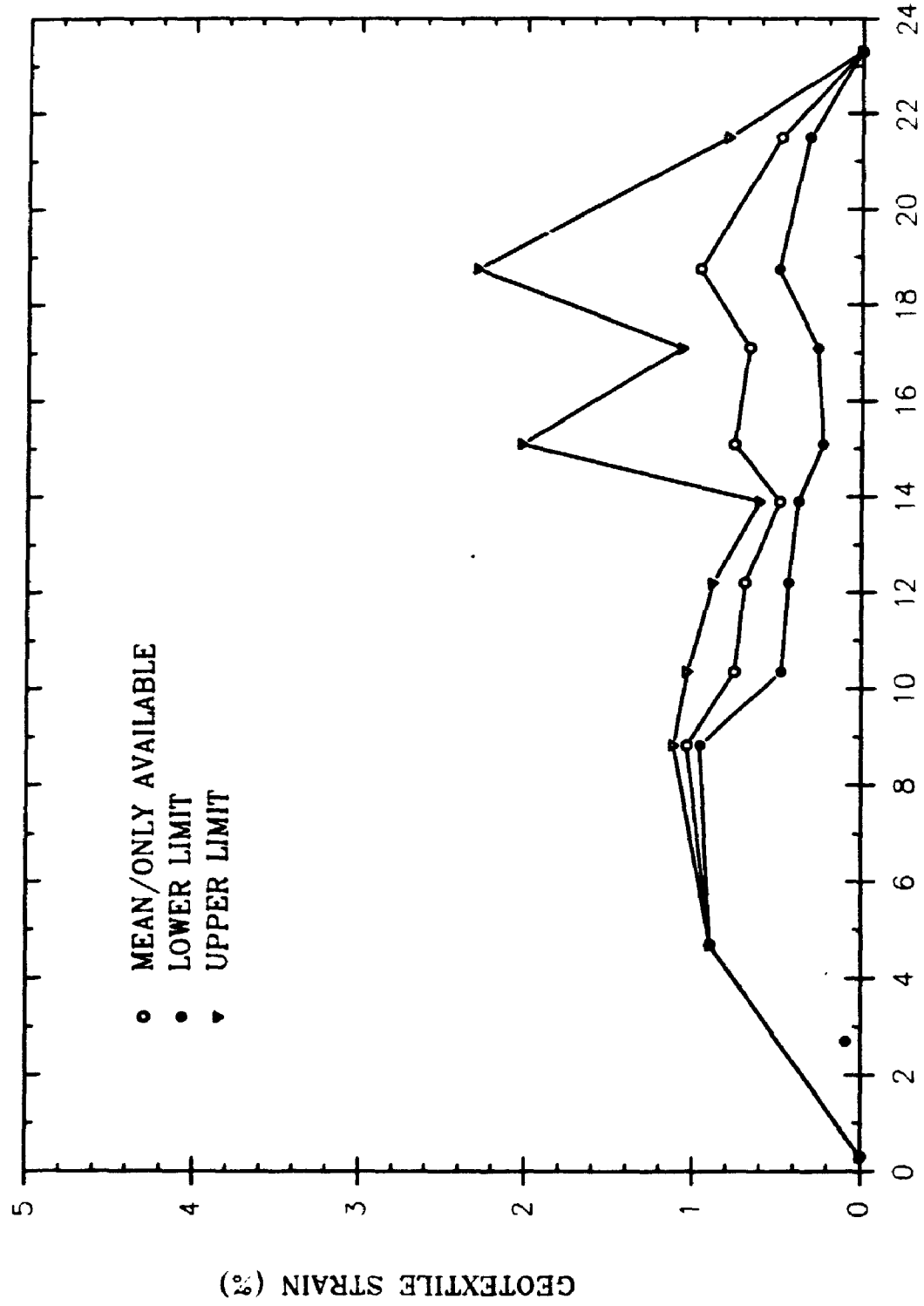

FIG. 5.29 GEOTEXTILE STRAIN DISTRIBUTION AT EMBANKMENT THICKNESS = 4.1 m (468 HOURS)

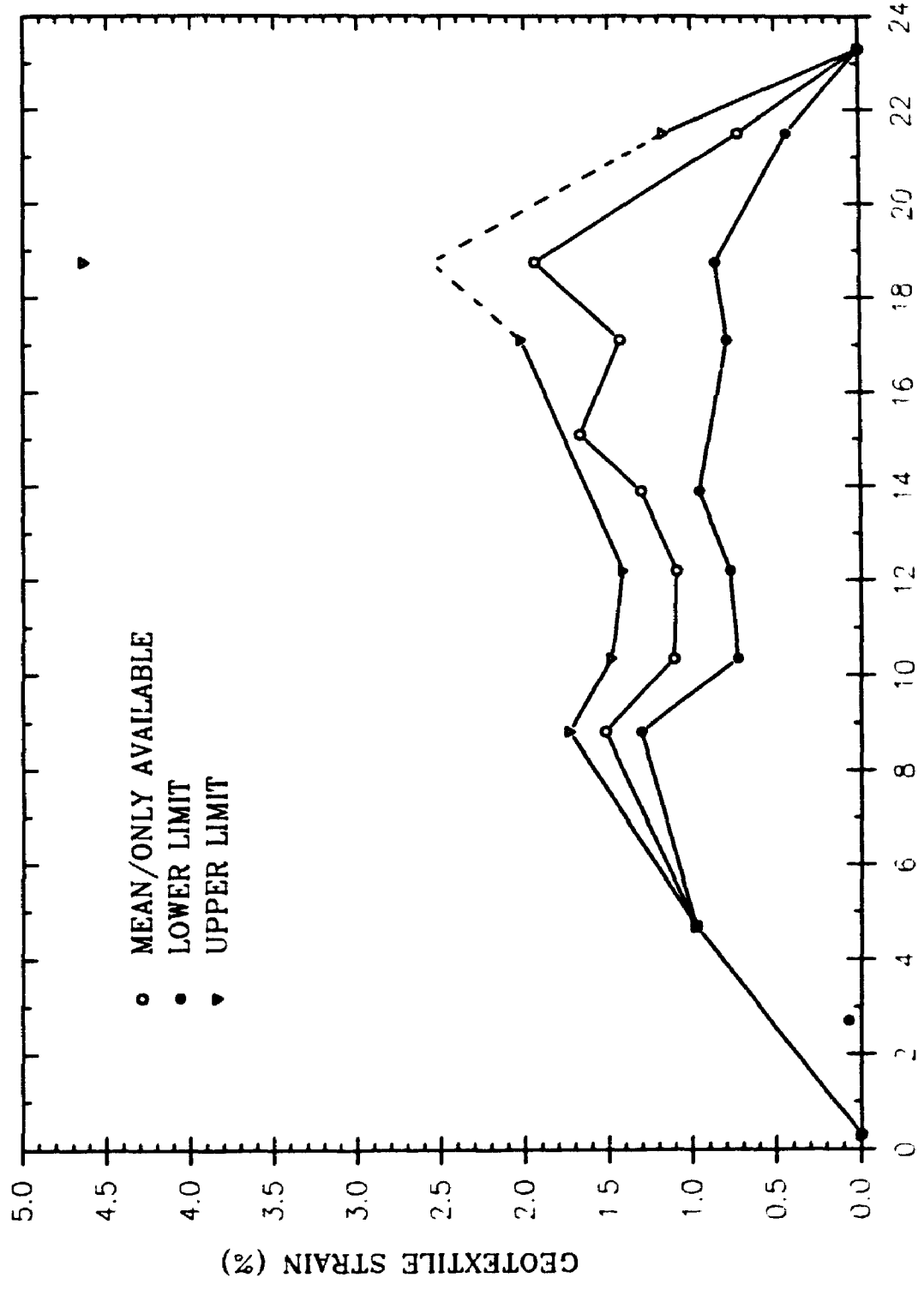

FIG. 5.30 GEOTEXTILE STRAIN DISTRIBUTION AT EMBANKMENT THICKNESS = 5.0 m (472 HOURS)

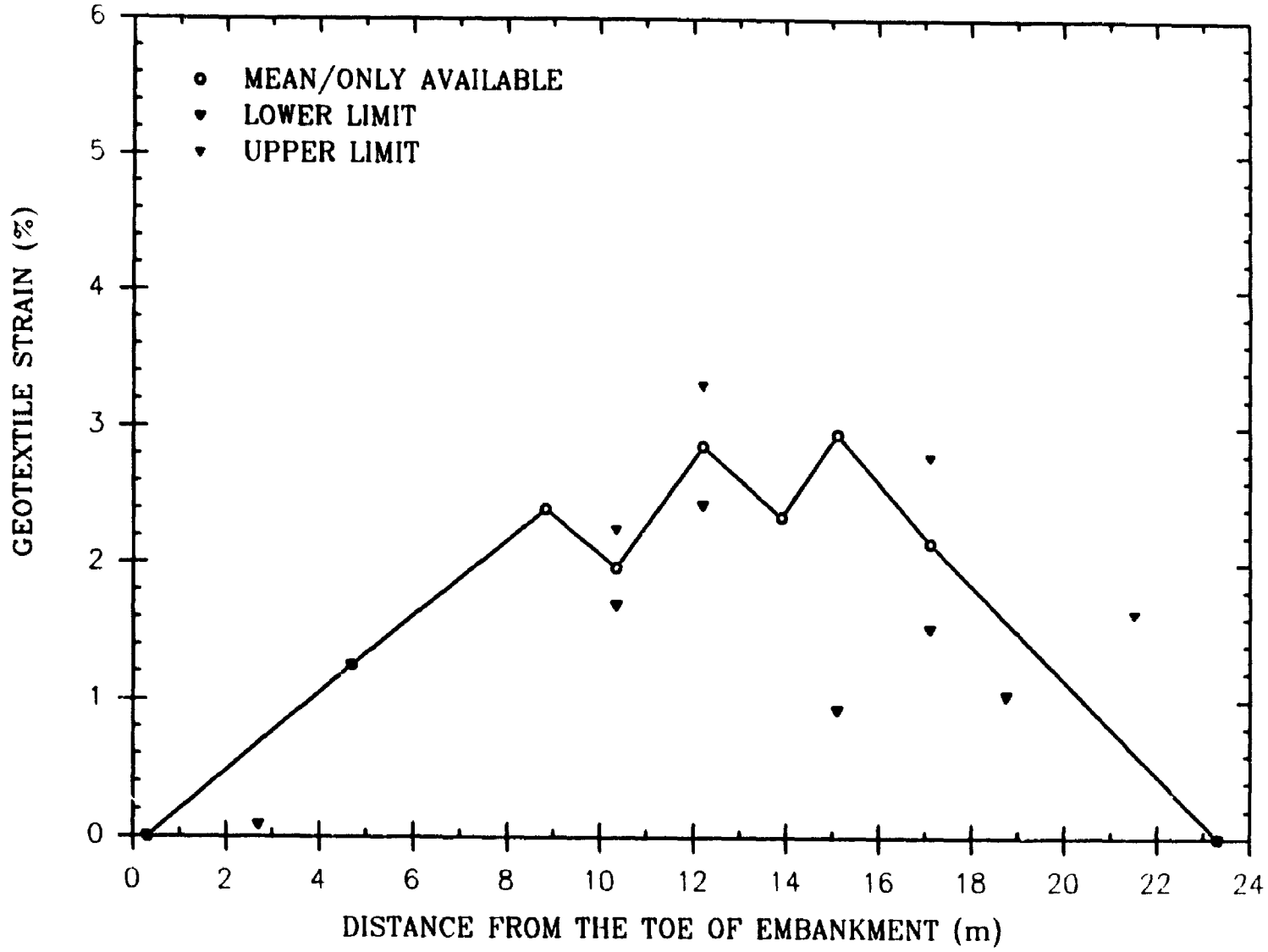

FIG. 5.31 GEOTEXTILE STRAIN DISTRIBUTION AT EMBANKMENT THICKNESS = 5.7 m (475 HOURS)

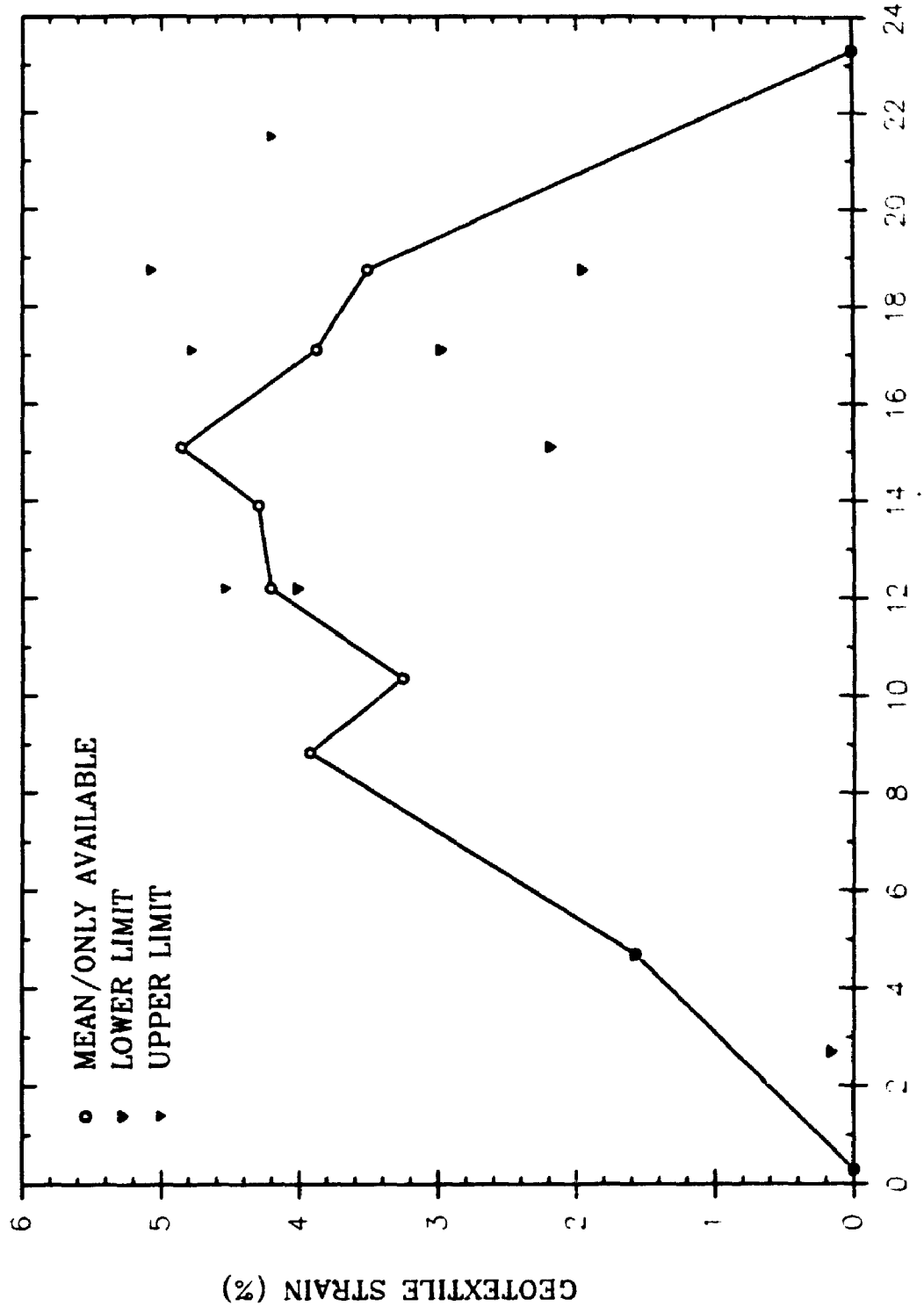

FIG. 5 32 GEOTEXTILE STRAIN DISTRIBUTION AT EMBANKMENT THICKNESS = 5 7 m (490 HOURS)

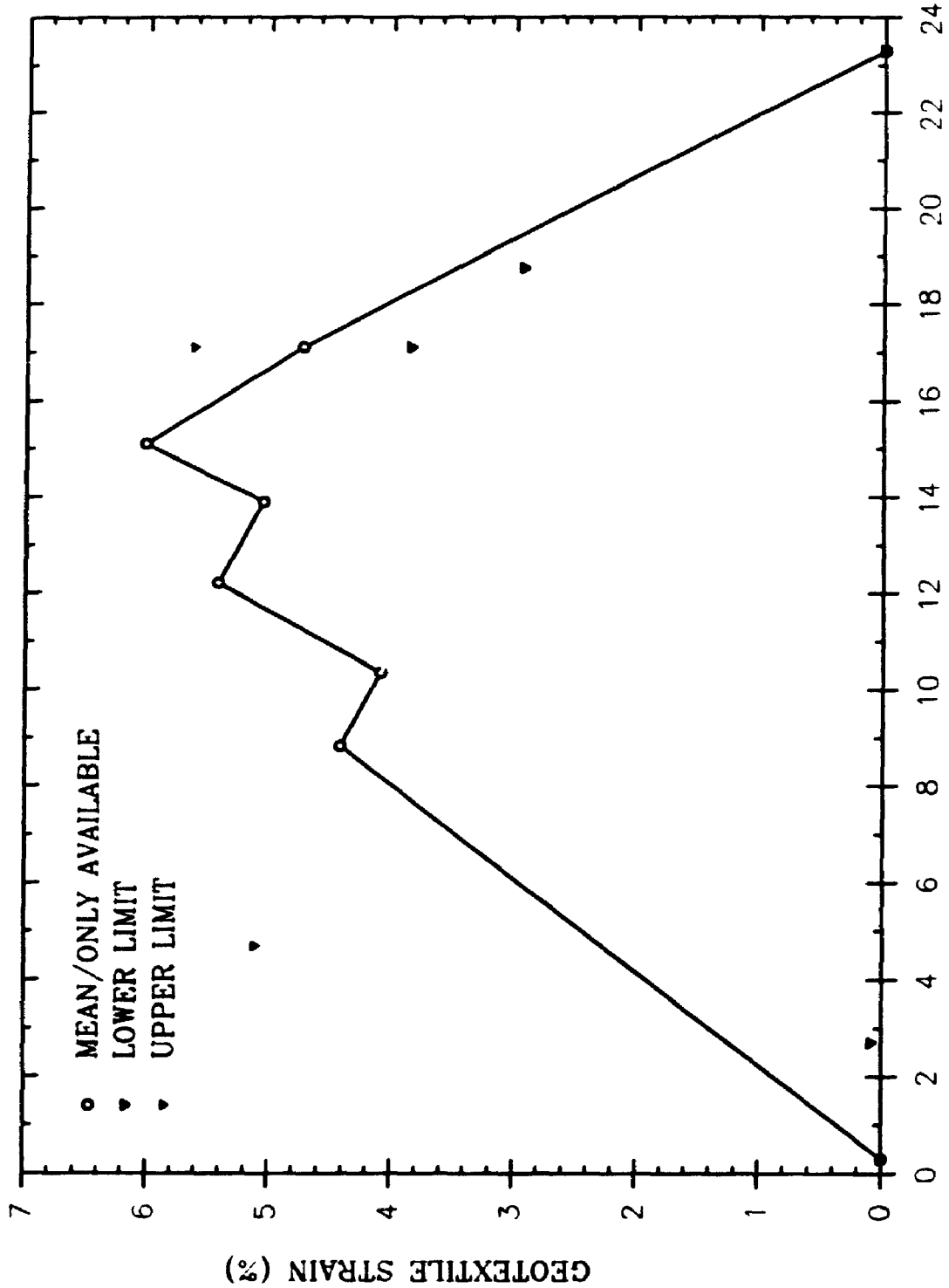

FIG. 5.33 GEOTEXTILE STRAIN DISTRIBUTION AT EMBANKMENT THICKNESS = 7.0 m (493 HOURS)

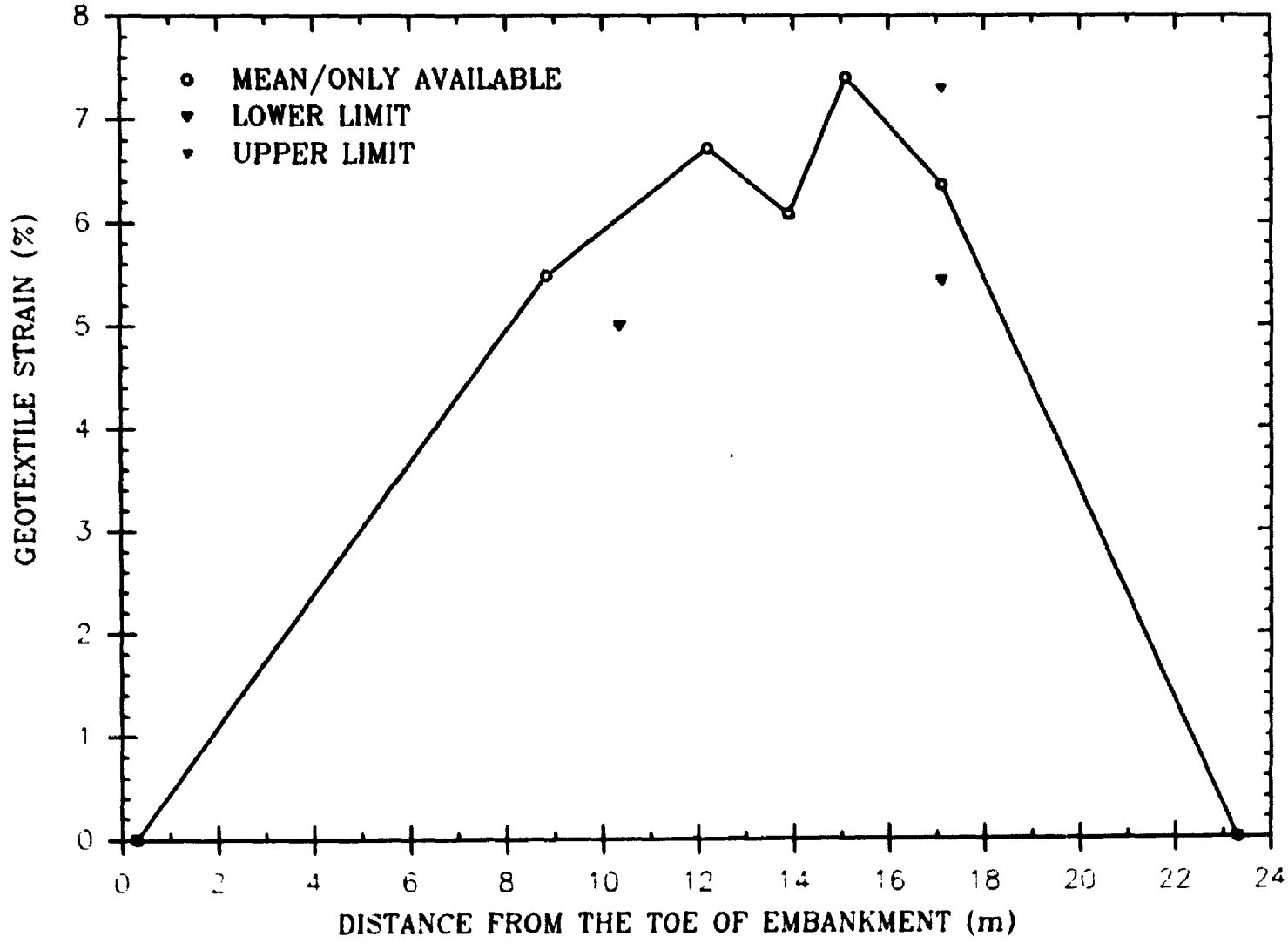

FIG 5 34 GEOTEXTILE STRAIN DISTRIBUTION AT EMBANKMENT THICKNESS = 7 5 m (495 HOURS)

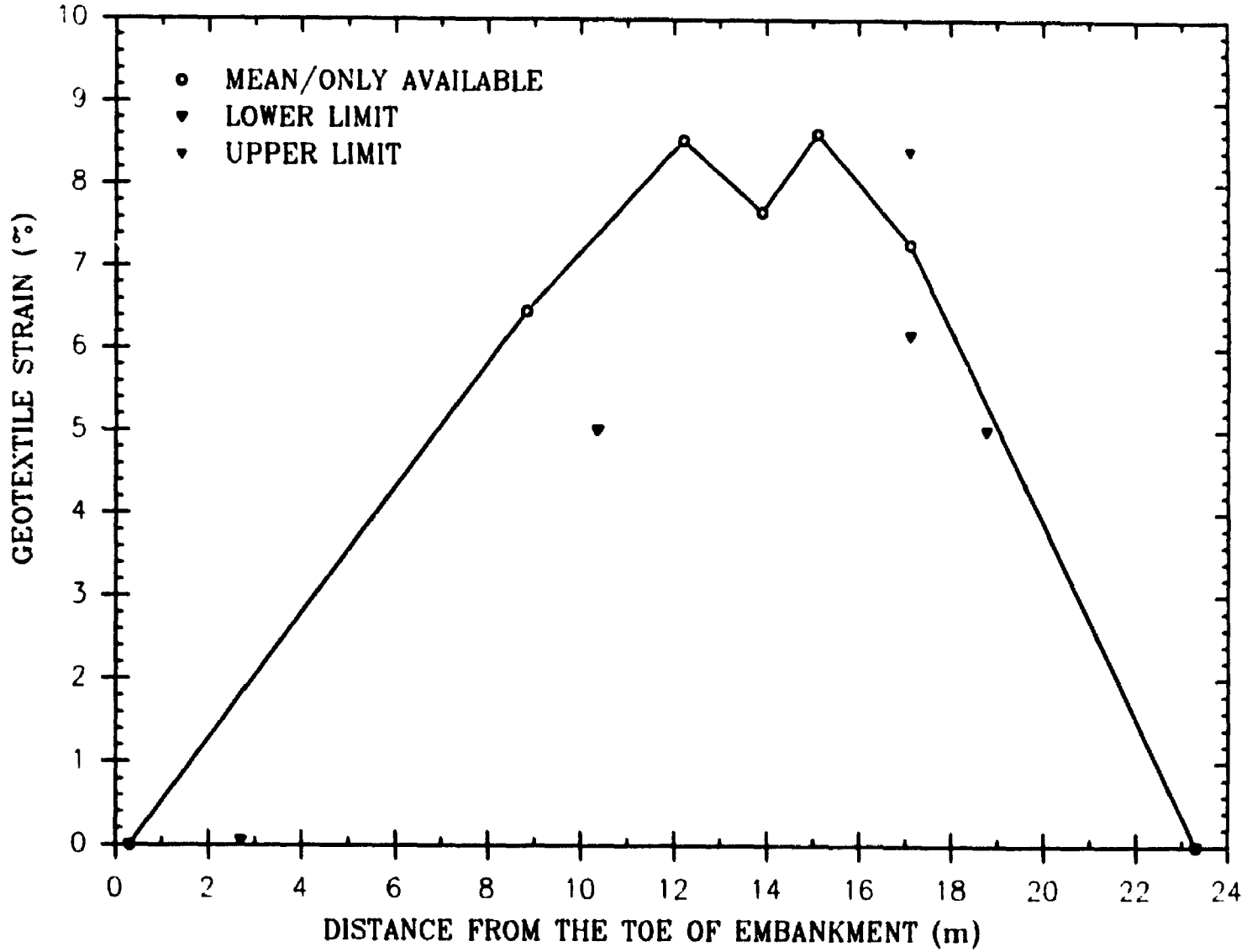

FIG. 5.35 GEOTEXTILE STRAIN DISTRIBUTION AT EMBANKMENT THICKNESS = 8.2 m (498 HOURS)

Figs. 5.26, 5.27 and 5.28 clearly indicate that the strains were less than about 1.3% when the embankment was constructed up to 3.4 m thickness. The largest strain (of about 4.7%) was observed about 18.75 m from the embankment toe at 5 m thickness (see Fig. 5.30). This value comes from the strain readings of rings 1 and 4 placed in the region 18 - 19.5 m from the toe. The trend of a sharp increase of strain from about 2% (at about 17.1 m from toe) to about 4.7% (at about 18.75 m from toe) and the sharp drop to about 1% (at about 21.5 m from toe), appears erroneous and it is the authors opinion that the largest strain of 4.7% is not realistic. The inferred largest strain (assessed by extrapolating the trends in the neighbouring regions) is expected to be about 3% (see Fig. 5.30).

A sharp drop of strain in the neighbourhood of 13.9 m (from the toe) is observed in the strain profiles, particularly during the early stages of construction (i.e. up to 3.4 m embankment thickness, see Figs. 5.26, 5.27 and 5.28), indicating a clear abrupt deviation from the trend exhibited in the neighbouring regions. These drops were due to the comparatively small strains observed in gauges 8, 19 and M4-M5 placed between 13.6 and 14.2 m from the toe during the early stages of construction. It is suspected that the geotextile in this region was subjected to some local pretension strain of about 0.1 - 0.4% (the range estimated, from Figs. 5.26, 5.27 and 5.28, as the difference between the expected strain for continuation of the same trend as the surrounding regions and the obtained strain readings) resulting in a zero shift and was the cause of the lower strain readings in these gauges. It should be noted that this zero shift is small compared to the strains obtained during the later stages of construction (say above 5 m thickness) and does not significantly affect the strain data of later stages of construction.

The strain profiles indicate that the maximum strain occurred between about 17 and 19 m from the toe when the embankment thickness was below 3.4 m (see Figs. 5.26, 5.27 and 5.28). The location of maximum strain along the geotextile shifted towards the

centre line of the embankment to between about 14 and 19 m when it was raised above 4.1 m thickness (see Figs. 5.29 and 5.30). When the embankment was raised above 5.7 m, it further shifted towards the centre line to about 12 - 15 m from the toe (see Figs. 5.31 to 5.35).

5.7 COMMENTS ON THE PERFORMANCE OF INSTRUMENTATION

The geotextile strain measurements proved to be very successful. Of the original 38 electrical gauges, 5 were lost during transport and placement of the fabric. Given the weight and bulky nature of the fabric, the nature of the gauges and the harsh environment, this is a remarkably low failure rate. Out of the remaining 33 gauges, 30 of them continued to function until an advanced state of failure (i.e. when the gauge or the cable were damaged due to large deformation). Five of the ring gauges also functioned reasonably well until an advanced stage of failure. The mechanical gauges performed very well and provided useful data during the entire construction and monitoring period. Five of the mechanical gauges continued to function until the embankment failed.

5.8 SUMMARY AND CONCLUSIONS

The instrumentation and field performance of the geotextile as a reinforcement to the test embankment constructed at Sackville, N.B. has been described. This embankment was instrumented with a number of piezometers, settlement plates, augers, heave plates and inclinometers and a total pressure cell. Details of this instrumentation, their responses and performance during construction have been described in chapter 4. A relatively high strength polyester woven geotextile (Nicolon style 68300) was used as reinforcement and it was instrumented with a number of electrical, electromechanical and mechanical gauges. The details of these gauges, their responses with the construction of

the embankment and their performance has been described in this chapter.

The strains were comparatively small (typically less than about 0.72%) up to an embankment thickness of 3.4 m. The strain increased to less than about 1%, 2% and 3% when the embankment thickness was increased to 4.1 m, 5.0 m and 5.7 m respectively suggesting the initiation of movement or (or yielding) of the foundation soil during the construction of the embankment above 4.1 m. Large increase of strain from about 3% to 4.5% was evident at 5.7 m thickness suggesting that the soil approached failure at about 5.7 m thickness. The maximum strain occurred between about 17 and 19 m from the toe when the embankment thickness was below 3.4 m but shifted towards the centre line of the embankment to between about 1[illegible] and 19 m when it was raised above 4.1 m thickness. When the embankment was raised above 5.7 m, it further shifted towards the centre line to about 12 - 15 m from the toe.

This field investigation indicates that the contribution of the geotextile to the stability of the embankment was not significant up to about 3.4 m thickness but its contribution increased gradually after about 4.1 m thickness. The strain increased to as high as about 8.5% when the embankment was raised to 8.2 m thickness. It was apparent that the role of geotextile in providing stability to the embankment increased substantially after 5.7 m thickness. It was concluded in chapter 4 that the construction of the embankment above 5.7 m thickness was possible only due to the influence of the geotextile and the reinforced embankment failed at a thickness of about 8.75 m (i.e. at a net height of 6.7 m). The strain data presented in this chapter also showed some evidence in support of this conclusion.

CHAPTER 6

LABORATORY INVESTIGATION AND SELECTION OF SOIL PARAMETERS FOR ANALYSES

6.1 INTRODUCTION

The extensive field testing programme for this project was described in chapter 3. In order to determine the additional soil parameters required for the analyses, a laboratory testing programme was also developed and carried out at the Geotechnical Laboratory of the University of Western Ontario. Some of the large (i.e. 200 mm) diameter undisturbed samples obtained with the use of an overcore drilling sampler developed at Laval University (see LaRochelle et al., 1980 for the details for the sampler) were used for this lab investigation (see Fig. 3.1 for the bore hole locations). The laboratory investigation consisted of the following:

1) preliminary tests to determine the grain size distribution, Atterberg limits, specific gravity and ash content;

2) triaxial compression tests;

3) direct simple shear tests;

4) consolidation tests; and

5) permeability tests.

The details of this laboratory investigation are reported in this chapter. These results are compared with the corresponding field test results and appropriate soil parameters selected for use in the analyses. It is noted that the results of the laboratory tests performed to determine the strength parameters of the fill materials used for this test embankment were reported in Chapters 3 and 4; and the results of tensile tests performed on the geotextile and the direct shear tests to determine the geotextile - fill interface properties were reported in Chapter 5.

6.2 PRELIMINARY TESTS

Index tests, hydrometer and sieve analyses, ash content and specific gravity tests were carried out on samples obtained from various depths. ASTM standard procedures were adopted in performing these tests. The grain size distribution of the samples tested are shown in Fig. 6.1 and the results of index tests are plotted on the plasticity chart shown in Fig. 6.2. Summarized in Table 6.1 are the results from all these tests. Ash contents were determined by burning off the organic components of the soil samples in a high temperature oven and (100 - ash content, expressed in percent) was considered as the approximate value of the organic content.

6.3 TRIAXIAL COMPRESSION TESTS

6.3.1 Introduction

To identify the presence of any anisotropy, conventional isotropically consolidated undrained (CIU) triaxial tests (with pore pressure measurement) were performed on samples (obtained at 1.8 m depth) trimmed at three different orientations. Similarly, unconsolidated undrained (UU) quick triaxial tests were also performed on samples (from

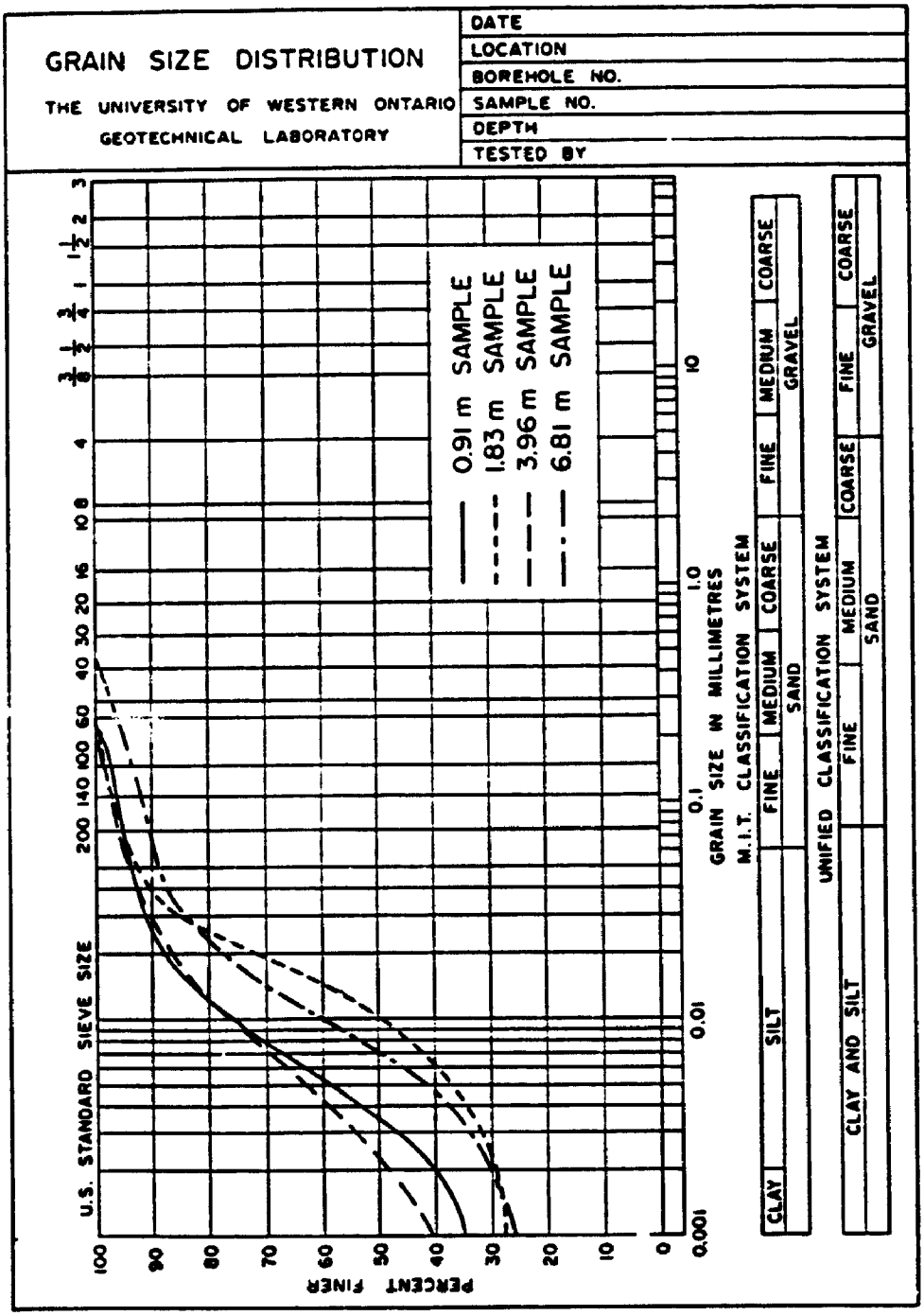

FIG. 6.1 GRAIN SIZE DISTRIBUTION OF SAMPLES FROM DIFFERENT DEPTHS

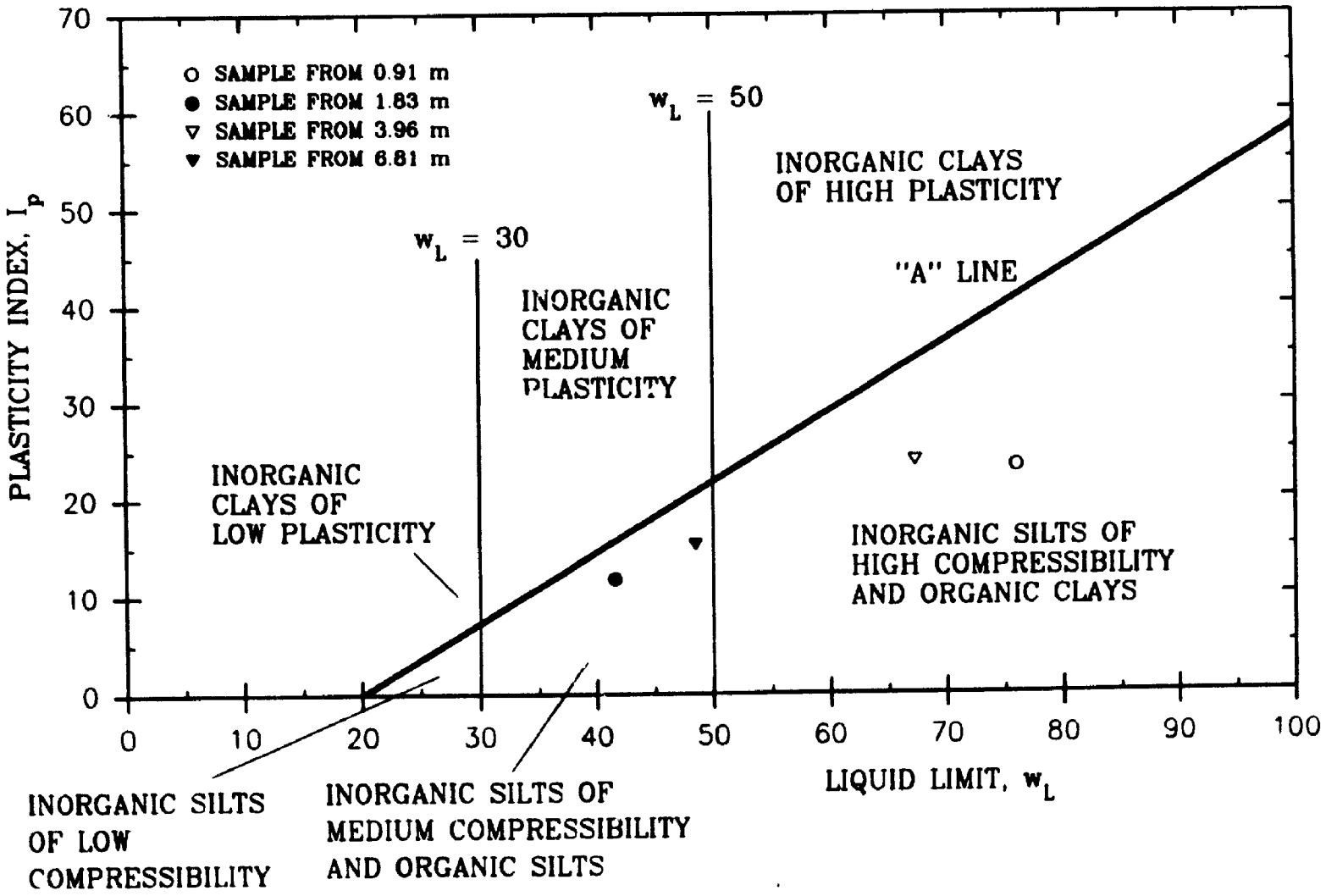

FIG. 6.2 THE PLASTICITY CHART (AFTER CASAGRANDE, 1948)

Table 6.1 Geotechnical properties of the foundation soil - results from the preliminary tests

Depth (m)	Description of soil	Natural water content (%)	w_p (%)	w_L (%)	I_p (%)	I_L (%)	* Organic content (%)	% clay	% Silt	Acti-vity	G_s
0.91	Matrix of fine Fibrous material in organic silty clay, grey, high compressibility	74.4	52.6	76.0	23.4	0.93	10.4	40	54	0.59	2.62
1.83	Brown organic clayey silt, medium compressibility	41.7	29.8	41.6	11.8	1.0	3.7	30	63	0.39	2.68
3.96	Grey organic silty clay, high compressibility	60.2	43.4	67.3	23.9	0.70	9.0	48	47	0.50	2.65
6.81	Reddish brown organic clayey silt, medium compressibility	43.5	33.2	48.5	15.3	0.67	4.9	30	61	0.51	2.69

* : Organic content determined as (100 - Ash content in percent).
w_p : Plastic limit.
w_L : Liquid limit.
I_p : Plasticity index.
I_L : Liquidity index.

2.36 m depth) trimmed at different orientations.

To obtain the undrained and drained strength parameters, undrained deformation modulus, and the variation of these parameters with depth, CAU (i.e. K_o consolidated undrained) triaxial tests with pore pressure measurement were performed on vertical samples obtained from three different depths. To define the shear strength envelope completely, two additional tests were performed on vertically trimmed samples (from 6.81 m depth) with anisotropic consolidation pressures equal to the estimated insitu effective stresses at 13.8 and 23.4 m depths. A CAD (i.e. K_o consolidated drained) test was also performed to determine the effective stress parameters (such as c', ϕ', E' and ν') for comparison with the parameters (c' and ϕ') determined from CAU tests and the field test results obtained from the self boring pressuremeter (i.e. for parameters such as c', ϕ' and E'). Details of these tests and the results are presented in the following sections.

6.3.2 General information of the triaxial tests performed

All the triaxial tests were performed with Wykeham Farrance equipment and the procedures followed were generally those described by Bishop and Henkel (1962). Carefully trimmed cylindrical specimens of soil measuring approximately 50 mm in diameter by 100 mm in length were used for these tests. After each sample was weighed and measured, it was carefully placed in the triaxial cell with filter paper and porous stones, top and bottom. It was also fitted with an all round slotted filter paper jacket (except for the UU triaxial tests) to enhance drainage during the consolidation phase of the test and the specimen was encased in a thin cylindrical latex rubber membrane. The sample was tested when the consolidation was considered to be complete.

A back pressure of 100 kPa was applied to saturate the soil samples. The degree of

saturation, as indicated by Skempton's $\overline{B}$ value ($\overline{B} = \frac{\Delta u}{\Delta \sigma_3} = 1.0$ if saturated) calculated from the measurements, was checked for each test. The estimated insitu effective horizontal stress was used as the consolidation pressure for the CIU, CAU and CAD tests. For the CAU and CAD tests, the axial stress applied during consolidation corresponded to the estimated insitu effective vertical stress. Periodic volume change readings were taken during the consolidation phase of the CIU, CAU and CAD tests. The estimated total overburden stress was used as the cell pressure for the UU triaxial tests.

A large number of pneumatic and Casagrande type piezometers were installed at the site several weeks (about 1 to 3 months) prior to the commencement of construction and they were monitored periodically as reported in Chapter 3. Based on the initial pore pressure measurements from these piezometers, the water table was found to be about 0.4 m below the ground level. This was used in the estimation of the insitu effective stresses. An average K_o (defined as the ratio of the horizontal effective stress to the vertical effective stress) value of 0.78 (see the NRC data given in Table 3.1) was also used.

The axial load was measured using a load cell located in the head of the plunger within the triaxial cell and the pore water pressure was measured using a pressure transducer at the base of the sample. A data acquisition system (Vishay Instruments - Model 2150) and a chart recorder (Soltec Corp. - Model 3306) were used to collect the data which allowed continuous monitoring of the axial load, cell pressure and pore water pressure during the entire duration of each test.

6.3.3 Results of CIU and UU Tests Performed to Verify Anisotropy

The term anisotropy is generally used to describe the variation of soil properties, whether it be strength, deformation, compressibility or permeability, with direction. The

anisotropy of clays is intimately connected with their structure, which depends on the environmental conditions during which the soil is deposited as well as the stress changes subsequent to deposition (Lo, 1965). It has been demonstrated (e.g. Rosenquist, 1959) that the clays deposited in salt water acquire an open card house structure with the particles randomly oriented. In a fresh water deposit, the structure is somewhat dispersed and a certain degree of parallelism is achieved between the clay particles. Thus it has been postulated that in the former case the clay is more or less isotropic at a macroscopic scale, while in the latter case, the clay will possess some inherent anisotropy (Lo, 1965). The soil under investigation is from an area of intertidal salt marsh deposit and therefore expected to behave almost isotropically with respect to the strength and deformation characteristics. For the purpose of examining the strength variation with direction, a series of CIU strain controlled triaxial tests were performed on samples trimmed vertically (i.e. i = 0), horizontally (i.e. i = 90^{o}) and at 45^{o} to the vertical (i.e. i = 45^{o}). The rate of strain used in the tests was about 2.46%/hr and each test lasted for about 9 hours.

Shown in Figures 6.3 to 6.6 are the deviator stress ($\sigma_1 - \sigma_3$), pore water pressure, principal stress ratio (σ_1'/σ_3') responses with axial strain and the variation of ($\sigma_1' - \sigma_3'$)/2 with ($\sigma_1' + \sigma_3'$)/2 for the CIU tests. A summary of the CIU test results is shown in Table 6.2. The CIU test for the sample oriented at i = 45^{o} was repeated in order to check the reproducibility of the tests and to verify consistency of test results (i.e. tests 2 and 9) and it could be observed that the results were very close, particularly until about 8% strain. There was some deviation in the responses mentioned above at large strains (say > 8%) which started well after the failure of the samples but the trends were similar until the tests were terminated.

In the triaxial tests, failure may be defined using two different criteria, namely the maximum principal stress ratio criteria and the maximum deviator stress criteria. In both

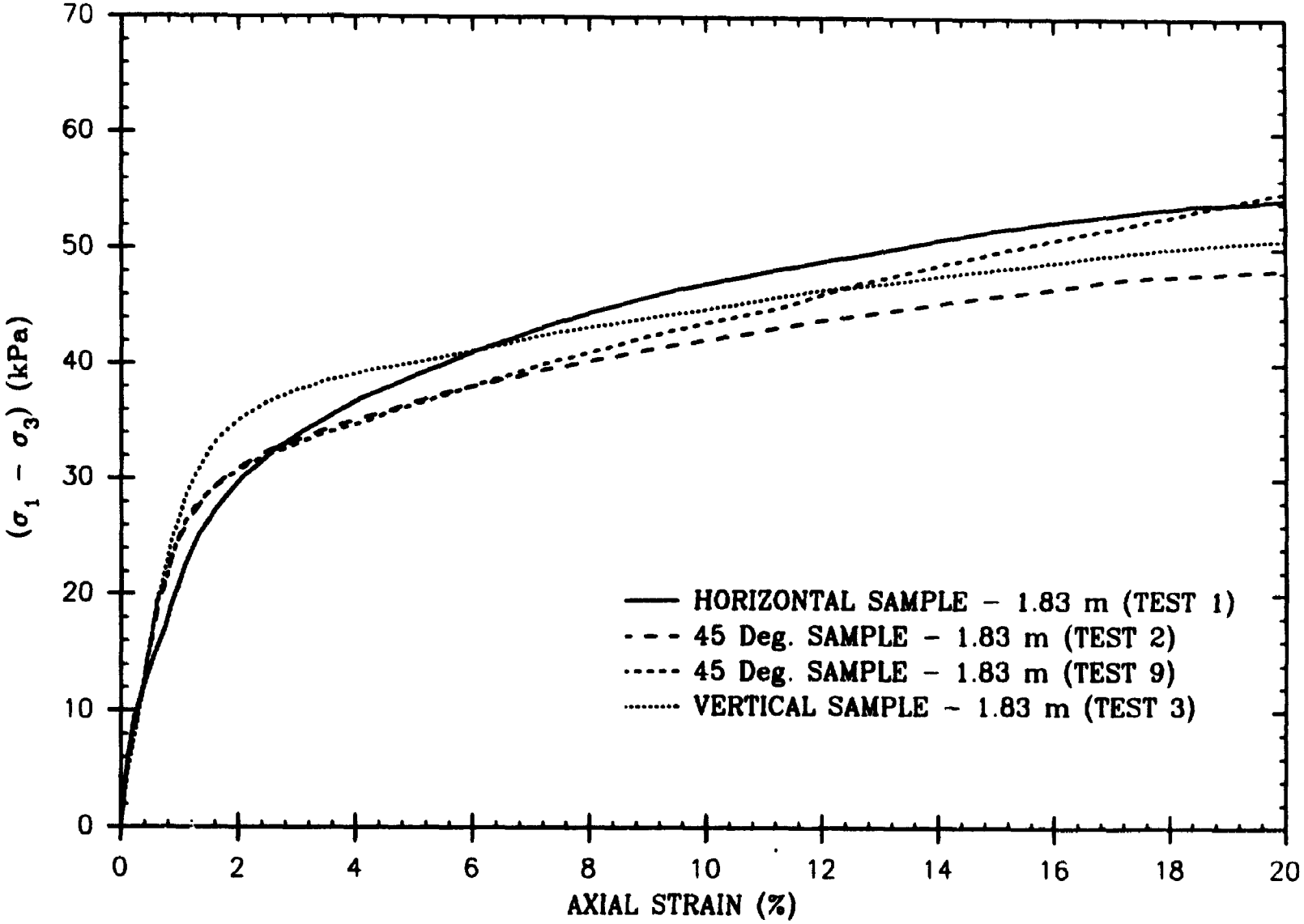

FIG. 6.3 VARIATION OF $(\sigma_1 - \sigma_3)$ Vs. AXIAL STRAIN - CIU TRIAXIAL TEST RESULTS

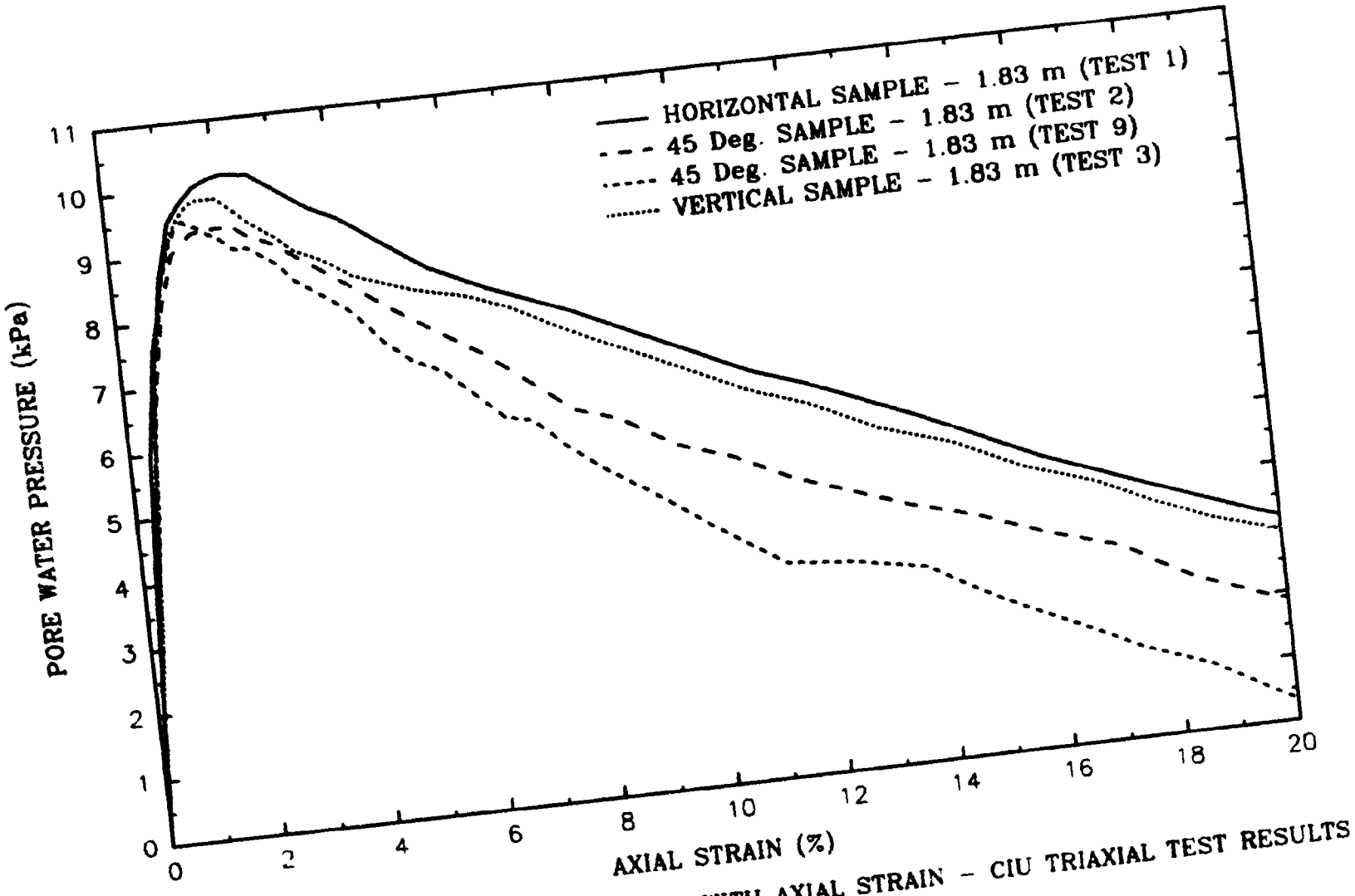

FIG. 6.4 VARIATION OF PORE WATER PRESSURE WITH AXIAL STRAIN - CIU TRIAXIAL TEST RESULTS

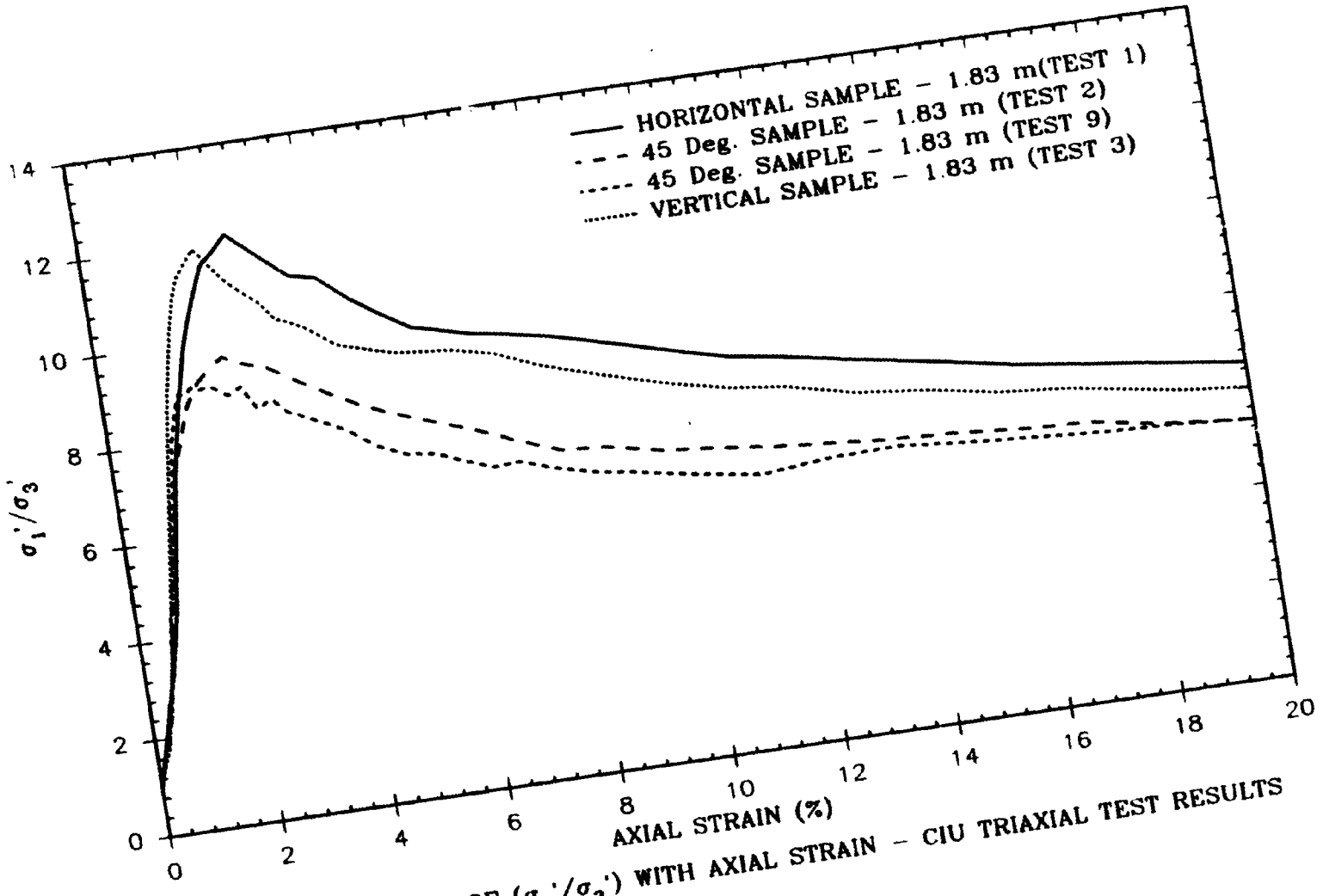

FIG. 6.5 VARIATION OF (σ_1'/σ_3') WITH AXIAL STRAIN – CIU TRIAXIAL TEST RESULTS

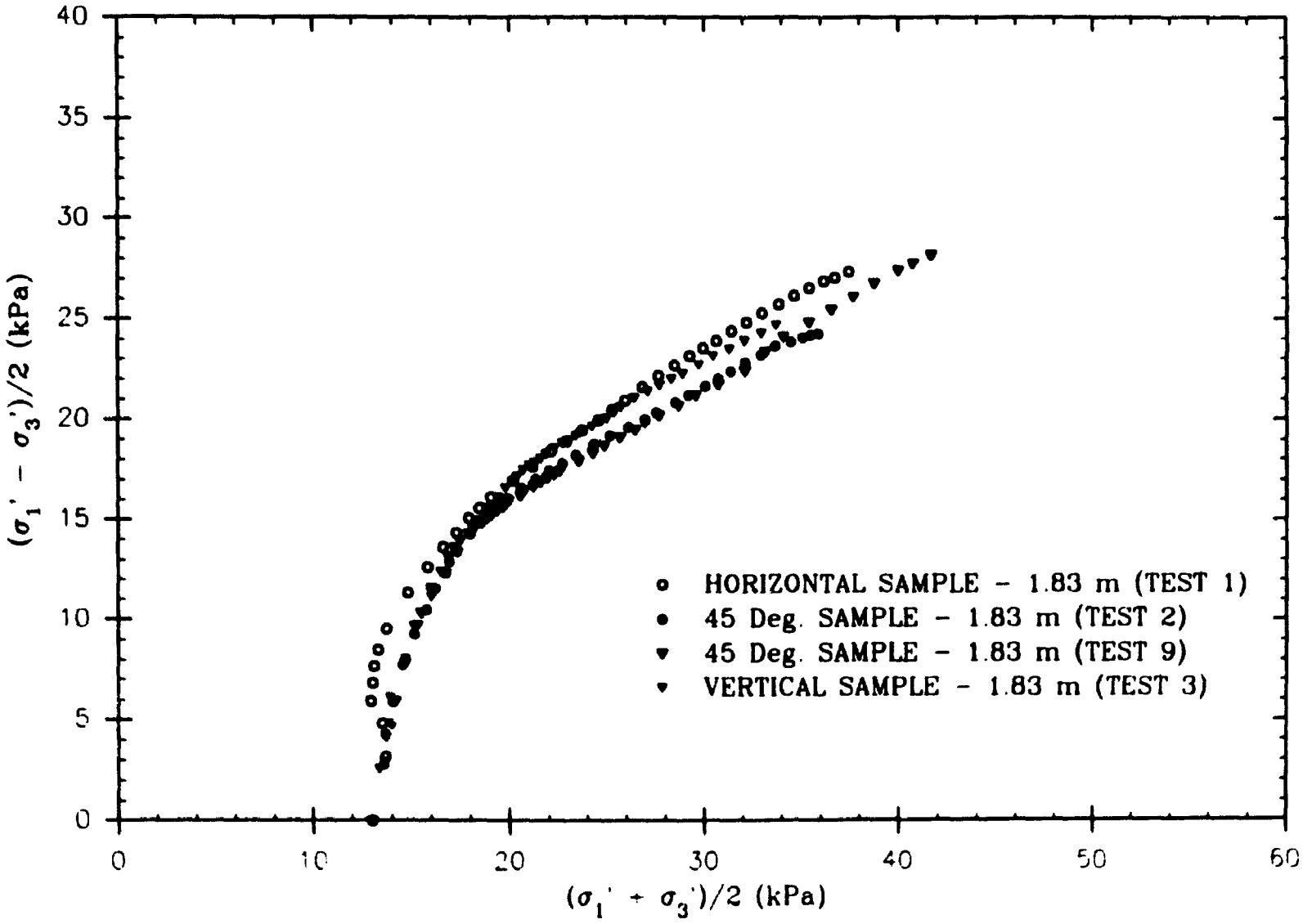

FIG 6.6 VARIATION OF $(\sigma_1' - \sigma_3')/2$ Vs. $(\sigma_1' + \sigma_3')/2$ - CIU TRIAXIAL TEST RESULTS

Table 6.2 Summary of CIU Triaxial test results

Test #	Type of test	Depth of sample (m)	Water content (%)	Cons. pressure (KPa)		Volume change during cons. (%)	C_u (KPa)	** E (MPa)	Approx. axial strain at failure (%)	A_f	Failure mode
				σ_1'	σ_3'						
1	CIU	1.83 (i=90°)	40.9	13	13	2.13	* 16.13	3.50	2.58	.31	Bulging
2	CIU	1.83 (i=45°)	40.2	13	13	2.16	* 15.74	3.45	2.20	.30	Bulging
9	CIU	1.83 (i=45°)	38.9	13	13	1.93	* 15.09	3.76	1.84	.31	Bulging
3	CIU	1.83 (i=0)	40.1	13	13	2.15	* 17.48	3.33	1.98	.28	Bulging

i = 90° (horizontal)
i = 0 (vertical)
* = Max. principal stress ratio failure criteria used.
** = Secant modulus at 1/3 of failure stress.

criteria, failure is deemed to have occurred when the maximum value is reached. However, the deviator stress responses did not indicate any maximum, at least until 20% strain, and failure was interpreted using the maximum principal stress ratio criteria only (see Figures 6.3 and 6.5). Failure strains ranged between 1.8 and 2.6%. It is interesting to note that all the curves seem to be approaching a post-peak principal stress ratio in the order of 3.0. The pore water pressure initially showed a large increase, nearly until failure, followed by a continuous decrease (see Fig 6.4). The occurrence of the maximum pore pressures coincided reasonably well with failure interpreted using the maximum principal stress ratio criteria.

The variation of $(\sigma_1' - \sigma_3')/2$ with $(\sigma_1' + \sigma_3')/2$ was consistent, each test showing similar trend for the stress path (see Fig. 6.6). The samples exhibit overconsolidated behaviour and ϕ' is estimated to range between 30 and 32^0.

Based on these tests, it appears that the variation of the undrained shear strength and the secant modulus (defined at 1/3 of failure stress) with the orientation of the sample were not significant (typically < 10%) indicating that the soil is essentially isotropic in a macroscopic scale as far as the shear strength and deformation are concerned. This finding is consistent with the earlier discussion where it was expected to behave almost isotropically. However, it will be shown later that the permeability values exhibited anisotropic behaviour.

To further confirm the absence of strength anisotropy, a series of UU triaxial tests also were performed on samples trimmed at i = 0, 45^0 and 90^0. A strain rate of about 1.02%/min was used for these tests. The response of the deviator stress with strain for these tests were similar (see Fig. 6.7). A summary of the results of these tests is presented in Table 6.3. Failure occurred generally at large strains (> 15%). The variation in the

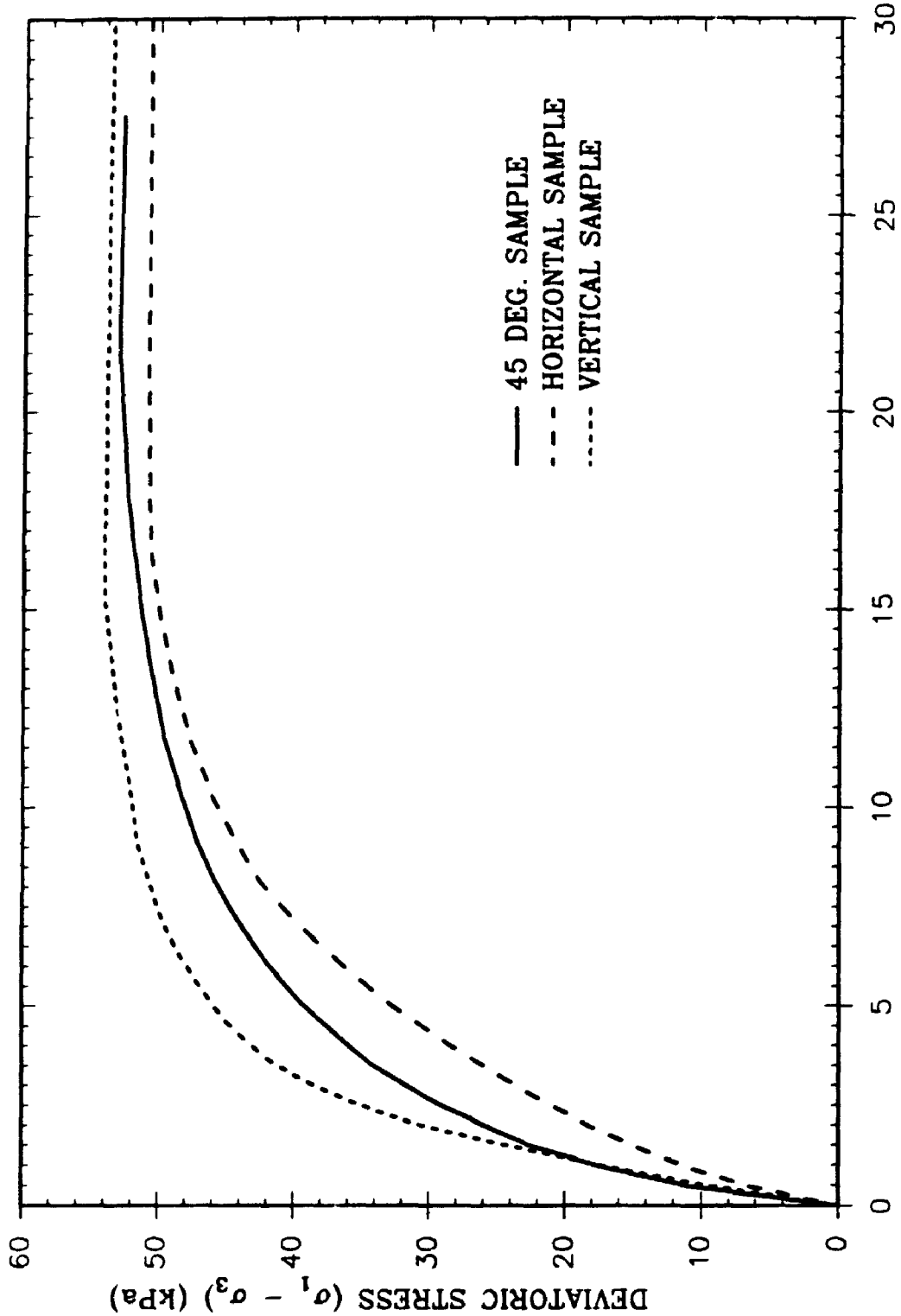

FIG. 6.7 VARIATION OF DEVIATORIC STRESS Vs. AXIAL STRAIN - UU TRIAXIAL TEST RESULTS

Table 6.3 Summary of UU Triaxial Test Results.

Depth (m)	Sample orientation i(°)	Natural water content (%)	Cell pressure (KPa)	Undrained shear strength (KPa)	Approx. axial strain at failure (%)	Mode of failure
2.36	0 (vertical)	40.0	39.0	27.0	15.3	Bulging
2.36	45	39.0	39.0	26.5	21.4	Bulging
2.36	90 (horizontal)	39.5	39.0	25.4	18.0	Bulging

undrained shear strength with the orientation of the sample was again relatively small suggesting that the strength of the soil is essentially isotropic for all practical purposes.

6.3.4 Results of CAU Tests

The deviator stress ($\sigma_1 - \sigma_3$), pore water pressure, and the principal stress ratio (σ_1'/σ_3') responses with axial strain for the strain controlled K_o consolidated undrained (CAU) triaxial tests performed on samples from various depths are shown in Figures 6.8 to 6.10. The stress path followed during each test is shown, as the plot of $(\sigma_1' - \sigma_3')/2$ versus $(\sigma_1' + \sigma_3')/2$, in Fig. 6.11. For ease of comparison, the stress path followed in the CAD test (discussed in the following section) is also presented in this figure. Here again, a strain rate of about 2.46%/hr was used for the CAU tests and each test lasted for about 9 hours. Two tests were performed for the samples from each depth to verify the repeatability of the tests and the results are shown for these duplicate tests on Figures 6.8 to 6.11 and they are summarized in Table 6.4.

The sample at 0.91 m depth was a fibrous organic silty clay soil which failed at a large strain of about 21% (see the plot of deviator stress with strain shown in Fig. 6.8). The pore water pressure variation also showed similar trend as the deviator stress (see Fig. 6.9). However, the principal stress ratio variation was peculiar, the maximum value reaching infinity (due to the minor principal stress (σ_3') decreasing from a positive to a negative value) and hence suddenly dropping to a negative value from infinity before reaching a constant negative value at large strain. It was not possible to interpret failure in the usual manner using the principal stress ratio criteria for the tests performed on samples from 0.91 m depth and therefore the (σ_1'/σ_3') response for these tests are not shown in Fig. 6.9.

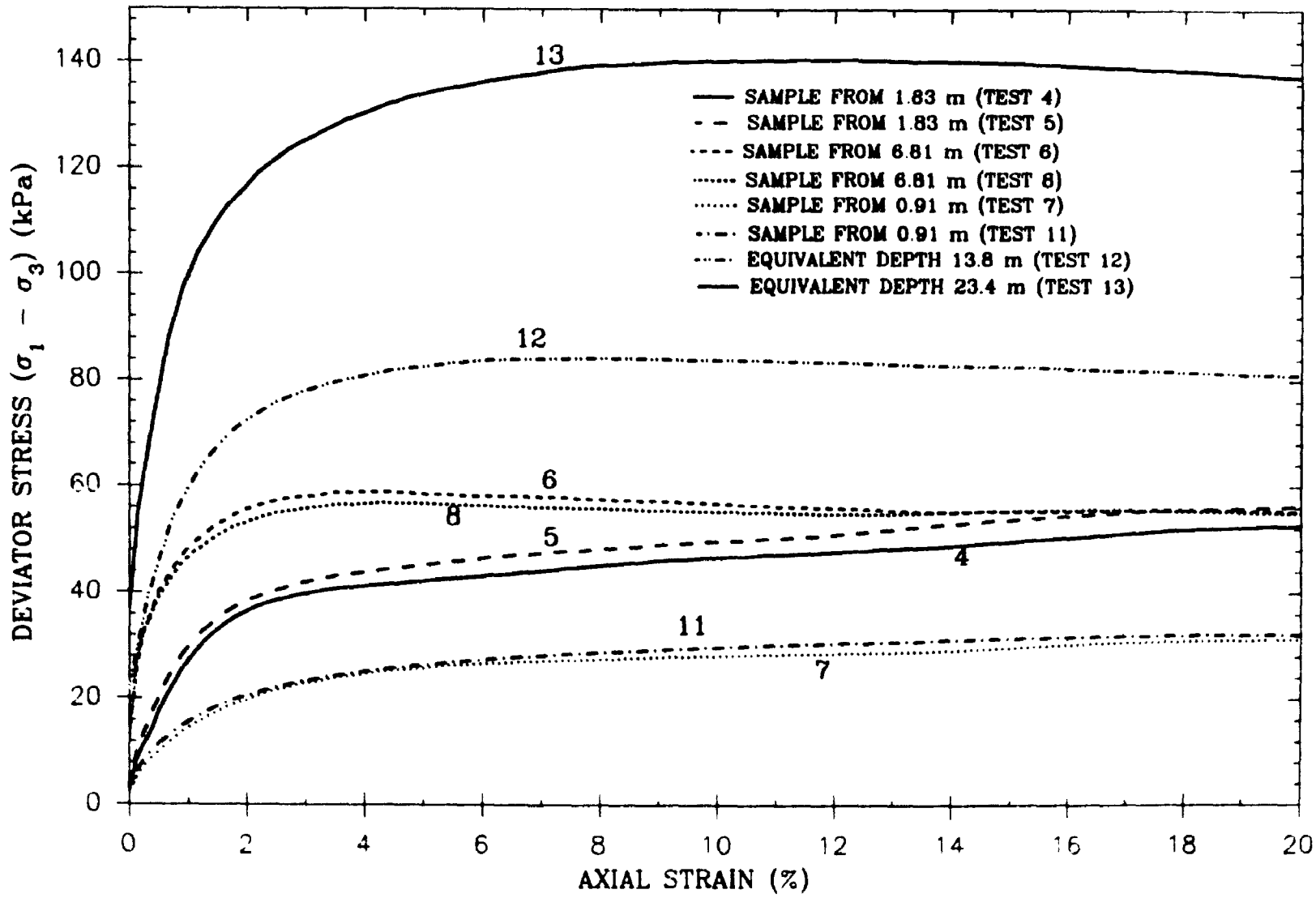

FIG. 6.8 VARIATION OF DEVIATOR STRESS Vs. STRAIN - CAU TRIAXIAL TEST RESULTS

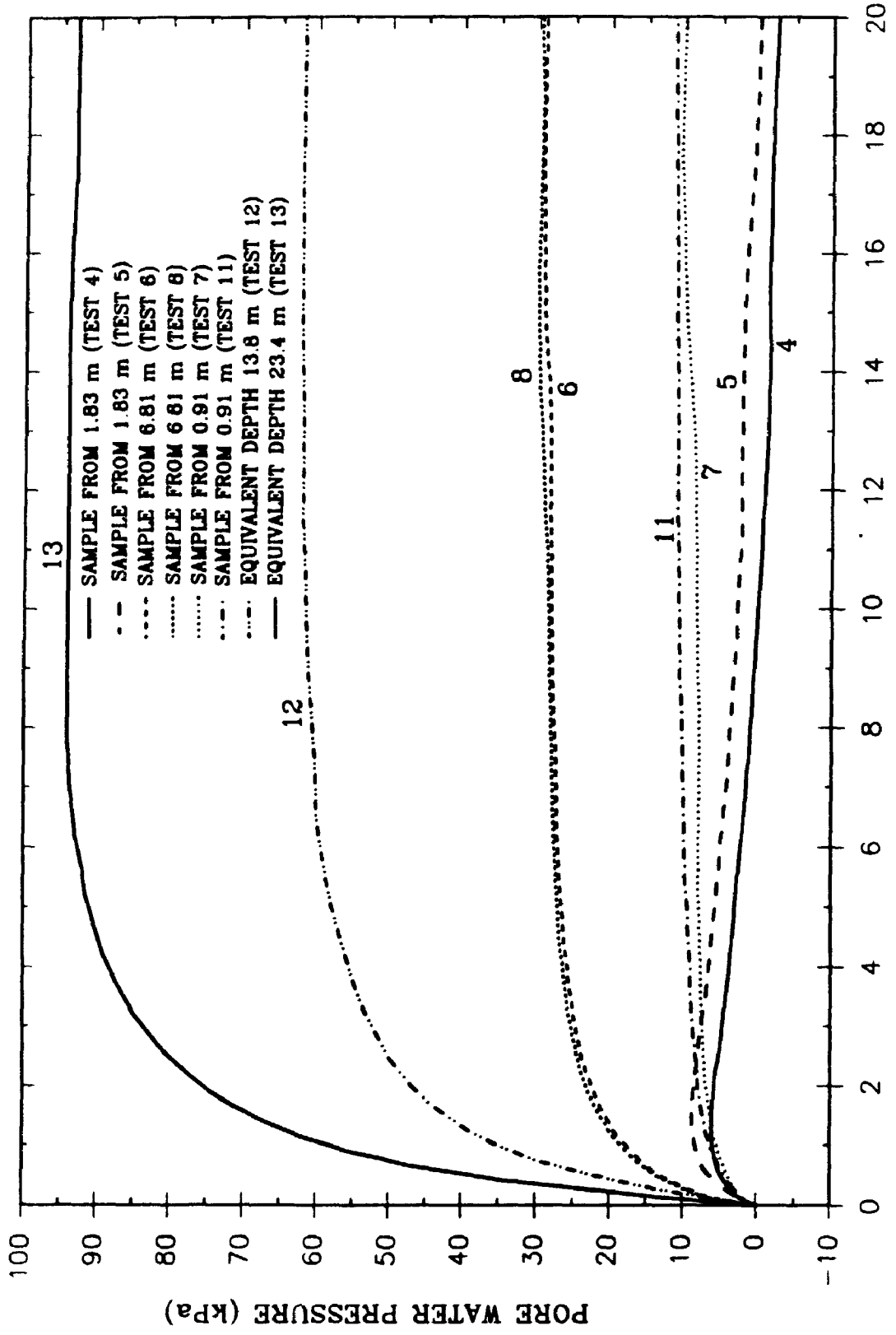

FIG. 6.9 VARIATION OF PORE WATER PRESSURE WITH AXIAL STRAIN – CAU TRIAXIAL TEST RESULTS

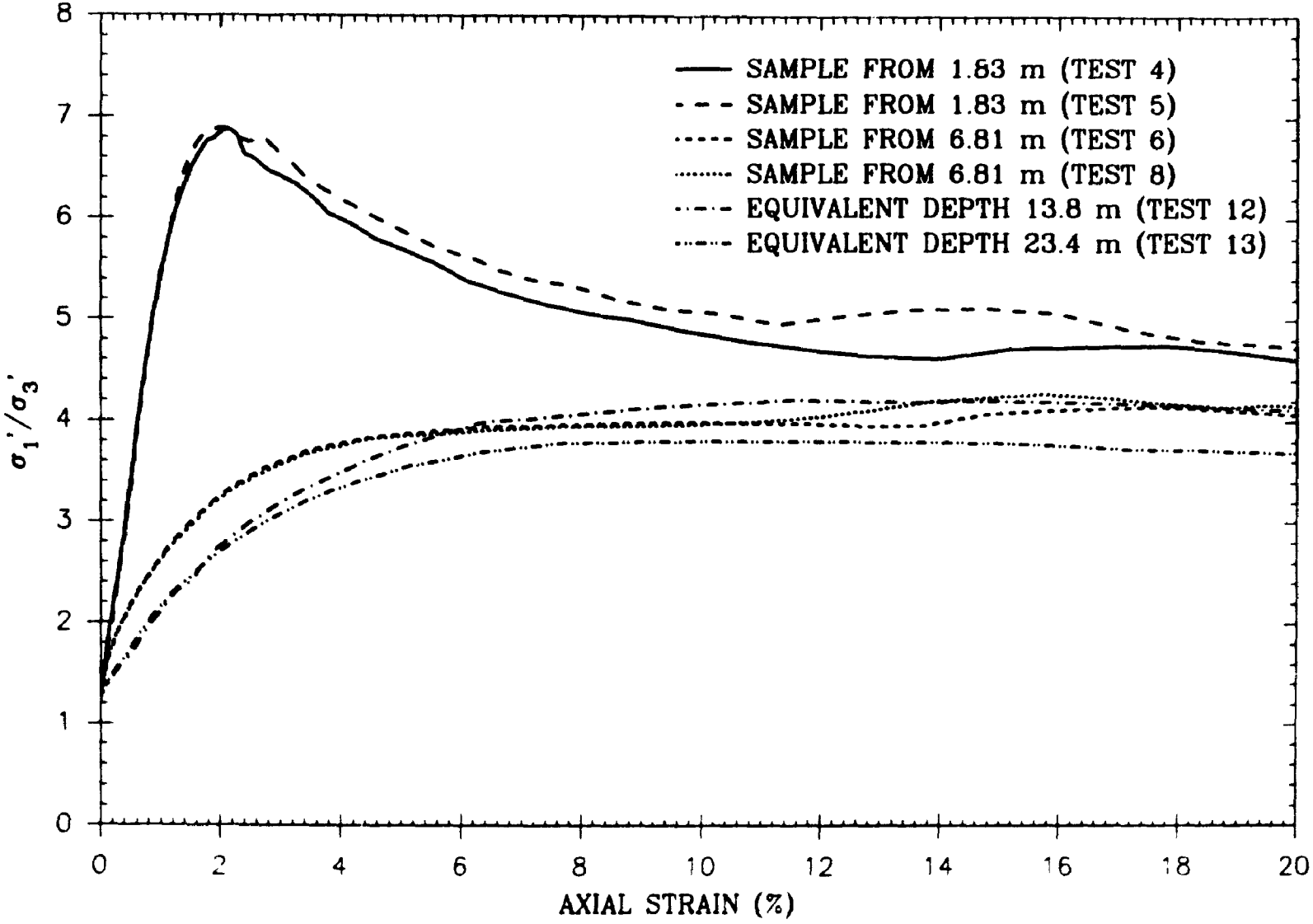

FIG. 6.10 VARIATION OF σ_1'/σ_3' WITH AXIAL STRAIN – CAU TRIAXIAL TEST RESULTS

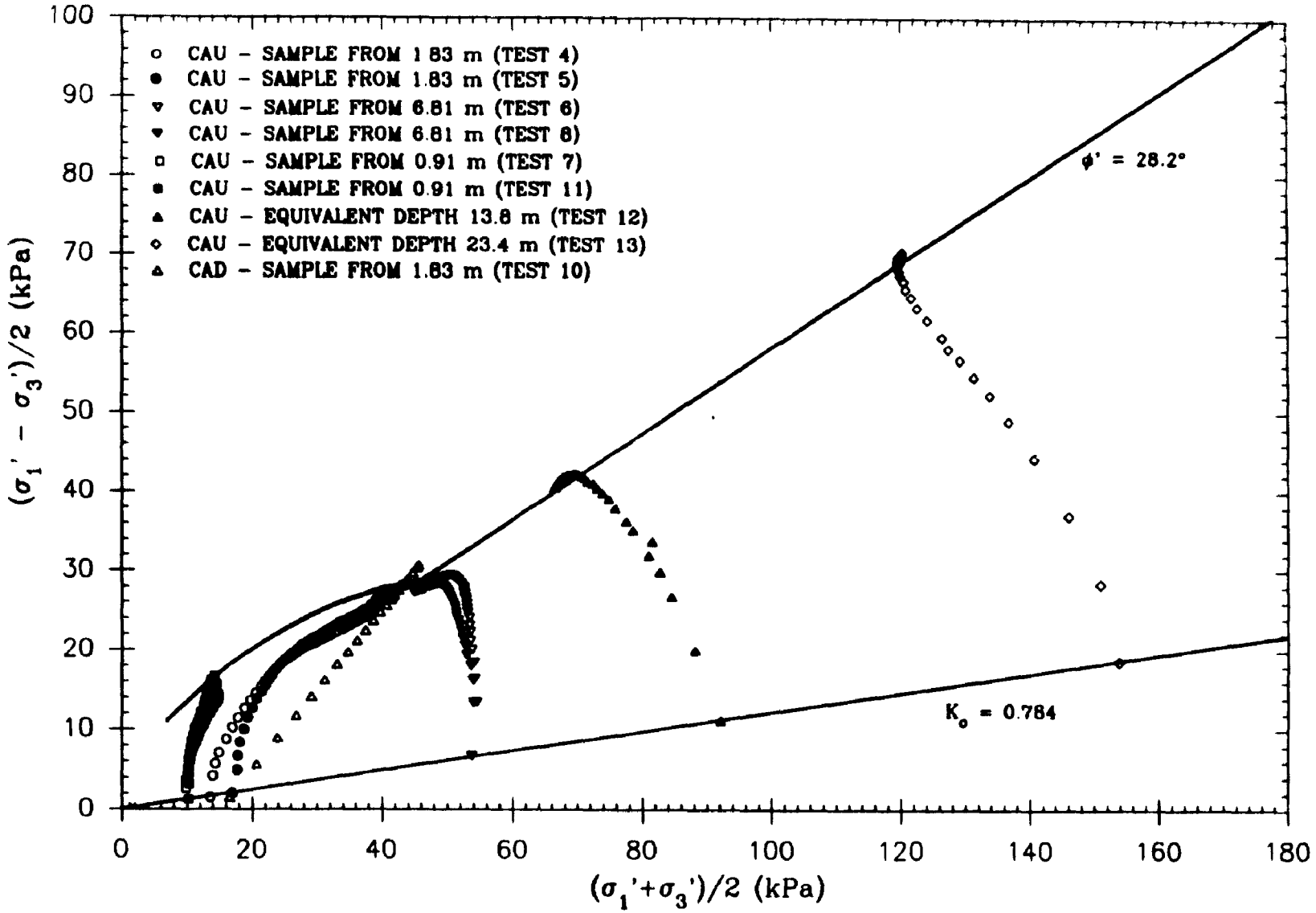

FIG. 6.11 VARIATION OF $(\sigma_1'+\sigma_3')/2$ Vs. $(\sigma_1-\sigma_3')/2$ - RESULTS OF CAU AND CAD TRIAXIAL TESTS

Table 6.4 Summary of CAU and CAD triaxial test results

Test #	Type of test	Depth of sample (m)	Water content (%)	Cons. pressure (KPa)		Volume change during cons. (%)	C_u (KPa)	** E_u or E' (MPa)	Approx. axial strain at failure (%)	A_f	Failure mode
				σ_1'	σ_3'						
4	CAU	1.83	40.3	15	12	2.71	* 18.65	3.08	2.15	.15	Bulging
5	CAU	1.83	40.7	19	15	2.44	* 19.15	3.87	1.97	.22	Bulging
6	CAU	6.91	45.9	60	47	5.97	27.9	9.70	4.20	.44	Bulging
8	CAU	6.91	43.6	60	47	5.74	27.84	11.0	4.30	.47	Bulging
7	CAU	0.91	74.4	11	9	2.83	15.7	1.73	21.2	.32	Bulging
11	CAU	0.91	79.0	11	9	3.56	16.1	1.96	20.3	.35	Bulging
12	CAU	*** 13.8	45.0	103	81		42.2	8.28	7.88	.72	Bulging
13	CAU	*** 23.4	44.2	172	135		70.3	12.70	12.22	.94	Bulging
10	CAD	183	40.5	19	15	2.53		2.88	6.40		Bulging

* Max. principal stress ratio failure criteria used.
** Secant modulus at 1/3 of failure stress.
*** Equivalent depth for the cons. pressures applied.

The tests on samples from 1.83 depth did not show clear maximum values for the deviator stress and the failure was interpreted using the maximum principal stress ratio criteria. These samples showed clear peaks for the principal stress ratio variation at low strain (of about 2%) suggesting that the soil dilates and is overconsolidated. A very small post peak decrease in strength (see Fig. 6.8) was observed in the tests with the samples from 6.81 m depth (i.e. tests 6 and 8) and the tests on samples of equivalent depth of 13.8 and 23.4 m (i.e. tests 12 and 13). The pore water pressures increased initially and then stayed more or less constant afterwards for these tests. The principal stress ratio response also was of similar nature suggesting that this soil is normally consolidated (or at most lightly over consolidated). The samples from 1.83 m showed significant continuous decrease in pore water pressures after the maximum and indicated negative pore pressures at large strains.

It is evident from the stress paths plotted as the variation of $(\sigma_1' - \sigma_3')/2$ with $(\sigma_1' + \sigma_3')/2$ that the samples from 6.81 m depth were normally consolidated or lightly over consolidated and the samples from 0.91 and 1.83 m were overconsolidated. The effective friction angle (ϕ') was found to be 28.2^o in the normally consolidated range. However, the K_o consolidated undrained and drained tests performed on samples from 0.91 and 1.83 depth indicated a mean value of $\phi' = 25.2^o$.

6.3.5 Results of CAD Tests

The deviator stress $(\sigma_1 - \sigma_3)$ and volumetric strain $(\Delta V/V_o)$ responses obtained for the strain controlled K_o consolidated drained (CAD) triaxial test performed on a sample from 1.83 m depth are shown in Fig. 6.12. A strain rate of about 0.246%/hr was used for this test and the sample failed at about 6.4% axial strain.

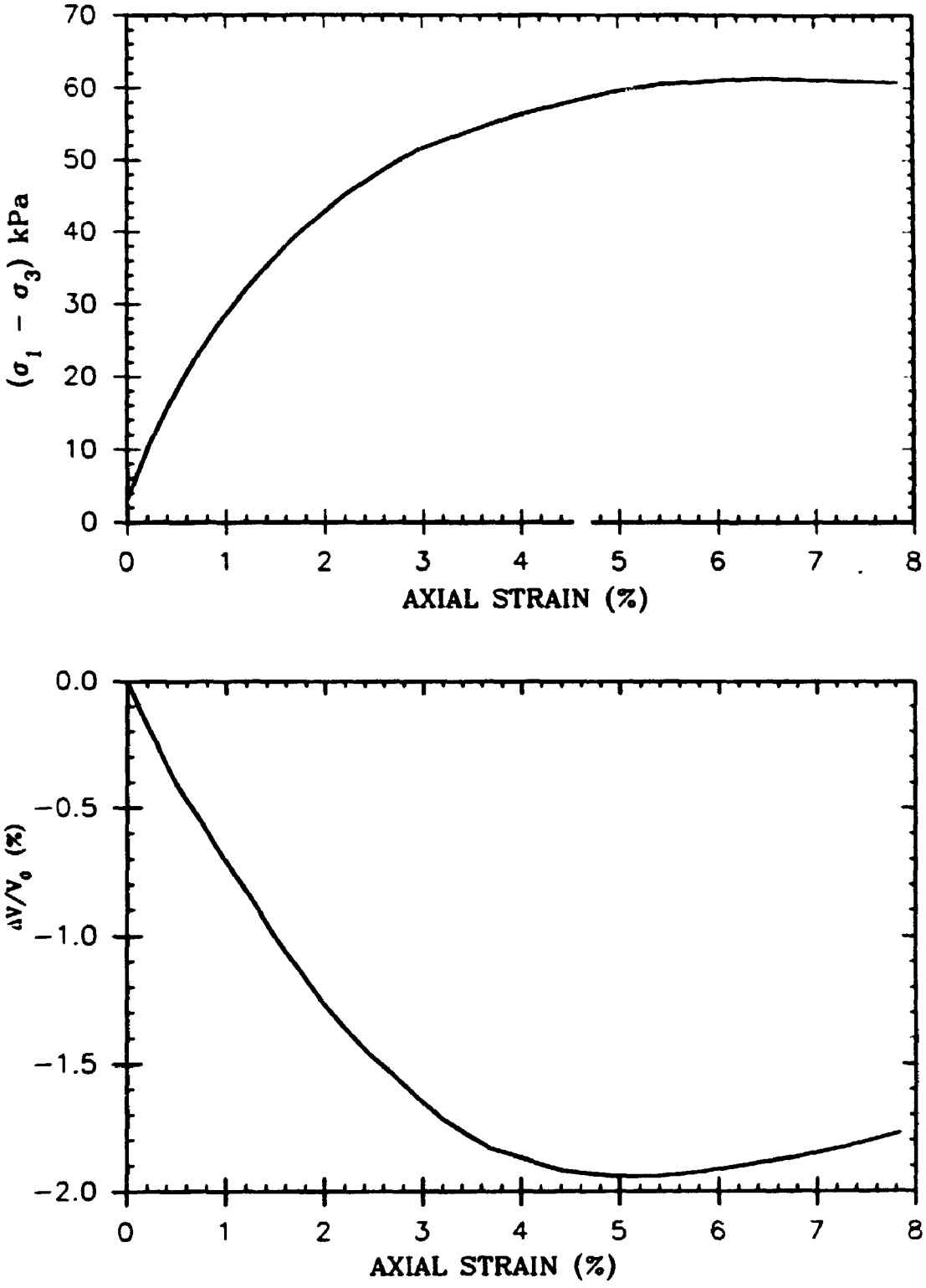

FIG. 6.12 CAD TEST RESULTS – SAMPLE DEPTH 1.83 m
(a) VARIATION OF $(\sigma_1 - \sigma_3)$ WITH AXIAL STRAIN
(b) VARIATION OF $\Delta V/V_0$ WITH AXIAL STRAIN

The sample underwent a volume decrease (to a volumetric strain of about 1.94%) until about 5.0% axial strain followed by an increase in volume or dilatancy. The initial volumetric strain response could be approximated to be linear (say up to about 3% axial strain) and the Poisson's ratio (ν), calculated from the volumetric strain ($\varepsilon_v = \Delta V/V_o$) and axial strain ($\varepsilon$) with the relationship

$$\nu = 0.5\,(1 - (\varepsilon_v/\varepsilon))$$

is about 0.21 for this region. The value of ν ranged between 0.31 and 0.35 (with a mean value of 0.33) for the range of axial strain between 5.0 and 6.4%. The value of the secant modulus was determined to be 2.88 MPa which corresponds reasonably well with those determined by NRC using the self boring pressuremeter (see Fig. 6.22).

6.4 DIRECT SIMPLE SHEAR TESTS

6.4.1 Introduction

For the purpose of examining the behaviour of the foundation soil in simple shear as well as to determine the shear strength parameters for comparison with the triaxial test results and the data from the field investigation, a series of constant volume direct simple shear (DSS) tests were performed on vertical samples obtained from various depths. Several types of simple shear test apparatus have been developed, but for reasons of convenience and the availability, the Norwegian Geotechnical Institute (NGI) Simple Shear Apparatus (Model h-12) was used for this investigation. Details regarding the use of this apparatus have been presented elsewhere (Bjerrum and Landva, 1966; Geonor, 1968). General information about the tests and the results of the tests performed are discussed in the following sections.

6.4.2 General information about the Simple Shear Tests Performed

In the NGI apparatus, a cylindrical specimen (of about 8 cm Dia. by 2 cm thick) confined in a reinforced rubber membrane is placed and clamped into the testing apparatus by means of top and bottom filter holders. The porous stones used at the top and bottom, between the specimen and the filter holder, have grids of built-in small pins that can be pressed into the specimen, thus preventing sliding between the filter holders and the specimen. The bottom holder is fastened to the base of the apparatus and prevents any movement of the bottom of the sample. The top holder, which is fastened to the top of the sample and to the apparatus, can move vertically under applied loads and horizontally under applied lateral displacement.

Vertical loads are applied to the specimen via a lever arm and hanger system (see Fig. 6.13 for the schematic of the apparatus). The magnitude of the vertical load is measured with a load cell and vertical displacement measured with a vertical dial gauge. Horizontal displacement is provided by a geared motor assembly which moves the yoke horizontally applying lateral displacement to the specimen. The horizontal shear force generated during shearing was measured with a load cell and horizontal displacements measured with a horizontal dial gauge. These load cells and dial gauges were monitored continuously with the use of a data acquisition and chart recorder.

The apparatus was designed to perform constant vertical stress (i.e. equivalent to a drained test when performed sufficiently slow) and constant volume tests. The constant volume test is equivalent to an undrained test. Undrained conditions are simulated by maintaining a constant specimen height. The change in vertical load induced by maintaining the specimen volume constant is equal to the change in pore pressure. Constant volume tests were performed on vertical samples from different depths using a

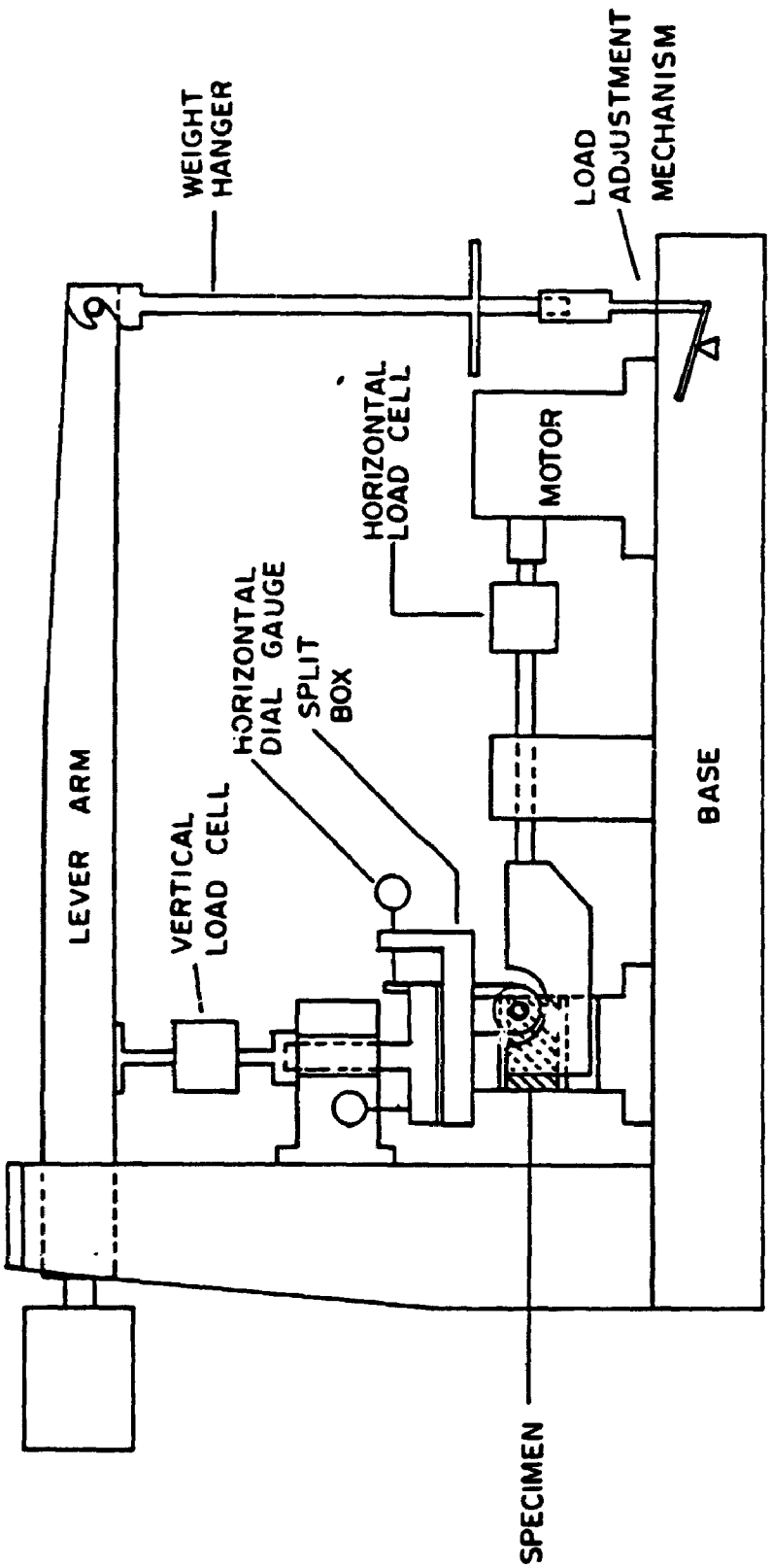

FIG. 6.13 SCHEMATIC OF SIMPLE SHEAR APPARATUS

constant rate of horizontal displacement equal to 1.98 mm/hr.

All the specimens were trimmed as out-lined in the operation manual of the simple shear apparatus. At the beginning of each test, the specimen was consolidated to its corresponding insitu effective overburden pressure. The amount of consolidation was measured by observing vertical movements with a dial gauge. Calibration curves determined by Johnson (1984) were used to account for the vertical and horizontal mobilities of the apparatus. The elastic resistance provided by the reinforced rubber membrane is also accounted for in the calibration of the horizontal load. The results from the constant volume simple shear tests are presented in the following section.

In essence, therefore, the apparatus attempts to simulate a state of plane strain in simple shear by applying uniform boundary displacements. However, the actual state of stress within the specimen during shearing is not completely described. Only vertical and horizontal loads are measured providing one point on the Mohr circle of stress. The sample experiences displacement conditions but complementary shear stress on the vertical sides of the sample may not be provided. The absence of these shear stresses has caused considerable controversy about the actual internal state of stress within the sample.

Several researchers (Budhu, 1984; Prevost and Hoeg, 1976; Wood et al., 1979; and Duncan and Dunlop, 1969, among others) have attempted to completely describe the state of stress within a soil specimen tested in the simple shear apparatus. The results of exhaustive analyses have still not provided accepted answers about the state of stress within the sample. However, the following points have been agreed upon: (i) the boundaries of the simple shear specimen are not subject to uniform stress, (ii) the inner portion of the specimen is subject to a stress condition which closely approximates one of simple shear stress (at least for strains less than 5%), (iii) the reinforced membrane does

not have adequate stiffness, bulging occurs and the diameter of the sample does not remain constant - a prerequisite for plane strain deformation, and (iv) slip between sample and the top and bottom plates results in a more non-uniform stress distribution.

The uncertainties regarding the actual state of stress within the sample tested in the NGI simple shear stress apparatus requires that the failure values and moduli obtained be used with some degree of caution. A comparative study of results obtained in the NGI device, standard triaxial cell, and hollow cylinder device by Saada and Townsend (1981) indicated that for both sands and clays under static and dynamic conditions, the NGI device led to modulus and shear strength values that were smaller (in the order of 10%) than those obtained in the other two devices. A similar conclusion was made more recently by Airey and Wood (1987) for DSS tests on clays using the Geonor apparatus. In this light, it appears that the shear strength and moduli obtained for the foundation soil in this investigation are likely to be the lower bound.

6.4.3 Results of the Simple Shear Tests

Consolidated constant volume DSS tests were performed on samples obtained from 0.91 m, 1.83 m, 3.96 and 6.81 m depth. Two tests were performed on the samples from 1.83 m to check the reproducibility of the test results. The variation of shear stress with the shear strain obtained from these tests are shown in Fig. 6.14 and the stress paths followed during the tests are shown in Fig 6.15 as the variation of shear stress with normal test. A summary of the results is presented in Table 6.5 and the following observations are made from the results:

(i) The results, including the stress strain plots as well as the stress paths, of the two tests performed on the samples from 1.83 m depth were very close. This in turn

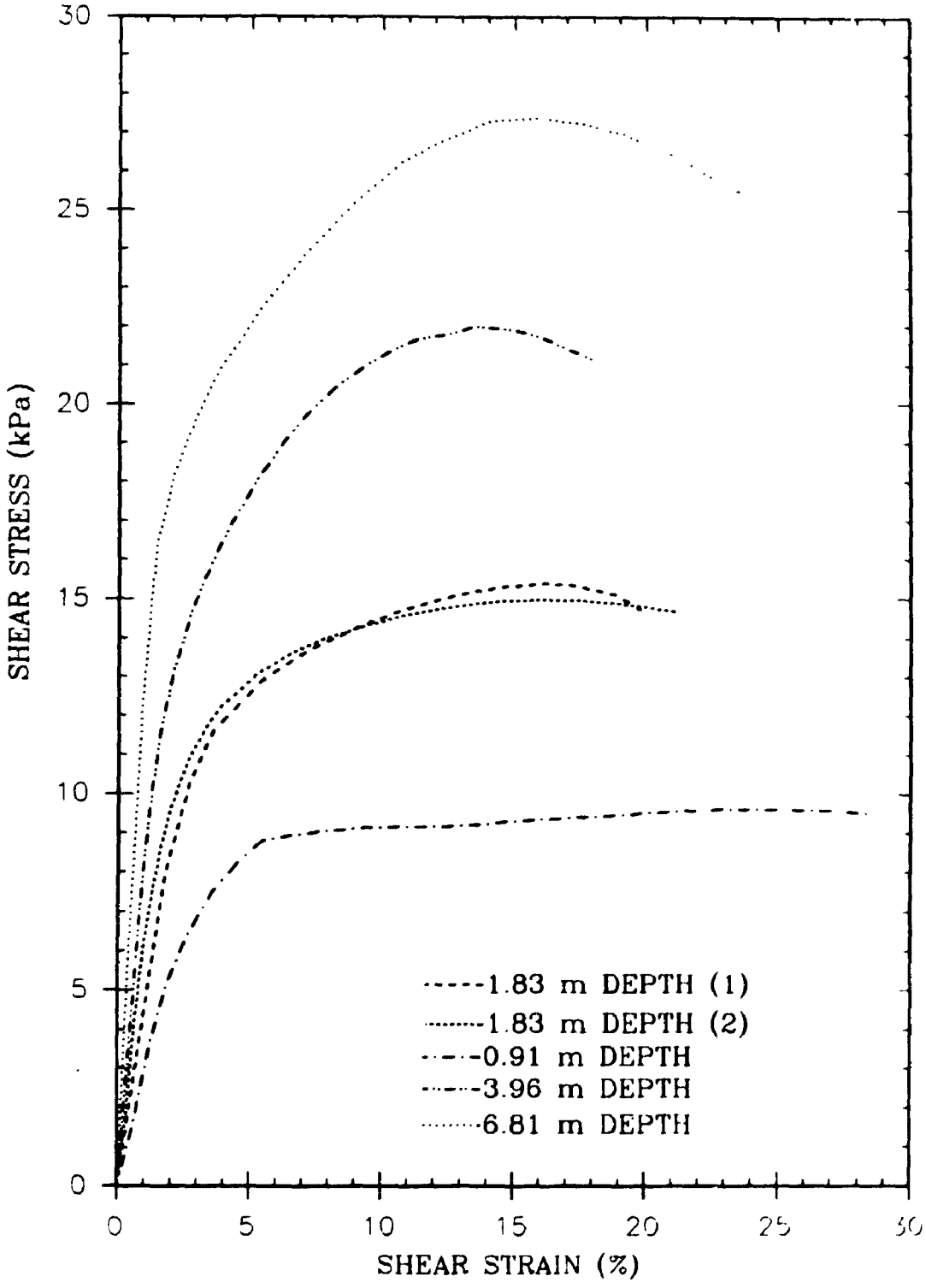

FIG. 6.14 VARIATION OF SHEAR STRESS WITH SHEAR STRAIN - SIMPLE SHEAR TEST RESULTS

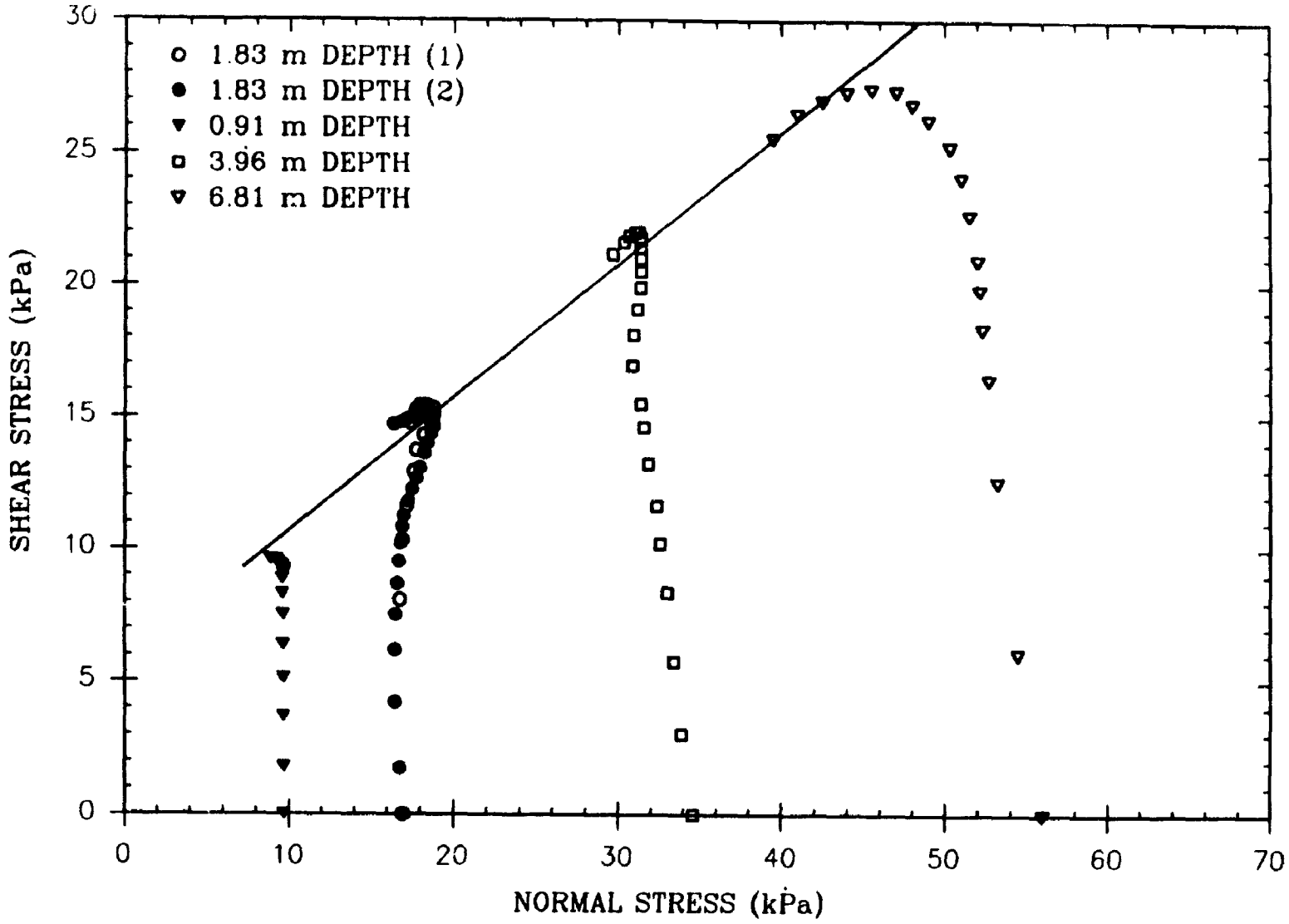

FIG. 6.15 VARIATION OF SHEAR STRESS WITH NORMAL STRESS - CONSOLIDATED CONSTANT VOLUME SIMPLE SHEAR TEST RESULTS

Table 6.5 Summary of Direct Simple Shear test results.

Depth of sample (m)	Natural water content (%)	Vertical cons. stress (kPa)	** Volume change during cons. (%)	C_u (KPa)	Approx. shear strain failure (%)	* Shear Modulus G (kPa)
0.91	86.8	9.2	4.63	9.62	24.0	280
1.83(1)	41.7	17.0	3.62	15.4	15.8	480
1.83(2)	40.6	17.0	3.86	15.0	16.0	620
3.96	60.2	34.6	5.47	22.0	13.5	820
6.81	43.5	56.0	5.95	27.4	15.6	1500

* Secant at 1/3 of maximum shear stress.
** Assuming no lateral deformation during consolidation.

confirms the consistency of the test results.

(ii) The samples generally failed at large shear strains (above 10% strain).

(iii) The sample from 0.91 m depth indicated a reasonably flat shear stress-strain response after about 6% shear strain. This (fibrous organic silty clay) sample (of high compressibility) indicated failure at a very large shear strain of about 24%.

(iv) The samples from 3.96 and 6.81 m depth showed significantly larger post peak decreases in shear stress compared to the samples from 1.83 and 0.91 m depth.

(v) The value of ϕ' estimated from the constant volume tests at large shear distortions by assuming $\tau/\sigma = \tan\phi'$ indicated a ϕ' value of 26.7^{o}. This value of ϕ' is quite close to the value of 28.2^{o} determined from the CAU triaxial tests. A similar finding was reported by Airey and Wood (1987) from the tests performed on normally consolidated kaolin.

The difficulties involved in interpreting simple shear test results due to the uncertainties of the actual state of stress of the sample were discussed in section 6.4.2. However, the following two consistent observations made during this testing program may be considered as indications that uniform shear strain and stresses were approximated:

(i) The porous stones used in this apparatus contained a grid of built-in small pins which were pressed into the specimen mainly to ensure nonslippage between the specimen and the apparatus. After testing and on careful separation of the porous stones, it was consistently observed that the grid of holes left in the specimen remained undistorted. This suggests that there was no significant slippage between the specimen and the

apparatus.

(ii) Observation of the sample configuration after the test indicated that an approximate simple shear configuration was obtained even at large shear strains (i.e. above 20%).

Variation of the undrained shear strength with depth obtained from the DSS tests will be compared with the similar results from the triaxial tests in a later section (see section 6.7.1).

6.5 CONSOLIDATION (OEDOMETER) TESTS

6.5.1 Introduction

To study the consolidation characteristics of the foundation soil, consolidation (oedometer) tests were performed on samples from different depths. These tests were carried out using conventional equipment with fixed oedometer rings and double drainage. A conventional load increment ratio of 1 was used for these tests and each individual load increment was applied for 24 hours (i.e. the loading increments were doubled every 24 hours). The details of the tests performed, procedure used and the results obtained from these tests are presented in the following section.

6.5.2 General details and the results of the consolidation tests

A total of four consolidation tests were performed on samples from 0.91, 1.83 and 6.81 m depths. One sample from each depth was trimmed vertically and an additional sample from 1.83 m depth was trimmed horizontally. A detailed description of the

consolidation test procedure can be found elsewhere (see Bowles, 1978 and Head, 1982), however, a brief summary is outlined here. The specimens were carefully trimmed using the standard consolidation ring (i.e. the specimen size is 50 mm diameter by 15 mm thick). The oedometer rings were lightly greased to reduce side friction. Initial water contents were obtained using the sample trimmings. Each specimen was then placed in the oedometer with filter paper and porous stones above and below to permit drainage. The tests were conducted with the samples submerged in water to prevent drying of the samples.

Each specimen was loaded through a porous loading cap and vertical deformations of the top surface of the cap were measured at specified time intervals using a dial gauge. Load was applied in increments (i.e. every 24 hours) using the following sequence 25, 50, 100, 200, 400, 800 and 1600 kPa and unloaded in the reverse order of the same sequence. Appropriate corrections were applied to the dial readings to account for the deformation of the apparatus.

Dial reading versus square-root of time for each loading increment was plotted for each test. These curves were used to determine t_{90}, the time for 90% primary consolidation, using Taylor's square-root-of-time method. Dial reading versus log time was also plotted for each increment in order to determine the t_{50} and t_{100}, the time for 50% and 100% primary consolidation respectively, using the Casagrande's method. However, the determination of t_{50} and t_{100} using Casagrande's method was quite ambiguous (except for the sample from 0.91 m depth) and therefore only the t_{90} obtained using the Taylor's method was used for all further calculations.

The void ratio (e) versus log consolidation pressure (i.e. $\log\sigma'$) curves obtained from these tests are shown in Figure 6.16 and the variation of the log of permeability with

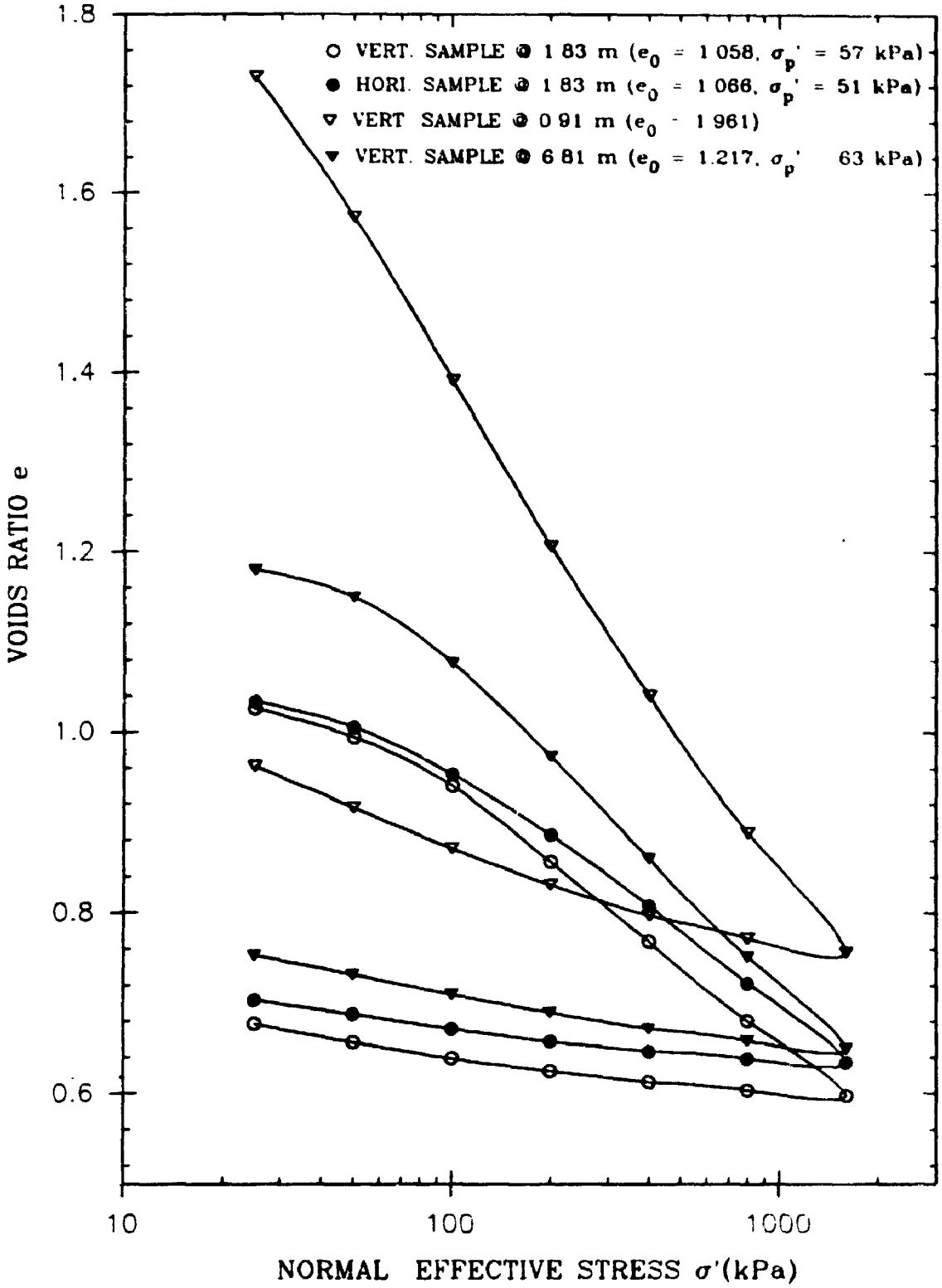

FIG. 6.16 VARIATION OF VOIDS RATIO WITH EFFECTIVE STRESS

the voids ratio are shown in Fig. 6.17. From the e - logσ' curves, the most probable value of the preconsolidation pressure (σ_p') was estimated for each sample using the Casagrande's method. The summary of the results from the consolidation tests are presented in Table 6.6. The e - logσ' curve for the sample from 0.91 m was more or less a straight line and it was not possible to determine its σ_p' using conventional methods (Casagrande, 1936; Schmertman 1955; Burmister 1942 and 1951; Janbu et al, 1981). The sample was apparently heavily overconsolidated and generally σ_p' is poorly defined for such soils (Crawford, 1986). Furthermore, it appears that the standard load increments used for these tests were not small enough in the low stress range for the determination of σ_p' for such shallow samples. The estimated insitu effective stress for the sample from 0.91 m depth was only about 9 kPa and the first load increment used for the tests was from zero (i.e. no seating load applied at the beginning) to 25 kPa. However, it was attempted to use the work per unit volume - effective stress relationship method proposed by Becker et al. (1987) to determine the σ_p' (see Fig. 6.18). The most probable values of the σ_p' obtained using this method are also presented in Table 6.6. These values correspond reasonably well with the values obtained using the Casagrande method for the other samples.

The values of the compression index, C_c, determined from the e - logσ' curves are in reasonably good agreement with those determined using the empirical relationship developed by Terzaghi and Peck;

$$C_c = 0.009\ (w_L - 10),$$

where w_L = the liquid limit expressed in percent.

The permeabilities decreased with the decrease in void ratio as expected (see Fig. 6.17).

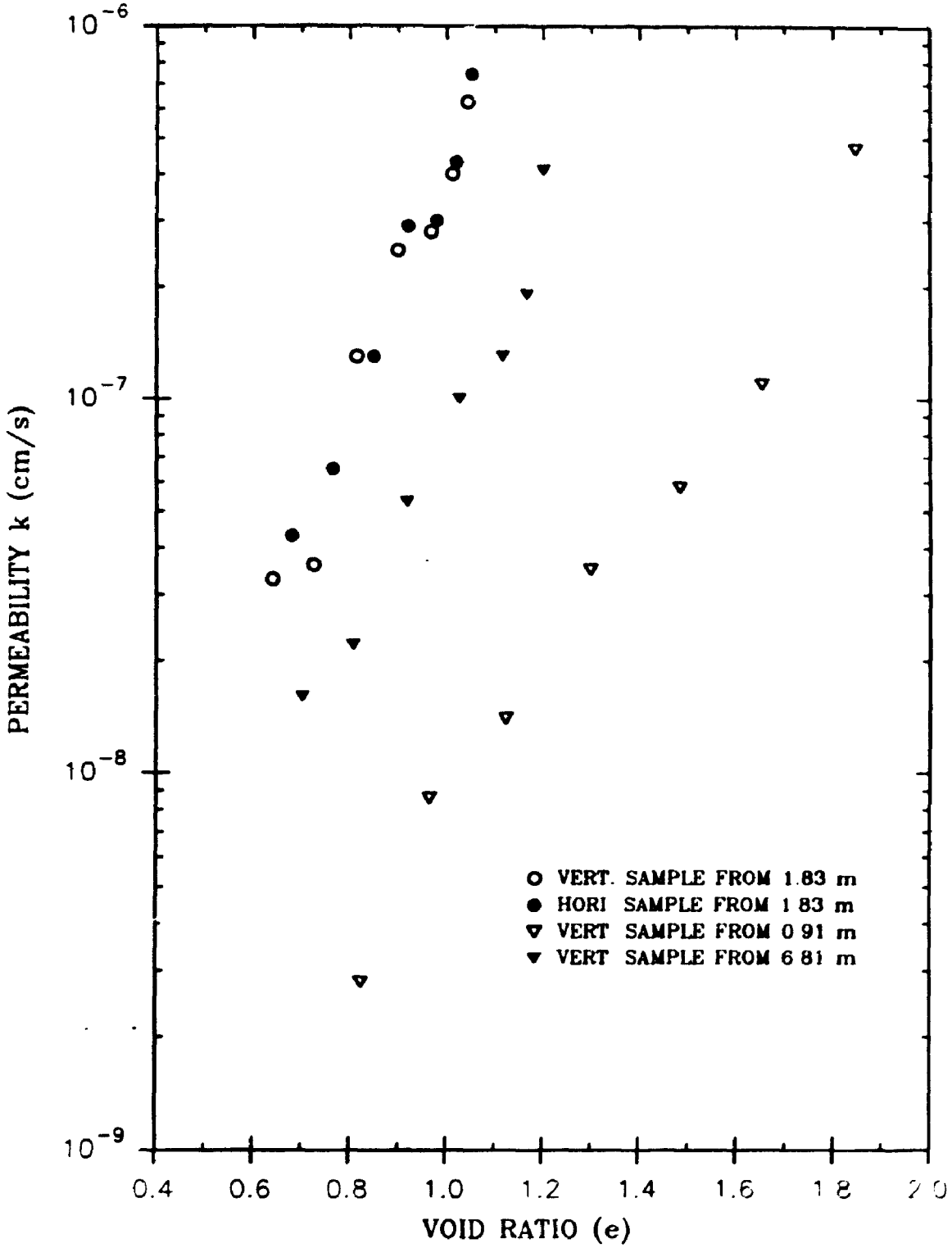

FIG. 6.17 VARIATION OF PERMEABILITY WITH VOID RATIO – CONSOLIDATION TEST RESULTS

Table 6.6 Summary of the results from consolidation tests.

Depth of sample (m)	Orientation of sample	C_c	C_R	σ_p' * (KPa)	Estimated σ_o' (KPa)	OCR [a]	σ_p' ** (KPa)	OCR [b]	C_c=0.009 (w_L-10)
0.91	Vertical	0.557	0.126		8.8		32	3.6	0.594
1.83	Vertical	0.255	0.049	57	16.0	3.6	62	3.9	0.284
1.83	Horizontal	0.286	0.040	51	12.5	4.1	53	4.2	0.284
6.81	Vertical	0.355	0.062	63	52.4	1.20	62	1.2	0.347

* Most probable value of the preconsolidation pressure using Caragrade's method.
w_L = Liquid limit in percent
** = Obtained using the work method proposed by Becker et al, 1987
σ_o' = Estimated normal effective stress.
σ_p' = Preconsolidation pressure.
a = With σ_p' obtained using Casegrande's method.
b = With σ_p' obtained using the work method of Becker et al, 1987

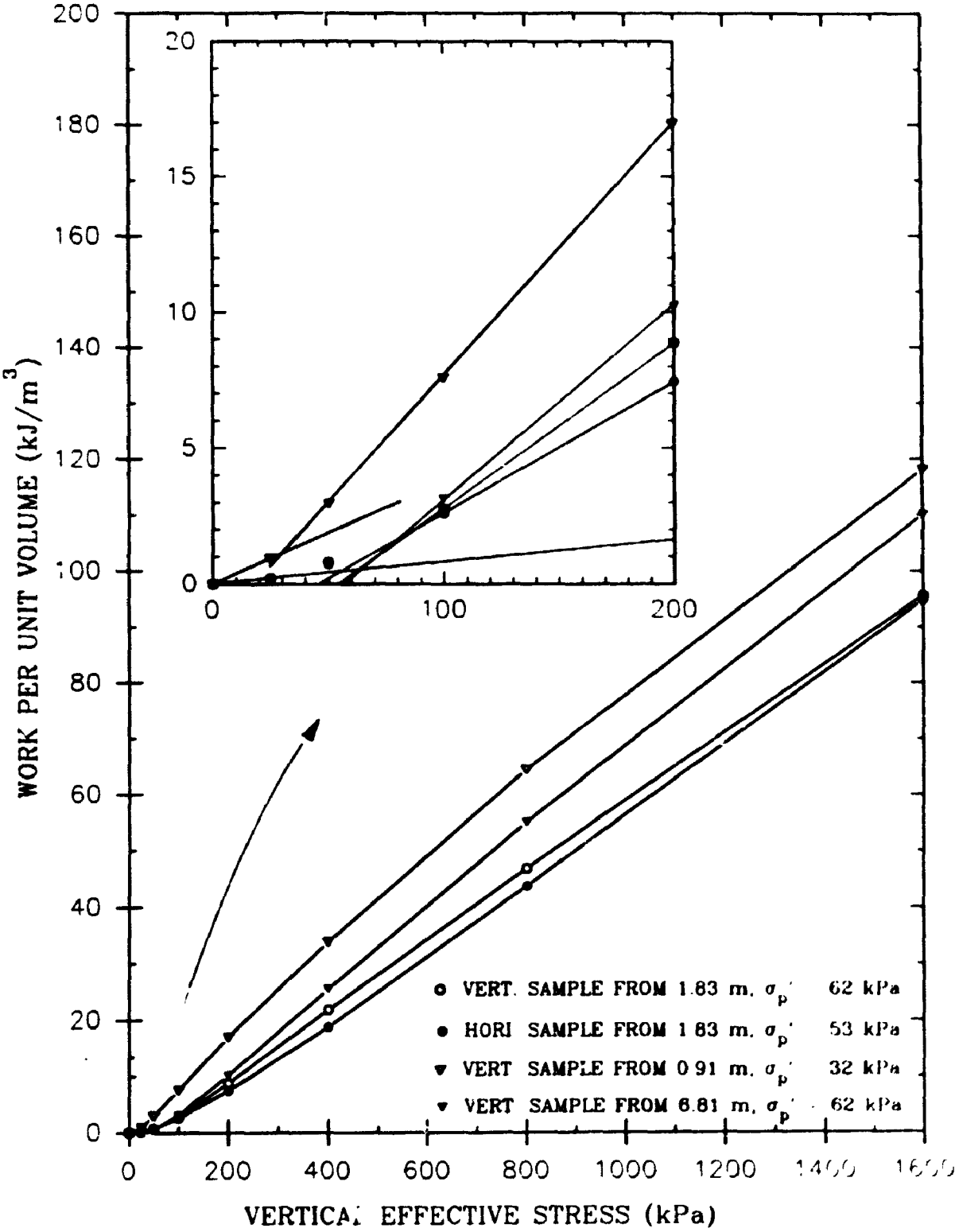

FIG. 6.18 WORK PER UNIT VOLUME INTERPRETATION OF CONS TEST RESULTS

Significantly larger decreases in the permeability were observed, particularly for the samples from 0.91 and 6.81 m depths, when the soil changes from an overconsolidated state to a normally consolidated state. Different curves fitted for the variation of permeability with the void ratio at the overconsolidated and normally consolidated states were used in the finite element analysis as reported in Chapters 8 and 9.

6.6 PERMEABILITY TESTS

6.6.1 Introduction

Constant head permeability tests were conducted on a vertical and a horizontal sample (both obtained from a depth of 2.57 m) at different confining/consolidation pressures to determine the permeabilities in the vertical and horizontal direction respectively and their variation with confining pressure. Triaxial type flexible wall permeameters (manufactured by Brainard-Kilman, Stone Mtn, GA30086, USA - Model S-480 Permeability cell and Model S500 Triaxial/Permeability panel with optional de-airing tank) were used for these tests. De-aired tap water was used as the permeant. Details of this apparatus and its operation are given in the operation manual provided by the manufacturer. Details of the tests performed and the results obtained are discussed below.

6.6.2 Details of the permeability tests performed and the results

The schematic of the triaxial permeability cell of the flexible wall permeability test apparatus used in this investigation is shown in Fig. 6.19. In these tests, the specimen is contained within a flexible (latex) membrane. Pressurized fluid surrounding the membrane applies a confining stress on the soil, and holds the membrane against the side of the sample while allowing sample deformation.

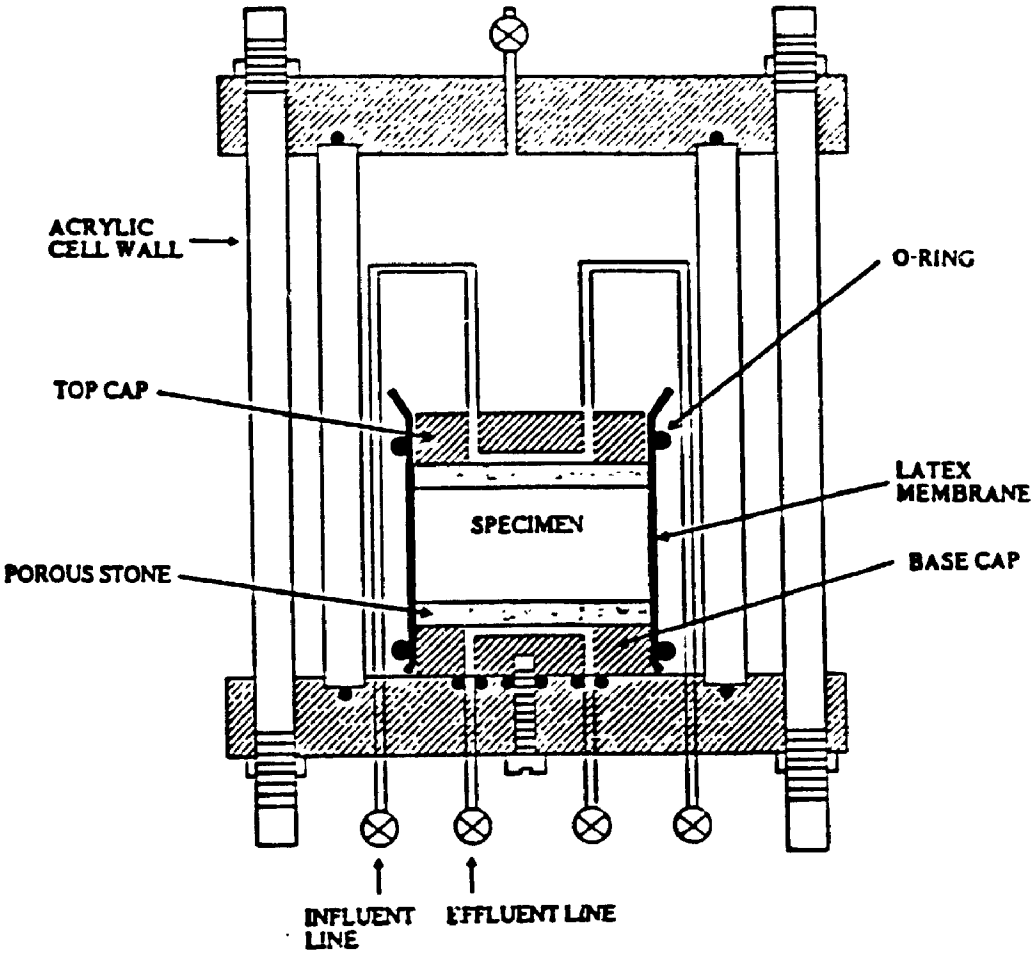

FIG. 6.19 SCHEMATIC OF FLEXIBLE WALL TRIAXIAL PERMEABILITY CELL

Cylindrical specimens (measuring about 70 mm Dia. by 100 mm long) were trimmed from the 200 mm Dia. undisturbed samples similar to the triaxial tests discussed previously and placed in the cell with filter paper and porous stone at the top and bottom. Each sample and the vertical sides of the porous stones were applied with a thin coating of (Dow Corning) high vacuum grease and encased in a latex membrane to eliminate side wall leakage. In order to ensure nonleakage of the permeant through the side wall, an additional layer of high vacuum grease was applied on the outer surface of the already placed membrane and the sample was encased in another latex membrane. The sample was then placed in the triaxial permeability cell and sealed at the ends with the use of "O" rings.

The samples were saturated with the application of (100 kPa) equal cell pressure and back pressure (i e. 100 kPa at both influent and effluent ends). The degree of saturation was checked similar to the triaxial tests and the samples were consolidated overnight at the required cell pressures (i.e. the cell pressure increased by the amount of consolidation pressure required but the influent and effluent pressures kept equal). Volume changes were monitored during saturation and consolidation phases of the tests. The influent and effluent pressures were set to the required values after consolidation, and the volume of water flow through the samples monitored periodically. A hydraulic gradient of 10 was used throughout this testing (i.e. to set the influent pressure) and each test at a particular confining pressure was continued for 5 to 6 days. Each sample was tested at 20, 50, 100 and 200 kPa consolidation/confining pressures.

The permeability was calculated from the rate of flow determined for each test. The summary of the permeability test results are presented in Table 6.7 and the variation of the permeability with the consolidation (i.e. confining) pressure obtained from these tests are shown in Fig. 6.20. For comparison purposes, the variation of the permeability

Table 6.7 Summary of results from permeability tests on samples from 2.57 m depth.

Confining pressure (KPa)	k_y (cm/s)	k_x (cm/s)	k_x/k_y
20	1.007E-6	2.564E-6	2.55
50	3.075E-7	1.276E-6	4.15
100	1.063E-7	6.688E-7	6.30
200	4.743E-8	4.289E-7	9

k_y = Permeability in the vertical direction.
k_x = Permeability in the horizontal direction.

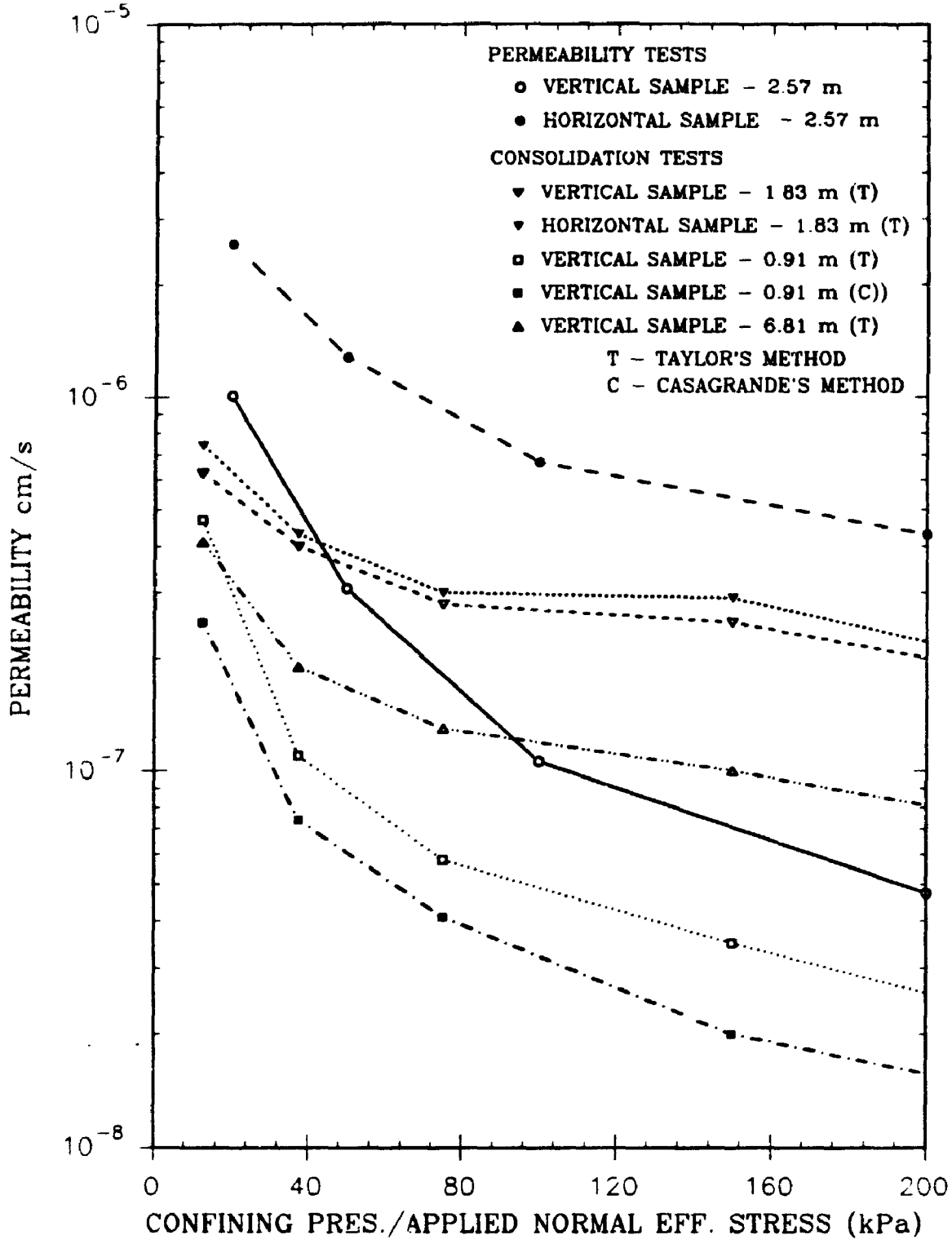

FIG. 6.20 VARIATION OF PERMEABILITY WITH CONFINING PRESSURE/ APPLIED NORMAL EFFECTIVE STRESS

with the applied normal effective stress obtained from the consolidation tests are also presented in this figure. The following observations are made from these results:

(i) The permeabilities decrease with the increase of either the confining stress or the normal effective stress.

(ii) Both the permeability tests and the consolidation tests indicate that the permeability is anisotropic, the horizontal permeability (k_h) is significantly greater than the vertical permeability (k_v). The permeability tests indicated that the ratio (k_h/k_v) increased from about 2.5 to 9 when the confining pressure was increased from 20 to 200 kPa. However, the consolidation tests on the vertical and horizontal samples from 1.83 m depth indicated that the (k_h/k_v) ratio to be in the order of only 1.2 (i.e. between 1.1 to 1.2).

(iii) The permeability tests indicated more dramatic decreases in (both vertical and horizontal) permeabilities with increasing confining pressure compared to the consolidation tests (e.g. see the results for samples from 1.83 m or 6.81 m depths). However, it is noted that this comparison is not strictly valid because the pressures applied in both the radial and axial directions for the samples tested in the triaxial permeability tests are equal to the confining pressure whereas the radial stress is unknown (and probably much smaller than the axial stress) in the consolidation tests. Furthermore, the sample used for the consolidation tests are much smaller than that used for the permeability tests. Despite these differences, however, comparison of the results between the permeability tests (on samples from 2.57 m depth) and the consolidation tests on the samples from 1.83 m depth (i.e. the closest sample depth to that of permeability test samples), indicate that the permeabilities from both test methods are of the same order of magnitude.

(iv) The sample from 0.91 m depth, a highly compressible fibrous organic silty clay, showed larger decrease in permeability with the applied normal effective stress compared to the samples from 1.83 and 6.81 m depths. It is also noted that the permeabilities determined using the Taylor's square-root-of-time method (i.e. for the determination of t_{90}) were larger than those determined using the Casagrande's log-time method (i.e. for the determination of t_{50} and t_{100}).

6.7 COMPARISON OF THE RESULTS FROM LAB INVESTIGATION WITH FIELD DATA

6.7.1 Variation of Undrained Shear Strength with Depth

The variation of the undrained shear strength (C_u) with depth (i.e. the shear strength profile) obtained from field vane tests as well as laboratory tests (i.e. both CAU triaxial tests and DSS tests) are shown in Fig. 6.21. The average as well as the range of the C_u values from the vane tests at locations V1, V2 and V3 in the main reinforced section of the embankment are plotted in this figure. The cone resistance (q_c) measured from the continuous (pencil) piezo-cone tests performed at the site of this embankment were reported in Chapter 3 (see Fig. 3.3b). These tests were performed at five locations and TM2, TM3 and TM4 are the only three of them which fall within the reinforced section of the embankment (see Fig 3.2 for the locations). The value of C_u could be interpreted from the cone resistance using the equation,

$$q_c = C_u N_c + \sigma_o$$

where N_c is a constant usually ranges between 6 and 14, and the term σ_o represents the total overburden pressure. The variation of C_u with the depth interpreted using this

equation for the mean of the cone resistance profiles at locations TM2, TM3 and TM4 is also shown in Fig. 6.21. It is noted that the shear strength profile interpreted using the above relationship could have significant variation depending on the value of N_c , which could be of different value for different types of soils. A value of $N_c = 8$ was used for this interpretation. A larger value of N_c (> 8) would result in much smaller shear strength between 3 and 8 m depths, and a smaller value of N_c (< 8) would indicate a larger shear strength, greater than the vane strength for depths greater than 10 m. Therefore, the interpretation shown in this figure represents a reasonable estimate for the shear strength profile (i.e. average for the locations TM2, TM3 and TM4).

The following observations are made from this figure:

(i) there was considerable variation in the C_u obtained from the vane tests performed at different locations indicating that the shear strength profile varies considerably with the location across the reinforced embankment section.

(ii) the average vane strength profile indicated an increase in C_u with depth between 2 and 3m followed by a decrease between 2 and 4 m depth. The overall trend was an increase of $C_u$with depth, for depths greater than 3 m, but with a relatively stiffer soil beneath 7 m depth.

(iii) the DSS showed significantly lower C_u values than the CAU tests for samples from shallow (i.e. < 2m) depth. It was discussed previously that the DSS tests would give lower bound values for the strength. However, the difference was not significant for the deeper samples (i.e. depth greater than 3 m).

(iv) the shear strength profile interpreted from the cone data indicated the existence

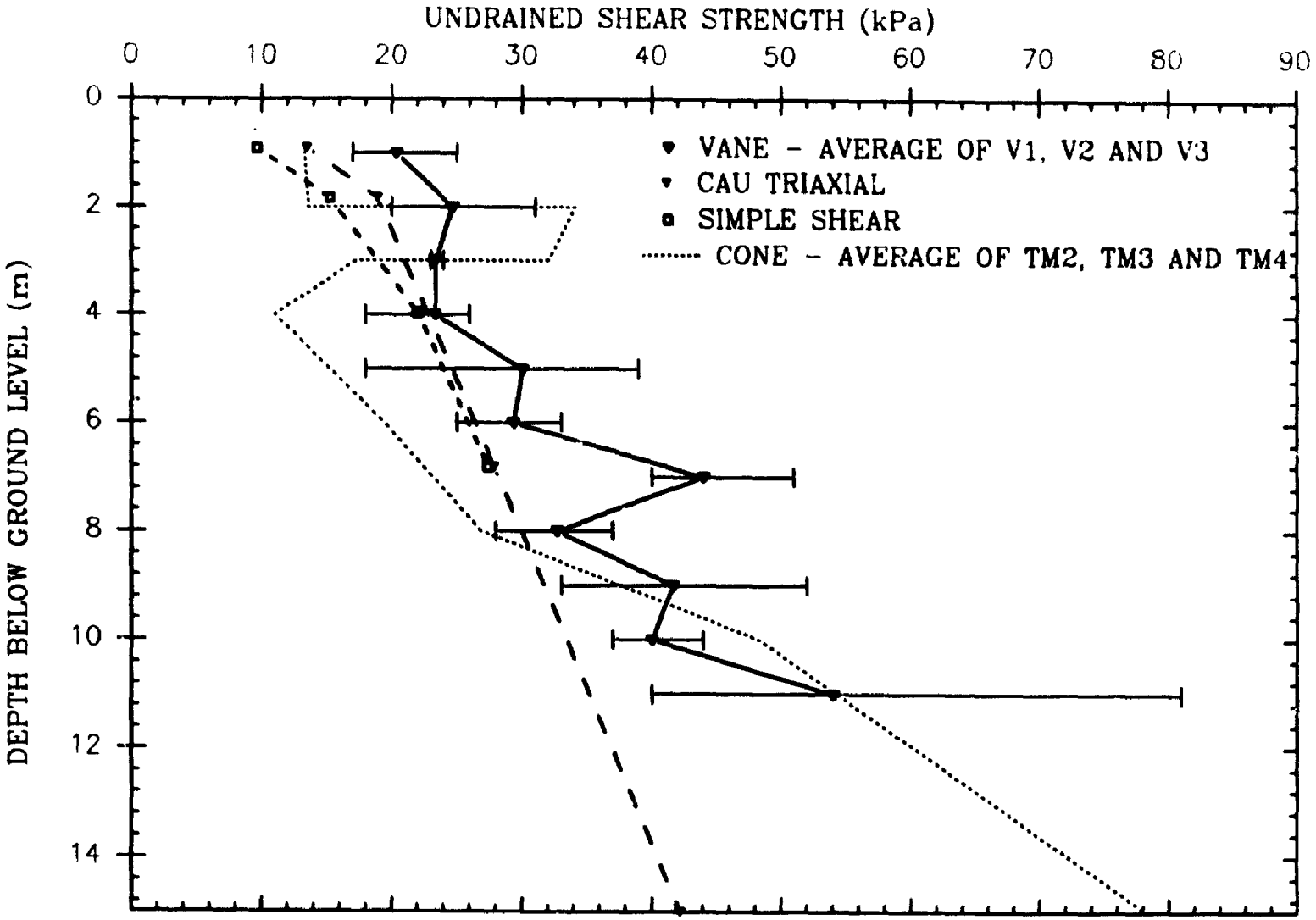

FIG. 6.21 VARIATION OF UNDRAINED SHEAR STRENGTH WITH DEPTH – SUMMARY OF ALL THE RESULTS

of a relatively stiffer stratum of soil between 2 and 3 m depth underlain by a weaker soil around 4 m depth. The cone shear strengths were less than those obtained from the other tests between 1 and 2 m as well as between 3 and 8 m depths.

(v) the C_u values obtained from CAU triaxial tests for shallow depth (< 2 m) were significantly lower than that obtained from the vane tests (i.e. the average as well as the lowest value of its range). However, the difference was not significant for depths greater than 3 m, considering the variation in the vane strength itself at different locations. The possible reasons for this discrepancy at shallow depth are

(a) disturbance of lab samples;

(b) strength anisotropy and strain rate during vane tests; and

(c) special nature of the soil such as the presence of fibrous material and/or organics in the soil.

Since the Plasticity Index of the particular soil ranged between 10 and 25%, Bjerrum's correction for the vane strength to account for (b) above is not significant (i.e. $\mu = 1$). Recent studies (e.g. Chandler, 1988) suggest that Bjerrum's relationship is appropriate for inorganic soils but they caution the use of such relationship for organic soils and other soils of special nature. Visual observation of the samples at shallow depth (up to about 1.5 m) as well as samples between 5.5 and 6.5 m showed the presence of significant quantity of organic fibrous material which would have resulted in an over estimation of the shear strength by the vane test. The soil at other depths also contained significant quantity of organics and it is believed that the Bjerrum's correction (factor of $\mu = 1$) is not directly applicable for these soils.

It is also possible that disturbance would result in an underestimate of the shear strength during lab investigation. However, it is not reasonable to expect more disturbance of the shallow sample than the deeper samples and the observation of close relationship between the vane strength and the strength obtained from lab tests for the soil below 3 m depth indicate that the sample disturbance was not significant. Moreover, the volume change during the consolidation phase of the CAU and CIU triaxial tests were less than 6% suggesting that the sample disturbance was not significant. Therefore, it is reasonable to consider the shear strengths obtained from the laboratory tests to be representative of the true behaviour.

From the discussion above, it is apparent that there is significant variation in the shear strength profile at different locations across the embankment. Considering all these variabilities, and the fact that the vane tests were relatively more specific to the test embankment configuration, it is appropriate to give more weight to the vane data for the C_u profile. However, the vane tests usually indicate a higher value for the shear strength and the average vane strength profile discussed earlier could therefore be considered as the upperbound. The CAU triaxial tests also indicated a reasonable estimate of the shear strength profile and it fell mostly within the range of variation of the vane strength. Considering the previous discussion about the various possibilities for the discrepancy between the lab results and the vane test results, it is believed that the actual shear strength variation with depth would lie between the shear strength profiles indicated by the average vane and the CAU tests.

6.7.2 Variation of the undrained and drained deformation modulus with depth

The variation of the undrained deformation (i.e. Young's) modulus (E_u) with depth

obtained from the CAU tests as well as the self boring pressure meter (SBP) tests during the field investigation are shown in Fig. 6.22. For ease of comparison, the drained modulus (E') obtained from the SBP tests and the CAD test are also shown in this figure. Both the lab tests and the field data indicate that the E_u as well as E' increased with depth and there is reasonably good agreement between the field data and the lab test results.

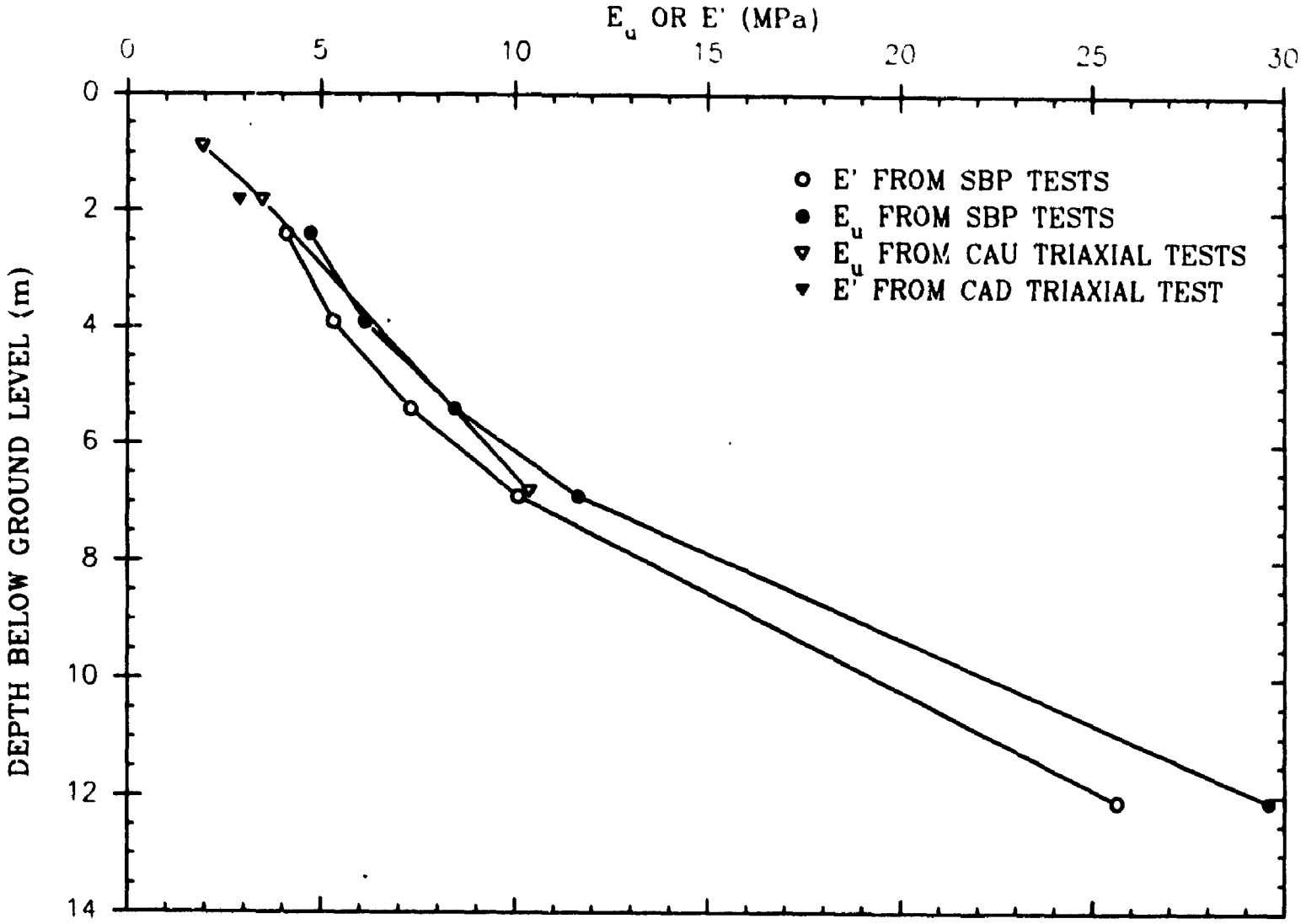

FIG. 6.22 VARIATION OF E_u AND E' WITH DEPTH – COMPARISON OF TRIAXIAL TEST RESULTS WITH SELF BORING PRESSURE METER (SBP) TEST RESULTS

CHAPTER 7

METHOD OF ANALYSIS

7.1 INTRODUCTION

Finite element analyses are used extensively in this thesis to theoretically predict the foundation soil pore pressures, deformations, geosynthetic reinforcement strains, and the stability of the test embankment constructed at Sackville, New Brunswick. A modified version of the program AFENA (A Finite Element Numerical Algorithm, Version 4.0) originally developed by Carter and Balaam (1990) based on the program structure proposed by Taylor (1977) was used for the analysis. The following modifications were made to perform the analysis reported in this thesis:

(i) implementation of high-order elements (i.e. 15-noded cubic strain triangular elements) for the elasto-plastic soil elements with Mohr-Coulomb failure criterion, and elasto-plastic soil elements with Modified Cam-clay material behaviour for consolidation analysis,

(ii) implemented appropriate modifications to perform finite deformation (i.e. large strain) elasto-plastic consolidation analysis using the Modified Cam-clay material behaviour for the foundation soil and Mohr-Coulomb failure criterion for the embankment fill material. The required modifications were made for the reinforcement bar element and the reinforcement-soil interface element to perform large deformation analysis,

(iii) made provision to change the permeability of the foundation soil when it changes from an over consolidated state to a normally consolidated state in addition to its

continuous change with the void ratio for the consolidation analysis.

and (iv) an approximate method to model the breakage of the reinforcement when the tensile force reaches the allowable limit.

Details regarding the AFENA program and actual models used are discussed in this chapter. The adequacy of the finite element mesh refinement was checked initially by analyzing a rigid footing problem for which the exact solution is known. Different element types were used for the descretization of the foundation soil and the embankment fill. Details regarding the choice of the actual element types used and the design of the finite element mesh are discussed in the following section.

7.2 ELEMENT SELECTION AND FINITE ELEMENT MESH DESIGN

There are many different types of finite elements which could potentially be used to represent the soil. It has been suggested by Sloan and Randolph (1982) that high-order elements are suitable for analysis of constant volume plasticity problems. In particular, they suggest that the finite elements with 15-noded cubic strain triangle, with "full" integration of the element stiffness matrices, is capable of modelling collapse behaviour accurately for both plane strain and axisymmetric loading. Using the theory developed by Nagtegaal et al. (1974), they established theoretically that high-order elements are capable of accommodating the large number of constraints on the nodal degrees of freedom that arise when incompressible models are employed. Sloan (1984) further showed that the above element is superior in predicting collapse heights accurately for both plane strain and axisymmetric conditions for constant volume plasticity problems compared to the other usual elements (such as for e.g. constant strain triangle, linear strain triangle, 4-noded quadrilateral and 8-noded quadrilateral elements). On the question of efficiency,

Sloan demonstrated, by analyzing a strip footing problem, that the cubic strain triangle solutions cost no more than equivalent solutions obtained using the 8-noded quadrilateral with reduced integration (for approximately the same accuracy of solution). This is because the integration rules that are available for triangular elements are particularly efficient, e.g. in plane strain, only 12 points are required to compute the element stiffness matrix exactly for the cubic strain triangle which has a quartic displacement expansion. A major advantage of using high order elements, with exact integration of the stiffness matrices, is that no problems are encountered with zero strain energy modes.

Based on the above considerations, it was decided to employ the use of 15-noded cubic strain triangular elements for the finite element descretization of the foundation soil. Since the cubic strain triangular elements require 16 points for full integration for axisymmetric cases, for convenience a 16 point integration rule was implemented for the plane strain analysis also. The embankment was constructed in small lifts and hence using the 15-noded cubic strain triangular elements for the finite element descretization of the embankment fill will require excessively large number of nodes (and therefore degrees of freedom) which would eventually result in very high computing cost. Therefore, in order to simulate the actual construction sequence adopted in the field and preserve the overall accuracy of the analysis at a reasonable computing cost, the embankment fill was descretized using a large number of constant strain triangular elements and the foundation soil was descretized with 15-noded cubic strain triangular elements. However, this arrangement of the finite element mesh involves some incompatibility at the boundary (or interface) between the embankment fill and foundation soil.

In order to check the adequacy of cubic strain triangular mesh refinement, a displacement analysis was performed for a rough rigid footing of width, B = 28.3 m on a cohesive deposit of depth, D = 14 m. A surface shear strength of 10 kPa (i.e. c_{uo} = 10

kPa), a rate of increase with depth, ρ_c= 2 kPa/m and a ratio of undrained modulus to undrained shear strength, E_u/c_u = 125 were adopted in the analysis. However, in order to assess any potential loss of accuracy due to the mixed use of constant strain and cubic strain triangular elements, a similar analysis was performed for the footing placed above 1 m of fill (of unit weight 18.5 kN/m^3 and represented by a layer of constant strain triangle mesh, formed in a crossed triangle formation) on the same 14 m foundation soil deposit with a similar strength profile (represented by 15-noded cubic strain triangle mesh) as shown in Fig. 7.1 (Note: the cubic strain triangle mesh was the same for both cases).

The results of these analyses in the form of the plot of footing load versus settlement are shown in Fig. 7.2. The collapse loads were compared with the solutions by Davis and Booker (1973) and Matar and Salencon (1977). The first case (i.e. case (1) in Fig. 7.2) indicated an error of about 4.6% in predicting the collapse load, suggesting that the cubic strain triangle mesh refinement is practically sufficient to predict the collapse load accurately. The second case (i.e. case (2) in Fig. 7.2) indicated an error of about 5.6% (after due consideration is given to the additional 18.5 kPa of applied load due to the weight of the 1 m thick fill) in the prediction of the collapse load of the footing.

These test analyses indicate the adequacy of the finite element mesh (with the foundation soil discretized with the 15-noded cubic strain triangular elements) for soil profiles similar to that examined. However, the foundation soil mesh was further refined to improve the accuracy for the actual reinforced embankment analyses reported in chapters 8 and 9 of this thesis. The layering of the triangular elements were chosen such that the actual variation of foundation soil properties with depth (based on the field vane and cone test results) could be represented by linear variations within each layer (to sufficient accuracy). The actual mesh used for the finite element analyses of the test embankment constructed at Sackville, New Brunswick is shown in Figures 7.3 and 7.4. It

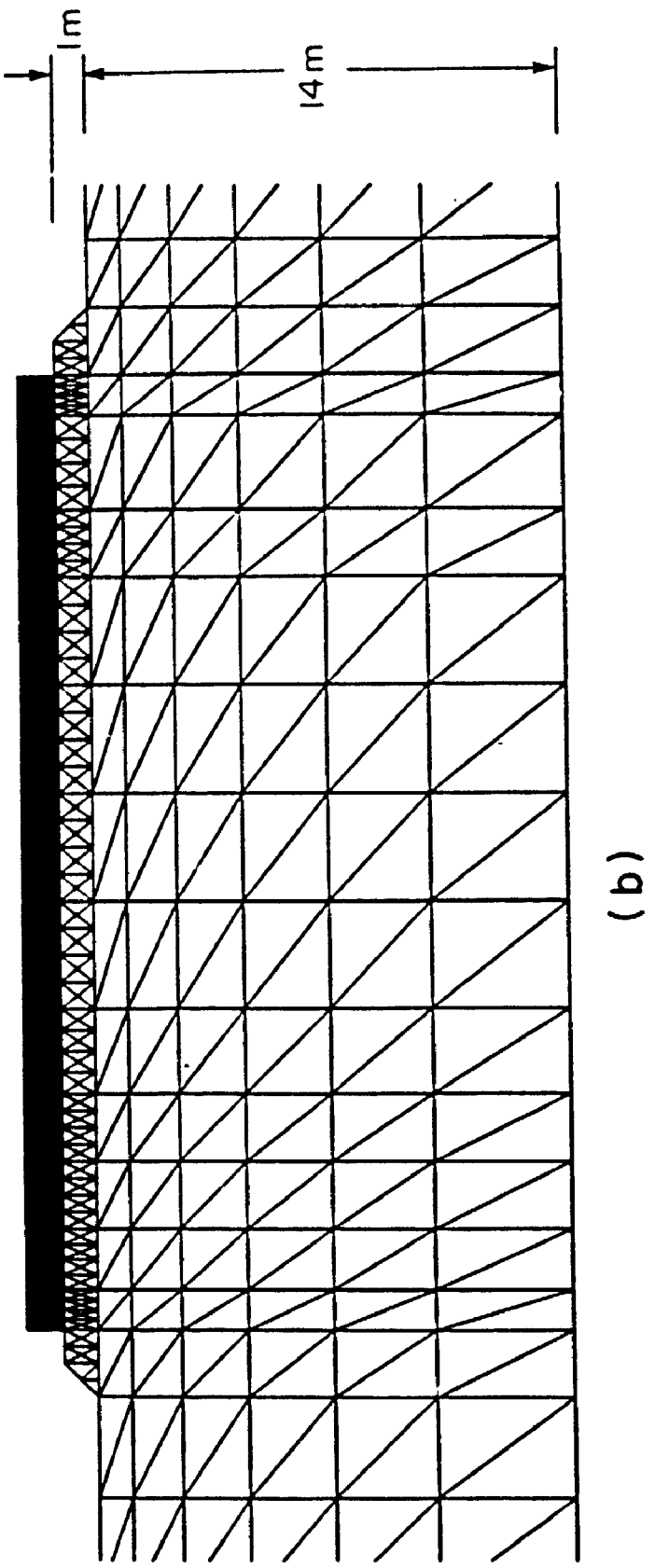

FIG. 7.1 FINITE ELEMENT MESH USED FOR THE ROUGH RIGID FOOTING TEST PROBLEM
(a) COMPLETE MESH (b) BLOW UP OF PART OF THE MESH

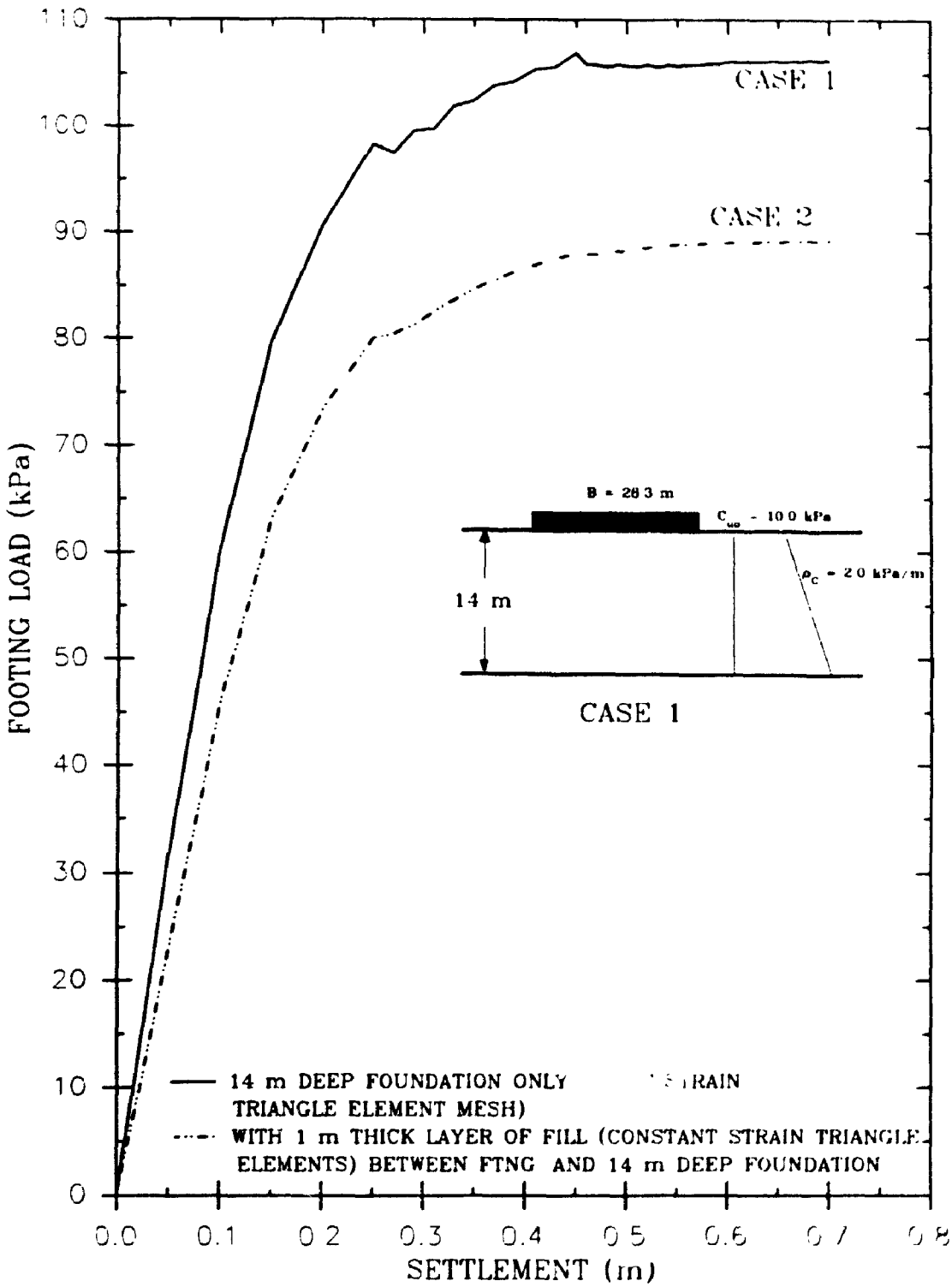

FIG. 7.2 LOAD vs SETTLEMENT PLOTS FOR ROUGH RIGID FOOTING TEST PROBLEMS

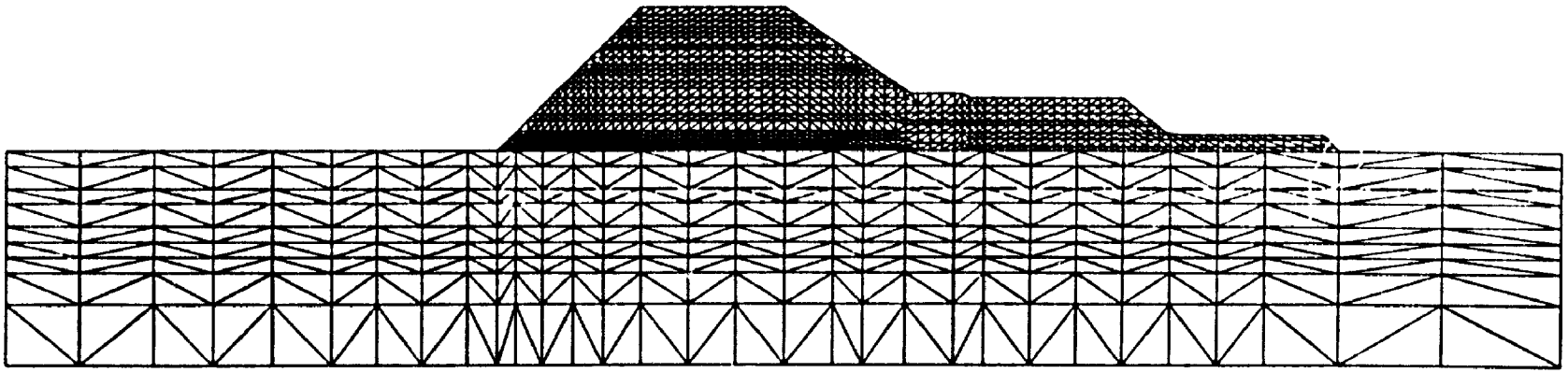

FIG. 7.3 THE FINITE ELEMENT MESH USED FOR THE REINFORCED EMBANKMENT ANALYSIS

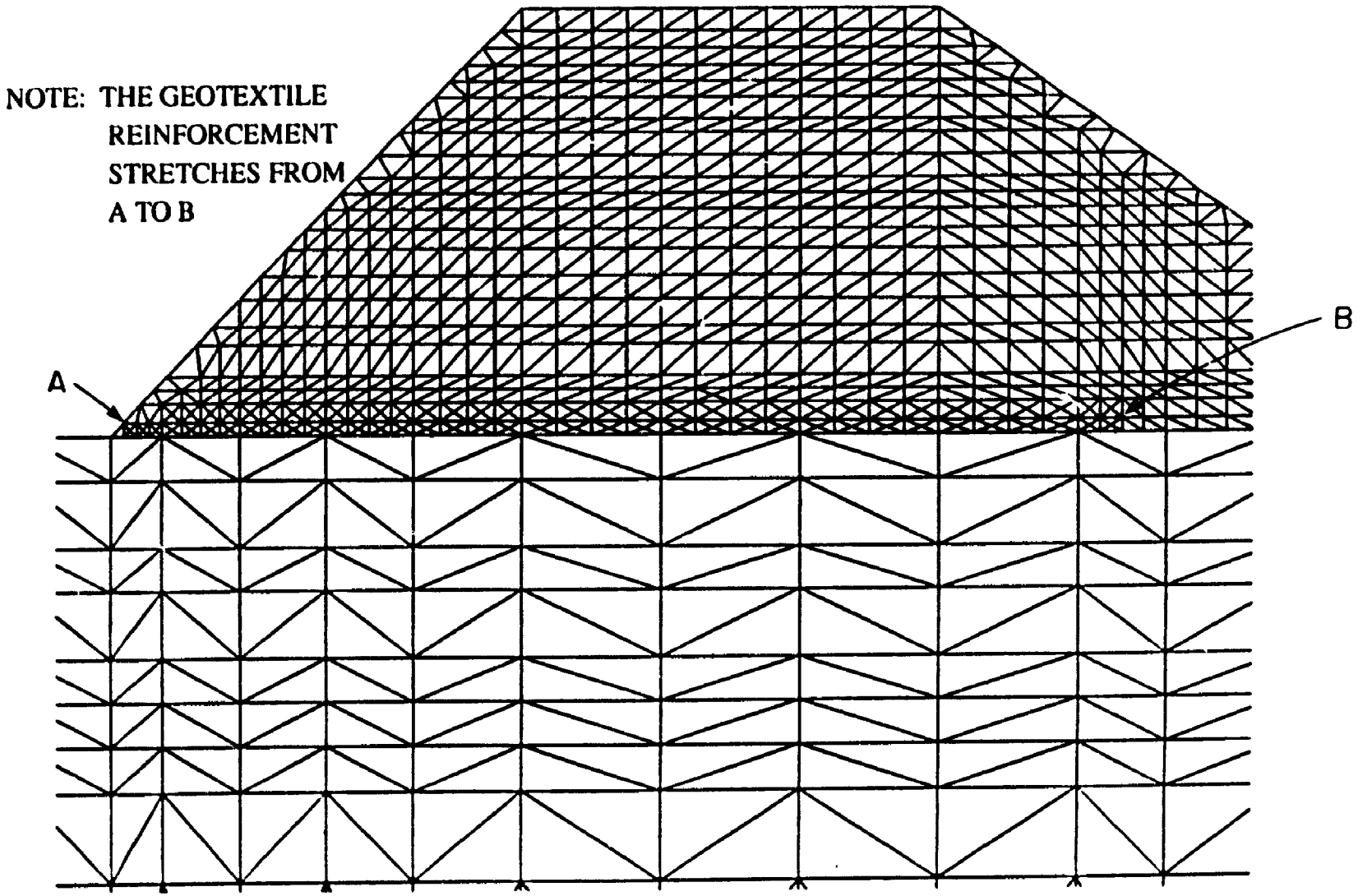

FIG. 7.4 PORTION OF THE FINITE ELEMENT MESH USED FOR THE REINFORCED EMBANKMENT ANALYSIS

consisted a total of 5624 nodes and 2509 elements which included 558 cubic strain triangle elements for representing the foundation soil and 1838 constant strain triangle elements for the embankment fill. The numerical simulation of embankment construction followed the actual construction sequence adopted in the field. A total of up to 400 load steps (or increments) were used in the analysis. The finite element mesh for the embankment fill was designed in such a way that the boundary of the fill element layers coincide with the actual lifts employed during the construction of the embankment in the field.

7.3 AFENA PROGRAM

For a steady-state, non-linear problem, the equations governing the incremental deformation of an elasto-plastic material subjected to known applied tractions and body forces during a load increment are non-linear and can be written in the form

$$\mathbf{K}\,\delta = \mathbf{f} \qquad (7.1)$$

where **K** is the tangent stiffness matrix

δ is the solution vector

and **f** is the incremental load vector

An approximate solution to these equations can be obtained using the FEM (Finite Element Method). The tangent stiffness approach is used in AFENA to solve the non-linear equations. This approach is straight forward, however it can be costly in computing since the tangent stiffness matrix must be assembled, factorized and solved for at each load step. For materials with a non-associated flow rule, the tangent stiffness matrix is

non-symmetric resulting in a considerable increase in both storage and computation time.

In AFENA, the consolidation behaviour is modelled numerically using the Biot consolidation theory. The non-linearity of the material behaviour (e.g. the Modified Cam-clay material behaviour of the foundation soil) is handled by adopting an incremental approach. This requires the use of a large number of small increments for accurate results. The finite element equations for this incremental analysis based on Small et al. (1976) are:

$$\begin{bmatrix} \mathbf{K} & -\mathbf{L}^T \\ -\mathbf{L} & -\alpha\Delta t\Phi \end{bmatrix} \begin{bmatrix} \Delta\delta \\ \Delta\mathbf{q} \end{bmatrix} = \begin{bmatrix} \mathbf{f} \\ \phi\mathbf{q}_o\Delta t + (1-\alpha)\Delta t\Phi\mathbf{q}_o \end{bmatrix} \qquad (7.2)$$

where δ is the time dependent nodal displacement vector, ϕ is the fluid stiffness matrix, $\mathbf{L}$ is the coupling matrix, α defines the particular integration rule used, $\mathbf{q}$ is the nodal excess pore pressure vector and $\mathbf{q_0} = \mathbf{q}$ ($t = t_0$) (i.e. the excess pore pressure at the beginning of the current increment). The stability of the integration scheme has been examined by Booker and Small (1975) who demonstrated that the process is unconditionally stable provided $\alpha \geq \frac{1}{2}$. In the absence of other data, it is usual to set $\mathbf{q}_{(t=0)} = 0$.

In AFENA, an 'extended' element stiffness matrix is calculated for the consolidation analysis to represent ($\mathbf{K}$ as well as) all the terms in the left hand side of equation (7.2). The value of α is assumed to be 1 and the term '$\phi\ \mathbf{q}_0\ \Delta t$' is calculated and added to the force vector in the right hand side of the equation.

7.4 THE DIFFERENT MODELS USED

Different models were used for the soil, geotextile reinforcement and the interface between the soil and the reinforcement. Details regarding these models are presented in this section.

7.4.1 Soil model

Different soil models were used for the foundation soil for the purposes of performing undrained and consolidation analyses. The details of these models are discussed below.

7.4.1.1 Soil model for undrained analysis

A non-linear elasto-plastic model was adopted for the soil. The Young's modulus of the soil was assumed to be either isotropic linear elastic or a parabolic function of the minor principal stress. The latter approach was accomplished using Janbu's equation (Janbu, 1963) viz.

$$\frac{E}{P_a} = K\left[\frac{\sigma_3}{P_a}\right]^m \qquad (7.3)$$

where E is the Young's modulus of the soil, P_a is the atmospheric pressure, σ_3 is the minor principal stress, and K and m are experimentally determined parameters.

Failure of the soil was modelled using the Mohr-Coulomb failure criterion (defined in terms of the cohesion intercept c and the angle of internal friction ϕ). The plastic strain rates were related by either an associated ($\phi = \psi$) or a non-associated ($\phi \neq \psi$) flow rule of

the form proposed by Davis (1968) (where ψ is the dilatancy angle). The formulation was such that if unloading was detected for a plastic element, then the element was returned to an elastic state. Elements having stresses which violate the yield criterion (i.e. in a state of stress outside the yield surface) were corrected back to the yield surface along a path normal to the yield surface. As mentioned in the previous section, two types of two dimensional plane strain elements were used to discretize the soil, namely the 15-noded cubic strain triangular elements for the foundation soil and 3-noded constant strain triangular elements for the embankment fill.

7.4.1.2 Soil model for consolidation analysis

Realistic computations of both the variation of strain in the reinforcement with time as well as the variation of displacements and pore pressures with time in clay foundations under reinforced embankments where significant consolidation takes place during construction require the use of numerical analyses with reliable constitutive models coupled with consolidation. The Cam-clay models (Schofield and Wroth, 1968; Roscoe and Burland, 1968) allow strength and compressibility to be treated within the elasto-plastic strain-hardening framework, using a small number of parameters for both drained and undrained analysis. Partially drained behaviour can also be modelled numerically using the Biot consolidation theory, as adopted in the AFENA program (Carter and Balaam, 1990) based on the coding given by Britto and Gunn (1987).

A Modified Cam-clay material behaviour coupled with Biot's consolidation is employed in this consolidation model. The details regarding the Modified Cam-clay material behaviour can be found elsewhere (e.g. Schofield and Wroth, 1968; Roscoe and Burland, 1968; Atkinson and Bransby, 1978) but a brief description of the parameters is given below (see also Fig. 7.5). Cam-clay uses four critical state parameters: λ, the

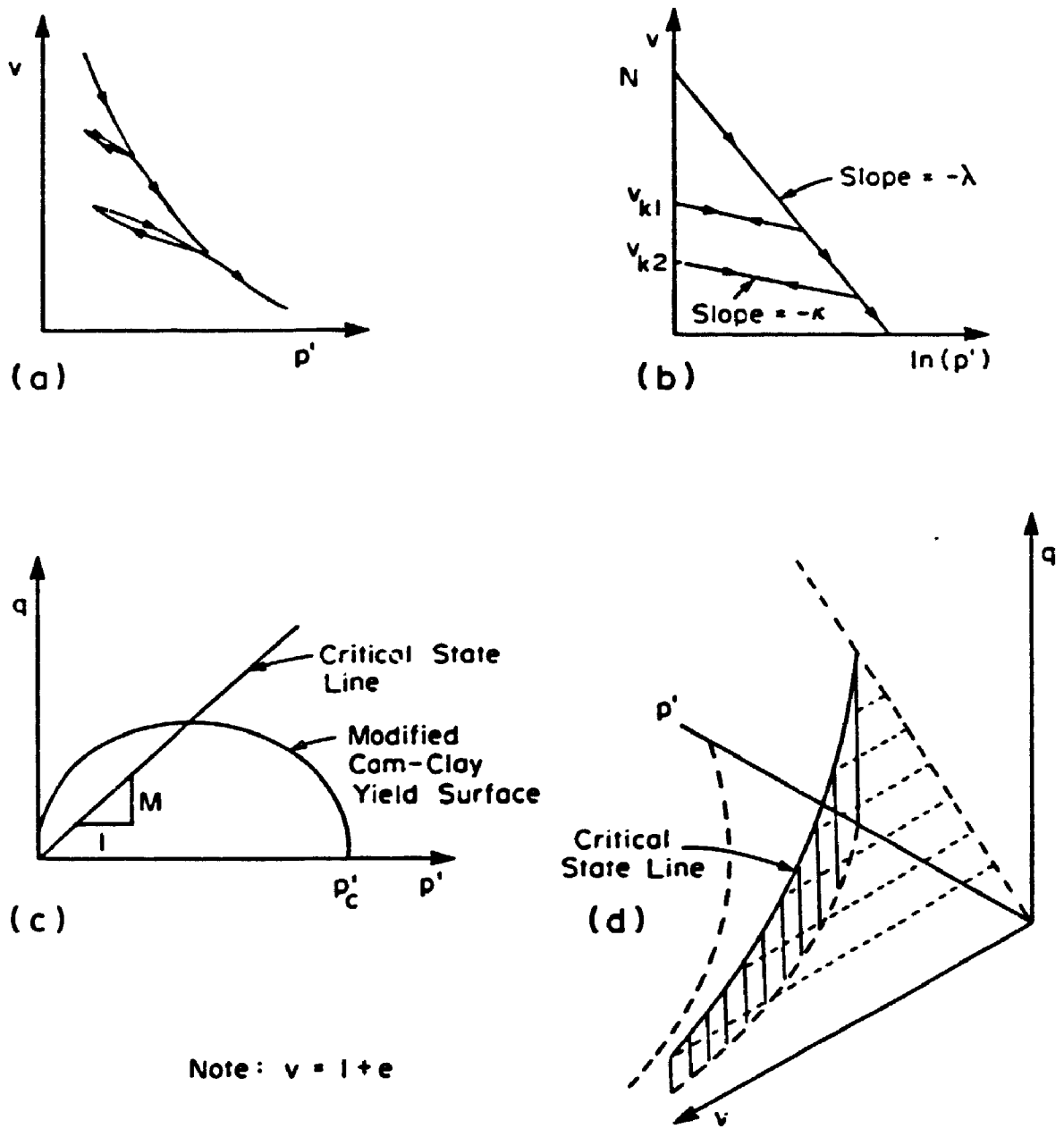

Note: v = 1 + e

FIG. 7.5 CRITICAL-STATE PARAMETERS BASED ON MODIFIED CAM-CLAY MODEL

gradient of the consolidation line in the e - ln p′ space, equal to $C_c/2.3$; κ, the gradient of the swelling line in the e - ln p′ space, equal to $C_s/2.3$; M, the value of the stress ratio q/p′ at the critical state condition; and e_{cs}, the void ratio at p′ = 1 kPa on the critical state line in the e - ln p′ space. The procedure for determining these parameters is discussed by Britto and Gunn (1987).

Some common criticisms (e.g. Tavenas, 1981) of the Cam-clay model are: (i) the assumption of a yield locus centred on the isotropic compression line whereas anisotropic consolidated clays exhibit yield loci approximately centred on the K_0 consolidation line (e.g. Parry and Nadarajah, 1973); (ii) the assumption of isotropic elastic rather than anisotropic elastic behaviour inside the yield locus; and (iii) the assumption of associated flow rules, which can be acceptable for isotropic soils but do not properly represent the behaviour of anisotropic natural clays. Despite these criticisms, the Modified Cam-clay model has been used in this research because of its mathematical simplicity, use a small set of parameters obtainable from standard laboratory tests, and its proven ability to model the behaviour of lightly over consolidated clays under stress paths corresponding to embankment loading (see for e.g. Wroth, 1977; Wood, 1982). The critical state models have been used successfully to predict the behaviour of unreinforced embankments constructed on soft soils (e.g. Almeida and Ortigao, 1982; Kavazanjan and Poepsel, 1984; Almeida et al., 1985; Indraratna et al., 1992) and its application for the prediction of the behaviour of reinforced embankments on soft soils is investigated in this thesis. Todate, all the analyses reported in the literature using this model employed a small strain theory whereas the current study also investigated the use of finite deformation theory as discussed later in this chapter.

The finite element formulation is based on Biot consolidation theory as discussed in section 7.3. Physical nonlinearity is handled by an incremental approach, which

requires the use of a larger number of small increments.

A coupled consolidation analysis requires values for the hydraulic conductivities in the horizontal (k_x) and vertical (k_y) directions. The hydraulic conductivity is not a soil constant and may change substantially with a change in void ratio. In AFENA, the following function is used to account for this change:

$$k_y = A * (B - e)^C \qquad (7.4)$$

where e is the current value of the void ratio and A, B and C are constants. However, the ratio k_x/k_y is assumed to remain constant.

It has been observed in previous investigations of the behaviour of unreinforced embankments on soft soils that the permeability of clay can decrease significantly when it changes from an over consolidated state to a normally consolidated state during the construction of the embankment and that this can alter the deformational pattern in the foundation soil (e.g. Leroueil et al., 1978a and 1978b). Therefore, appropriate modifications have been made in the program to allow variation of the permeability with void ratio during the over consolidated state according to the following function:

$$k_y = A1 * e^{B1} \qquad (7.5)$$

where A1 and B1 are constants, and hence according to the previous function (i.e. equation 7.4) when the soil stress state becomes normally consolidated. The constants A1, B1, A, B, and C are determined from laboratory tests (i.e. either directly from hydraulic conductivity tests or indirectly from consolidation tests) at the appropriate stress states.

7.4.2 Reinforcement model

The reinforcement was modelled using a series of one dimensional linear elastic bar elements. Although the breakage (snap) of the reinforcement could involve the redistribution of energy in the reinforcement prior to breakage, an approximate method was adopted for the redistribution of stresses. In this method the force in the reinforcement and its stiffness (i.e. for the element where breakage occurred) were decreased gradually in several steps without any overall addition of external load and with no significant advance in time until the entire force in the reinforcement vanished at the particular location of breakage.

7.4.3 Reinforcement-soil interface model

The reinforcement-soil interface was modelled using nodal compatibility joint elements, assumed to be rigid plastic and non-dilatant (i.e. $\psi = 0$). Provision was made for slip between the reinforcement and the soil above and/or below the reinforcement by incorporating interface slip elements above and below the reinforcement. For each reinforcement node there was a soil node above and a soil node below the reinforcement. Thus, slip could occur independently above and/or below the reinforcement. At each point in the interface, the displacement of the soil and reinforcement were compatible until the interface shear stress reached the shear strength defined by a Mohr-Coulomb yield criterion at the interface. Once the shear strength was reached, slip (i.e. differential tangential displacement between the soil and reinforcement) occurred at this location.

7.5 FINITE DEFORMATION ANALYSIS

A finite deformation elasto-plastic consolidation analysis was performed for the

prediction of the behaviour of the reinforced test embankment constructed at Sackville, New Brunswick and to study the sensitivity of the predictions to various parameters. The theory adopted for this analysis and the finite element formulations are discussed in this section.

7.5.1 General

In the infinitesimal theory of elastic-plastic deformations, it is possible to define strain in a unique and unambiguous way. However, this is not true when the deformations are large since a variety of co-ordinate systems may be used which will inevitably result in different definitions of strain. In continuum mechanics, the deformation of a body subjected to large displacements is usually described by either a Lagrangian or an Eulerian reference system. Both these systems have been used in the finite element analysis of large strain problems (e.g. Hibbitt et al., 1970; Carter et al., 1977). The choice of the system depends mainly on material behaviour that is being modelled and could be influenced by the ease with which the appropriate material properties can be measured. The Lagrangian approach is best suited to those problems where the constitutive law may be written in terms of total deformation of the material and therefore lends itself to the description of materials with a natural reference state. The Eulerian description, however, is well suited to the analysis of material for which the constitutive laws are conveniently expressed in terms of stress and strain rates, as is often the case in soil mechanics. The finite element formulations using the Eulerian description were adopted for the large strain analysis reported in this thesis.

The basis of the Eulerian approach is to consider the velocity of a material point, u_i, in the current configuration, to be related to the co-ordinate of the material point x_i (relative to some fixed reference), and the time t in a relationship of the form:

$$u_i = u_i(x_i\ t) \tag{7.6}$$

The deformation of the material is described by the rate of deformation tensor defined as:

$$d_{ij} = \frac{\partial u_i}{\partial x_j} \tag{7.7}$$

For a mathematical description of material behaviour to be consistent within the framework of continuum mechanics, it is necessary that the stress rate used in the constitutive equation should be 'objective'. This condition requires that the stress rate must vanish under conditions of rigid body motion. Prager (1961) showed that the definition of 'objectivity' is not sufficiently restrictive to give a unique definition of stress rate and several different 'objective' stress rates have been proposed (e.g. Jaumann, 1911; Truesdell, 1953; and Oldroyd, 1950). Amongst these, the Jaumann definition has been widely accepted for use in large strain computations in recent years. This popularity stems from the desirable feature of the Jaumann definition that vanishing of the stress state implies stationary behaviour of the stress invariants. The original form of the Jaumann stress rate, as defined by:

$$\hat{\sigma}_{ij} = \dot{\sigma}_{ij} - \sigma_{ik}\dot{\omega}_{jk} - \sigma_{jk}\dot{\omega}_{ik} \tag{7.8}$$

has been adopted in this study also. The superior dot denotes the Cauchy total stress rate and ω_{ij} is the skew-symmetric spin tensor:

$$\dot{\omega}_{ij} = \frac{1}{2}\left[\frac{\partial u_i}{\partial x_j} - \frac{\partial u_j}{\partial x_i}\right] \tag{7.9}$$

It has been shown that the Jaumann stress rate may give rise to physically unrealistic solutions to problems where shear strains become very large (Dienes, 1979). However, most geometrically non-linear soil mechanics problems do not involve large shear strains and the shear strains expected in the analysis reported in this thesis are not sufficiently large to justify the additional complexity of any modification.

These incremental formulations with 'rate' quantities require that the solution be obtained by following the actual loading path. Ideally, the approach of obtaining finite deformation (i.e. geometrically non-linear) solutions will be compatible with the non-linear models such as the elasto-plastic formulations based on the tangent stiffness matrix (which is related to the tangent constitutive matrix D_T) used in the infinitesimal deformation (i.e. small strain) analysis discussed in the previous section.

7.5.2 Finite element equations for large strain analysis

The finite element solution procedure reported by Carter et al. (1977) using Jaumann's definition of stress rate was implemented in AFENA. The Jaumann definition of stress rate expressed in Cartesian co-ordinate system for a 2-D (plane strain) case will be given by the following equation:

$$\hat{\dot{\sigma}} = \dot{\sigma} + \begin{bmatrix} 0_{(3,3)} & \begin{matrix} -\sigma_{xy} \\ \sigma_{xy} \\ \frac{1}{2}(\sigma_{xx} - \sigma_{yy}) \end{matrix} \end{bmatrix} \begin{bmatrix} \dot{\varepsilon}_x \\ \dot{\varepsilon}_y \\ \dot{\gamma}_{xy} \\ \dot{\omega} \end{bmatrix} = \dot{\sigma} + \begin{bmatrix} 0_{(3,3)} & \begin{matrix} -\sigma_{xy} \\ \sigma_{xy} \\ \frac{1}{2}(\sigma_{xx} - \sigma_{yy}) \end{matrix} \end{bmatrix} \dot{\varepsilon}^a \qquad (7.10)$$

In AFENA, the 'objective' stress rate vector ($\hat{\sigma}$), is featured by an augmented constitutive matrix, D_T^a and the strain rate vector ($\dot{\varepsilon}^a$) (augmented to include the additional term for the spin rate, ω, as shown in the above equation) given by the following relationship:

$$\dot{\sigma} = \begin{bmatrix} & & \sigma_{xy} \\ D_{T\,(3,3)} & & -\sigma_{xy} \\ & & \frac{1}{2}(-\sigma_{xx}+\sigma_{yy}) \end{bmatrix} \begin{bmatrix} \dot{\varepsilon}_x \\ \dot{\varepsilon}_y \\ \dot{\gamma}_{xy} \\ \dot{\omega} \end{bmatrix} = D_T^a \dot{\varepsilon}^a \qquad (7.11)$$

where, σ represents the augmented stress rate for large strain analysis, and D_T is the non-augmented tangent constitutive matrix.

For large strain consolidation analysis, the numerical solution method proposed by Carter et al. (1979) was adopted in this study. In this method, a general linear relationship of the form given below was used:

$$\hat{\sigma}_{ij} + \dot{p}\delta_{ij} = D_{ijkl} l_{kl} \qquad (7.12)$$

where, p is the pore pressure at time t (taken positive when compressive),

δ_{ij} is the Kronecker delta, and

D_{ijkl} are the material constants for the drained behaviour of the soil.

An alternate form of equation (7.12) for the corrected stress rate would be:

$$\dot{\sigma}_{ij} = D_{ijkl}\dot{l}_{kl} + \sigma_{ik}\dot{\omega}_{jk} + \sigma_{jk}\dot{\omega}_{ik} - \dot{p}\delta_{ij} \qquad (7.13)$$

The finite element equations for an approximate solution of the above tensor equation developed by Carter et al. (1979) are given below:

$$\begin{bmatrix} \mathbf{Q} & -\mathbf{L}^T \\ -\mathbf{L} & -\alpha\Delta t\Phi \end{bmatrix} \begin{bmatrix} \Delta\delta \\ \Delta\mathbf{q} \end{bmatrix} = \begin{bmatrix} \mathbf{f} \\ \phi\mathbf{q}_o\Delta t + \mathbf{n}\Delta t \end{bmatrix} \qquad (7.14)$$

where, Q represents the augmented tangent stiffness matrix for the soil skeleton and **n** represents the time gradient for the change in location. This equation was used, in a similar manner as the small strain consolidation analysis, and by augmenting the tangent constitutive matrix and strain vector as used in the case of total stress (or steady state) large strain analysis discussed earlier in this section (i.e using equation 7.11). The total pressure and effective stress changes due to the change in geometry were also considered accordingly.

For the large strain analyses, the geometry (i.e. the nodal co-ordinates) were updated at the end of each load increment. Modifications were also made to update the length of the geotextile reinforcement bar elements and to change the orientation of the slip plane of the reinforcement - soil interface elements for each increment.

CHAPTER 8

COMPARISON OF CALCULATED AND OBSERVED BEHAVIOUR OF THE TEST EMBANKMENT

8.1 INTRODUCTION

One of the advantages of full scale instrumented structures and the measurements obtained from them is that they provide a basis for calibrating methods of analyses. The validity of the numerical model (for the large strain elasto-plastic consolidation analysis with Modified cam-clay material behaviour) described in chapter 7 may be assessed, in part, by a comparison of calculated and observed field behavior. In this chapter, the results of the finite element analysis performed using this model for the geotextile reinforced section of the test embankment is discussed in comparison with the field observations. The results of a similar analysis performed for the unreinforced embankment is also briefly discussed in this chapter.

8.2 COMPARISON OF THE OBSERVED AND PREDICTED BEHAVIOUR OF THE REINFORCED EMBANKMENT

8.2.1 Numerical Details

A fully coupled large strain Biot consolidation finite element analysis was performed for the reinforced test embankment constructed at Sackville, New Brunswick. In this analysis, the foundation soil was modelled as a consolidating elasto-plastic Modified Cam-clay material and the embankment fill was modelled as an elasto-plastic

material with Mohr-Coulomb failure criterion. The geotextile was modelled as a series of linear elastic bar elements and the geotextile-fill interface was modelled using nodal compatibility joint elements. The analysis allowed for slip at the fill-geotextile interface both below and above the geotextile. The details regarding these models and the finite element mesh used were described in chapter 7.

The properties of the foundation soil, embankment fill, geotextile reinforcement and the geotextile-fill interface used for this analysis are presented in the following section. The numerical construction of the reinforced embankment followed as nearly as possible the actual construction sequence adopted in the field (by turning on gravity of the appropriate series of embankment fill elements). A total of up to 400 load increments were used in this analysis.

8.2.2 Selection of Parameters

The properties of the foundation soil used for this analysis is shown in Table 8.1. These properties were selected on the basis of laboratory test results reported in chapter 6. A ϕ' value of 28.2° determined from CAU triaxial tests performed on the samples from various depths reported in chapter 6 was adopted in this analysis (i.e. the value of M = 1.12 using the relationship, $M = \frac{6 \sin\phi'}{3 - \sin\phi'}$). The values for parameters λ, κ and e_{cs} were based on the results of consolidation tests performed on the samples from 1.83 and 6.81 m depths (e.g. using the relationship, $\lambda = C_c/2.303$ and the procedure described by Britto and Gunn, 1987 to evaluate e_{cs}). The vane and cone tests performed in the field indicated the existence of a soft layer in the region of about 4 m depth (see Fig. 6.21 in chapter 6). Therefore, the estimated values of these parameters using empirical relationships (e.g. $C_c = 0.009(w_L - 10)$) based on the index properties determined for the sample from 3.96 m (see Table 6.6 in chapter 6) were adopted for the layer of soil from 3.5 to 5m depth.

Table 8.1 Foundation soil parameters adopted for the analysis

Depth (m)	γ (kN/m^3)	M	κ	λ	e_{cs}	ν	K_o	OCR
0 - 1	15.2	1.12	0.055	0.242	2.21	0.3	0.68	1.0
1 - 2.5	17.8	1.12	0.021	0.111	1.30	0.3	0.68	3.6
2.5 - 3.5	17.8	1.12	0.027	0.154	1.59	0.3	0.71	1.2
3.5 - 5	16.0	1.12	0.045	0.224	1.80	0.3	0.77	1.0
5 - 6	17.0	1.12	0.027	0.154	1.59	0.3	0.79	1.2
6 - 7	17.0	1.12	0.027	0.154	1.59	0.3	0.81	1.2
7 - 8	17.0	1.12	0.027	0.154	1.59	0.3	0.82	1.2
8 - 10	17.0	1.12	0.027	0.154	1.59	0.3	0.84	1.2
10 - 14	17.0	1.12	0.027	0.154	1.59	0.3	0.88	1.2

The K_o values were selected on the basis of the results from self boring pressure meter tests conducted by NRC (courtesy Dr. K.T. Law) reported in chapter 3. The OCR values were also selected on the basis of consolidation test results reported in chapter 6. However, an OCR value of 1.0 was adopted for the soft layer of soil between 3.5 and 5 m depth. As discussed in chapters 3 and 4, vertical cuts were made on the ground up to a depth of 1 to 1.2 m (on an approximately 1.3 to 1.8 m square grid using a chain saw) to reduce the effect of the root mat (i.e. to minimize the fill required to construct the embankment until failure). To simulate the effect of these cuts on the soil near the surface, an OCR value of 1.0 was assumed for the 0 to 1 m depth layer of soil.

As discussed previously in chapter 7, provision was made in the program for the permeability of the foundation soil to vary with the void ratio according to either eqn. 7.4 or eqn. 7.5 depending on whether the soil is at overconsolidated or normally consolidated state. Since the foundation soil contained large portion of silt (i.e. between 47 and 63%) and 4 to 10% organics, the permeability of this soil was expected to range between 10^{-5} and 10^{-7} cm/s with a mean value of about 10^{-6} cm/s. In the absence of site specific field data and the availability of only limited amount of lab data for the over consolidated state, the permeability was assumed to be constant at 10^{-6} cm/s when the soil is overconsolidated. However, the permeability of the soil was allowed to vary with the void ratio when the soil become normally consolidated according to eqn. 7.4 (see chapter 7). The constants of these equations (for the permeabilities to be evaluated in m/day) determined on the basis of the results of consolidation tests (performed on the samples from 1.83 and 6.81 m depths) are summarized in Table 8.2. The results of permeability tests indicated that the ratio of the horizontal permeability to the vertical permeability (i.e. k_x/k_y) could range between 2.5 and 9 for the variation of consolidation pressure from 20 to 200 kPa (see Table 6.5). A value of 4 was selected for the permeability ratio in this analysis. However, a higher value of 10 was assumed for the layer between 0 and 1 m

Table 8.2 The constants to describe the variation of permeability with void ratio.

	Normally consolidated			Over consolidated		k_x/k_y
Depth (m)	A	B	C	A1	B1	
0 - 1	0.5769E-3	5.1033	0.1006	0.00864	0.0	10.0
1 -3.5	0.5769E-3	5.1033	0.1006	0.00864	0.0	4.0
3.5 -5	0.5769E-3	5.1033	0.1006	0.00864	0.0	10.0
5 - 14	0.7413E-4	4.8574	0.6033E-9	0.00864	0.0	4.0

k_x = permeability in the horizontal direction
k_y = permeability in the vertical direction
A, B, C, A1 and B1 are constants for the evaluation of permeability in m/day according to equation 7.4 and 7.5

depth where vertical cuts were made.

The layer of soil between 3.5 and 5 m depth was soft and highly compressible. This type of soil generally exhibits anisotropic behaviour which cannot be modelled accurately using the Modified Cam-clay material model. However, to simulate its behaviour in an approximate manner, an OCR value of 1 was adopted for this layer of soil. Consequently, this layer of soil would behave normally consolidated from the beginning of construction of the embankment and would therefore assume a lower permeability compared to the surrounding soil (which is initially over consolidated). This may result in an under estimation of the permeability of this soil during the early stages of construction. Moreover, such soft soil layers are likely to have significantly higher anisotropy in permeability. Therefore a higher permeability ratio (i.e. k_x/k_y) value of 10 was assumed for this layer of soil.

A locally available fill material (gravelly silty sand with some clay) was used for the construction of most part of the embankment. However, a good quality granular fill material was used both below and above the geotextile (for a total thickness of about 0.7 m) to allow adequate interaction between the geotextile and the surrounding fill as discussed in chapter 4. The properties of these fill materials used in the analyses are summarized in Table 8.3. The unit weights given in this table were based on field density measurements and the shear strength properties were obtained from direct shear tests performed in the lab.

The stiffness, J, and the tensile strength of the geotextile reinforcement were determined to be 1920 kN/m and 216 kN/m from tensile tests performed on the samples of the geotextile (see chapter 5 for details). The geotextile-granular fill interface friction angle (ϕ'_{int}) was determined to be 41.9° from direct shear tests as discussed in chapter 5.

Table 8.3 Embankment fill parameters.

		First 0.7m thickness	All the fill other than the first 0.7m thickness
Material properties	c′ (kPa)	0	17.5
	ϕ'	43°	38°
	ψ	8°	7°
	γ (kN/m^3)	18.0	19.6
	ν	0.35	0.35
Janbu's equation	K	100	100
	m	0.5	0.5

These values were adopted in this analysis for the parameters of the geotextile and the geotextile-fill interface.

8.2.3 Comparison of vertical and horizontal deformations

The settlement and heave (i.e. vertical deformation) responses predicted from the finite element analysis are compared with the corresponding field observations in Figs. 8.1 and 8.2. It can be seen that there is reasonably good agreement between the predicted vertical deformations and field observations up to about 8.2 m embankment thickness (i.e. until about 500 hours) for the settlement responses and up to 9.5 m thickness (i.e. until about 570 hours) for the heave responses. The settlement and heave evaluated from the analysis were small (typically less than 0.3 m) until 3.4 m thickness followed by a large increase during the construction of the embankment from 3.4 to 5.7 m thickness. This suggest that the response is more or less elastic until about 3.4 m thickness. However, the predicted settlements were significantly larger than those observed in the field during the early stages of construction (i.e. up to about 3.4 m thickness).

The settlement indicated from the analysis at plate 7S was slightly greater than that at 8S for thicknesses between 1.3 and 8.2 m whereas the settlements observed in the field were more or less the same at these locations up to about 8.2 m thickness (i.e. until about 512 hours). The results from the analysis also indicated the same trend of larger settlement at 8S compared to that at 7S for embankment thickness greater than 8.2 m similar to that observed in the field. However, the settlement indicated in the analysis was significantly lower than that observed in the field at thickness $\geq 8.2m$. Larger increase in settlement and heave were observed in the field during the brief period of construction stoppage at 8.2 m thickness compared to that predicted in the analysis. This is apparently due to comparatively smaller consolidation deformations indicated in the analysis. Very

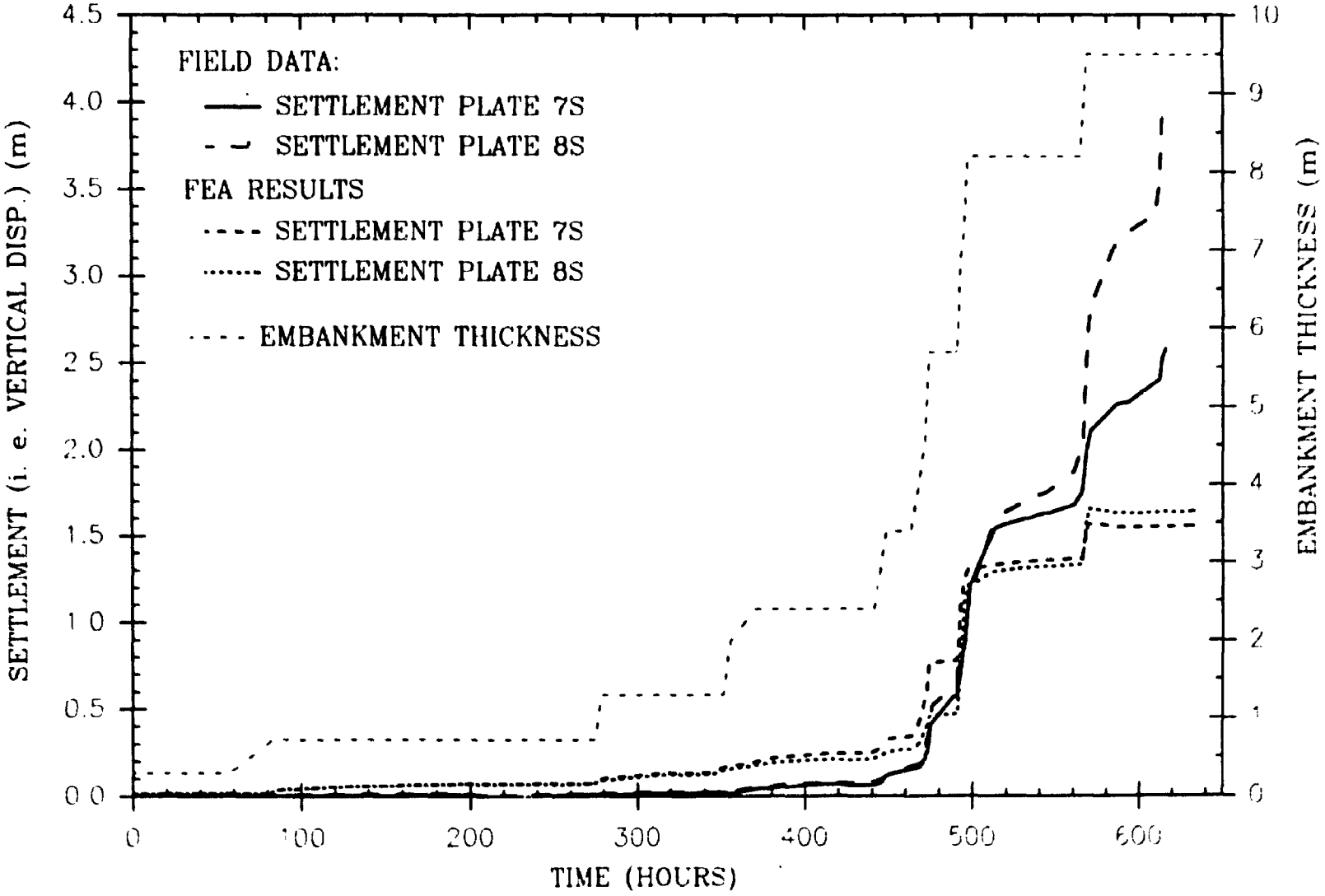

FIG 8.1 VARIATION OF SETTLEMENT WITH TIME FOR SETTLEMENT PLATES 7S AND 8S – COMPARISON OF FEA RESULTS WITH FIELD DATA

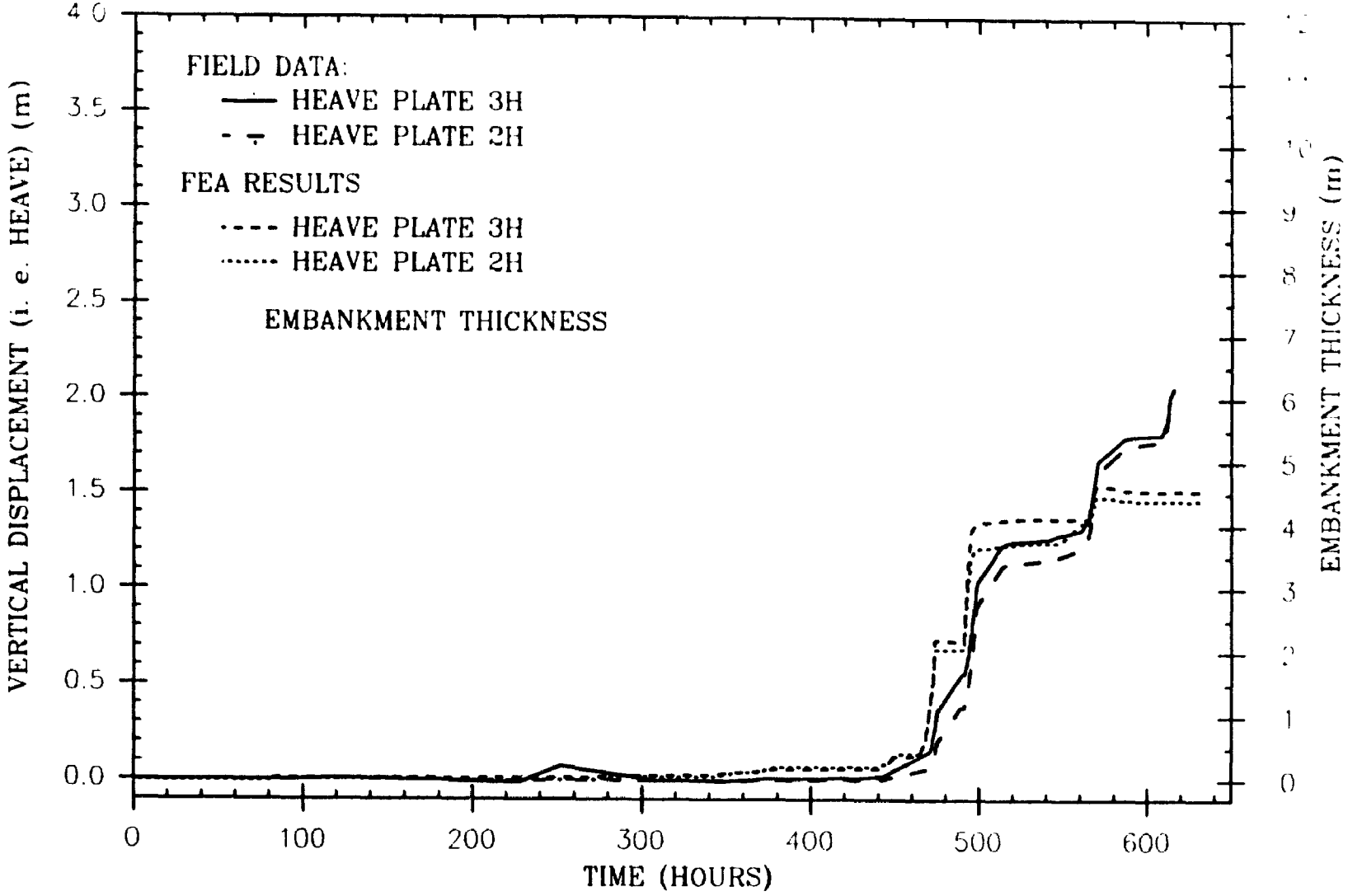

FIG. 8.2 VARIATION OF VERTICAL DISPLACEMENT WITH TIME FOR HEAVE PLATES 2H AND 3H – COMPARISON OF FEA RESULTS WITH FIELD DATA

large increase in settlement was observed at location 8S in the field during the construction of the embankment from 8.2 to 9.5 m thickness and a plastic type of failure of the foundation soil was interpreted at 8.75 m thickness as previously discussed in chapter 4. However, the analysis indicated only a moderate increase of settlement during this construction phase and there was no evidence for the failure of the foundation soil.

The discrepancy between the vertical deformations at large embankment thicknesses (i.e. say > 8.2 m thickness) indicate that the large strain finite element model used in this investigation is not suitable to predict the plastic type of failure encountered during the construction of this test embankment. However, it will be shown in chapter 9 that the plastic type of failure observed in the field for this test embankment can be predicted quite accurately by a small strain undrained analysis with a Mohr-Coulomb failure criterion.

The vertical displacements examined so far were for the settlements and heaves at different locations on the ground surface. Shown in Fig. 8.3 are the comparison of settlements calculated at the locations of augers 9A, 10A and 11A (placed at 2, 4 and 6 m depths respectively - see Fig. 4.1 in chapter 4 for additional details regarding the location) with the corresponding field data. The calculated settlement at auger 9A agreed reasonably well with the measured values up to about 8.2 m thickness, similar to the settlement responses at the ground surface discussed previously. The calculated settlement at augers 10A and 11A agreed well with the field measurements only up to about 3.4 m thickness. The settlement at these deep locations were underpredicted by the analysis after 3.4 m thickness and the difference between the calculated and measured values widened with increasing thickness. This discrepancy between the calculated and measured values indicate that the large strain finite element model used in this investigation is not suitable to predict the vertical deformations at large depth (i.e. say > 4

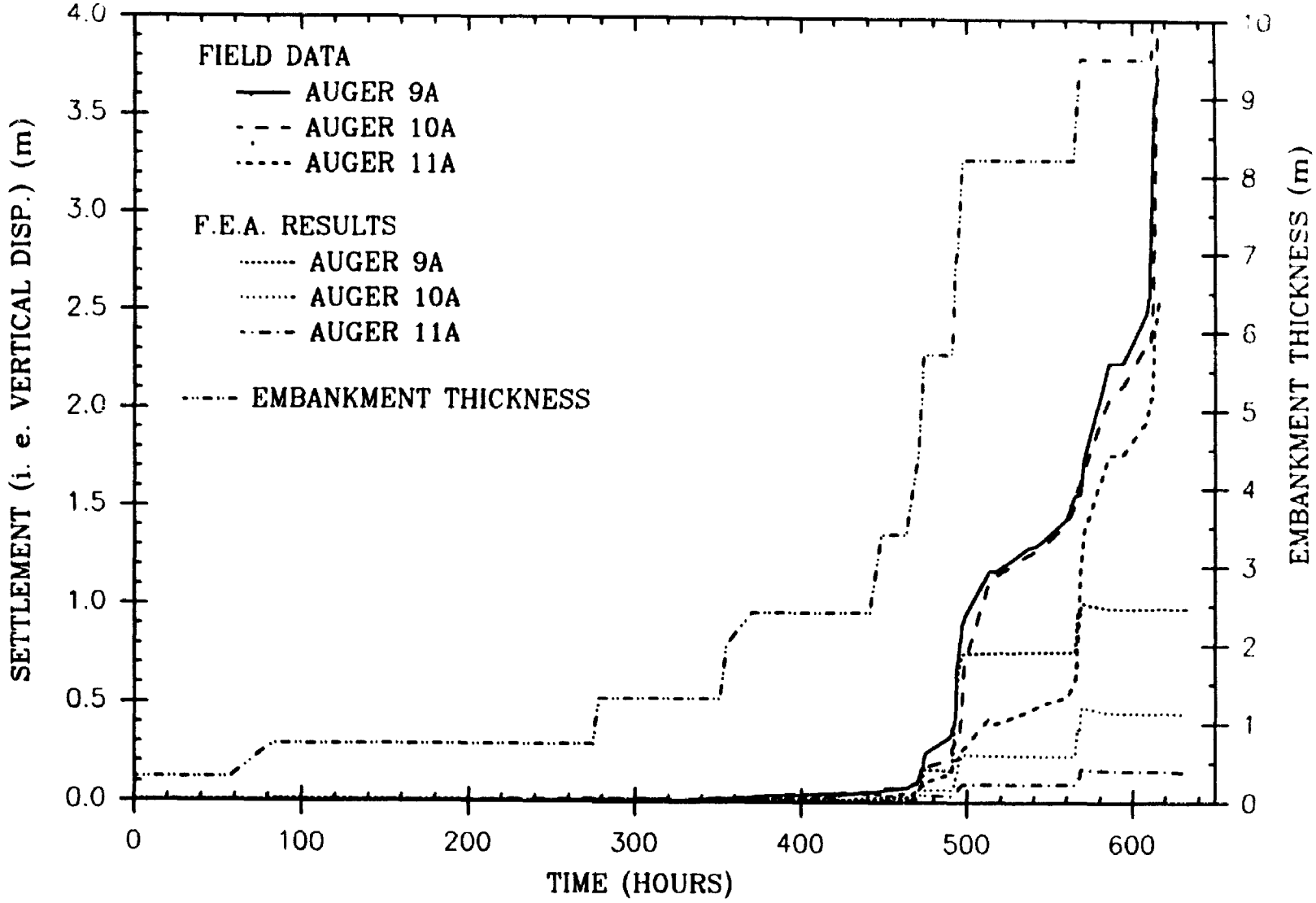

FIG. 8.3 VARIATION OF SETTLEMENT WITH TIME FOR AUGERS 9A, 10A AND 11A

m depth) after the overall elastic response of the foundation soil (i.e. after about 3.4 m thickness).

The horizontal deformations predicted from the analysis at different embankment thicknesses along the vertically placed inclinometer at the toe (i.e. inclinometer 221) are compared with the field observations in Fig. 8.4. This figure indicates reasonably good agreement between the predicted horizontal deformations and the field observations at 2.4 m embankment thickness. The predicted horizontal deformations near the ground surface were significantly lower than the observed values at 3.4 and 5.4 m thicknesses. However, there was reasonably good agreement between these responses at depths greater than about 2.5 m. The horizontal deformations were under-predicted significantly at inclinometer 231 at 2.4 and 3.4 m thicknesses (see Fig. 8.5). The prediction at 5 m thickness was reasonably close to the field observations but significantly lower near the ground surface (say up to a depth of about 3 m). Computed horizontal displacements appeared to be restrained at the foundation-embankment interface, thus differing in shape from the observed curves.

Difficulties associated with calculations of lateral deformations of foundations were discussed by Poulos (1972). Predicted horizontal displacements were usually much larger than the measurements and Poulos listed the possible reasons for the discrepancies: (1) the difficulty of estimating Poisson's ratio of the soil; (2) anisotropy of the soil; (3) nonlinear stress-strain behaviour of soil; (4) nonhomogeneity of soil; (5) neglect of certain factors such as the effect of embankment stiffness and foundation roughness or more generally, incorrect assumptions made regarding the stresses applied to the soil by the foundation or embankment. Poulos (1972) also pointed out that the sensitivity of the horizontal movements to the factors listed above is considerably greater than that of vertical displacements. It appears that factors (2) and (5) listed by Poulos (1972) are

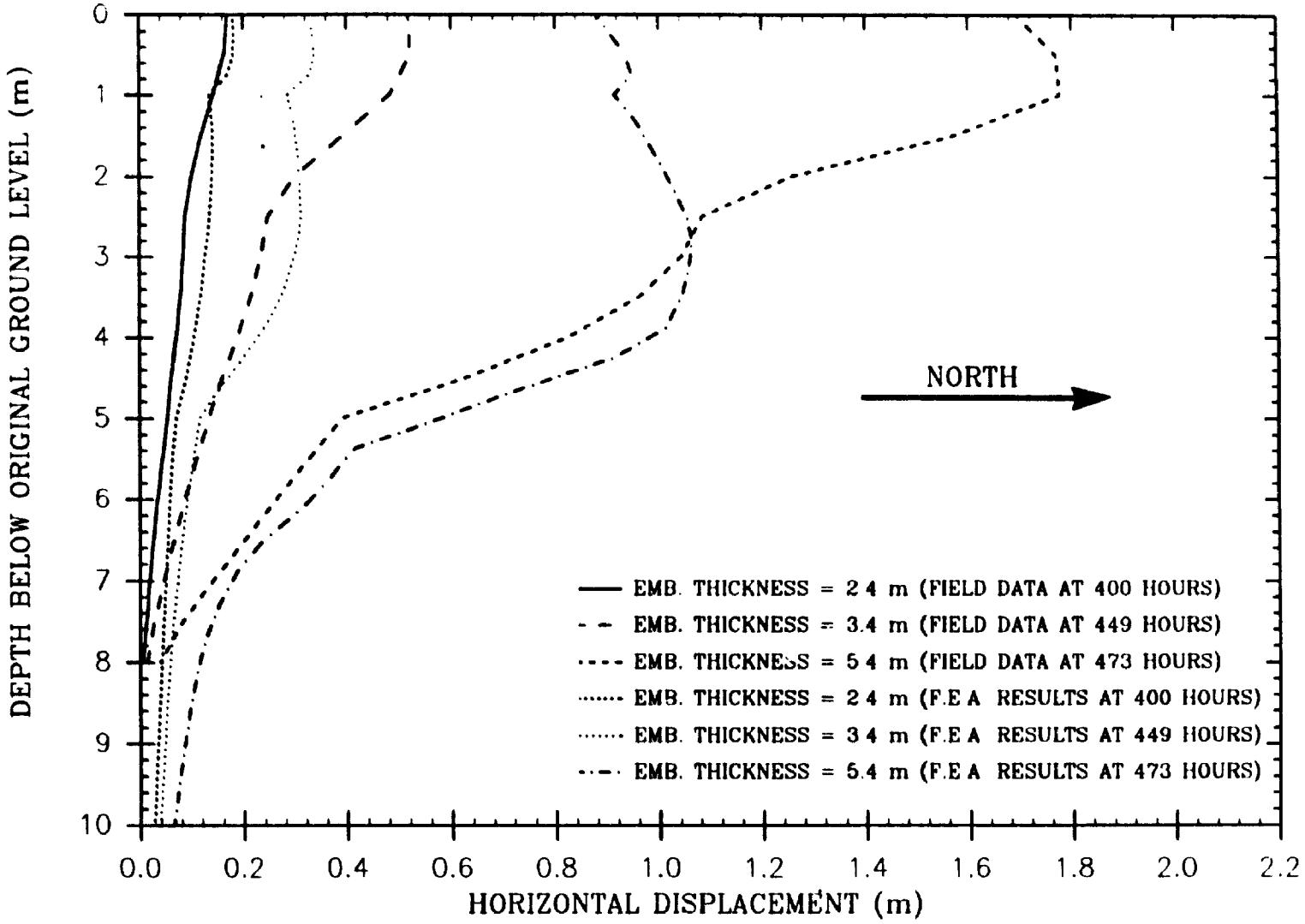

FIG. 8.4 COMPARISON BETWEEN FIELD DATA AND F.E.A. RESULTS OF HORIZONTAL DISPLACEMENTS AT INCLINOMETER 22I

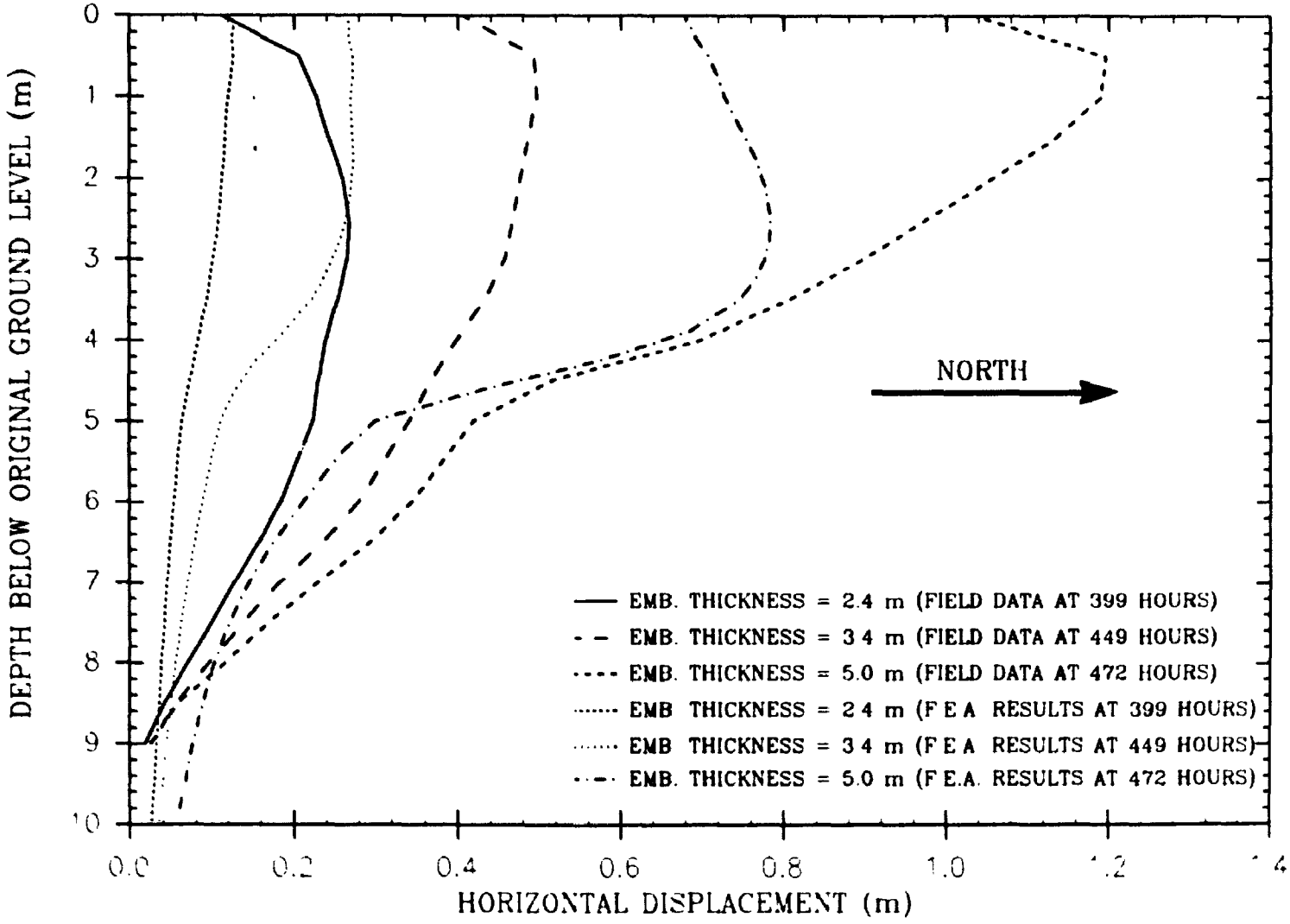

FIG 8.5 COMPARISON BETWEEN FIELD DATA AND F.E.A RESULTS OF HORIZONTAL DISPLACEMENTS AT INCLINOMETER 231

relevant to the analysis reported here.

The lateral displacements developed in clay foundations during construction under 21 different embankments were investigated by Tavenas et al. (1979) who attributed the over prediction (from the undrained analyses) to the development of significant consolidation at the beginning of any embankment construction. They concluded that the lateral deformations developed initially would be in conformity to the theory of elasticity (when the foundation soil is over consolidated) and undrained shear distortions develop near the end of construction when the clay foundation has become partly or entirely normally consolidated. The large strain fully coupled consolidation finite element model developed for the analysis of the Sackville test embankment reported here considered these factors by using two different functions for the variation of the permeability of the foundation soil with the void ratio depending on whether the soil is over consolidated or normally consolidated as discussed in chapter 7.

Despite the advances in the understanding of the behaviour of soft clays under embankment loading due to the extensive research during the past two decades, still it had not been possible to predict the vertical and horizontal deformations and the excess pore pressures developed in the foundation soil concurrently (i.e. in the same analysis with the same soil parameters). More recent studies on unreinforced embankments on soft soils have considered the consolidation effects with the use of coupled consolidation finite element analysis. However, the predicted lateral displacements were significantly higher than the measured values and the shape of the horizontal displacement profile with depth was also significantly different from the measurements (e.g. Almeida et al., 1986; Indraratna et al., 1992). The analysis reported in this chapter considered the effects of consolidation using a large strain formulation with Modified cam-clay material behaviour using higher order finite elements. In general, there was reasonably good agreement

between the predicted and computed horizontal displacements. However, the agreement was less satisfactory near the ground surface where the horizontal displacements were under predicted significantly.

As was discussed previously in chapters 3 and 4, vertical cuts were made in the crust (i.e. up to a depth of 1 to 1.2 m from the ground surface in an approximately 1.3 to 1.8 m square grid) to reduce the effect of the root mat. The effect of these cuts are likely to be the cause of the much larger horizontal deformations observed in the field near the ground surface (see Fig. 8.4). One may suspect that the large horizontal deformation in the foundation soil near the ground surface may have resulted in significant slip between the foundation and the embankment. However, there was no evidence for actual slip occurring at this interface (e.g. the inclinometers placed on the shoulder and the crest of the embankment did not indicate any evidence of slip at the interface).

The foundation soil can open up along these vertical cuts near the surface when subjected to tensile stresses (i.e. resulting in a non-continuum material with slots near the ground surface) and again close up and come into contact when subjected to compressive stresses. There could also be vertical relative movement along these cuts. Therefore, the actual effect of these cuts (i.e. vertical slots up to a depth of about 1 m) on the behaviour of the embankment could be complex and modelling them is beyond the scope of this thesis. However, an attempt was made to approximately model the effect of these cuts on the behaviour of the embankment by assigning a lower value of OCR (= 1.0) for the layer of soil from 0 to 1 m depth. Although this attempt appears to have given reasonable predictions, there was significant discrepancy between the field observations and the predictions for the vertical and horizontal deformations. These cuts are likely to cause anisotropic behaviour of the soil near the ground surface and the actual Poisson effect in this part of the foundation soil is also not known. The relatively simple Modified cam-

clay material behaviour used in this study to model the foundation soil is an isotropic model and the inadequacy of this numerical model to represent the soil where vertical cuts were made is expected to be the cause for the discrepancies between the predicted and observed lateral deformations near the ground surface.

The OCR value of 1.0 used for the layer of soil where vertical cuts were made (i.e. 0 to 1 m depth) would indicate yielding of this soil right from the beginning of construction of the embankment and result in larger deformation (than that indicated during a typical elastic response). This is expected to be the cause for the over prediction of the vertical deformations at low embankment thicknesses (i.e. < 3.4 m thickness) discussed earlier.

8.2.4 Comparison of excess pore pressures in the foundation soil

The excess pore water pressures evaluated at different locations in the foundation soil from the analysis are compared with the field observations in Figures 8.6 to 8.10. It can be seen from these figures that the predicted excess pore pressures from this analysis were generally higher than those observed in the field. The difference between the predicted and observed excess pore pressures were moderate up to about 5.7 m embankment thickness but were larger at thicknesses greater than 5.7 m. However, there was reasonably good agreement between the observed excess pore pressures and the predicted values at piezometers located beneath the shoulder of the embankment (see Figs. 8.9 and 8.10).

The importance of considering the effects of consolidation on the excess pore pressures developed in clay foundations under embankments was suggested by the research workers al Laval (e.g. Leroueil et al. 1978). These suggestions were considered

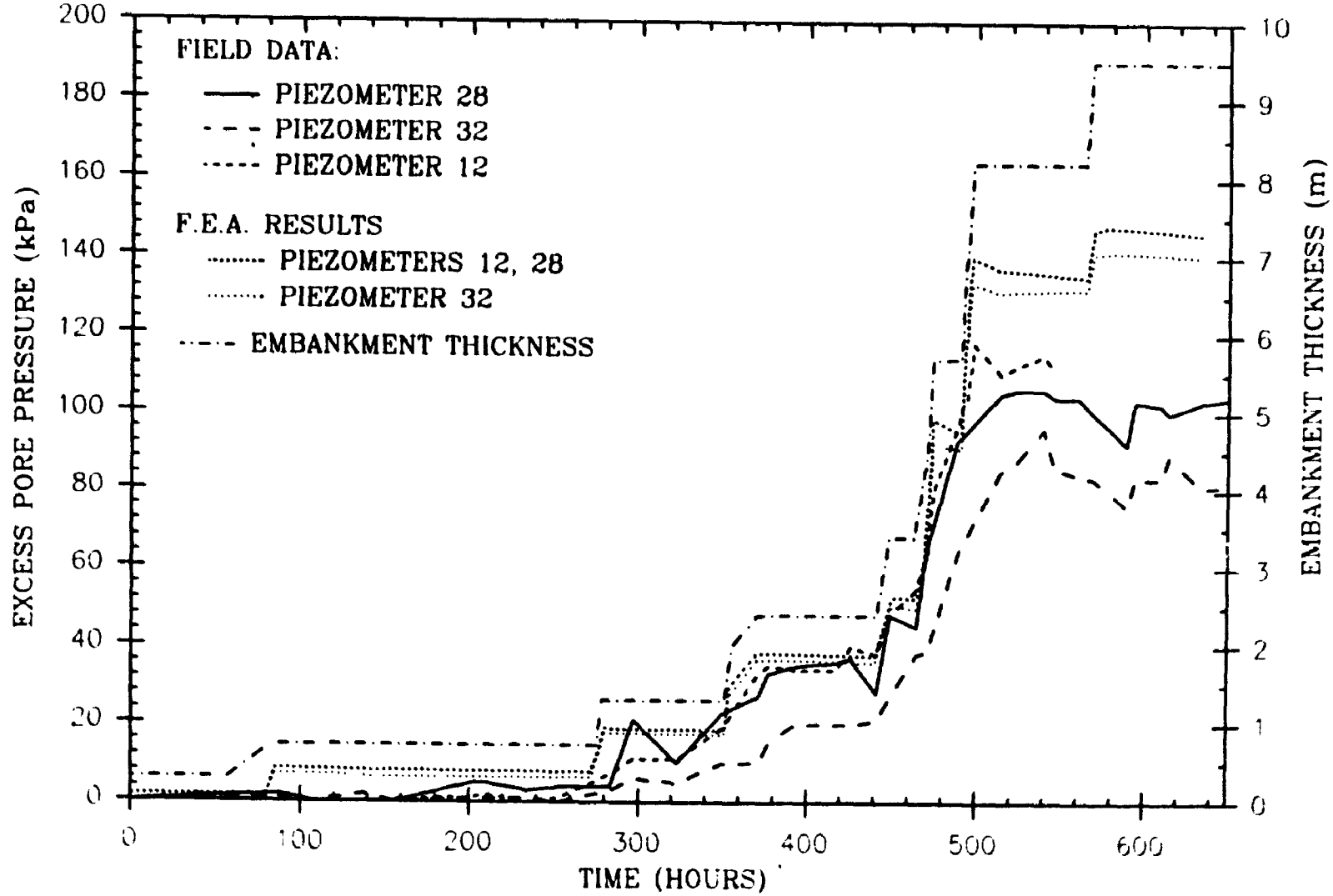

FIG 8 6 VARIATION OF EXCESS PORE PRESSURE WITH TIME FOR PIEZOMETERS 28, 32 AND 12 – COMPARISON OF F E.A RESULTS WITH FIELD DATA

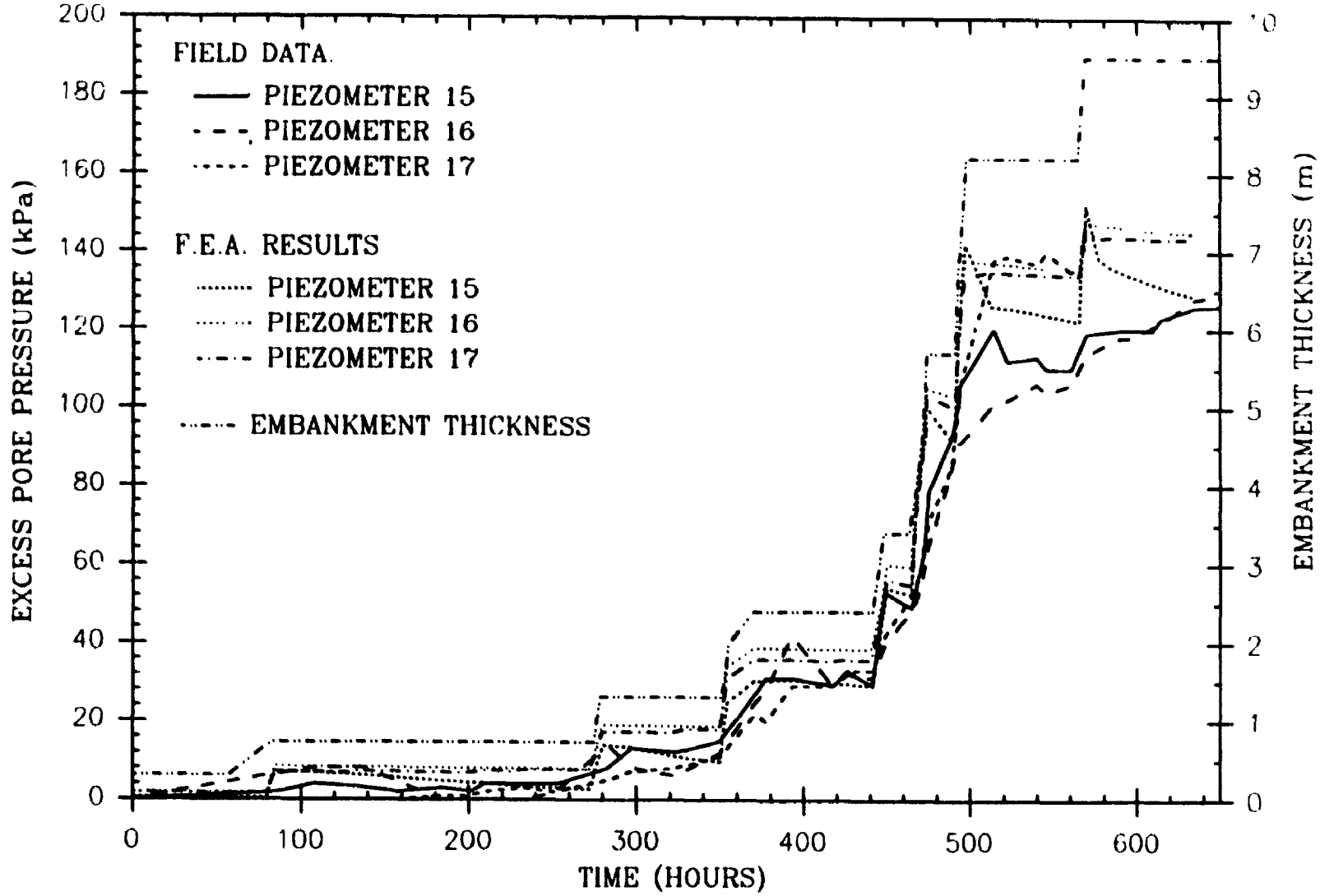

FIG. 8.7 VARIATION OF EXCESS PORE PRESSURE WITH TIME FOR PIEZOMETERS 15, 16 AND 17 – COMPARISON OF FEA RESULTS WITH FIELD DATA

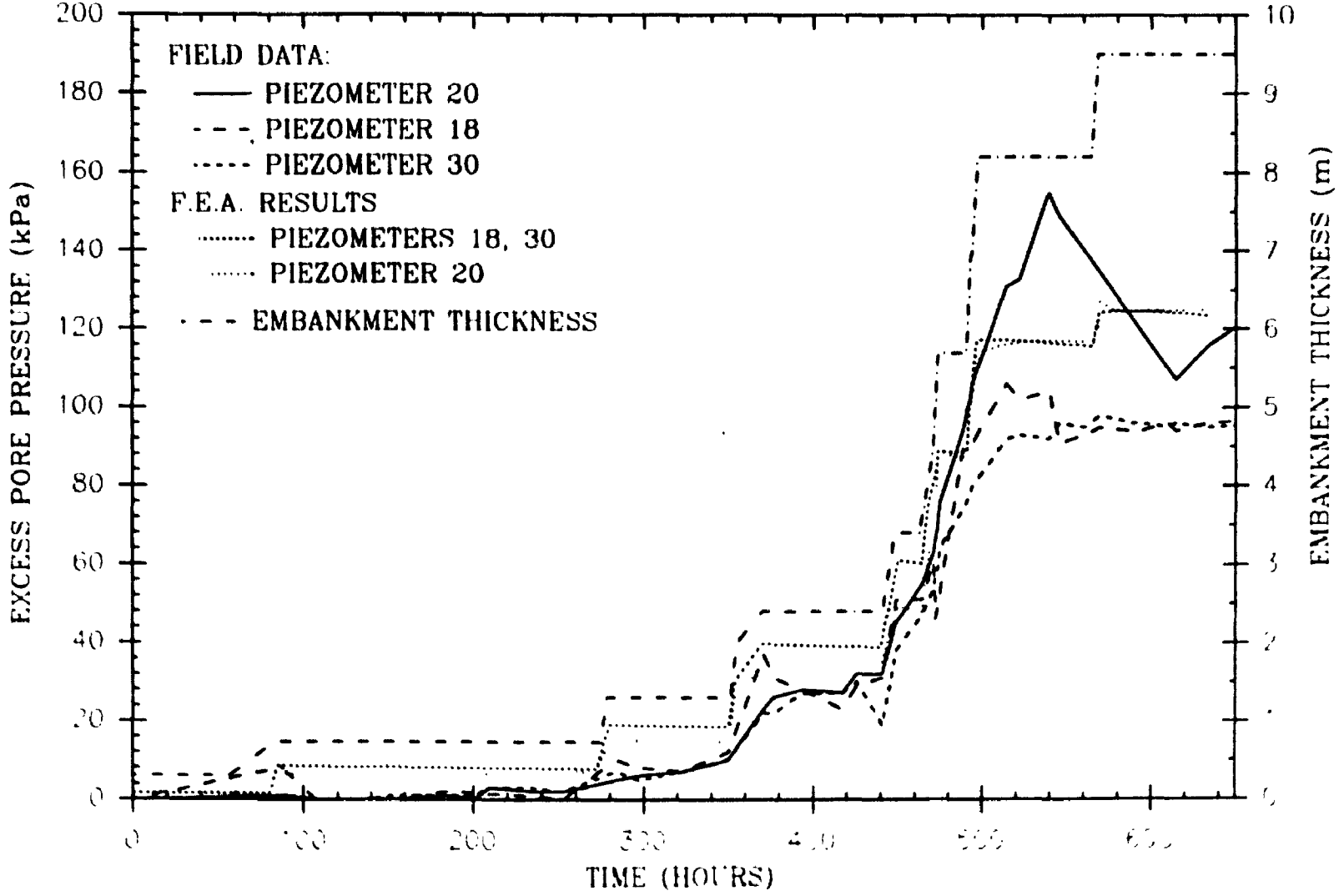

FIG 8.8 VARIATION OF EXCESS PORE PRESSURE WITH TIME FOR PIEZOMETERS 18, 30 AND 20 – COMPARISON OF F.E.A. RESULTS WITH FIELD DATA

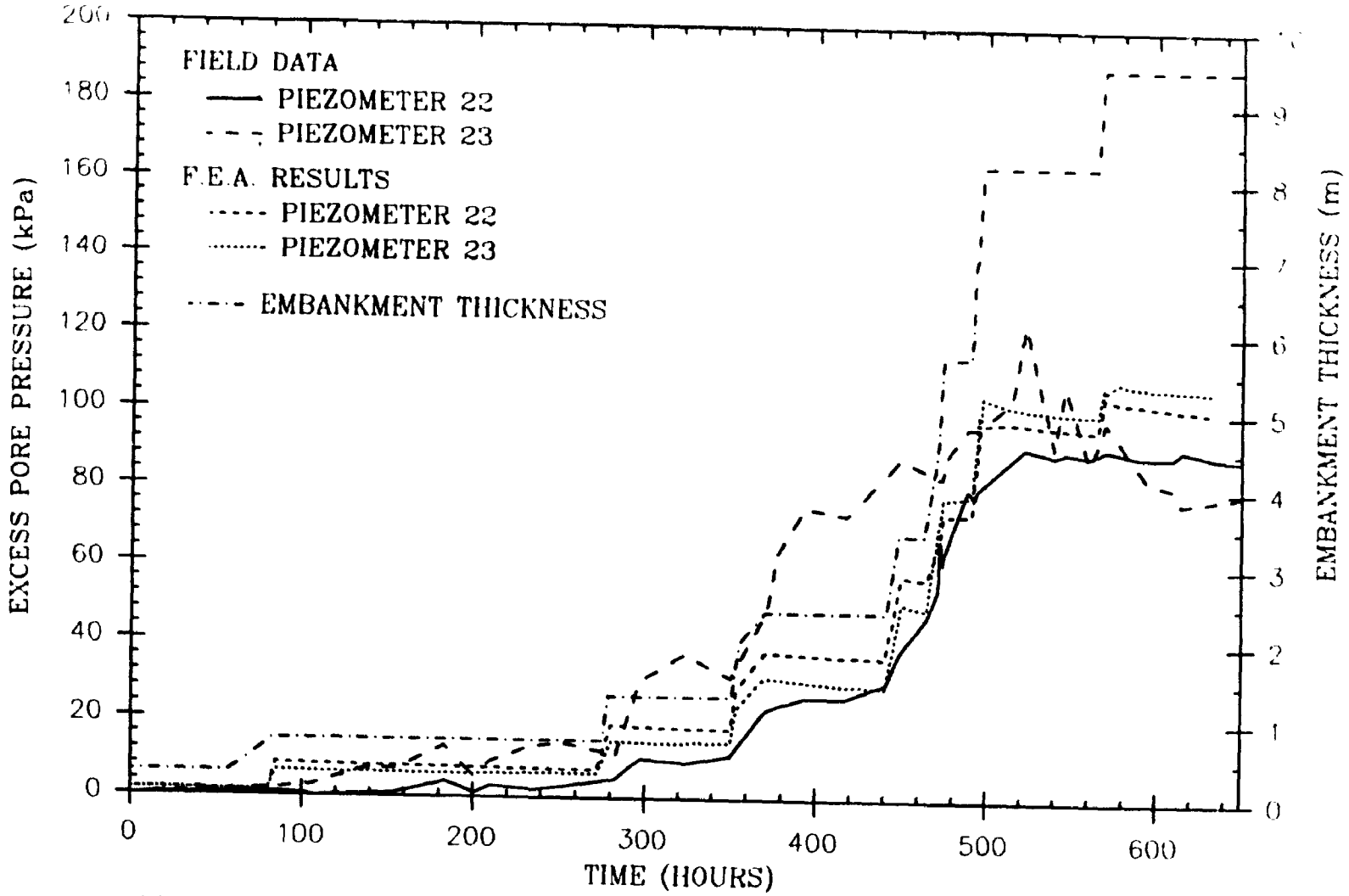

FIG. 8.9 VARIATION OF EXCESS PORE PRESSURE WITH TIME FOR PIEZOMETERS 22 AND 23 – COMPARISON OF F.E.A. RESULTS WITH FIELD DATA

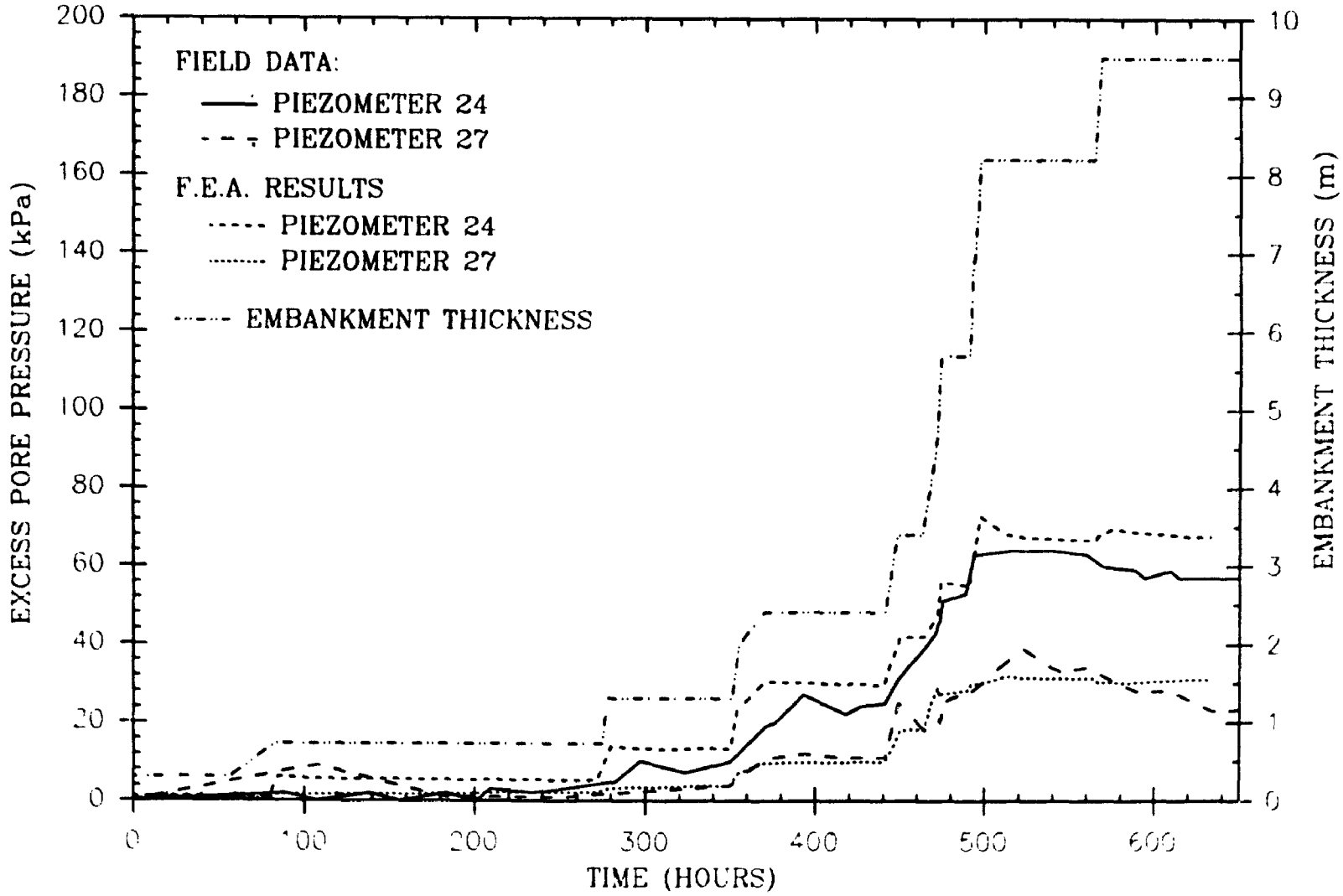

FIG 8.10 VARIATION OF EXCESS PORE PRESSURE WITH TIME FOR PIEZOMETERS 24 AND 27 – COMPARISON OF F.E.A. RESULTS WITH FIELD DATA

in the consolidation finite element model used in the analysis reported here as discussed previously (i.e. the change of the permeability or the coefficient of consolidation when the foundation soil changes from an initially overconsolidated state at low embankment thickness to normally consolidated state). However, still the computed excess pore pressures were higher than those measured in the field (see Figs. 8.6 to 8.8).

The effect of changing the permeability of the foundation soil on the behaviour of this reinforced embankment is examined in chapter 9. The results of this analysis indicated that the predictions could be improved significantly by increasing the permeability values for the foundation soil. However, such variations need to be justified with field or laboratory measurements of permeability in order to be considered here for comparison with the observed field responses.

Initial analysis of the Cubzac-les-Ponts embankment in France (Magnan, 1984) also indicated similar higher excess pore pressures than the measured values. However, subsequent analysis of this embankment assuming the pore fluid to be compressible and with the assumption of the degree of saturation equal to 98% in all the foundation soil is reported to have resulted in good agreement between the calculated and measured excess pore pressures and settlements (Leroueil et al., 1990). The samples used for the triaxial tests reported in chapter 6 indicated the initial degree of saturation to be between 97% to 99%. The discrepancies between the calculated and observed excess pore pressures in the Sackville test embankment also can be attributed in part to an underestimation of the actual coefficients of permeability of the soil, and partly to the compressibility of the pore fluid and incomplete saturation of the soil at Sackville, New Brunswick.

There were no in-situ field measurements of permeability and the permeability of the foundation soil used in the analysis were based on conventional one dimensional

consolidation tests (performed on 50 mm Dia. and 15 mm thick specimens) on samples obtained from one bore hole (i.e. indicated as Laval sample in Fig. 3.2). Moreover, due to the limitation on the quantity of samples available for investigation at U.W.O., special consolidation tests (such as the consolidation test using Rowe's apparatus) could not be performed. As discussed previously in chapter 3, the shear strength varied over the site at different locations quite significantly as indicated by the vane and cone tests performed at several locations. This suggest the possibility for a three dimensional variation of the permeabilities across the site. Coupled with this is the possibility of the existence of (micro) fissures in the soil, particularly in the significantly overconsolidated soil near the surface (say up to about 3.5 m), which could result in higher permeability values and higher horizontal to vertical permeability ratios. Based on the available information, the analysis reported here considered the ground surface as the only free draining boundary. However, the possibility of the existence of relatively more permeable silt layers or seams could not be ruled out.

Based on the investigation of the excess pore pressures developed in the foundation soils beneath the centre line of embankments, Leroueil et al. (1978a and 1978b) proposed an empirical approach to evaluate the excess pore pressures along the centre line of embankments where no rotation of principal stresses were expected. They suggested that the consolidation effects would be significant during early stages of construction when the foundation soil is overconsolidated and the excess pore pressure changes in the foundation soil would be in accordance to $\overline{B} = 1$ (i.e. at constant vertical effective stress) when the soil become normally consolidated. Clearly, the concept of $\overline{B} = 1$ at normally consolidated state is not applicable for the reinforced test embankment constructed at Sackville, New Brunswick where it was observed that B reached a peak value (ranging between 0.8 and 0.9) at about 488 hours (i.e. at 5.7 m fill thickness) and decreased rapidly afterwards as discussed previously in chapter 4 (see Figs. 4.11 and

4.12). This type of discrepancy has been reported by Folkes and Crooks (1985) for six other case histories which demonstrated that the effective stress path can vary widely depending on factors such as imposed stress level, rate of construction and boundary drainage conditions, contrary to a single effective stress path considered by Leroueil et al. (1978b), and consequently the parameter $\overline{B}$ does not provide an adequate basis for determining the effective stress state in a soft clay.

The Modified Cam-clay material behaviour adopted in the numerical model assumes an associated flow rule and that the yield locus to be centred on the isotropic compression line as discussed previously in chapter 7 (see Fig. 7.5). This assumption is valid for normally consolidated isotropic soils and the yield locus has been found to be approximately centred on the K_o consolidation line for many natural clays (e.g. Parry and Nadarajah, 1973; Leroueil et al. 1978b; Tavenas, 1981). The discrepancies between the calculated and measured excess pore pressures could also be partly due to such limitations of the Modified Cam-clay material model used in this analysis. Despite these limitations, the Modified Cam-clay material model was used in this analysis because of its mathematical simplicity for implementation in numerical codes, use of a small set of parameters obtainable from standard laboratory tests and above all its proven ability to give reasonable predictions of the behaviour of lightly overconsolidated clays under stress paths corresponding to embankment loading (e.g. Wood, 1982) as discussed previously in chapter 7.

8.2.5 Comparison of geotextile strains

The variation of geotextile strain with embankment thickness predicted from the analysis at different locations across the geotextile are compared with the similar data obtained from field measurements in Figs. 8.11 to 8.15 It can be observed that there were

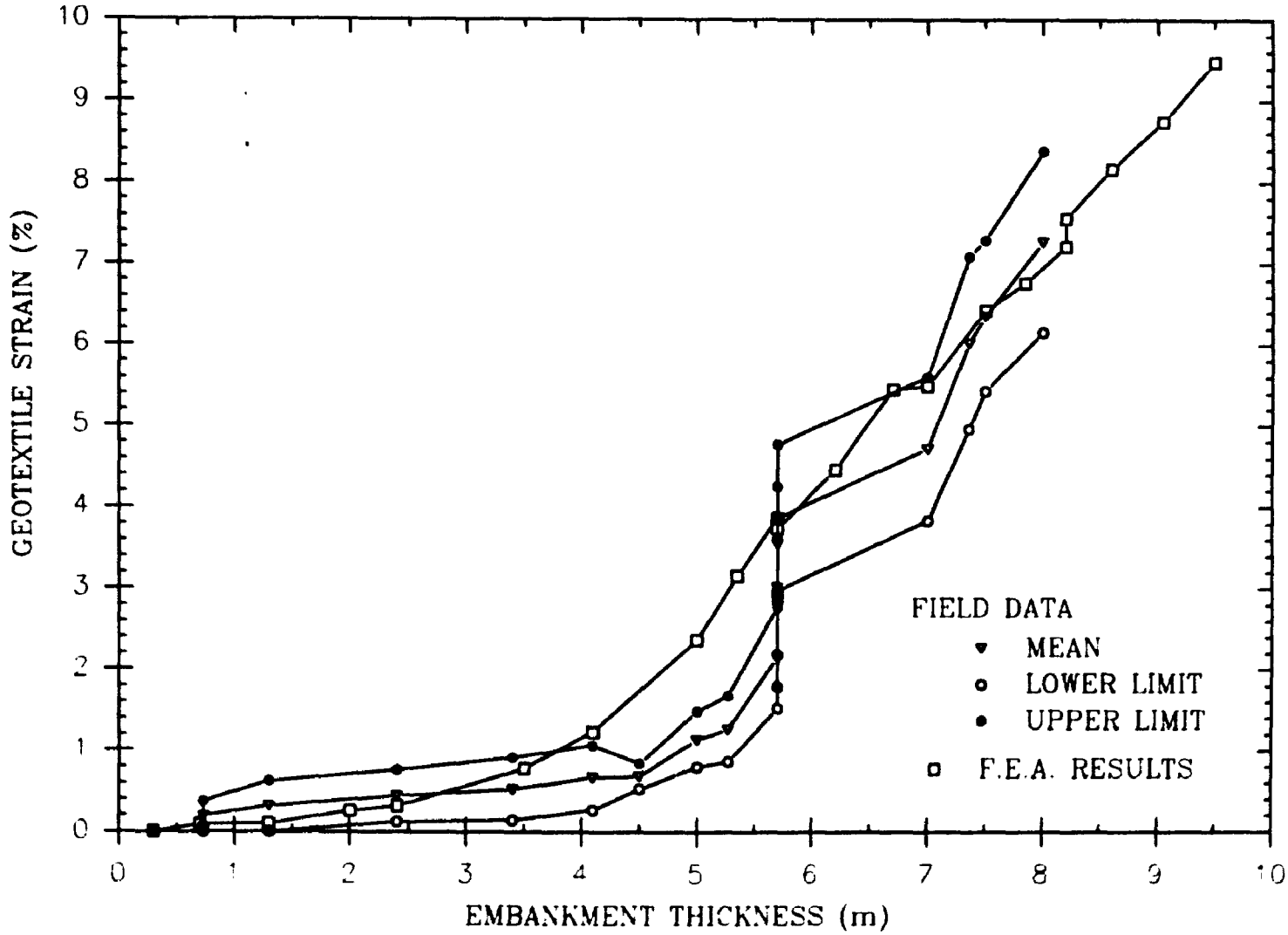

FIG. 8.11 VARIATION OF GEOTEXTILE STRAIN WITH EMBANKMENT THICKNESS AT 17.1 m FROM EMBANKMENT TOE – COMPARISON OF F.E.A. RESULTS WITH FIELD DATA

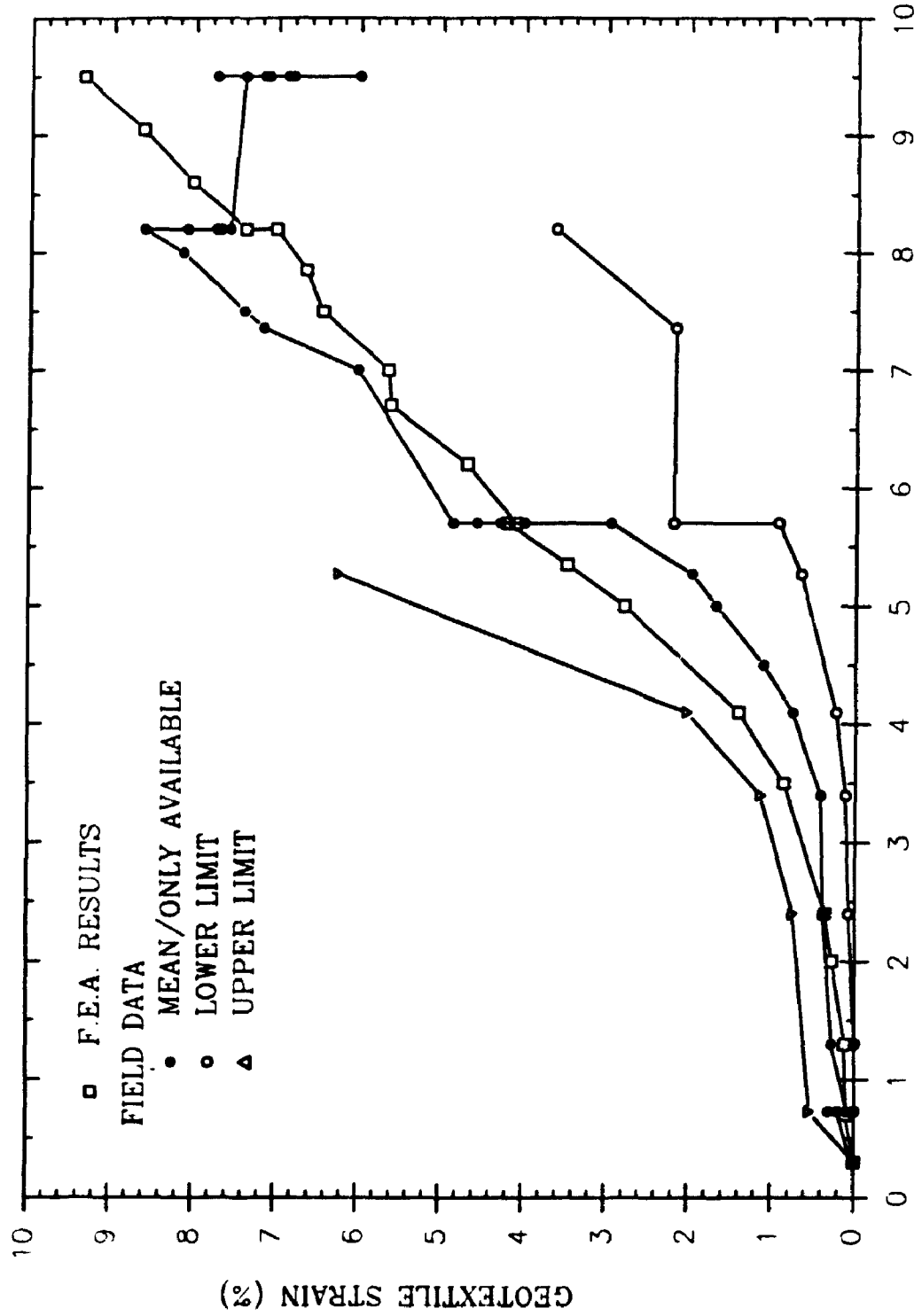

FIG. 8.12 VARIATION OF GEOTEXTILE STRAIN WITH EMBANKMENT THICKNESS AT 15.1 m FROM EMBANKMENT TOE – COMPARISON OF F.E.A. RESULTS WITH FIELD DATA

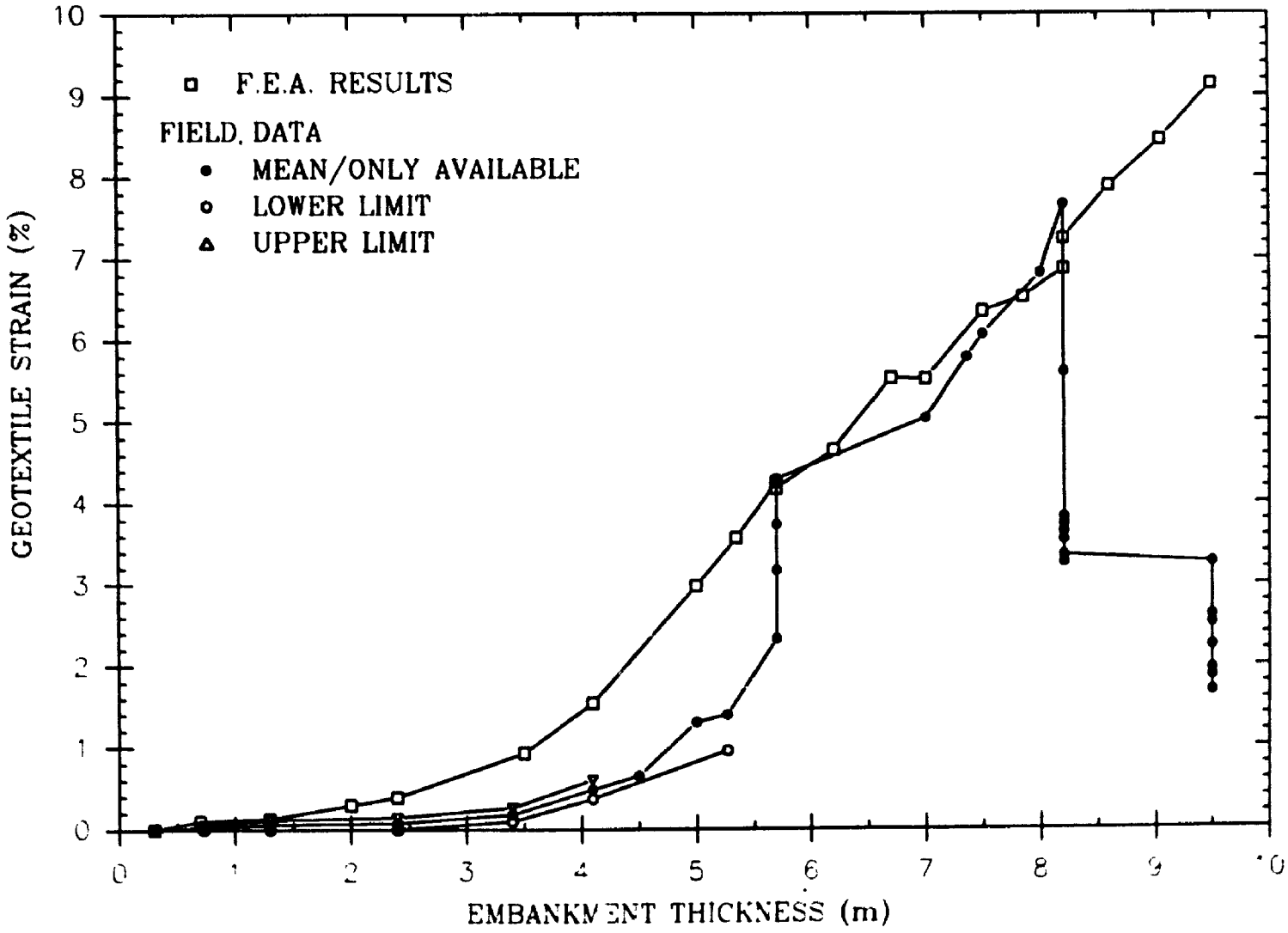

FIG. 8.13 VARIATION OF GEOTEXTILE STRAIN WITH EMBANKMENT THICKNESS AT 13.9 m FROM EMBANKMENT TOE – COMPARISON OF F E A RESULTS WITH FIELD DATA

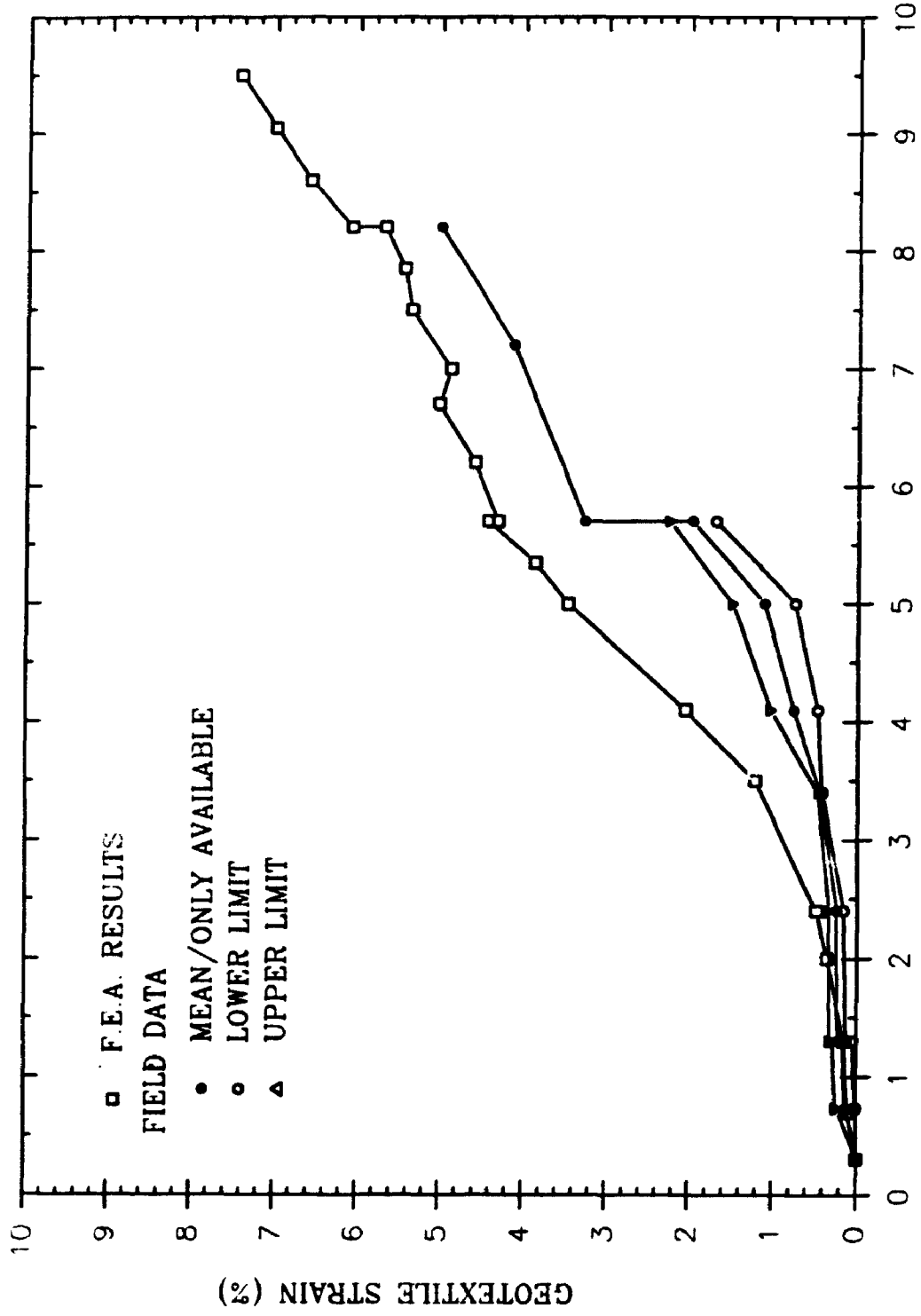

FIG. 8.14 VARIATION OF GEOTEXTILE STRAIN WITH EMBANKMENT THICKNESS AT 10.3 m FROM EMBANKMENT TOE - COMPARISON OF F.E.A. RESULTS WITH FIELD DATA

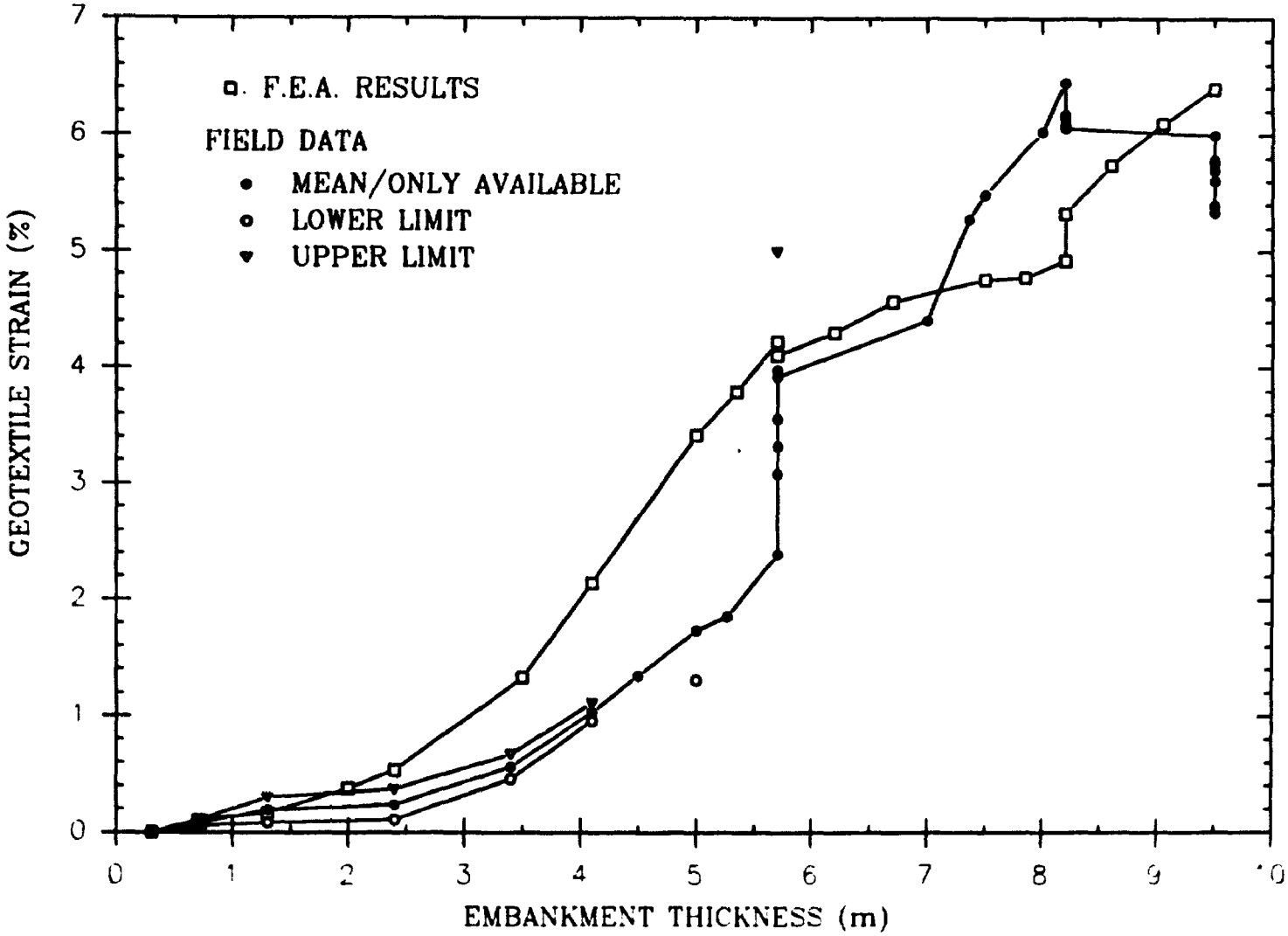

FIG. 8.15 VARIATION OF GEOTEXTILE STRAIN WITH EMBANKMENT THICKNESS AT 8.8 m FROM EMBANKMENT TOE - COMPARISON OF F.E.A. RESULTS WITH FIELD DATA

reasonably good agreement between the calculated strains and the measured values at the locations 15.1 and 17.1 m from the toe (see Figs. 8.11 and 8.12). The predicted strains were higher, particularly between 2.4 and 5.7 m embankment thickness, at locations 13.9 and 8.8 m from the toe of embankment (see Figs. 8.13 and 8.15). The predicted strains at 10.3 m from the toe were higher than the measured values for embankment thickness greater than 2.4 m (Fig. 8.14). However, these discrepancies were not large to be concerned considering the difficulties involved in the instrumentation and monitoring of strain in a geotextile.

The analysis indicated a very small decrease in strain during the brief period of construction stoppage at 5.7 m thickness. The improvement in the stability of the foundation soil due to the consolidation process during this period and the consequent decreased dependency on the geotextile for its stability is expected to be the cause of this behaviour indicated in the analysis (see Figs. 8.11 to 8.15). However, the field measurements indicated large increase in strain during this brief stoppage of construction at 5.7 m thickness.

Shown in Figs. 8.16 to 8.21 are the comparison between the calculated geotextile strain distributions across the geotextile at different embankment thicknesses with the similar data obtained from the field measurements. The location where the maximum strain occur indicated from the analysis was close to the toe of embankment at low embankment thickness (e.g. say at 2.4 m thickness) and shifted towards the centre line of the embankment when the thickness was increased up to 5.7 m. The small strain undrained finite element analysis performed for this reinforced embankment also indicated a similar pattern of geotextile strain variation which will be discussed later in chapter 9. The field measurements indicated an opposite trend of maximum strain occurring close to the other edge of geotextile and shifting towards the centre line with

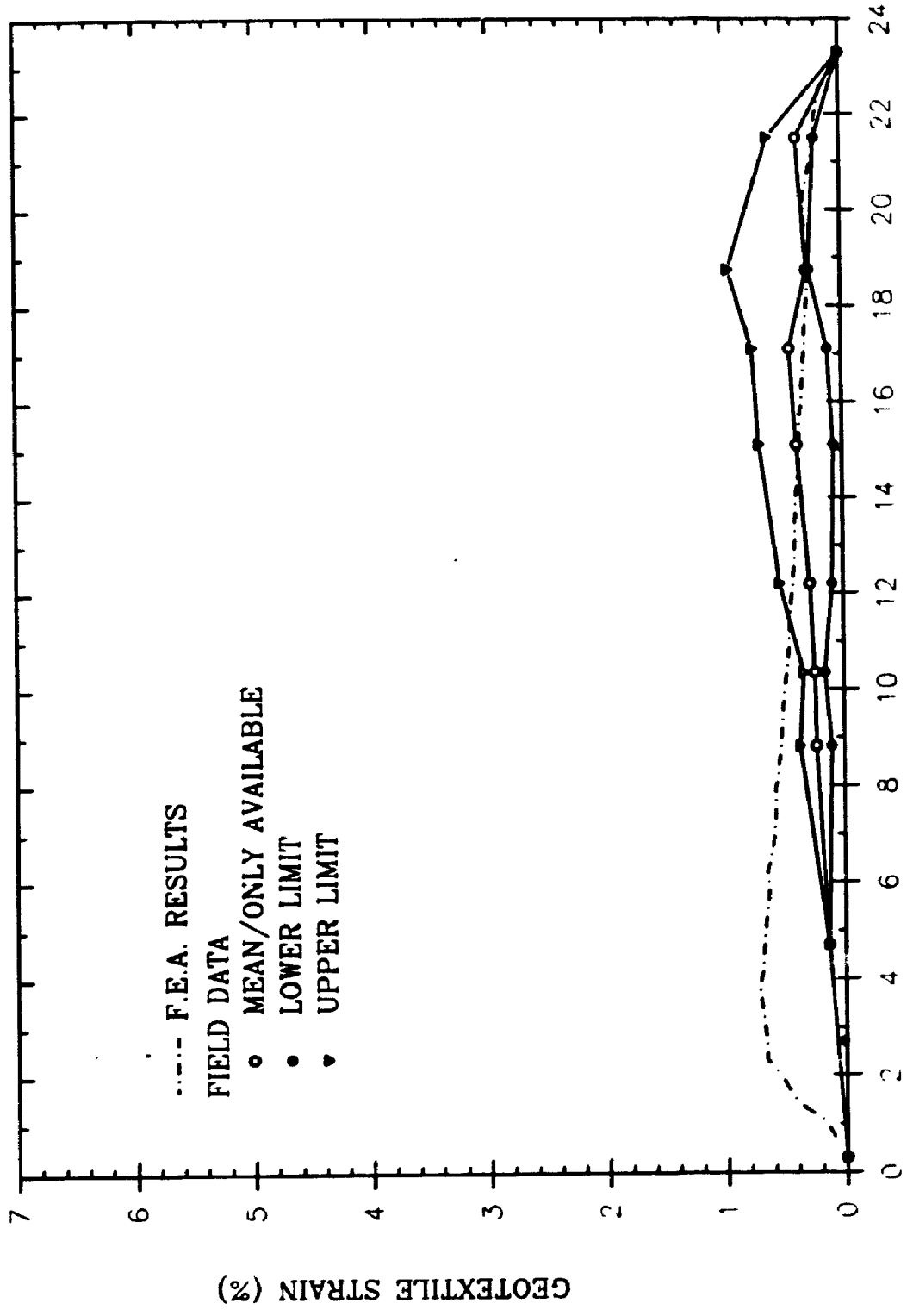

FIG 8.16 COMPARISON OF PREDICTED GEOTEXTILE STRAIN DISTRIBUTION WITH FIELD DATA AT EMBANKMENT THICKNESS = 2.4 m (272 HOURS)

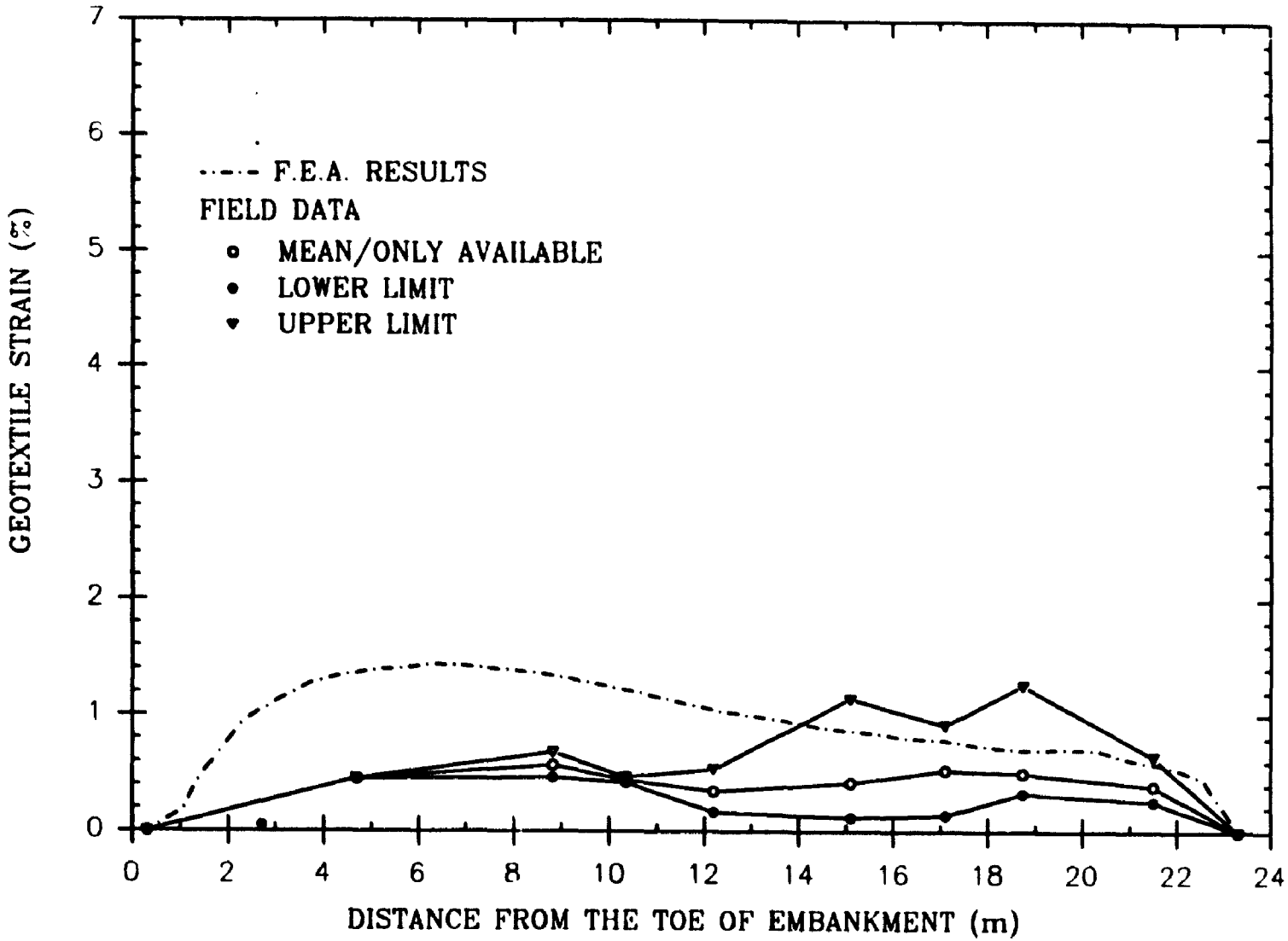

FIG. 8.17 COMPARISON OF PREDICTED GEOTEXTILE STRAIN DISTRIBUTION WITH FIELD DATA AT EMBANKMENT THICKNESS = 3.4 m (448 HOURS)

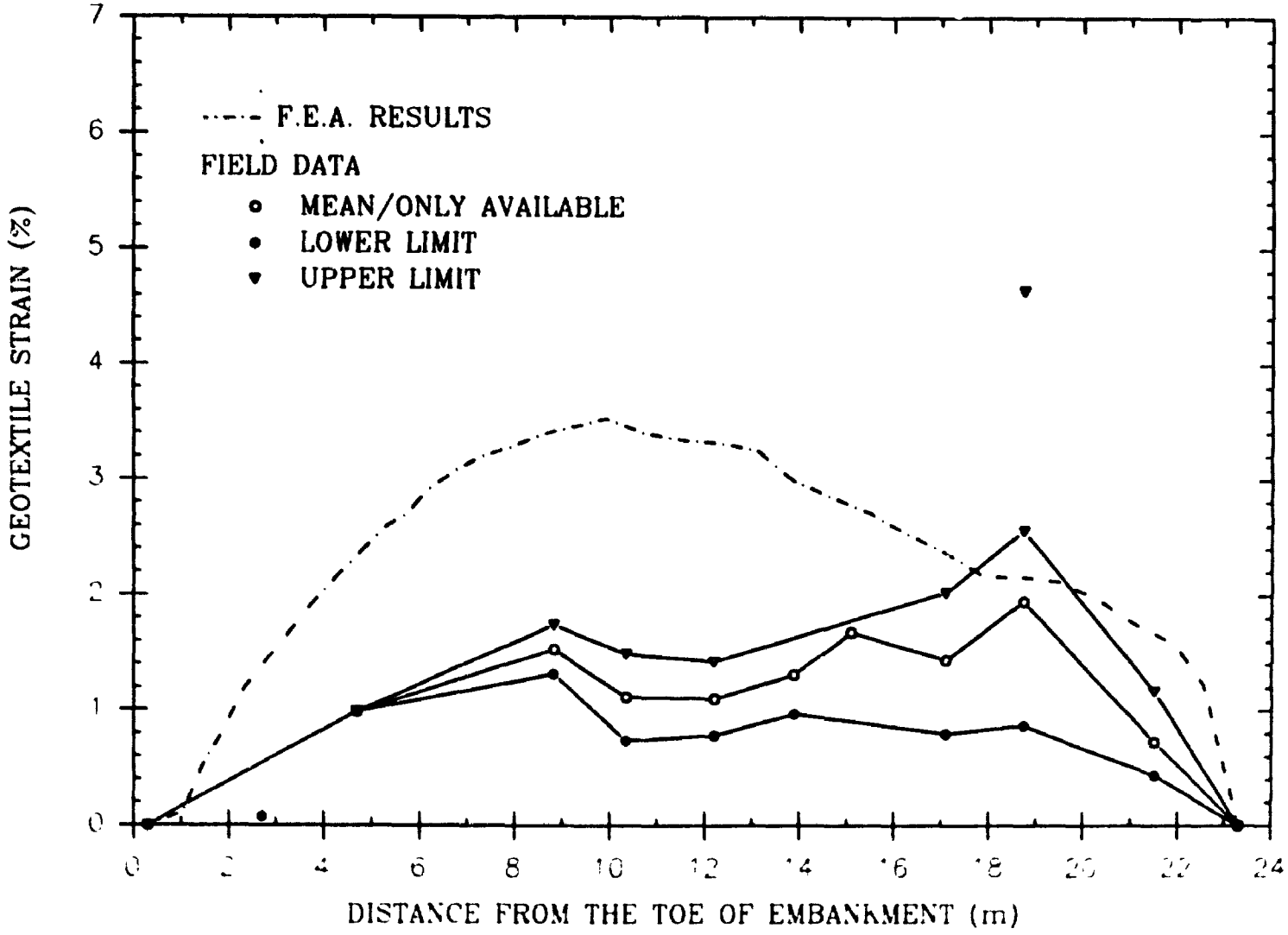

FIG 8.18 COMPARISON OF PREDICTED GEOTEXTILE STRAIN DISTRIBUTION WITH FIELD DATA AT EMBANKMENT THICKNESS = 5 m (472 HOURS)

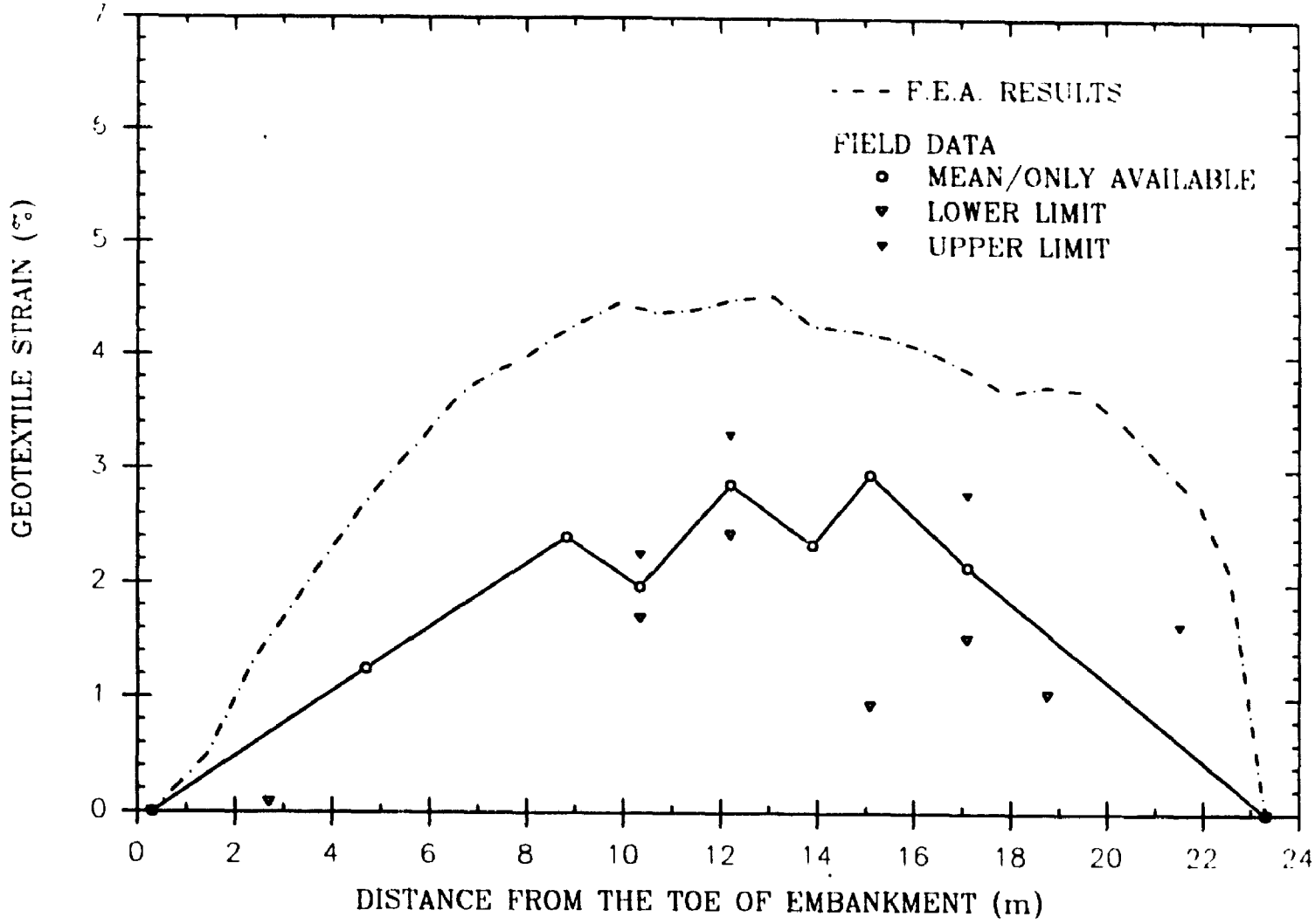

FIG. 8 19 COMPARISON OF PREDICTED GEOTEXTILE STRAIN DISTRIBUTION WITH FIELD DATA AT EMBANKMENT THICKNESS = 5.7 m (475 HOURS)

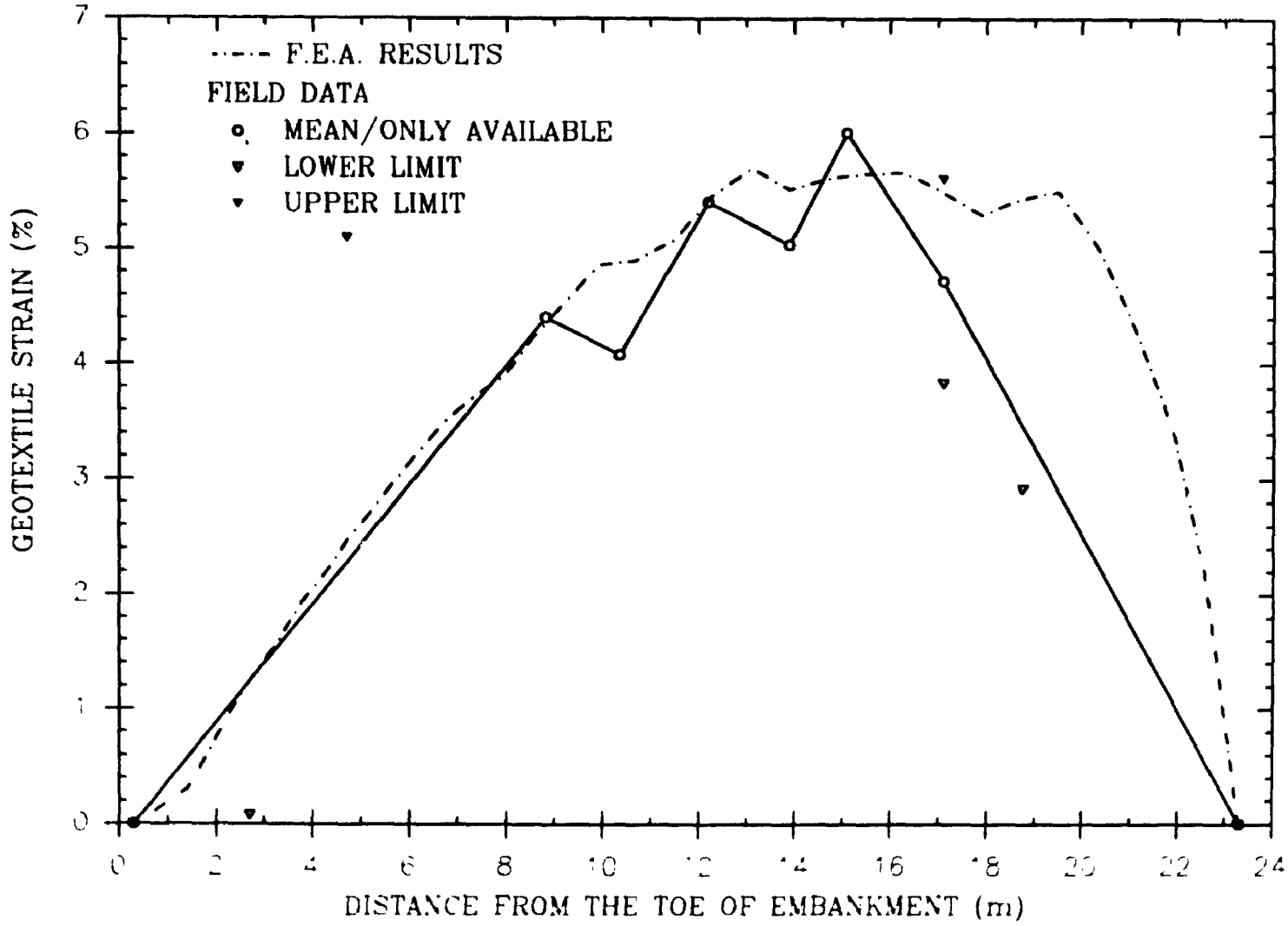

FIG 8.20 COMPARISON OF PREDICTED GEOTEXTILE STRAIN DISTRIBUTION WITH FIELD DATA AT EMBANKMENT THICKNESS = 7 m (493 HOURS)

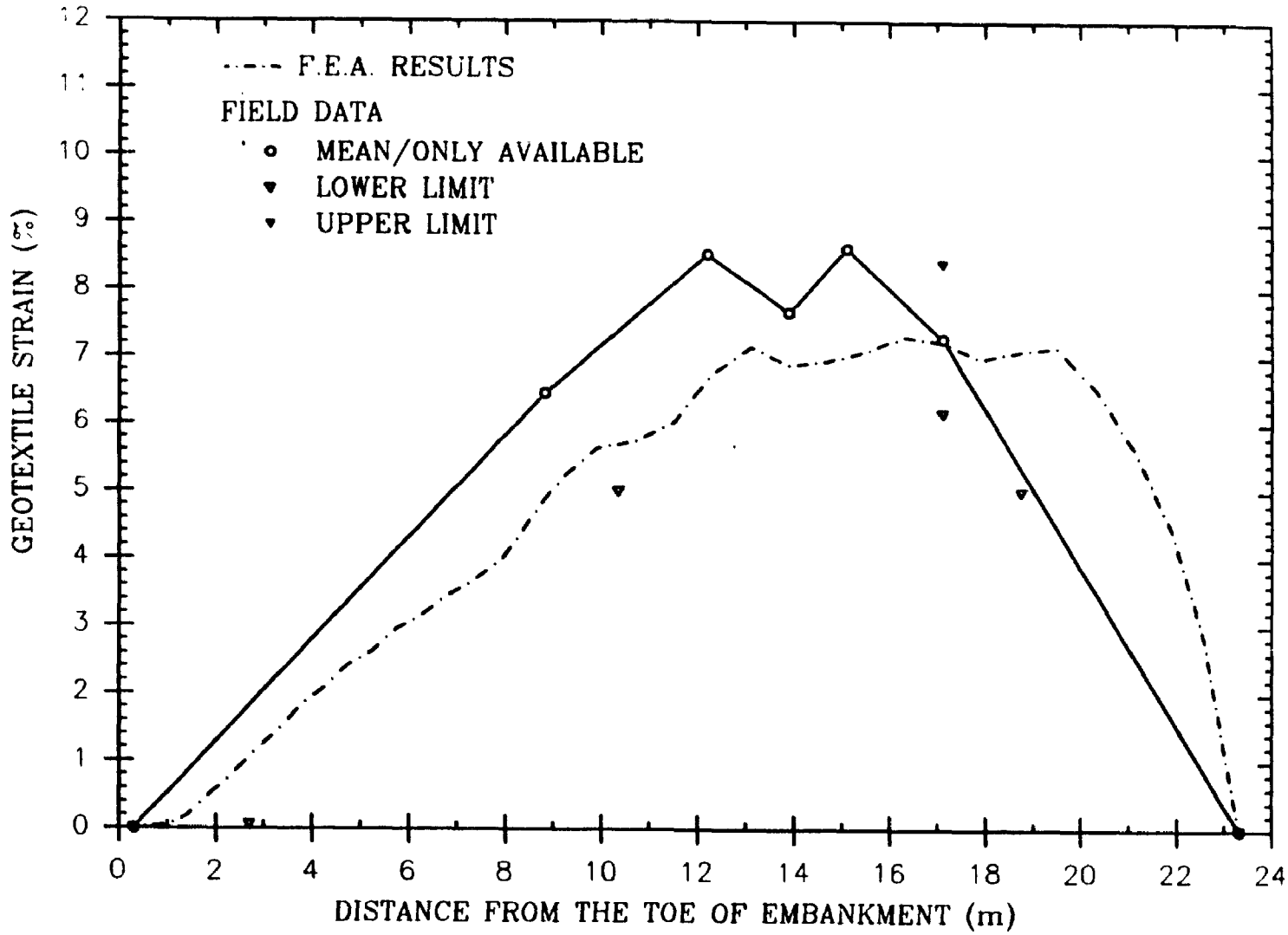

FIG. 8.21 COMPARISON OF PREDICTED GEOTEXTILE STRAIN DISTRIBUTION WITH FIELD DATA AT EMBANKMENT THICKNESS = 8.2 m (498 HOURS)

increasing embankment thickness up to 5.7 m. However, the magnitude of the predicted maximum geotextile strains agreed reasonably well with those indicated by the field measurements up to about 3.4 m thickness (see Figs. 8.16 and 8.17). The maximum strain indicated from the analysis were higher than those indicated in the field at 5 and 5.7 m thicknesses (see Figs. 8.18 and 8.19). Both the analysis and the field measurements did not indicate any significant further shifting of the location of maximum strain for thicknesses greater than 5.7 m. There was good agreement between the predicted geotextile strain distribution and the field measurements at higher embankment thicknesses (> 5.7 m) up to 8.2 m (see Figs. 8.20 and 8.21).

As previously discussed, the vertical cuts made on the soil near the ground surface (to reduce the effect of the root mat) could alter the behaviour of the foundation soil significantly and the actual influence of these cuts on the behaviour of the reinforced embankment could be complex. The effect of these cuts is expected to be the cause for the discrepancies between the predicted and observed strain distribution across the geotextile at low embankment thickness (say < 5.7 m). The field observations indicated that the role played by the geotextile reinforcement in providing stability increased substantially after 5.7 m thickness as discussed in chapters 4 and 5. It appears that the effect of the cuts on the geotextile strain responses were not significant after 5.7 m thickness.

The field observations indicated large increase in strain at 8.2 m thickness and it was hypothesized that the geotextile either tore or yielded at about 498 hours (i.e. during the brief period of construction stoppage at 8.2 m thickness) between 11.8 and 12.6 m from the toe (see chapter 5 for more details). However, the analysis did not indicate this type of tearing or yielding of the geotextile even when the embankment was constructed up to 9.5 m thickness.

8.2.6 Summary and discussion

The results from the large strain fully coupled Biot consolidation analysis using the finite element method of the geotextile reinforced embankment constructed at Sackville, New Brunswick have been compared with the field measurements. There was reasonably good agreement between the calculated vertical displacements at the ground surface and the field measurements up to about 8.2 m embankment thickness. Both the analysis and the field observations indicated an overall elastic response up to about 3.4 m thickness but the calculated settlements were significantly higher than the measured values during this elastic phase. The settlements and heaves indicated from the analysis after reaching 8.2 m thickness were significantly lower than those indicated in the field.

The settlement at depth greater than about 4 m in the foundation soil were underpredicted by the analysis after 3.4 m thickness and it appears that the large strain elasto-plastic finite element model used in this investigation is not suitable to predict the vertical deformations at large depth after the overall elastic response of the foundation soil.

The calculated excess pore water pressures were significantly higher than those indicated in the field. The difference between the calculated excess pore pressures and the field measurements were moderate up to 5.7 m thickness but the difference became larger during further construction of the embankment. However, there was reasonably good agreement between the calculated excess pore pressures and the field measurements at the piezometers located beneath the shoulder of the embankment. The difference between the calculated and measured excess pore pressures were attributed to an underestimation of the actual coefficients of permeability of the soil, and partly to the compressibility of the pore fluid and incomplete saturation of the soil at Sackville, New Brunswick.

The calculated lateral displacements at the toe of the embankment agreed reasonably well with the field measurements but were lower near the ground surface (say up to about 3 m depth). The predicted lateral displacements at inclinometer 231 (located on the shoulder of the embankment) were lower than the field measurements up to about 3.4 m thickness. The agreement was reasonably good at 5 m thickness but the calculated lateral displacements were lower than the field measurements near the ground surface.

The maximum geotextile strains indicated from the analysis at different stages of construction agreed reasonably well with the field measurements up to about 8.2 m thickness. There was a difference between the pattern of the strain distribution across the geotextile reinforcement indicated from the analysis and those obtained from field measurements at low embankment thicknesses (i.e. say up to about 5 m thickness). Reasonably good agreement was observed between the predicted strain distributions and the field measurements at higher embankment thicknesses (i.e. after reaching 5.7 m thickness). Large increase in geotextile strain was observed in the field during the brief period of construction stoppage at 5.7 m thickness whereas the analysis indicated a very small decrease in strain.

As discussed previously, a relatively large increase in settlement was observed in the field during the brief period of construction stoppage at 5.7 m thickness. This can be attributed to the time dependent viscous effects in the foundation soil and undrained creep. The large increase in geotextile strain observed in the field during the same period suggests that the geotextile began to play a significant role in providing stability to the embankment during this period.

The discrepancies between the calculated and observed geotextile strains and the horizontal deformations in the foundation soil were attributed mainly to the vertical cuts

made on the ground up to a depth of about 1 to 1.2 m (on an approximately 1.3 to 1.8 m square grid on plan) to minimize the effect of the root mat on the amount of fill required to construct the embankment until failure. As previously discussed, these cuts would result in a complex behaviour of the foundation soil near the ground surface and modelling them is beyond the scope of this thesis. The effect of these cuts was considered approximately by assigning a lower value of OCR (= 1) for the 0 to 1 m depth layer of foundation soil.

The predictions agreed reasonably well with the field measurements for the vertical and horizontal deformations at the ground surface, excess pore pressures in the foundation soil and the strains developed in the geotextile reinforcement until the embankment was constructed up to about 8.2 m thickness. The large increases in displacements and the geotextile strain observed in the field during the brief period when no additional fill was placed at 8.2 m thickness and the subsequent failure of the embankment at 8.75 m thickness (as discussed in chapter 4) could not be predicted by the large strain finite element model used here. The large displacements observed in the field at these higher embankment thicknesses could be partly due to viscous and creep effects in the soil which were not considered in the numerical model. Similarly, one may suspect the existence of creep in geotextile as a contributory factor for the large increase in strain observed during the brief periods of construction stoppage at 5.7 and 8.2 m thicknesses. The creep effects in the geotextile were not modelled in this analysis. However, the type of geotextile used was made of 100% polyester and is expected not to have any significant creep for the relatively short time intervals involved. The definition of the term "failure" is quite debatable and one may define failure based on an acceptable limit for the settlements and heaves. The settlements and heaves on the ground surface predicted from the analysis (as well as those observed in the field) exceeded 1.5 m when the embankment was constructed up to 8.2 m thickness and the embankment could be considered to have already failed or passed the performance limit at this stage. Moreover, in routine

construction projects, at least in theory, embankments are not constructed until such large settlements and heaves of the ground. Therefore, in general, the application of the numerical model adopted here appears good for predicting the behaviour of embankments on soft soils.

It appears that the predictions could be improved further by modelling the vertical cuts made on the foundation soil near the ground surface and also by considering the effects of initial incomplete saturation of the foundation soil. Additional investigation regarding the in situ permeabilities and drainage conditions could also result in the improvement of the predictions.

The natural soils are mostly anisotropic and overconsolidated (e.g. Tavenas, 1981) and the Modified Cam-clay material behaviour used here does not model these aspects as discussed previously. As discussed previously in chapter 6, the CIU and UU triaxial tests performed on samples trimmed at different inclinations did not indicate any significant anisotropy with respect to the undrained shear strength and undrained Young's modulus. However, due to the limitation on the quantity of samples available for investigation at U.W.O., these tests were performed on the samples from a particular depth only (i.e. for samples from about 2 m depth) and no additional special tests were performed. For the same reason, it was not possible to perform any special tests (such as the consolidation test using Rowe's apparatus or the triaxial tests to determine the actual yield locus) and only standard tests were performed to determine the parameters required for the analysis using the Modified Cam-clay material model. Therefore, it is also recommended that the anisotropic effects need to be further investigated and included in any future improvement of the model.

As discussed in chapter 3, the length of the embankment constructed was only 25

m (due to budgetary constraints). Moreover, the soil strength varied over the site significantly as indicated by the NRC cone test data and the field vane test data. These limitations are not likely to give ideal plane strain conditions and the actual behaviour observed in the field may have been influenced by three dimensional effects. However, the analysis reported here assumes plane strain conditions and therefore a 3 dimensional analysis is also recommended for possible improvement of the predictions in future.

8.2.7 Conclusions

The results from a fully coupled large strain elasto-plastic Biot consolidation analysis with Modified Cam clay material behaviour had been compared with the field measurements for the reinforced test embankment constructed at Sackville, New Brunswick. Details regarding this model were presented in chapter 7. The parameters of the soil and the geotextile were selected on the basis of laboratory tests and in situ field measurements which were discussed at the beginning of this chapter.

Reasonably good overall agreement was obtained between the predictions and the field measurements for the settlements, heaves, horizontal displacements and geotextile strains. The agreement was less satisfactory for excess pore pressures which were over predicted after about 5.7 m thickness. The settlements in the foundation soil at depth greater than about 4 m were underpredicted after 3.4 m thickness. The large displacements and large increases in geotextile strains observed in the field after reaching 8.2 m thickness could not be predicted satisfactorily from this analysis.

The reasonable agreement between the predicted and observed behaviour of this reinforced embankment suggest that the large strain finite element model adopted here could be used to predict the general behaviour of such embankments on soft soils

successfully. However, the predictions could be improved further by modelling the vertical cuts made on the foundation soil near the ground surface, viscous and creep effects in the soil and also by considering the effects of initial incomplete saturation of the foundation soil. The possible anisotropic behaviour of the foundation soil also needs to be investigated and included in the numerical model. Additional investigation regarding the in situ permeabilities and drainage conditions could also result in the improvement of the predictions.

8.3 COMPARISON OF THE OBSERVED AND PREDICTED BEHAVIOUR OF THE UNREINFORCED EMBANKMENT

8.3.1 General

As discussed in chapter 3, the reinforced embankment was failed before the unreinforced embankment and hence this may have had some influence on the field response of the unreinforced embankment. The extent of this influence is not known. A more accurate method to analyze this embankment would be to perform a three dimensional analysis; however this is beyond the scope of this thesis. Rather, the (plane strain) large strain finite element model developed for the consolidation analysis of the reinforced embankment is used here to examine the behaviour of the unreinforced embankment. The unreinforced embankment was constructed in four stages as discussed in chapter 3. It was constructed up to 3.4 m thickness in the first three stages. The final stage of construction until failure was commenced about 15 days after the start of construction of this embankment. Due to the considerable amount of time left in between these stages, there could have been significant consolidation and consequently an undrained approximation for the behaviour of this embankment may not be valid. Therefore, only the consolidation analysis discussed above was performed for this

embankment.

The soil samples used for the laboratory investigation reported in chapter 6 were obtained from a bore hole located beneath the reinforced embankment (indicated as Laval sample in Fig. 3.2). There was no determination of soil parameters specifically made for the soil beneath the unreinforced embankment. The NRC cone data and the field vane data indicated that the soil strength varied over the site and it was approximately 30% higher beneath the unreinforced embankment compared to that beneath the reinforced embankment as discussed in chapter 3. The only available site specific data for the unreinforced embankment is the undrained shear strength from the field vane tests performed at locations V4, V5 and V6 (see chapter 3 for additional details regarding field vane tests and the results). Although there are empirical correlations between the field vane strength and the critical state parameters, their validity for the soil at Sackville, New Brunswick is not known (due to significant organic content and high compressibility) and therefore they are not used.

The limitation on the application of the plane strain approximation for the observed field behaviour would itself preclude actual comparison between the measured and calculated responses using the numerical models discussed in chapter 7. Therefore, for completeness and to have at least a qualitative assessment of the behaviour of the unreinforced embankment, the same material parameters used earlier for the analysis of the reinforced embankment were used for the analysis of the unreinforced embankment also. Consequently, only a brief examination is presented for the comparison between the calculated and measured responses of the unreinforced embankment. However, it is noted that this thesis is mainly concerned with the behaviour of the reinforced embankment and the limitations encountered in the analysis as well as the field behaviour do not affect the findings of this thesis.

8.3.2 Numerical details

The mesh used for the finite element analysis of the unreinforced embankment is shawn in Fig. 8.22. It consists a total of 4635 nodes and 1683 elements which included 486 cubic strain triangle elements for representing the foundation soil and 1197 constant strain triangle elements for the embankment fill. The unreinforced embankment was numerically constructed as closely as possible in the actual construction sequence adopted in the field by turning on gravity of the appropriate series of embankment fill elements. A total of up to 300 load increments were used in the analysis. The finite element mesh for the embankment fill was designed in such a way that the boundary of the fill element layers coincide as closely as possible with the actual lifts employed during the construction of the embankment in the field.

A fully coupled large strain elasto-plastic consolidation finite element analysis was performed for the unreinforced test embankment constructed at Sackville, New Brunswick. In this analysis, the foundation soil was modelled as a consolidation elasto-plastic Modified Cam-clay material and the embankment fill was modelled as an elasto-plastic material with Mohr-Coulomb failure criterion. The details regarding the finite element model were described in chapter 7. The material parameters of the foundation soil as well as the embankment fill were the same as adopted for the analysis of the reinforced embankment examined earlier (see section 8.2.2 and tables 8.1 to 8.3). However, only one kind of fill material was used for the entire construction of this unreinforced embankment (i.e. the similar fill material used for the construction of the reinforced embankment after 0.7 m thickness).

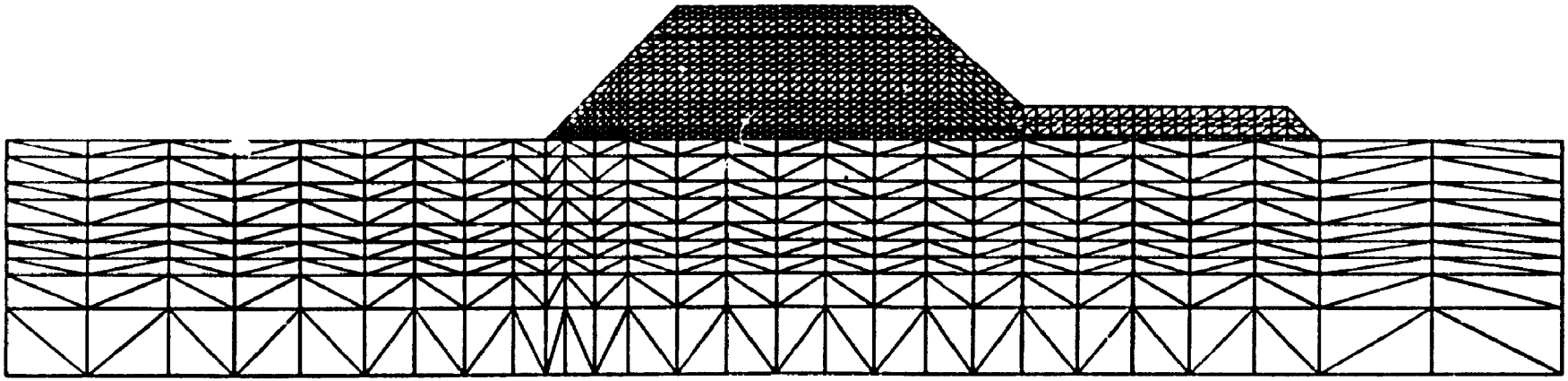

FIG. 8.22 THE FINITE ELEMENT MESH USED FOR THE UNREINFORCED EMBANKMENT ANALYSIS

8.3.3 Comparison of calculated and observed responses

The settlement and heave responses obtained from the finite element analysis are compared with the corresponding data from field measurements in Figs. 8.23 and 8.24. For comparison purposes, the variation of embankment thickness with time is also shown in these figures. It can be seen that the calculated settlements and heaves of the ground were significantly higher than the measured values in the field throughout the construction and monitoring period. This is apparently due to the comparatively larger plasticity in the foundation soil indicated in the analysis. However, both the field and calculated responses indicate similar pattern of variation for the vertical displacements. The analysis ran into some numerical problem just after the brief period of construction stoppage at 6.25 m. Large settlements and heaves were indicated at this stage which also could be an indication of failure of the embankment (i.e. at about 5.4 m thickness).

The parameters of the foundation soil used in this analysis were the same as previously used in the analysis of the reinforced embankment whereas the field vane and cone tests indicated a higher undrained shear strength values (of . out 30%) for the soil beneath the unreinforced embankment than that beneath the reinforced embankment (see chapter 3 for details regarding undrained shear strength). The higher undrained shear strength could reflect in significantly higher OCR values for the soil beneath the unreinforced embankment than those currently used which could in turn result in significantly reduced plasticity in the foundation soil. This is apparently the main cause for the discrepancies between the calculated and measured vertical displacements reported above.

The increase in the settlement during the brief period of construction stoppage at 6.25 m thickness observed in the field were significantly larger than that indicated in the

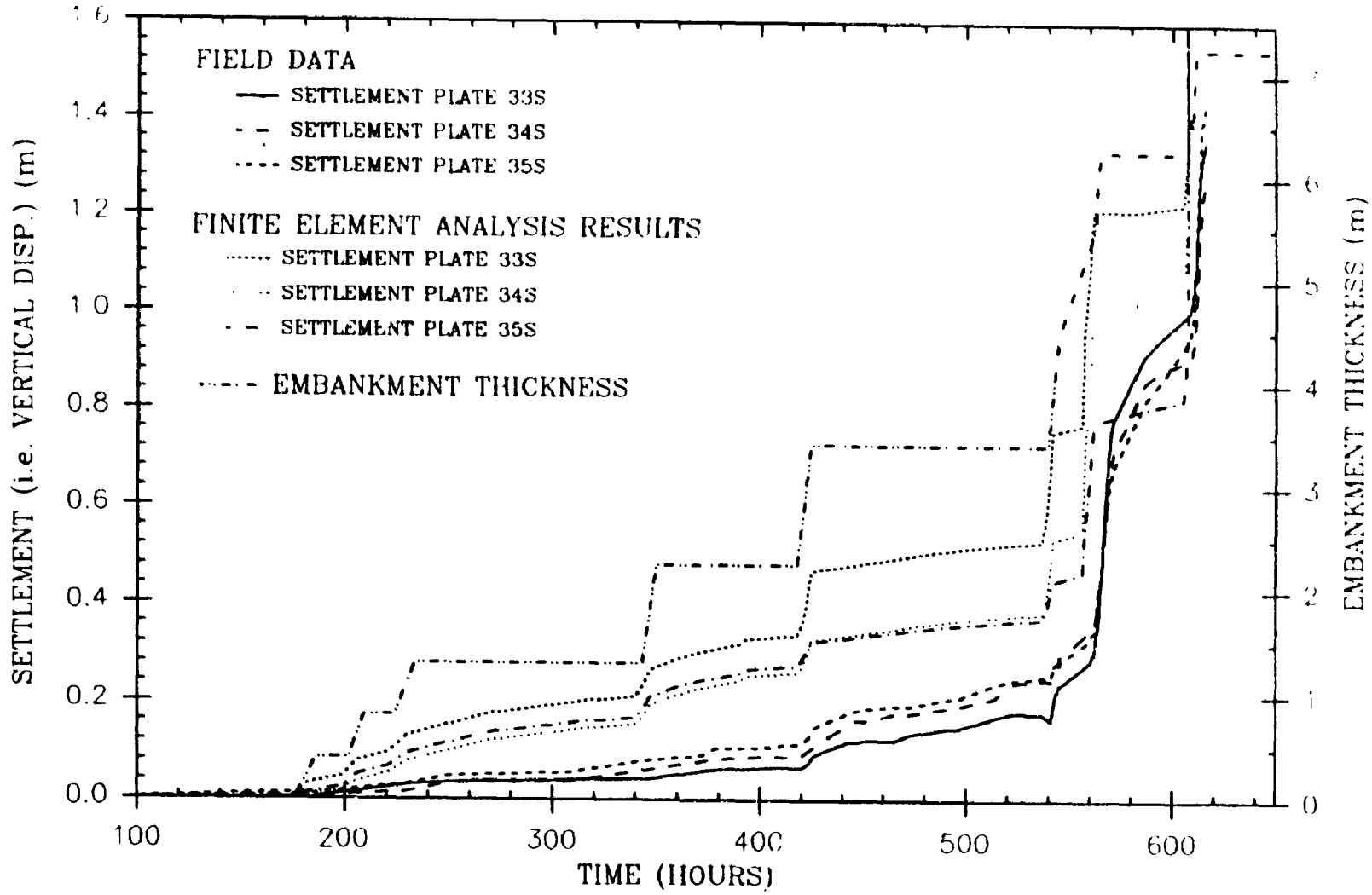

FIG. 8.23 VARIATION OF SETTLEMENT WITH TIME FOR SETTLEMENT PLATES 33S, 34S AND 35S – COMPARISON BETWEEN FIELD DATA AND F E.A. RESULTS

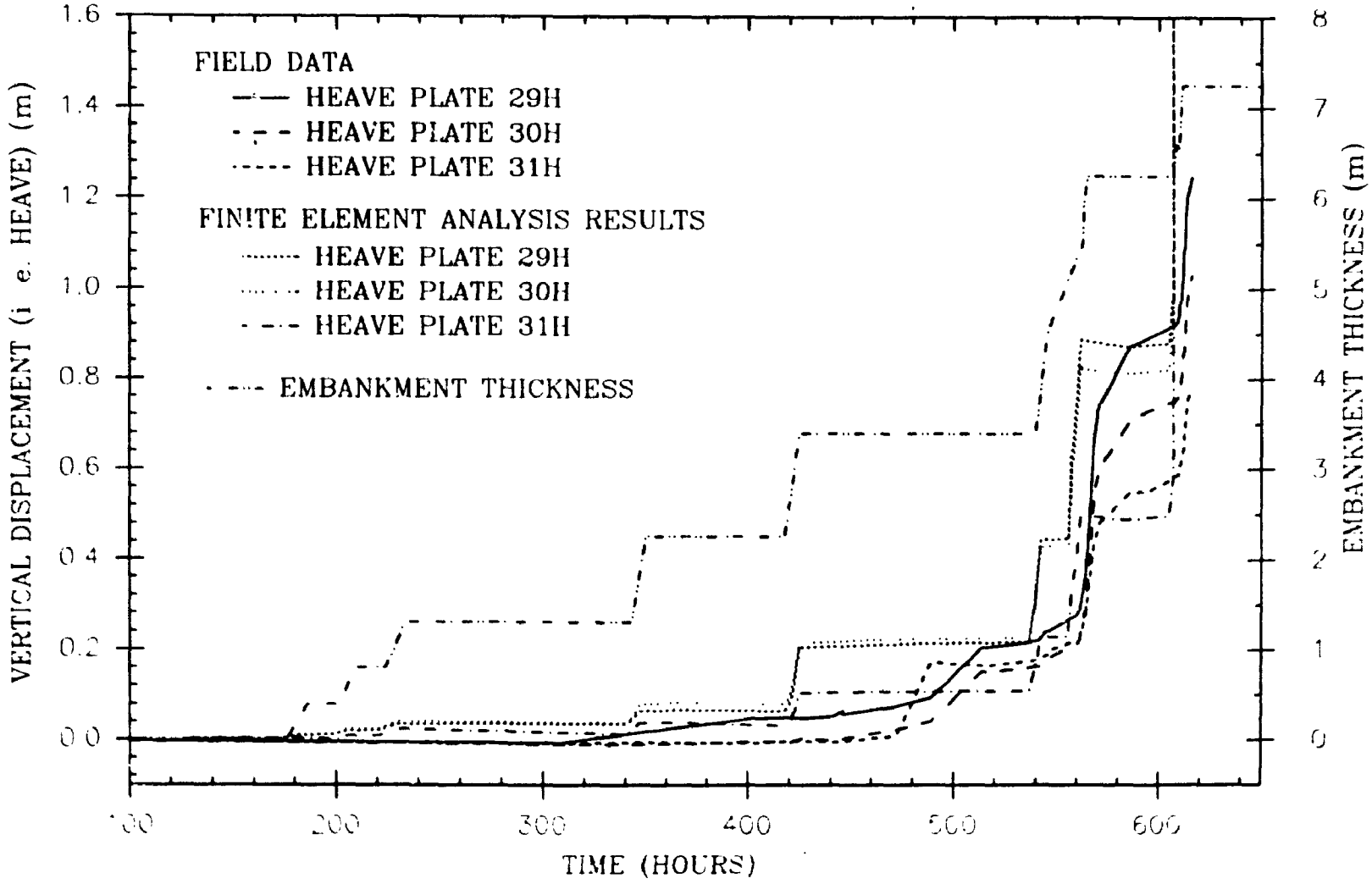

FIG 8.24 VARIATION OF VERTICAL DISPLACEMENT WITH TIME FOR HEAVE PLATES 29H, 30H AND 31H - COMPARISON BETWEEN FIELD DATA AND F E A RESULTS

analysis. This large increase in settlement observed in the field can be due to many factors such as time dependent undrained creep in the soil and visco-plastic type of behaviour of the soil. These aspects were not considered in the numerical model being used currently and are likely the causes for the above discrepancy.

Shown in Figs. 8.25 and 8.26 are the comparison of calculated horizontal displacements at inclinometer locations 501 and 511 with those measured in the field. The calculated maximum horizontal displacements were larger than the measured values but the general pattern of the variation of horizontal displacement with depth agreed reasonably well with the measured responses. However, for embankment thicknesses greater than 3.4 m, the horizontal displacements at inclinometer 511 were lower than the measured values at depths greater than 4 m. This suggest that the finite element analysis underpredicts the dispiacements at higher depth. One possible explanation for this discrepancy is the significance of anisotropy of the foundation soil and the limitation of the Modified Cam-clay to model this anisotropic behaviour.

The excess pore pressures indicated from the analysis at selected piezometer locations are compared with the field measurements in Figs. 8.27 to 8.29. It can be seen that the calculated excess pore pressures were higher than the measured values at low embankment thicknesses (up to about 3.4 m) but agreed reasonably well afterwards. The calculated buildup of excess pore pressures were higher than the field observations during the early stages of construction (say up to 3.4 m thickness). The possible reasons for these discrepancies are the incomplete saturation of the soil, compressibility of the pore fluid and the under estimation of hydraulic conductivity. As discussed previously, the OCR values of the foundation soil adopted in the current analysis were the same as used earlier for the reinforced embankment analysis whereas the actual OCR of the soil beneath the unreinforced embankment were expected to be higher. The hydraulic conductivity values,

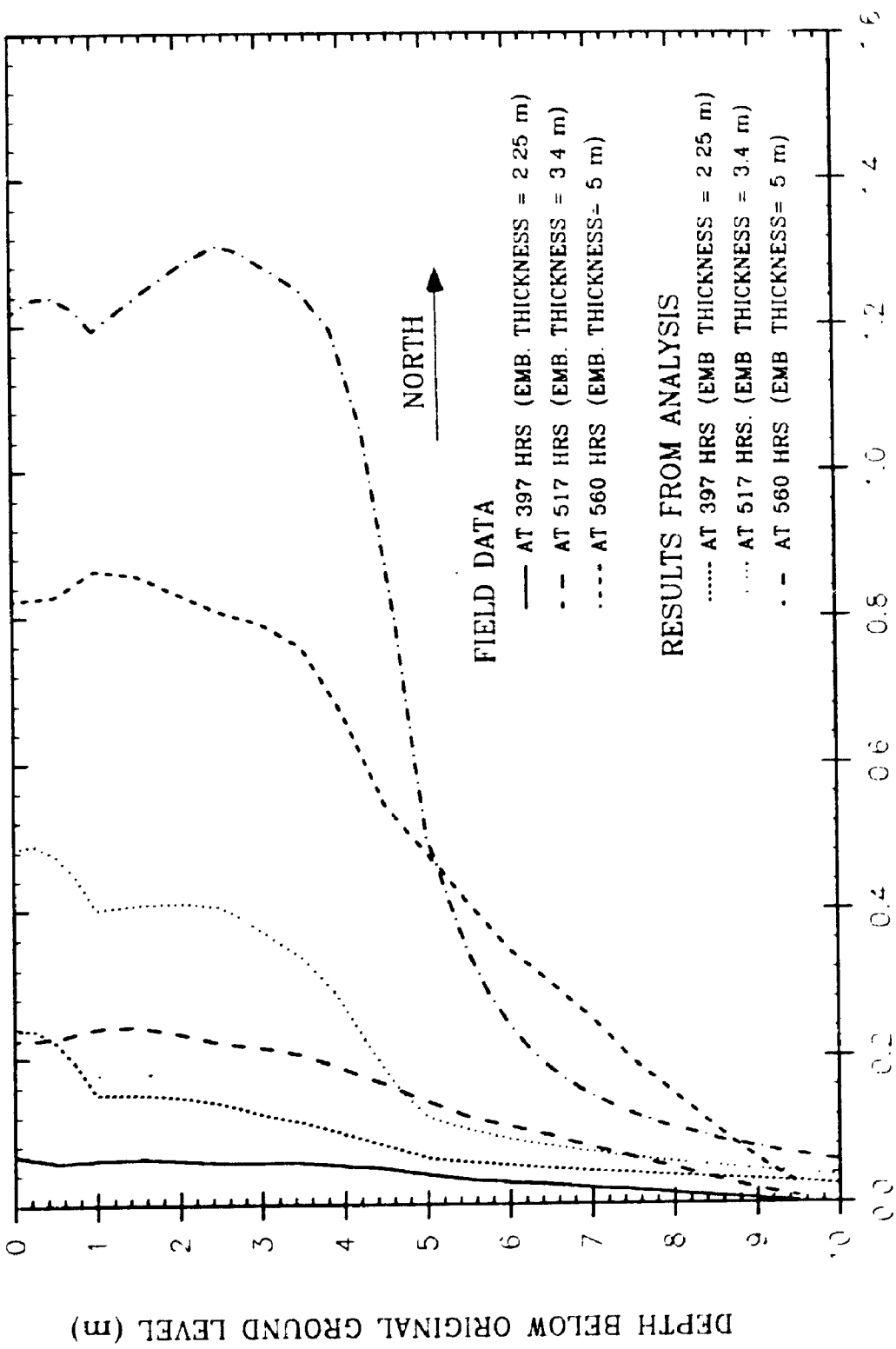

FIG. 8.25 VARIATION OF HORIZONTAL DISPLACEMENT WITH DEPTH AT DIFFERENT THICKNESSES FOR INCLINOMETER 501 – COMPARISON BETWEEN FIELD DATA AND F E A RESULTS

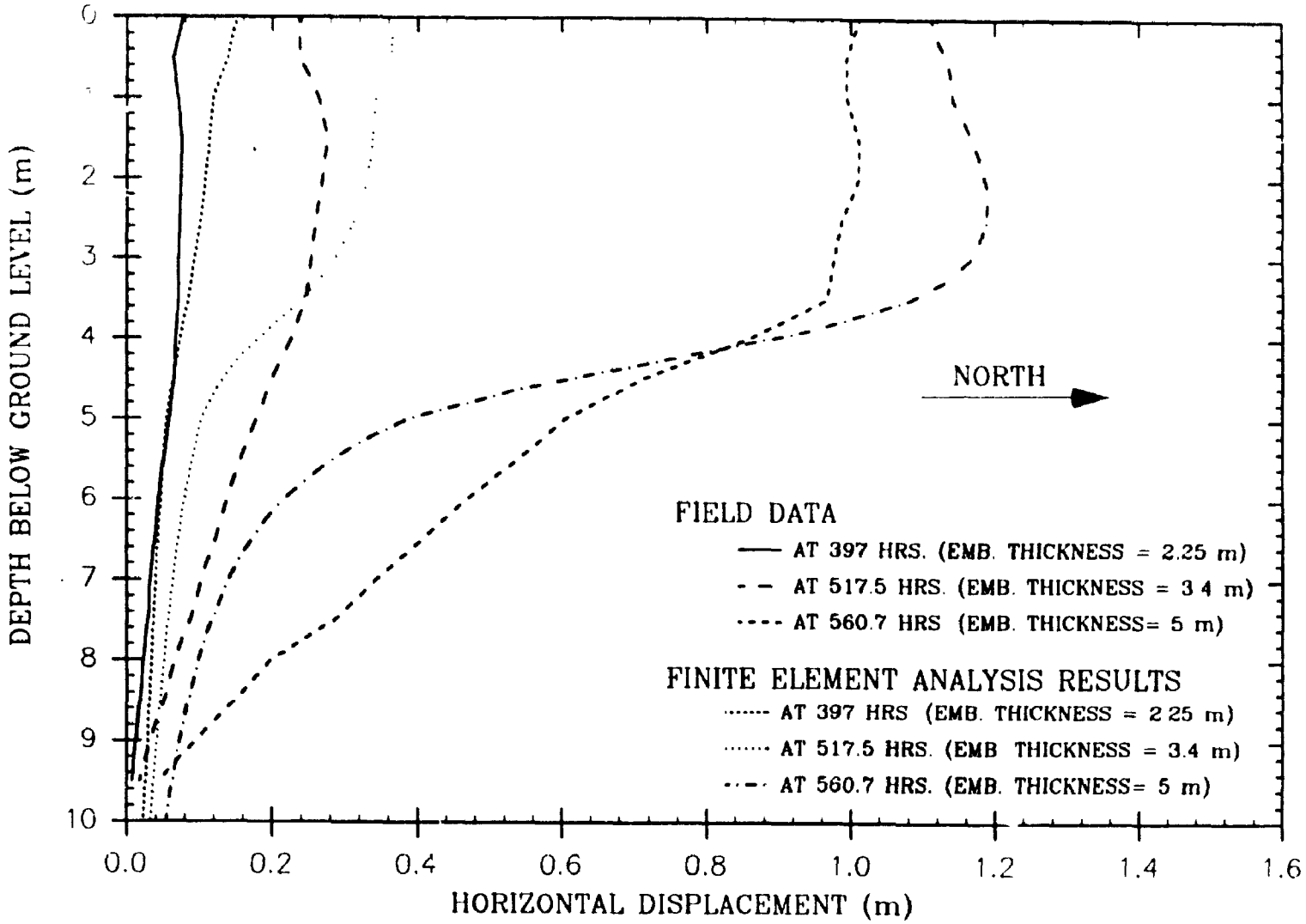

FIG. 8.26 VARIATION OF HORIZONTAL DISPLACEMENT WITH DEPTH AT DIFFERENT THICKNESSES FOR INCLINOMETER 511 – COMPARISON BETWEEN FIELD DATA AND F.E.A. RESULTS

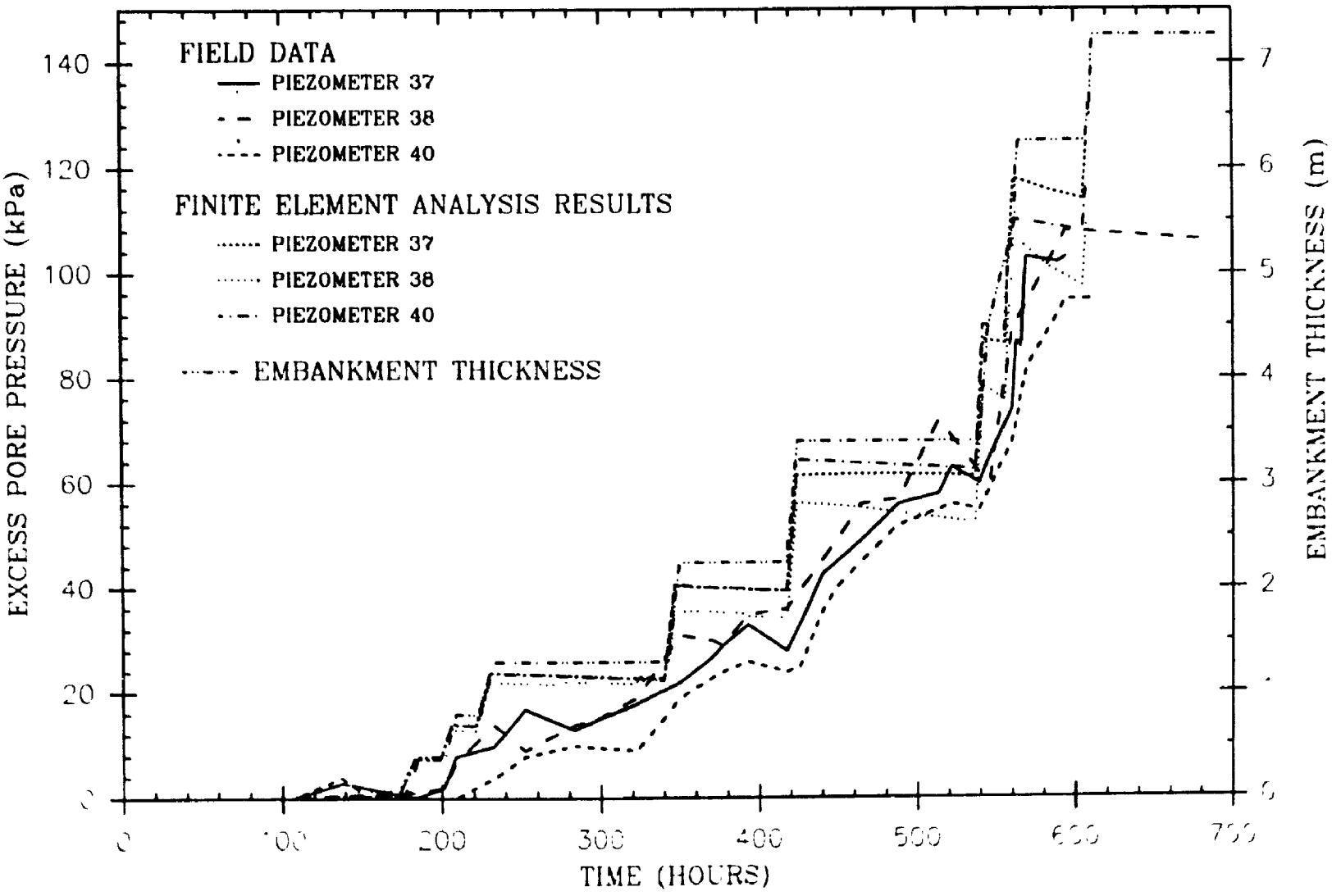

FIG 8.27 VARIATION OF EXCESS PORE PRESSURE WITH TIME FOR PIEZOMETERS 37, 38 AND 40 – COMPARISON BETWEEN FIELD DATA AND F E A RESULTS

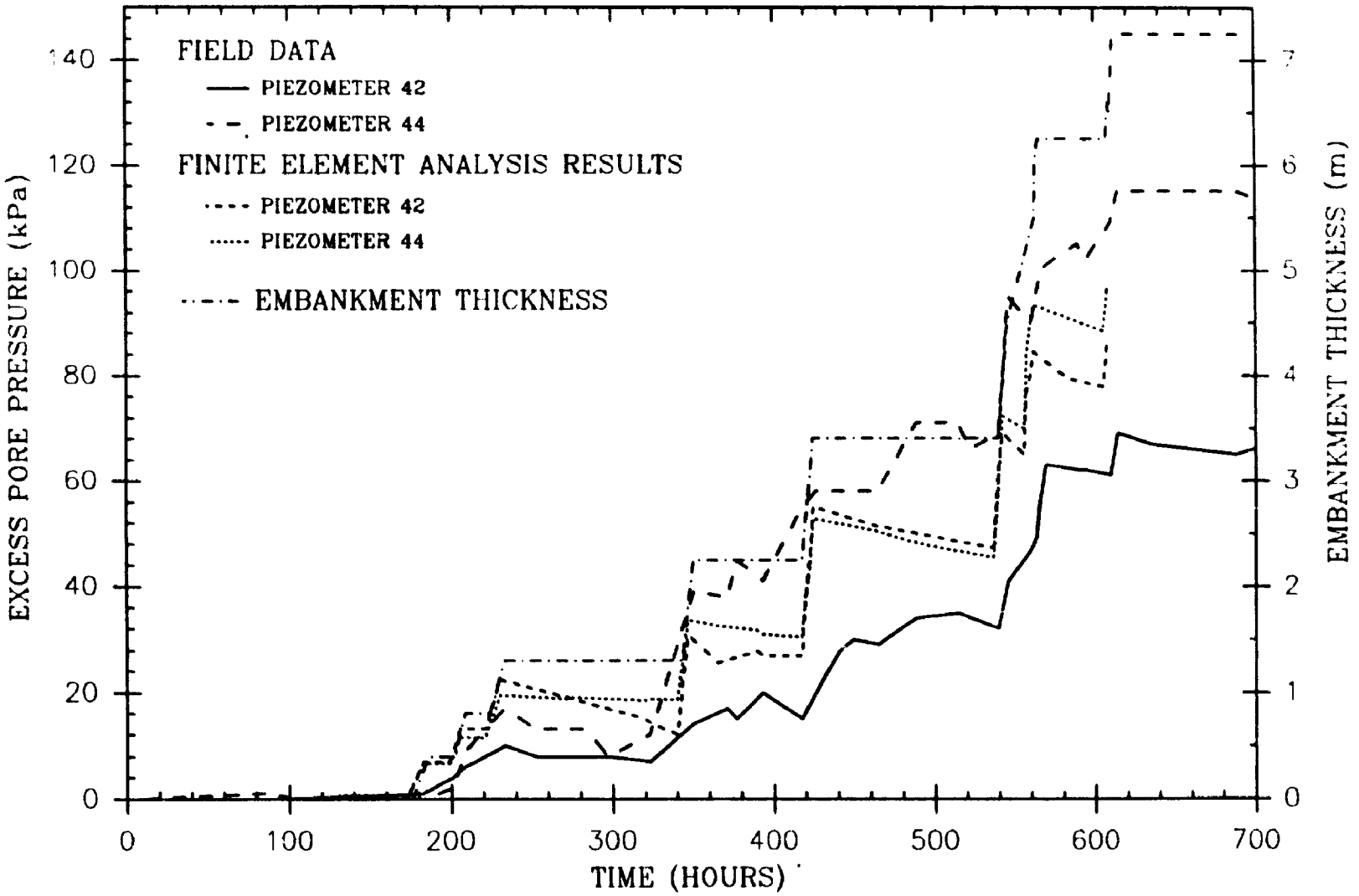

FIG. 8.28 VARIATION OF EXCESS PORE PRESSURE WITH TIME FOR PIEZOMETERS 42 AND 44 – COMPARISON BETWEEN FIELD DATA AND F.E.A. RESULTS

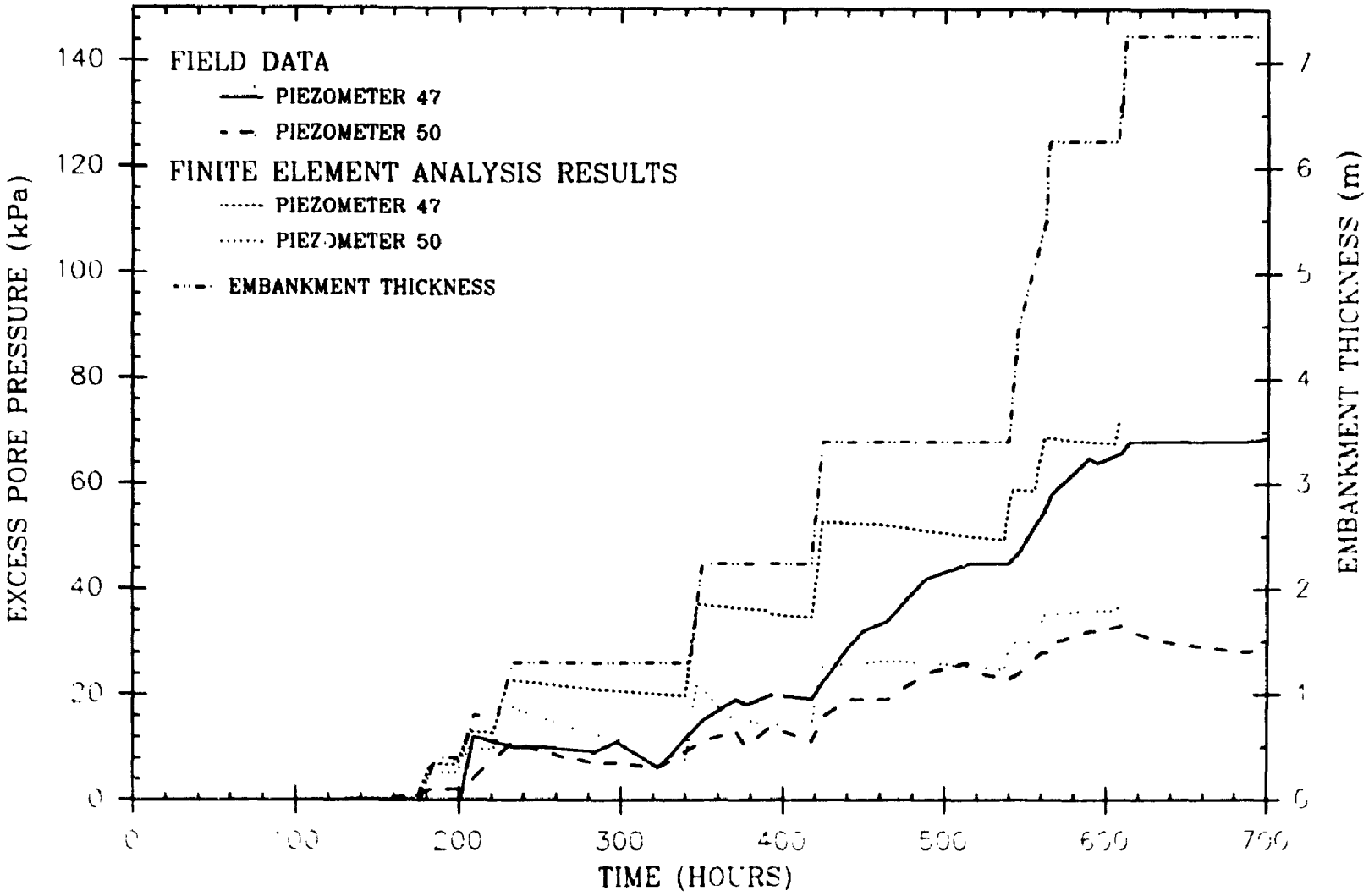

FIG 8.29 VARIATION OF EXCESS PORE PRESSURE WITH TIME FOR PIEZOMETERS 47 AND 50 – COMPARISON BETWEEN FIELD DATA AND F E A RESULTS

being dependent on whether the soil is normally consolidated or overconsolidated, would therefore be under estimated due to the lower OCR values currently used. This is apparently the cause for the under estimation of hydraulic conductivity at low embankment thickness discussed earlier.

8.3.4 Summary and conclusions

The results of the fully coupled large strain elasto-plastic consolidation finite element analysis of the unreinforced embankment have been compared with the field measurements. The possible three dimensional effects due to the construction of the reinforced embankment until failure (prior to the unreinforced embankment) and the variation of soil properties over short distances within the site were discussed previously. Consequent to this shortcoming and the use of the same soil parameters used previously for the analysis of the reinforced embankment (due to the constraint of insufficient data regarding the parameters of the soil beneath the unreinforced embankment), only qualitative comparisons were made between the calculated and observed responses.

The calculated settlement, heave and horizontal displacement responses showed similar pattern of variation as observed in the field but were overpredicted. However, the horizontal displacements were underpredicted in the analysis at large depth apparently due to anisotropy of the soil and the limitation of the Modified Cam-Clay to model this.

The calculated excess pore pressures were higher than the measured values at low embankment thicknesses up to about 3.4 m apparently due to incomplete saturation of the soil and under estimation of hydraulic conductivity of the soil. However, the general pattern of excess pore pressure variations with time agreed reasonably well with the measured responses for thicknesses greater than 3.4 m.

In summary, the calculated pattern of variations of vertical and horizontal displacements and the excess pore pressures in the foundation soil agreed reasonably well with those indicated from field measurements. This general agreement on the pattern of observed and calculated responses suggest that the large strain elasto-plastic Biot consolidation finite element model adopted here may also be used for the analysis of unreinforced embankments on soft soils.

CHAPTER 9

SENSITIVITY STUDY ON THE BEHAVIOUR OF REINFORCED EMBANKMENT

9.1 INTRODUCTION

One of the advantages of the finite element analysis is that it readily and inexpensively allows consideration of the effects of changing the soil parameters. The comparison between the calculated and observed performance of the reinforced embankment described in chapter 8 provides some confidence in the analysis and the selection of soil parameters. However, the effect of changing various parameters on the deformation and the excess pore pressure in the foundation soil as well as the geotextile strains are examined in this chapter. In particular, the effects of over consolidation ratio (OCR), effective friction angle (ϕ'), coefficient of earth pressure at rest (K_o), Poisson's ratio and the permeability of the foundation soil and the effective friction angle of the embankment fill (i.e. the ϕ' of the sandy fill used below and above the geotextile) are examined.

As discussed in chapter 2, it has been found in previous investigations (such as for example Rowe and Soderman, 1984) that an elasto-plastic soil model with a Mohr-Coulomb failure criterion is suitable for the analysis and successful prediction of the behaviour of reinforced embankments on soft soils. To examine how the prediction would be for the reinforced test embankment constructed at Sackville, New Brunswick, a small strain undrained (i.e. $\phi = 0$) finite element analysis was performed using this model. A mean undrained shear strength profile between the results from field vane, CAU triaxial and constant volume DSS tests was used for this analysis. The results of this analysis is

presented in this chapter. The effect of changing the undrained shear strength profile for the foundation soil and the use of a large strain finite element analysis using this model on the predicted performance of the reinforced embankment are also examined in this chapter.

9.2 UNDRAINED FINITE ELEMENT ANALYSES

9.2.1 The effect of changing the undrained shear strength profile

A small strain undrained finite element analysis was performed using an elasto-plastic soil model with a Mohr-Coulomb failure criterion. A mean undrained shear strength profile (referred to as Run 1 hereafter and in all the figures) between the results from field vane, CAU triaxial and constant volume DSS tests (referred to as mean strength hereafter) was used for this analysis. To study the effect of changing the undrained shear strength profile of the foundation soil on the behaviour of the reinforced embankment, an additional small strain undrained finite element analysis was performed. The undrained shear strength profile obtained from the cone tests (i.e the average undrained shear strength inferred from the cone tests at TM2, TM3 and TM4 as discussed in chapter 6 - hereafter referred to as cone strength profile) was adopted for this analysis (i.e. run2). The undrained shear strength profiles used for the two different analyses (i.e. Run 1 and Run 2) are shown in Fig. 9.1. All other properties of the foundation soil used were the same for both these analyses and are summarized in Table 9.1. The saturated unit weights given in this table were measured in the lab and the Young's modulus and K_0 values were obtained from the self boring pressure meter test results of NRC (courtesy Dr. K.T. Law). The Poisson's ratio of the soil was assumed to be 0.48 for all the undrained analyses. The properties of the embankment fill, geotextile reinforcement and the geotextile-fill interface were the same as those used for the consolidation analysis reported in chapter 8.

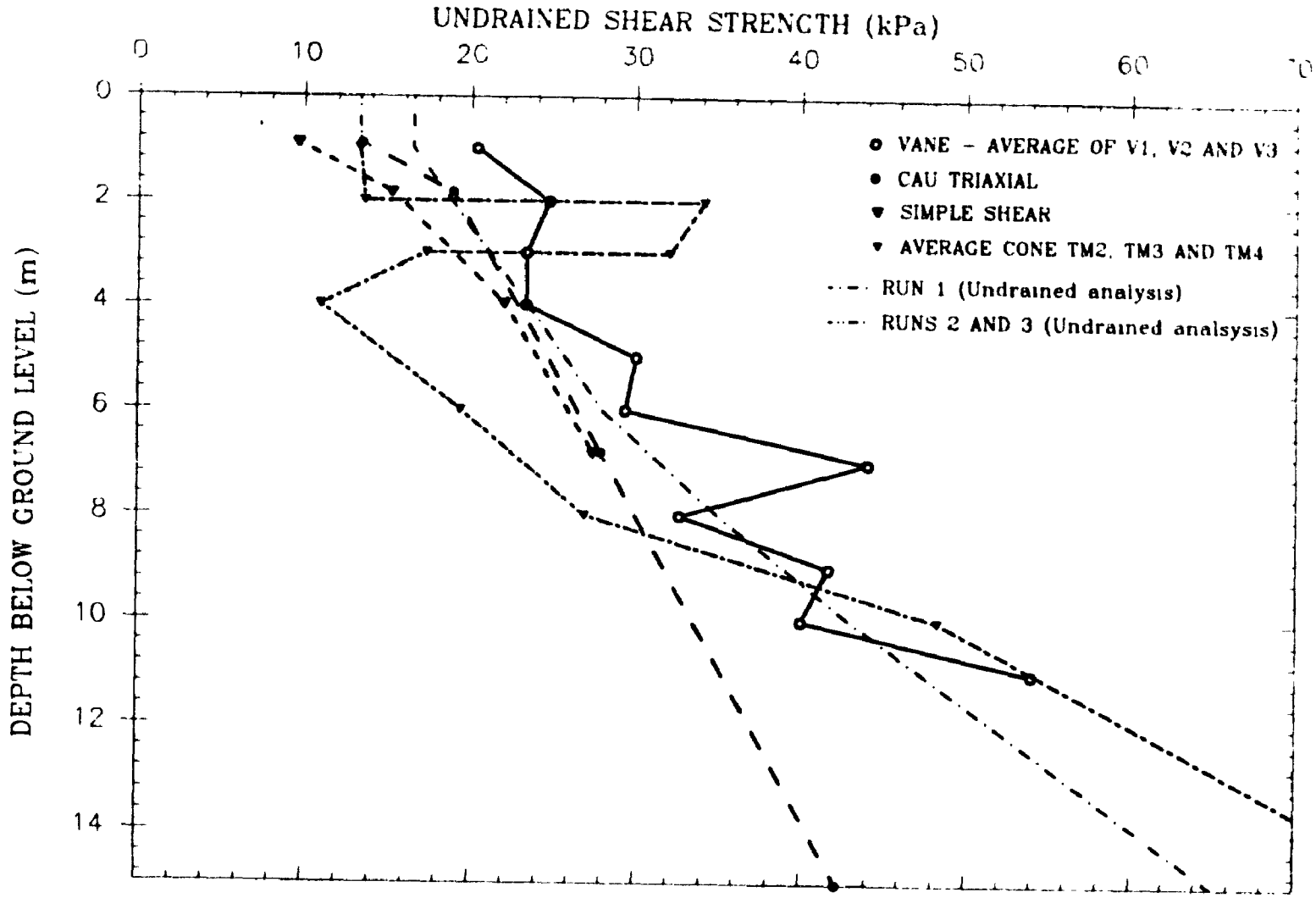

FIG. 9.1 VARIATION OF UNDRAINED SHEAR STRENGTH WITH DEPTH - DATA USED FOR UNDRAINED ANALYSIS

Table 9.1 Foundation soil parameters used for undrained analysis

Depth (m)	γ (kN/m^3)	E (kPa)	EGRAD (kPa/m)	K_o
0 - 1	15.2	2085	0	0.68
1 - 2.5	17.8	2085	1543	0.68
2.5 - 3.5	17.8	4400	1380	0.71
3.5 - 5	16.0	5780	1380	0.77
5 - 6	17.0	7850	1380	0.79
6 - 7	17.0	9230	1380	0.81
7 - 8	17.0	10610	2100	0.82
8 - 10	17.0	12710	2400	0.84
10 - 14	17.0	17510	3300	0.88

E = Young's modulus at the surface of the layer
EGRAD = Rate of increase of Young's modulus with depth

However, to examine the effect of using a large strain finite element formulation instead of the small strain approach, a large strain undrained finite element analysis (referred to as Run 3) was also performed with the same undrained shear strength profile (i.e. the same data as in Run 2 above) for the foundation soil. All other properties of the foundation soil and the properties of the geotextile, embankment fill and the interface between the geotextile and embankment fill adopted for this analysis were the same as in Run 2. The details regarding the finite element mesh and the models used for the soil, geotextile reinforcement and the reinforcement-fill interface were described in chapter 7.

The variation of net embankment height (= embankment thickness - settlement) with embankment thickness is shown in Fig. 9.2 for all the three cases discussed above. The net embankment height reached a maximum value of about 5 m at location 7S (for the corresponding embankment thickness of 6.2 m) in Run 2 compared to about 7.6 m at both locations 7S and 8S (for the corresponding embankment thickness of 8.8 m) in Run 1. These maximum values indicate a plastic type failure, the type predicted for reinforced embankments on soft soils by Rowe and Soderman (1987). For the purpose of easy comparison, the corresponding data obtained from the field investigation in also shown in Fig. 9.2. The construction of the embankment was stopped for brief periods at 8.2 and 9.5 m thicknesses in the field and a clear maximum for the net embankment height similar to those obtained in the small strain undrained analyses is not apparent However, the failure thickness of the reinforced embankment was interpreted as 8.75 m (see discussion in chapter 4) and the corresponding maximum net embankment height (inferred by constructing a smooth curve for the field response) is about 7.4 m. It can be observed that during the brief construction stoppages, considerable deformation continued to occur as is evident from the net embankment height vs. thickness response. This is due to the time dependent viscous effects in the foundation soil and undrained creep, as discussed previously in chapter 8. However, the failure thickness of 8.8 m predicted in Run 1 using

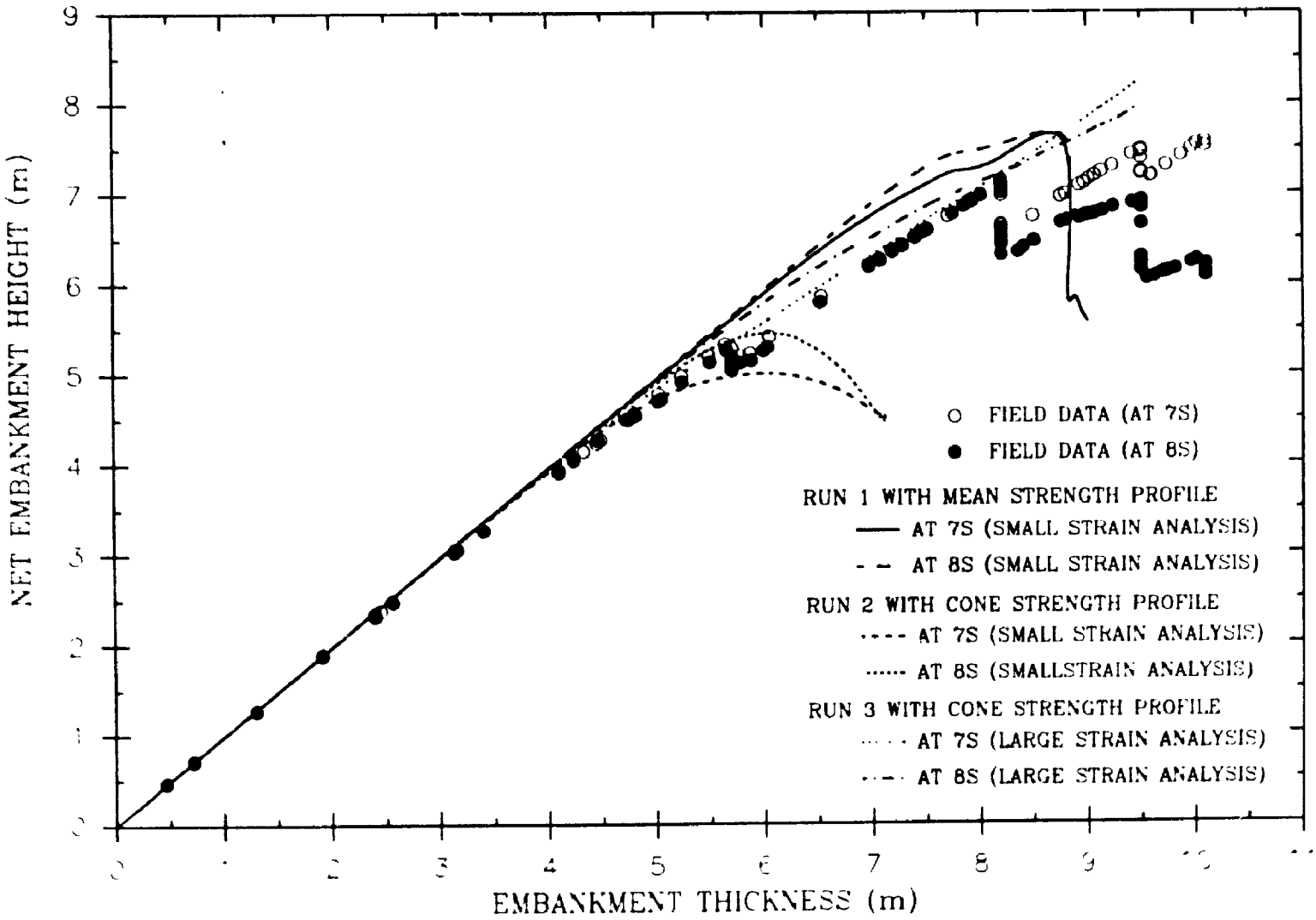

FIG 9.2 VARIATION OF NET EMBANKMENT HEIGHT WITH EMBANKMENT THICKNESS AT LOCATIONS 7S AND 8S – UNDRAINED FINITE ELEMENT ANALYSIS RESULTS

a mean shear strength profile for the foundation soil agrees well with the observed failure thickness of 8.75 m in the field. This close prediction of the failure thickness suggest that the small strain undrained finite element analysis can be used successfully to predict the failure thickness of the reinforced embankments on such soft soil.

The large strain analysis conducted in Run 3 with the similar data as Run 2 predicted the net embankment height well, indicating better agreement than that obtained in the small strain analysis with the mean strength profile, until about 8.2 m thickness. However, it did not indicate (the plastic type of) failure of the embankment when it was constructed up to 9.5 m thickness (i.e. the failure thickness > 9.5 m). Fig. 9.2 further indicates that the net embankment height response is essentially elastic up to about 3 m embankment thickness in Run 2 compared to about 4 m thickness in Run 1 and 3.4 m thickness in Run 3. Comparing the calculated responses with the field response, it is evident that the elastic response is well predicted in both runs 1 and 3.

The horizontal displacements in the foundation soil at the toe of the embankment at different embankment thicknesses obtained from the three undrained finite element analyses discussed above are shown in Figures 9.3 and 9.4. The horizontal displacements indicated in all the three analyses were small (typically less than 0.1 m) until about 3.4 m thickness. Significantly increased horizontal displacements were obtained at 5 m embankment thickness in both runs 2 and 3. However, Run 1 indicated a relatively small horizontal displacement (a maximum of about 0.12 m) even at 5.7 m thickness (see Fig. 9.4). In contrast, a maximum horizontal displacement of about 1.8 m was observed at this location in the field at 5.4 m thickness (see chapter 4).

The horizontal displacements evaluated in runs 2 and 3 were nearly the same at 5 m thickness. Run 2 indicated large increase in horizontal displacement during the

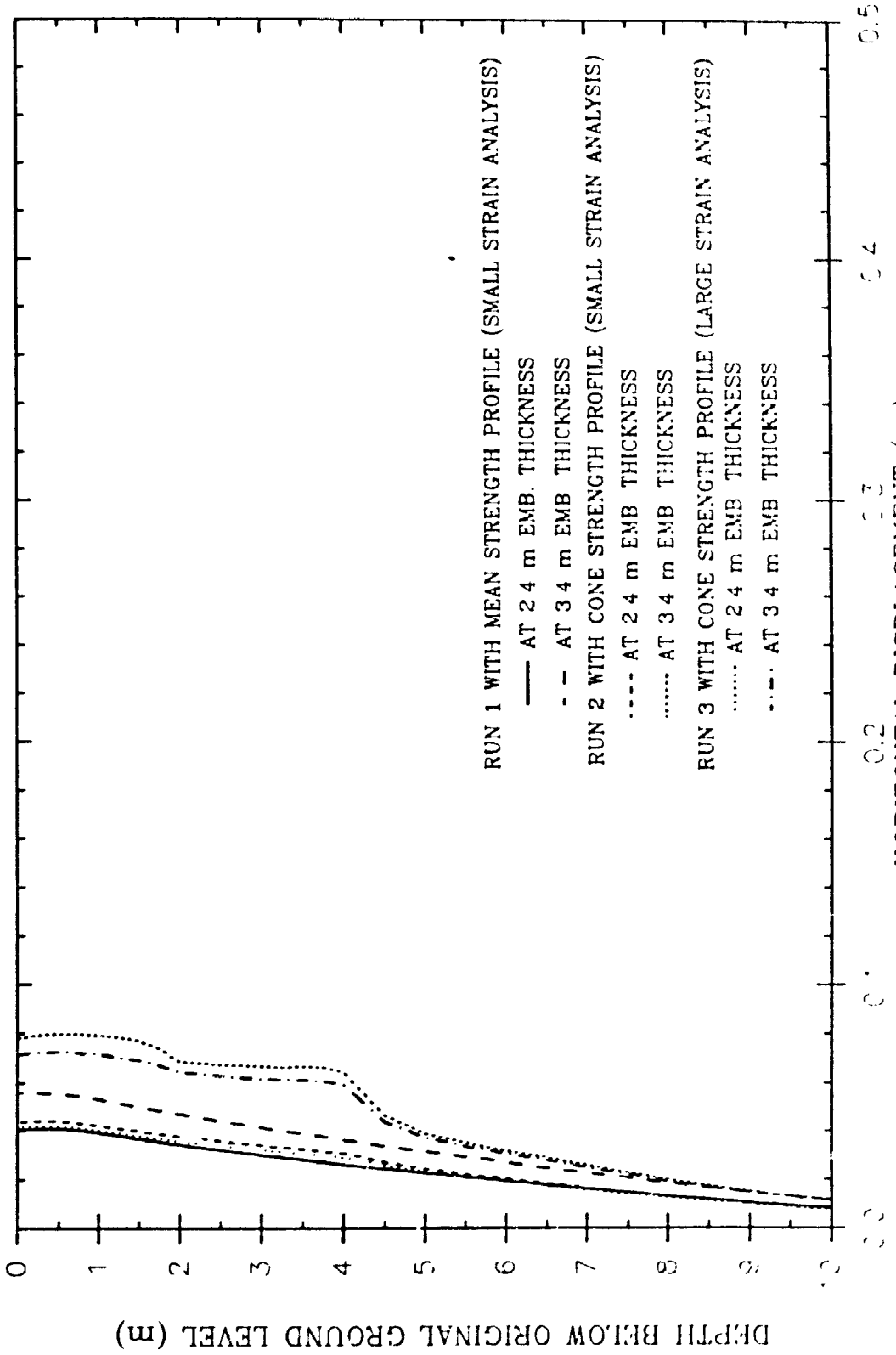

FIG. 9.3 VARIATION OF HORIZONTAL DISP WITH DEPTH AT LOCATON 221 – UNDRAINED FINITE ELEMENT ANALYSIS RESULTS

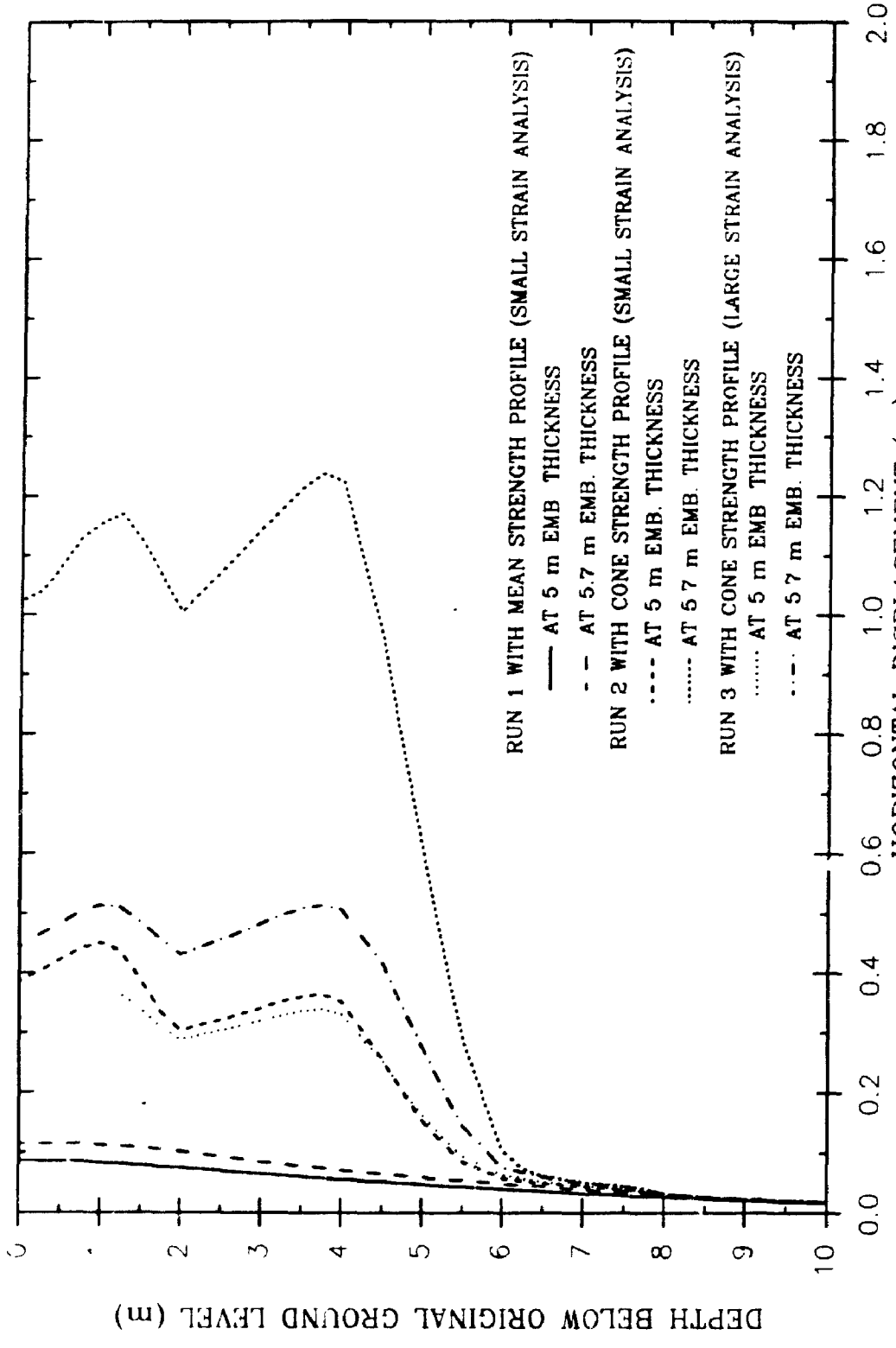

FIG. 9.4 VARIATION OF HORIZONTAL DISP. WITH DEPTH AT LOCATON 22I
– UNDRAINED FINITE ELEMENT ANALYSIS RESULTS

construction of the embankment from 5 to 5.7 m thickness (the maximum horizontal displacement increased from 0.45 to 1.25 m) due to increased growth of plasticity in the foundation soil. A marginal increase in the horizontal displacement was indicated in Run 3 (i.e. the maximum horizontal displacement increased from 0.37 to 0.52 m). Since the same parameters were used in both runs 2 and 3, they showed similar pattern of horizontal displacement variation with depth. The large strain analysis (i.e. Run 3) indicated much lower horizontal displacement than that observed in the field (see chapter 4 for the field response). The magnitude of the maximum horizontal displacement indicated at 5.7 m thickness in Run 2 was also significantly lower but somewhat comparable to that observed in the field (e.g. a maximum horizontal displacement of about 1.8 m was observed in the field at 5.4 m thickness).

The strain distribution across the entire width of the geotextile reinforcement evaluated at different embankment thicknesses are shown in Figs. 9.5 and 9.6. The geotextile strain indicated in all three analyses were small (maximum values less than 0.65%) at 3.4 m embankment thickness. The maximum strains were obtained between about 4 and 6 m from the toe of the embankment. The field observations also indicated similar maximum values (typically less than about 0.72% up to 3.4 m thickness) for the geotextile strain but the peak strains occurred between 17 and 19 m from the toe. Large difference in the geotextile strains between the three analyses were indicated at 5.7 m thickness. At this thickness, Run 1 indicated a maximum geotextile strain of only about 1% (at about 7.9 m from the toe). Run 2 indicated a maximum geotextile strain of about 5.2% whereas the large strain analysis with the same material properties indicated a maximum strain of about 3% at 5.7 m thickness. Both these analyses (i.e. runs 2 and 3) indicated that the maximum strain would occur between 10 and 14 m from the toe. In contrast, a maximum strain of about 4.5% was observed in the field which occurred between 12 and 15 m from the toe. The small strain undrained analysis with the mean

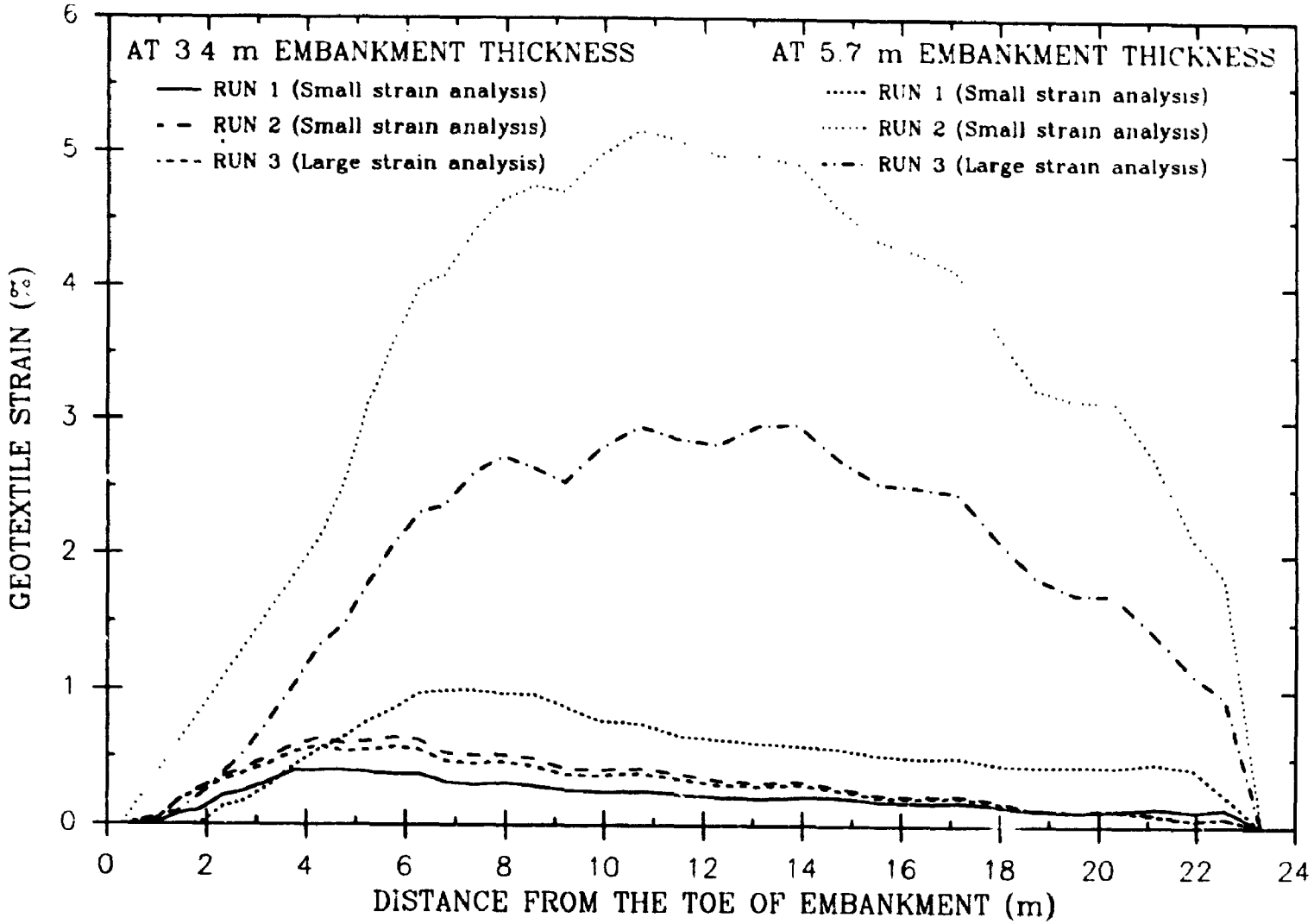

FIG. 9.5 GEOTEXTILE STRAIN DISTRIBUTION AT EMBANKMENT AT 3.4 AND 5.7 m THICKNESSES – UNDRAINED FINITE ELEMENT ANALYSIS RESULTS

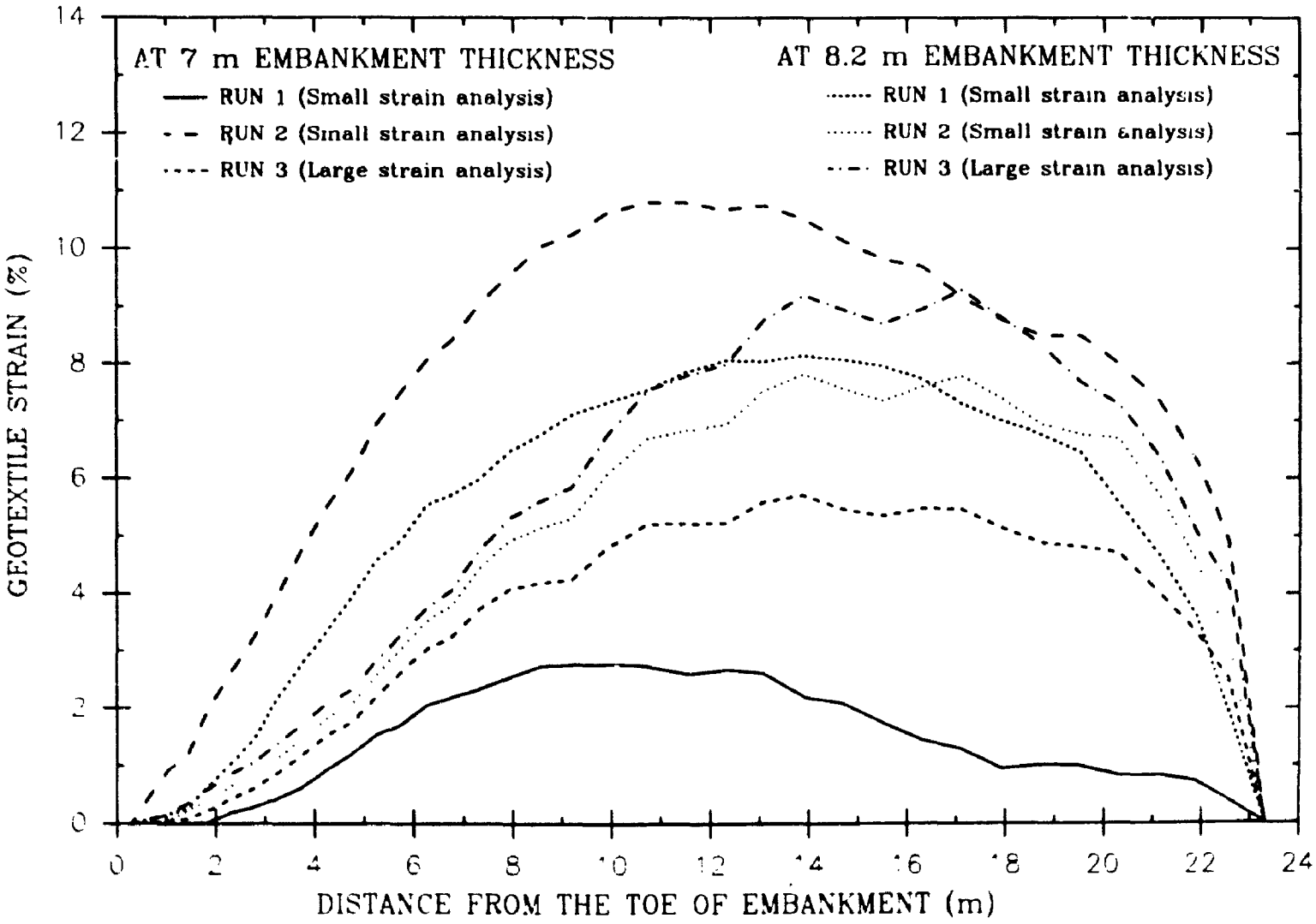

FIG 9.6 GEOTEXTILE STRAIN DISTRIBUTION AT DIFFERENT EMBANKMENT THICKNESSES – UNDRAINED FINITE ELEMENT ANALYSIS RESULTS

strength profile significantly underpredicts the geotextile strain at 5.7 m thickness. However, a similar analysis with the cone strength profile gave a reasonable prediction of the geotextile strain.

All the three analyses indicated the occurrence of maximum geotextile strain between about 10 and 14 m from the toe when the thickness was increased to 7 m (see Fig. 9.6). Large increase in the geotextile strain was indicated in Run 2 during the construction of the embankment from 5.7 to 7 m thickness. The maximum force in the geotextile reached the allowable limit (of 216 kN/m) at 7.12 m thickness in this run (i.e. at about 13.1 m from the toe). The embankment could not be numerically constructed further after unloading the geotextile force at the location of breakage. However, the embankment indicated a plastic type failure well before that at 6.2 m thickness as discussed previously.

The large strain analysis with the cone strength profile (Run 3) indicated a maximum strain of about 5.7% at 7 m thickness which agrees reasonably well with the maximum strain of 6% indicated in the field. The small strain analysis with the mean strength profile (Run 1) underpredicted the geotextile strain at 7 m thickness also (i.e. the maximum strain indicated in the analysis was 2.8% compared to the 6% observed in the field). However, the strains indicated at 8.2 m thickness in runs 1 and 3 (i.e. the maximum strains of 8.2 and 7.8% respectively which occurred at 13.9 m from the toe in both runs) agreed reasonably well with the maximum strain of 8.6% (which occurred between 12 and 15 m from the toe) observed in the field. In the field investigation, the geotextile strain increased significantly during the brief period of stoppage of construction at 8.2 m thickness (as discussed previously in chapter 5) but was not modelled in these undrained analyses.

Run 1 indicated a large increase in the geotextile force during the construction

after 8.2 m thickness and the maximum force reached the allowable limit (of 216 kN/m) at 8.8 m thickness. The embankment also failed at 8.8 m thickness, subsequent to the breakage of the reinforcement (which occurred at 13.9 m from the toe). Run 3 indicated a maximum geotextile strain of about 9.3% (at about 14 m from the toe) at 9.5 m thickness and had not indicated either the failure of the embankment or the breakage (or snap) of the geotextile, at least up to 9.5 m thickness.

9.2.2 Summary and discussion

The results of both small strain and large strain undrained finite element analyses performed for the reinforced test embankment constructed at Sackville, New Brunswick using an elasto-plastic soil model with a Mohr-Coulomb failure criterion have been examined. The results of these analyses indicate that the settlement and lateral deformation responses of the foundation soil and the geotextile strain responses are highly dependent on the shear strength profile of the foundation soil. The small strain analysis (Run 1) with the mean undrained strength profile (between the field vane and the CAU triaxial and constant volume DSS tests in the lab) predicted the failure of the embankment quite accurately. However, the predicted horizontal deformations from this analysis were very small, at least until 5.7 m thickness. There was significant difference between the calculated net embankment heights and those indicated from field measurements when the embankment thickness was greater than 5.7 m due to the under prediction of settlements in the analysis. For the type of foundation soil under investigation and the construction sequence adopted in the field, the effects of consolidation would be important and are also expected to be part of the cause for the discrepancies between the calculated and measured settlements.

The small strain analysis with the mean undrained shear strength profile inferred

from the cone tests at TM2, TM3 and TM4 (i.e. Run 2) underpredicted the failure thickness. However, when the same strength profile was used with a large strain analysis, the embankment did not indicate failure (at least up to 9.5 m thickness). The predicted horizontal deformations from the small strain analysis with the cone strength profile (i.e. Run 2) were quite comparable to those observed in the field. However, the predicted lateral deformations from the large strain analysis, for the same strength profile, were lower than those observed in the field, particularly near the ground surface (see chapter 4 for the field responses).

All the three undrained analyses predicted the magnitude of the maximum geotextile strains quite accurately up to about 3.4 m thickness (i.e. during the elastic behaviour of the foundation soil). However, the maximum strains were indicated between 4 and 6 m from the toe of the embankment in these analyses whereas in the field they occurred between 17 and 19 m from the toe. All the three undrained analyses indicated the occurrence of maximum strain in the geotextile between 10 and 14 m from the toe of the embankment for thicknesses greater than 5.7 m which agreed well with field observations where it occurred between 12 and 15 m from the toe.

The small strain analysis with the cone strength profile gave reasonable predictions of the geotextile strain up to 5.7 m thickness but indicated larger strains afterwards. This analysis indicated a plastic type of failure of the embankment at 6.2 m thickness as discussed previously. The large strain analysis with the cone strength profile underpredicted the geotextile strains at 5.7 m thickness but gave reasonable predictions afterwards up to about 8.2 m thickness. However, neither breakage of the reinforcement nor the failure of the embankment was indicated in this analysis at least up to 9.5 m thickness.

The small strain analysis with the mean strength profile underpredicted the geotextile strains significantly for thicknesses above 3.4 m and up to about 7 m thickness but gave a reasonable prediction at 8.2 m thickness. Large increase in the geotextile force was indicated in this analysis during the construction after 8.2 m thickness and the embankment failed at 8.8 m thickness subsequent to the breakage of the reinforcement. In the field investigation, large increases in the geotextile strain were observed during the brief periods of construction stoppage at 5.7 and 8.2 m thicknesses. As discussed in chapter 5, the geotextile either tore or yielded at 8.2 m thickness (i.e. at about 498 hours) between 11.8 and 12.6 m from the toe of embankment.

As discussed in chapters 3 and 4, vertical cuts were made on the ground up to a depth of about 1 to 1.2 m (on an approximately 1.3 to 1.8 m square grid on plan) to minimize the effect of the root mat on the amount of fill required to construct the embankment to failure (i.e. due to budgetary constraints). These cuts would result in a complex behaviour of the foundation soil near the ground surface and modelling them explicitly is beyond the scope of this thesis. However, to consider the effects of these cuts in an approximate manner, the shear strength of the soil between 0 and 1 m depth was assumed to be constant and equal to the shear strength evaluated at 1 m depth. The discrepancies between the calculated geotextile strains discussed above, particularly during the early stages of construction up to about 5.7 m thickness, could be mainly due to the effect of these cuts. The effects of consolidation, which were not modelled in these undrained analyses, also could be a contributory factor for the discrepancies between the measured geotextile strains.

The effects of the vertical cuts and the significance of consolidation could be contributory factors for the discrepancies between the calculated and measured horizontal deformations. However, the comparatively much smaller horizontal deformations

indicated in the analysis with the mean strength profile suggest that there could be additional factors need to be considered in order to get good agreement between the calculated and measured horizontal displacements. Extensive research into the behaviour of unreinforced embankments on soft clays during the past two decades has indicated that it is important to consider the change of state of these soft foundation soils from an overconsolidated to a normally consolidated state (e.g. Leroueil et al. 1978b). This cannot be considered in the Mohr-Coulomb material model used in these undrained analyses but was considered in the large strain coupled consolidation analysis using Modified Cam-clay material behaviour reported previously in chapter 8. However, the computing cost for an undrained analysis was significantly lower than the effective stress (consolidation) analysis reported in chapter 8.

In the final assessment, the small strain undrained analysis with the mean strength profile (between the field vane and the laboratory tests) was the one which gave overall better results (among the three undrained analyses reported here). It accurately predicted the failure of the embankment but underpredicted the settlement after 5.7 m thickness. The horizontal deformations and geotextile strains were under predicted up to at least 5.7 m.

9.2.3 Conclusions of undrained analyses

The undrained analyses performed for the reinforced embankment constructed at Sackville, New Brunswick with different undrained shear strength profiles suggest that the mean shear strength profile (between the field vane and the CAU triaxial and constant volume DSS tests in the lab) was appropriate for the prediction of failure of this embankment. However, this small strain analysis under predicted the settlements, especially after about 5.7 m thickness. The predicted horizontal deformations and the

geotextile strains were lower than those measured in the field. Despite the difficulties caused by the vertical cuts made on the soil near the ground surface, it appears that the undrained model used here cannot predict these vertical and horizontal deformations and geotextile strains concurrently unless provisions are made to account for the effects such as consolidation and change of state from over consolidated to normally consolidated behaviour of the soil. These effects were considered in the effective stress (coupled Biot consolidation) analysis with Modified Cam-clay material behaviour reported in chapter 8.

9.3 SENSITIVITY STUDY USING CONSOLIDATION ANALYSIS

9.3.1 General

To investigate the effect of different assumptions regarding the various soil parameters, three series of fully coupled large strain Biot consolidation finite element analyses were performed. In these consolidation analyses, the foundation soil was modelled as a consolidation elasto-plastic Modified Cam-clay material. The properties of the foundation soil used for the first analysis (hereafter referred as Case 1) are shown in Table 9.2. These properties were selected on the basis of laboratory test results reported in chapter 6 (e.g. ϕ' from the CAU triaxial tests which was used to evaluate the value of M using the relationship, $M = \frac{6 \sin\phi'}{3 - \sin\phi'}$ and λ from the consolidation test results using the relationship, $\lambda = C_c/2.303$) and the insitu test results (e.g. K_o values from the self boring pressure meter tests conducted by NRC, courtesy Dr. K.T. Law). The embankment fill was modelled as an elasto-plastic material with Mohr-Coulomb failure criterion. The properties of the fill material used in the analyses were the same as reported in chapter 8. The details regarding the finite element mesh and the models used for the soil, geotextile reinforcement and the reinforcement-fill interface were described in chapter 7. The properties of the geotextile reinforcement and the geotextile-fill interface were also the

Table 9.2 Foundation soil parameters used for the analysis - Case 1.

Depth (m)	γ (kN/m^3)	M	κ	λ	e_{cs}	ν	K_o	OCR
0 - 1	15.2	1.12	0.055	0.242	2.21	0.33	0.68	5.6
1 - 2.5	17.8	1.12	0.021	0.111	1.30	0.33	0.68	3.6
2.5 - 3.5	17.8	1.12	0.023	0.122	1.37	0.33	0.71	1.2
3.5 - 5	16.0	1.12	0.024	0.133	1.45	0.33	0.77	1.2
5 - 6	17.0	1.12	0.026	0.143	1.52	0.33	0.79	1.2
6 - 7	17.0	1.12	0.027	0.154	1.59	0.33	0.81	1.2
7 - 8	17.0	1.12	0.027	0.154	1.59	0.33	0.82	1.2
8 - 10	17.0	1.12	0.027	0.154	1.59	0.33	0.84	1.2
10 - 14	17.0	1.12	0.027	0.154	1.59	0.33	0.88	1.2

same as used in chapter 8.

The permeability of the foundation soil was allowed to vary with the void ratio according to either eqn. 7.4 or eqn. 7.5 (see chapter 7) depending on whether the soil is at overconsolidated or normally consolidated state. The constants of the two equations used were determined from the results of the two consolidation tests performed on the samples from 1.83 and 6.81 m depths. These equations were fitted to the consolidation test results (see Fig. 9.7) in order to evaluate the constants. The values of these constants (for the permeabilities to be evaluated in m/day) used for the various layers of the foundation soil are summarized in Table 9.3. The permeability test results indicated that the ratio of the horizontal permeability to the vertical permeability (i.e. k_x/k_y) range between about 2.5 and 9 (see Table 6.5). A value of 4 was selected for the permeability ratio in Case 1.

The results of the first analysis (i.e. Case 1) is discussed in the following sections with due comparison with the results obtained from the analyses performed with the variations of different soil parameters. The analyses reported in the following sections consider the construction of the embankment only up to 5.7 m thickness since it was at this point that the embankment began to show signs of distress and, for practical purposes, one would not normally wish to add fill beyond this point. In all the analyses reported, the embankment was numerically constructed according to the actual sequence adopted in the field for the construction of the reinforced test embankment at Sackville, New Brunswick (i.e. up to 5.7 m thickness).

9.3.2 Series 1: The effects of changing the OCR and the Poisson's ratio of the foundation soil

In this series of analyses the effects of changing the OCR is investigated first

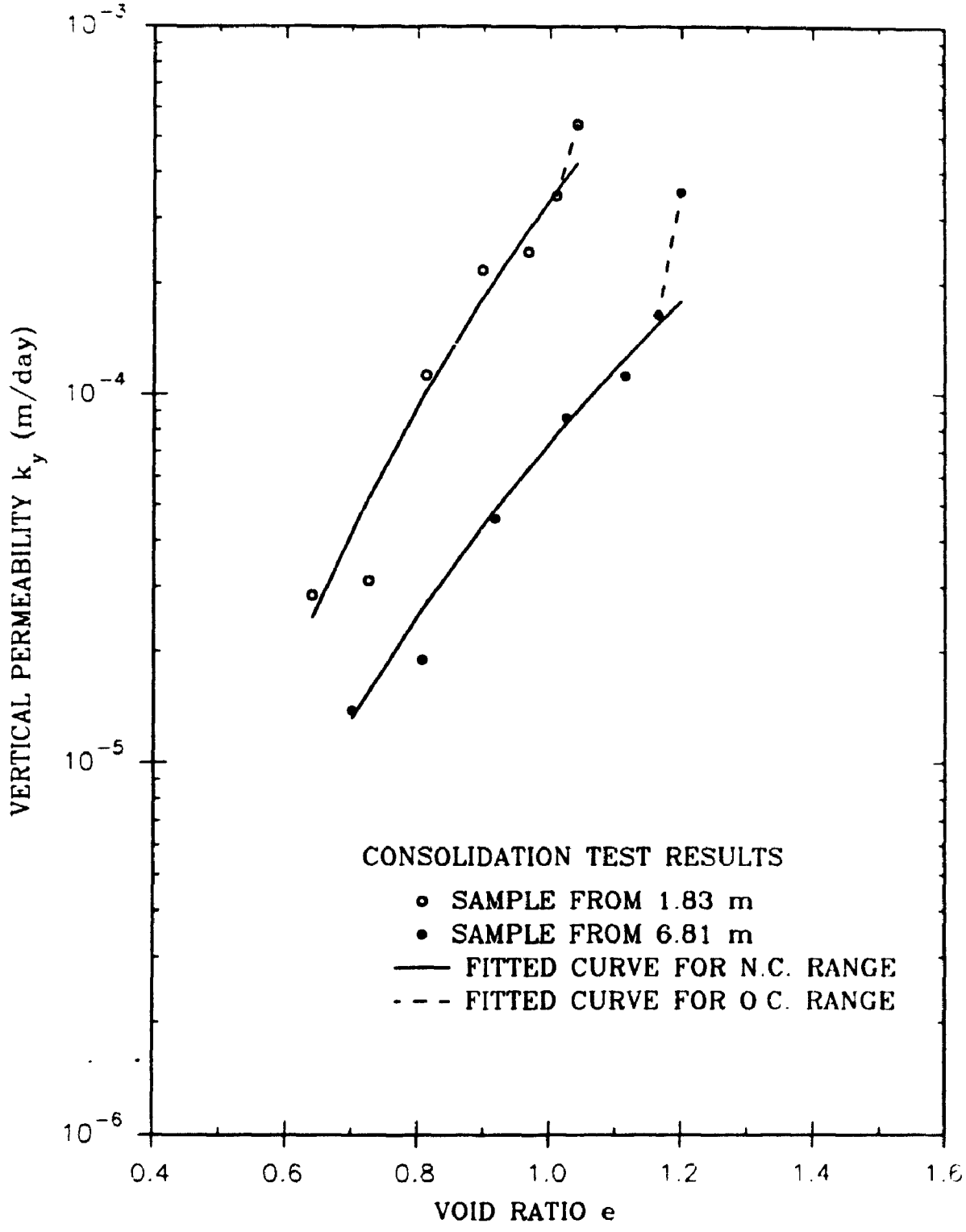

FIG. 9.7 VARIATION OF PERMEABILITY WITH VOIDS RATIO USED FOR THE FINITE ELEMENT ANALYSIS

Table 9.3 The constants to describe the variation of permeability with void ratio.

	Normally consolidated			Over Consolidated		k_x/k_y
Depth (m)	A	B	C	A1	B1	
0 - 5	0.5769E-3	5.1033	0.1006	0.3206E-3	8.6848	4.0
5 - 14	0.7413E-4	4.857	0.6033E-9	0.3601E-4	10.193	4.0

k_x = permeability in the horizontal direction
k_y = permeability in the vertical direction
A, B, C, A1 and B1 are constants for the evaluation of permeability in m/day according to equations 7.4 and 7.5

followed by an examination of the effects of changing the Poisson's ratio of the foundation soil. The effect of assuming that the soil deposit has a constant OCR value with depth of 1.2 is examined as Case 2. All other soil and geotextile properties were the same as for Case 1. Case 1 represents the situation where a crust exists at the ground surface whereas Case 2 represents the situation where a crust does not exist.

To examine the effects of changing the Poisson's ratio (v) of the foundation soil on the deformational and excess pore pressure responses, another analysis was performed. In this analysis (Case 3) the Poisson's ratio was decreased to 0.21 from the value of 0.33 considered for both Cases 1 and 2. All other soil and geotextile parameters were the same as used in Case 2.

The settlement and heave responses with time evaluated at selected locations for the three analyses are shown in Figs. 9.8 and 9.9. The variation of embankment thickness with time is also superimposed on these figures. The settlement and heave evaluated from the three cases considered were small (typically less than 0.3 m) until 3.4 m thickness followed by a large increase during the construction of the embankment from 3.4 to 5.7 m thickness. This suggest that the response is more or less elastic until about 3.4 m thickness. Case 2 showed a significantly larger increase in settlement compared to Case 1 during the construction of the embankment from 3.4 to 5.7 m thickness. A similar observation can be made with respect to the heave responses (see Fig. 9.9). It is therefore apparent that the OCR values of the soil near the ground surface can have a significant effect on the settlement of the embankment and heave of the ground near the embankment. Moreover, it can be inferred from these analyses that the existence of an overconsolidated crust near the ground surface (Case 1) can reduce the settlement and heave. However, the responses for Case 3 were not very different from that obtained in Case 2 (with a Poisson's ratio of 0.21 giving slightly less settlement than for $v = 0.33$) suggesting that uncertainty

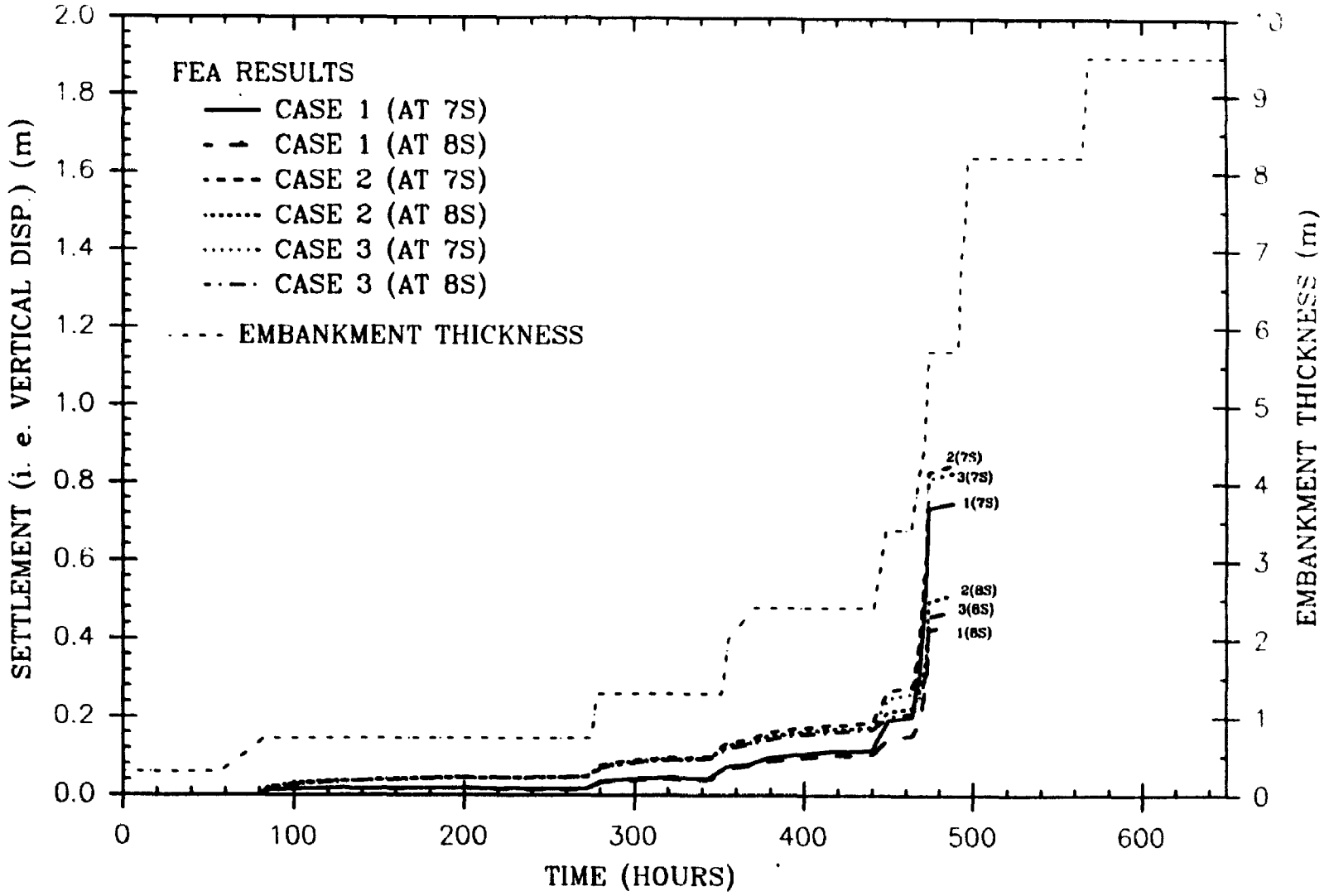

FIG. 9.8 VARIATION OF SETTLEMENT WITH TIME AT LOCATIONS 7S AND 8S

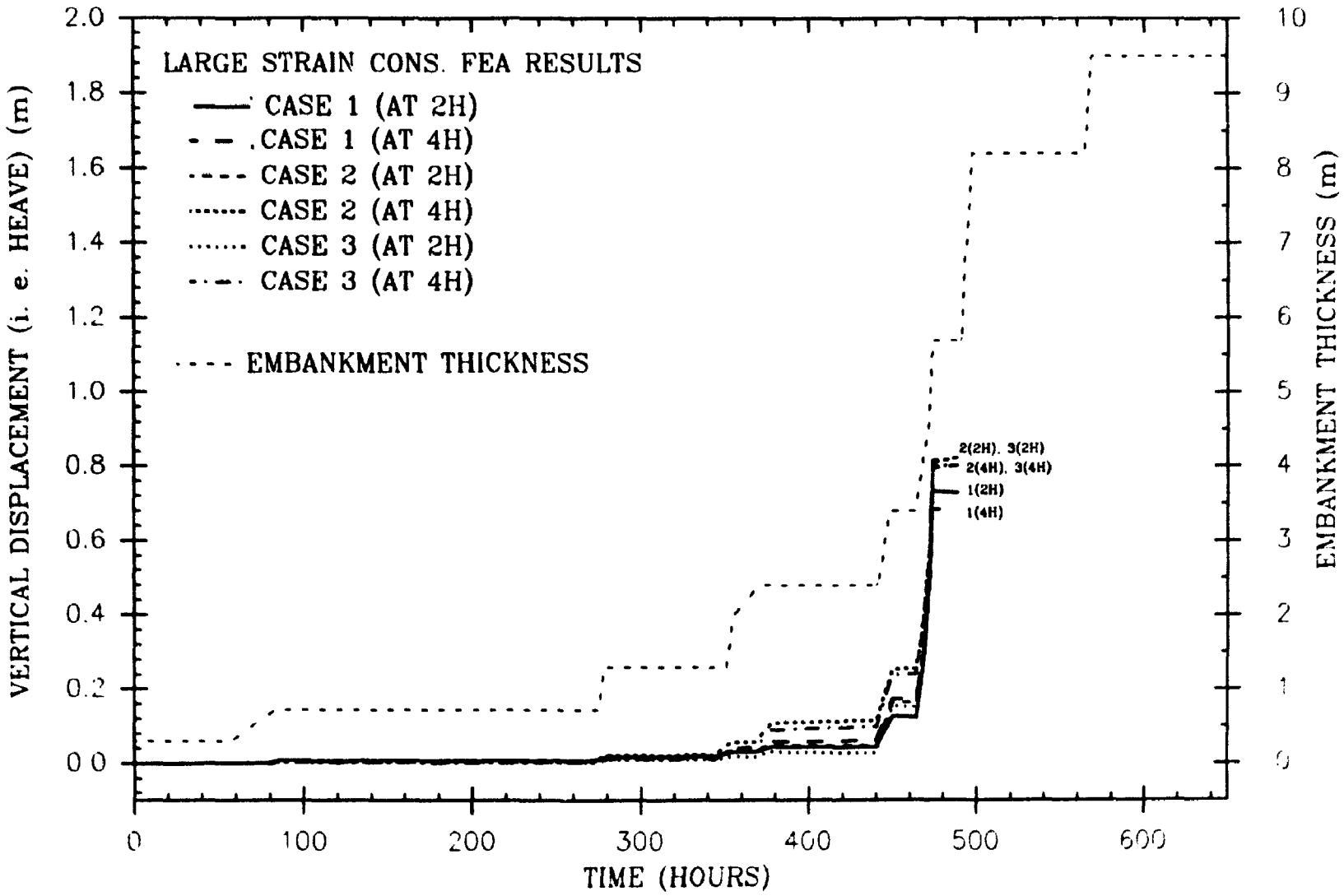

FIG 9.9 VARIATION OF VERTICAL DISPLACEMENT WITH TIME AT LOCATIONS 2H AND 4H

regarding Poisson's ratio will only have a modest effect on the settlement and heave responses.

The horizontal deformations in the foundation soil at the toe of the embankment (at different embankment thicknesses) as calculated from this series of analyses are shown in Figs. 9.10 and 9.11. Case 1 indicated lower horizontal deformations compared to the other two cases suggesting that the presence of an overconsolidated crust (i.e. higher OCR values for the foundation soil near the ground surface) would reduce the horizontal deformations in the foundation soil. Case 3 ($\nu = 0.21$) gave smaller horizontal deformation compared to Case 2 ($\nu = 0.33$) until about 3.4 m thickness (see Fig. 9.10), i.e. during the period when overall behaviour of the embankment is elastic. The difference between the horizontal deformations evaluated in these two cases (i.e. Cases 2 and 3) were not significant at higher embankment thicknesses (see Fig. 9.11 for the responses at 5 and 5.7 m). This is apparently due to the fact that the lateral deformations at these higher embankment thicknesses are dominated by plastic deformations (i.e. plasticity) in the soil which does not depend on the Poisson's ratio significantly.

The excess pore pressure in the foundation soil did not show any significant difference in the responses for the variation of OCR and Poisson's ratio examined in this series of analyses (see Figs. 9.12 and 9.13). Similarly, the strain developed in the geotextile reinforcement did not change significantly due to a change in ν of the foundation soil from 0.33 to 0.21 (see the geotextile strain distributions across the geotextile shown in Figs. 9.14 and 9.15) even for low embankment thicknesses when the overall behaviour of the embankment was elastic. The strain developed in the geotextile was lower in Case 1 (i.e. when higher OCR values were used for the foundation soil near the ground surface) compared to the other two cases suggesting that the existence of a crust would result in a lower geotextile strain.

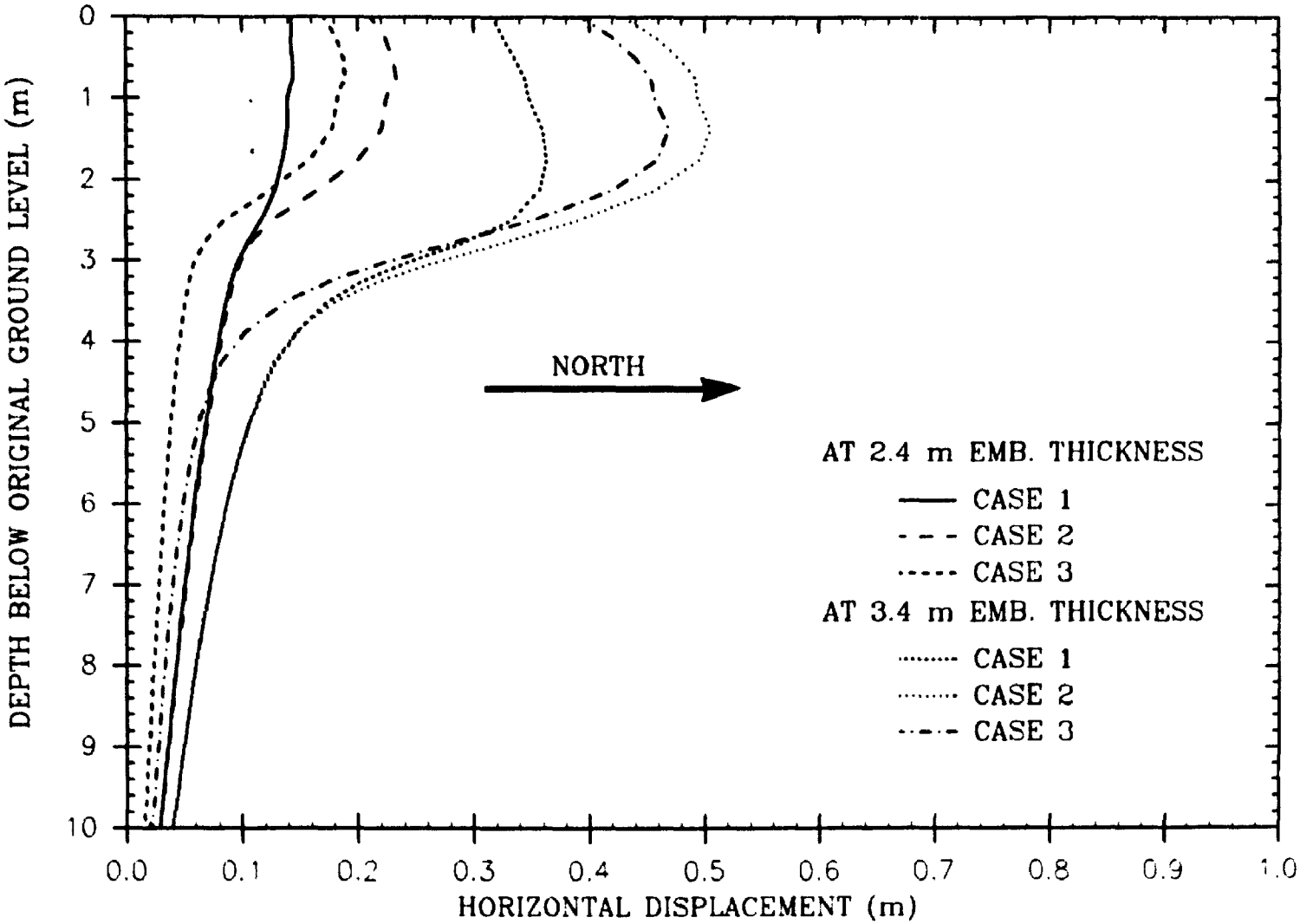

FIG 9 10 VARIATION OF HORIZONTAL DISP. WITH DEPTH AT 2.4 m AND 3 4 m EMB THICKNESSES (i.e. AT 400 AND 449 HOURS) AT THE TOE OF EMBANKMENT

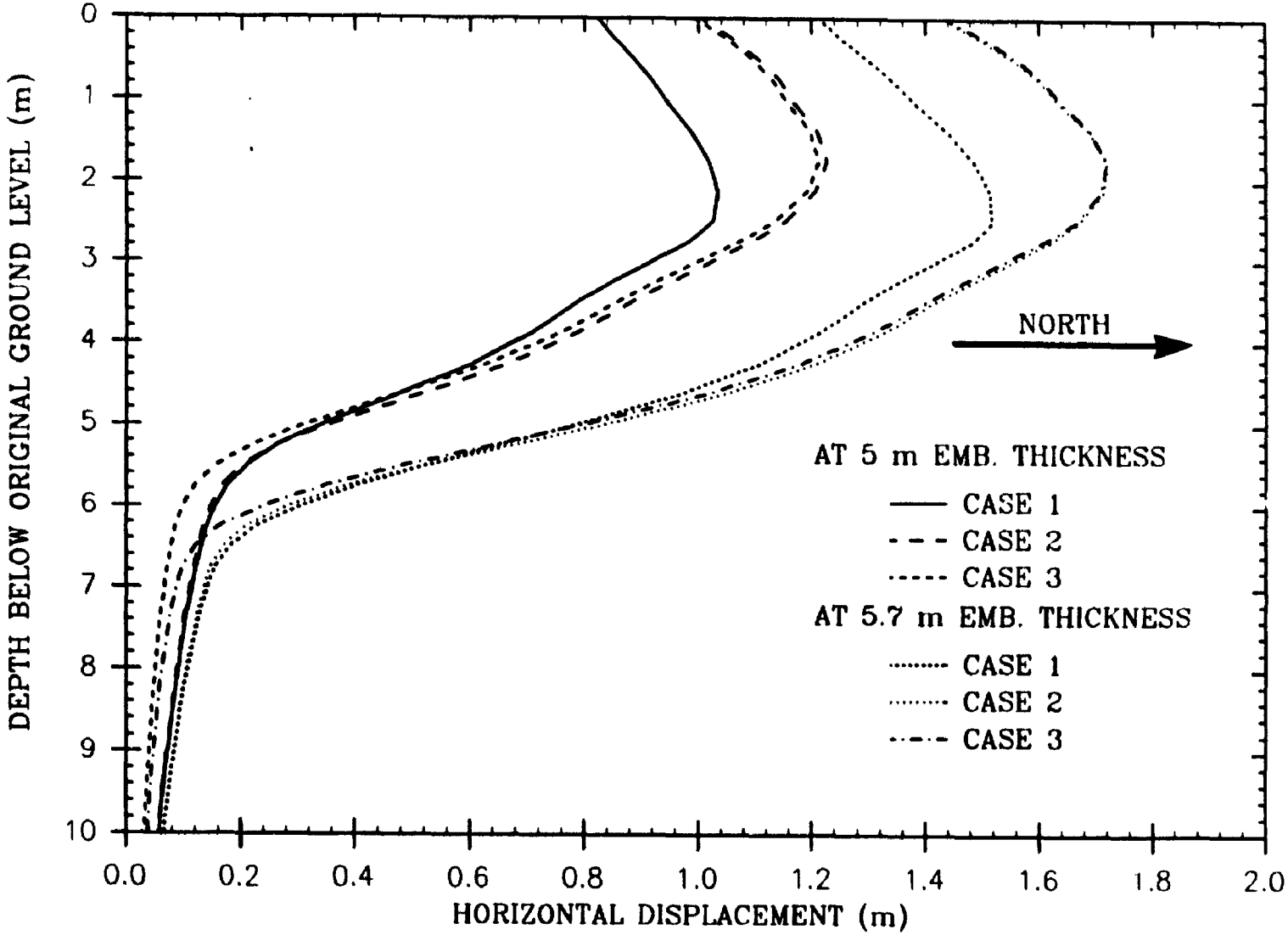

FIG. 9.11 VARIATION OF HORIZONTAL DISP. WITH DEPTH AT 5 m AND 5.7 m EMB. THICKNESSES (i.e. AT 472 AND 475 HOURS) AT THE TOE OF EMBANKMENT

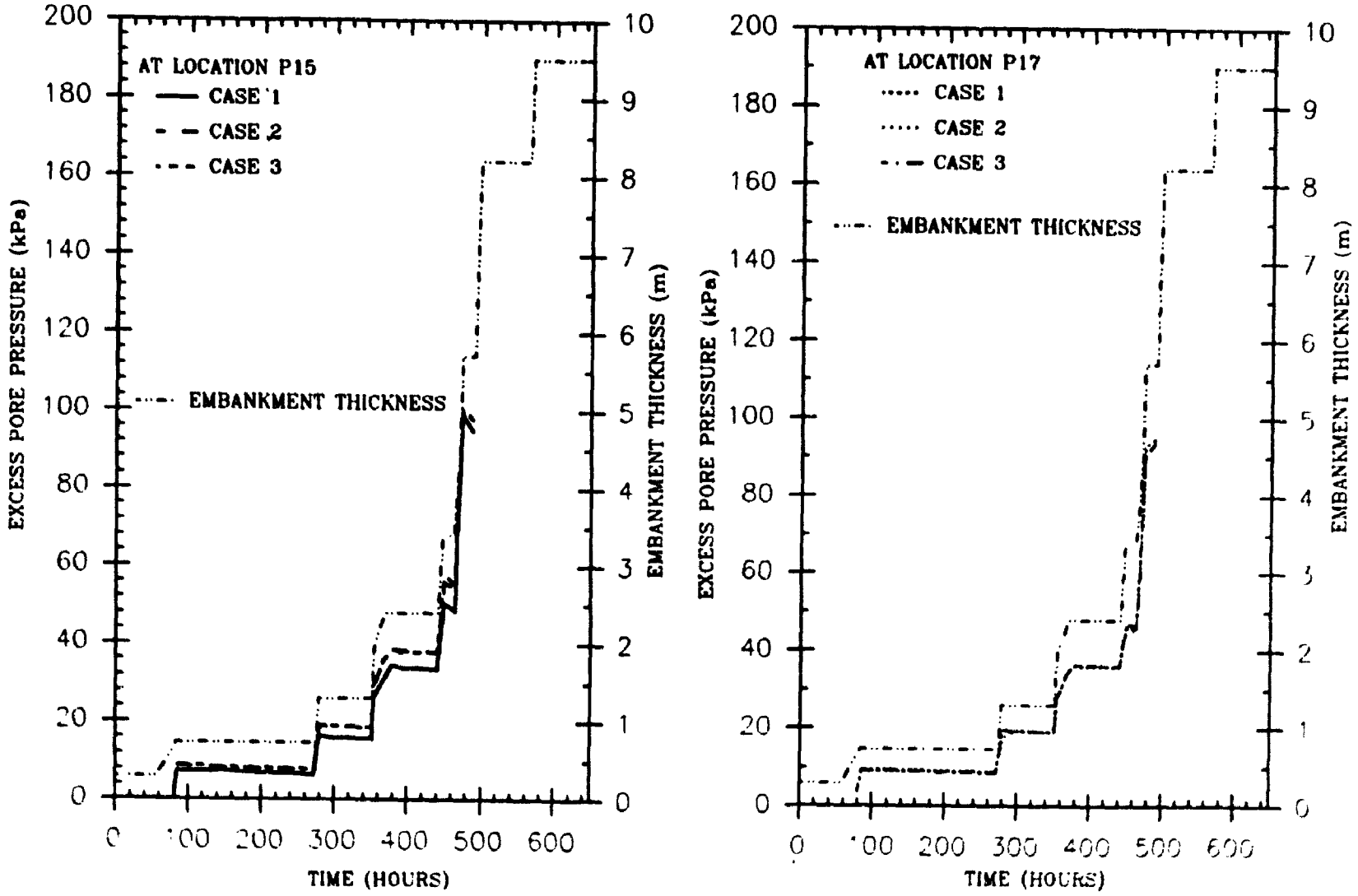

FIG. 9.12 VARIATION OF EXCESS PORE PRESSURE WITH TIME AT LOCATIONS P15 AND P17

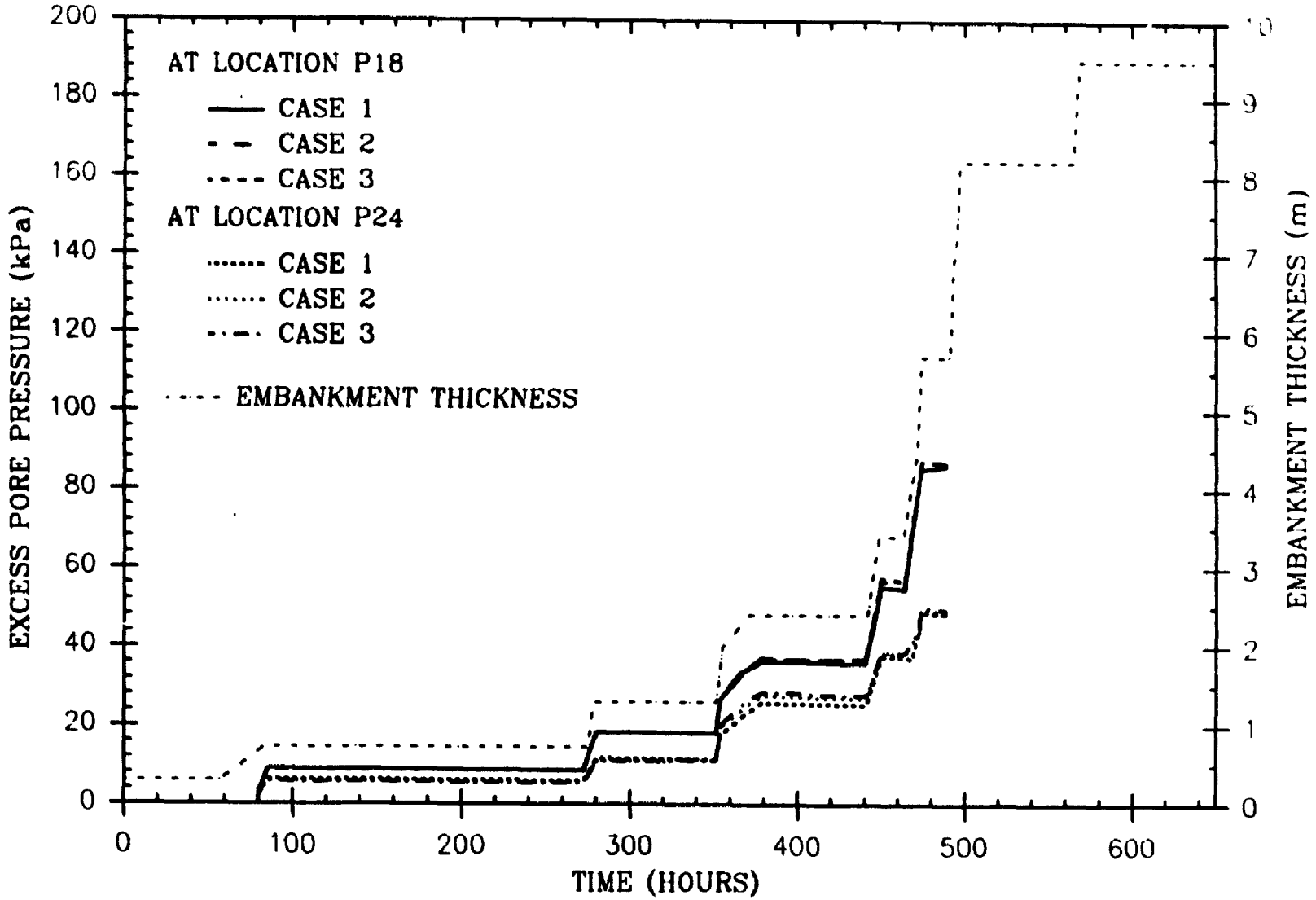

FIG. 9.13 VARIATION OF EXCESS PORE PRESSURE WITH TIME AT LOCATIONS P18 AND P24

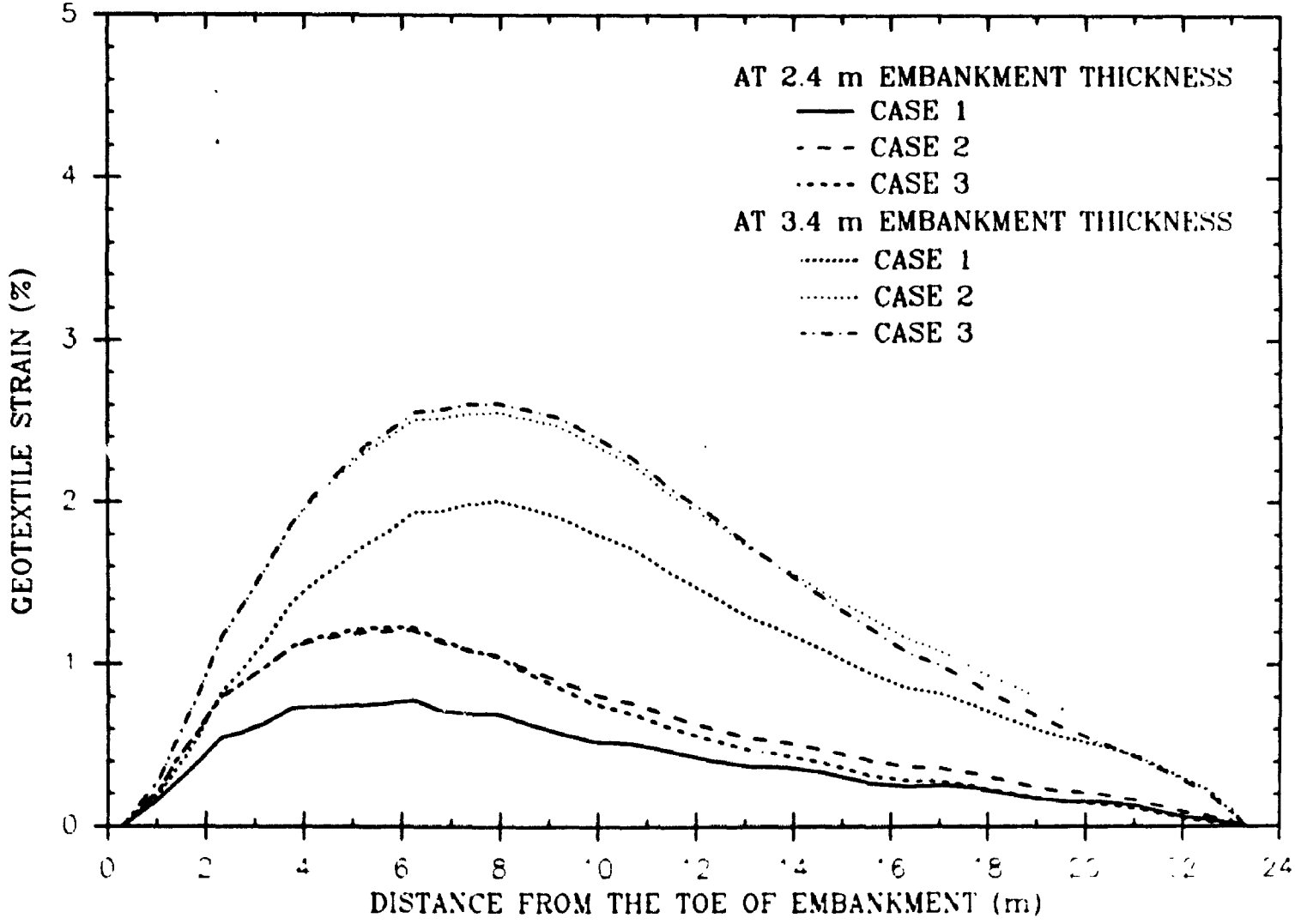

FIG 9 14 GEOTEXTILE STRAIN DISTRIBUTION AT EMBANKMENT AT 2 4 AND 3 4 m THICKNESSES – LARGE STRAIN CONS FINITE ELEMENT ANALYSIS RESULTS

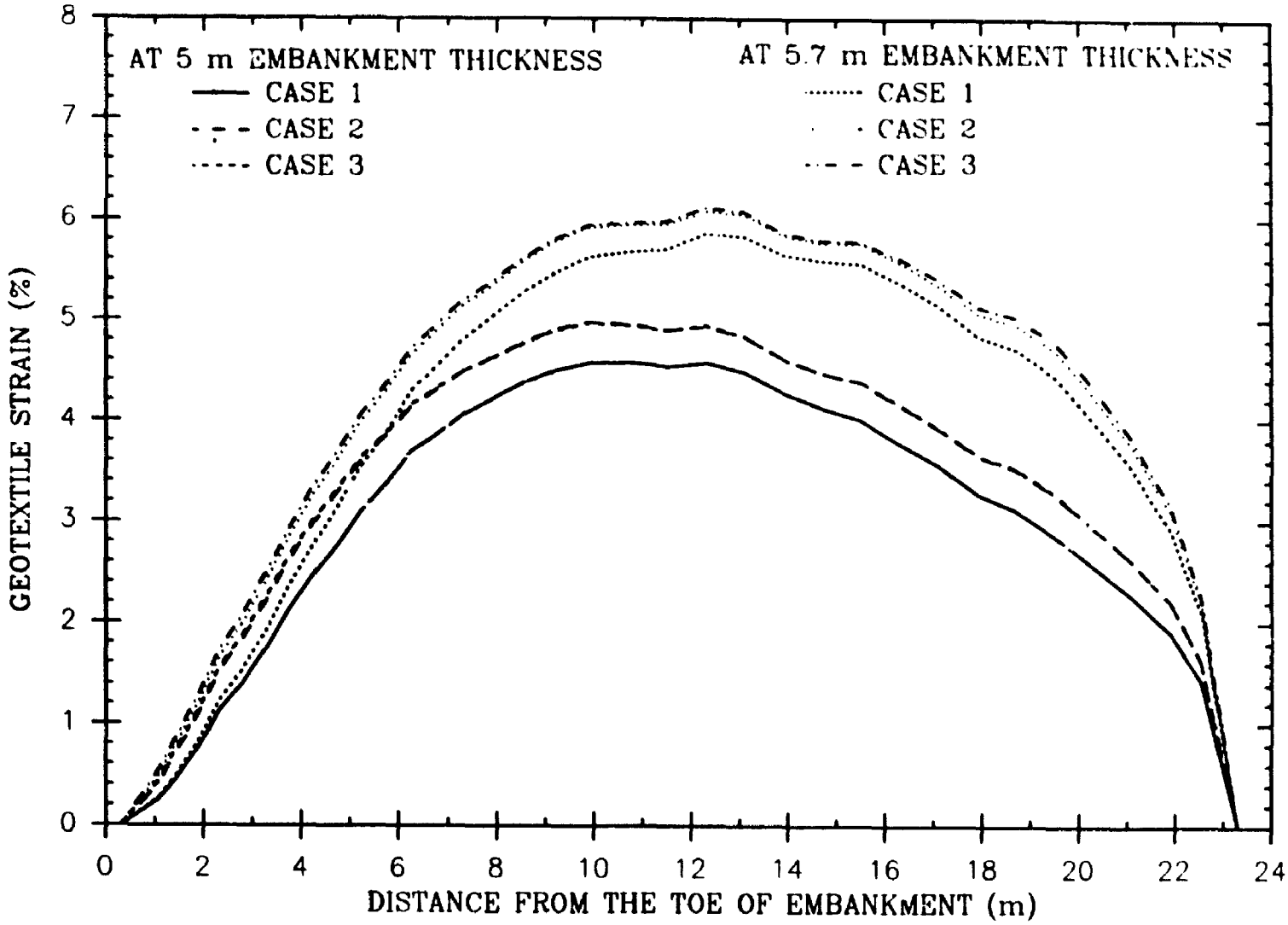

FIG. 9.15 GEOTEXTILE STRAIN DISTRIBUTION AT EMBANKMENT AT 5 AND 5.7 m THICKNESSES – LARGE STRAIN CONS. FINITE ELEMENT ANALYSIS RESULTS

9.3.3 Series 2: The effects of changing ϕ', K_o and OCR of the foundation soil

The effects of changing the effective friction angle (ϕ'), K_o (the horizontal to vertical effective stress ratio at rest) and OCR of the foundation soil on the calculated behaviour of the reinforced test embankment are examined in this section. The effect of changing the ϕ' of the foundation soil from a value of 28.2^o (i.e. M = 1.12) adopted in Case 1 - 3 analyses reported earlier, to 25.2^o (i.e. M = 0.992) is examined first as Case 4. All other soil and reinforcement parameters were the same as those previously adopted for Case 1.

Two additional analyses were also performed, one in which only the K_o values were changed (Case 5) and one in which both K_o and OCR values were changed (Case 6). The results for these two cases will be compared with those from Case 4. The K_o values used in all the previous analyses (i.e. Cases 1 to 4) were based on results from the site investigation (i.e. the self boring pressure meter tests conducted by NRC). For Cases 5 and 6, the K_o values were estimated using the following empirical relationship proposed by Mayne and Kulhawy (1982):

$$K_o = \frac{\sigma_{VO}'}{\sigma_{HO}'} = (1 - \sin\phi_{tc}') \, OCR^{\sin\phi_{tc}'} \qquad (9.1)$$

For Case 6, the OCR values were estimated on the basis of the mean undrained shear strength from the field vane tests conducted at locations V1, V2 and V3 (see chapter 3 for the details regarding the vane tests performed) using the following empirical relationship proposed by Mayne and Mitchell (1988):

$$OCR = \alpha_{VST} \left(\frac{c_u}{\sigma_{vo}'} \right)_{VST} \qquad (9.2)$$

An α_{vsl} value of 3.22 (as suggested by Kulhawy and Mayne, 1990) and ϕ' value of 25.2° were adopted for estimating K_0 and/or OCR. The consequent variation of OCR and K_0 with depth for different layers of the foundation soil for Cases 5 and 6 are summarized in Table 9.4. It is noted that the K_0 values shown in this table were obtained by fitting a third order polynomial to the values estimated using eqn. 9.1. All other parameters adopted for Cases 5 and 6 were the same as for Case 4 (including ϕ').

The settlement and heave responses with time evaluated from these analyses at different locations on the ground surface are shown in Figures 9.16 to 9.19. Small settlements and heaves (typically less than about 0.2 m) were indicated up to about 2.4 m thickness in all the four cases considered in this series of analyses. These responses were very close up to about 2.4 m thickness particularly for Cases 1, 4 and 5. However, Case 6 indicated lower settlements even at low embankment thicknesses compared to the other three cases. This difference in the settlement behaviour in Case 6 at low embankment thickness was also evident in the heave responses and is a direct result of the higher value of OCR used (see Table 9.4). Large increases of settlement and heave during the construction of the embankment from 2.4 to 3.4 m as well as from 3.4 to 5.7 m thickness were indicated in Cases 1, 4 and 5 whereas Case 6 indicated this type of large increases (but still smaller in magnitude compared to the other cases) only after 3.4 m thickness. The difference between Case 6 and the other cases are apparently due to delayed initiation of significant plasticity in the foundation soil (i.e. predominantly elastic deformations at least up to 3.4 m thickness).

Case 4 gave larger settlements than Case 1, with the maximum settlement at 5.7 m thickness having increased from about 0.74 to 0.9 m (i.e. indicating an increase of about 20%) as a result of the decrease in the ϕ' of the foundation soil from 28.2° to 25.2°. The decrease of ϕ' would indicate a decrease in the slope of the critical state line in $p' - q$

Table 9.4 OCR and K_o values adopted for cases 5 and 6.

Depth (m)	Case 5 OCR	K_o	Case 6 OCR	K_o
0 - 1	5.6	0.83	7.0	0.83
1 - 2.5	3.6	0.83	5.1	0.83
2.5 - 3.5	1.2	0.83	3.0	0.83
3.5 - 5	1.2	0.69	2.4	0.69
5 - 6	1.2	0.62	2.3	0.62
6 - 7	1.2	0.60	2.4	0.60
7 - 8	1.2	0.59	2.2	0.59
8 - 10	1.2	0.59	2.0	0.59
10 - 14	1.2	0.59	1.9	0.59

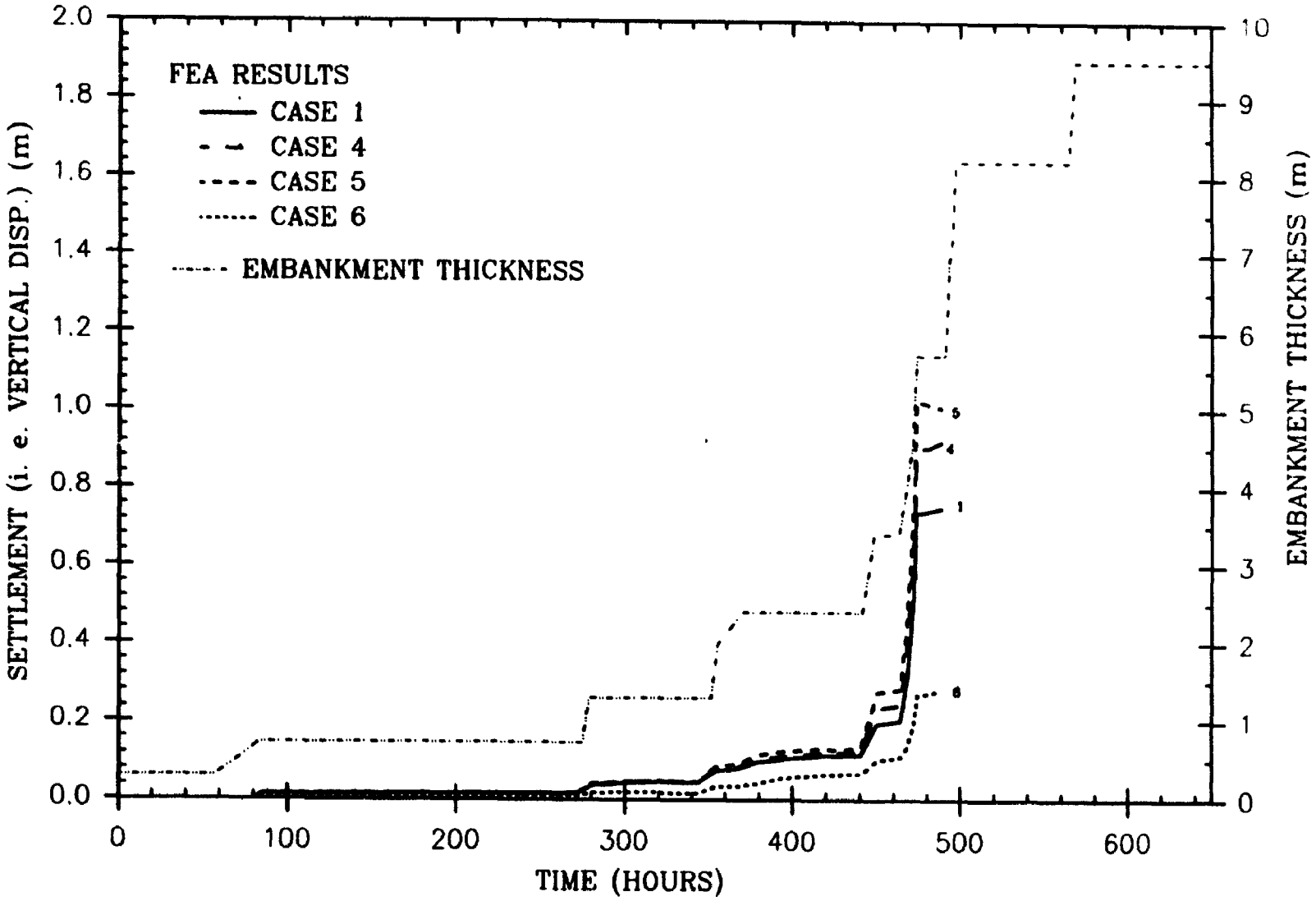

FIG. 9.16 VARIATION OF SETTLEMENT WITH TIME AT LOCATIONS 7S

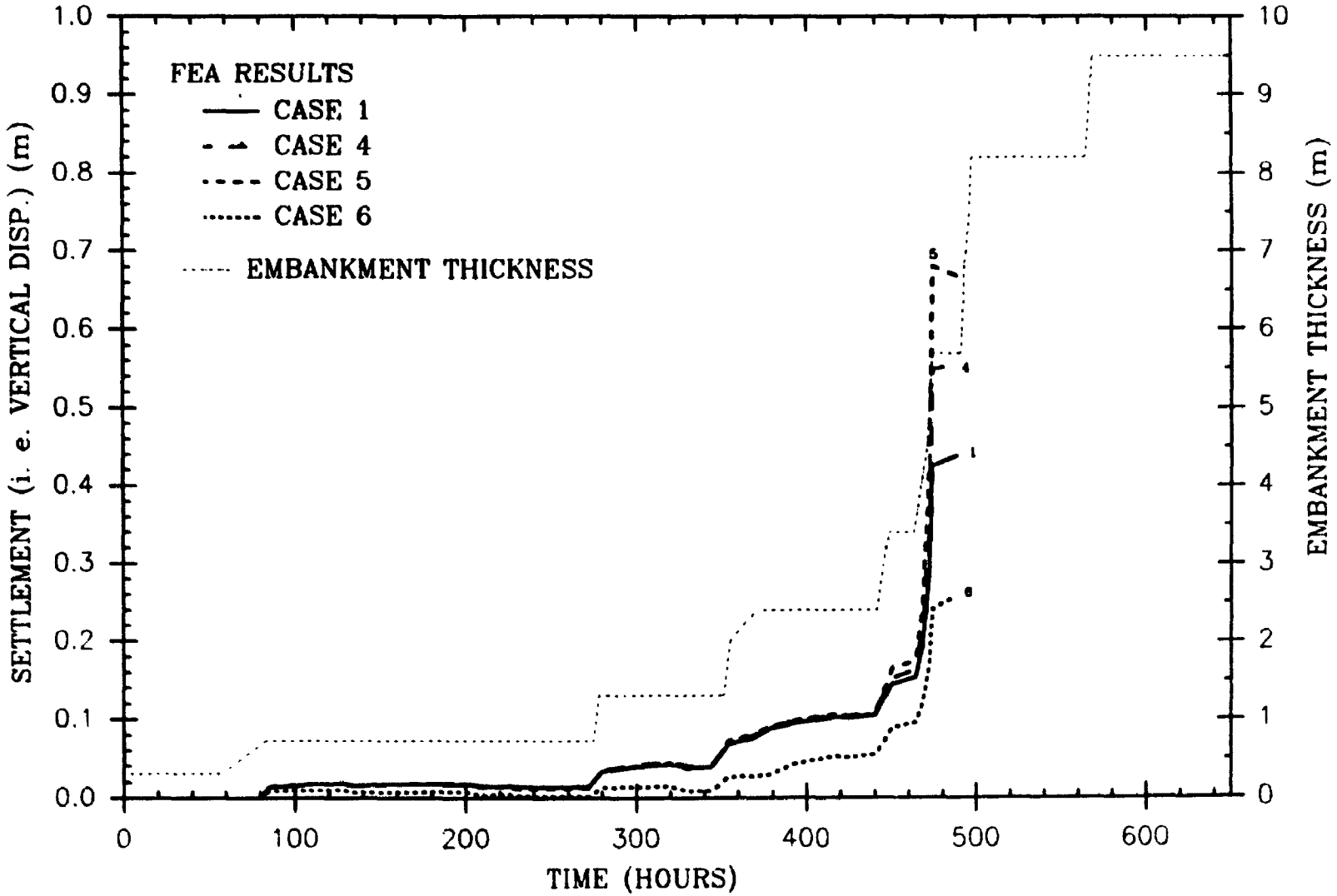

FIG. 9.17 VARIATION OF SETTLEMENT WITH TIME AT LOCATIONS 8S

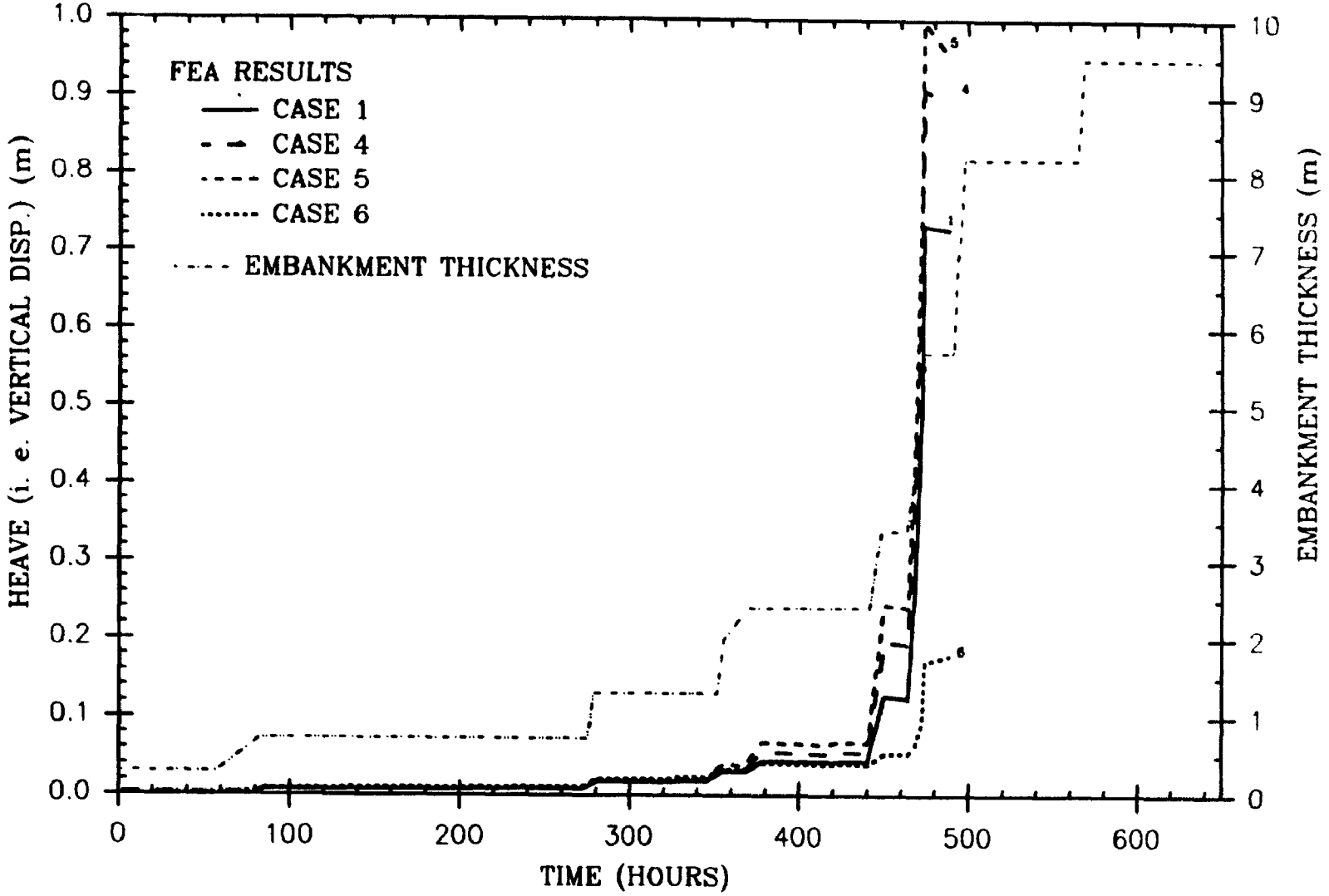

FIG. 9.18 VARIATION OF HEAVE AT LOCATION 2H WITH TIME

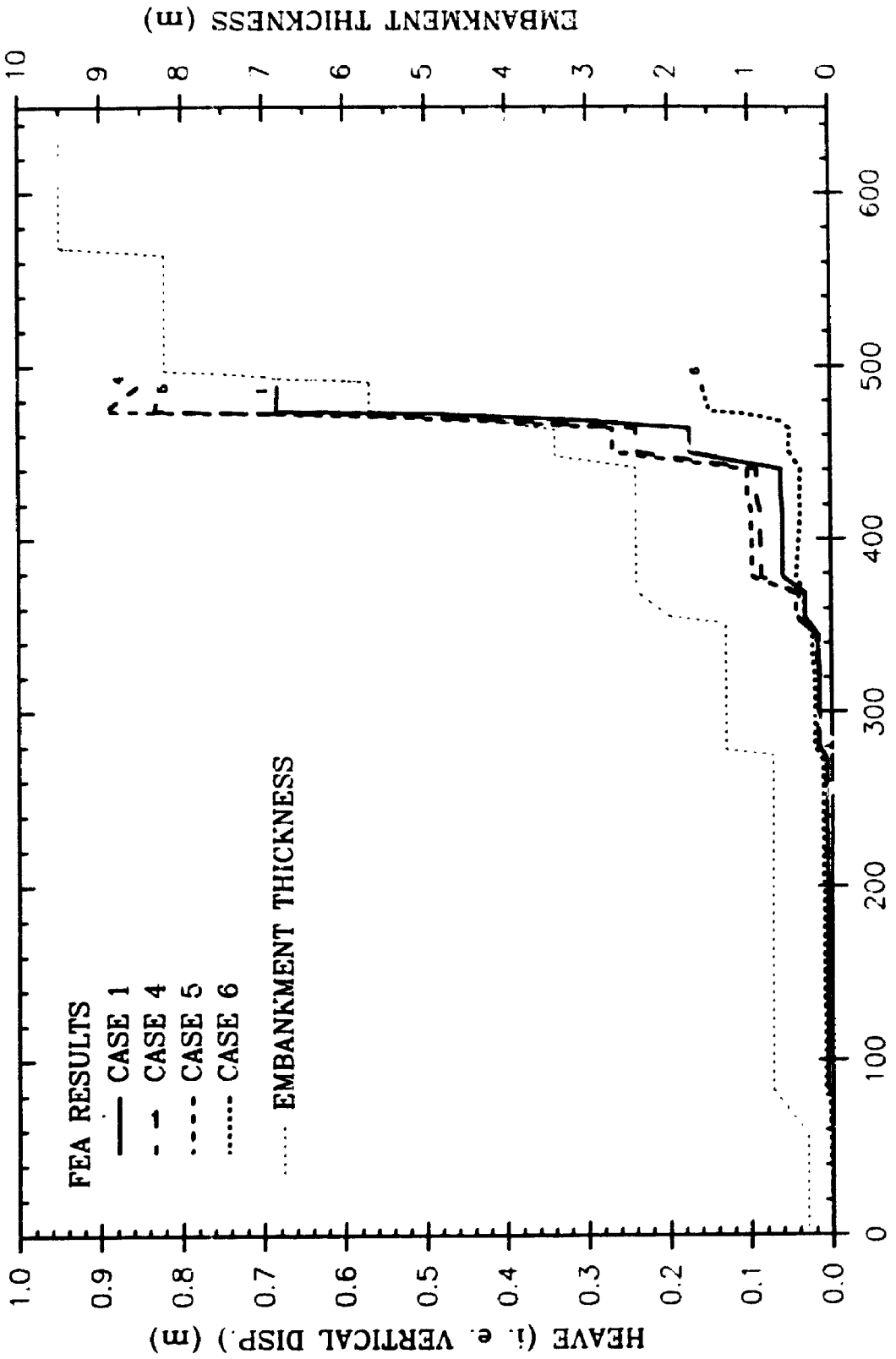

FIG. 9.19 VARIATION OF HEAVE AT LOCATION 4H WITH TIME

space (i.e. decrease in the value of M) and a shrinkage in the yield surface (i.e. smaller ellipse). Consequently, the plasticity in the foundation soil gets increased due to the decrease in ϕ' and this is apparently the cause for the increased displacements in Case 4 compared to that in Case 1.

Similar observations of larger settlement (and heave) for thicknesses greater than 3.4 m could be made between Cases 4 and 5 (e.g. the maximum settlement indicated at 5.7 m thickness increased from a value of about 0.9 m in Case 4 to about 1.02 m in Case 5, representing an increase of about 10%) suggesting that changing the K_o values of the foundation soil can have a significant influence on the predicted behaviour of the embankment. The higher OCR values used in Case 6 give rise to small settlements (and heaves) even at higher embankment thicknesses (maximum settlement of the order of 0.3 m at 5.7 m thickness compared to a maximum of about 1.06 m in Case 5).

The K_o values were increasing with depth (from 0.68 to 0.88) in Case 4 but they were decreasing with depth (from 0.83 to 0.59) in Case 5, as can be seen in Tables 9.1 and 9.4. The initial stress state would be different for these two cases due to the changes of K_o values. Consequently, there could be significant difference in the development and growth of plasticity in the foundation soil between Cases 4 and 5. This is apparently the cause for the changes in the behaviour of the embankment seen between Cases 4 and 5.

The horizontal deformations in the foundation soil at the toe of the embankment were small (typically less than 0.21 m) up to about 2.4 m thickness for all the four cases considered here (see Fig. 9.20). In general, the horizontal deformations obtained in Case 5 were larger than those in Case 4 which, in turn, were larger than in Case 1 (see Figs. 9.20 to 9.22). In Case 1, the maximum horizontal deformation increased from 0.21 to 0.36 m during the construction of the embankment from 2.4 to 3.4 m thickness and it further

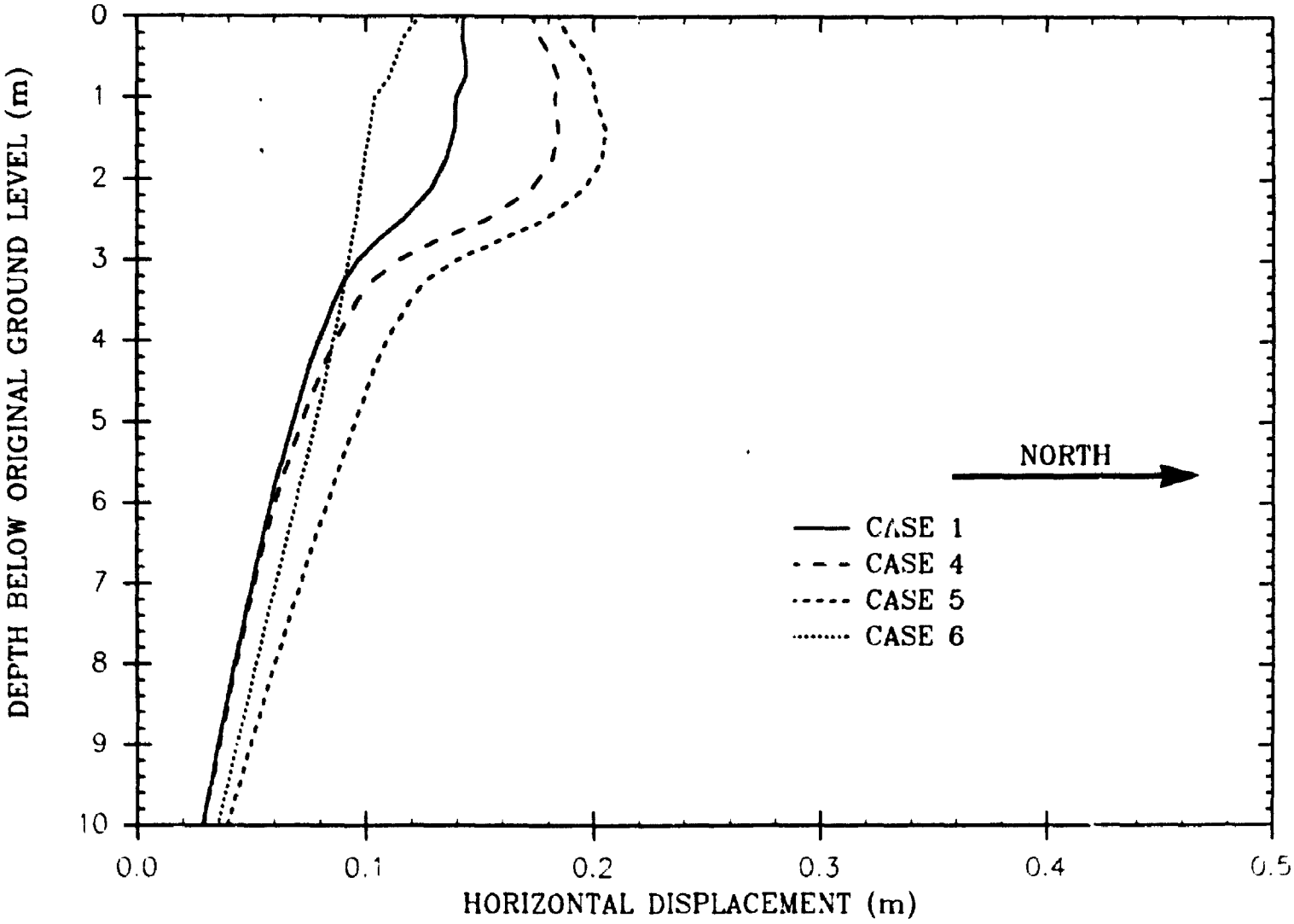

FIG. 9.20 VARIATION OF HORIZONTAL DISP. WITH DEPTH AT 2.4 m EMB. THICKNESS (i.e. AT 400 HOURS) AT THE TOE OF EMBANKMENT

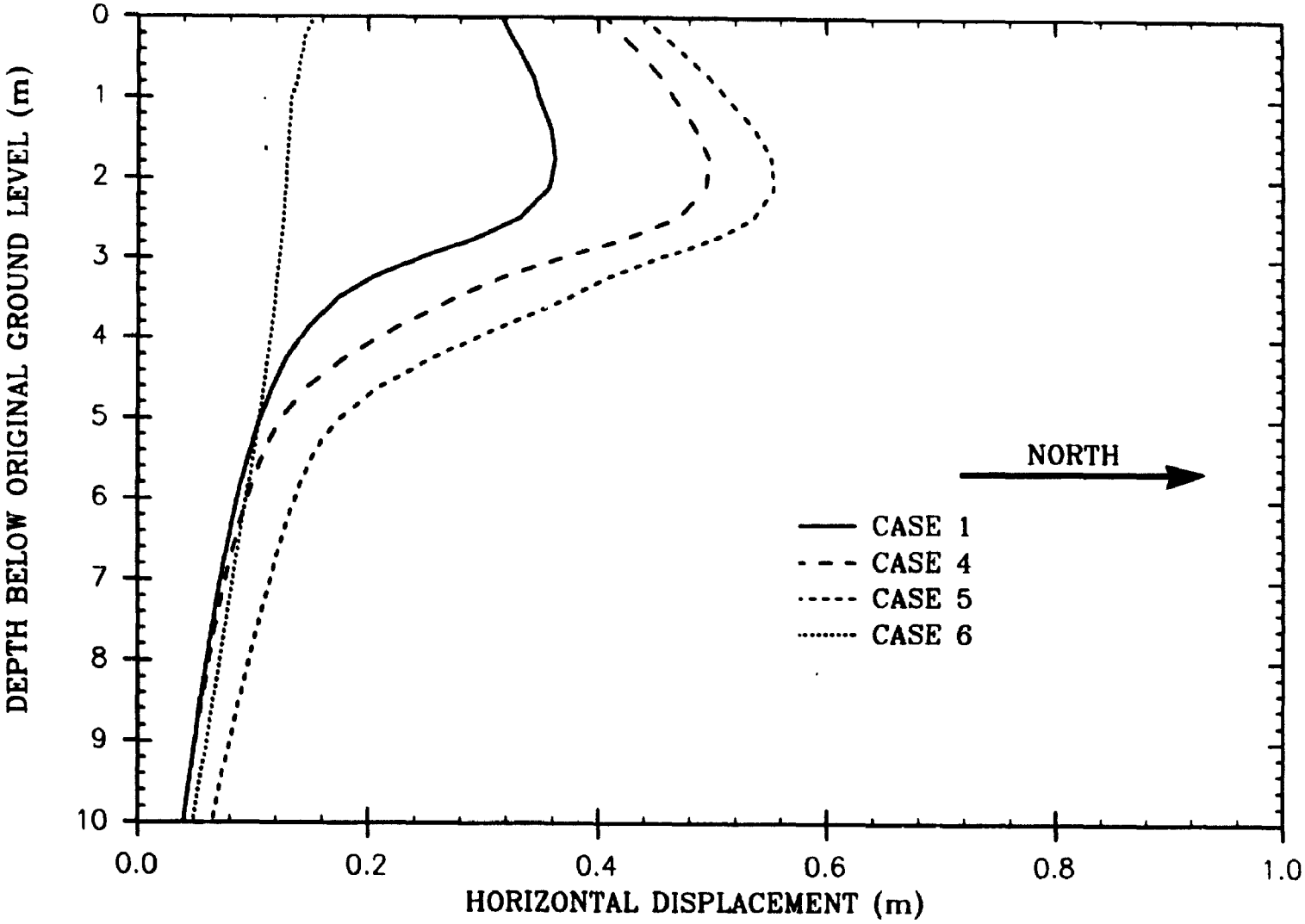

FIG. 9.21 VARIATION OF HORIZONTAL DISP. WITH DEPTH AT 3.4 m EMB. THICKNESS (i.e. AT 449 HOURS) AT THE TOE OF EMBANKMENT

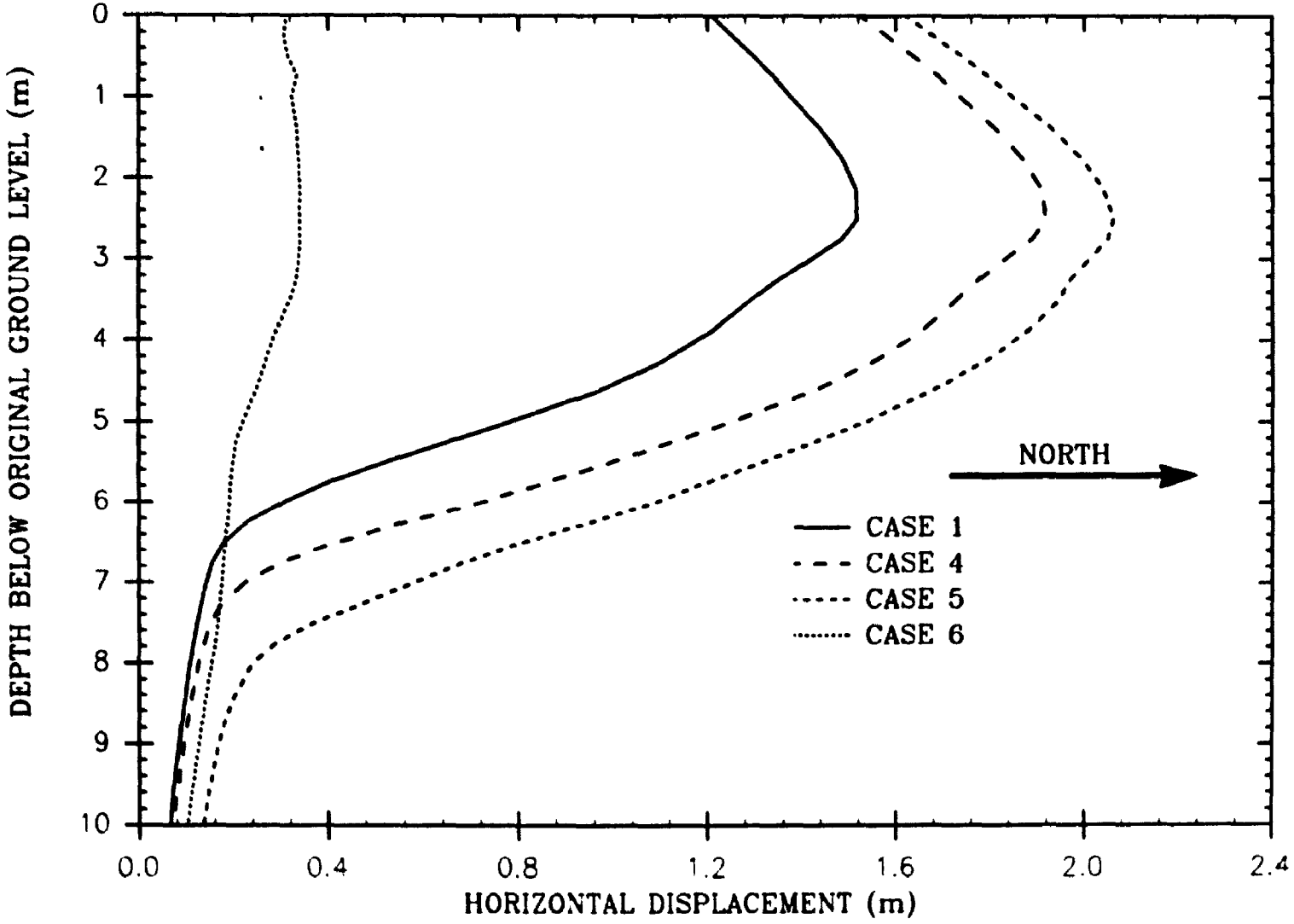

FIG. 9.22 VARIATION OF HORIZONTAL DISP. WITH DEPTH AT 5.7 m EMB. THICKNESS (i.e. AT 475 HOURS) AT THE TOE OF EMBANKMENT

increased to 1.52 m at 5.7 m thickness. The maximum horizontal deformation increased from 0.5 to 1.92 m during the construction of the embankment from 3.4 to 5.7 m in Case 4, indicating an increase of the horizontal deformation in excess of 25% between Cases 4 and 1 (i.e. for a 3^0 decrease in the ϕ' of the foundation soil). Comparison of the results between Cases 4 and 5 shows that a change in the assumed K_o values of the foundation soil can also alter the horizontal deformations significantly. The horizontal displacements indicated in Case 5 were larger than those indicated in Case 4 and the differences were evident at all depths (e.g. the maximum horizontal displacement increased from a value of 1.92 m indicated at 5.7 m thickness in Case 4 to about 2.06 m in Case 5, representing a change of about 7%). The difference in the development of plasticity in the foundation soil caused by the K_o changes is apparently the cause for these changes in the horizontal displacement responses.

In Case 6, the increase in the horizontal deformations were very small during the construction of the embankment from 2.4 to 3.4 m thickness (i.e. the maximum horizontal deformation increased from 0.12 to only 0.15 m) suggesting an elastic behaviour of the embankment up to at least 3.4 m thickness. A significant increase in the horizontal deformation was predicted for the construction of the embankment from 3.4 to 5.7 m thickness. However, the horizontal deformations obtained in Case 6 were much smaller than those obtained in Case 5 (e.g. a maximum of only 0.34 m for Case 6 compared to 2.06 m for Case 5 at 5.7 m thickness). These large variations suggest that the OCR profile of the foundation soil is crucial for the accurate determination of the horizontal deformations in the foundation soil.

The responses with time of the excess pore pressures in the foundation soil did not show any significant difference between the different cases considered in this series of analysis until about 350 hours (i.e. 1.3 m thickness) (see Figs. 9.23 to 9.25). Slight

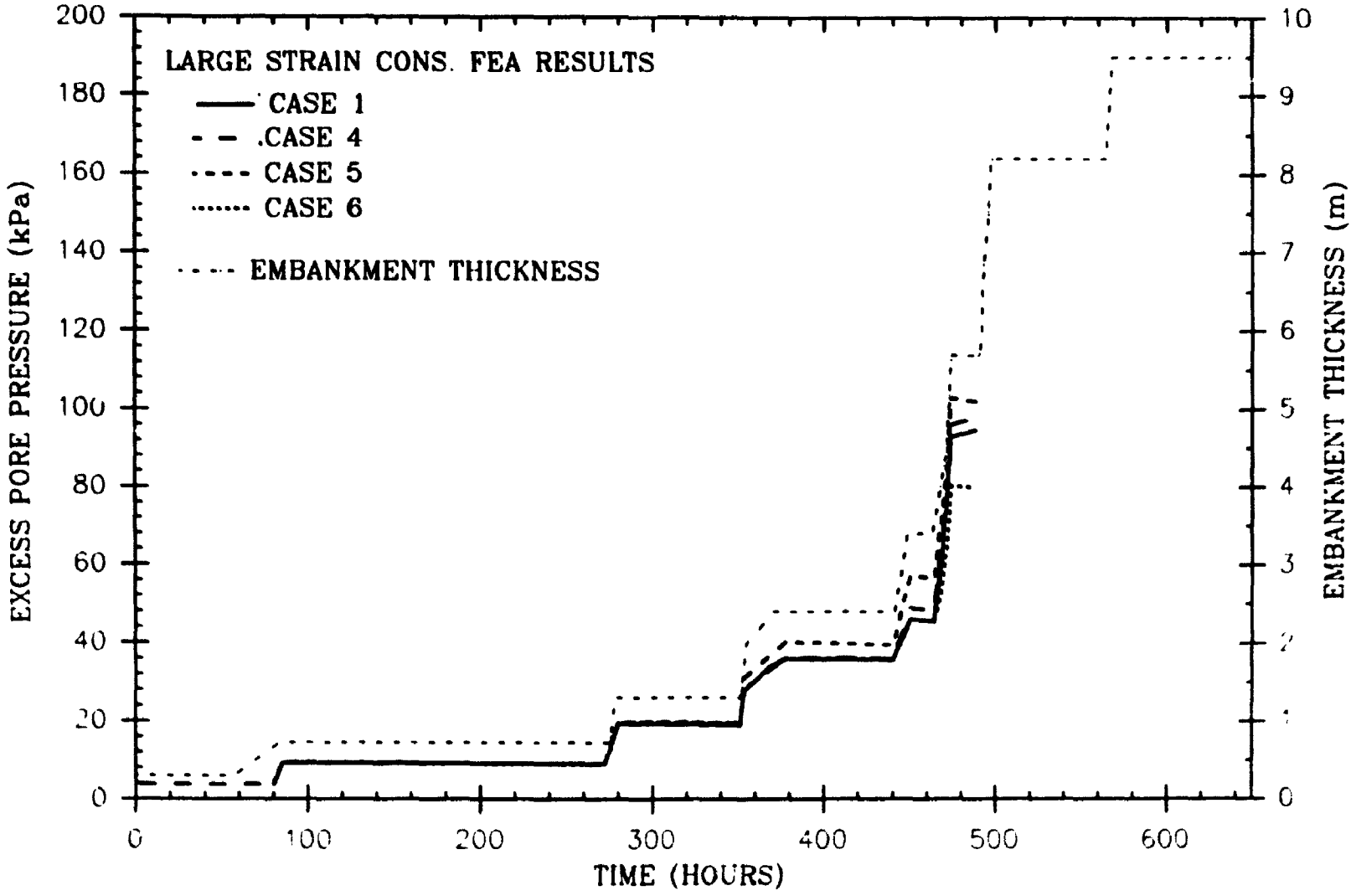

FIG 9.23 VARIATION OF EXCESS PORE PRESSURE WITH TIME AT LOCATION P17

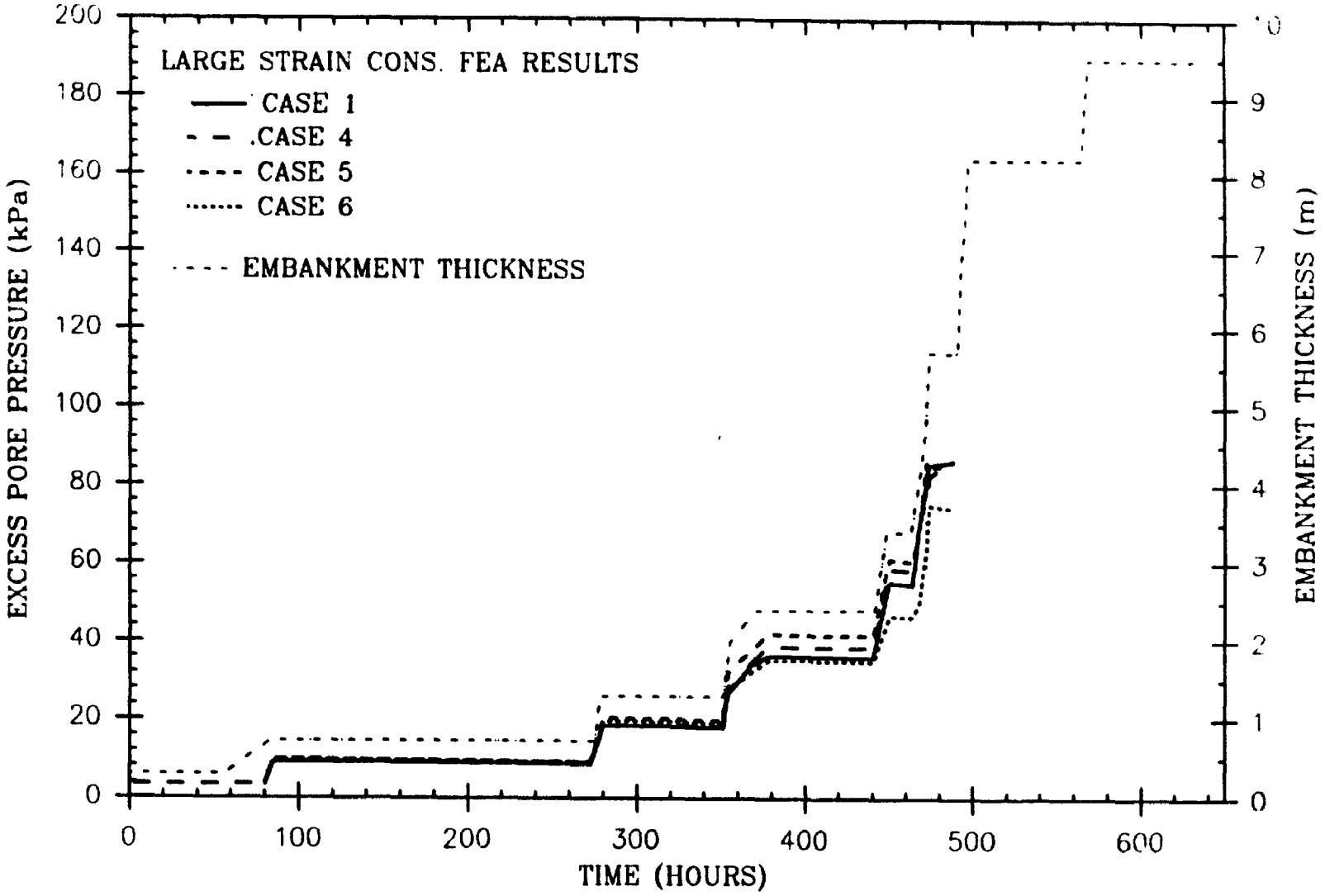

FIG. 9.24 VARIATION OF EXCESS PORE PRESSURE WITH TIME AT LOCATION P18

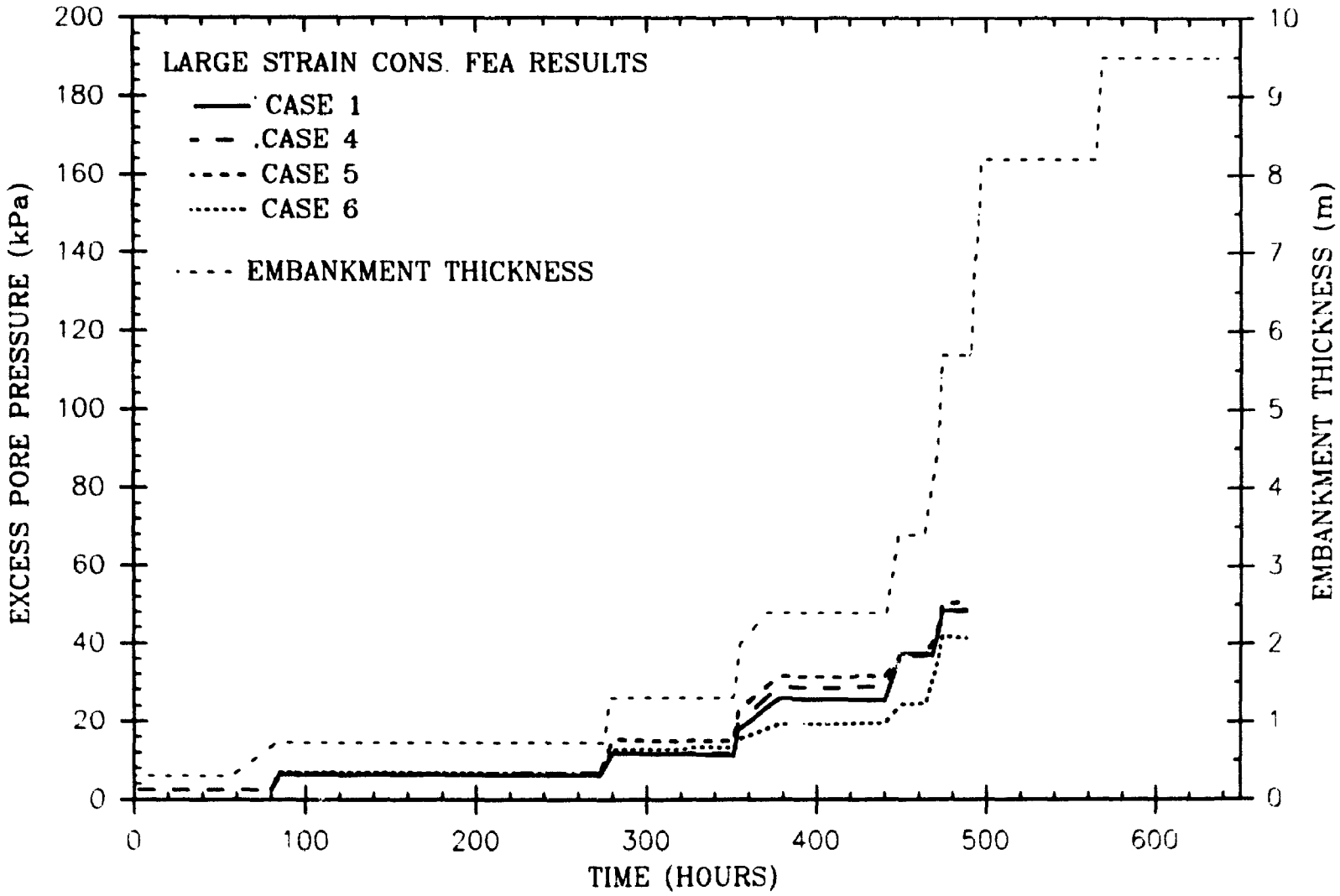

FIG. 9.25 VARIATION OF EXCESS PORE PRESSURE WITH TIME AT LOCATION P24

variations in the responses between Cases 1, 4 and 5 were indicated at some locations (e.g. at location P18) for thicknesses above 2.4 m. Slightly increased excess pore pressures were indicated in Case 4 compared to Case 1 as well as in Case 5 compared to Case 4 at locations P18 and P24 for thicknesses greater than 2.4 m. However, the difference in the excess pore pressures between Cases 1, 4 and 5 were not significant when the embankment was constructed to 5.7 m thickness.

Lower excess pore pressures compared to Case 5 were indicated in Case 6 at all the locations for thicknesses above 3.4 m. As previously noted, the foundation soil experienced much larger plastic deformations in Cases 1, 4 and 5 compared to Case 6 for thicknesses above 3.4 m. The difference in the pore pressure responses between Cases 5 and 6 is a result of the differences in OCR and the consequent difference in hydraulic conductivity controlling the pore pressure response (see eqns. 7.4 and 7.5).

The smaller value of ϕ' used in Case 4 gave rise to higher strains in the geotextile reinforcement when compared to Case 1 at least up to 3.4 m thickness (see Figs. 9.26 to 9.28). The deformations, excess pore pressures and geotextile strain responses suggest that the foundation soil is yielding at a thickness of about 3.4 m for both Cases 1 and 4 and that after this yielding, the geotextile reinforcement playing a major role in providing stability to the embankment. Large increases in the geotextile strain were calculated for Cases 1 and 4 during the construction of the embankment from 3.4 to 5.7 m (apparently due to yielding of the foundation soil as noted above). The strain distributions across the geotextile for these cases were very close when the embankment was constructed to 5.7 m thickness. At this thickness, Cases 1 and 4 both had a maximum geotextile strain of about 6% at a point between 12 and 14 m from the toe of the embankment. The difference in K_o values considered between Cases 4 and 5 showed only a moderate difference in the strain distribution across the geotextile reinforcement. Thus, for the embankment configuration

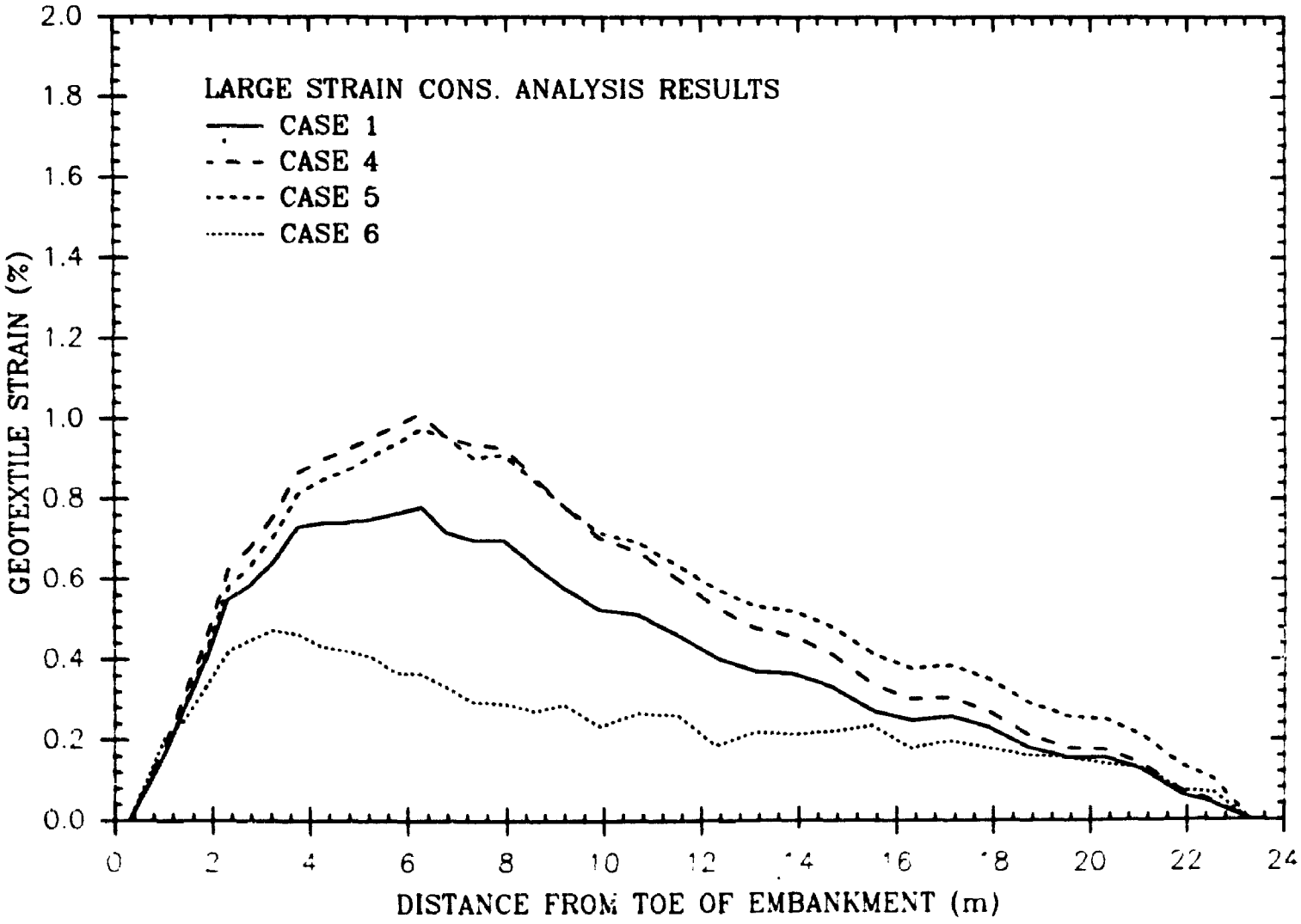

FIG. 9 26 GEOTEXTILE STRAIN DISTRIBUTION AT EMBANKMENT THICKNESS = 2 4 m - (372 HOURS)

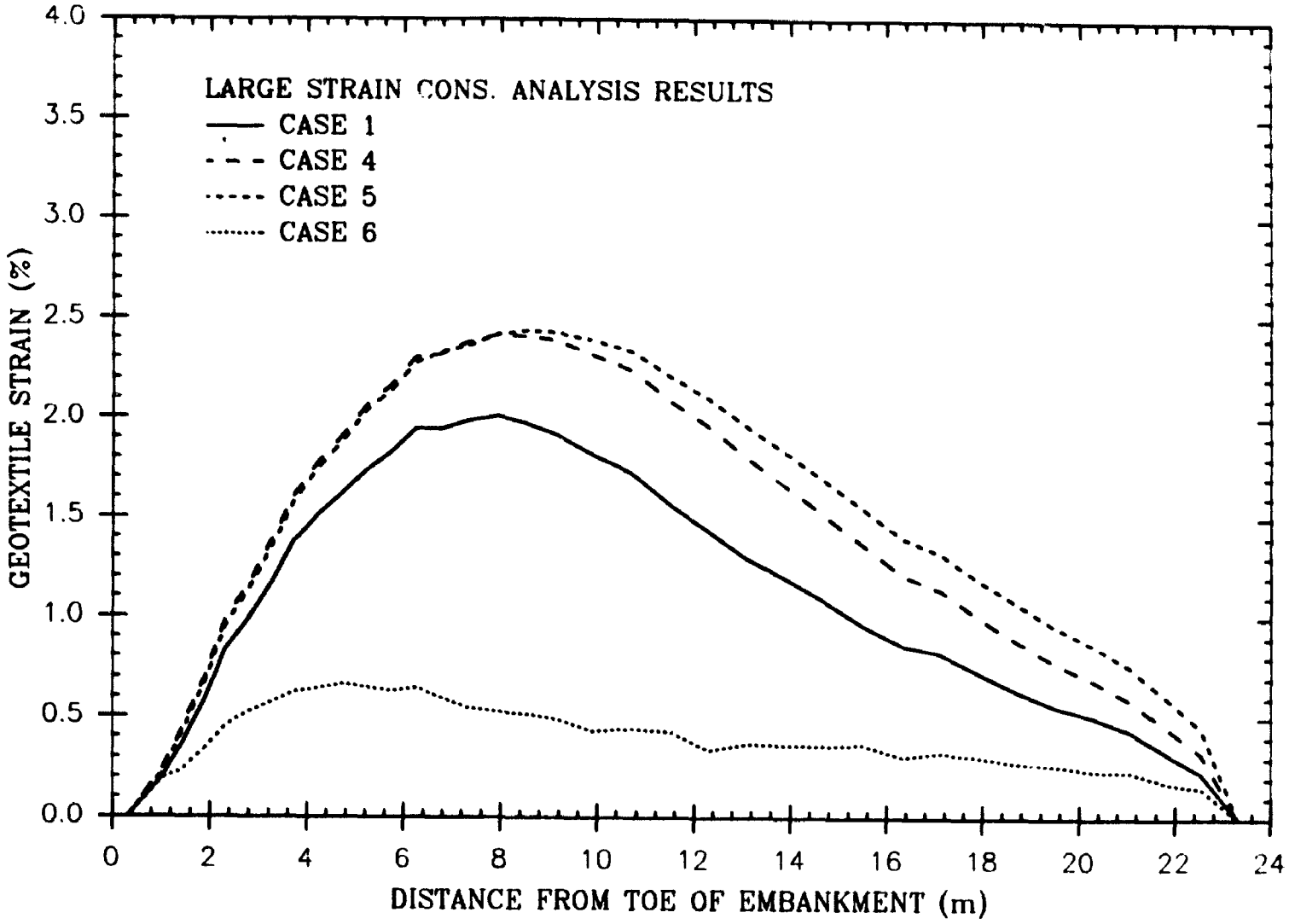

FIG. 9.27 GEOTEXTILE STRAIN DISTRIBUTION AT EMBANKMENT THICKNESS = 3.4 m – (448 HOURS)

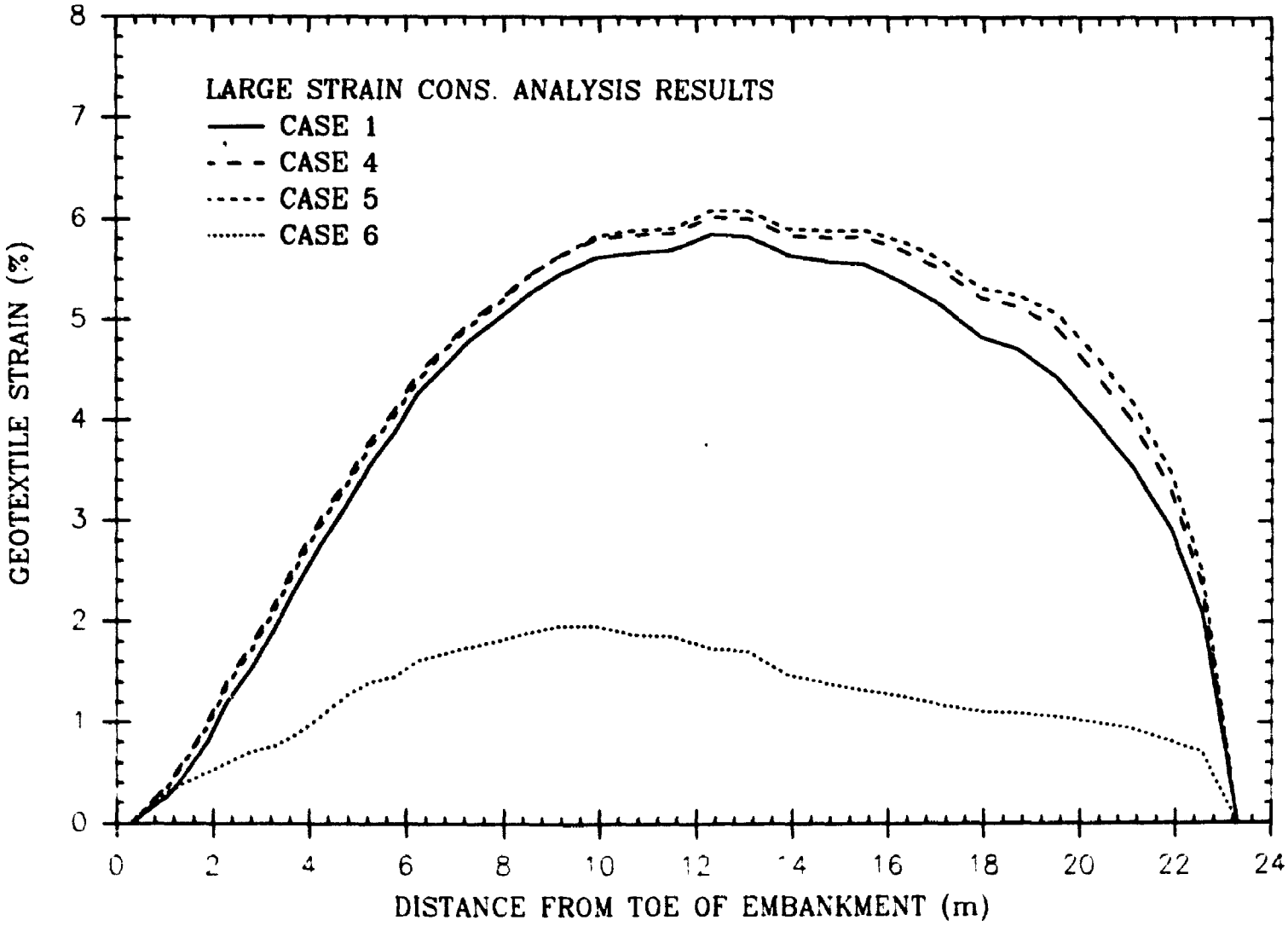

FIG 9.28 GEOTEXTILE STRAIN DISTRIBUTION AT EMBANKMENT THICKNESS = 5.7 m – (475 HOURS)

considered here the calculated geotextile strain distribution tended to be very similar for the different values of ϕ' and K_o considered.

The higher OCR values used for the foundation soil in Case 6 resulted in the development of lower strains in the geotextile reinforcement, at least up to 5.7 m thickness. The maximum strain developed in the geotextile increased from about 0.44 to 0.67% when the embankment was constructed from 2.4 to 3.4 m thickness and it further increased to about 2% when constructed to 5.7 m thickness. Although plasticity has developed in the foundation soil, it is apparent that the foundation soil is not experiencing uncontained plastic flow at 5.7 m thickness in this Case and the stability of the embankment does not depend entirely on the geotextile reinforcement. The results of this series of analyses also indicates that the OCR of the foundation soil can have an important effect on the strain developed in the geotextile reinforcement at different stages of construction of the embankment.

9.3.4 Series 3: The effects of changing the permeability of the foundation soil and ϕ' of the embankment fill

The effects of changing the permeability of the foundation soil and the ϕ' of the embankment fill on the behaviour of the reinforced embankment were examined in this series of analyses. To study the effects of changing the permeability of the foundation soil, the horizontal to vertical permeability ratio was increased from the value of 4 used previously to 10. In addition, the vertical permeability of all layers of the foundation soil during the overconsolidated state was considered to be constant at 10^{-6} cm/s. However, the permeabilities were allowed to vary with the void ratio when the soil becomes normally consolidated in a similar manner to that previously considered (see Table 9.3). The results of the large strain finite element analysis performed with these permeability

changes (hereafter referred to as Case 7) are compared with the results from Case 1 analysis reported earlier. All other soil and geotextile parameters were the same as those adopted in Case 1.

To examine the effects of changing the ϕ' of the embankment fill, an analysis was performed with the ϕ' of the fill material used below and above the geotextile reinforcement (i.e. the fill material used for the first 0.7 m thickness of the embankment) decreased from the value of 43^{o} adopted in previous cases of analyses (e.g. Case 1 and 7) to 30^{o}. In this analysis (hereafter referred to as Case 8), the ϕ' of the geotextile-fill interface was also decreased to 30^{o} (from a value of 41.9^{o} used previously, see Table 8.2). All other soil and geotextile properties were the same as adopted in Case 7.

The settlement and heave responses with time evaluated from the large strain elasto-plastic consolidation analyses using the FEM for the above two cases are compared with Case 1 in Figs. 9.29 and 9.30. The settlements and heaves were comparatively small (typically less than 0.3 and 0.2 m respectively) up to about 3.4 m thickness due to the essentially elastic behaviour of the foundation. However, both Cases 7 and 8 gave increased settlements when compared to Case 1 after about 350 hours (1.3 m thickness). This is due to increased consolidation resulting from the higher permeabilities used for the foundation soil in these cases. The heave responses did not show any significant difference up to about 2.4 m thickness.

The settlement and heave responses were very close for Cases 7 and 8 up to about 3.4 m thickness. Large increases in settlement and heave were indicated in all the three cases examined here for thicknesses above 3.4 m, due to large plastic deformations in the foundation soil as previously discussed. Case 7 gave rise to larger settlement than Case 1. Case 8 gave even larger deformations. The heave responses indicated an opposite trend of

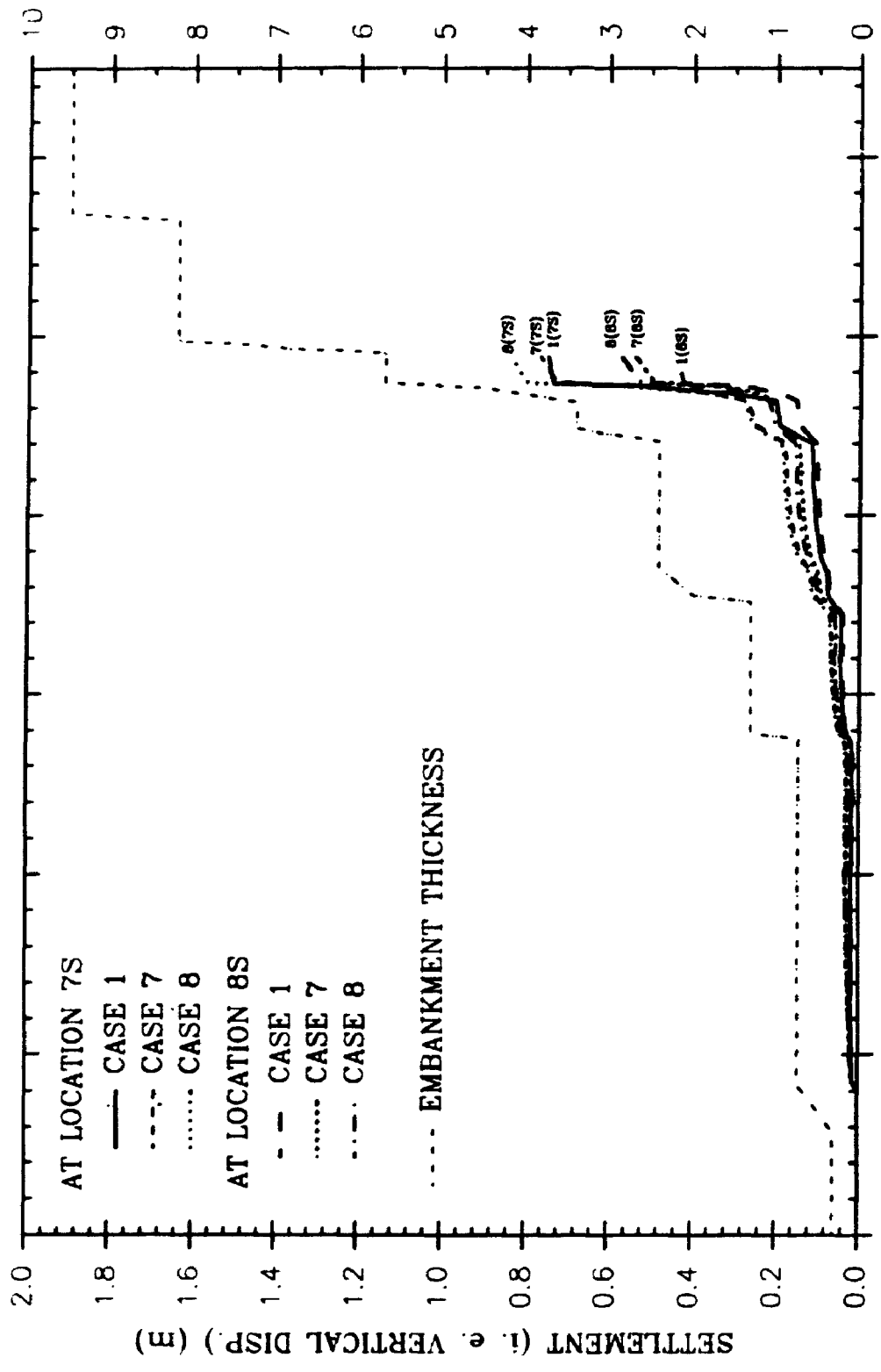

FIG. 9.29 VARIATION OF SETTLEMENT WITH TIME AT LOCATIONS 7S AND 8S

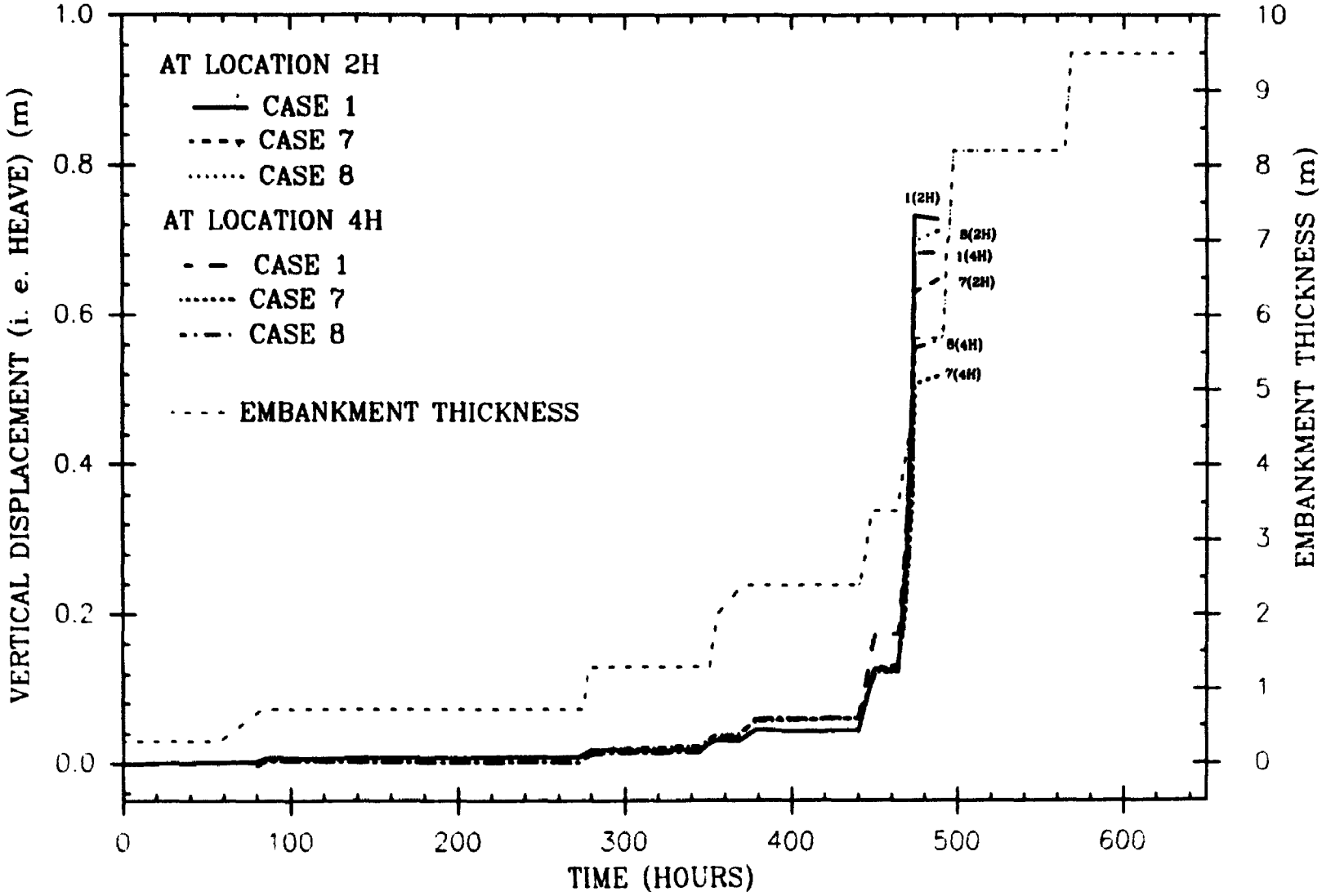

FIG 9.30 VARIATION OF VERTICAL DISPLACEMENT WITH TIME AT LOCATIONS 2H AND 4H

smaller heave in Case 7 compared to Case 1 and even smaller heave in Case 8 compared to Case 7. Thus, the calculated settlements increase significantly when the permeabilities of the foundation soil are increased and when the ϕ' of the fill material (and the geotextile-fill interface) are decreased. An opposite trend could be expected for the heave of the ground near the toe of the embankment at thicknesses above 3.4 m.

The horizontal deformations in the foundation soil at the toe of the embankment were very similar for all three cases (i.e. Cases 1, 7 and 8) up to about 2.4 m thickness (see Fig. 9.31) indicating that the changes of permeability of the foundation soil (i.e. Case 7) and ϕ' of the fill material (i.e. Case 8) considered here did not alter the horizontal deformations significantly up to about 2.4 m thickness. However, significantly lower horizontal deformations for the first 3 m depth of the foundation soil were indicated for Case 7 compared to Case 1 at 3.4 m thickness. The increased permeability for the foundation soil adopted in Case 7 (compared to Case 1) could result in increased consolidation thereby strengthening the soil, particularly for the soil near the surface, which is closer to the drainage boundary. In turn, this reduces the plasticity in the foundation soil and the lateral movement. No significant difference between Cases 7 and 8 were indicated at 3.4 m thickness indicating that the change in fill friction angle ϕ' considered here does not significantly change the horizontal deformations up to about 3.4 m thickness.

Large increases in the horizontal deformations were indicated during the construction of the embankment from 3.4 to 5.7 m for all three cases (see Fig. 9.32). Significantly reduced horizontal deformations were indicated in Case 7 compared to Case 1 for thicknesses above 3.4 m and the difference between the magnitude of horizontal deformations increased with increasing embankment thickness (e.g. the maximum deformation was 1.52 m in Case 1 whereas it was 1.12 m in Case 7 at 5.7 m thickness).

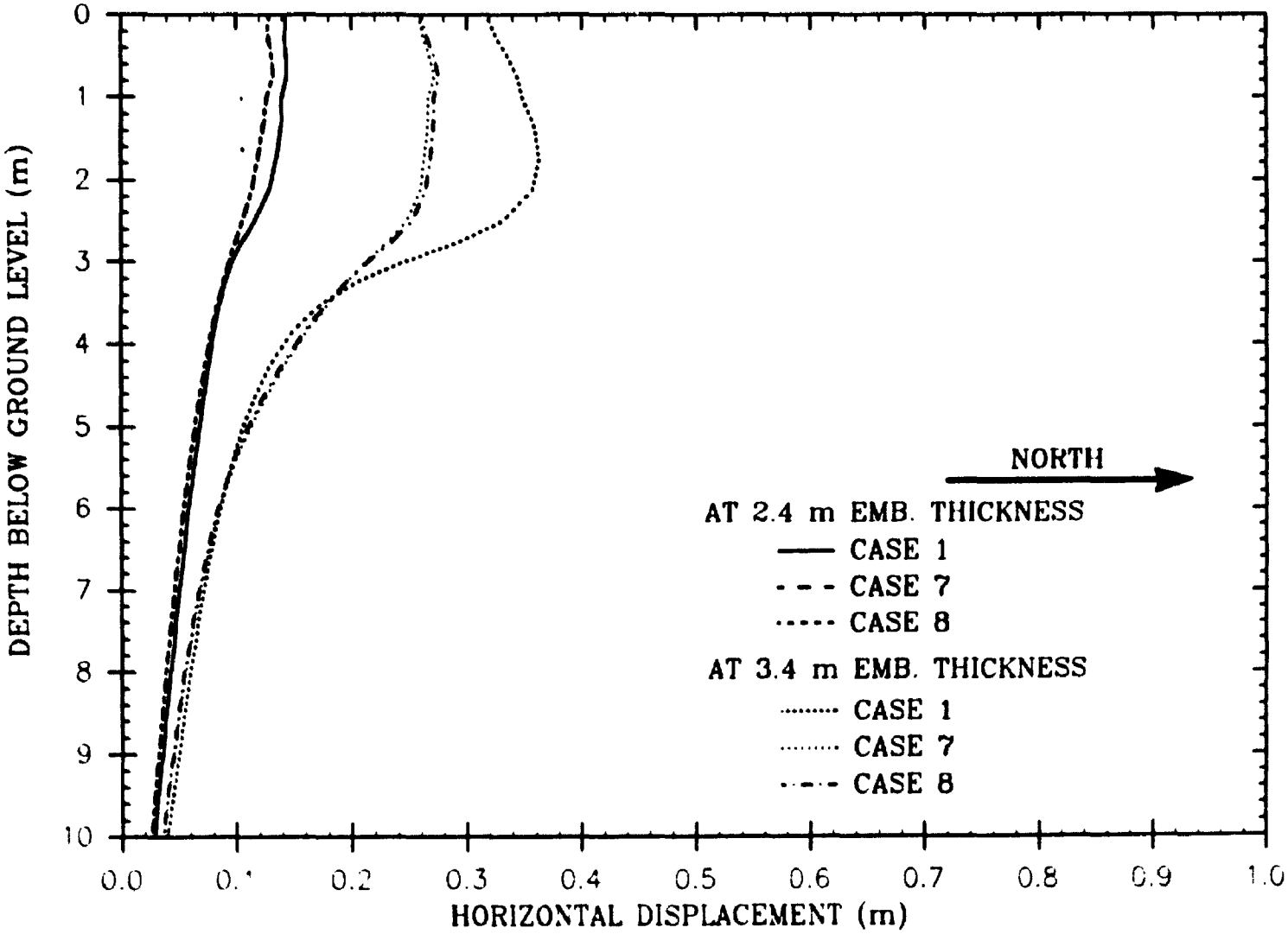

FIG 9.31 VARIATION OF HORIZONTAL DISP. WITH DEPTH AT 2.4 AND 3.4 m EMB THICKNESSES (i.e. AT 400 AND 449 HOURS) AT THE TOE OF EMBANKMENT

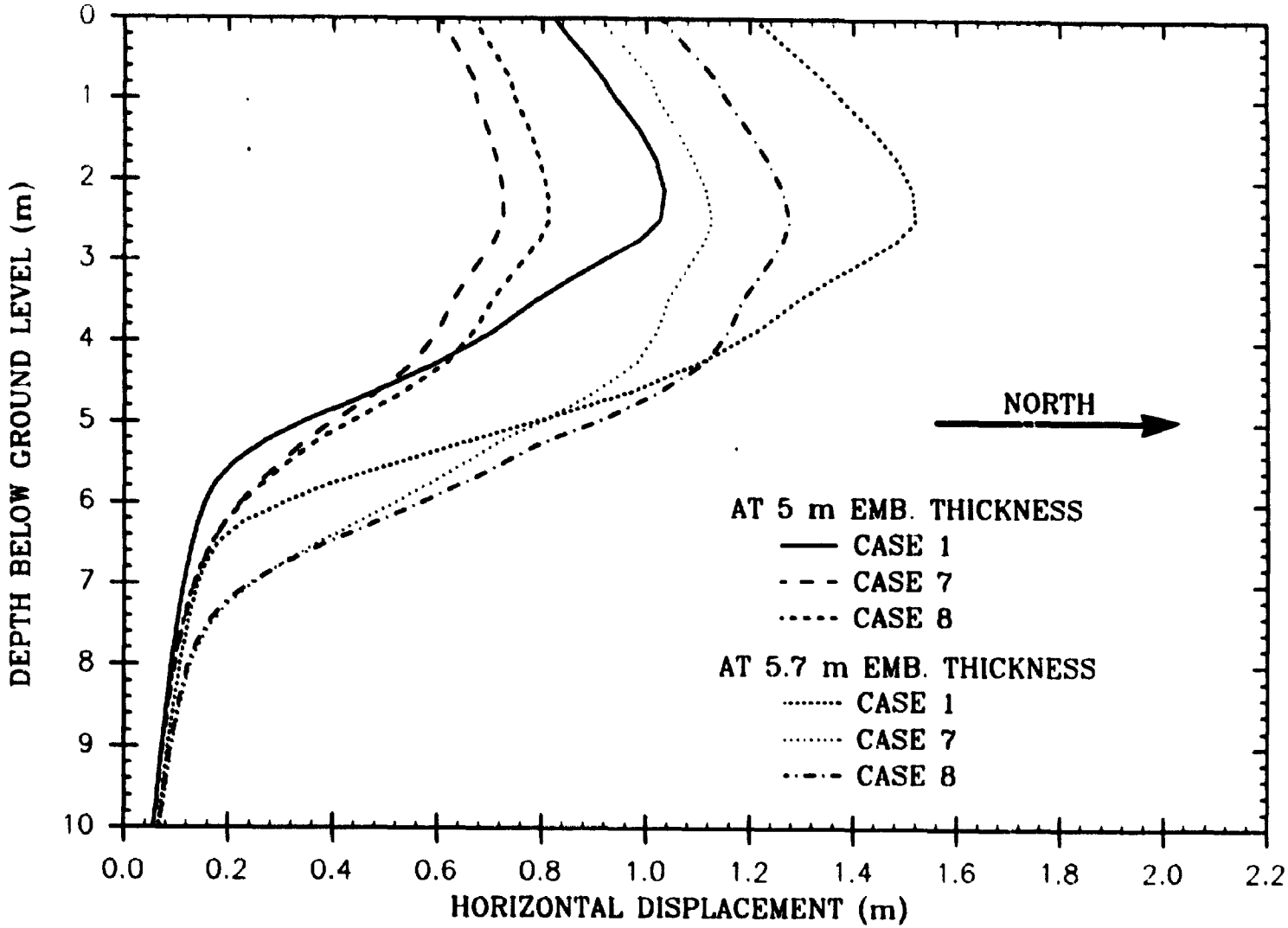

FIG. 9.32 VARIATION OF HORIZONTAL DISP. WITH DEPTH AT 5 AND 5.7 m EMB. THICKNESSES (i.e. AT 472 AND 475 HOURS) AT THE TOE OF EMBANKMENT

The difference in the development of plastic region in the foundation soil, as discussed earlier, is the cause for this behaviour. Case 8 with lower ϕ' for the fill resulted in increased horizontal deformation compared to Case 7 for fill thickness above 3.4 m.

The excess pore pressures in the foundation soil were quite different in Cases 1 and 7 (see Figs. 9.33 and 9.34). Larger dissipation of excess pore pressures at location P15 compared to P17 which is at a deeper location (i.e. at a larger distance from the drainage boundary) are clearly indicated. Again, larger dissipation of excess pore pressures are indicated in Cases 7 and 8 compared to Case 1, particularly during the brief stoppages of construction at 0.7, 1.3 and 2.4 m embankment thicknesses. Cases 7 and 8 with higher permeabilities for the foundation soil indicated much lower excess pore pressures compared with Case 1 even at higher embankment thicknesses. These differences in the excess pore pressure responses suggest that the permeability of the foundation soil can have a significant effect on the calculated excess pore pressures that develop at different stages of construction of the embankment for typical embankment construction rates.

The excess pore pressure responses in Cases 7 and 8 were essentially the same up to 5.7 m embankment thickness. This behaviour suggest that the changes of ϕ' of the fill considered between these cases would not significantly alter the excess pore pressures that develop in the foundation soil.

The strain developed in the geotextile reinforcement decreased in Case 7, compared to that obtained for Case 1 (see Figures 9.35 and 9.36 for the strain distributions across the geotextile for the different cases considered in this series of analyses). A decrease in the ϕ' of the fill (i.e. Case 8 compared with Case 7) resulted in an increase in the strain developed in the geotextile. The differences between the strain responses were not significant at low embankment thicknesses (say up to about 2.4 m thickness) but the

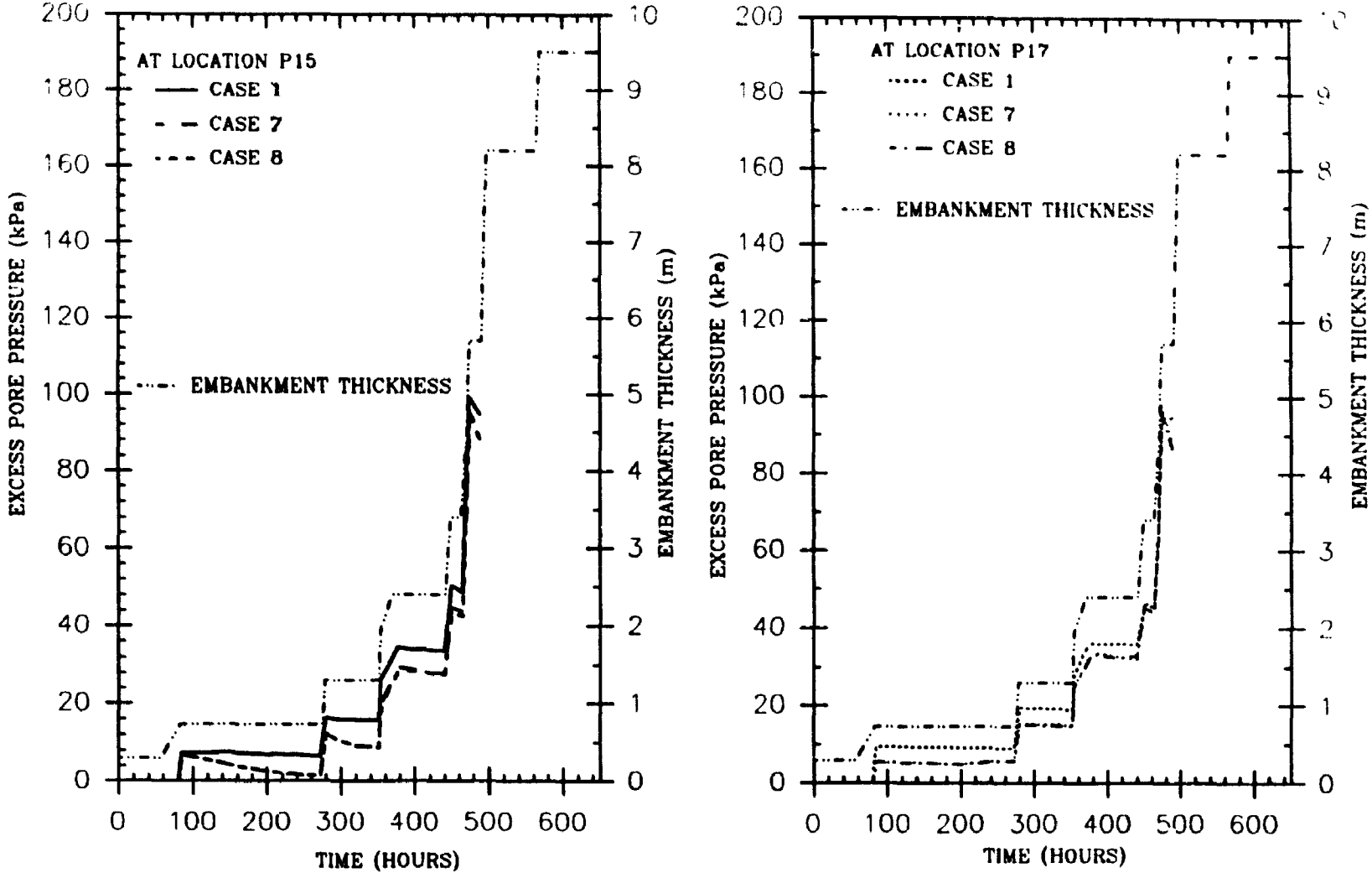

FIG. 9.33 VARIATION OF EXCESS PORE PRESSURE WITH TIME AT LOCATIONS P15 AND P17

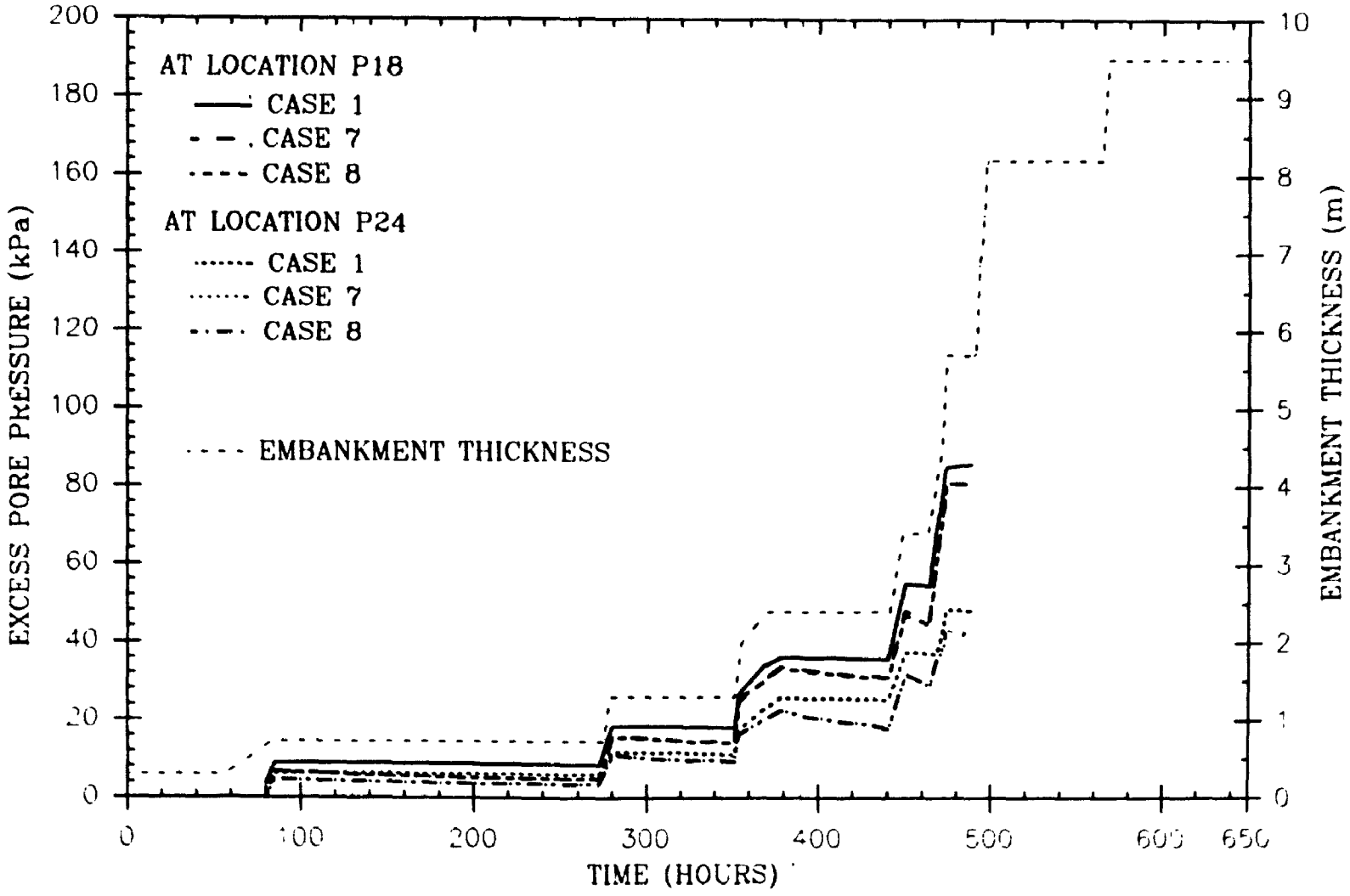

FIG 9.34 VARIATION OF EXCESS PORE PRESSURE WITH TIME AT LOCATIONS P18 AND P24

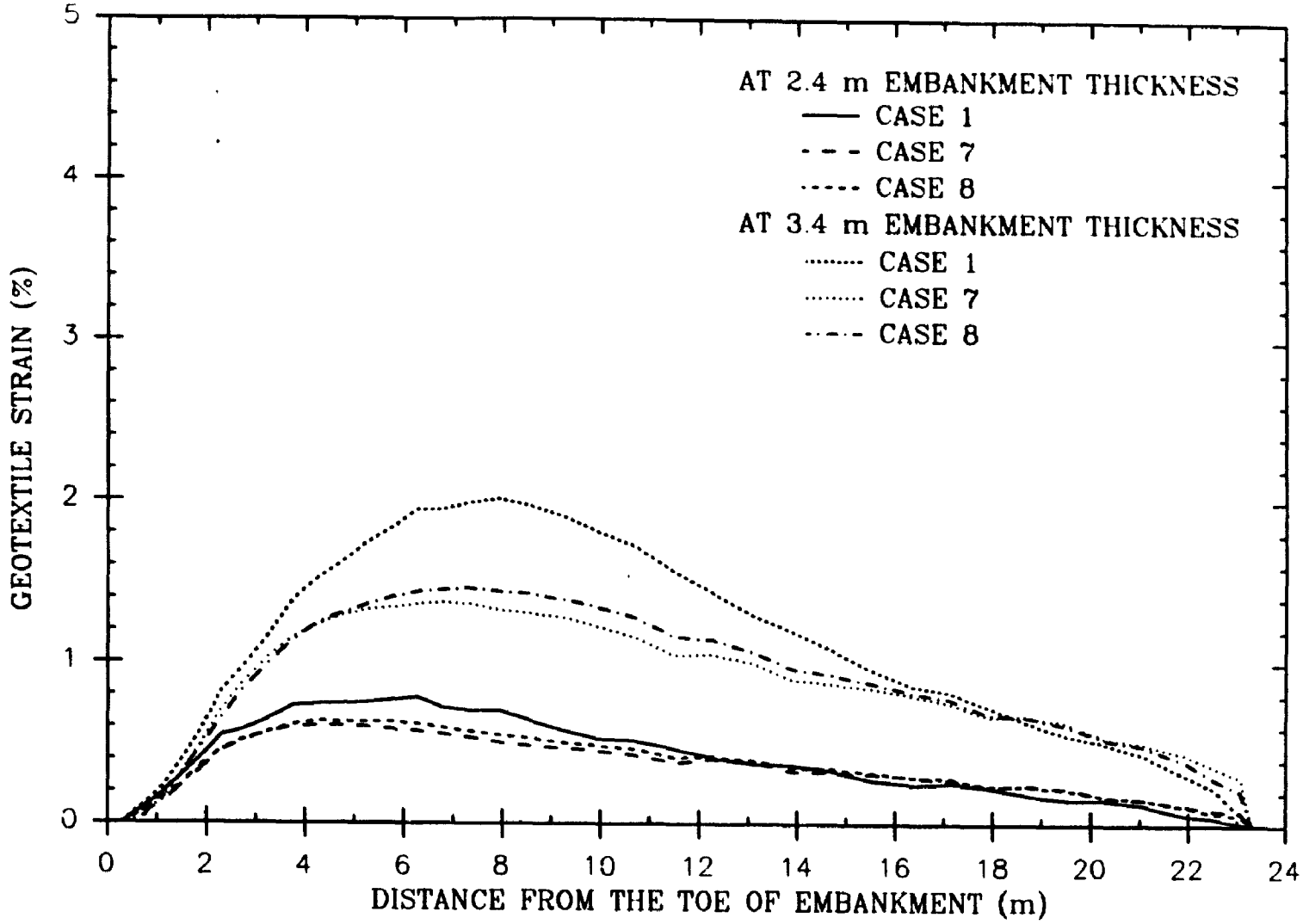

FIG. 9.35 GEOTEXTILE STRAIN DISTRIBUTION AT 2.4 AND 3.4 m EMBANKMENT THICKNESSES – LARGE STRAIN CONS. FINITE ELEMENT ANALYSIS RESULTS

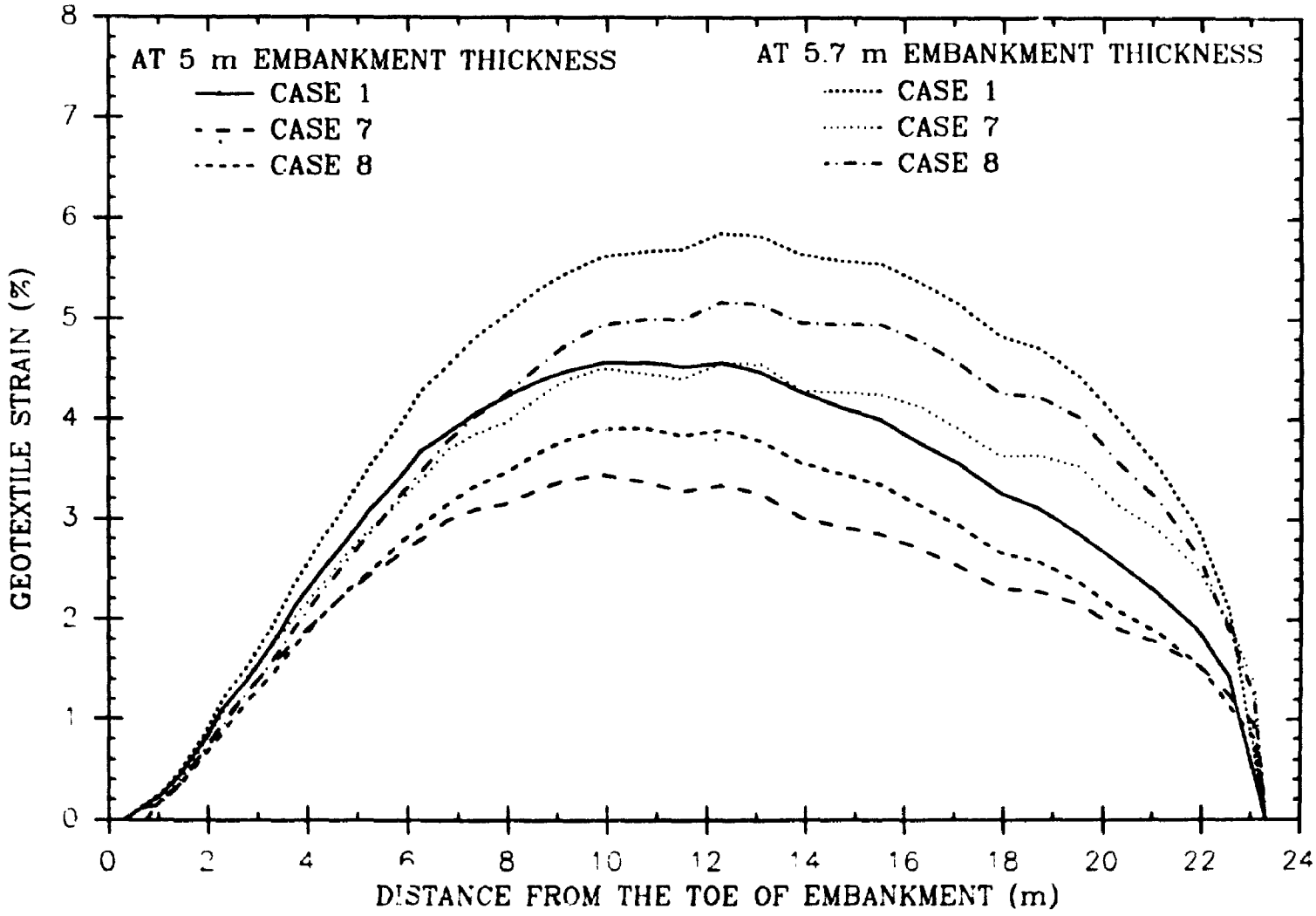

FIG. 9.36 GEOTEXTILE STRAIN DISTRIBUTION AT 5 AND 5.7 m EMBANKMENT THICKNESSES – LARGE STRAIN CONS. FINITE ELEMENT ANALYSIS RESULTS

differences increased with increasing embankment thickness. A similar pattern of variations were observed in the horizontal deformations in the foundation soil. As discussed previously, the higher permeability of the foundation soil would cause increased consolidation which in turn would result in increased strength and reduced plasticity in the soil. This is apparently the cause of decreased deformations and geotextile strain in Case 7 compared to Case 1.

Unfortunately, no data are available in the literature on the horizontal earth pressures developed in a settling fill containing a geotextile reinforcement. However, the horizontal earth pressure near the base of the fill could be expected to be $K\gamma H$ (where γ is the unit weight of fill, K is a coefficient of earth pressure and H is the thickness of fill). The coefficient K may range between K_o ($= 1 - \sin\phi'$) and K_a (i.e. the active state). When the friction angle, ϕ', of the fill (as well as the geotextile-fill interface) are decreased, both K_o and K_a ($= \frac{1 - \sin\phi'}{1 + \sin\phi'}$) would increase (but K_a would increase by a larger amount than that of K_o). It may be expected that K would increase when ϕ' is decreased, resulting in increased horizontal pressure in the embankment fill. When there are large movements in the foundation soil, the horizontal earth pressure at the base of the fill could be expected to approach $K_a\gamma H$ (i.e. active condition). As previously discussed, large movements in the foundation soil were evident at higher embankment thicknesses (say > 3.4 m, when significant plastic deformations were observed in the foundation soil). Therefore, the horizontal pressure at the base of the fill could be expected to increase resulting in an increase in the lateral thrust imposed on the foundation soil by the embankment when ϕ' of the fill is decreased. This would result in a larger force transferred to the geotextile, which is included in the embankment to provide additional stability to both the embankment and the foundation, and an increased shear transferred to the foundation soil. This is apparently the cause for the increased strain in the geotextile and larger lateral deformation in the foundation soil in Case 8 compared to Case 7 for the decrease of ϕ' of

the fill which were obvious at embankment thicknesses greater than 3.4 m (see Fig. 9.36).

9.3.5 Summary and discussion of consolidation analyses

A series of large strain consolidation analyses were performed to examine the effects of changing the OCR and the Poisson's ratio (v) of the foundation soil. These analyses indicated an overall elastic response for the embankment up to about 3.4 m thickness. The vertical and horizontal deformations were indicated to be small (typically less than 0.3 m) at low embankment thicknesses followed by large deformations for thicknesses above 3.4 m.

A change in the value of the Poisson's ratio of the foundation soil from 0.33 to 0.21 was examined in this series of analysis. The results of these analyses suggest that the settlement and heave at the ground surface, excess pore pressures in the foundation soil and the strain developed in the geotextile does not depend greatly on the Poisson's ratio of the foundation soil for all embankment thicknesses. The horizontal deformation in the foundation soil is affected by Poisson's ratio under essentially elastic condition (i.e. up to about 3.4 m thickness) and is not much affected thereafter (i.e. at thicknesses above 3.4 m, for this test embankment). Therefore, in an overall sense, the uncertainty regarding the Poisson's ratio wouldn't affect the results significantly, particularly after 3.4 m thickness when the responses are dominated by plasticity in the foundation soil. The Modified Cam - clay material model adopted in these analyses assumes an associated flow rule and isotropic behaviour as discussed previously in chapters 7 and 8.

The higher OCR values for the foundation soil near the ground surface (the existence of a typical crust) would result in a greatly reduced settlement and heave of the ground and the strain development in the geotextile even at higher embankment

thicknesses. It is therefore concluded that a good estimation of the OCR values of the foundation soil is crucial for accurate evaluation of the vertical and horizontal deformations as well as the strain developed in the geotextile. The excess pore pressures developed in the foundation soil did not vary significantly, at least up to 5.7 m thickness, for the v and OCR changes examined in series 1 analyses.

Effects of changing the ϕ', K_o and OCR of the foundation soil on the behaviour of the reinforced embankment were examined in series 2 analyses. A decrease of ϕ' from 28.2^o to 25.2^o indicated increases in the settlement (of the order of 20%) and heave of the ground and lateral deformation (in the order of 25% at the toe of embankment) in the foundation soil. Slightly increased excess pore pressures were indicated for this change of ϕ' of the foundation soil for embankment thicknesses between 2.4 and 3.4 m, apparently during the transition from predominantly elastic to plastic behaviour of the embankment. However, the difference was not significant when the embankment was constructed to 5.7 m thickness (i.e. the foundation soil apparently yielding at this stage). Increased geotextile strains were also indicated up to about 3.4 m thickness but no significant difference was evident at 5.7 m thickness.

The K_o values used in all the analyses discussed so far (i.e. Cases 1 to 4 and that reported in chapter 8) were based on field measurements (i.e. self boring pressuremeter tests conducted by NRC). However, the effects of changing the K_o values on the behaviour of the embankment was also examined in this sensitivity study. The K_o values evaluated using an empirical relationship proposed by Mayne and Kulhawy (1982) on the basis of field vane undrained shear strength were used in Case 5 (i.e. using eqn. 9.1) as previously discussed. Significant increases in settlement and heave of the ground as well as horizontal displacement in the foundation soil were observed for the above change in K_o. However, the changes indicated for the responses of excess pore pressures in the

foundation soil and the strain in the geotextile reinforcement were quite moderate. Therefore, a design based on such estimated values of K_o may result in a significant overprediction of vertical and horizontal displacements in the foundation soil as well as some moderate differences in the excess pore pressures in the foundation soil and the strain in the geotextile.

The OCR values used in Cases 1 to 5 were based on laboratory investigation reported in chapter 6. However, in many design situations, it is estimated on the basis of field vane undrained shear strength. The effects of using such estimated OCR values were investigated as Case 6. In this case, the OCR of the foundation soil evaluated using a typical empirical relationship (e.g. using eqn. 9.2 proposed by Mayne and Mitchell, 1988; and Kulhawy and Mayne, 1990) was used.

The OCR changes of the foundation soil considered between Cases 5 and 6 indicated large variations in the settlement and heave at the ground surface, lateral deformation in the foundation soil and the strain in the geotextile reinforcement. Significantly reduced settlements and heave as well as much smaller horizontal deformations and geotextile strains even at 5.7 m thickness were indicated for the changes of OCR considered here. Significantly reduced excess pore pressures were also indicated for embankment thicknesses above 3.4 m. It was apparent that the development of plasticity in the foundation soil is highly dependent on the OCR profile of the foundation soil which would alter the deformations in the foundation soil and the strain in the geotextile reinforcement. Therefore, a design based on such estimated values of OCR may result in a significant underprediction of vertical and horizontal displacements in the foundation soil as well as the strain in the geotextile.

The effects of increasing the permeability of the foundation soil and decreasing the

ϕ' of the embankment fill material were examined in series 3 analysis. The results indicated that the settlements would increase for either of these changes. The difference between the settlement responses are small at low embankment thicknesses (say < 3.4 m thickness) when an overall elastic behaviour is indicated for the behaviour of the embankment. The heave at the ground near the toe of the embankment indicated an opposite trend, for the changes considered in this series of analysis, compared to the settlement responses.

The calculated strain developed in the geotextile reinforcement decreased as a result of an increase in the permeability of the foundation soil. The geotextile strain increased as a result of a decrease in ϕ' of the embankment fill. These strain changes indicated were small at low embankment thicknesses but the differences increased with increasing embankment thickness, apparently with the growth of plasticity in the foundation soil. A similar pattern of changes were indicated for the horizontal deformations in the foundation soil at the toe of the embankment.

The excess pore pressures were greatly reduced due to the increase in permeabilities of the foundation soil considered here. These changes were evident at all embankment thicknesses suggesting that the uncertainties regarding permeabilities of the foundation soil would have a significant effect on the calculated excess pore pressures. The decrease in the ϕ' of the embankment fill considered here did not have much effect on the excess pore pressures developed in the foundation soil.

The limitations of the Modified Cam-clay to model the behaviour of natural soils were discussed previously in chapter 8. Due to these limitations, the sensitivity of various parameters examined may not be directly applied to soils which cannot be approximated with Modified Cam-clay material behaviour (e.g. highly anisotropic and/or

overconsolidated soils).

9.3.6 conclusions of consolidation analyses

The change of Poisson's ratio of the foundation soil from 0.33 to 0.21 did not indicate any significant change in the responses except the horizontal displacements during the overall elastic behaviour of the foundation soil (i.e. up to about 3.4 m thickness). Therefore, the uncertainty regarding the Poisson's ratio wouldn't affect the results of the analysis significantly.

The results indicated that the ϕ', K_o and OCR of the foundation soil are all important parameters and therefore should be measured or estimated cautiously for the accurate evaluation of settlement behaviour of the embankment, the deformations and excess pore pressures in the foundation soil and the strain in the geotextile reinforcement.

In many design situations, several parameters of the foundation soil are estimated using empirical relationships. One common situation is the estimation of the required design parameters on the basis of field vane undrained shear strength. The effects of using such estimated K_o and OCR values (on the basis of vane strength) were also investigated in this study. The results of this investigation indicate that a design based on such estimated values of K_o may result in a significant overprediction of vertical and horizontal displacements in the foundation soil as well as some moderate differences in the excess pore pressures in the foundation soil and the strain in the geotextile. A design based on the estimated values of OCR may result in large variations in the calculated vertical and horizontal displacements and excess pore pressures in the foundation soil as well as the strain in the geotextile. Therefore, considerable caution is required in the design of reinforced embankments on such soft compressible organic clayey silt deposits when such

design is based on vane strength.

A decrease in the effective friction angle of the embankment fill increases the calculated strain developed in the geotextile and horizontal and vertical displacements in the foundation soil. However, it may not have any significant effect on the excess pore pressures developed in the foundation soil.

The uncertainties regarding permeabilities of the foundation soil would have a significant effect on the calculated excess pore pressures, the vertical and horizontal displacements in the foundation soil and the strain developed in the geotextile reinforcement.

CHAPTER 10

CONCLUSIONS AND RECOMMENDATIONS

10.1 CONCLUSIONS

A test embankment was constructed until failure on a soft compressible organic clayey silt deposit between Sackville and Aulac in the Province of New Brunswick, Canada in September/October 1989. This embankment consisted of an unreinforced and a geotextile reinforced section and each section was instrumented with piezometers, settlement plates, augers, heave plates, inclinometers and a total pressure cell. A relatively high strength polyester woven geotextile was used as reinforcement and it was instrumented with three types of strain gauges. The site conditions, instrumentation, construction, monitoring and field performance of these embankments were investigated. A laboratory investigation was also performed to determine the parameters of the fo ndation soil, embankment fill and the geotextile reinforcement.

A numerical model was developed to perform fully coupled large strain elasto-plastic consolidation analysis with Modified cam-clay material behaviour using 15-noded cubic strain triangular elements. This finite element model was used to back analyze the above test embankments. Rigorous finite element analyses were also performed to study the sensitivity of embankment behaviour to variations in the foundation soil and embankment fill properties. In particular, the influence of the variation of over consolidation ratio (OCR), the coefficient of earth pressure at rest (K_o), angle of internal friction, Poisson's ratio and the permeability of the foundation soil as well as the effective friction angle of the embankment fill were examined. Both small strain and large strain undrained finite element models were also used to back analyze the reinforced

embankment and the effect of changing the undrained shear strength profile on the behaviour of this embankment was examined.

The following conclusions can be drawn from this study.

1. The field performance of full scale unreinforced and geotextile reinforced embankments constructed on a soft compressible organic clayey silt have been investigated. Geotechnical instruments such as piezometers, inclinometers, settlement plates, settlement augers, heave plates and total pressure cells were used successfully to monitor the behaviour of these embankments.

2. The unreinforced embankment behaved elastically up to a thickness of about 3.4 m and it approached failure at a thickness of about 6.1 m. The failure was of plastic (or visco-plastic) type and no classical type abrupt failure was encountered during the construction of this embankment.

3. The height to which the unreinforced embankment could be constructed (i.e. 6.1 m thickness) was substantially less than the 9.2 m failure thickness (and below the range 7.0 - 11.4 m, determined for the range of vane strengths) indicated from conventional limit equilibrium analysis based on vane strength data. Therefore, considerable caution is required for the design of embankments on such soft organic clayey silt deposits if such design is based on vane strength and on the use of simple limit equilibrium design procedures. It is suggested that this may be evidence of time-dependent progressive failure in the soil.

4. The geotextile reinforcement had been successfully instrumented with electrical, electromechanical and mechanical gauges to monitor the strain during the

construction of the reinforced embankment.

5. The reinforced embankment behaved elastically up to about 3.4 m thickness. The horizontal deformation, geotextile strain and excess pore pressure responses suggested that the foundation soil approached failure at a thickness of about 5.7 m. It was possible to construct the embankment above 5.7 m only because of the influence of the geotextile, and the reinforced embankment failed at a thickness of about 8.75 m. This was a plastic-type failure and no classical type of abrupt failure was encountered during the construction of this embankment. There was evidence of time dependent (progressive) failure in the foundation soil for embankment heights above 5.7 m.

6. The failure thickness of 8.75 m for the reinforced embankment indicated from the field investigation is significantly above the 8.2 m determined from limit equilibrium analysis on the basis of average vane strength profile (and well within the range of 6.6 - 11.1 m determined from the range of vane strength profile). This suggest that the relative benefits of reinforcement may be even greater for the type of soil investigated in this test embankment (soft compressible organic clayey silt) than they are for perfectly plastic or work hardening soils.

7. A fully coupled large strain elasto-plastic Biot consolidation finite element model was developed to perform an effective stress analysis which appears to be suitable for the investigation of consolidation behaviour of reinforced and unreinforced embankments on soft soils.

8. Reasonably good overall agreement was obtained between the predictions made using the above finite element model and the field measurements for settlements,

heaves, horizontal displacements and geotextile strains. The agreement was less satisfactory for excess pore pressures which were over predicted after about 5.7 m thickness. The settlements in the foundation soil at depth greater than about 4 m were underpredicted after 3.4 m thickness. The large displacements and large increases in geotextile strains observed in the field after reaching 8.2 m thickness could not be predicted satisfactorily from this analysis.

9. The uncertainty regarding the Poisson's ratio of the foundation soil wouldn't affect the results of a consolidation analysis significantly. However, it could have some influence on the horizontal deformations during the overall elastic behaviour of the foundation soil.

10. The effective friction angle (ϕ'), K_o and OCR of the foundation soil are all important parameters and therefore should be measured or estimated cautiously for the accurate evaluation of settlement behaviour of the embankment, the deformations and excess pore pressures in the foundation soil and the strain in the geotextile reinforcement.

11. The use of estimated K_o and OCR values on the basis of vane strength were examined in the sensitivity study. The results of this investigation indicate that a design based on estimated values of K_o may result in a significant overprediction of vertical and horizontal displacements in the foundation soil as well as some moderate differences in the excess pore pressures in the foundation soil and the strain in the geotextile. A design based on the estimated values of OCR may result in large variations in the calculated vertical and horizontal displacements and excess pore pressures in the foundation soil as well as the strain in the geotextile. Therefore, considerable caution is required in the design of reinforced

embankments on such soft compressible organic clayey silt deposits when such design is based on vane strength.

12. The uncertainties regarding permeabilities of the foundation soil would have a significant effect on the calculated excess pore pressures and may result in significant changes in the vertical and horizontal displacements in the foundation soil and the strain developed in the geotextile reinforcement.

13. A decrease in the effective friction angle of the embankment fill may result in significant increases in the strain developed in the geotextile and horizontal and vertical displacements in the foundation soil. However, it may not have any significant effect on the excess pore pressures developed in the foundation soil.

14. The failure of the reinforced embankment could be predicted accurately by a small strain undrained finite element analysis using the mean shear strength profile between the field vane and the CAU triaxial and constant volume simple shear tests in the lab. This analysis underpredicted the settlements after 5.7 m thickness. The horizontal deformations and geotextile strains were also underpredicted.

10.2 RECOMMENDATIONS

Future work is required to accurately model the vertical cuts made on the foundation soil near the ground surface. The improvement of the numerical model to consider the viscous/creep effects and progressive failure as well as the effects of initial incomplete saturation of the foundation soil are also recommended. Further laboratory investigation would also be needed to determine the parameters required to model these effects.

The possible anisotropic behaviour of the foundation soil also need to be investigated and included in the numerical model. Additional investigation regarding the in situ permeabilities and drainage conditions is also desirable for possible improvement of the predictions.

Other well instrumented field studies should also be analyzed in order to further validate and refine the numerical model used in this thesis.

REFERENCES

Airey, D.W. and Wood, D.M. (1987). An evaluation of direct simple shear tests on clay. Geotechnique 37, No. 1, pp 25-35.

Almeida, M.S.S. and Ortigao, J.A.R. (1982). "Performance and finite element analysis of a trial embankment on soft clay." Proceeding of the International Symposium on Numerical Models in Geomechanics, Zurich, Switzerland, pp. 548-558.

Almeida, M.S.S., Davies, M.C.R. and Parry, R.H.G. (1985). "Centrifuged embankments on strengthened and unstrengthened clay foundations." Geotechnique, Vol. 35(4), pp. 425-441.

Almeida, M.S.S., Britto, A.M. and Parry, H.G. (1986). Numerical modelling of a centrifuged embankment on soft clay. Canadian Geotechnical Journal, Vol. 23, pp. 103-114.

Andrawes, K.Z., McGown, A., Mashhour, M.M. and Wilson-Fahmy, R.F. (1980). "Tension resistant inclusions in soils." Journal of Geotechnical Engineering Division, ASCE, Vol. 106, No. GT12, pp. 1313-1326.

Atkinson, J.H. and Bransby, P.L. (1978). The Mechanics of Soils - An Introduction to Critical State Soil Mechanics, McGraw-Hill, London, U.K.

Becker, D.E., Crooks, J.H.A., Been, K., and Jefferies, M.G. (1987). Work as a criterion for determining in situ and yield stresses in clays. Canadian Geotechnical Journal, Vol. 24, pp 549-564.

Bell, J.R., Greenway, D.R. and Vischer, W. (1977). "Construction and analysis of a fabric reinforced low embankment on muskeg." Proceedings, 1st. International Conference on the Use of Fabrics and Geotechnics, Paris, France, pp. 71-76.

Bishop, A.W. 1967. Progressive failure - with special reference to the mechanism causing it. Proc. Geotech. Conf., Oslo, Vol. 2, pp. 142-150.

Bjerrum, L. and Landva, A. (1966). Direct simple shear tests on a Norwegian quick clay. Geotechnique, Vol. 16, No. 1, pp 1-20.

Bjerrum, L. (1967). Progressive failure in slopes of over-consolidated plastic clay and clay shales. Proc. A.S.C.E., Vol. 93, SM5, pp. 1-49.

Bjerrum, L. (1972). Embankment on soft ground. Proceedings, ASCE Specialty Conference on Performance of Earth and Earth-Supported Structures, Volume 2, pp. 1-54.

Bjerrum, L. (1973). Problem of soil mechanics and construction on soft clays. Proceedings of the 8th International Conference on Soil Mechanics and Foundation Engineering, Moscow, State of the Art Report. Vol. 3, pp. 111-159.

Bonaparte, R. and Christopher, B.R. (1987). "Design and construction of reinforced embankments over weak foundations." Transportation and Research Record, No. 1153, pp. 26-39.

Boutrup, E. and Holtz, R.D. (1983). "Analysis of embankments on soft ground reinforced with geotextiles." Proceedings of the VIII European Conference on Soil Mechanics and Foundation Engineering, ECSMFE, Helsinki, Finland, pp. 469-472.

Brakel, J., Coppens, M., Maagdenberg, A.C. and Risseuw, P. (1982). "Stability of slopes constructed with polyester reinforcing fabric, test section at Almere, Holland 1979." Proceedings of Second International Conference on Geotextiles, Las Vegas, Nevada, U.S.A., Vol. 3, pp. 727-732.

Britto, A.M. and Gunn, M.J. (1987). Critical state soil mechanics via finite elements. Ellis Horwood, Chichester, England.

Budhu, M. (1984). Nonuniformities imposed by simple shear apparatus. Canadian Geotechnical Journal, Vol. 21.

Burmister, D.M. (1942). Laboratory investigation of soils at Flushing Meadow Park. Transactions of the American Society of Civil Engineers, **107**: 187.

Burmister, D.M. (1951). The application of controlled test methods in consolidation testing. Symposium on Consolidation Testing of Soils. American Society for Testing and Materials, Special Technical Publication 126, p. 83.

Carter, J.P., Booker, J.R. and Davis, E.H. (1977). "Finite deformation of an elasto-plastic soil."International Journal of Numerical and Analytical Methods in Geomechanics, Vol. 1, pp. 25-43.

Carter, J.P., Booker, J.R. and Small, J.C. (1979). "The analysis of finite elasto-plastic consolidation." International Journal of Numerical and Analytical Methods in Geomechanics, Vol. 3, No. 2, pp. 107-130.

Carter, J.P. and Balaam, N.P. (1990). AFENA - A general finite element algorithm - User's Manual, School of Civil and Mining Engineering, University of Sydney, N.S.W. 2006, Australia.

Casagrande, A. (1936). The determination of the preconsolidation load and its practical significance. Proceedings, First International Conference on Soil Mechanics and Foundation Engineering, Cambridge, Vol. 3, pp 60-64.

Chandler, J.R. (1988). The insitu measurement of the undrained shear strength of clays using the field vane. Vane shear strength testing in soils: Field and laboratory studies (STP 1014), ASTM, Philadelphia, pp 13-44.

Crawford, C.B. (1986). State of the art: Evaluation and interpretation of soil consolidation tests. Consolidation of soils: Testing and evaluation, A symposium sponsored by ASTM Committee D-18 on Soil and Rock, Ft. Lauderdale, Fla., ASTM Special Publication 892, pp 71-103.

Davis, E.H. (1968). "Theories of plasticity and failure of soil masses." Chapter 6 in Soil Mechanics - Selected Topics, I.K. Lee (Ed.), Butterworths.

Davis, E.H. and Booker, J.R. (1973). "The effect of increasing strength with depth on the bearing capacity of clays." Geotechnique, Vol. 23, No. 4, pp. 551-563.

Dienes, J.K. (1979). "On the analysis rotation and stress rate in deforming bodies." Acta Mechanica, 32: 217-232.

Draft CGSB Standard, (1986). Draft of the new test method CAN/CGSB-148.1 No. 7.2-M - Tensile properties of geotextile fabric - 200 mm wide strip method, Methods for testing geotextiles and geomembranes, Canadian General Standards Board, Ottawa, Canada.

Enka Industrial Systems Group. (1987). "Design guidelines for reinforced embankments on soft subsoil using Stabilenka reinforcing mats." Arnhem, The Netherlands.

Fisher, D.G. (1982). The behaviour of foundations on non-homogeneous soils. M. E. Sc. Thesis. The University of Western Ontario, London, Ontario, Canada.

Fisher, D. G., Rowe, R. K. and Lo, K. Y. (1982). Prediction of second stage behaviour of the Gloucester Test Fill - Part 1: Predictions. Research Report GEOT-3-82, Faculty of Engineering Science, University of Western Ontario

Fisher, D. G., Rowe, R. K. and Lo, K. Y. (1982). Prediction of second stage behaviour of the Gloucester Test Fill - Part 2: Method of Analysis. Research Report GEOT-4-82, Faculty of Engineering Science, University of Western Ontario

Folkes, D.J. and Crooks, J.H.A. (1985). Effective stress paths and yielding in soft clays below embankments. Canadian Geotechnical Journal, Vol. 22, pp. 357-374.

Fowler, J. (1982). "Theoretical design considerations for fabric reinforced embankments." Proceedings of Second International Conference on Geotextiles, Las Vegas, Nevada, U.S.A., Vol. 2, pp. 665-670.

Geonor. (1968). Description and instruction for use of Direct simple shear test apparatus (Model h-12), Geonor, Oslo, Norway.

Haliburton, T.A. (1981). "Use of engineering fabric in road and embankment construction." Seminar on The Use of Synthetic Fabrics in Civil Engineering, Toronto, Ontario, pp. 66-94.

Head, H.K. (1982). Manual of soil laboratory testing. John Wiley and Sons, New York, USA.

Hibbitt, H.D., Marcal, P.V. and Rice, J.R. (1970). "A finite element formulation for problems of large strain and large displacement." Int. J. Solids and Structures, 6:1060-1086.

Hird, C.C. and Kwok, C.M. (1989). "Finite element studies of interface behaviour in reinforced embankments on soft ground." Computers and Geotechnics, Vol. 8, No. 2, pp. 111-131.

Humphrey, D.N. and Holtz, R.D. (1989). "Effect of surface crust on reinforced embankment." Proceedings of Geosynthetic '89 Conference, San Diego, U.S.A., pp. 136-147.

Indraratna, B., Balasubramaniam, A.S. and Balachandran, S. (1992). "Performance of test embankment constructed to failure on soft marine clay." ASCE Journal of Geotechnical Engineering, Vol. 118, No.1, pp. 12-33.

Ingold, T.S. (1982). "An analytical study of geotextile reinforced embankments." Proceedings of Second International Conference on Geotextiles, Las Vegas, Nevada, U.S.A., Vol. 2, pp. 683-688.

Janbu, N. (1963). "Soil compressibility as determined by oedometer and triaxial tests." Proceedings of the European Conference on Soil Mechanics and Foundation Engineering, Wiesbaden, Germany, Vol. 1, pp. 19-25.

Janbu, N., Tokheim, O., and Senneset, K. (1981). Consolidation test with continuous loading. Proceedings, 10th International Conference on Soil Mechanics and Foundation Engineering, Stockholm, Vol. 1, pp 645-654.

Jaumann, G. (1911). Sitzungsberichte akad. Wiss. Wien., 120:385.

Jewell, R.A. (1982). "A limit equilibrium design method for reinforced embankments on soft foundations." Proceedings of Second International Conference on Geotextiles, Las Vegas, Nevada, U.S.A., Vol. 2, pp. 671-676.

Johnson, K. (1984). A preliminary study of testing procedures used in the determination of major peat design parameters. ES500 M. Eng. Project Report, The University of Western Ontario, London, Ontario.

Kaniraj, S.R. and Abdullah, H. (1992). "Reinforcement force in embankments on soft soils." Proceedings of the International Symposium on Earth Reinforcement Practice, Fukuoka, Kyushu, Japan, pp. 254-250.

Kavazanjian, E. and Poepsel, P.H. (1984). "Numerical analysis of two embankment foundations." Proceedings, ASCE Symposium on Sedimentation Consolidation Models, San Francisco, CA, pp. 84-106.

Keenan, G. H., Landva, A. O., Valsangkar, A. J. and Comier, R. J. (1986). Performance and failure of test embankment on organic silty clay, Proc. Conf. on Building on Marginal and Derelict Land, Glasgow, The Institution of Civil Engineers, Vol. 2, pp. 417-428.

Kirby, C. R. and Lambe, T. W. (1972). Design of embankment soft soils. MIT Research Report, R72-36, Soils Publication 307.

Kulhawy, F.H. and Mayne, P.W. (1990). Manual on estimating soil properties for foundation design. Electric Power Research Institute EL-6800, Project 1493-6, Final Report prepared by Cornell University.

La Rochelle, P., Trak, B., Tavenas, F. and Roy, M. (1974). Failure of a test embankment on a sensitive champlain clay deposit. Canadian Geotechnical Journal, 11, pp 142-164.

Leroueil, S., Tavenas, F., Trak, B., La Rochelle, P. and Roy, M. (1978a). Construction pore pressures in clay foundations under embankments. Part I: the Saint-Alban test fills. Canadian Geotechnical Journal, 15, pp 54-65.

Leroueil, S., Tavenas, F., Mieussens, C. and Peignaud, M. (1978b). Construction pore pressures in clay foundations under embankments. Part II: generalized behaviour. Canadian Geotechnical Journal, 15, pp 66-82.

Leroueil, S., Magnan, J.P. and Tavenas, F. (1990). Embankments on soft clays. Ellis Horwood Series in Civil Engineering, Geotechnics Section, Ellis Horwood Ltd., England.

Lo, K.Y. (1965). Stability of slopes in anisotropic soils. Journal of the Soil Mechanics and Foundation Division, ASCE, Vol. 91, No. SM4, pp 85-106.

Lo, K. Y. (1966). The stress-strain pore pressure relationship of normally consolidated clays. Ph.D. Thesis. University of London, England.

Lo, K.Y. (1972). An approach to the problem of progressive failure. Canadian Geotechnical Journal, Vol. 9, pp. 407-429.

Low, B.K., Wong, K.S., Lim, C. and Broms, B.B. (1990). "Slip circle analysis of reinforced embankments on soft ground." International Journal of Geotextiles and Geomembranes, Vol. 9, No. 1, pp. 165-181.

Magnan, J.P. (1984). Modelisation numerique du comportement des argiles lolles naturelles. These de Doctorat es Sciences. Universite Paris VI, Paris, France.

Marche, R. and Chapuis, R. (1974). Controle de la stabilite des remblais par la measure des desplacements horizontaux. Canadian Geotechnical Journal, 11, pp. 182-201.

Matar, M. and Salencon, J. (1977). "Capacite portante a une semelle filante sur sol purement coherent d'epaisseur limitee et de cohesion variable avec la profondeur." Annales de l'Institute Technique du Batiment et des Travaux Publics, Supplement No. 352, Serie: Sols et Fondations, No. 143, pp. 95-107.

Mayne, P.W. and Kulhawy, F.H. (1982). K_o - OCR relationships in soil. Journal of the Geotechnical Engineering Division, ASCE, Vol. 108, No. GT6, pp. 851-872.

Mayne, P.W. and Mitchell, J.K. (1988). Profiling of overconsolidation ratio in clays by field vane. Canadian Geotechnical Journal, Vol. 25, No. 1, pp. 150-157.

Milligan, V. and La Rochelle, P. (1984). "Design methods for embankments over weak soils." Symposium on Polymer Grid Reinforcement in Civil Engineering, Institute of Civil Engineers, London, England, Paper No. 3.4, pp. 95-102.

Monnet, J., Gourc, J.P. and Mommes, M. (1986). "Study of soil geotextile interaction - a reinforced embankment." Proceedings of the International Symposium on Numerical Models in Geomechanics, Ghent, pp. 539-542.

Mylleville, B.L.J. and Rowe, R.K. (1988). "Simplified undrained stability analysis for use in the design of steel reinforced embankments on soft foundations." GEOT-3-88, Research Report, Geotechnical Research Centre, Faculty of Engineering Science, The University of Western Ontario, London, Ontario, 123p.

Mylleville, B.L.J. and Rowe, R.K. (1991). "On the design of reinforced embankments on soft brittle clays." Proceedings of Geosynthetics '91, Atlanta, Georgia, U.S.A., pp. 395-408.

Mylleville, B.L.J. (1991). "Behaviour of heavily reinforced embankments on soft foundations." Ph.D. Thesis, The University of Western Ontario, London, Ontario.

Nagtegaal, D.J., Parks, D.M. and Rice, J.R. (1974). "On numerically accurate finite element solutions in the fully plastic range." Comp. Meth. Appl. Mech. Engrg., 4, pp. 153-177.

Ohta, H., Mochinaga, R. and Kurihara, N. (1980). "Investigation of soft foundations with surface reinforcement." Proceedings of the 3rd Australia-New Zealand Conference on Geomechanics, Wellington, New Zealand, Vol. 1, pp. 123-128.

Oldroyd, J.G. (1950). "On the formulation of rheological equations of state." Proc. Roy. Soc., 200, pp. 523-541.

Ortigao, R. J. A., Werneck, M. L. G. and Lacerda, W. A. (1983). Embankment failure on clay near Rio De Janeiro. ASCE Journal of the Geotechnical Engineering Division, 109, No. 11, pp 1460-1479.

Parry, R.H.G. and Nadarajah, V. (1973). "Observations in laboratory prepared lightly overconsolidated kaolin." Geotechnique, 24, pp. 345-357.

Poulos, H.G. (1972). Difficulties in prediction of horizontal deformations of foundations. ASCE Journal of the Soil Mechanics and Foundations Division, Vol. 98 (SM8), pp. 843-848.

Prager, W. (1961). "An elementary discussion of definitions of stress rate." Quart. Appl. Math., Vol. 18, pp. 403-407.

Prevost, J.H. and Hoeg, K. (1976). Reanalysis of simple shear soil testing. Canadian Geotechnical Journal, Vol. 13, pp

Rampton, V. N. and Paradis, S. (1981). Quarternary geology of Amherst - Map area 21H, New Brunswick. Mineral Development Branch, Department of Natural Resources, Fredericton, New Brunswick, Map report 81-3.

Roscoe, K.H. and Burland, J.B. (1968). "On the generalized behaviour of 'wet' clay." In Engineering plasticity. Edited by J. Heyman, and F. Lecckie. Cambridge University Press, London, England, pp. 535-609.

Rosenquist, I.Th. (1959). Physico-chemical properties of soils: Soil-water systems. Journal of the Soil Mechanics and Foundation Division, ASCE, Vol. 85, No. SM2, Proc. Paper 2000.

Rowe, R.K. (1982). "The analysis of an embankment constructed on a geotextile." Proceedings of Second International Conference on Geotextiles, Las Vegas, Nevada, U.S.A., Vol. 2, pp. 677-682.

Rowe, R.K. (1984). "Reinforced embankments: analysis and design." Journal of Geotechnical Engineering Division, ASCE, Vol. 110, No. 2, pp. 231-247.

Rowe, R.K. and Soderman, K.L. (1984). Comparison of predicted and observed behaviour of two test embankments. Geotextiles and Geomembranes, Vol. 1, pp. 143-160.

Rowe, R.K. and Soderman, K.L. (1985). "An approximate method for estimating the stability of geotextile-reinforced embankments." Canadian Geotechnical Journal, Vol. 22, No. 3, pp. 392-398.

Rowe, R.K. and Soderman, K.L. (1987). "Stabilization of very soft soils using high strength geosynthetics: the role of finite element analyses." International Journal of Geotextiles and Geomembranes, Vol. 6, No. 1, pp. 53-80.

Rowe, R. K. and Soderman, K. L. (1987). Reinforcement of embankments on soils whose strength increases with depth. Proceedings of Geosynthetics '87, New Orleans, pp. 266-277.

Rowe, R.K. and Soderman, K.L. (1988). Stabilization of very soft soils using high strength geosynthetics: The role of finite element analysis. Geotextiles and Geomembranes, Vol. 6, No. 1.

Rowe, R.K., MacLean, M.D. and Soderman, K.L. (1984). "Analysis of a geotextile-reinforced embankment constructed on peat." Canadian Geotechnical Journal, Vol. 21, No.3, pp. 563-576.

Rowe, R.K., Ho, S.K. and Fisher, D.G. (1985). Determination of soil-geotextile interface strength properties. Proc. 2nd canadian Symposium on Geotextiles and Geomembranes, Edmonton, pp. 25-34.

Rowe, R.K. and Mylleville, B.L.J. (1989). "Consideration of strain in the design of reinforced embankments." Proceedings of Geosynthetic '89 Conference, San Diego, U.S.A., pp. 124-135.

Rowe, R.K. and Mylleville, B.L.J. (1990). "Implications of adopting an allowable geosynthetic strain in estimating stability." Proceedings of 4th International Conference on Geotextiles and Geomembranes, The Hague, The Netherlands, pp. 131-136.

Saada, A.S. and Townsend, F.C. (1981). State of the art: Laboratory strength testing of soils. Laboratory shear strength of soil. American Society for Testing and Materials, pp 7-77.

Schimelfenyg, P., Fowler, J. and Leshchinsky, D. (1990). Fabric reinforced containment dike, New Bedford superfund site. Proceedings of the 4th. International Conference on Geotextiles Geomembranes and Related Products, The Hague, Netherlands., Volume 1, pp. 149-154.

Schmertmann, J.M. (1955). The undisturbed consolidation of clay. Transactions of the American Society of Civil Engineers, **120**: 1201.

Schofield, A.N. and Wroth, C.P. (1968). Critical state soil mechanics. McGraw-Hill, London, England

Sloan, S.W. and Randolph, M.F. (1982). "Numerical prediction of collapse loads using finite element methods." International Journal of Numerical and Analytical Methods in Geomechanics, Vol. 6, pp. 47-76.

Sloan, S.W. (1984). "Plastic collapse calculations using high-order elements." Proceedings of Int. Conf. Accuracy Estimates and Adaptive Refinements in Finite Element Computations (ARFEC), Lisbon, pp. 301-313.

Sluimer, G. and Risseew, P. (1982). A strain gauge technique for measuring deformations in geotextiles. Proceedings of the Second International Conference on Geotextiles, Las Vegas, U.S.A., pp. 835-838.

Study Centre for Road Construction (SCW). (1981). Stability of slopes constructed with polyester reinforcing fabric. Arnhem, The Netherlands.

Tavenas, F. (1981). "Some aspects of clay behaviour and their consequences on modelling techniques." American Society for Testing and Materials, Special Technical Publication No. 740, pp. 667-677.

Tavenas, F. Chapeau, C., La Rochelle, P. and Roy, M. (1974). Immediate settlements of three test embankments on champlain clay. Canadian Geotechnical Journal, 11, pp 109-141.

Tavenas, F., Mieussens, C. and Bourges, F. (1979). Lateral displacements in clay foundations under embankments. Canadian Geotechnical Journal, 16, pp 532-550.

Tavenas, F. and Leroueil, S. (1980). The behaviour of embankments on clay foundations. Canadian Geotechnical Journal, 17, pp 236-260.

Taylor, D.W. (1948). Fundamentals of soil mechanics. John Wiley and Sons, New York.

Taylor, R.L. (1977). "Computer procedures for finite element analysis." Chapter 24 in The Finite Element Method, 3rd Edition., O.C. Zienkiewicz, McGraw-Hill.

Terzaghi, K. (1936). Stability of slopes of natural clay. Proc. 1st Int. Conf. Soil Mechanics, Vol. 1, pp. 161-165.

Terzaghi, K. and Peck, R.B. (1948). Soil mechanics in engineeing practice. John Wiley and Sons, New York.

Truesdell, C. (1953). "The mechanical foundations of elasticity and fluid dynamics." J. Rat. Mech. Analys., Vol. 2, pp. 593-616.

Wood, D.M. (1982). "Choice of models for geotechnical predictions." Technical Report CUED/D-SOILS TR126, Engineering Department, Cambridge University, Cambridge, England.

Wood, D.M., Drescher, A. and Budhu, M. (1979). On the determination of stress state in the simple shear apparatus. ASTM Geotechnical Testing Journal, 2(4), pp 211-221.

Wroth, C.P. (1977). "The predicted performance of soft clay under a trial embankment loading based on the Cam-clay model." In Finite Elements in Geomechanics, Ed. by G. Gudehus, John Wiley & Sons, Chapter 6, pp. 191-208.